Faculty of Engineering and Science

Department of Civil and Construction Engineering

Modelling of Sludge Dewatering in Non-Mechanical Systems under Feeding and Non-Feeding Conditions

Huong Yu Zhe

0000-0003-4337-868X

This thesis is presented for the Degree of
Doctor of Philosophy
of
Curtin University

June 2024

DECLARATION

To the best of my knowledge and belief, this thesis contains no material previously published by any other person except where due acknowledgment has been made.

This thesis contains no material which has been accepted for the award of any other degree or diploma in any university.

_____

Huong Yu Zhe

25 March 2024

ACKNOWLEDGEMENT

I want to acknowledge the Faculty of Engineering and Science, Curtin University Sarawak Malaysia, for allowing me to complete my PhD research in Modelling of Sludge Dewatering in Non-Mechanical Systems under Feeding and Non-Feeding Conditions. Also, I would like to acknowledge the Fundamental Research Grant Scheme (FRGS/1/2020/TK0/CURTIN/03/3) by the Ministry of Higher Education Malaysia for the financial support of this research study. I completed my PhD journey smoothly without financial concerns with the scholarship provided. Further, I sincerely thank my supervisors, Dr. Tan Yee Yong, Prof. Tang Fu Ee, and Prof. Agus Saptoro, for their guidance and advice throughout the study. Thanks to Dr. Tan Yee Yong for his time and patience in commenting on this research study under step-by-step supervision. Moreover, I would like to express my gratitude to the laboratory technician, Miss Yuana, for her assistance in doing my laboratory work and to research students Chok Kah Chun, Sabrina Hii, and Chong Jia Xuan, for their help in completing the laboratory-scale STRB in treating septage. Last but not least, many thanks to my family for being supportive during my PhD study, allowing me sufficient time to complete the research.

ABSTRACT

The challenging issue of septage treatment could be due to the higher organic content and low dewaterability of existing treatment systems. The high variability in sludge characteristics and quantity of septage treated hindered the treatment system's performance. A sludge treatment reed bed (STRB), an engineered system modified from the natural wetland, can treat different high organic content sludge. A STRB that meets the treatment requirements has been successfully constructed for this project. The final TS content of the retained solids was at least 20%, which complies with the standard set by the government (Department of Environment). Moreover, the overall effluent TS and COD removals were 82% and 96%, respectively, indicating that the overall STRB performance was favorable. The initial sludge deposit layer thickness affected the effluent flux significantly from the experiment. A thicker sludge deposit thickness has reduced the infiltration and effluent flux, regardless of the loading conditions. The most optimal loading regime was under 100 kg TS/m^2.year SLR and a 6-day resting period, where the bed sustained sufficient moisture for slow dewatering and treatment processes. Meanwhile, the formulated model successfully simulated the hydraulic dynamics in the STRB, which were associated with the moving-boundary conditions due to ponding and sludge accumulation. The average Mean Absolute Error (MAE) and Root Mean Square Error (RMSE) values were 0.039022 and 0.055862, respectively, indicating the robustness of the proposed model in simulating the effluent flux in different flow cases. The strong R2 value of 0.9620 further confirmed the consistency and reliability of the simulation. However, the simulated evapotranspiration rate was relatively low, and the water loss to the atmosphere is only significant in a long-term effect. The model also simulated the sludge accumulation and stabilization of the sludge deposit layer during feeding and non-feeding periods. The flux overprediction in the late phase of the resting period highly influenced the simulated sludge deposit layer thickness, while the simulated organic content matched the measured Total Volatile Solids (TVS) content. In addition, the parametric study revealed the importance of hydraulic load, hydraulic head, saturated hydraulic conductivity, and sludge deposit layer thickness to the overall STRB performance with a limited range.

PUBLICATIONS

1. Huong, Y. Z., Tan, Y. Y., Tang, F. E., & Saptoro, A. (2023). Modelling of Hydraulic Dynamics in Sludge Treatment Reed Beds with Moving Boundary Condition. MATEC Web of Conferences, EDP Sciences, 377, 01013. https://doi.org/10.1051/matecconf/202337701013

2. Tan, Y. Y., Huong, Y. Z., Tang, F. E., & Saptoro, A. (2023). A review of sewage sludge dewatering and stabilisation in reed bed system: towards the process-based modelling. *International Journal of Environmental Science and Technology*. https://doi.org/10.1007/s13762-023-05063-9
3. Huong, Y. Z., Tan, Y. Y., Tang, F. E., & Saptoro, A. (2023). DEWATERING AND STABILIZATION OF SLUDGE RESIDUE IN SLUDGE TREATMENT REED BEDS TREATING SEPTAGE. *Science International*, 35(5), 653-657.
4. Huong, Y. Z., Tan, Y. Y., Tang, F. E., & Saptoro, A. (2024). Influence of sludge deposit layer on sludge treatment reed beds treating septage. *Journal of Water, Sanitation and Hygiene for Development*, washdev2024162. https://doi.org/10.2166/washdev.2024.162

5. Huong, Y. Z., Tan, Y. Y., Tang, F. E., & Saptoro, A. (2024). Modelling sludge dewatering in treatment reed bed considering sludge deposit formation. *Modeling Earth Systems and Environment*. https://doi.org/10.1007/s40808-023-01930-z

TABLE OF CONTENTS

LIST OF FIGURES

LIST OF TABLES

LIST OF ABBREVIATIONS

ADE	Advective-dispersion equation
ANOVA	Analysis of variance
ASM	Activated sludge model
ASTM	American Society for Testing and Materials
BOD	Biological oxygen demand
CCF	Compressible cake filtration
COD	Chemical oxygen demand
DO	Dissolved oxygen
ET	Evapotranspiration
FD	Finite difference / Flow delay
FE	Finite element
FMM	Fixed-mesh method
FP	Flux peak
HL	Hydraulic load
HLR	Hydraulic loading rate
HRC	Hydraulic retention curve
HRT	Hydraulic retention time
LAI	Leaf area index
MAE	Mean absolute error
MAE%	Mean absolute error percentage
MC	Moisture content
MMM	Moving-mesh method
PET	Potential evapotranspiration
PFP	Preferential flow pathway
PT	Potential transpiration
R^2	Coefficient of determination
RE	Richards' equation
RMSE	Root mean square error
RP	Resting period
SA	Sludge accumulation
SL	Shrinkage limit

SLR	Solids loading rate
SPAN	Suruhanjaya Perkhidmatan Air Negara
SRT	Solids retention time
SS	Suspended solids
STRB	Sludge treatment reed bed
T	Thickness
TS	Total solids
TSC	Total solids content
TSS	Total suspended solids
TVS	Total volatile solids
TVSC	Total volatile solids content
USEPA	United States Environment Protection Agency
VGM	van Genuchten-Mualem
VS	Volatile solids
WR	Water recovery

LIST OF ENGLISH SYMBOLS

h	Pressure head $[L]$
t	Time $[t]$
z	Vertical coordinate assumed positive upward $[L]$
K	Unsaturated hydraulic conductivity $[L/t]$
S	Source/sink term $[t^{-1}]$
n	VGM parameter of pore-size distribution $[Dimentionless]$
m	VGM parameter, $m = 1 - 1/n$ $[Dimentionless]$
K_s	Saturated hydraulic conductivity $[L/t]$
l	Mualem's empirical pore-connectivity parameter $[Dimentionless]$
S_{mo}	Source/sink terms for mobile region $[t^{-1}]$
S_{im}	Source/sink terms for immobile region $[t^{-1}]$
Γ_w	Water transfer rate between two regions $[t^{-1}]$
S_e	Effective saturated water content $[Dimentionless]$
S_e^{mo}	Effective saturated water content for mobile region $[Dimentionless]$
S_e^{im}	Effective saturated water content for immobile region $[Dimentionless]$
ET_0	Evapotranspiration rate $[L/t]$
ET_{rad}	Radiation (evaporation) $[L/t]$
ET_{aero}	Aerodynamic (transpiration) $[L/t]$
Δ	Slope of the saturated vapor pressure curve $[M/Lt^2T]$
R_n	Net radiation flux $[M/t^3]$
G	Soil heat flux $[M/t^3]$
c_p	Specific heat of dry air $[L^2/t^2T]$
e_s	Saturation vapor pressure $[M/Lt^2]$
e_a	Actual vapor pressure $[M/Lt^2]$
r_a	Aerodynamic resistance $[t/L]$
r_s	Surface resistance $[t/L]$
γ	Psychrometric constant $[M/Lt^2T]$
E_p	Potential soil evaporation $[L/t]$
T_p	Potential transpiration $[L/t]$
g	Root density function $[L^{-1}]$

z_R	Maximum root depth $[L]$
g_0	Root density at $z = 0$ $[L^{-1}]$
b	Decreasing coefficient of the distribution $[L^{-1}]$
F_{10}	Top 10% of root length density fraction $[Dimentionless]$
c	Solute concentration in aqueous solution $[M/L^3]$
s	Solute concentration adsorbed at solid surface $[M/L^3]$
D	Combined diffusion-dispersion coefficient $[L^2/t]$
q	Volumetric flux $[L^3/L^2t]$
R	Reaction term $[M/L^3t]$
D_d	Diffusion coefficient $[L^2/t]$
D_p	Dispersion coefficient $[L^2/t]$
D_0	Equivalent coefficient in free-water system $[L^2/t]$
a	Soil characteristic constant, $a = 0.001$ $[Dimentionless]$
b	Soil characteristic constant, $b = 10$ $[Dimentionless]$
D_L	Longitudinal dispersivity $[L]$
$\|q\|$	Absolute value of Darcian fluid flux density $[L/t]$
V	Average interstitial flow velocity $[L/t]$
s_e	Equilibrium concentration of solutes at adsorbed phase $[M/M]$
K_d	Distribution coefficient $[L^3/M]$
F	Mass fraction of all sites occupied in instantaneous equilibrium $[Dimentionless]$
s_k	Time-dependent concentration of solutes at adsorbed phase $[M/M]$
c_{mo}	Solute concentrations at mobile region $[M/L^3]$
c_{im}	Solute concentrations at immobile region $[M/L^3]$
s_{mo}^e	Equilibrium adsorbed solute concentrations at mobile region $[M/M]$
s_{im}	Adsorbed solute concentrations at immobile region $[M/M]$
s_{mo}^k	Adsorbed solute concentrations at kinetic sorption sites $[M/M]$
F_{mo}	Mass fraction of all sites occupied in instantaneous equilibrium at mobile region $[Dimentionless]$
f	Fraction of sorption sites in contact with mobile region $[Dimentionless]$
D_{mo}	Dispersion coefficient in mobile region $[L^2/t]$
q_{mo}	Volumetric fluid flux in mobile region $[L/t]$
R_{mo}	Reaction term at mobile region $[M/L^3t]$
R_{im}	Reaction term at immobile region $[M/L^3t]$

R_{mo}^{k}	Reaction term at mobile region of sorption sites $[M/L^3t]$
Γ_{s1}	Physical solute exchange rate $[M/L^3t]$
Γ_{s2}	Chemical kinetic sorption rate $[M/L^3t]$
$s_{mo,e}^{k}$	Equilibrium adsorbed solute concentrations on the solid surface at the mobile region $[M/M]$
$q_{l,c}$	Liquid flux on cake side of interface $[L^3/L^2t]$
$q_{l,s}$	Liquid flux on sludge side of interface $[L^3/L^2t]$
$q_{s,c}$	Solid flux on cake side of interface $[L^3/L^2t]$
$q_{s,s}$	Solid flux on sludge side of interface $[L^3/L^2t]$
$q_{l,m}$	Permeation flux of filtrate through the medium (filtrate flux) $[L^3/L^2t]$
k	Cake permeability coefficient $[L^2]$
p	Pressure $[M/Lt^2]$
k^0	Permeability coefficient at zero compression stress, $p_s = 0$ $[L^2]$
p_a	Scaling factor $[Dimentionless]$
S_O	Dissolved oxygen (O_2 or DO) $[M/L^3]$
S_I	Inert soluble organic material $[M/L^3]$
S_S	Readily biodegradable organic substrates $[M/L^3]$
S_N	Dinitrogen (N_2) $[M/L^3]$
S_{NH}	Ammonium (NH_4^+-N) and ammonia (NH_3-N) nitrogen $[M/L^3]$
S_{NO}	Nitrate (NO_3^--H) and nitrite (NO_2^--H) nitrogen $[M/L^3]$
S_{HCO}	Bicarbonate (HCO_3^-) $[M/L^3]$
S_{PO}	Inorganic soluble phosphorus $[M/L^3]$
X_I	Inert particulate organic material $[M/L^3]$
X_S	Slowly biodegradable substrates $[M/L^3]$
X_H	Heterotrophic organisms $[M/L^3]$
X_A	Autotrophic organisms $[M/L^3]$
i	Iteration number $[Dimentionless]$
N	Number of nodes $[Dimentionless]$
a ; b	Specific coordinates at two extreme locations $[L]$
z_i	Differential of vertical coordinate with respect to time, $z_i(t) = dz_i/dt$ $[L/t]$
q_a	Liquid flux at medium surface $[L^3/L^2t]$
q_0	Prescribed liquid flux $[L^3/L^2t]$

t_0	Initial time $[t]$
t_e	End of loading period $[t]$
t_s	Total simulation time $[t]$
W	Amount of water in medium profile $[L]$
j	Iteration number, $j = i - 1,\ i,\ i + 1$ $[Dimentionless]$
C	Specific moisture capacity $[L^{-1}]$
MB	Mass balance $[t]$
R_{mo}	Reaction term in mobile region $[M/L^3t]$
J	Total flux of solute $[M/L^3t]$
c_0	Concentration of influent liquid $[M/L^3]$
h_i	Prescribed pressure head $[L]$

LIST OF GREEK SYMBOLS

θ	Volumetric water content $[L^3/L^3]$
θ_r	Residual water content $[L^3/L^3]$
θ_s	Saturated water content $[L^3/L^3]$
α	VGM parameter related to inverse of air-entry pressure $[Dimentionless]$
θ_{mo}	Mobile water content $[L^3/L^3]$
θ_{im}	Immobile water content $[L^3/L^3]$
ω	First-order rate coefficient $[t^{-1}]$
λ	Latent heat of vaporization $[L^2/t^2]$
ρ_a	Atmospheric density $[M/L^3]$
γ	Psychrometric constant $[M/Lt^2T]$
α_1	Compensation coefficient $[Dimentionless]$
α_2	Water stress coefficient $[Dimentionless]$
θ_{wilt}	Wilting point $[L^3/L^3]$
ρ	Soil bulk density $[M/L^3]$
μ_1	Rate constant for first-order decay in liquid phase $[Dimentionless]$
μ_2	Rate constant for first-order decay in adsorbed phase $[Dimentionless]$
γ_1	Zero-order production term in liquid phase $[Dimentionless]$
γ_2	Zero-order production term in adsorbed phase $[Dimentionless]$
α_k	First-order rate coefficient $[t^{-1}]$
ω_{s1}	First-order rate constant for physical process $[t^{-1}]$
ω_{s2}	First-order rate constant for chemical process $[t^{-1}]$
ε_c	Particle volume fraction on cake side of interface $[Dimentionless]$
ε_s	Particle volume fraction on sludge side of interface $[Dimentionless]$
μ	Viscosity of liquid $[M/Lt]$
α_c	Specific cake resistance $[L/M]$
ρ_s	Density of solids $[M/L^3]$
ε_s^0	Solid porosity at zero compression stress, $p_s = 0$ $[Dimentionless]$
α^0	Specific cake resistance at zero compression stress, $p_s = 0$ $[L/M]$
β	Solid material characteristic of compressibility $[Dimentionless]$
$\emptyset$	Solid material characteristic of compressibility $[Dimentionless]$

v_i Hydraulic velocity $[L/t]$

γ_i Function of fractional integral constant in time $[Dimentionless]$

δ Dependent variable [L]

δ_a Prescribed tolerance $[L]$

CHAPTER 1: INTRODUCTION

1.1 Background

Parallel to the development of technologies worldwide, environmental pollution has become inevitable. Further, water pollution due to domestic and municipal waste has also greatly impacted the environment. Sludge is a semi-solid slurry in volatile and suspended forms from various wastewater treatment processes. Septic sludge, or septage, is the mixture of sediments and blackwater removed from the septic tank. It is regarded as one of the most common sewage sludges in developing countries (Tayler, 2018). According to statistics, septage management issues have been an emerging challenge in most developing countries, as 2.7 billion people worldwide still rely on septic tanks as the on-site sanitation system. The number is expected to rise to 5 billion by the end of 2030 (Jain *et al.*, 2022).

In most countries, septage is treated by either the centralized or decentralized approach (Mladenov *et al.*, 2022). Both techniques are appropriate for septage management, but the application depends on a country's economic and environmental aspects. The centralized treatment system is preferred in densely populated urban areas with limited land availability, as it is usually a large-scale mechanical system that can provide a high volume of septage management (Tayler, 2018). However, the suburban and rural areas with a lower population density may favor the decentralized method, where septage management is implemented near the households, and the treatment facilities are much smaller. The decentralized approach saves transportation costs, which is utilized for capital investment in constructing more decentralized plants in the local area (Hube & Wu, 2021). A study also recommended that rural areas with large land availability adopt a decentralized treatment approach to reduce overall operational and maintenance costs (Yang *et al.*, 2021).

Among the various existing technologies for septage treatment, the sludge treatment reed bed (STRB) has been well-known for its ease of construction and operation, low operational and maintenance costs, as well as high dewatering and contaminant removal efficiency, making it an ideal system for decentralized septage

management (Joshi *et al.*, 2020; Mustafa & Ali, 2019; Ni *et al.*, 2020). Indeed, standard mechanical technologies for dewatering could be promising for septage treatment due to the application of high-pressurized techniques to force the liquid out. However, a STRB is always capable of achieving comparable rates of dewatering compared to mechanical dewatering, yet it does not require a high energy input and is potentially chemical-free (Carvalho *et al.*, 2017; Nielsen & Larsen, 2016; Tayler, 2018).

Nonetheless, there are still many gaps in operating the STRB to achieve the desirable sludge dewatering and stabilization performance in the long run. Further, forming of the sludge deposit layer on top of the reed bed is always an issue to the system's hydraulic performance, subsequently affecting the overall performance efficiency (Khomenko *et al.*, 2019). The incremental sludge deposit thickness due to continuous sludge loading reduces layer permeability, leading to severe retention of influent sludge on the bed surface. As a result, the start of discharge flow is prolonged, and the infiltration flux decreases over feeding-resting periods.

Therefore, an in-depth understanding of the interaction between the buildup of sludge deposits and operational parameters, such as loading rate and resting period, is crucial to the success of the STRB. In addition, it is essential to understand the relationship between the shrinkage limit of the sludge deposit and its mineralization. Both factors contribute to the formation of cracks on the surface of the sludge layer, subsequently affecting the dewatering efficiency (Khomenko *et al.*, 2019). However, the experimental data is complex due to the high capital cost of constructing the STRB. Thus, the introduction of simulation in predicting the outcomes of hydraulics and the associated sludge deposit effects is needed to save the costs, time, and workload of experiments.

1.2 Problem Statements

A centralized septage treatment plant is consistently implemented in areas with high population density due to the limitation of high capital and operational expenditures (Jung *et al.*, 2018). Therefore, the introduction of decentralized and non-mechanical dewatering technology, such as sludge treatment reed beds (STRBs), is a promising alternative for septage management (Kołecka *et al.*, 2018). Such systems have been

widely applied to dewater the sludge by drainage and evapotranspiration (ET) under low-pressure conditions (Tayler, 2018). Despite extensive studies regarding the dewatering efficiency, STRB is yet to be explored thoroughly (Tan *et al.*, 2017; Tan *et al.*, 2020). The lack of understanding of the effects of operational and design parameters on treatment efficiencies limits the application of STRBs in practice, in which the overloading and lack of non-feeding phases have been reported as operational issues of STRBs (Brix, 2017). In addition, the influence of the loading rates and non-feeding period is strongly linked to the buildup of sludge deposits, which progressively decreases the dewatering capacity as the deposited layer increases in thickness (Tan *et al.*, 2020).

Several process-based models were developed in the past decades to investigate the hydraulic flow in similar systems, particularly in vertical flow constructed wetlands, using software such as HYDRUS (Langergraber *et al.*, 2009; Langergraber & Šimůnek, 2005) and CFD (Rajabzadeh *et al.*, 2015). In hydraulic simulations, Richards' equation (RE) is commonly used to describe the unsaturated hydraulic flow in the porous medium, as in the STRB. Generally, the RE is associated with the van-Genuchten model (VGM) to predict the corresponding water content, hydraulic conductivity, and pressure head. However, these models assumed the sludge deposit as a fixed layer, resulting in over-prediction of the dewatering capacity. This assumption is somewhat valid when the amount of influent solids concentration is low, but it causes a critical problem in simulation when the solid content is high.

In particular, the thickness and hydraulic properties of the sludge deposit layer are highly variable due to the settlement and accumulation of particles during the feeding period (Tan *et al.*, 2017). Accordingly, a typical discretization of these equations by the fixed-mesh method (FMM) has resulted in over-prediction of the hydraulic flow. The top boundary condition is always treated as stationary in the FMM. In such a situation, the sludge loaded on top of the reed bed is assumed to be constant in volume. Thus, the sludge level remains unchanged. Moreover, the FMM simulation could not describe the changes in the thickness of the sludge deposit layer. The changes in the sludge deposit layer thickness are always affected by gravity drainage and evapotranspiration. Therefore, the compressible cake filtration (CCF) theory is identified and is believed to impact the

simulation of dewatering performance in STRB significantly (Friedrich *et al.,* 2022; Höfgen *et al.*, 2019). The CCF uses the moving mesh method (MMM), where the solution nodes constantly change according to monitor function's equation nodes. Such an adaptive mesh refinement scheme improves the drawback of the FMM, as it involves moving boundary conditions. Hence, the numerical simulation studies of the STRB are incorporated with the MMM regarding the moving boundaries of the sludge deposit layer and sludge ponding (Bruce, 2011; Lee *et al.*, 2015; Tang, 2005).

The hydraulic properties of the sludge deposit layer are highly dependent on the organic content. The high volatile solids (VS) sludge fed on STRBs results in sludge deposit layers with low permeability and limited dewatering efficiency (Khomenko *et al.*, 2019). The system efficiency may be overestimated due to discounting the high organic matter in the sludge deposits. Further, this would eventually lead to an extensive reduction in the percolation rate and permanent ponding. Accordingly, the simulation of dewatering dynamics in low-pressure systems should consider the kinetics of sludge mineralization. Moreover, the sludge deposit layer cracks due to the continuous moisture loss during the non-feeding period (Tan *et al.*, 2017). The shrinkage limit of the sludge deposit is believed to relate to sludge mineralization, where the sludge deposit with high organic content cracks easily due to the higher shrinkage limit.

Therefore, a process-based model is developed in this study to determine the hydraulic properties and the dynamics of drainage flow in STRBs. Due to the variability of the sludge deposit layer, the simulation treats the system as a moving boundary problem, and a CCF concept is considered. In addition, the shrinkage limit of the sludge deposit is studied as it is crucial for understanding deformability regarding the composition and water content. This study would contribute to knowledge in STRBs and bridge the theory and practice of the learning.

1.3 Research Questions

In this project, a fundamental model is proposed to investigate the mechanism of sludge dewatering under a low-pressure condition and the hydraulic properties of sludge

deposits under both feeding and non-feeding conditions. The research questions of this study are as follows:

1. How does the sludge deposit accumulation affect the hydraulic properties and dewatering dynamics of the reed beds operated under varying solid loading rates and resting periods?
2. How can the dewatering dynamics of septic sludge under low-pressure conditions and the hydraulic properties of the sludge deposit under feeding and non-feeding conditions, be robustly simulated by integrating a range of modeling theories?
3. What are the limitations of implementing the compressible cake filtration theory and the moving mesh method in the model to simulate the specific resistance and moving-boundary condition in sludge dewatering for loading rates and influent characteristics? What are the approaches to mitigate these limitations and enhance the robustness of the model?
4. How do the parameters of sludge mineralization and shrinkage limit affect the sludge dewatering and associated deformation of sludge deposits under non-feeding conditions?

1.4 Aim and Objectives

In project aims to develop a mechanistic model that can incorporate the moving boundaries of the hydraulic load with respective discharge flux and the sludge deposit layer with mineralization. Further, a laboratory-scale STRB is constructed and operated to obtain necessary data for results calibration and validation. These aims would be achieved with the following objectives:

1. To determine the influence of sludge deposit accumulation on the hydraulic properties and dewatering dynamics in the laboratory-scale reed beds under varying solid loading rates and resting periods.
2. To formulate and validate a fundamental model for the dewatering dynamics of septic sludge under low-pressure conditions and hydraulic properties of sludge deposit under feeding and non-feeding conditions.

3. To examine the applicability and robustness of implementing the compressible cake filtration theory and moving mesh method in the simulation of septic sludge dewatering.
4. To assess the effect of sludge mineralization and the shrinkage limit on the septic sludge dewatering and associated deformation of sludge deposit.

This study uses MATLAB® Simulink R2023b to develop a mechanistic model to simulate the hydraulic flow and solute transport in the STRB. The moving mesh method is considered in the simulation of hydraulic flow and sludge deposit formation is a novel approach in the study area. Six laboratory-scale STRBs were constructed to acquire experimental results for calibration and validation of the model, as well as interpretation and analysis of the model developed. Septage is used in this project study, so the term "sludge" refers to septage hereafter. Moreover, the shrinkage limit of the sludge deposit upon dewatering and mineralizing is investigated to gain insight into the relationship between the deformation and mineralization of the sludge deposit and its impact on the performance of STRB. In the end, a parametric analysis with different loading rates and resting periods is conducted through simulation to improve the applicability and robustness of the system.

1.5 Research Significance

Many countries use mechanical systems in dewatering sludge to reduce treatment duration and land distribution. However, the operational cost of running a mechanical system is higher than the capital cost in the long term. The STRB is an alternative non-mechanical system to dewater sludge under low-pressure conditions. It requires less operation and maintenance costs throughout the lifespan. The STRB is an environmentally friendly solution, but it is not widely utilized in Malaysia. The study of STRB provides an understanding of non-mechanical sludge treatment that can be implemented in municipal and industry areas.

To date, little work has been carried out to formulate a model for sludge dewatering in non-mechanical systems such as STRB, and previous works have yet to comprehensively consider the influence of the sludge deposit layer (Tan *et al.*, 2023). The

solids settling on the bed surface accumulate and compact the sludge deposit layer, reducing the layer permeability over time. The limited hydraulic conductivity deteriorates the STRB performance by prolonging the sludge retention time on the bed surface. As a result, the discharge effluents are slow but clean, and the final solids are high in moisture content (MC), affecting the STRB operation economically and timewise. Therefore, it is crucial to understand the sludge deposit layer with associated infiltration flux and MC.

The simultaneous integration and utilization of moving mesh and compressible cake filtration concepts provide a novel idea for modeling sludge dewatering under low-pressure conditions. The infiltration flux is directly related to the pressure head of the hydraulic load and the permeability of the sludge deposit layer. Thus, applying moving boundary conditions reduces flux overprediction as the theory complies with the changes in the temporary sludge ponding level and sludge deposit layer thickness. Therefore, this study develops and presents a fundamental model for the dynamics of sludge dewatering through gravity drainage and evapotranspiration under low-pressure conditions, in which the hydraulic properties of sludge deposit under feeding and non-feeding conditions are considered.

The findings of this research facilitate the design and operation of low-pressure STRB systems in the local context. The STRB operating duration requires months to accumulate sufficient data. Meanwhile, the simulation study allows instant results prediction when sufficient input parameters are provided. The simulation study shortens the experimental duration in determining the optimal loading rates and sludge characteristics on the dewatering efficiency in STRB. The sludge loading rate differs for climatic countries (Gholipour *et al.*, 2022), and is always affected by the sludge density. Insufficient and excessive sludge loading would lead to underperformance in sludge dewatering due to crack occurrence and ponding conditions.

Moreover, the proposed model considers the shrinkage limit of the sludge deposit and sludge mineralization, which provides insightful information about the relationship between dewatering dynamics and the deformation of sludge deposits during the non-feeding period. The sludge deposit cracks during the resting period, leading to influent septage bypassing the STRB. Such an unwanted circumstance is believed to be caused by

the high organic content and shrinkage limit of the sludge deposit layer. Hence, understanding the sludge deposit shrinkage limit would avoid cracks.

In summary, the research outcomes provide a solid foundation for future research directions in the optimization of sludge dewatering technologies and contribute knowledge to the simulation of sludge deposit formation in low-pressure systems. The knowledge from this research also contributes to the design and operation parameters of this sustainable technology to solve the septage management issue in Malaysia.

1.6 Scope and Limitation

This study presents the construction, implementation, and outcomes of numerical modeling of STRBs with the combination of fixed and moving boundaries of the sludge deposit layer on top of the reed bed and the hydraulic flows due to the varying sludge ponding levels. The experimental data are collected from the laboratory-scale STRB to calibrate and validate the simulated results. The scope of the study is as follows:

- The proposed model is developed using MATLAB® Simulink R2023b to predict the hydraulic flow for dewatering dynamics with a moving sludge deposit layer in a laboratory-scale STRB system. The study's outcome prioritizes the simulation's precision, followed by computational efficiency and mathematical optimization.
- The proposed model is developed and conceptualized to prioritize practicality. The comprehensiveness of the equations and the selection of the numerical approach used in the proposed model are based on the simulation's applicability, versatility, accuracy, and computation time, as well as the literature available on the subject.
- The proposed model is developed in tandem with the laboratory-scale STRB system. Hence, the upper and lower boundary conditions are temporal flux-and-pond and free drainage.
- The proposed model is developed as a mechanistic model to relate the hydraulic behavior and sludge deposit to the dewatering efficiency and treatment performance. Thus, the quantification of heat transfer, oxygen restoration, organic

carbon cycle, alkalinity consumption, water loss during the resting period, and microbial community development were outside the scope of the study.

- The proposed model is developed, calibrated, and validated based on the error analysis of the measured data rather than the existing models in the literature for its accuracy and efficiency as the operating conditions and sludge characteristics differ for STRBs.

1.7 Thesis Outline

The ultimate objective of this project study is to develop a mechanistic model to estimate the moving boundaries due to the compressible sludge deposit layer and the associated hydraulic flow with the aid of laboratory-scale experimental data for the calibration and validation needed. Meanwhile, the sludge stabilization of the sludge deposit layer is predicted via the mentioned model, and a parametric study for the different loading and resting periods is carried out.

In **CHAPTER 2**, the status quo of wastewater management in Malaysia is addressed. Several different types of existing technologies for dewatering and biological treatment are discussed. Furthermore, an overview of the STRB and its performance efficiencies is presented. The recent studies of the STRB worldwide are also presented in detail. Moreover, a literature review on the existing numerical models and moving mesh method (MMM) due to compressible sludge deposit layer is presented.

CHAPTER 3 presents the configurations of the laboratory-scale experimental rigs and procedures, as well as the laboratory tests and analyses. The operational regime employed in this study and the sampling analysis protocols are presented. The experiment's configuration can be separated into sludge deposits and effluents. The components' dewatering efficiency, water content, and mineralization are discussed. A list and diagrams of the probe and equipment used are included to complete the methodology. On the other hand, this chapter also discusses the theory, and features employed in the proposed mechanistic model. The assumptions and limitations of the model are summarized. The model is subdivided into hydraulic, transport, and kinetics modules. The governing equations such as mixed form Richards' equation (RE),

velocity-based RE, Penman-Monteith equation, advection-dispersion equation (ADE), compressible cake filtration (CCF) model, and activated sludge model (ASM) are included in the proposed model and associated by the MMM. Then, each module's numerical implementation, initial conditions, and boundary conditions for the development of MATLAB® simulation are demonstrated.

In **CHAPTER 4**, the hydraulic dynamics and treatment performance of the laboratory-scale STRB are reported. In the first section, the preliminary experimental results are presented to highlight the feasibility of the STRB system in septage treatment. The measured data obtained from the laboratory-scale reed bed system are analyzed according to water recovery (WR), delay of flow occurrence, and peak effluent flux. The effects of solids loading rate (SLR) and resting period on the sludge deposit layer thickness, moisture content (MC), total solids content (TSC), and total volatile solids content (TVSC) are also discussed. Moreover, the effluent quality, including COD, NO_3, pH, DO, and TS, with the associated treatment efficiencies are presented. In addition, the characteristics of raw septage used in the study are also explained. Lastly, the ANOVA study was conducted to determine the significance of the dependent variables over the SLRs and resting periods.

In **CHAPTER 5**, the results of the simulated hydraulic behavior from the proposed model are illustrated and discussed. The simulation setup, assumptions, procedure for calibration, and input parameters are introduced. Then, the error analysis between the simulated results and measured data is compared and analyzed. Moreover, the analysis of the influence of evapotranspiration (ET) and sludge accumulation (SA) rate of the compressible sludge deposit layer on hydraulic simulation is also discussed in this chapter. Moreover, the sludge stabilization is performed by applying activated sludge model no.3 (ASM3). The kinetic model for the sludge deposit stabilization is completed to assess the possible growth and decay of the microorganisms in the sludge deposit. Hence, the organic content of sludge stabilization is compared between the measured and simulated data. Finally, the MMM and FMM simulations are compared to prove the robustness of applying moving boundary conditions in STRBs.

In **CHAPTER 6**, the parametric study is conducted for varying hydraulic loads, heads, saturated conductivities, and sludge deposit thicknesses on the effluent flux, sludge deposit layer thickness and MC, sludge stabilization, and potential ET rate. The manipulated variables are obtained from the calibrated hydraulic model, with SLR and resting period ranging from 50 to 450 kg/m^2/year and 3 to 30 days, respectively. Meanwhile, the analyzed hydraulic pressures ranged from -7 to -30 cm, whereas the saturated conductivities of the sludge deposit layer were tested from 0.0009 to 0.1269 cm/min. Additionally, the sludge deposit layer thicknesses ranged from 4 to 20 cm. The other constant variables are estimated from the consistency of tested experimental data, such as sludge and sludge deposit porosities, density, thickness, and initial COD concentration.

CHAPTER 2: LITERATURE REVIEW

2.1 Wet and Dry Sanitation Systems

Excreta is defined as any waste created and discharged by human bodies, such as liquid urine and solid faeces containing relatively high organic matter. Hence, the term "sanitation system" is describes the treatment process in collecting and disposing of excreta (Jain *et al.*, 2022). The method of sanitation can be classified into two major systems: the dry and the wet sanitation systems, as shown in Figure 2.1 (Tayler, 2018).

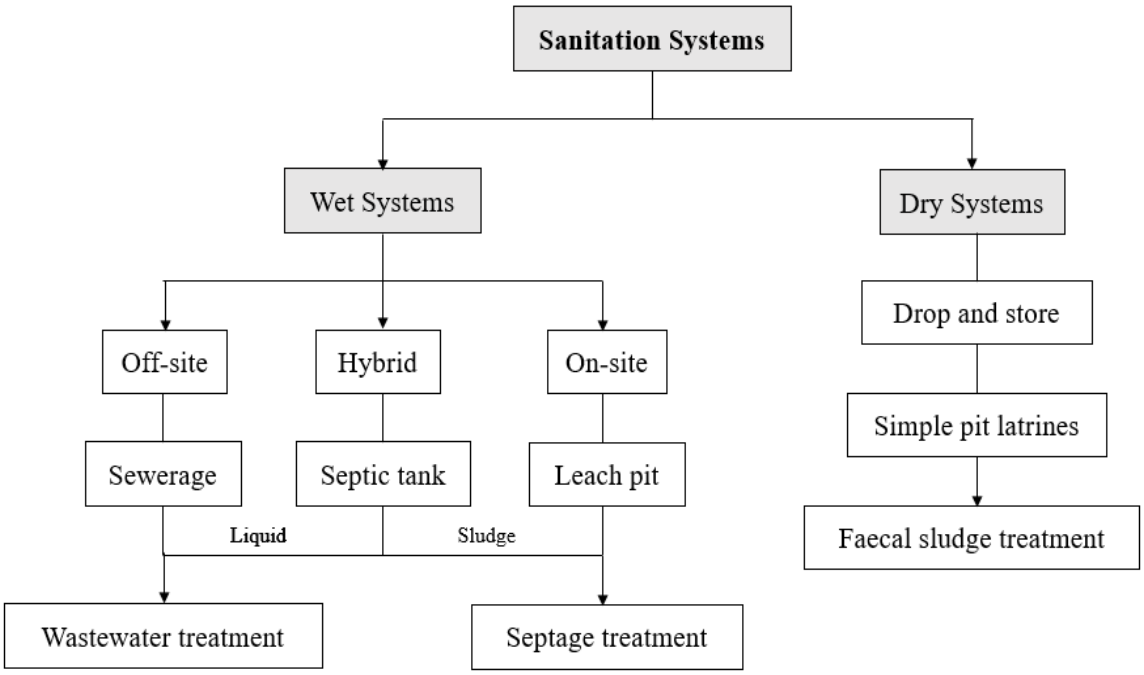

Figure 2.1: Sanitation Systems.
Note: Adapted from "Faecal Sludge and Septage Treatment – A guide for low- and middle-income countries," by Tayler, K., *Practical Action Publishing,* 2018.

The dry sanitation system is commonly known as a direct-drop toilet, while the wet or water-borne sanitation system works by discharging the excreta through discharge pipes with liquid. The significant difference between the two systems is that the dry sanitation system does not involve water to flush away the excreta but collects them by putting a pit or vault under the toilet directly (Gupta *et al.*, 2023).

In the wet system, the mixture of faeces, urine, and flush water is known as black water. The black water was retained in a septic tank and required further treatment. In developing countries such as Malaysia, the septic tank is always the first choice to be implemented (Tan *et al.*, 2023). The relatively low capital and maintenance costs of the septic tank allows domestic affordability (Krzyk & Drev, 2023).

The wet sanitation system is categorized into three major disposal systems. The on-site sanitation system collects and retains the solid waste in a pit or tank, thus allowing the liquid waste to diffuse into the ground. In contrast, an off-site system collects and retains solid and liquid wastes in a container before removing them through a sewer system (Tayler, 2018). Combining on-site and off-site sanitation systems is then known as a hybrid system. In most countries, the hybrid system is always preferable for domestic sanitation, where the solid waste is collected and retained on-site while the liquid waste is sent off-site (Conaway *et al.*, 2023).

2.2 Sludge Characteristics

Sewage sludge from various sources, including septic tanks, pit latrines, and sewage treatment plants, shows considerable variability in its characteristics. Septic sludge often has high total solids (TS), typically exceeding 10,000 mg/L, with variability influenced by factors such as tank dimensions, desludging frequency, and climate (Tan *et al.*, 2017). Further, faecal sludge from pit latrines generally exhibits even higher TS concentrations and variable volatile solids (VS) ratios, reflecting different stabilization processes (Jain *et al.*, 2022; Osei *et al.*, 2019). In contrast, surplus-activated sludge from sewage treatment plants has lower TS compared to septic sludge but can still have high chemical oxygen demand (COD) levels, indicating significant organic pollution (Wang, Zhao, *et al.*, 2022; Zhong *et al.*, 2021)

Key quality parameters, such as TS, VS, and COD, are essential for designing and operating sludge treatment systems. Heavy metal concentrations are typically low in septic and faecal sludges but can be higher in surplus-activated sludge, which requires careful monitoring (Chandana & Rao, 2022). Additionally, emerging pollutants like antibiotics and polycyclic aromatic hydrocarbons (PAHs) have been reported,

complicating sludge management (Cui *et al.*, 2015; Ma *et al.*, 2020; Ma *et al.*, 2021). Therefore, effective treatment systems must address these variables to ensure compliance with environmental standards and optimize sludge handling processes.

2.3 The Importance of Sludge Treatment

People require clean and safe drinking water to survive. Untreated sludge possesses bacteria and heavy metals. Many alternatives to treating the sludge include reed beds (Parde *et al.*, 2021) and lagoons (Owusu-Twum & Sharara, 2020). The bacteria and any other microorganisms can be easily removed throughout the wastewater treatment process, but the heavy metals require specific techniques for removal. For instance, ion exchange (Bashir *et al.*, 2019), chemical precipitation (Zhang & Duan, 2020), membrane filtration (Efome *et al.*, 2019), and adsorption (Chai *et al.*, 2021) are the common approaches to retain or filter the heavy metals. Hence, the primary purposes of wastewater treatment are (Karia *et al.*, 2023):

- To reduce the chemical oxygen demand (COD), biological oxygen demand (BOD_5), suspended solids (SS), oil and grease (O&G), and nutrients such as phosphorus (P), ammonia nitrogen (NH_4-N), and nitrate (NO_3) to comply with national environmental regulations.
- To reduce the water content in the sludge to a point where a dried solid is produced, ensuring that it is easier, cheaper, and safer to handle and transport.

In Malaysia, a standard for wastewater effluent discharge and sludge treatment requirements is formulated according to the National Water Services Commission or Suruhanjaya Perkhidmatan Air Negara (SPAN). These discharge standards are then partitioned into Standard A and B according to the Environmental Quality Act, which specifies the water release to upstream and downstream waterbodies, respectively. The Malaysia's standards of wastewater effluent discharge limits (ppm or mg/l) are given in Table 2.1 (SPAN, 2008). The main objective of the existence of these standards is to ensure the limitation of the contaminants discharged to any water bodies, so that the parameters of BOD_5, SS, COD, NH_4-N, NO_3, P, and O&G comply with the national

environmental regulations (SPAN, 2008). The allowable discharge concentrations are lower in the upstream to minimize the pollution dealt to the downstream waterbodies.

Table 2.1: Malaysia's wastewater effluent discharge standards.
Note: Adapted from "Malaysia Sewerage Industry Guidelines – Sewage Treatment Plants," by SPAN, *National Water Services Commission, Ministry of Energy, Water and Communications*, 2008.

Parameter	Effluent discharge to river or stream (ppm)		Effluent discharge to stagnant water [ponds and lakes] (ppm)	
	Standard A (upstream)	Standard B (downstream)	Standard A (upstream)	Standard B (downstream)
BOD_5	10-20	20-50	10-20	20-50
SS	20-50	40-100	20-50	40-100
COD	60-120	100-200	60-120	100-200
NH_4-N	5-10	10-20	2-5	2-5
NO_3	10-20	20-50	5-10	5-10
P	N/A	N/A	2-5	5-10
O&G	2-5	5-10	2-5	5-10

On the other hand, the treated sludge must have a total solid content of not more than 4.0% in liquid form and attain a minimum of 20% dry solid content before disposal or use for any other purposes (Tayler, 2018). In Malaysia, the sludge treatment process follows the sequence of thickening, stabilizing, conditioning, and finally dewatering, as shown in Figure 2.2, to meet the requirements stipulated by the Department of Environment (SPAN, 2008).

A typical sludge treatment and disposal strategy can be separated into three main stages (Tayler, 2018). In stage one, the untreated sludge is screened to remove relatively large solid particles that can deteriorate the treatment plant. Then, a primary thickener, such as a centrifuge or gravity thickener, is installed to increase the dry solids content from 1% to 6%, approximately by removing the volume of free water. Biological treatment of thickened sludge involves either aerobic or anaerobic digestion to stabilize and reduce sludge volume. Aerobic digestion uses oxygen to decompose organic matter, while anaerobic digestion breaks down sludge in the absence of oxygen, producing biogas and stabilized sludge. In stage two, the thickened sludge is optionally conditioned using chemicals initially before dewatering. There are two types of dewatering:

mechanical dewatering, such as belt press and centrifuge press, and non-mechanical dewatering, such as drying beds and sludge lagoons. In stage three, the dried sludge is finally used for land reclamation land application or sent to a landfill site for disposal.

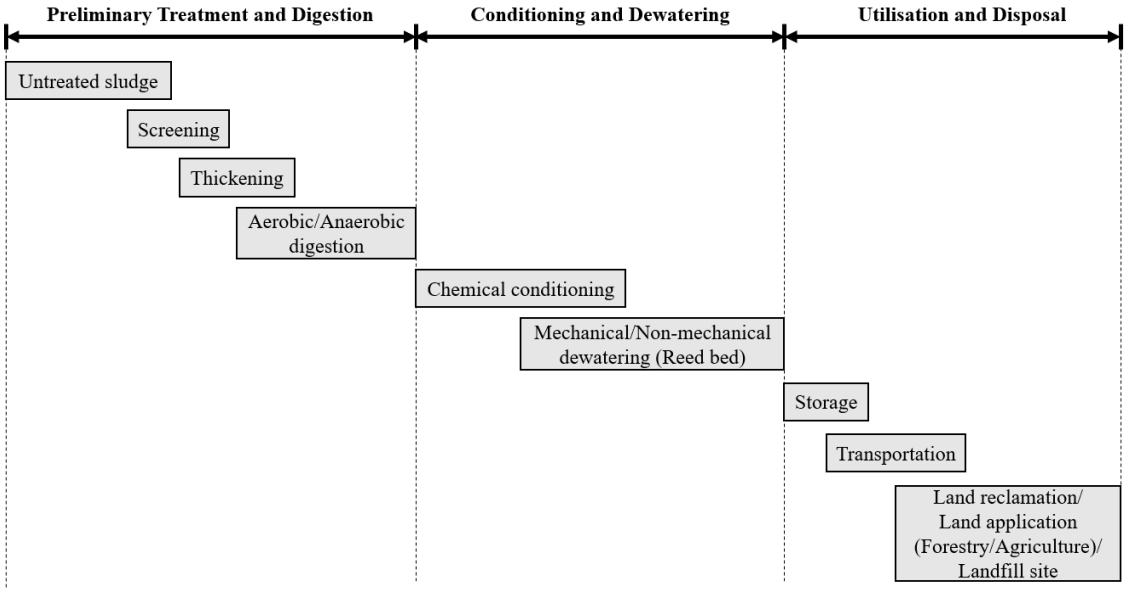

Figure 2.2: Sequence of sludge treatment process.
Note: Adapted from "Faecal Sludge and Septage Treatment – A guide for low- and middle-income countries," by Tayler, K., *Practical Action Publishing,* 2018.

2.4 Centralized versus Decentralized Treatment

Most existing septage treatment plants are centralized, using one plant serving a town, city or even district. However, many environmentalists including private researchers and government authorities, have raised critical concerns about implementing the decentralization of septage treatment. The advantages and disadvantages of the centralized and decentralized approaches are listed in Table 2.2 (Tayler, 2018).

Table 2.2: Centralized versus decentralized approaches.
Note: Adapted from "Faecal Sludge and Septage Treatment – A guide for low- and middle-income countries," by Tayler, K., *Practical Action Publishing,* 2018.

Centralized approach	Decentralized approach
Advantages	
• A larger centralized treatment plant requires relatively low capital and	• Reduced haul distances, thus reducing transport costs and haulage time.

operational costs. • A small number of centralized plants are easy to manage and maintain compared to many decentralized plants. • More lands are saved and can be used for other means.	• Extra individual economic income, where the treated liquid and solids can be used for agricultural purposes. • Smaller loadings allow for more straightforward and cheaper technologies to be employed.
Disadvantages	
• Longer haul distances lead to an increase in transport costs. • The relatively high loading on a single plant complicates the treatment technologies. • A large and sophisticated plant requires skilled operators, increasing the maintenance cost.	• Possess difficulties searching for an appropriate decentralized location and opposition from people living near the proposed site. • Difficulties in managing, monitoring, and maintaining the distributed sites. • Potential risk of insufficient loading to cover up the cost of technologies.

In summary, the decentralized approach has a higher potential to be beneficial for a developing country due to its lower maintenance and transportation costs, as well as promising extra income for private industry (Capodaglio *et al.*, 2017; Jung *et al.*, 2018; Sharma & Sharma, 2018). In addition, the final dried solids can be further processed to manufacture fertilizer for vegetation. This fertilizer could be organic or inorganic, depending on the types of sludge treated.

2.5 Types of Existing Technologies

Generally, the sludge treatment processes can be categorized into solids-liquid separation and liquid-liquid separation (Singh & Gurjar, 2023). In solid-liquid separation, the solids waste is extracted from the sludge in mechanical or non-mechanical ways (Tayler, 2018). Many types of technologies exist for solids-liquid separation depending on one's willingness and preference. However, the selection of technologies and the implementation techniques are critically important for proper sludge treatment.

Table 2.3 and Table 2.4 present the standard technologies and brief descriptions for solids-liquid and liquid-liquid separations used worldwide. Among them, mechanical presses and gravity thickeners are widely used in industry for solid extraction. In contrast,

applications such as anaerobic ponds and sludge treatment reed beds are commonly used for liquid treatment in wastewater management. Unlike solids-liquid extraction, the primary mechanism applied in liquid-liquid separation is entirely depends on microorganisms and probably chemicals (Tayler, 2018). Thus, chemical-free technologies are always the first choice regarding a developing country's decision.

Table 2.3: Solids-liquid separation techniques.
Note: Adapted from "Faecal Sludge and Septage Treatment – A guide for low- and middle-income countries," by Tayler, K., *Practical Action Publishing,* 2018.

Types	Description	Reference
Sludge drying beds	Separation of solid and liquid via settling, evaporation, and filtration.	May Cua (2019)
Anaerobic ponds	Separation of solid and liquid with organic load reduction.	Adwet *et al.* (2019)
Imhoff tanks	Design for solid-liquid separation on top of the settled solids digestion.	Gabr (2022)
Settling-thickening tanks	A rectangular batch tank includes the surface water for further liquid treatment.	Shahid *et al.* (2022)
Mechanical presses	Use pressure to remove the liquid from the sludge through a filter cloth or fine sieve.	Bień and Bień (2022)
Gravity thickeners	Utilize the most general settling mechanism.	Fawell *et al.* (2021)
Decanting drying beds	Remove the water by both decanting and evaporation.	Elbaza *et al.* (2021)

Table 2.4: Liquid-liquid separation techniques.
Note: Adapted from "Faecal Sludge and Septage Treatment – A guide for low- and middle-income countries," by Tayler, K., *Practical Action Publishing,* 2018.

Types	Description	Reference
Anaerobic		
Anaerobic ponds	Utilizes the anaerobic bacteria to decompose organic compounds.	Putro *et al.* (2020)
Anaerobic baffled reactor	An improved septic tank consists of baffles to increase the contact time between sludge and organic matter.	Khalekuzzaman *et al.* (2019)
Upflow anaerobic sludge blanket reactor	It depends on the anaerobic bacteria in the sludge blanket to convert organic materials into biogas, thus flowing upward through the reactor.	Sierra *et al.* (2019)

Aerobic		
Facultative ponds	A shallow pond possesses an aerobic zone to contact with oxygen in the air.	Ho *et al.* (2019)
Aerated lagoons	A lagoon that consists of artificial aeration to promote biological decomposition.	Malovanyy *et al.* (2018)
Sludge treatment reed beds (STRB)	An artificial wetland removes the organic matter through vegetation.	Li *et al.* (2020)
Trickling filters	Deploy a range of media that promotes a biofilm for decomposing the organic matter.	Yang *et al.* (2019)
Rotating biological contactors	A biological fixed film attached to a disk which rotates slowly in the sludge.	Waqas and Bilad (2019)
Activated sludge reactor	Employ a multi-chamber reactor unit comprising intensively concentrated microorganisms to degrade organic materials continuously.	Sánchez *et al.* (2018)
Sequencing batch reactor	Use one or more batch reactors to decompose the organic matter intermittently.	Li *et al.* (2019)
Moving-bed biofilm reactor	An advanced technology combines both biofilm and activated sludge processes.	Ashkanani *et al.* (2019)
Oxidation ditches	A modified activated sludge biological treatment process employs relatively long solids retention times (SRTs) to degrade organic matter.	Luo *et al.* (2021)

In addition, studies have shown that the sludge dewatered via belt presses or centrifuges delivered a lower dry solid content of 15-24% and 15-20%, respectively, whereas the sludge treated by STRB has reached a dry solid content of 25-40% (Nielsen & Larsen, 2016). Therefore, several comparisons among the standard wastewater treatment options can be found in Table 2.5 (Nielsen & Larsen, 2016; Tayler, 2018).

Table 2.5: Comparison between mechanical and non-mechanical methods.
Note: Adapted from "Operational strategy, economic and environmental performance of sludge treatment reed bed systems – based on 28 years of experience," by Nielsen, S., and Larsen, J.D., *Water Sci Technology*, 2016.

Solids-liquid separation methods	**Typical solids content of dried sludge**	**Percentage reduction in liquid strength**	
		TSS	**BOD**

Sludge treatment reed beds	At least 20% depending on the climate and retention time.	95%	70 – 90%
Anaerobic ponds	Typically, 10%	Perhaps 80%	Around 60% at 20°C depending on temperature.
Belt presses	Typically, 12 – 35% depending on the type of sludge.	30 - 60%	30 – 50%
Gravity thickening in hopper-bottomed tanks	4 – 10% but typically 6%.	30 - 60%	30 – 50%

2.6 Sludge Treatment Reed Beds (STRBs)

The sludge treatment reed bed (STRB) is one of the most promising alternative solutions for sewage sludge treatment, especially in tropical and sub-tropical countries (Al-Rashdi *et al.*, 2024; Varma *et al.*, 2021). The other common names used for the STRB are constructed wetlands, treatment wetlands, artificial wetlands, etc. (Carvalho *et al.*, 2017). STRB involves sedimentation, filtration, evapotranspiration, evaporation, and adsorption. STRBs can remove a large amount of BOD, COD, and TN (Al-Ajalin *et al.*, 2020a; Haydar *et al.*, 2020; Salem *et al.*, 2022).

The STRB is an engineered system modified from natural wetlands that can dry the sludge and treat the wastewater by drainage and evapotranspiration (ET) under low-pressure conditions (Tayler, 2018). According to Nielsen and Larsen (2016), STRBs designated for sludge dewatering and mineralization have existed in Europe since the late 1980s (Carvalho *et al.*, 2017).

The STRB uses both physical and biochemical processes to treat the sludge (Nielsen, 2023). The sludge is fed intermittently on top of the reed bed, and liquid is allowed to diffuse downwards through the bed, where a multi-layered granular substrate filter is found. Thus, the solid waste is physically retained on the bed surface, producing a layer of sludge deposit, while the liquid waste is discharged from the bottom of the bed (Tan *et al.*, 2017). A schematic diagram of a typical STRB is displayed in Figure 2.3.

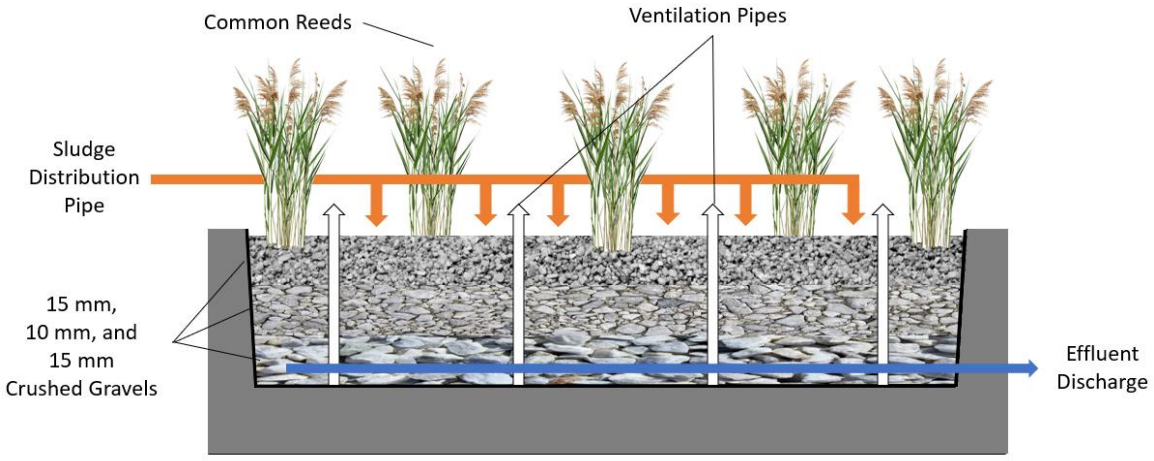

Figure 2.3: Schematic diagram of STRB.

The STRB has become popular and is commonly implemented in many countries to treat wastewater. It delivers a great outcome on environmental, economic, and operational requirements, unlike mechanical sludge dewatering approaches that use relatively high-pressure systems to force the water out. Studies have shown that the sludge dewatered via STRB can achieve a 25-40% dried solid content, comparable to mechanical dewatering techniques (Nielsen & Larsen, 2016; Nielsen & Stefanakis, 2020). Moreover, biological treatment occurs throughout the dewatering processes in the STRB, which makes it preferable to mechanical treatment. The concentration of TS, COD, and BOD removal in the effluent of STRBs was more efficient than that of the pressurized techniques (Tayler, 2018).

Therefore, the capital cost of a common STRB is often higher than that of a mechanical dewatering device. Still, they offer benefits such as less energy usage, are naturally chemical-free, and produce relatively high-density biosolids (Nielsen & Larsen, 2016). However, the overall cost of wastewater treatment by mechanical techniques is higher than that of the STRB by at least 50%, mainly due to the high energy input required (Nielsen & Stefanakis, 2020). Further, the operating costs can be reduced by up to 90% with the implementation of STRB (Stefanakis, 2020). Therefore, the STRB is widely regarded as an eco-friendly solution for sludge treatment, due to its natural processes and economic and operational benefits (Kołecka *et al.*, 2016).

Figure 2.4 shows the factors affecting the STRB performance, such as sludge characteristics (Tan *et al.*, 2023), system operating conditions (Gholipour *et al.*, 2022), substrate media (Jain *et al.*, 2022), macrophytes (Osei *et al.*, 2019), and sludge deposit layer (Huong *et al.*, 2024a). Moreover, pH (Sánchez *et al.*, 2021) and temperature (Ji *et al.*, 2020) are some additional factors affecting the STRB performance.

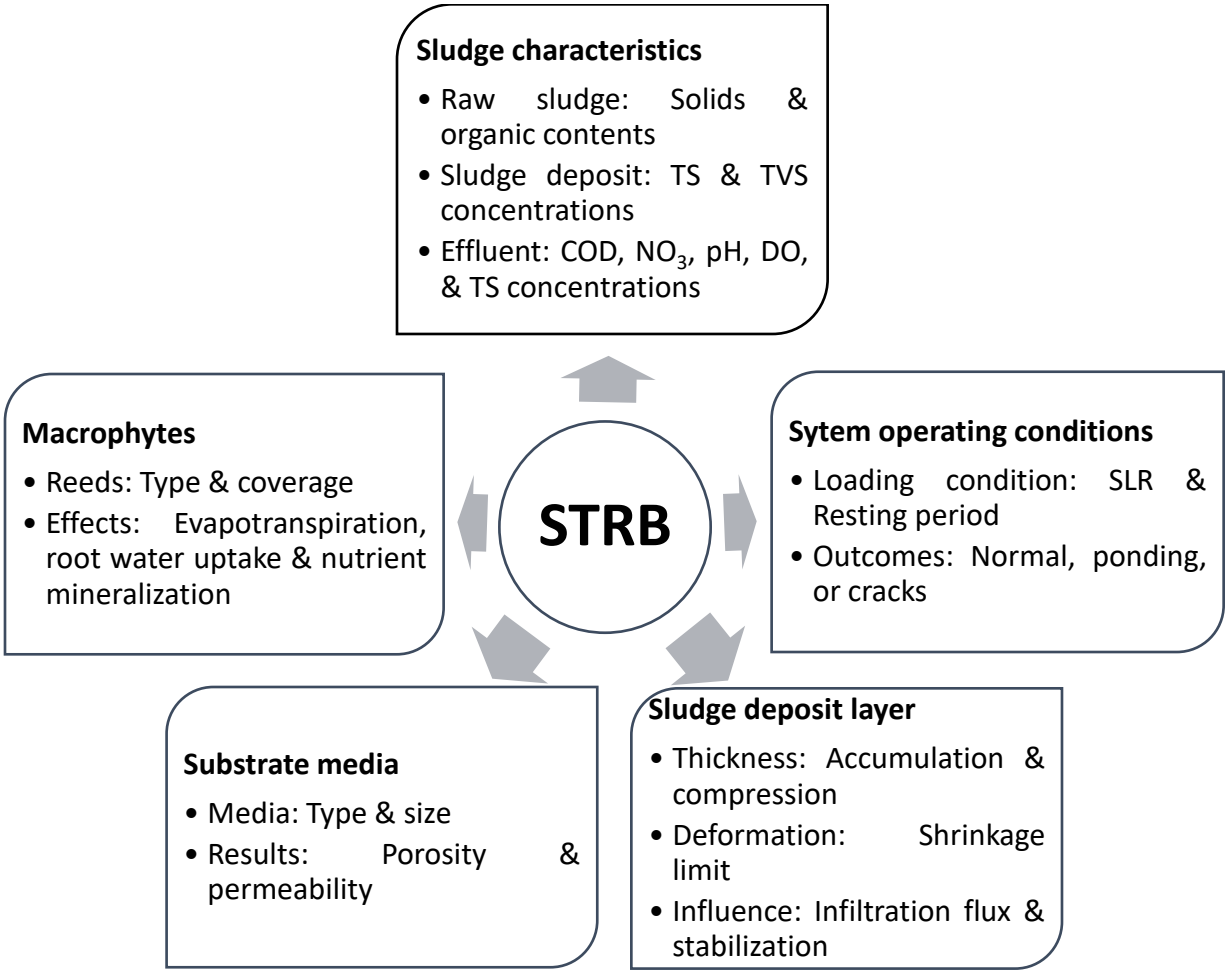

Figure 2.4: Factors affecting the sludge treatment reed bed (STRB).

In summary, raw sludge with high solid and organic contents is deemed to increase TS and total volatile solids (TVS) accumulated in sludge deposit layer, improving effluent quality, due to the thickened layer. Sludge accumulation directly increases the sludge deposit layer thickness, while compression and deformation due to hydraulic load and low shrinkage limit decrease its thickness. The sludge deposit layer cracks whenever the moisture content is lower than the shrinkage limit, influencing

infiltration flux and sludge deposit stabilization (Khomenko *et al.*, 2019). The type and size of substrate medium used in STRB system also affect overall porosity and permeability, subsequently impacting the infiltration flux and effluent quality. The size of the substrate medium increases from top to bottom, aiming to filter different sizes of solids. In contrast, the type and coverage of macrophytes affect evapotranspiration rate, root water uptake, and nutrient mineralization. This helps to remove sludge deposit moisture and enhance biological treatment. Further, an optimal SLR and resting period ensure a normal case flow (Tan *et al.*, 2017). By means, a relatively small SLR and long resting period would lead to cracks in the sludge deposit layer. Whereas an extensively high SLR and short resting period would result in ponding conditions. Additionally, unfavored pH condition of the STRB leads to retardation in macrophyte growth, resulting in reduced mineralization. This affects the overall evapotranspiration and the effluent quality. Lastly, temperature also affects the STRB performance. The evapotranspiration rate is high under hot climatic conditions, where the moisture loss to the surrounding increases, enhancing the drying of the sludge deposit.

2.7 The Sludge Deposit Layer and the Compressible Cake Theory

The influent septic sludge often contains volatile solids (VS). The VS contains active microorganisms crucial for decomposing organic matter in the sludge (Das *et al.*, 2023). The breakdown of organic materials is essential for the growth of plants and directly affects the purification process of wastewater treatment. During infiltration, the VS are retained on the bed surface, while the wastewater diffuses through the filter medium and is discharged from the bottom of the bed. The VS accumulates by settling, forming the sludge deposit layer, which increases the infiltration duration and improves water distribution. Upon sufficient sludge deposit layer thickness, the water retaining in the sludge deposit prevents the occurrence of cracks. Hence, the sludge deposit layer positively impacts system efficiency (Khomenko *et al.*, 2019; Tan *et al.*, 2017).

However, as the STRB is continuously operated, the sludge deposit layer gradually increases in thickness as time passes. As a result, the top boundary condition of a STRB varies with time, complicating the system and affecting its efficiency. Moreover,

the sludge deposit layer changes its structure due to compression caused by drag forces acting on the retained particles by the imposed hydraulic flow (Tien *et al.*, 1997). Such a situation is described by the compressible cake filtration (CCF) theory, in which the changes in sludge deposit thickness and structure have affected the filtration performance (Tan *et al.*, 2017). The CCF is further described in **Section 2.15**.

Meanwhile, it has also been stated that the hydraulic properties of a sludge deposit layer are highly dependent on the organic content. In contrast, a sludge deposit layer with high VS would have low permeability and limit the dewatering efficiency (Khomenko *et al.*, 2019). The reduced percolation was caused by the sludge deposition on the surface bed, which reduces the effective porosity due to the permanent attachment of biofilm onto the filter medium and reed roots development, which obstructs the medium pores. These occurrences decrease available pore space and change the medium's hydraulic properties, subsequently altering the water flow and causing system malfunctioning (Pucher & Langergraber, 2018). Despite these undesirable effects, the growth of bacteria within the media is necessary to degrade wastewater pollutants efficiently.

2.8 Substrate Media

In a full scale sludge treatment reed bed (STRB) system, multiple reed beds are arranged in parallel to facilitate an alternating loading and resting cycle, with typically eight to twenty-four beds used depending on the required dewatering and stabilization duration (Brix, 2017; Nielsen & Larsen, 2016). The choice of substrate media such as gravel, sand, or industrial by-products significantly affects influent infiltration, retention time, filtration efficiency, and leachate purification. Gravel, being common due to its availability and low cost, supports good permeability but may limit pollutant removal due to its coarse nature (Brix, 2017; Kołecka *et al.*, 2016). Sand, with smaller grain sizes, provides better filtration but lower permeability, and is often used as a top layer for improved pollutant removal and to prevent clogging (Panuvatvanich *et al.*, 2009; Wang, Liu, *et al.*, 2019). Industrial by-products like zeolite and activated carbon are used for enhanced sorption but are less common due to cost and availability concerns (Greenway *et al.*, 2022; Wang, Jiang, *et al.*, 2022).

The substrate media depth in STRBs typically exceeds 0.5 m, with most systems falling between 0.60 and 0.69 m. While varying depths have been used depth alone has a limited effect on performance, and the choice of materials and their properties is more crucial (Magri *et al.*, 2016; Uggetti *et al.*, 2010). For instance, a system with a 0.75-m substrate depth achieved similar results to one with a o.40-m depth, indicating that while a depth between 0.40 and 0.50 meters is generally sufficient, material selection is more critical for effective sludge dewatering leachate purification (Afifi *et al.*, 2015; Panuvatvanich *et al.*, 2009).

2.9 Evapotranspiration (ET) in Sludge Treatment Reed Beds (STRBs)

The STRB dewaters through three crucial mechanisms: evaporation, evapotranspiration (ET), and drainage system. Evaporation occurs instantaneously on top of the reed bed, which results in a drier solids sludge by reducing the water content in the sludge deposit. Moreover, ET by plants is the major contributor to the dewatering process in hot and dry climatic countries (Tayler, 2018). Generally, plants that include reeds (*Phragmites species*) and cattails (*Typha species*) are selected for the STRB. These plants are suggested as they can to grow from rhizomes, at which their shoots produce new stems, increasing plant density over time (Tayler, 2018).

The existence of vegetation ensures the increase of TS content in the final dried solids sludge by 2-6%, as compared to unplanted systems (Bui *et al.*, 2019). Also, Hu (2021) has reported that the average water loss in planted STRBs is approximately 60-70% higher than that in the unplanted STRBs (S. Hu *et al.*, 2021). A relatively high ET rate is believed to aid in dewatering, where the water is absorbed through the vegetation and released as water vapor into the atmosphere (Stefanakis, 2020). According to statistics, the final dried sludge can achieve up to 40% of TS content if the ET rate is high enough to overcome the influent wastewater applied (Brix, 2017).

Generally, potential evapotranspiration (PET) is a measurement used to predict the actual amount of water loss through plants (Xiang *et al.*, 2020). The quantity of PET is usually measured by Hargreaves (Gentilucci *et al.*, 2021), Priestly-Taylor (Han *et al.*, 2021), and Penman-Monteith equations. These equations often result in similar PET

values, but different regional characteristics may lead to data deviation (Amatya *et al.*, 2018; Odusanya *et al.*, 2018). However, the Penman-Monteith equation shows a better PET result as it includes the weather data (Abeysiriwardana *et al.*, 2022; Dlouhá *et al.*, 2021; Paredes *et al.*, 2020). The inclusion of weather data provides an accurate estimation of the PET, covering a wide range of climates (Mostafa *et al.*, 2023). Predicting the PET using the Penman-Monteith equation in Malaysia is preferable due to its hot and humid environment.

2.10 Mineralization in Sludge Treatment Reed Beds (STRBs)

In STRBs, sludge mineralization represents the biological treatment, where the organic materials are converted into macronutrients such as nitrogen (N) and phosphorus (P). Generally, these nutrients are converted through biomass decomposition by microorganisms (bacteria) in soil or any other medium. The properties of substrate media play an essential role in controlling the influent infiltration, thus affecting the retention time for bacteria interaction (Tan *et al.*, 2023). The gravel and sand are always preferred to be used as the substrate media, as they are abundantly available, have promising performance in retaining pollutants, and are relatively low in cost.

The bacteria found in the STRB are categorized into autotrophs and heterotrophs at which the former is known as a producer that is capable of generating their own food from raw materials and energy. In contrast, the latter is known as a consumer that obtains energy from the foods consumed (Huang *et al.*, 2021). The nitrogen cycle describes the production and consumption of nitrogen, which is governed by nitrification and denitrification. Nitrosomonas and Nitrobacter are the two nitrifying bacteria responsible for the nitrification (Mellbye *et al.*, 2018). The nitrification process involves the oxidation of ammonia or ammonium to nitrite and oxidizes to nitrate. The bio-reaction equations are as follows (Mpongwana *et al.*, 2019):

$$2NH_4^+ + 3O_2 \rightarrow 2NO_2^- + 4H^+ + 2H_2O \quad (2.1)$$

$$2NO_2^- + O_2 \rightarrow 2NO_3^- \quad (2.2)$$

In contrast, the denitrification process is the reversed reaction of nitrification, where the nitrites are converted to nitrogen by accepting electrons to balance the reaction equation, as follows:

$$NO_3^- \rightarrow NO_2^- \rightarrow NO + N_2O \rightarrow N_2 \quad (2.3)$$

$$2NO_3^- + 10e^- + 12H^+ \rightarrow N_2 + 6H_2O \quad (2.4)$$

The phosphorus cycle in the soil is governed by the $H_2PO_4^-$ and HPO_4^{2-} ions originated from the phosphoric acid, H_3PO_4. The overall reaction equation is:

$$H_3PO_4 \rightarrow H_2PO_4^- \rightarrow HPO_4^{2-} \quad (2.5)$$

At the end of the decomposition of biomass, the nutrients are released, and ready for the uptake by plants. In STRB, this reaction is considered a "win-win" process, where the plants gain the nutrients for growth while the unwanted pollutants are removed in the reed bed, thus producing lower BOD and COD contents in the effluent.

2.11 Loading Regime

In STRBs, the sludge is fed intermittently in batches, where the loading rate governs the overall system performance. Optimal sludge loading ensures system performance, but excessive sludge loading jeopardizes the sludge dewatering efficiency. The loading rate controls the buildup of sludge residue and its associated stabilization, making it a crucial parameter in determining the bed dimensions and resting period (Tan *et al.*, 2023). The sludge loading regime is always measured by solids loading rate (SLR) or hydraulic loading rate (HLR). However, the SLR is preferred for its accuracy in determining the bed capacity for sludge loading.

In tropical regions, the SLRs for the STRB systems are usually high, ranging from 100 to 350 kg/m^2/year (Bui *et al.*, 2019). However, it is proven that a relatively high SLR significantly reduces the dewatering efficiency of STRB from 66.56% to 22.82% when the SLR increases from 100 to 350 kg/m^2/year (Tan *et al.*, 2017). Furthermore, the excessively high SLR would lead to a clogging condition, where the sludge ponding is

permanent. In such an unwanted condition, the resting period should be extended to ensure sufficient liquid loss via drainage and evapotranspiration to meet the targeted dewatering efficiency. In addition, the SLR of 100 kg/m^2/year has been analyzed to be appropriate for the STRB in tropical countries (Gholipour *et al.*, 2022).

To ensure that the STRB system meets the requires SLR, the sludge is managed and applied to the bed in a controlled manner. The SLR, expressed as kilograms of total solids per meter square per year, is initially determined based on the bed's capacity to handle sludge without compromising performance (Tan *et al.*, 2023). This calculation considers the volume of sludge to be processed, the expected dewatering efficiency, and the physical characteristics of the STRB (Jain *et al.*, 2022).

Sludge is introduced to the STRB intermittently in batches, rather than continuously, to manage the accumulation of solids effectively (Bui *et al.*, 2019). Each batch is carefully measured to align with the desired SLR. Monitoring systems or manual checks ensure that the amount of sludge applied does not exceed the bed's capacity (Tan *et al.*, 2017). If the SLR becomes too high, which could lead to reduced dewatering efficiency and clogging, adjustment are made by either reducing the sludge volume per batch or extending the resting periods between loading cycles (Gholipour *et al.*, 2022). These adjustments help manage sludge buildup and promote adequate dewatering.

Resting periods are crucial for allowing the bed to naturally dewater and stabilize the sludge (Uggetti *et al.*, 2010). During these periods, the bed facilitates liquid loss through drainage and evapotranspiration. The length of these periods is adjusted based on the SLR and the bed's performance to ensure that the sludge is treated effectively (Panuvatvanich *et al.*, 2009). Additionally, regular maintenance and optimization are performed to ensure ongoing efficiency. This includes inspecting for clogging, adjusting loading rates as needed, and maintaining the effectiveness of the substrate media for filtration and treatment (Kołecka *et al.*, 2016). By managing these factors, the STRB can effectively meet the required SLR, ensuring optimal sludge dewatering and stabilization.

2.12 Resting Period

The resting period is the drying period between loading periods to ensure adequate sludge dewatering and stabilization in STRBs (Tan *et al.*, 2023). During the resting period, the sludge dewaters through drainage initially followed by moisture content (MC) reduction via evapotranspiration towards the end. There are no standard design criteria for the resting period. Usually, the resting period is longer than the loading period to ensure sufficient sludge dewatering. Thus, a weekly basis loading regime with a one-day loading period followed by a six-day resting period is always adopted for STRBs (Bui *et al.*, 2018; Osei *et al.*, 2019; Wang, Jiang, *et al.*, 2022). A relatively short resting period would lead to temporary surface ponding, while a slightly longer resting period would cause cracks on the sludge deposit layer (Khomenko *et al.*, 2019). Figure 2.5 shows the example of cracks on the sludge deposit layer. Minor cracks on the sludge deposits can boost the percolation rate, but severe cracks would lead to sludge bypassing the substrate medium.

Minor cracks in the sludge deposit layer typically occur when the resting period is slightly extended beyond the optimal duration. These cracks are relatively small and shallow, often appearing on the surface of the sludge layer. While they may seem detrimental, minor cracks can be beneficial in certain contexts. They enhance the percolation rate of leachate by creating additional pathways for liquid to drain away from the sludge (Khomenko *et al.*, 2019). This increased drainage can improve the overall dewatering process and promote more efficient sludge stabilization. Additionally, minor cracks can facilitate air circulation, which aids in aerobic decomposition of organic matter. However, if not managed properly, these cracks can gradually expand, potentially leading to more significant issues.

Figure 2.5: Crack occurrence on the sludge deposit layer.

In contrast, severe cracks are more problematic and usually result from an excessively long resting period. These cracks are deep and wide, penetrating through the sludge deposit layer and sometimes extending down to the underlying substrate medium (Khomenko *et al.*, 2019). Severe cracking can disrupt the sludge's structural integrity and lead to several issues. One major concern is the bypassing of sludge through these large cracks, which reduces the contact between the sludge and the substrate medium, impairing the treatment efficiency. Thus, bypass can result in incomplete dewatering and stabilization, as the untreated sludge may escape the intended treatment processes. Furthermore, severe cracks can lead to uneven drying and increase the risk of surface ponding if the cracks allow for localized accumulation of leachate. This undermines the overall effectiveness of the STRB system and may require additional management efforts to rectify the problem.

In summary, while minor cracks can enhance the dewatering process and improve air circulation, severe cracks pose a risk to the system's effectiveness by allowing sludge to bypass treatment and leading to uneven drying and potential ponding. Properly managing the resting period is essential to balance these effects and ensure the efficient operation of STRBs.

2.13 System Performance

A STRB can remove pollutants such as TSS, BOD, COD, TN, and TP for different kinds of sludges ranging from domestic to industry in both urban and rural areas (Moreira & Dias, 2020; Przydatek & Wota, 2020). It can also remove a large composition of organic materials containing nutrients and water content, producing high-quality biosolid and treated wastewater. According to statistics, the high concentrations of COD in the sludge can be reduced by at least 60%, and the majority of the ammonium nitrogen would be nitrified (Brix, 2017). Moreover, up to 25% of the organic materials can be removed via the sludge mineralization in the STRB (Nielsen & Larsen, 2016).

As reported by Moreira and Dias (2020), STRB is believed to be promising in eliminating pharmaceutical compounds, hormones, and wastewater toxicity. Also, it can remove most of the heavy metals found in influent sludge, which may inhibit reeds' growth in the STRB. According to Nielsen and Stefanakis (2020), heavy metals are likely bound to the gravel media, with less than 16% of the final heavy metal mass filtered and discharged through the drainage system of the bed. Therefore, the final sludge product of a STRB, with low hazardous organic compounds and heavy metal content, allows the sludge residue to be used in agricultural activities (Nielsen & Larsen, 2016).

Several removal efficiencies of the STRB reported by researchers in recent studies can be seen in Table 2.6. The size of a reed bed is predominated by factors such as type of sludge, macrophytes, solids/hydraulic loading rate (SLR/HLR), and hydraulic retention time (HRT). It is noticed that the *Phragmites species* has been widely used in research, proving its applicability to treat different sludges in STRB. The hydraulic retention time of less than a week further confirmed that prolonging resting periods is unfavorable. In addition, the TS and COD removals of at least 80% and 90%, respectively, revealed that the STRB is excellent in sludge treatment.

Table 2.6: Recent studies on the performance of STRB.

Reference	Type of Sludge	Macrophytes	SLR / HLR	HRT (days)	Size (m^3)	Initial Concentration		Removal Efficiency (%)
Gholipour *et al.* (2024)	Domestic	*Arundo donax*	43.59 kg TS/m^2/yr	-	0.96 x 1.16 x 1.00	**TSS** **COD** **BOD** **TN** **TP**	= - = 20,749 ± 6,128 mg/L = - = 1,187 ± 423 mg/L = 4,097 ± 1,390 mg/L	- 99.0 - 86.0 99.0
Prost-Boucle *et al.* (2023)	Industrial	*Heliconia psittacorum* + *Cyperus papyrus*	32 kg TS/m^2/yr / 0.15 m/d	-	-	**TSS** **COD** **BOD** **TN** **TP**	= 3,260 ± 1,060 mg/L = 14,641 ± 2,973 mg/L = 6,843 ± 1,125 mg/L = 262 ± 67 mg/L = 145 ± 91 mg/L	92.0 96.0 - - -
Jóźwiakowska and Bugajski (2023)	Domestic	*Phragmites australis*	0.8 m^3/d	-	-	**TSS** **COD** **BOD** **TN** **TP**	= - = - = - = - = -	81.0 89.0 95.0 66.0 76.0
Singh *et al.*	Faecal	*Canna indica*	30 L/d	2	0.76 x 0.76 x 0.53	**TSS**	= 309 ± 66.3 g/m^2/day	65.0

(2023)						**COD** **BOD** **TN** **TP**	= 713 ± 443.9 g/m^2/day = 150 ± 65.7 g/m^2/day = - = -	87.0 88.0 - -
Al-Ajalin *et al.* (2022)	Domestic	*Lepironia articulata* + *Scirpus grossus*	-	-	-	**TSS** **COD** **BOD** **TN** **TP**	= - = 496 to 616 mg/L = - = 3 to 18 ppm = 1 to 8 ppm	- 85.6 - 75.8 58.3
Saeed *et al.* (2022)	Municipal	*Phragmites sp.*	30 kg TS/m^2/yr / 20 L/week	5	0.91 x 0.61 x 0.45	**TSS** **COD** **BOD** **TN** **TP**	= 2,619.2 ± 2,743.3 mg/L = 2,847.4 ± 1,317.5 mg/L = 145.5 ± 82.3 mg/L = 79.7 ± 37 mg/L = 188.3 ± 33.6 mg/L	98.0 99.0 96.0 89.0 99.0
Torrens *et al.* (2021)	Faecal	*Phragmites australis*	5.6 cm/d	-	4.70 x 0.70 x 0.60	**TSS** **COD** **BOD** **TN** **TP**	= 765 to 19,537 mg/L = 3,514 to 16,785 mg/L = 520 to 4,750 mg/L = 1,038 to 3,752 mg/L = 62 to 874 mg/L	94.3 73.9 75.5 69.5 81.6
Al Falahi *et*	Domestic	*Scirpus*	9 L/d	5	1.00 x 0.60 x 0.05	**TSS**	= -	-

***al.* (2021)**		*grossus*				**COD** **BOD** **TN** **TP**	= 182.7 ± 1.5 mg/L = - = 7.5 ± 1.6 mg/L = 30.7 ± 10 mg/L	88.2 - 72.9 83.2
S. Hu *et al.* (2021)	Domestic + Leachate	*Phragmites australis*	90 kg $TS/m^2/yr$ / 3 L/d	5	0.30 x 0.20 x 0.50	**TSS** **COD** **BOD** **TN** **TP**	= - = - = - = - = -	- 99.6 - 94.9 95.0
Haddis *et al.* (2020)	Faecal	*Cyperus papyrus*	0.8 m^3/d	4	8.00 x 2.00 x 0.60	**TSS** **COD** **BOD** **TN** **TP**	= 188.40 ± 193.08 mg/L = 412.83 ±92.76 mg/L = 223.74 ± 61.93 mg/L = - = -	76.9 65.2 80.6 - -
Al-Ajalin *et al.* (2020a)	Domestic	*Scirpus grossus* + *Lepironia articulata*	35 – 45 cm	5	2.00 x 1.00 x 1.00	**TSS** **COD** **BOD** **TN** **TP**	= 13.90 ± 2.97 mg/L = 234.00 ± 19.80 mg/L = 118.10 ± 14.00 mg/L = - = 5.04 ± 0.25 mg/L	99.0 96.9 99.7 - 99.5
Al-Ajalin *et*	Domestic	*Scirpus*	35 ± 0.87	1	2.00 x 1.00 x 1.00	**TSS**	= 13.90 ± 2.97 mg/L	99.0

***al.* (2020b)**		*grossus*	cm			**COD** **BOD** **TN** **TP**	= 234.00 ± 19.80 mg/L = 118.10 ± 14.00 mg/L = - = 5.04 ± 0.25 mg/L	96.6 99.7 - 99.6
Moreira and Dias (2020)	Faecal	-	-	-	-	**TSS** **COD** **BOD** **TN** **TP**	= 63 to 798 mg/L = 119 to 1339 mg/L = 42.6 to 904.0 mg/L = 39.2 to 205.0 mg/L = 3.4 to 30.7 mg/L	87.0 89.0 93.0 70.0 72.0
Fu *et al.* (2020)	Domestic	*Kandelia candel*	0.034 $m^3/m^2/d$	1.45	$0.55 \times 0.15^2 \times \pi$	**TSS** **COD** **BOD** **TN** **TP**	= - = - = - = 15 mg/L = -	- - - 96.2 -
Feng *et al.* (2020)	Faecal	*Iris pseudacorus*	6 L	3	$0.65 \times 0.10^2 \times \pi$	**TSS** **COD** **BOD** **TN** **TP**	= - = 374.17 mg/L = - = 83.84 mg/L = -	- 95.0 - 73.0 -
Khalifa *et al.*	Faecal	*Phragmites*	2 m^3/d	0.33	10.00 x 2.00 x 0.65	**TSS**	= 291 mg/L	88.5

(2020)		*australis*				**COD** **BOD** **TN** **TP**	= 231 mg/L = 157 mg/L = - = 2.82 mg/L	88.0 88.0 - 85.0
Kabir *et al.* (2020)	Faecal	-	5 m^3/d	3	4.60 x 3.70 x 1.20	**TSS** **COD** **BOD** **TN** **TP**	= - = - = - = 140 mg/L = 320 mg/L	- 94.0 94.0 63.0 82.0
Khan *et al.* (2020)	Hospital	*Phragmites australis*	110 - 120 mm/d	-	1.50 x 0.65 x 0.50	**TSS** **COD** **BOD** **TN** **TP**	= 272 ± 49 mg/L = 942 ±117 mg/L = 205 ± 25 mg/L = 3.6 ± 0.77 mg/L = 5.33 ± 0.9 mg/L	98.0 94.0 96.0 - 79.0
Jehawi *et al.* (2020)	Domestic	*Scirpus grossus*	-	3	1.00 x 2.00 x 1.00	**TSS** **COD** **BOD** **TN** **TP**	= 39.86 ± 5.20 mg/L = 72.42 ±10.22 mg/L = - = 7.08 ± 0.80 mg/L = 2.84 ± 0.16 mg/L	- - - 84.7 71.0
Hu *et al.*	Domestic	*Phragmites*	45.6 kg	2	0.30 x 0.20 x 0.50	**TSS**	= -	-

(2020)		*australis*	TS/m^2/yr			**COD** **BOD** **TN** **TP**	= - = - = - = -	99.1 - 91.5 91.0
Tan *et al.* (2020)	Faecal	*Phragmites karka*	125 kg TS/m^2/yr	-	-	**TSS** **COD** **BOD** **TN** **TP**	= 9,438.89 ± 6,646.11 mg/L = 4,549.39 ± 2,477.49 mg/L = - = 192.28 ± 104.08 mg/L = -	98.0 99.0 - 96.6 -
Trein *et al.* (2019)	Faecal	*Cynodon dactylon Pers*	13 m^3/d / 0.43 m^3/m^2/yr	-	-	**TSS** **COD** **BOD** **TN** **TP**	= 415 ± 0.91 mg/L = 467 ± 0.52 mg/L = 286 ± 0.34 mg/L = 42 ± 0.24 mg/L = -	85.0 72.0 80.0 60.0 -
Jóźwiakowski *et al.* (2019)	Domestic	*Phragmites australis*	0.45 – 38 m^3/d	-	-	**TSS** **COD** **BOD** **TN** **TP**	= 403 mg/L = 780 mg/L = 417 mg/L = 151 mg/L = 31.6 mg/L	83.5 85.4 89.7 65.2 66.6
Shen *et al.*	Domestic	*Iris tectorum*	7.5 L	3	0.60 x 0.10^2 x π	**TSS**	= -	51.1

(2019)		*Maxim*				**COD** **BOD** **TN** **TP**	= 65.72 ± 3.26 mg/L = - = 20.85 ±0.64 mg/L = 1.10 ± 0.08 mg/L	- - 81.5 93.6
Li *et al.* (2018)	Domestic	-	0.46 m/d	1.4	-	**TSS** **COD** **BOD** **TN** **TP**	= 104.4 ± 13.7 mg/L = 181.6 ± 41.6 mg/L = 90.6 ± 19.7 mg/L = 29.1 ± 6.0 mg/L = 3.0 ± 0.6 mg/L	82.1 72.6 81.8 63.7 75.6
de Rozari *et al.* (2018)	Faecal	*Melaleuca quinquenervia* + *Cymbopogon citratus*	-	-	0.24	**TSS** **COD** **BOD** **TN** **TP**	= - = - = - = 2.9 to 4.0 mg/L = -	- - - 87.0 -
Bui *et al.* (2018)	Faecal	*Phragmites karka*	11.04 cm/d	-	-	**TSS** **COD** **BOD** **TN** **TP**	= 173.4 mg/L = 118.1 mg/L = - = 2.8 mg/L = -	97.9 99.4 - 78.6 -
Kim *et al.*	Faecal +	*Phragmites*	37 kg	-	-	**TSS**	= 14,320 ± 737 mg/L	99.5

(2017)	Leachate	*australis*	TS/m^2/yr / 11 cm/d			**COD** **BOD** **TN** **TP**	= 17,168 ± 457 mg/L = - = 742 ± 26 mg/L = 217 ± 21 mg/L	98.3 - 94.9 94.8
Karolinczak and Dąbrowski (2017)	Faecal	*Phragmites australis*	0.01 – 1.26 kg TSS/m^2/yr	-	-	**TSS** **COD** **BOD** **TN** **TP**	= 1,094 ± 3,841 mg/L = 2,599 ± 3,763 mg/L = 1,280 ± 2,174 mg/L = 221.0 ± 103.7 mg/L = 30.2 ± 22.7 mg/L	91.0 82.0 82.0 47.0 93.6
Panwar and Makvana (2017)	Domestic	*Phragmites karka*	75 m^3/d	-	-	**TSS** **COD** **BOD** **TN** **TP**	= 696.38 ± 56.62 mg/L = 122.83 ± 16.81 mg/L = 98.77 ± 25.93 mg/L = 26.00 ± 10.94 mg/L = -	80.2 78.6 69.5 69.5 -
Tan *et al.* (2017)	Faecal	*Phragmites karka*	350 kg TS/m^2/yr	-	1.51	**TSS** **COD** **BOD** **TN** **TP**	= 42,693 ± 29,812 mg/L = 35,526 ± 21,002 mg/L = - = 4,549 ± 2,477 mg/L = -	98.1 98.0 - 94.7 -

2.14 Numerical Models of Treatment by STRBs

Despite the promising advantages of the STRB, high capital costs always restrict its experimental studies. In recent years, many numerical models have been created as simulation tools to save time and workload for experimental research that has been conducted. Many process-based models were developed to simulate the wastewater treatment system, particularly in vertical flow constructed wetlands or sludge treatment reed beds (Mancuso & Fioreze, 2018). For instance, HYDRUS-CW2D (Jayswal & Rodríguez, 2021), HYDRUS-CWM1 (Nawaz *et al.*, 2019), and CFD (Hua *et al.*, 2018), are the most commonly used numerical simulators in recent studies.

The numerical models used in STRBs have described the wastewater treatment processes by integrating several sub-models, including hydraulic, reactive transport, plants, biochemical reaction, and substrate clogging (Yuan *et al.*, 2020). In summary, the hydraulic sub-model described the dynamics of water flow. In contrast, the reactive transport sub-model simulated the transport of dissolved and particulate contaminants between the solid and liquid phases in the system. Moreover, biochemical and plant sub-models describe the fate of water and pollutants throughout the treatment process.

Several standard process-based models, descriptions, and sub-models are summarized in Table 2.7 (Yuan *et al.*, 2020). These models are promising in estimating the hydraulic flow in STRBs. However, these tools are “black box” models requiring input-output data to simulate the process and system. HYDRUS has been well-known for decades due to its relatively stable and reliable performance in modeling hydraulic dynamics. HYDRUS has served as the basis for developing other hydraulic models and has significantly increased the number of modified models worldwide. Thus, the hydraulic and solute transport models implemented in the simulation were found to be varied for each novel model.

Table 2.7: Common numerical models for simulating STRBs.
Note: Adapted from "Numerical Models of Subsurface Flow Constructed Wetlands" Review and Future Development," by Yuan, C., Huong, T., Zhao, X., and Zhao, Y., *Sustainability*, 2020.

Model	**HYDRUS-CW2D**	**HYDRUS-CWM1**	**BIO_PORE**	**CWM1-RETRASO**	**FITOVERT**	**CFD**
Software	HYDRUS		COMSOL Multiphysics™	RetrasoCodeBright	MATLAB	COMSOL Multiphysics
Types	Vertical and Horizontal Flow		Horizontal Flow	Horizontal Flow	Vertical Flow	Vertical Flow
Hydraulic	Saturated and unsaturated (Richards' equation)		Saturated (Darcy's equation)	Saturated and unsaturated	Saturated and unsaturated (Richards' equation)	Saturated (Brinkman's equation)
Reactive transport	Advection-dispersion equation with adsorption		Fick's law with attachment and detachment rates	Darcy's law and Fick's law	Bresler's equation and numerical analysis	Advection-dispersion equation
Bio-chemical	CW2D	CWM1	Modified version of CWM1	CWM1	ASM1	ASM1
Plant	Oxygen release and solute uptake		Oxygen release and nutrient uptake	-	-	-
Reference	Langergraber and Šimůnek (2005)	Langergraber *et al.* (2009)	Samsó and Garcia (2013)	Llorens *et al.* (2011)	Giraldi *et al.* (2010)	Rajabzadeh *et al.* (2015)

However, the existing models described the hydraulic system as a fixed domain where a uniform mesh was assumed (Huong *et al.*, 2023b). The top mesh, where the bed surface was found, is loaded with sludge that drains continuously upon feeding. The drainage and evapotranspiration processes reduce the sludge ponding level significantly. Hence, the existing approaches were said to overestimate the hydraulic performance, where the actual infiltration and dewatering rates are much smaller. Further, the continuous sludge loading also leads to an extensive increase in the sludge deposit layer thickness. The sludge accumulation on the bed surface increases the top mesh layer upon sludge particle settlement, followed by the thickness reduction due to evapotranspiration during the resting period.

The conventional approach considered the increment of sludge deposit layer thickness obtained from the equation and reform to become a new mesh of the top boundary in the simulation to impose a flow resistance (Tan *et al.*, 2023). Nonetheless, this method is less robust when the solid loading rate is high, as the newly formed sludge deposit thickness is comparable to the existing sludge deposit layer. The sludge deposit layer is rich in organic matter and is highly compressible (Wang, Jiang, *et al.*, 2022). The compression of the sludge deposits extensively reduces the permeability of the layer (Höfgen *et al.*, 2019). Hence, these changes in the top mesh thickness are crucial to be included in the model simulation.

The moving boundary condition at the top mesh layer is critical in developing a feasible solution in the hydraulic module. Instead of the conventional fixed mesh method (FMM), a novel approach as known as the moving mesh method (MMM) is more suitable for a range of one-dimensional moving boundary problems, including the finite difference Richards' equation (RE) model (Lee *et al.*, 2015). This moving mesh finite difference RE has successfully predicted the hydraulic flow in STRBs (Bruce, 2011; Huong *et al.*, 2023b). In addition, the compressible cake filtration (CCF) theory was able to describe the compressibility of the sludge cake. The CCF model has been successfully applied to the sludge deposit layer in STRBs (Höfgen *et al.*, 2019; Pergam & Briesen, 2023).

Reviewing the literature on numerical models for STRBs reveals several key outcomes and areas for improvement. Advances in modeling have introduced a diverse range of tools, such as HYDRUS-CW2D, HYDRUS-CWM1, and CFD, which integrate various sub-models, covering hydraulic dynamics, reactive transport, plant growth, biochemical reactions, and substrate clogging, to simulate complex interactions in STRBs. The adoption of the MMM over traditional FMM has enhanced simulation accuracy, particularly in capturing dynamic boundary changes due to sludge accumulation. Additionally, incorporating CCF theory has improved the understanding of sludge compressibility and its impact on hydraulic performance, leading to more reliable models like HYDRUS.

Despite these advancements, there are notable knowledge gaps that need addressing. Many models still rely on fixed domain assumptions, which can lead to inaccuracies in simulating dynamic sludge changes. There is a need for more detailed models that account for the full spectrum of sludge properties and long-term behavior. Calibration and validation challenges persist, with many models requiring extensive data that may not always be available. Furthermore, integrating climatic, operational, economic, and environmental factors into simulations remains an area for development. Simplifying complex models and improving their accessibility for practical use in field settings are also crucial for enhancing their application and effectiveness.

2.15 The Compressible Cake Filtration (CCF) Theory

The existing STRB and related numerical models are primarily developed for wastewater treatment, while the models for sludge treatment still need to be developed. The simulation typically does not consider sludge deposit or filtration cake buildup. This assumption is reasonable for wastewater treatment due to low-influent total suspended solids (TSS) concentration. Still, it is essential for the sludge treatment, as the TSS concentration in sludge is much higher, especially for the septic sludge. The formulation of the sludge deposit on the top surface of the bed increases the specific cake resistance, possibly bringing substantial changes to the hydraulic flow through the medium (Tan *et al.*, 2017).

In STRBs, the compression of sludge deposits plays a crucial role in influencing system performance. As sludge accumulates on the bed surface, the increasing thickness of the sludge layer results in greater pressure being applied to the underlying sludge. This pressure, combined with the force of the fluid flowing through the sludge, causes the sludge particles to be compressed. The compressive force reduces the porosity of the sludge, which is the amount of open space between particles. As a result, the ability of the sludge layer to allow water to pass through decreases, leading to reduced permeability. This reduced permeability means that water flow through the sludge deposit slows down, making it more difficult for the system to process wastewater effectively. This process is described by the compressible cake filtration (CCF) theory (Höfgen *et al.*, 2019). The porosity, permeability, and specific cake resistance of a compressible sludge deposit always vary due to the applied load and fluid drag. At the same time, these parameters remain constant for an incompressible sludge deposit (Tiller & Yeh, 1987). Consequently, the sludge deposit undergoes compression and eventually deformation. Figure 2.6 shows a schematic illustration of the CCF mechanism.

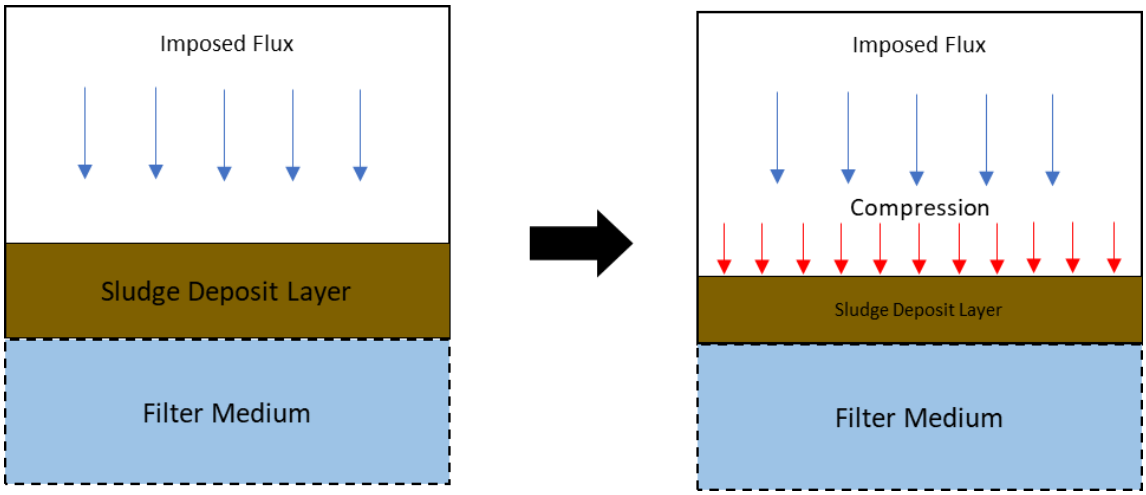

Figure 2.6: Compression of sludge deposit.

The deformation of the sludge deposit significantly affects the sludge dewatering and wastewater treatment performances. Besides sludge deposit compression, the deformation of the sludge deposit is also caused by the continuous loss of moisture during non-feeding periods and may eventually lead to cracks in the layer (Khomenko *et al.*, 2019; Tan *et al.*, 2017). The ET by vegetation may also aid in its occurrence. The

shrinkage of the sludge deposit usually causes cracks, allowing the influent to "bypass" the sludge deposit layer and accelerating the drainage flow in the following feeding. Such a deformation in sludge deposit creates a "preferential flow pathway" (PFP), which positively impacts the system's permeability but negatively affects the overall treatment efficiency. This is believed to be related to the organic content in the sludge deposit, where a sludge deposit with high volatile solids (VS) would result in a low permeability system, leading to less water diffusing into the sludge deposit (Khomenko *et al.*, 2019). Thus, the shrinkage limit of the sludge deposit layer before it cracks is essential in determining the sustainability and longevity of the bed for septage treatment.

Therefore, a numerical model should be able to simulate a system that can incorporate the changes in the thickness of the sludge deposit layer towards improving its robustness. The consideration of moving boundaries due to the CCF and the shrinkage limit of the sludge deposit should be considered.

2.16 The Shrinkage Limit (SL) of the Sludge Deposit Layer

The shrinkage limit (SL) of the sludge deposit layer plays a vital role in describing its deformability based on its composition and water content. The SL of the sludge deposit layer is the maximum durable stress before it can no longer maintain its shape (Pergam & Briesen, 2023). Thus, the SL determines the critical point before the sludge deposit layer cracks. It is the minimum water content required to sustain the sludge deposit layer in its original shape.

However, a higher organic content of the sludge deposit layer results in higher compressibility and SL (Obour *et al.*, 2018; Reichert *et al.*, 2018). The accumulation of VS increases the sludge deposit thickness and the volume of effective pores, thus retaining more water in the sludge deposit layer (Zahermand *et al.*, 2020). Subsequently, the water detaining on top of the bed ponds temporarily reduces the water recovery of the reed bed system at the end of treatment. This situation retards the sludge infiltration rate and impacts the system performance negatively. Therefore, conditioning with oxidation reagents may be necessary to improve its dewaterability (Yu *et al.*, 2017). However, this

is not environmentally friendly, and additional processes are required to remove the reagents added.

In some cases, the ponding lasts for the entire resting period, which causes a clogging condition. Such a scenario is uneconomic and inefficient. In fact, ponding conditions reduce the infiltration rate and lengthen the treatment duration. Therefore, experiments are required to investigate the relationship between sludge mineralization and the SL of the sludge deposit layer. This critical SL can then act as a reference for the STRB to maintain the moisture of the sludge deposit layer in the future.

2.17 The Moving Mesh Method (MMM)

In a conventional model simulation, mesh and differential equations are often solved simultaneously to generate new nodes and solutions. This method discretizes the mesh and differential equations using the fixed mesh method (FMM) and a simple Picard iteration approach (Dehghan & Shirilord, 2020; Tisdell, 2019). The final solutions are rearranged into a tri-diagonal matrix to further input into the software, such as MATLAB, to simulate the subsequent spatial and temporal nodes. This method successfully simulated the hydraulic dynamics and reactive transport in the porous medium (Li & Hodges, 2021; Lu *et al.*, 2022).

However, the proposed method for solving the simulation in this study is based on the MMM, where the mesh and solution are varied simultaneously in such a way that a fixed number of nodes remain concentrated in regions of rapidly variated solution (Lee *et al.*, 2015; Tang, 2005). The moving mesh method (MMM) is an alternative to the FMM, where it is an adaptive method of moving mesh (Koncz *et al.*, 2021), that is capable of simulating the fluid dynamic related problems (Duan *et al.*, 2020; Kannan *et al.*, 2019). With the implementation of this method, there is no longer a need to interpolate dependent variables from the old mesh. A simple illustration of the refinement method by MMM is displayed in Figure 2.7 (Bisheh-Niasar & Ameri, 2018). According to MMM, the mesh points relocate, thus changing the original positions based on the monitor function while keeping the number of nodes constant (Bazilevs *et al.*, 2023). Hence, the MMM is a promising technique nowadays for the solution of moving boundaries. The

comparisons between fixed and moving meshes can be seen in Table 2.8 (Tang, 2005). The MMM improves time efficiency by excluding the interpolations of meshes, thus reducing the number of iterations.

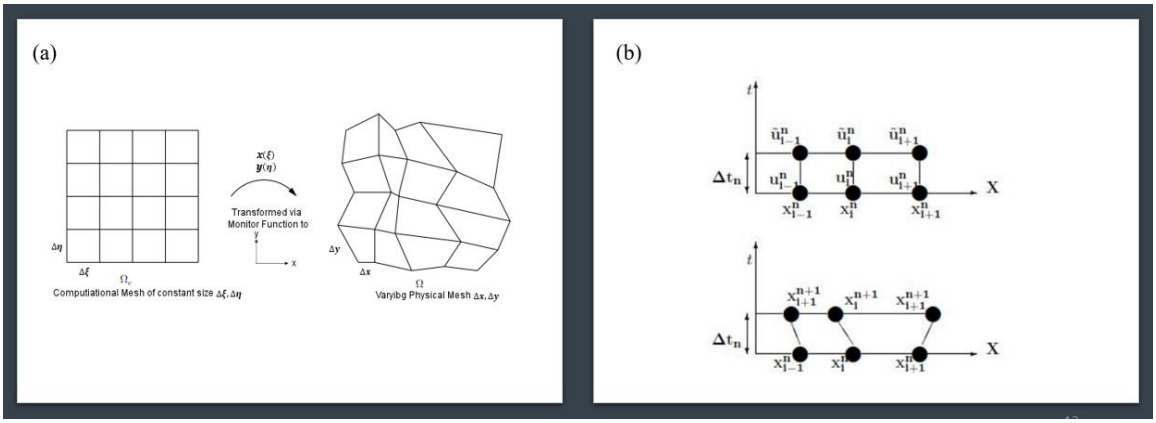

Figure 2.7: Refinement using MMM by FD approach.
Note: Adapted from "Moving mesh Non-standard Finite Difference Method for Non-linear Heat Transfer in a Thin Finite Rod," by Bisheh-Niasar, M., and Ameri, M. A., *Applied and Computational Mechanics*, 2018.

Table 2.8: A comparison between fixed and moving meshes.
Note: Adapted from "Moving mesh methods for computational fluid dynamics," by Tang, T., *Contemp. Math.*, 2005.

	Fixed Mesh	**Moving Mesh**
Method	• *h*-refinement method – The most common method at which the spatial mesh is refined by repeated subdivision of the intervals of a fixed mesh. • *p*-refinement method – By this method, the degree of polynomial order of shape functions is increased.	• *r*-refinement method – This method is well known as the moving mesh method (MMM) where it relocates the grid points in a mesh at each time step.
Algorithm	Solution and mesh selection	Solution and mesh-redistribution
Discretization	Finite difference and element	Finite difference, element, and volume
Interpolation	Required	Not required
Stiffness	Low	High
Time Integration	Explicit	Implicit

In contrast to FMM, the method of discretization in the MMM can be done by finite difference (FD) (Lapidus & Pinder, 1982; Von Rosenberg, 1969), finite element (FE) (Li, 2022; List & Radu, 2016), or finite volume (FV) (Bassetto *et al.*, 2022; Cardiff & Demirdžić, 2021). The changes in the spatial mesh due to moving boundary conditions further complicate the system's ability to simulate the desirable solution. However, the MMM discretizes the meshes regarding the actual space, element, and volume changes and has managed to ideally describe the moving boundary condition. Particularly in RE of hydraulic flow, the meshes can be discretized through a velocity-based equation with the MMM by the FD approach (Bruce, 2011). In dealing with the same problem, Lee *et al.* (2015) successfully implemented the FE approach to solve the velocity-based RE but with a different type of discretized equation. However, this study implements the FD rather than the FE method, as the FEs are generally preferable and superior for higher-order and dimensional problems.

2.18 Summary of Literature Review

Management of the sanitation system in Malaysia has always been an issue for the country's development. Decentralized wastewater management systems offer better economic advantages. Among all the existing technologies, the STRB performs outstanding in wastewater and sludge treatments. While studies of modeling and simulation of hydraulic flow and contaminant transport for the STRB have become prevalent among researchers, the compressibility of the sludge deposit needs to be addressed in the modeling. The CCF theory describes the compressibility of the sludge deposit by the moving boundary condition, where the increase in actual thickness of the sludge deposit is due to the continuous settling and deposition of solid sludge. Upon infiltration, the subsequent decrease in the sludge deposit thickness is caused by the compression due to the imposed flux and the water loss by ET. Thus, this project would feature a model incorporating the CCF theory based on the MMM to derive a robust and practical model to simulate the moving boundary condition of the changes in sludge deposit layer thickness and sludge ponding.

Furthermore, the shrinkage limit of the sludge deposit is an essential parameter in determining the performance of the sludge deposit layer in STRBs. The shrinkage limit of the sludge deposit indicates the ability of the reed bed to sustain the treatment processes. A high organic content in the sludge deposit is believed to lead to increased shrinkage limit due to more water in the sludge deposit. The VS contained in the organic matter increases the porosity of the sludge deposit, which detains more water from diffusing through the reed bed and affects the system's performance. The sludge deposit layer with a high organic content has been shown to crack during the non-feeding period due to water loss by drainage and ET effects.

This study creates a one-dimensional dual-porosity variably saturated model by applying some innovations such as MMM and CCF. The dual-porosity variably-saturated model is developed to estimate the gravity drainage flow in a STRB in the treatment of sludge, in which the Richards' equation (RE) and van Genuchten-Mualem's (VGM) model are employed to describe the unsaturated flow and hydraulic properties of the medium, respectively (Tan *et al.*, 2017). Moreover, the mechanism of evapotranspiration (ET) is described by the Penman-Monteith equation, where potential transpiration (PT) is required for root water uptake (Allen *et al.*, 1998). In addition, the solute transport is explained by the Advection-Dispersion Equation (ADE), with the inclusion of sludge mineralization related to bio-kinetic analysis in such a way that the production and decay of bacteria in the sludge deposit and within the medium are taken into consideration (Bresler, 1973; Gujer *et al.*, 1999). Finally, the shrinkage limit of the sludge deposit is studied to obtain the correlation between the sludge mineralization and the deformation of the sludge deposit layer.

CHAPTER 3: RESEARCH METHODOLOGIES

3.1 Experimental Rigs

A laboratory-scale sludge treatment reed bed (STRB) system was constructed next to the Wastewater Treatment Plant of Curtin University Malaysia. The purpose of the laboratory experimental work was to collect data for use in calibrating and validating the proposed process-based model that describes the hydraulic performance of STRBs and the associated changes in sludge deposition characteristics. The system comprises six reed beds with the same substrate profile and vegetation. This study adopted the operational parameters of three solids loading rates (SLRs) and five resting periods (RPs). The parameters used to evaluate the performance included the thickness, moisture content (MC), total solids, and volatile solids of the sludge deposit layer. A thorough experimental flowchart can be found in Figure 3.1.

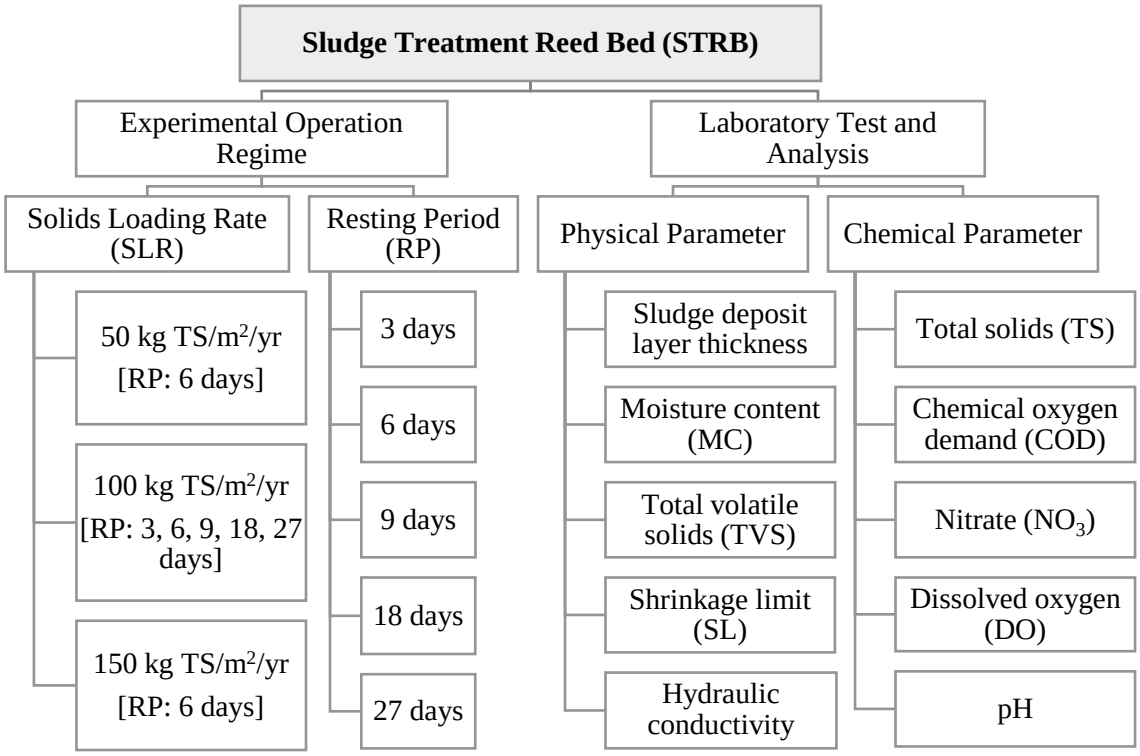

Figure 3.1: STRB for septage treatment experimental flowchart.

3.1.1 Pre-treatment and Storage

The septage used in this study was retrieved from the septic tanks of local households. The collection of septic sludge was performed by a desludging truck provided by a local company, as shown in Figure 3.2 to Figure 3.5.

Figure 3.2: Desludging truck.

Figure 3.3: Excessive septic sludge.

Figure 3.4: Desludging process.

Figure 3.5: Empty septic tank after desludging.

The septage collected at the household, was then transferred to the experimental site at Curtin University Malaysia. The septage was stored in a 400-gallon polyethylene water tank, as shown in Figure 3.6 to Figure 3.8.

Figure 3.6: Transferring the septage into a storage tank.

Figure 3.7: Process of filling the septage.

Figure 3.8: Septic sludge storage tank.

3.1.2 Sludge Treatment Reed Beds

Figure 3.9 to Figure 3.11 show the setup of the STRB system constructed in this study as per the design recommendation established in Bui's research (Bui *et al.*, 2019).

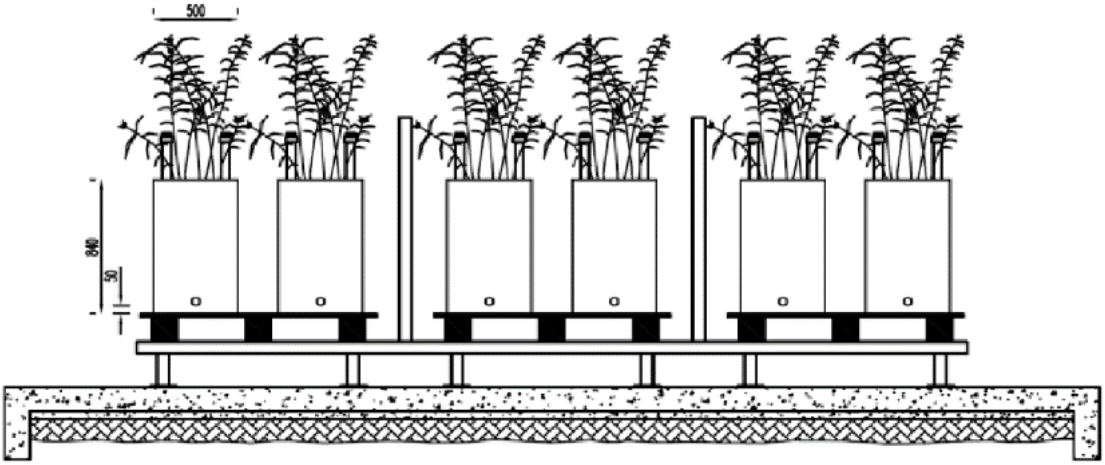

Figure 3.9: Cross-sectional illustration of laboratory-scale STRBs.
Note: Adapted from "Dewatering and Mineralization of Sludge in Vertical Flow Constructed Wetlands: A Review," by Bui, J. J. X., Tang, F. E., Tan, Y. Y., Wong, K. S., and Saptoro, A., *IOP Conference Series: Materials Science and Engineering*, 2019.

Figure 3.10: Actual experimental illustration of laboratory-scale STRBs.

Figure 3.11: Inside view of the STRB during acclimatization.

A total of six beds were constructed to investigate the influence of different SLRs and resting periods. The STRB was constructed in a 55-gallon water barrel with a surface area of 0.196 m^2 and a height of 0.84 m, as shown in Figure 3.12 (Bui et al., 2019). The additional information on the bed is given in Table 3.1 (Bui et al., 2019).

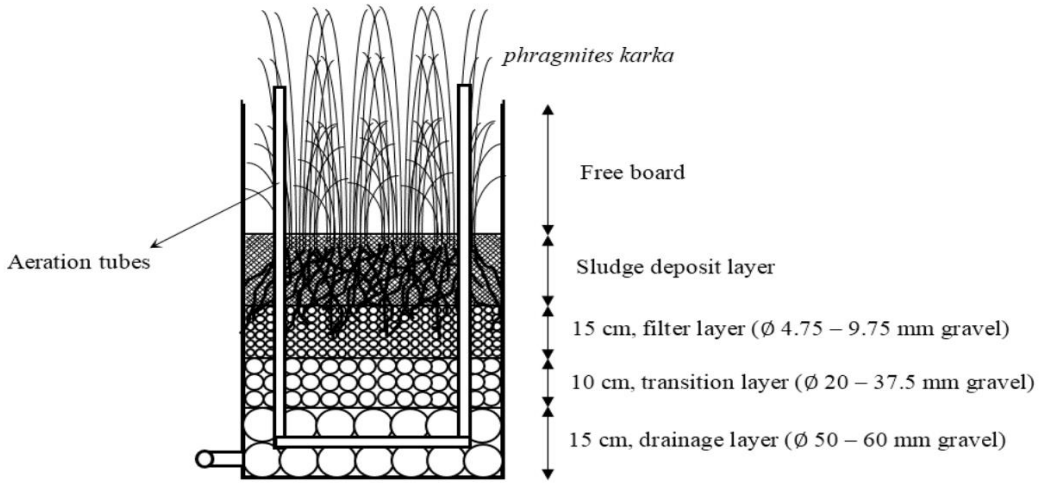

Figure 3.12: Enlarged cross-sectional view of a STRB.
Note: Adapted from "Dewatering and Mineralization of Sludge in Vertical Flow Constructed Wetlands: A Review," by Bui, J. J. X., Tang, F. E., Tan, Y. Y., Wong, K. S., and Saptoro, A., *IOP Conference Series: Materials Science and Engineering*, 2019.

The substrate is a 0.4 cm granular medium constructed by different sizes of crushed limestone. The substrate profile consists of (from bottom to top) 0.15 m coarse aggregates (diameter 50 – 60 mm), 0.10 m medium-sized aggregates (diameter 25 - 37.5 mm), and 0.15 m small-sized aggregates (diameter 4.75 - 9.75 mm). The selection of crushed limestone as the substrate material is based on cost consideration and availability in the local area (Bui *et al.*, 2019; Tan *et al.*, 2017). Each bed was planted with fourteen common reeds (*Phragmites karka*). The common reed was selected due to its extensive root development, effective rhizome system, excellent productivity, efficient water absorption, tolerance to weather, and resistance against toxins (Kołecka *et al.*, 2016).

Table 3.1: Additional information of STRB.

Parameter	**Dimensions**	**Units**
Diameter (D)	500	mm
Height (h)	840	mm
Average outlet height from base (h_0)	50	mm
Average surface area (A)	196349.5	mm^2

Meanwhile, two perforated pipes have been installed vertically in the substrate to allow air exchange in the substrate, which is a typical setup in STRBs. Furthermore, each

bed was installed with an outlet valve located at the bottom of the bed. Six containers were placed at the discharge outlets to collect the treated sludge effluent.

3.1.3 Acclimatization of STRBs

Before the experiments, the raw septage was screened to remove gross solids that may clog the substrate to reduce the risk of clogging. Then, the STRBs were acclimatized for a month to stimulate the growth of microorganisms and macrophytes. The growth of microorganisms promotes enzyme activity and stabilizes the microbial structure (Xing *et al.*, 2020). Thus, microbial acclimatization increased the amount of bacteria in the STRB and formed a stable biofilm layer for sludge mineralization.

The acclimatization process is described as follows. The discharge valve at the bottom of the bed was closed before loading. The septage was filled until the water level was above the top surface of the reed bed. After the acclimatization period, the septage held in each reed bed was discharged by removing the discharge plugs at the bottom of the beds. Meanwhile, the formation of sludge deposits can be observed after the discharge of the impounding septage. Additionally, significant growth of the macrophytes in the STRB was also detected.

3.1.4 Experiment Phase

Six laboratory-scale STRBs were constructed to treat the septage under different loading regimes. The reed beds were labelled from 1 to 6, as shown in Figure 3.13. Table 3.2 summarizes the SLRs and resting periods applied to the reed beds. The experiment was completed in two phases. The preliminary treatment was conducted for a month to enhance the development of the biofilm, followed by the main treatment, which was operated on for two months.

In the literature, the solids loading rates (SLRs) of a STRB usually fall within the range of 100 to 350 kg/m^2/year (Carneiro *et al.*, 2022; Jain *et al.*, 2022; Tan *et al.*, 2017). However, the optimal SLR for a STRB is highly dependent on the climate. It has been confirmed that the SLR of 100 kg/m^2/year was most suitable for tropical regions where

the climate is relatively hot (Gholipour *et al.*, 2022). A higher SLR would lead to clogging conditions, causing the STRB system to malfunction. Hence, the tested SLRs were selected to be 50, 100, and 150 kg/m^2/year to investigate the effect of SLRs towards hydraulic performance.

Furthermore, the resting period is usually longer than the feeding period in the STRB system (Carneiro *et al.*, 2022; Kim *et al.*, 2017; Torrens *et al.*, 2021). Economically, the loading-resting cycle was commonly done on a weekly basis to save capital and operational costs (Tan *et al.*, 2023). This led to a resting period of 7 days in a cycle. In this project, the septage treatment was performed by the "feed-and-drain" mechanism, where the septage was fed to the reed bed directly at once. Hence, 1 out of 7 days of the resting period was assumed to be the feeding period, which resulted in 1/6 days of the feeding/resting period (Carneiro *et al.*, 2022). Moreover, a relatively short resting period would lead to prolonged waterlogging conditions and an extensively long resting period is believed to have caused cracks on the sludge deposit layer (Khomenko *et al.*, 2019; Tan *et al.*, 2017). Thus, the resting periods used in the experiments ranged from 3 to 27 days to determine the optimum resting period.

In addition, the effect of initial sludge deposit layer thickness on the overall treatment performance was also studied. Thus, Bed 2 would have twice the initial sludge deposit layer thickness of Bed 5. The other conditions of the bed were kept constant and tested with a SLR of 100 kg/m^2/year and a resting period of 6 days.

Before any loadings, the thickness of the sludge deposit was measured with a ruler. The septage in the storage tank was stirred manually to ensure homogeneity. The raw septage was fed slowly from the top of the STRB and percolated through the filter medium.

Figure 3.13: Actual experimental rig and set-up.

Table 3.2: Experimental operating regime.

Bed	SLR	Resting Period	Total Sludge (TS/loading)
Phase 1			
1	50 kg TS/m^2/year	6 days	0.16 kg TS
2	100 kg TS/m^2/year		0.33 kg TS
3	150 kg TS/m^2/year		0.49 kg TS
4	100 kg TS/m^2/year	3 days	0.16 kg TS
5		6 days	0.33 kg TS
6		9 days	0.49 kg TS
Phase 2			
1	50 kg TS/m^2/year	6 days	0.16 kg TS
2	100 kg TS/m^2/year		0.33 kg TS
3	150 kg TS/m^2/year		0.49 kg TS
4	100 kg TS/m^2/year	18 days	0.98 kg TS
5		27 days	1.47 kg TS
6		9 days	0.49 kg TS

The septage volume loaded for each bed was determined before the experiment. The total volume of septage required is based on the concentration of TS. Thus, 50 ml of the raw septage was collected from the storage tank to test for the TS concentration, as shown in Equation (3.1). Then, the respective volume of septage required (hydraulic load) is calculated as shown in Equation (3.2). Since the septage concentration was tested prior to the loading, the hydraulic load calculated from the TS concentration differed for each

loading. The overall loading volume required for each bed under various TS concentrations is summarized in Table 3.3.

$$TS\ (mg/L) = \frac{(Initial\ sample\ weight - final\ sample\ weight)\ mg}{50\ ml} \times 1000\left(\frac{ml}{L}\right) \quad (3.1)$$

$$Hydraulic\ load\ (L/loading) = \frac{Total\ sludge\ (mg/loading)}{TS\ (mg/L)} \quad (3.2)$$

Table 3.3: Summary of loading volume.

Tested sludge TS according to loading regime (mg/L)	Bed 1 (ml)	Bed 2 (ml)	Bed 3 (ml)	Bed 4 (ml)	Bed 5 (ml)	Bed 6 (ml)
Phase 1						
18780	8710	17420	26140	8710	17420	26140
29967	5460	10917	16380	5460	10917	16380
55780	2930	5870	8800	2930	5870	8800
20365	8030	16070	24110	8030	16070	24110
Phase 2						
10796	15150	30310	45470	90940	110000	45470
17507	9345	18690	28040	56080	84120	28040

3.1.5 Assessment of Hydraulic Behavior

The STRB was operated by means of free drainage, where the effluent discharged freely in the experiments. The time was recorded when a new batch of raw septage was loaded into the reed bed. The effluent discharged through the drainage pipe was collected in the container, as shown in Figure 3.14.

Figure 3.14: Collection of effluent from drainage pipe.

The volume of the effluent was measured with respect to the feeding time using a 500 ml measuring cylinder with a minimum scale of 5 ml. Generally, the effluent volumes were recorded at 1-minute intervals to plot the effluent flux at the beginning of the draining processes. The volume measurement frequency was reduced over the experiment, depending on whether the flow rate dropped gradually or drastically. Ideally, the time interval for volume measurements was increased from 1 to 5 minutes, then increased to 10 and 30 minutes as the flow rate decreased over the experiment. The hydraulic assessment on the loading is restricted to 6 hours due to technical limitations and safety concerns. The effluent flow rate and the percentage of water recovery of each loading cycle were determined as shown in Equations (3.3) and (3.4):

$$Effluent\ Flux\ (cm/min) = \frac{Collected\ volume\ (cm^3)}{Surface\ area\ (cm^2) \times Time\ interval\ (min)} \quad (3.3)$$

$$Water\ Recovery\ \% = \frac{Total\ volume\ of\ effluent\ (l)}{Volume\ of\ influent\ (l)} \times 100\% \quad (3.4)$$

3.1.6 Assessment of Sludge Deposit Layer

In addition to the hydraulic behavior, the characteristics of the sludge deposit were also monitored throughout the experiment. The variations of sludge deposit thickness were measured before and after the feeding period and during the non-feeding period. The sludge deposit thickness was measured by penetrating a wooden stick into the sludge deposit. The marks on the penetrated depth were then measured using a ruler, as illustrated in Figure 3.15. Thus, the changes in sludge deposit thickness can be determined, as shown in Equation (3.5).

$$Changes\ in\ sludge\ deposit\ layer\ thickness\ (cm) = (Final\ measurement - Initial\ measurement)cm \quad (3.5)$$

Figure 3.15: Measurement of sludge deposit thickness.

3.2 Laboratory Test and Analysis

The effluent was collected in the container from the drainage pipe during each loading with respective resting period and SLR. The effluent sample collected daily was then transferred to a 300-ml disposable BOD bottle with a plastic cap. Meanwhile, the collection of 20 g sludge deposit was performed daily from three different points in the reed bed. Upon the completion of the treatment processes, the sludge deposit samples,

and the effluents were sent to the laboratory for test and analysis. The sludge deposit sample was tested for its changes in thickness, MC, total solids, volatile solids, and shrinkage limit. On the other hand, the effluent was analyzed for dissolved oxygen, nitrate, chemical oxygen demand, pH, and total solids. The overall removal efficiency is calculated as shown in Equation (3.6).

$$\%\ Removal\ Efficiency = \frac{C_i V_i - C_e V_e}{C_i V_i} \times 100\% \tag{3.6}$$

where V_e and V_i are the volumes of effluent and influent (L), C_i and C_e are the concentrations of influent and effluent (mg/L), respectively. The standards, probe and equipment used for each test and analysis, is summarized in Table 3.4.

Table 3.4: Probe and equipment used for test and analysis.

Parameter	Probe and Equipment
Moisture Content (MC)	Oven (ASTM D2216 2019)
Total Volatile Solid (TVS)	Furnace (USEPA method 1684)
Shrinkage Limit (SL)	Oven (ASTM D4318-17)
Total Solids (TS)	Oven (ASTM D2216 2019)
Chemical Oxygen Demand (COD)	HACH DRB 2000 digital reactor and HACH DR2800 spectrophotometer (USEPA reactor digestion method 8000)
Nitrate (NO_3)	HACH HQ40d portable multimeter with NO_3 probe
pH	HACH HQ40d portable multimeter with pH probe
Dissolved Oxygen (DO)	HACH HQ40d portable multimeter with IntelliCAL™ LDO101 standard luminescent / Optical dissolved oxygen (LDO) probe

3.2.1 Moisture Content (MC)

Moisture content (MC) of a sludge deposit is crucial to understanding the infiltration rate and dewatering efficiency. The MC of the sludge deposit sample was determined via the standard method of the American Society for Testing and Materials (ASTM) D2216 2019, also well-known as the oven-drying method. 20 g of sludge deposit was collected directly from the reed bed using a soil core sampler. Then, the sample was weighed using a digital balance in the lab before putting in an oven for 24 hours. The drying temperature was set

to be 105 ± 5 ℃, as shown in Figure 3.16. Figure 3.17 shows the dried sludge sample before and after the oven test. The initial and final weight of the sample was weighed and recorded. Hence, the MC of the sludge deposit is determined as shown in Equation (3.7).

$$MC\ (\%) = 100\% - \left[\frac{(Initial\ sample\ weight - final\ sample\ weight)\ mg}{(Initial\ sample\ weight)\ mg} \times 100\%\right] \quad (3.7)$$

Figure 3.16: Oven with set temperature 105℃.

Figure 3.17: Dried sludge sample before (left) and after (right) oven test.

3.2.2 Total Volatile Solids (TVS)

Total volatile solids (TVS) are the organic materials present in wastewater. TVS determines the organic content in a wastewater or sludge sample. TVS can be obtained via reheating the dried TS sludge in a furnace, with a set temperature of 550 ℃ for 1 hour, according to the standard of the United States Environmental Protection Agency (USEPA) method 1684. Figure 3.18 shows the dried sludge sample after furnace heating. Thus, the initial and final weight of the sample was recorded. The relationship between TS and TVS is stated in Equations (3.8) and (3.9).

$$TVS\ (\%) = \frac{\left(TS\ weight - Sample\ weight\ after\ drying\ in\ 550℃\ furnace\ for\ 1\ hour\right) mg}{TS\ weight} \times 100\% \quad (3.8)$$

$$TVS\ (mg/L) = \frac{\left(TS\ weight - Sample\ weight\ after\ drying\ in\ 550℃\ furnace\ for\ 1\ hour\right) mg/L}{TS\ weight} \times 1000\left(\frac{ml}{L}\right) \quad (3.9)$$

Figure 3.18: Dried sludge sample after furnace test.

3.2.3 Shrinkage Limit (SL)

Shrinkage limit (SL) determines the maximum durable stress of a sample material before it deforms permanently. The ASTM D4318-17 method was practiced in determining the SL of the sludge deposit sample. This testing approach is known as the "rolling into thread" method. 20 g of sludge sample was retrieved from the reed bed using the soil core sampler and brought to the lab. The sludge deposit sample was reshaped and rolled into a 3-mm diameter thread. The rolling process was repeated until the thread crumbled. When the thread can no longer maintain its shape, the sample is well prepared for the oven-drying method. The exact temperature and duration features for the oven were used to dry

the sample, and then the initial and final weight of the sample was recorded. Hence, the shrinkage limit of the sludge deposit can be determined using Equation (3.10) as follows:

$$Shrinkage\ Limit\ (\%) = \frac{(Initial\ sample\ weight - final\ sample\ weight)\ mg}{(Initial\ sample\ weight)\ mg} \times 100\% \quad (3.10)$$

3.2.4 Total Solids (TS)

Total solids (TS) are always present in wastewater treatment effluent. TS is used to describe the total suspended solids found in wastewater. TS can be evaluated using the same method used to determine MC. Thus, the oven-drying method of standard ASTM D2216 2019 was used. Approximately 50 ml of effluent sample was retrieved from the drainage system of the reed bed. Then, the sample was transferred to a moisture can and weighed before being put in the oven for 24 hours. The drying temperature was set to be 105 ± 5 ℃ as well. The initial and final weight of the sample was weighed and recorded using the digital electronic balance, as shown in Figure 3.19. Figure 3.20 indicates the dried effluent sample after the oven test. Hence, the TS concentration of the samples is determined as shown in Equations (3.11) and (3.12).

$$TS\ (\%) = \left(\frac{(Initial\ sample\ weight - final\ sample\ weight)\ mg}{(Initial\ sample\ weight)\ mg} \times 100\%\right) \quad (3.11)$$

$$TS\ (mg/L) = \frac{(Initial\ sample\ weight - final\ sample\ weight)\ mg}{(Initial\ sample\ volume)\ ml} \times 1000\left(\frac{ml}{L}\right) \quad (3.12)$$

Figure 3.19: Digital electronic balance.

Figure 3.20: Dried effluent sample before (left) and after (right) oven test.

3.2.5 Chemical Oxygen Demand (COD)

Chemical oxygen demand (COD) is one of the methods used to determine the organic contaminants in wastewater treatment. COD describes the amount of DO in the wastewater oxidized chemically. In COD analysis, a HACH DR2800 spectrophotometer, as shown in Figure 3.21, with the standard of USEPA reactor digestion method 8000 was implemented. Both distilled water (blank) and wastewater sample (2 ml) were prepared and added into the high range (HR) COD digestion reagent vials (20 to 1,500 mg/L). Then, the samples were put into a HACH DRB 2000 digital reactor, as illustrated in Figure 3.22 with a set temperature of 150 ℃ for 2 hours. In the end, the concentrations of the sample vials were compared to the blank, and the results were recorded for further analysis.

Figure 3.21: HACH DR2800 spectrophotometer.

Figure 3.22: HACH DRB 2000 digital reactor.

3.2.6 Nitrate (NO_3)

Nitrate (NO_3) is an essential nutrient for the growth of plants. The decomposition of ammonia and ammonium to nitrate would increase the NO_3 content in the effluent. However, the strength of NO_3 conversion is still dominated by the successful decomposition of ammonia and ammonium in the system. Generally, the NO_3 composition is expected to increase in the effluent during the treatment. Thus, a HACH HQ40d portable multimeter with a NO_3 probe was used for the determination of NO_3 content in the effluent, as illustrated in Figure 3.23.

3.2.7 pH

The pH value is a common indicator of wastewater quality and characteristics. A lower pH value indicates a high acidity content of the liquid, while a higher pH represents a high alkalinity content. In addition, a pH value of 7 reveals a neutral condition of the liquid. Thus, a HACH HQ40d portable multimeter with a pH probe was used for the evaluation, as indicated in Figure 3.23.

Figure 3.23: HACH HQ40d portable multimeter with pH probe (left) and NO_3 probe (right).

3.2.8 Dissolved Oxygen (DO)

Dissolved oxygen (DO) measures the amount of oxygen dissolved in water. DO is significant in determining the effluent quality in a wastewater treatment process. Effluents with low DO content always find poor-quality solutions, especially septic sludge containing high organic matter. Then, a HACH HQ40d portable multimeter with IntelliCAL™ LDO101 standard luminescent / Optical dissolved oxygen (LDO) probe was directly inserted into the bottle with an effluent sample to measure the DO concentration, as shown in Figure 3.24 and Figure 3.25.

Figure 3.24: HACH HQ40d portable multimeter with IntelliCAL™ LDO101 standard luminescent / Optical dissolved oxygen (LDO) probe (left).

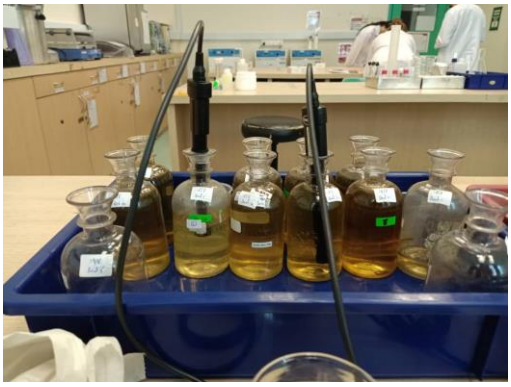

Figure 3.25: Reading and evaluating of effluent concentrations using portable multimeter with respective probes.

3.3 Analysis of Variance (ANOVA)

The analysis of variance (ANOVA) is a well-known statistical approach to evaluate several independent variables by comparing them to mean values (Burger, 2023). Hence, the ratio indicates the feature's strength is linked to the group variables, as shown in Equation (3.13).

$$F\ (\lambda) = \frac{S_B^2(\lambda)}{S_W^2(\lambda)} \tag{3.13}$$

where $S_B^2(\lambda)$ and $S_W^2(\lambda)$ are the sample variance between groups (Mean Square Between, MSB) and within groups (Mean Square Within, MSW), respectively, given in Equations (3.14) and (3.15).

$$S_B^2(\lambda) = \sum_{i=1}^{K} n_i \frac{\left(\left(\sum_{j=1}^{n_i} \frac{f_{ij}(\lambda)}{n_i}\right) - \left(\sum_{i=1}^{K}\sum_{j=1}^{n_i} \frac{f_{ij}(\lambda)}{\sum_{i=1}^{K} n_i}\right)\right)^2}{df_B} \tag{3.14}$$

$$S_W^2(\lambda) = \sum_{i=1}^{K}\sum_{j=1}^{n_i} \frac{\left(f_{ij}(\lambda) - \left(\sum_{i=1}^{K}\sum_{j=1}^{n_i} \frac{f_{ij}(\lambda)}{\sum_{i=1}^{K} n_i}\right)\right)^2}{df_W} \tag{3.15}$$

and the degrees of freedom for MSB and MSW are $df_B = K - 1$ and $df_W = N - K$, respectively. Whereas K is the number of groups and N is the total number of samples. The frequency of the λ th feature in the j th sample in the i th group is denoted by $f_{ij}(\lambda)$, and the number of samples in the i th group is denoted by n_i.

By implementing ANOVA, the variance distribution with a 95% confidence level is considered critical to the response (Veernapu & Cherukuri, 2023). Hence, the significance variables are the technique parameters with a p-value of less than 0.05.

3.4 Summary of Experimental and Laboratory Works, and Existing Limitations

In this study, the system configurations of all laboratory-scale STRBs were designed to be identical. The variables included the operating regime, including loading rate and resting period. These parameters have been reported in the literature as the factors that directly affect the system performance. However, this research study aims to investigate the impact of sludge deposit buildup on the system performance. Thus, the factor of the operating regime is considered a passive parameter which directly or indirectly influences the experimental outcomes. In addition to the operating regime, another factor that significantly influences the experimental results is the influent characteristics, which were not controlled in the experiment. The sludge used in this study was directly withdrawn from the households so that the sludge characteristics might vary throughout the experiment.

Furthermore, there are six laboratory-scale STRBs, and each bed was operated for an average of thirteen repetitions, where a total of 78 sets of data were collected. During each data collection, four tests (thickness, MC, organic content, and shrinkage limit) and five influent and effluent quality analyses (DO, NO_3, COD, TS, and pH) were carried out for the model calibration and validation. Meanwhile, the volume of the effluent collected from the bottom of the reed bed, with respective time intervals, would be used to validate the hydraulic conductivity of the numerical modeling. The expected color change of the effluent collected is noticed, as presented in Figure 3.26. The stage sampling shows that the effluent concentrations were inconsistent throughout the treatment as the filtration improved across time. Moreover, the total volume of effluent is collected to determine the water recovery of each bed. Additionally, the ANOVA test was performed to assess the significance of dependent variables on independent variables.

Figure 3.26: Sample effluents collected with respect to time.

After calibrating and validating the model, further analysis of parametric studies would be conducted to investigate the effects of the varying operating regimes (different SLRs and resting periods) on the dewatering efficiencies and hydraulic properties of the sludge deposit layer. Several SLRs (50 to 600 kg/m^2/year) with 50 kg/m^2/year of septic sludge intervals were studied, and a range of resting periods from 3 to 36 days are to be investigated as well. From the parametric studies, an optimum operating regime would be obtained and tested experimentally. Lastly, the treatment performance with the implementation of the optimum operating regime was investigated and compared with those suggested in the literature review.

3.5 Model Development

A conventional hydraulic model considers fixed boundary conditions, where it neglects the changes in the top boundary of the mesh. Temporary sludge ponding and deposit accumulation alter the top layer thickness, leading to moving boundary conditions. The difference in surface ponding level due to drainage and evapotranspiration causes variation in hydraulic heads, thus affecting the subsequent hydraulic conductivity of the infiltration flow through the sludge deposit layer (Brindt & Wallach, 2020). Further, the increase in sludge deposit layer thickness also reduces the saturated hydraulic conductivity of the layer. The compression of the sludge deposit due to continuous loading further reduces the permeability of the sludge deposit layer (Höfgen *et al.*, 2019). Therefore, a hydraulic model should be able to simulate the infiltration flow and associated solute transport in a STRB under moving boundary conditions.

Hence, necessary data, such as the sludge deposit's peak effluent flux and moisture content (MC), were obtained from the laboratory-scale STRB to calibrate and validate the model. The set of essential features of the proposed model are summarized as follows:

- A variably saturated flow module is essential to describe the hydraulic behavior of STRB with an intermittent feeding mode.
- The proposed model should incorporate appropriate boundary conditions, including batch feeding, surface ponding, and free drainage.
- The moving boundary condition should be applied to describe the sludge ponding and the formation of sludge deposits on the bed surface over the experiment.
- The substrate should be a filter medium with a fixed boundary condition.
- The accumulation and compression of sludge deposit on the surface of the reed bed and its associated impact on the hydraulic behavior should be considered.
- The root water uptake and water loss due to evapotranspiration should be included in the water balance.
- The bio-kinetic module should include sludge mineralization to describe the changes in organic content.

In this project, a laboratory-scale STRB is constructed to validate the model simulation created. Figure 3.27 presents the project flow to produce model simulation and the conduction of experiments. After the calibration and validation of the model, a parametric study would be done on different SLRs of feeding and non-feeding periods. The overall flowchart of research activities for the project is shown in Figure 3.28. Moreover, the flowcharts for hydraulic and solute transport modules are presented in Figure 3.29 and Figure 3.30.

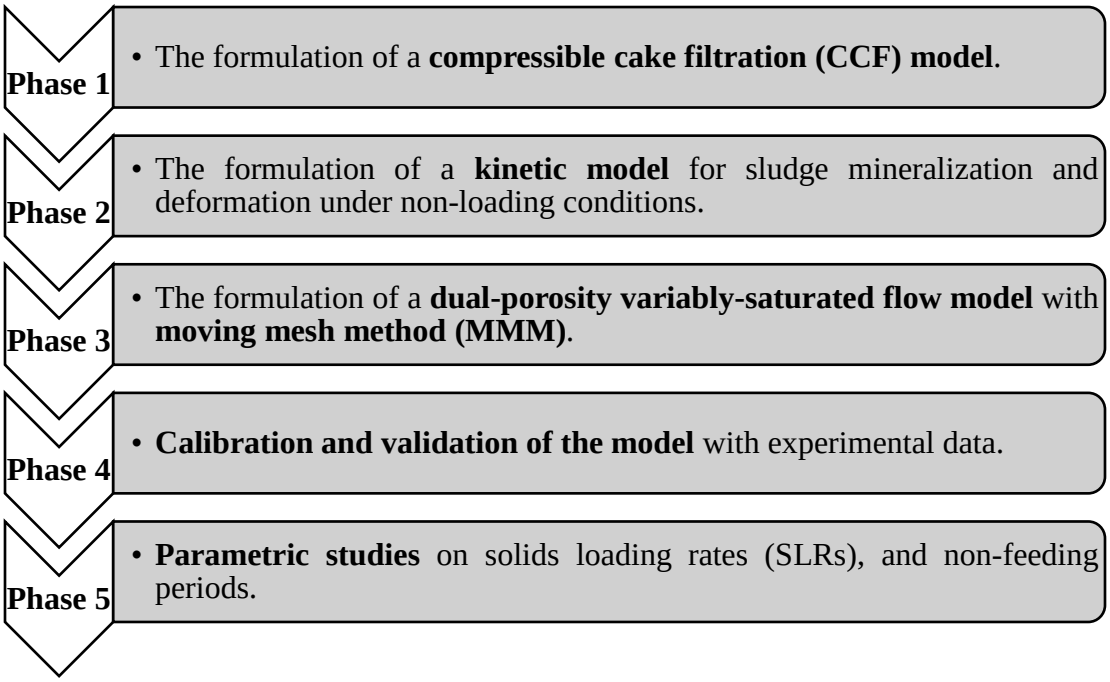

Figure 3.27: Project flowchart.

Figure 3.31 shows the framework for integrating process-based modeling of STRBs under the moving mesh method (Tan *et al.*, 2023). In this study, the hydraulic module adopted a dual-porosity variably saturated flow model to describe the unsaturated transient flow. The Richards' equation simulates the hydraulic flow in the substrate media and the associated volumetric water content. The Penman-Monteith equation estimates the potential evapotranspiration rate of water loss to the atmosphere. The Compressible Cake Filtration (CCF) model simulates the increment of sludge deposit

layer thickness. Lastly, the Activated Sludge Model is used to simulate the degradation of organic matter in the sludge deposits.

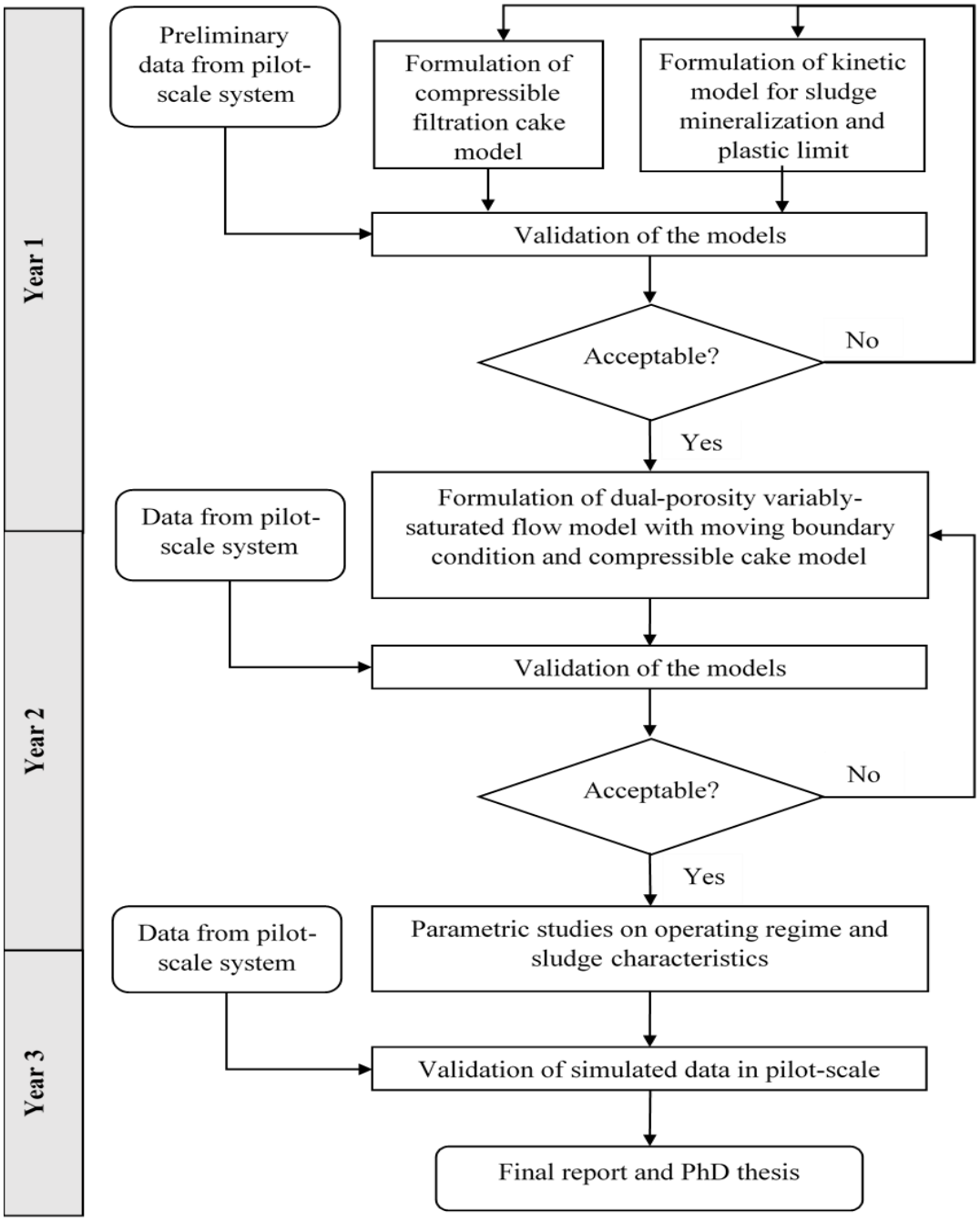

Figure 3.28: Flowchart of research activities.

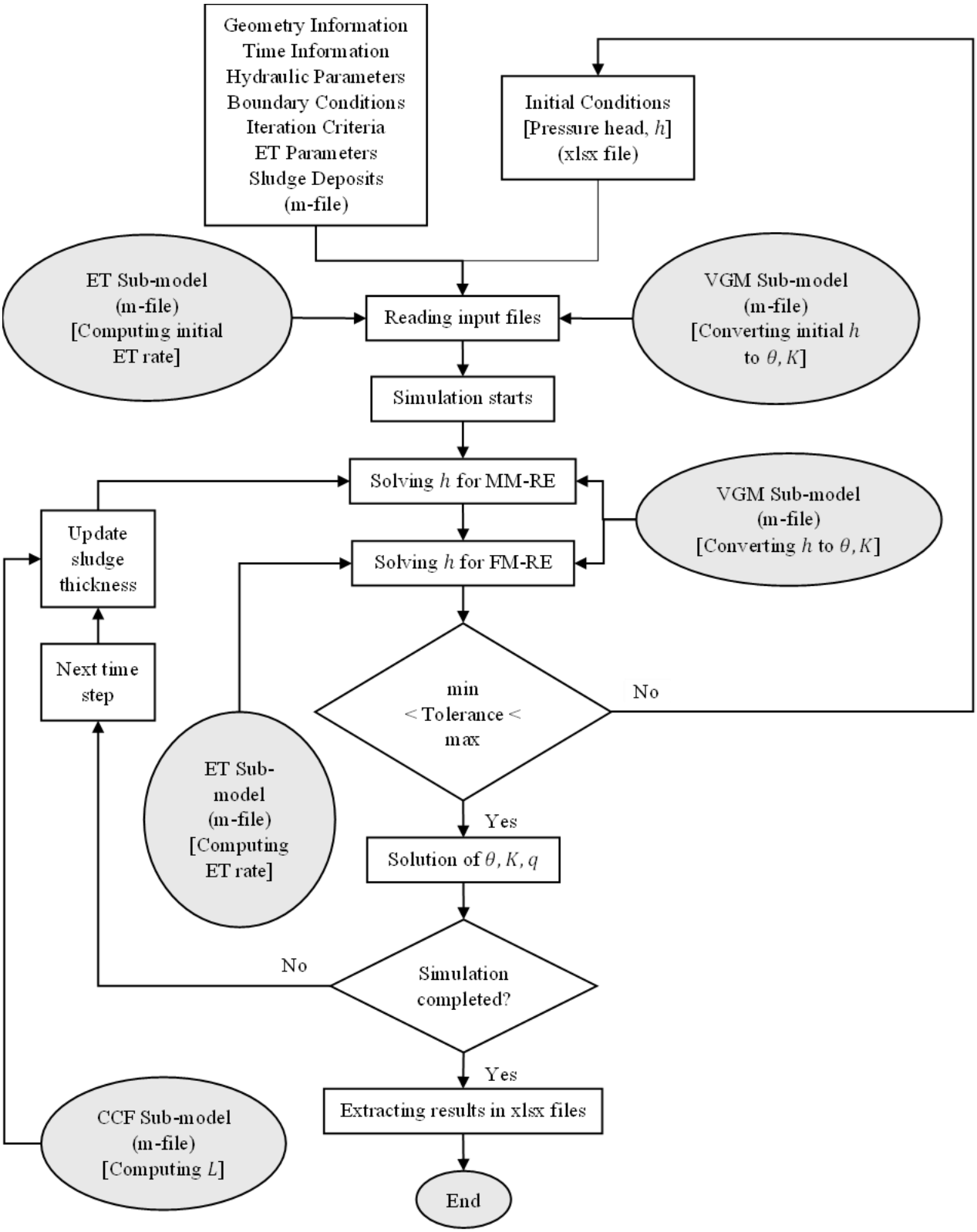

Figure 3.29: Flowchart for hydraulic module.

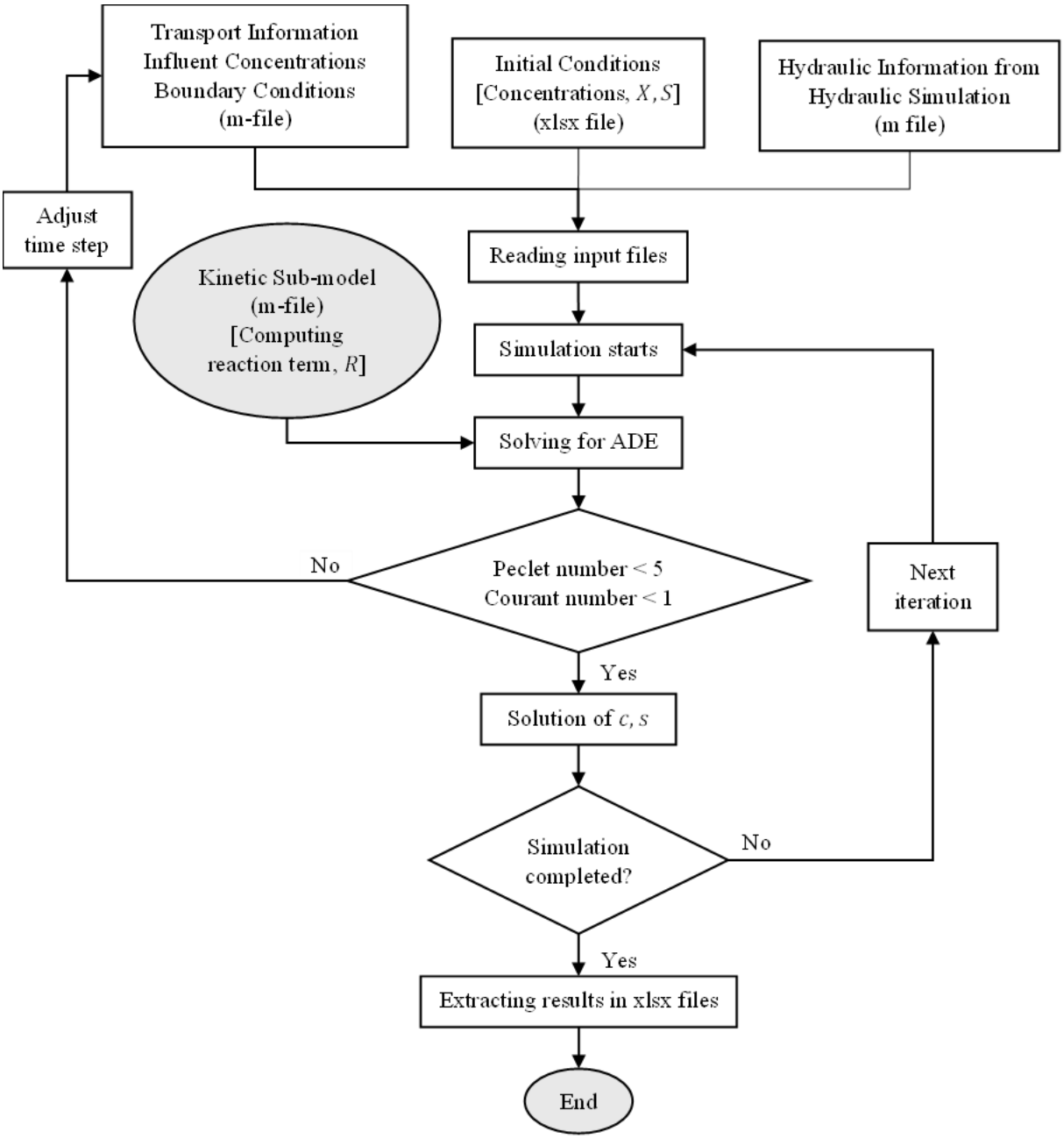

Figure 3.30: Flowchart for solute transport module

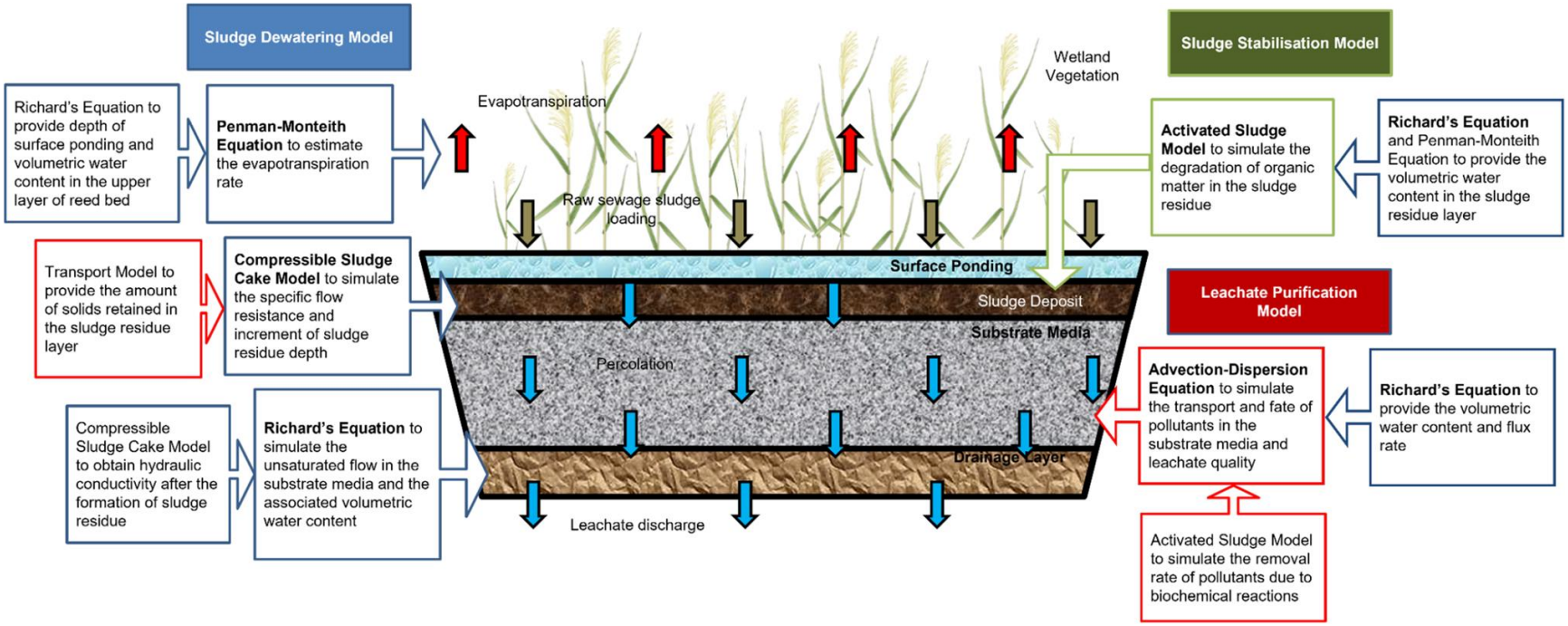

Figure 3.31: Integration of process-based modeling of STRBs.

Note: Adapted from "A review of sewage sludge dewatering and stabilization in reed bed system: toward the process-based modelling," by Tan, Y. Y., Huong, Y. Z., Tang, F. E., and Saptoro, A., *International Journal of Environmental Science and Technology*, 2023.

As usual, the very first step of the simulation is to read the input files to initialize the set variables and coding in the model. These files include information on geometry, time, hydraulic properties, boundary conditions, iteration criteria, sludge quality, and solute transport properties. However, the initial condition for pressure head and solute concentrations are imported from an Excel file (xlsx.) for the model initialization. The model simulation always starts from the hydraulic module to the solute transport module, in which the computation of model simulation is accommodated simultaneously with the VGM, ET, CCF, and kinetic sub-models. The simulation repeats the same written procedure (program code) in every time step until the prescribed final simulation time has been reached. Lastly, the simulated results are saved into several separate Excel files with a file extension of xlsx.

As the simulation initializes, several matrices are created to store the arrays of the simulated data for hydraulic behavior and contaminant transport, where the associated input information is the geometry and time. The modeling of the hydraulic and solute transport is coded in the same MATLAB® file (m-file), as the solute transport is always correlated with the hydraulic flow. The same hydraulic data is then used for the simulation of the solute transport module with different input variables and coding. In the model, the VGM model was employed for the computation of initial water content and the subsequent hydraulic conductivity based on the prescribed initial head distribution and hydraulic characteristics. Moreover, the ET model estimates the rate of water uptake by plants and the water loss to the atmosphere. The kinetic model is applied to the solute transport module, where the fate of contaminant concentrations is modeled according to the resultant hydraulic flow.

This study investigates a combination of moving and fixed mesh discretization of the RE and ADE. Hence, the STRB system is partitioned into three layers: the sludge ponding layer, the sludge deposit layer, and the reed bed substrate layer. The MMM is implemented in the top layer due to the ponding occurrence and in the second layer of the sludge deposition. Simultaneously, the CCF model is applied to the second layer, where the thickness of the sludge deposit increases or decreases due to the continuous sludge deposition and the water loss via ET, respectively. According to the moving mesh

principle, the mesh size constantly changes, not the mesh number. Thus, the changes in the upper mesh are the most apparent. For the remaining layers, the FMM is implemented as the filter medium of the reed bed, which is always stationary. A better illustration of the mentioned layers is shown in Figure 3.32.

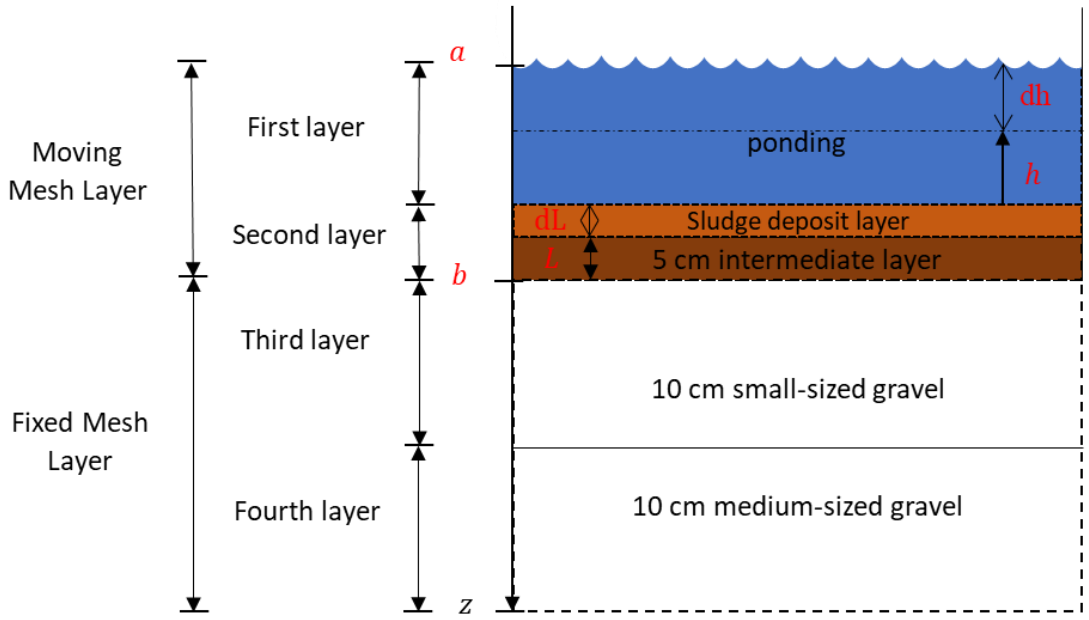

Figure 3.32: Combination of moving and fixed mesh layers.

The pressure head (h) in the next time step is solved using the velocity-based RE for the moving mesh layer, followed by the modified Picard iteration approach for the fixed mesh layer. The bottom fluxes estimated via the MMM are then used as the input fluxes for the FMM. Thus, the convergence of the solution is obtained by comparing the residual of the solution to the prescribed minimum tolerance in the FMM. Then, the resultant pressure head calculates water content and flux in the mobile and immobile regions. If convergence fails within the maximum set iterations, the residual would be compared to the prescribed maximum tolerance. However, if the solution cannot converge even to the maximum tolerance, the simulation is terminated and regarded as a failure. In case of successful convergence, the simulation continues, and the simulated data is temporarily stored in previously created matrices. The same procedure is repeated until the end of the prescribed duration. Eventually, the simulated data output is saved and displayed in Excel files as soon as the simulation is completed.

In the solute transport module, the resultant water content and water flux are exported from the hydraulic module and utilized as input variables for the simulation. Since the solute transport module uses the output of the hydraulic module as an input, the computation of ADE is carried out directly without the necessity of an iterative algorithm. However, the simulation of the reactive transport of a particular component is carried out independently with the accommodation of a kinetic model at each iteration step. The computation of the following component is started after the solution of the aqueous concentration and sorbed concentration of a particular component has been acquired. In addition, stability constraints are set to ensure the precision and robustness of the model. The simulation stops if the conditions are undesirable, where the Courant number, ($C_r > 1$) or Peclet number, ($P_e > 5$) is observed. Thus, the spatial and temporal size for the discretization must be corrected to prevent numerical dispersion. The iterative procedure is repeated until the prescribed simulation time ends, and the simulated data is stored in the set matrices before exporting to Excel files.

3.6 The Hydraulic Module of the Model

The hydraulic flow in STRBs is meant to be partially obstructed by the substrate medium, leading to unsaturated transient flow. The unwanted particles are retained on the bed surface, thus treating the sludge by filtration. The dual-porosity variably saturated flow model describes the unsaturated flow in mobile and immobile regions of the substrate medium. Hence, the Richards' equation is used to explain the unsaturated flow in the STRB, incorporating the plant sub-model (Penman-Monteith equation), sludge sub-model (Compressible Cake Filtration), and bio-kinetic sub-model (Sludge Stabilization) in the dual-porosity variably saturated flow model.

3.6.1 Richards' Equation

Richards' equation (RE) (Richards, 1931) has been widely used in the research on transient water flow processes in unsaturated soils (Bassetto *et al.*, 2022; Brunone *et al.*, 2003; Mladenov *et al.*, 2022). The RE can be expressed in three forms, namely, head-based (h), moisture content-based (θ), and mixed form (Celia & Bouloutas, 1990).

According to Brunone *et al.* (2003), a fundamental limitation was discovered for h-based RE with specific moisture capacity, $C(h) = d\theta/dh$ $[L^{-1}]$, where the hydraulic properties yield a realistic behavior only within a relatively small range of pressure heads. Thus, θ-based RE was derived from the former equation with the concept of water diffusivity, $D(\theta) = K(h)/C(h)$ $[L^2/t]$. However, based on the findings of Celia and Bouloutas (1990), a mixed form of RE exhibits consistently reliable and robust numerical solutions for unsaturated flow. Therefore, the mixed form of RE is selected as the governing unsaturated flow equation of the numerical simulation in this study.

A mixed form of RE that comprises the effect of gravity and water pressure to relate the variation of volumetric water content within a partially saturated porous medium $(\partial\theta/\partial t)$ $[t^{-1}]$ is presented as Celia and Bouloutas (1990):

$$\frac{\partial\theta}{\partial t} = \frac{\partial}{\partial z}\left[K(h)\frac{\partial h}{\partial z}\right] + \frac{\partial K(h)}{\partial z} - S \tag{3.16}$$

where θ denotes the volumetric water content $[L^3/L^3]$, $K(h)$ denotes the unsaturated hydraulic conductivity $[L/t]$, z denotes the vertical coordinate assumed positive upward $[L]$, t denotes the time $[t]$, and h denotes the pressure head $[L]$. In numerical modeling, the volumetric water content and unsaturated hydraulic conductivity are considered system variables, and the coordinates and time are the independent variables. Further, the term S is introduced as a source/sink term $[t^{-1}]$ to indicate root water uptake or water loss via ET (Casulli & Zanolli, 2010). The detailed derivation of the RE is given in **Appendix A**.

RE is a partial differential equation with nonlinear behavior. Therefore, the analytical solution is only limited to certain boundary conditions. Accordingly, two general numerical approximations have been applied to solve the RE: finite differences (FD) and finite elements (FE) methods. FD is often used for RE discretization as it involves one-dimensional problem simulation (Farthing & Ogden, 2017).

3.6.2 Unsaturated Hydraulic Conductivity

In vadose zone flow and transport studies, the unsaturated hydraulic conductivity decreased with the volumetric water content as the hydraulic pressure decreased (Beulke *et al.*, 2002). Such a relationship describes the hydraulic properties in STRBs. Several well-known parametric non-linear models were established for unsaturated flow in porous media, such as the viscous coupling, Corey, and van Genuchten-Mualem models. However, the van Genuchten-Mualem model was selected for this study due to its robustness in describing unsaturated hydraulic conductivity and volumetric water content (Sheng *et al.*, 2019).

The hydraulic properties are typically defined by the pore size distribution model (Mualem, 1976) incorporated with the water retention function (van Genuchten, 1980) for hydraulic conductivity under unsaturated conditions, known as the van Genuchten-Mualem function. Based on Mualem (1976) findings, a model of the relative hydraulic conductivity function of unsaturated porous media was derived from the soil water retention curve, which is based on the relationship and assumption that the length is proportional to the radius of the inter-connected pores (Ghanbarian *et al.*, 2016). Thus, the porosity of a gravel is always proportional to its size. This model was considered desirable by many other researchers in the same field, as these unsaturated hydraulic conductivities are notoriously tricky to measure. The linear coefficient relationship eases the determination of unsaturated hydraulic conductivity in the porous media. Thus, Mualem's model was suggested for use together with the analytical model of van Genuchten.

In 1980, van Genuchten developed the soil water retention equation, $\theta(h)$, given as (van Genuchten, 1980):

For $h \leq 0$,
$$\theta(h) = \theta_r + \frac{\theta_s - \theta_r}{[1 + |\alpha h|^n]^m} \tag{3.17}$$

For $h \geq 0$,
$$\theta(h) = \theta_s \tag{3.18}$$

Hence, the combined van Genuchten-Mualem's (VGM) hydraulic conductivity equation, $K(h)$ $[L/t]$ is presented as (van Genuchten, 1980):

For $h \leq 0$,
$$K(h) = K_s \left[\frac{\theta(h) - \theta_r}{\theta_s - \theta_r}\right]^l \left\{1 - \left[1 - \left(\frac{\theta(h) - \theta_r}{\theta_s - \theta_r}\right)^{\frac{1}{m}}\right]^m\right\}^2 \quad (3.19)$$

For $h \geq 0$,
$$K(h) = K_s \quad (3.20)$$

In addition, a specific moisture capacity, $C(h)$ $[L^{-1}]$ is known as (van Genuchten, 1980):

For $h \leq 0$,
$$C(h) = \alpha n m \frac{\theta_s - \theta_r}{[1 + |\alpha h|^n]^{m+1}} |\alpha h|^{n-1} \quad (3.21)$$

For $h \geq 0$,
$$C(h) = 0 \quad (3.22)$$

where $\theta(h)$ is the volumetric water content $[L^3/L^3]$ at pressure head, h $[L]$; θ_r and θ_s are the residual and saturated water contents, respectively $[L^3/L^3]$; α $[L^{-1}]$ is related to the inverse of the air-entry pressure; n is a measure of the pore-size distribution (van Genuchten, 1980); $m = 1 - 1/n$; K_s is the saturated hydraulic conductivity $[L/t]$; and $l = 1/2$ is an empirical pore-connectivity parameter (Mualem, 1976). Also, it should be noted that θ_r, θ_s, K_s, α, n, and $m \geq 1$ are material parameters which affect the shape of the soil hydraulic functions and satisfy $0 \leq \theta_r < \theta_s$ and K_s, $\alpha > 0$.

Therefore, this model is used in this study for the hydraulic simulation, based on the assumption of the proportionality between the pore radius and the inter-connected length, which relates to the availability of the gravel parameters used in the experiment.

3.6.3 Dual-Porosity Model for Hydraulic Flow

Generally, Richards' Equation (RE) is still used to describe the variably saturated water flow, while the solute transport is simulated via the advective-dispersion equation (ADE). The equilibrium and non-equilibrium flow explain the hydraulic flow and solute transport

in the single-porosity and dual-porosity medium (Šimůnek & van Genuchten, 2008). The conceptual physical illustrations of several equilibrium and non-equilibrium models are displayed in Figure 3.33 (Šimůnek & van Genuchten, 2008). The equilibrium model assumes a uniform water and solute flow in a medium. However, the non-equilibrium model describes the dual-porosity hydraulic behavior in a medium with mobile and immobile regions. Such a model includes the water exchange between the mobile and immobile regions, which improves the accuracy of the dual-porosity variably saturated flow model.

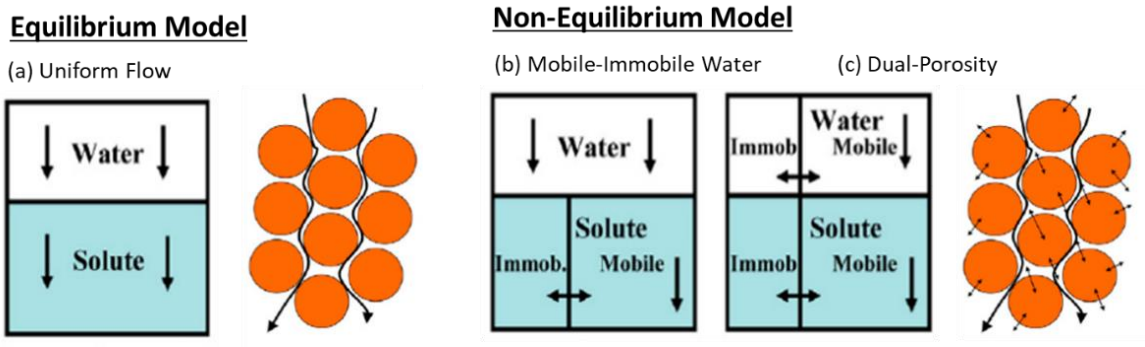

Figure 3.33: Conceptual physical equilibrium and nonequilibrium models for water flow and solute transport.
Note: Adapted from "Modelling Nonequilibrium Flow and Transport Processes Using HYDRUS," by Šimůnek, J., and van Genuchten, M. T., *Vadose Zone Journal*, 2008.

The limitation of the single-porosity model in describing the unsaturated flow in the porous medium has been reported in which the porous media flow and transport processes cannot be effectively described based on the assumptions of uniform flow and transport (Arbogast, 1992; McCarter *et al.*, 2019; Pucher & Langergraber, 2018; Tan *et al.*, 2017). Indeed, the single-porosity model eases the hydraulic simulation as it involves fewer parameter and assumes the hydraulic flow through a medium with only a single porous domain (Ooi *et al.*, 2018). However, this is unsuitable for the model simulation in the STRB system due to inconsistent porosity in the substrate medium and possible cracks on the sludge deposits. Hence, a new one-dimensional dual-porosity model has been developed (Gerke & van Genuchten, 1993a, 1993b). The dual-porosity model aims to study the variably saturated water flow and solute transport in the porous medium that involves two intersecting continua: a fracture pore system and a matrix pore system

(Gerke & van Genuchten, 1993a, 1993b). The mobile and immobile regions represent the macro and micropores in the STRB to describe the matrix pore and fracture pore systems, respectively.

Based on the dual-porosity conceptualization, the liquid phase in the system is partitioned into two regions: mobile, θ_{mo} and immobile, θ_{im} (van Genuchten & Wierenga, 1976). Hence, a total water content formulation, θ $[L^3/L^3]$ is given as:

$$\theta = \theta_{mo} + \theta_{im} \tag{3.23}$$

Then, the dual-porosity equation for water flow is combined with the RE to explain further the water flow in the macropores (fracture pores) and matrix pores (Šimůnek *et al.*, 2003; Šimůnek & van Genuchten, 2008). Thus, the formulated functions for mobile and immobile regions, respectively, are presented as:

Mobile: $$\frac{\partial \theta_{mo}(h_{mo})}{\partial t} = \frac{\partial}{\partial z}\left[K(h_{mo})\frac{\partial h_{mo}}{\partial z}\right] + \frac{\partial K(h_{mo})}{\partial z} - S_{mo} - \Gamma_w \tag{3.24}$$

Immobile: $$\frac{\partial \theta_{im}(h_{im})}{\partial t} = -S_{im} + \Gamma_w \tag{3.25}$$

where S_{mo} and S_{im} are the source/sink terms for the mobile and immobile regions $[t^{-1}]$, respectively, and Γ_w is the water transfer rate between the two regions $[t^{-1}]$.

According to several studies, the mass transfer rate of water flow, Γ_w between the two regions (mobile and immobile) is a first-order rate equation, that is based on the difference in effective water contents of the two regions (Gerke & van Genuchten, 1993b; Šimůnek *et al.*, 2003; Šimůnek *et al.*, 2001). Therefore, the water transfer rate equation, Γ_w and the general effective saturated water content equation, S_e are expressed as:

$$\Gamma_w = \frac{\partial \theta_{im}(h_{im})}{\partial t} = \omega(S_e^{mo} - S_e^{im}) \tag{3.26}$$

$$S_e(h) = \frac{\theta(h) - \theta_r}{\theta_s - \theta_r} \tag{3.27}$$

where θ_{im} is the water content in the immobile region based on the pressure head differences, h_{im}; ω is the first-order rate coefficient $[t^{-1}]$; S_e^{mo} and S_e^{im} are the effective saturated water content for mobile and immobile regions, respectively. Also, it should be noted that the water tends to transfer from mobile to immobile regions when the value of Γ_w is positive and vice versa.

3.6.4 Sink Term – Evapotranspiration (ET)

Evapotranspiration (ET) has been used broadly in agriculture to describe the two processes involved: evaporation and transpiration. Evaporation is a process where the liquid water changes its phase to water vapor, thus being removed from the soil surface. On the other hand, transpiration is water loss to the atmosphere through the leaf stomata in vapor form. Generally, evaporation and transpiration co-occur and are influenced by solar radiation, relative humidity, wind speed, and air temperature (Jensen *et al.*, 1990).

There are a large number of empirical methods developed by researchers worldwide in purpose of estimating the potential evapotranspiration (PET) for different climates, such as Turc method (Turc, 1961), Blaney-Criddle method (Blaney & Criddle, 1962), Penman-Monteith method (Monteith, 1965; Penman, 1948), Priestley-Taylor method (Priestley & Taylor, 1972), and Pan method (Christiansen Jerald, 1968). However, it has been determined that the modified Penman-Monteith method (FAO-56 Penman-Monteith) offers the best results among all the stated empirical methods (Allen *et al.*, 1998). This modified method is altered based on the assumption and reference crop of 0.12-m high in a comprehensive report by the Food and Agriculture Organization of the United Nations (FAO-56 Paper). Thus, the method is relatively accurate in estimating the PET in various locations and climates, even under insufficient data (Chen *et al.*, 2022; Xiang *et al.*, 2020).

The Penman-Monteith's combination equation for reference evapotranspiration rate, ET_0 $[L/t]$ based on the addition of radiation (evaporation), ET_{rad} and aerodynamic (transpiration), ET_{aero}, which is presented as (Allen *et al.*, 1998):

$$ET_0 = ET_{rad} + ET_{aero} = \frac{1}{\lambda}\left[\frac{\Delta(R_n - G) + \rho_a c_p \frac{(e_s - e_a)}{r_a}}{\Delta + \gamma\left(1 + \frac{r_s}{r_a}\right)}\right] \tag{3.28}$$

where λ is the latent heat of vaporization $[L^2/t^2]$; Δ is the slope of the saturated vapor pressure curve $[M/Lt^2T]$; R_n is the net radiation flux $[M/t^3]$; G is the soil heat flux $[M/t^3]$; ρ_a is the atmospheric density $[M/L^3]$; c_p is the specific heat of dry air $[L^2/t^2T]$; $(e_s - e_a)$ is the vapor pressure difference between saturation and actual $[M/Lt^2]$; r_a and r_s are the aerodynamic and surface resistances $[t/L]$, respectively; and γ is the psychrometric constant $[M/Lt^2T]$. Also, it should be noted that $\lambda = 2.45\ MJ/kg$ at 20℃, $\Delta = \partial e/\partial T$ where e is saturated vapor pressure in kPa and T is the temperature in $°C$, $c_p \sim 1.013 \times 10^{-3}\ MJ/kg$℃, e_s is computed by taking the mean at a minimum and maximum air temperature in ℃, e_a is the ambient vapor pressure in kPa, r_a and r_s are resistances of evaporating water vapor from the vegetation and soil surfaces into the air, respectively, and $\gamma \sim 0.066\ kPa/$℃ that is proportional to atmospheric pressure $101.3kPa$. The detailed steps and calculations are presented in **Appendix B**.

However, the Penman-Monteith's combination equation for PET estimation is based on an ideal situation, where (a) the vegetation is fully covering the ground and with homogeneous height; (b) there is an aerodynamically rough surface for ET; (c) there is sufficient supply of water and nutrients (Xiang *et al.*, 2020). Therefore, it could be problematic for the numerical simulation later, as the vegetation may not completely cover the ground. To ease the numerical simulation, the ET can be separated and redefined into two primary processes, evaporation and transpiration, based on the leaf area index (LAI) by Beer-Lambert law (Varado *et al.*, 2006). Thus, the potential soil evaporation, E_p $[L/t]$ and potential transpiration, T_p $[L/t]$ are shown as follow:

$$E_p = PET \exp(-a_{b1} LAI) \tag{3.29}$$

$$T_p = PET[1 - \exp(-a_{b1} LAI)] \tag{3.30}$$

where $a_{b1} = 0.5$ is a coefficient that represents the radiation by the vegetation, and LAI is the leaf area index based on the fraction of leaf area coverage to that of the soil surface.

Furthermore, the sink term, S, in the RE is the water loss via ET. The sink term included here is the root water uptake (water extraction) by the plants, where a linear function has been developed based on the potential transpiration rate, T_p (Lai & Katul, 2000; Li *et al.*, 2001). Thus, the linear function of the sink term, $S(\theta, z, t)$ $[t^{-1}]$ is formulated as:

$$S(\theta, z, t) = \alpha_1(\theta)\alpha_2(\theta)g(z)T_p(t) \tag{3.31}$$

where z is the depth $[L]$, t is the time $[t]$, θ is the volumetric water content $[L^3/L^3]$, $\alpha_1(\theta)$ and $\alpha_2(\theta)$ are the empirical coefficient between [0, 1] contributing to compensation mechanism and water stress, respectively, whereas $g(z)$ is the root density function $[L^{-1}]$.

The formulations of empirical coefficient contributed to the compensation mechanism, $\alpha_1(\theta)$ and water stress, $\alpha_2(\theta)$ are:

$$\alpha_1(\theta) = Max\left(\frac{\theta(z)}{\theta_s - \theta_{wilt}}; \frac{\int_0^z \theta(z)dz}{\int_0^{z_R} \theta(z)dz}\right) \tag{3.32}$$

$$\alpha_2(\theta) = \left(\frac{\theta(z) - \theta_{wilt}}{\theta_s}\right)^{\frac{\gamma}{\theta(z)-\theta_{wilt}}} \tag{3.33}$$

where θ_{wilt} is the wilting point $[L^3/L^3]$, z_R is the maximum root depth $[L]$, and $\gamma = 0.01$ is a parameter that contributed to the sharpness of the stress function. For better illustration, the distance between z and z_R for the root depth as indicated in Figure 3.34.

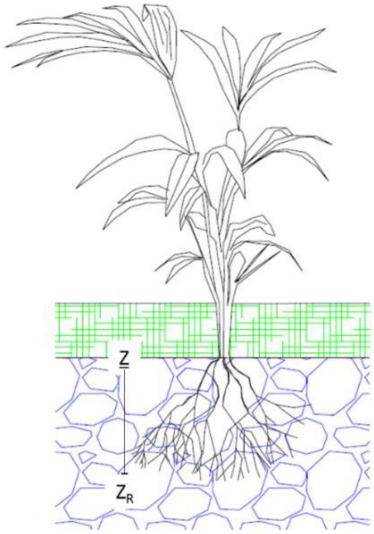

Figure 3.34: Root depth between z and Z_R.
Note: Adapted from "Dewatering and Treatment of Septage Using Vertical Flow Constructed Wetlands," by Tan, Y. Y., Tang, F. E., Ho, C. L. I., and Jong, V., *Technologies*, 2017.

On the other hand, the root density function, $g(z)$ is given as:

$$g(z) = g_0 \frac{\exp(-bz)\,[1.5 + 0.5\exp(-bz)]}{1 + \exp(-bz)} \tag{3.34}$$

$$b = \frac{24.66\,(F_{10})^{1.59}}{Z_R} \tag{3.35}$$

where g_0 is the root density at $z = 0\,[L^{-1}]$, b is a decreasing coefficient of the distribution $[L^{-1}]$, and F_{10} is the top 10% of root length density fraction in the root zone.

3.7 Solute Transport Module of the Model

3.7.1 Advective-Dispersion Equation (ADE)

The transport of solutes in porous media undergoes various processes such as advection, diffusion, and dispersion. In general, any solute transported through a porous medium entirely depends on the average flow pattern, rate of molecular diffusion, and the ability of the porous medium to spread or deviate the solutes from average flow (Bresler, 1973;

Healy, 1990). In addition, these processes are also involved in mechanisms such as rate-limiting sorption and desorption (physical reaction), as well as chemical reactions (Nielsen *et al.*, 1986). The solute transport in porous media is highly affected by the interactions between the solute and the solid (substrate). Thus, the transport model must have linear or non-linear equilibrium isotherms for these interactions. Generally, linear equilibrium adsorption is applied to the system if the adsorption rate exceeds the hydraulic flow. However, if the condition is unfavored, a kinetic model (non-linear equilibrium), such as Langmuir and Freundlich isotherm models, would better describe the solute transport model (Fetter Jr, 2000; Healy, 1990; McCarter *et al.*, 2019).

The soil-water systems in the unsaturated zone are always complex. On the one hand, this system is seldom in a stable equilibrium state but in a constant flux (q) situation. On the other hand, the degree of soil-water saturation (θ) is often varying with time (t) and space (z). As a result, the flow parameters such as suction head (h) and hydraulic conductivity (K) are affected, thus further sophisticating the system. Therefore, according to Bresler (1973) and Nielsen *et al.* (1986), a parabolic type of partial differential equation, as known as the advection-dispersion equation (ADE) with the inclusion of the adsorption term, has been developed to consider the mentioned processes simultaneously, and it is given as:

$$\frac{\partial \theta c}{\partial t} + \rho \frac{\partial s}{\partial t} = \frac{\partial}{\partial z}\left(\theta D \frac{\partial c}{\partial z} - qc\right) + R \tag{3.36}$$

where θ is the volumetric water content $[L^3/L^3]$; c is the solute concentration in aqueous solution $[M/L^3]$; t is the time $[t]$; ρ is the soil bulk density $[M/L^3]$; s is the solute concentration adsorbed at solid surface $[M/L^3]$; z is the vertical coordinate assumed positive downward $[L]$; D is the combined diffusion-dispersion coefficient $[L^2/t]$; q is the volumetric flux $[L^3/L^2t]$; and R is the reaction term.

The combined diffusion-dispersion coefficient, D is obtained from the following formula:

$$D = D_d + D_p \tag{3.37}$$

where D_d $[L^2/t]$ is the diffusion coefficient and D_p $[L^2/t]$ is the dispersion coefficient, respectively. Thus, the respective diffusion coefficient, D_d and dispersion coefficient, D_p can be found as:

$$D_d(\theta) = D_0 a e^{b\theta} \tag{3.38}$$

$$D_p(q) = D_L|q| \tag{3.39}$$

where D_0 is the equivalent coefficient in the free-water system $[L^2/t]$, $a = 0.001$ and $b = 10$ are the empirical constants that characterize the soil in particular, D_L is the longitudinal dispersivity $[L]$, and $|q|$ is the absolute value of the Darcian fluid flux density $[L/t]$. Moreover, the volumetric flux, q $[L/t]$ is given by:

$$q = V\theta \tag{3.40}$$

where q is the imposed flux $[L/t]$, V is the average interstitial flow velocity $[L/t]$, and θ is the volumetric water content $[L^3/L^3]$. Furthermore, the reaction term, R $[M/L^3t]$ is usually estimated by zero- or first-order rate terms as follow:

$$R = -\mu_1\theta c - \mu_2\rho s + \gamma_1\theta + \gamma_2\rho \tag{3.41}$$

where μ_1 and μ_2 are the rate constants for first-order decay in the liquid and adsorbed phases, respectively, whereas γ_1 and γ_2 are the zero-order production terms for the two phases, respectively.

Additionally, it has been determined by Nielsen *et al.* (1986) that a desirable solute transport model should have considered two linear adsorption sites, at which one is an instantaneous process governed by the equilibrium adsorption and the other is a time-dependent process with first-order kinetics (non-equilibrium), respectively. Their hydrogeology research incorporates the linear equilibrium adsorption model into the solute transport model. Accordingly, the instantaneous adsorption of the solutes onto the surface of the porous medium could be explained based on the simple linearity between s_e and c, as follows:

$$s_e = K_d c \tag{3.42}$$

where s_e is the equilibrium concentration of solutes at adsorbed phase $[M/M]$, K_d is the distribution coefficient obtained from the slope of the isotherm curve $[L^3/M]$, and c is the concentration of solute at the free phase $[M/L^3]$. Therefore, when Equation (3.42) is inserted into Equation (3.36), it gives a typical instantaneous equilibrium of ADE distribution as follows:

$$(\theta + \rho K_d)\frac{\partial c}{\partial t} = \frac{\partial}{\partial z}\left(\theta D \frac{\partial c}{\partial z} - qc\right) + R \tag{3.43}$$

Meanwhile, in consideration of time-dependent first-order kinetics $(\partial s_k/\partial t)$, the formula distribution is revised as:

$$\frac{\partial s_k}{\partial t} = \alpha_k[(1-F)K_d c - s_k] \tag{3.44}$$

where α_k is the first-order rate coefficient $[t^{-1}]$, F is the mass fraction of all sites occupied in instantaneous equilibrium, and s_k is the time-dependent concentration of solutes at adsorbed phase $[M/M]$. Also, it should be noted that the two-site sorption concept is based on the addition of equilibrium and first-order kinetics adsorption, $s = s_e + s_k$, and $F = 0$ when the overall process is time-dependent, while $F = 1$ when an instantaneous process is assumed. Therefore, a two-site kinetic model of ADE distribution by taking into consideration of both instantaneous and time-dependent processes is determined by adding Equation (3.44) to the LHS of Equation (3.43), as shown below:

$$(\theta + F\rho K_d)\frac{\partial c}{\partial t} + \alpha\rho[(1-F)K_d c - s_k] = \frac{\partial}{\partial z}\left(\theta D \frac{\partial c}{\partial z} - qc\right) + R \tag{3.45}$$

3.7.2 Dual-Porosity Model for Solute Transport

Equation (3.36) is mathematically equivalent to a dual porosity model for solute transport in both mobile and immobile regions of a porous medium (Nielsen *et al.*, 1986; Šimůnek

et al., 2003; Šimůnek & van Genuchten, 2008). Identical to the dual-porosity model for water flow, the total solute transport, θc $[M/L^3]$ is given as:

$$\theta c = \theta_{mo} c_{mo} + \theta_{im} c_{im} \tag{3.46}$$

where θ is the volumetric water content θ $[L^3/L^3]$, c_{mo} and c_{im} are the solute concentrations at the mobile and immobile regions $[M/L^3]$, respectively. Moreover, the two-site sorption model $(s = s_e + s_k)$ is divided into mobile and immobile regions, as well as kinetic sorption sites with respect to the total adsorbed concentration at equilibrium, where the new sorption models are given as:

Mobile: $$s_{mo}^e = F_{mo} K_d c_{mo} \tag{3.47}$$

Immobile: $$s_{im} = F_{mo} K_d c_{im} \tag{3.48}$$

Kinetics: $$s_{mo}^k = (1 - F_{mo}) K_d c_{mo} \tag{3.49}$$

where s_{mo}^e is the equilibrium adsorbed solute concentrations at the mobile region $[M/M]$; s_{im} is the adsorbed solute concentrations at the immobile region $[M/M]$; s_{mo}^k is the adsorbed solute concentrations at the kinetic sorption sites $[M/M]$; and F_{mo} is the mass fraction of all sites occupied in instantaneous equilibrium at the mobile region.

Hence, the dual-porosity formulation incorporated with the ADE model for solute transport can be redefined and separated into mobile and immobile regions, as well as kinetic sorption sites, respectively, as displayed below:

Mobile: $$\frac{\partial \theta_{mo} c_{mo}}{\partial t} + \rho f \frac{\partial s_{mo}^e}{\partial t} = \frac{\partial}{\partial z}\left(\theta_{mo} D_{mo} \frac{\partial c_{mo}}{\partial z} - q_{mo} c_{mo}\right) + R_{mo} - \Gamma_{s1} - \Gamma_{s2} \tag{3.50}$$

Immobile: $$\frac{\partial \theta_{im} c_{im}}{\partial t} + \rho (1 - f) \frac{\partial s_{im}}{\partial t} = R_{im} + \Gamma_{s1} \tag{3.51}$$

Kinetic:
$$\rho f \frac{\partial s_{mo}^{k}}{\partial t} = R_{mo}^{k} + \Gamma_{s2} \tag{3.52}$$

where f is the fraction of sorption sites in contact with the mobile region; D_{mo} is the dispersion coefficient in the mobile region $[L^2/t]$; q_{mo} is the volumetric fluid flux in the mobile region $[L/t]$; R_{mo}, R_{im}, and R_{mo}^{k} are the reaction terms at the mobile and immobile regions, as well as sorption sites $[M/L^3t]$, respectively; and Γ_{s1} and Γ_{s2} are the solute transfer rates between the two regions that account for physical and chemical processes, respectively $[M/L^3t]$. Also, it should be that $f = 1$ when the sorption site is fully exposed to the mobile water and $f = 0$ when there is no water flow.

In addition, the solute transfer rates between the mobile and immobile regions, Γ_{s1} and Γ_{s2} for physical solute exchange and chemical kinetic sorption, are found as:

Physical:
$$\Gamma_{s1} = \omega_{s1}(c_{mo} - c_{im}) \tag{3.53}$$

Chemical:
$$\Gamma_{s2} = \omega_{s2}\rho\left(s_{mo}^{k} - s_{mo,e}^{k}\right) \tag{3.54}$$

where ω_{s1} and ω_{s2} are the first-order rate constants responsible for physical and chemical processes $[t^{-1}]$, respectively, and $s_{mo,e}^{k}$ is the equilibrium adsorbed solute concentrations on the solid surface at the mobile region $[M/M]$.

3.8 Formation of the Sludge Deposit Layer

Sludge is often described physically as a solid-liquid mixture in which the solids are either free suspension or closely packed (Sørensen *et al.*, 1996). In some specific cases, the porous structure undergoes deformation due to the deposition of the solid sludge on the medium surface, subsequently changing its porosity, permeability, and flow resistance. According to several past studies, these sludge deposit formations are thickened and compressed due to the continuous deposition of solid sludge (Sørensen *et al.*, 1996; Stamatakis & Tien, 1991; Tien *et al.*, 1997; Tiller & Yeh, 1987).

3.8.1 Mass Balances

According to the literature, the permeability and porosity of a sludge deposit are highly related to the compressibility imposed. When the thickness of the sludge deposit increased and was followed by compression, its hydraulic conductivity was significantly reduced (Bandelt Riess *et al.*, 2021; Jafari *et al.*, 2019). Hence, the change in the sludge deposit layer thickness alters the top boundary condition of a STRB system. The waterlogging condition causes the increment in sludge thickness upon feeding, while the thickness reduces due to compression by hydraulic loads on top of the sludge deposits. Water loss via drainage and evapotranspiration also aids in the thickness reduction during the resting period.

A compressible cake filtration (CCF) model is formulated to describe the buildup of sludge deposits under low-pressure conditions for a range of loading rates and sludge characteristics. Generally, the model can be divided into two stages: sludge deposit formation and sludge deposit deformation. In the proposed model, the solid particles in the influent are retained on the top surface of the filter medium by sedimentation and filtration, resulting in sludge accumulation during the feeding period. The formation of the sludge deposit is then thickened and compressed due to the continuous deposition of solid sludge, directly varying the permeability of the filter medium. Therefore, the CCF model is a function of the settling rate of particles and specific cake resistance to describe the sludge dewatering under low-pressure conditions accurately (Sørensen *et al.*, 1996; Stamatakis & Tien, 1991; Tien *et al.*, 1997; Tiller & Yeh, 1987).

The thickness of the sludge deposit layer at the sludge-cake interface, L can be found directly from the sludge deposit growth rate, dL/dt. Thus, by considering the sludge deposit thickness is increased by δL over a time interval of δt, the mass balances of liquid and solids are given as (Tien *et al.*, 1997):

Liquid: $$\left(q_{l,c} - q_{l,s}\right)\delta t = \delta L[(1 - \varepsilon_c) - (1 - \varepsilon_s)] \tag{3.55}$$

Solid: $$\left(q_{s,c} - q_{s,s}\right)\delta t = \delta L(\varepsilon_c - \varepsilon_s) \tag{3.56}$$

where $q_{l,c}$ and $q_{l,s}$ are the liquid fluxes on the cake and sludge side at the interface $[L^3/L^2t]$, respectively; $q_{s,c}$ and $q_{s,s}$ are the solid fluxes on the said interface $[L^3/L^2t]$, respectively, whereas ε_c and ε_s are the particle volume fractions on the respective side of the interface. A better illustration is presented in Figure 3.35 to demonstrate the increased in thickness of the sludge deposit.

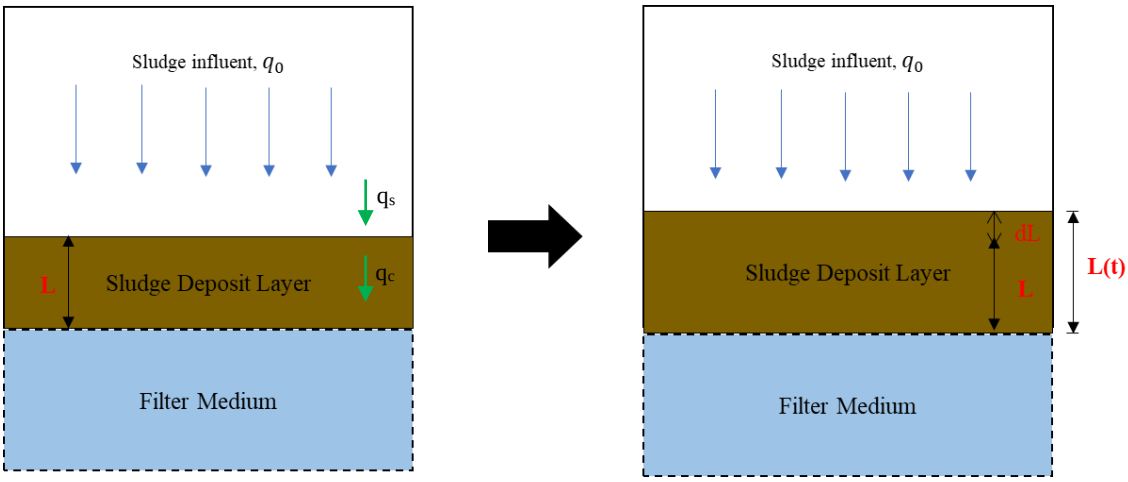

Figure 3.35: Thickness of sludge deposit layer.

Also, it should be noted that the addition of mass balances of both liquid and solid fluxes in the sludge deposit, is equivalent to that of the sludge and the flux infiltrated through the medium, respectively. Thus, the overall mass balance is known as (Tien *et al.*, 1997):

$$(q_{l,c} + q_{s,c}) = (q_{l,s} + q_{s,s}) = q_{l,m} = \left(\frac{k}{\mu}\frac{\partial p}{\partial z}\right)_{z=0} \tag{3.57}$$

where $q_{l,m}$ is the permeation flux of filtrate through the medium (filtrate flux) $[L^3/L^2t]$, μ is the viscosity of liquid $[M/Lt]$, z is the vertical elevation $[L]$, whereas the cake permeability coefficient, k $[L^2]$ and pressure, p $[M/Lt^2]$ are given by:

$$k = \frac{1}{\alpha_c \rho_s \varepsilon_s} \tag{3.58}$$

where α_c is the specific cake resistance $[L/M]$ and ρ_s is the density of solids $[M/L^3]$.

From the mass balance of Equation (3.57), the differential of the equation is derived for the estimation in changes of sludge deposit thickness over the resting period, which is expressed as follows:

$$\frac{dL}{dt} = \frac{q_{l,c} - q_{l,s}}{\varepsilon_s - \varepsilon_c} \tag{3.59}$$

where the volumetric fluxes, q_l and q_s are given by the Darcy's law as follows:

$$\left(\frac{q_l}{1-\varepsilon_s} - \frac{q_s}{\varepsilon_s}\right) = \frac{k}{(1-\varepsilon_s)\mu}\frac{\partial p}{\partial z} \tag{3.60}$$

Thus, the final expression for the change in the thickness of the sludge deposit layer is found as:

$$\frac{dL}{dt} = \frac{\varepsilon_c}{\varepsilon_c - \varepsilon_s}\left(\frac{k}{\mu}\frac{\partial h}{\partial z}\right)_L - q_{l,m} \tag{3.61}$$

A detailed derivation for Equation (3.61) is illustrated in **Appendix C**.

3.8.2 Constitutive Relationships

In estimating fluxes over the medium, the constitutive functional relationship among the porosity, ε, the cake permeability coefficient, k, the specific cake resistance, α, and the compressive stress, p_s must be established initially. These values could be either determined from literature or estimated via constitutive relationships. Power law functions have been proven to be in fair agreement with the measurements using a "compression-permeability cell" for various inorganic suspensions. This method of estimation is flexible for cases with significant pressure differences. Perhaps, when the solid compressibility is relatively high, it causes the coefficients in the power-law description to change with respect to the function of contact pressure. Therefore, these coefficients are determined by the power-law as (Tien *et al.*, 1997):

$$\varepsilon_s = \varepsilon_s^0 \left(1 + \frac{p_s}{p_a}\right)^{\beta} \tag{3.62}$$

$$k = k^0 \left(1 + \frac{p_s}{p_a}\right)^{-\emptyset} \tag{3.63}$$

$$\alpha = \alpha^0 \left(1 + \frac{p_s}{p_a}\right)^{-(\emptyset+\beta)} \tag{3.64}$$

where ε_s^0, k^0, and α^0 are the solid porosity, permeability coefficient, and specific cake resistance at zero compression stress, respectively. Meanwhile, p_a is a scaling factor, whereas β and $\emptyset$ are the solid material characteristics that specify the degree of compressibility. In addition to these coefficients, it should be noted that $\emptyset < 1$ represents low and moderate compressibility, while $\emptyset > 1$ means that the sludge deposit is highly compressible.

3.9 Kinetics Module of the Model

3.9.1 Bio-Kinetics

A bio-kinetic sub-model is created to describe the sludge mineralization and nutrient uptake by plants. These nutrients could be nitrogen and phosphorus obtained from the decomposition of organic materials, which are essential for the growth of plants. In many biological kinetic studies related to wastewater treatment, Activated Sludge Model 1 (ASM1) has become a standard guideline and reference for scientific and practical projects (Henze *et al.*, 1987). ASM1 was created mathematically to simulate the degradation of primary contaminants, such as organic matter and nitrogen, by means of biological and chemical decomposition. The ASM1 has been implemented in a series of computer codes to simulate the behavior of activated sludge systems in treating domestic wastewater.

Nonetheless, with over ten years of experience in the application of ASM1, it was found that this wastewater treatment model has some shortcomings as the technologies

advance. Therefore, a new model known as Activated Sludge Model No.3 (ASM3) was formulated to improve the model by combining the ASM1 and ASM2 (Gujer *et al.*, 1995; Henze *et al.*, 1999). In general, ASM3 is capable of predicting oxygen consumption, sludge production, nitrification, and denitrification of activated sludge systems (Gujer *et al.*, 1999). In addition, a thorough review of the existing kinetic models has confirmed that the Gujer matrix is the most suitable and desirable for the research application among all the other process-dedicated models (Tan *et al.*, 2021). There are many successful applications of ASM3 in the simulation of wastewater treatment, especially by biological reactors (Blomberg *et al.*, 2018; Kapumbe *et al.*, 2019; Simon-Várhelyi *et al.*, 2020).

3.9.2 Components

The thorough heterotrophic and autotrophic reactions, and the respective cycle flows, are illustrated in Figure 3.36 (Tan et al., 2021). The phosphorus reaction is neglected in the illustration as it does not involve any cycle. Moreover, all the components mentioned in the illustration, are listed in Table 3.5 and Table 3.6 (Gujer *et al.*, 1999).

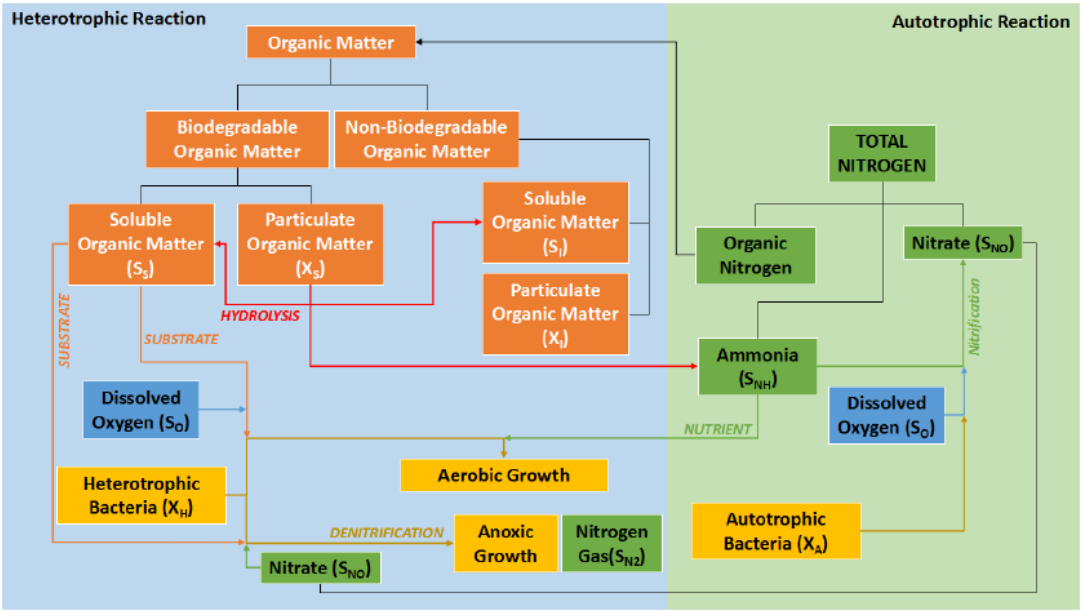

Figure 3.36: Heterotrophic and autotrophic reaction cycles.
Note: Adapted from "Process-based models for nitrogen dynamics in subsurface flow constructed wetlands: A state-of-the-art-review," by Tan, Y. Y., Tang, F. E., Saptoro, A., *Environmental Reviews*, 2021.

Table 3.5: Soluble components.
Note: Adapted from "Activated sludge model No. 3," by Gujer, W., Henze, M., Mino, T., and Loosdrecht, M. van, *Water Science and Technology*, 1999.

Components $[M/L^3]$	Denotation	Description
S_O	Dissolved oxygen (O_2 or DO)	The main components involved in the aerobic processes.
S_I	Inert soluble organic material	These are the organic materials that cannot be further degraded and are presented in the products of hydrolysis of particulate substrates, X_S.
S_S	Readily biodegradable organic substrates	This fraction of soluble components can be decomposed via biodegradation by heterotrophic organisms.
S_N	Dinitrogen (N_2)	The main product of denitrification.
S_{NH}	Ammonium (NH_4^+-N) and ammonia (NH_3-N) nitrogen	These are the main components that contribute to nitrogen sources in both aerobic and anoxic processes. However, only NH_4^+-N is assumed to be involved in the overall process.
S_{NO}	Nitrate (NO_3^--H) and nitrite (NO_2^--H) nitrogen	Nitrite is the final product of nitrification. Thus, only NO_3^-H is assumed to be involved in the overall process.
S_{HCO}	Bicarbonate (HCO_3^-)	This component is the alkalinity of the wastewater. It can be used for the indication of low pH conditions, besides to balance the ionic charges.
S_{PO}	Inorganic soluble phosphorus	One of the complementary nutrients for bacteria growth. Generally, it is assumed to be consisting of 50% $H_2PO_4^-$ and HPO_4^{2-} independent of pH.

Table 3.6: Particulate components.
Note: Adapted from "Activated sludge model No. 3," by Gujer, W., Henze, M., Mino, T., and Loosdrecht, M. van, *Water Science and Technology*, 1999.

Components $[M_{COD}/L^3]$	Denotation	Description
X_I	Inert particulate organic material	These are the undegraded materials, and maybe produced in the biomass decaying process.
X_S	Slowly biodegradable	These substrates must undergo hydrolysis for degradation. The products of hydrolysis are

	substrates	either biodegradable, S_S or inert, S_I soluble organics.
$\boldsymbol{X_H}$	Heterotrophic organisms	These are the organisms that consume carbon for growth. They are responsible for hydrolysis of particulate substrates, X_S.
$\boldsymbol{X_A}$	Autotrophic organisms	These organisms use inorganic compounds as energy sources, and carbon dioxide as carbon source for cell synthesis. They are dedicated for nitrification, and directly oxidized ammonium, S_{NH} to nitrate, S_{NO}.

3.9.3 Reactions

1. Hydrolysis (Gujer *et al.*, 1999):

In this process, all nitrogen obtained via the decomposition of ammonium and denitrification accounts for slowly biodegradable substrates (X_S). Also, it is assumed that the nitrogen is independent of the electron donor, and the heterotrophs dominated the overall reaction. Thus, the Monod equation of the hydrolysis is given as:

$$Process_1 = k_H \cdot \frac{\frac{X_S}{X_H}}{K_X + \frac{X_S}{X_H}} \cdot X_H \tag{3.65}$$

2. Aerobic growth of heterotrophs (Gujer *et al.*, 1999):

The aerobic growth of heterotrophs (X_H) fully relies on the digestion of the soluble and biodegradable organic materials for carbon sources, and the dissolved oxygen (S_O) is consumed as the terminal electron acceptor. Nonetheless, the growth of heterotrophs is also dependent on complementary nutrients such as nitrogen (S_{NH}, and S_{HCO}) and phosphorus (S_{PO}), as well as readily biodegradable substrates (S_S). Further, a maximum growth rate, μ_H is included in the process to limit the growth of the heterotrophs, whereas K stands for the saturation constant of respective components. Hence, the Monod-type growth rate equation is expressed as:

$$Process_2 = \mu_H \cdot \frac{S_O}{K_O + S_O} \cdot \frac{S_S}{K_S + S_S} \cdot \frac{S_{NH}}{K_{NH} + S_{NH}} \cdot \frac{S_{HCO}}{K_{HCO} + S_{HCO}} \cdot \frac{S_{PO}}{K_{PO} + S_{PO}} \cdot X_H \quad (3.66)$$

3. Anoxic growth of heterotrophs (Gujer *et al.*, 1999):

The anoxic growth of heterotrophs is identical to that of aerobic growth, but the respiration of heterotrophs depends on the denitrification. Thus, the soluble component of nitrite nitrogen (S_{NO}) is added to the equation. Meanwhile, a reduction factor, η_{NO} is also added into the expression, so that the reaction is fixed to be a limited denitrification process. Further, since the process is a reaction without oxygen, the fraction of the oxygen component is altered so that the amount of dissolved oxygen is within the saturated amount. Therefore, the overall expression of anoxic growth rate is:

$$Process_3 = \mu_H \cdot \eta_{NO} \cdot \frac{K_O}{K_O + S_O} \cdot \frac{S_S}{K_S + S_S} \cdot \frac{S_{NO}}{K_{NO} + S_{NO}} \cdot \frac{S_{NH}}{K_{NH} + S_{NH}} \cdot \frac{S_{HCO}}{K_{HCO} + S_{HCO}} \cdot \frac{S_{PO}}{K_{PO} + S_{PO}} \cdot X_H \quad (3.67)$$

4. Growth of autotrophs (Gujer *et al.*, 1999):

In the growth of autotrophs (X_A), these nitrifying organisms synthesize the cell to acquire carbon for energy, thus oxidizing the ammonium directly to nitrate. This process is also known as nitrification, which contributes fully to the growth of autotrophs. Moreover, it is also determined that the growth rate of autotrophs is generally slower compared to that of the heterotrophs. So, the overall reaction equation is given by:

$$Process_4 = \mu_A \cdot \frac{S_O}{K_{A,O} + S_O} \cdot \frac{S_{NH}}{K_{A,NH} + S_{NH}} \cdot \frac{S_{HCO}}{K_{A,HCO} + S_{HCO}} \cdot \frac{S_{PO}}{K_{A,PO} + S_{PO}} \cdot X_A \quad (3.68)$$

5. Lysis (Gujer *et al.*, 1999):

This process includes all the loss of energy and biomass, which are not required for the growth of the heterotrophs and autotrophs. Hence, the rates of the lysis for heterotrophs and autotrophs, respectively, are illustrated as:

$$Process_5 = b_H \cdot X_H \tag{3.69}$$

$$Process_6 = b_A \cdot X_A \tag{3.70}$$

The reference values of the mentioned kinetic parameters and relative units are shown in **Appendix D**.

3.9.4 Reaction Term for Solute Transport

The reaction term, R $[M/L^3t]$ in the solute transport module can be determined by the reaction processes listed previously. The first-order decay is assumed to be identical for both liquid and adsorbed phases, as well as the zero-order production term; thus, the new reaction term equation is given as (Bresler, 1973; Nielsen *et al.*, 1986):

$$R = -\mu(\theta c + \rho s) + \gamma(\theta + \rho) \tag{3.71}$$

where the first-order decay, μ and the zero-order production term, γ are known as:

$$\mu = Process_5 + Process_6 \tag{3.72}$$

$$\gamma = Process_1 + Process_2 + Process_3 + Process_4 \tag{3.73}$$

The model components and typical wastewater compositions are given in **Appendix E**.

3.10 Numerical Simulation

Generally, non-linear equations are discretized into linear forms so that they are described explicitly using the numerical approach before being plugged into computational software. The changes in sludge ponding level and sludge deposit layer thickness cause variance to the upper boundary conditions, where the conventional mesh

discretization approach would be inappropriate to describe the situation. In this study, numerical discretization is performed using a moving mesh finite difference (FD) method (Dorfi & Drury, 1987) using a velocity-based approach. This type of scheme is advantageous and has been proven effective in moving boundaries of the physical system (Bruce, 2011). Three types of adaptive strategies have been implemented in computational fluid dynamics (CFD) problems (Tang, 2005) which are:

- *h*-refinement method: The most common method, at which the spatial mesh is refined by repeated subdivision of the intervals of a fixed mesh.
- *p*-refinement method: By this method, the degree of polynomial order of shape functions is increased.
- *r*-refinement method: This method is known as the moving mesh method (MMM), which relocates the grid points in a mesh at each time step. In detail, this method can vary the mesh and the solution simultaneously in such a way that the mesh has a fixed number of nodes that remain concentrated in regions of rapidly variated solution.

According to Tang (2005), by implementing the *r*-method, there is no longer the need to interpolate dependent variables from the old mesh to the new mesh. As a result, this method is also called an "interpolation-free moving mesh method". Moreover, there are several advantages of MMMs, such as reducing time variation to allow for larger time steps due to mesh velocity, detecting, tracking, and resolving the moving boundaries, and all without the need for interpolation. However, it should be noted that since this study only deals with one-dimensional problems, finite differences are used instead of the finite element method, as the finite elements are generally considered superior for two- and three-dimensional problems (Tang, 2005).

This study comprehensively describes the hydraulic flow and solute transport by the moving mesh and fixed mesh. The moving mesh method is applied to the moving boundaries on top of the reed bed due to temporary ponding and sludge deposit accumulation, while the fixed mesh method continues subsequently, as the substrate layer of the reed bed remains unchanged over the treatment cycle. The application of MMM alters the spatial mesh distance, *dt* based on the actual sludge ponding on the bed surface,

whereas the *dt* remains at a fixed value in the fixed mesh layers. In this section, the discretization of moving and fixed mesh methods is presented in detailed equations for a thorough illustration of simulation steps.

In the discretization of numerical simulation, the terms with subscript i represents the iteration number of nodes, N, where $i = 1, 2, 3, \ldots, N$. Additionally, the superscript, n is to denote the iteration evaluated at the time, $t = n\Delta t$, thus $\Delta t = t^{n+1} - t^{n}$.

3.10.1 Moving Mesh Layer for Hydraulic Module

Figure 3.37 shows the schematic illustration of a STRB under moving boundary condition. Particularly in the hydraulic studies of the moving mesh method, the main concept is to keep the fractional amount of water between adjacent mesh points constant (Bruce, 2011).

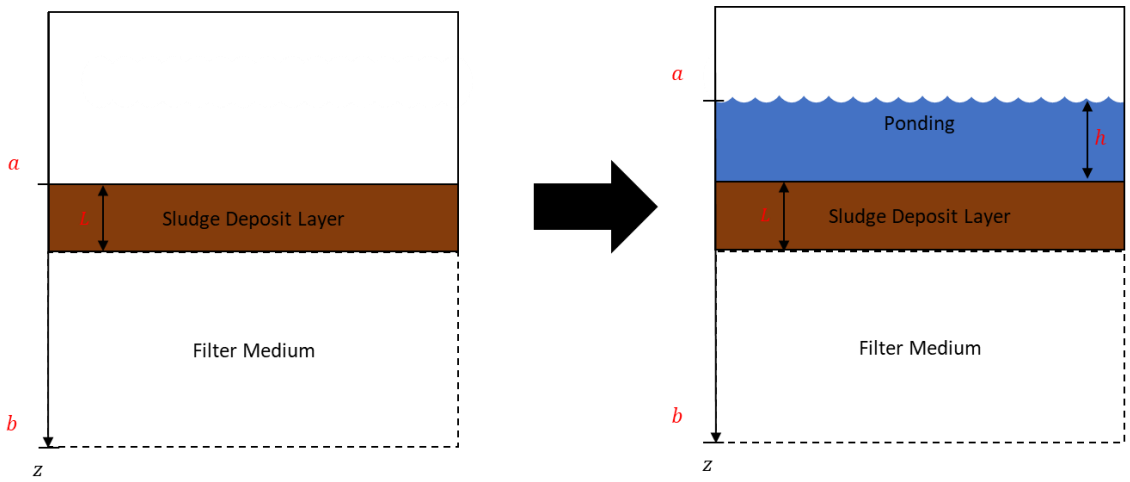

Figure 3.37: Boundary conditions of STRB with no ponding (left) and ponding (right).

Thus, the formulation of the conservative equation is given by:

$$\frac{\int_a^{z_i(t)} \theta dz}{\int_a^b \theta dz} = \gamma_i \tag{3.74}$$

where γ_i is constant in time. Then, the RE is reformulated into a velocity-based moving boundary of RE, as given by (Bruce, 2011):

$$v_i = \frac{dz_i}{dt} = \frac{1}{\theta}\left\{\gamma_i\left(K\left[\frac{\partial h}{\partial z}+1\right]_a^b + \left[\theta\frac{dz_i}{dt}\right]_a^b\right) - K\left[\frac{\partial h}{\partial z}+1\right]_a^{z_i(t)} + \left[\theta\frac{dz_i}{dt}\right]_a\right\} \quad (3.75)$$

where v_i is the hydraulic velocity $[L/t]$; z_i is the vertical coordinate assumed positive downward; t is the time $[t]$; θ is the volumetric water content $[L^3/L^3]$; γ_i is the function of fractional integral constant in time; K is the hydraulic conductivity $[L/t]$; h is the pressure head $[L]$; a and b are the specific coordinates at two extreme locations $[L]$ depending on the boundary conditions, respectively; and $z_i(t) = dz_i/dt$ is the differential of vertical coordinate with respect to time $[L/t]$. A thorough derivation of Equation (3.75) is given in **Appendix F**.

Meanwhile, when Equation (3.75) is presented in the form of dual-porosity model, specifically for the mobile region, is shown as (Bruce, 2011):

$$\frac{dz_i}{dt} = \frac{1}{\theta_{mo}}\left\{\gamma_i\left(K\left[\frac{\partial h_{mo}}{\partial z}+1\right]_a^b + \left[\theta\frac{dz_i}{dt}\right]_a^b - S_{mo} - \Gamma_w\right) - K\left[\frac{\partial h_{mo}}{\partial z}+1\right]_a^{z_i(t)} + \left[\theta\frac{dz_i}{dt}\right]_a + S_{mo} + \Gamma_w\right\} \quad (3.76)$$

where S_{mo} is the sink term for mobile region $[M/L^3t]$ and Γ_w is the water transfer rate $[M/L^3t]$.

3.10.2 Initial and Boundary Conditions for MMM–RE

The steady-state initial condition for the hydraulic model, is determined by the initial distribution of either pressure head or water content, as follows:

$$h(z,t) = h_i(z), \qquad t = t_0 \quad (3.77)$$

$$\theta(z,t) = \theta_i(z), \qquad t = t_0 \quad (3.78)$$

where h_i is the prescribed pressure head at elevation, z; θ_i is the prescribed water content regarding the pressure head and elevation, whereas t_0 is the time when the simulation starts.

In general, the boundary conditions of Dirichlet, which is also known as the first type (constant h or θ), and Neumann, which is also known as the second type (constant flux, q), may be applied to this method of simulation (Celia *et al.*, 1987; Gottardi & Venutelli, 1993; Vasconcellos & Amorim, 2001). According to the illustration shown in Figure 3.37, it can be deduced that the top boundary condition is set to be switching between the first and second types of boundary conditions, due to the intermittent loading mode, whereas the bottom boundary is a free drainage condition. The flux is given by Darcy's equation (Celia *et al.*, 1987; Gottardi & Venutelli, 1993; Vasconcellos & Amorim, 2001), as follows:

$$q = V\theta = \frac{dz}{dt}\theta = \left[K(h)\frac{\partial h}{\partial z} + K(h)\right] \tag{3.79}$$

Every reed bed has its own filtration capacity to receive loadings. When the hydraulic loading rates exceed the infiltration capacity, the top surface layer of the reed bed is completely saturated. In this case, the excessive influent sludge accumulates on top of the reed bed, resulting in temporary ponding. When no ponding occurs on top of the medium, the upper boundary condition is set to be a flux-controlled (Neumann type) boundary condition while head-controlled (Dirichlet type) is used in the opposite scenario. Thus, the top boundary conditions are:

$$q_a = \theta_a \frac{da}{dt} = q_0, \qquad t_0 \leq t \leq t_e \tag{3.80}$$

$$q_a = \theta_a \frac{da}{dt} = 0, \qquad t_e < t \leq t_s \tag{3.81}$$

$$\frac{dh}{da} = 0, \qquad t = t_0 \tag{3.82}$$

where q_a is the liquid flux at the medium surface, q_0 is the prescribed liquid flux input by the user, t_0 is the initial time, t_e is the end of the loading period, and t_s is the total simulation time. On the other hand, consideration of no imposed flux, and free drainage at the bottom, b of the reed bed, the lower boundary is then set to be a zero-gradient flux boundary condition, thus:

$$q_b = \theta_b \frac{db}{dt} = 0 \tag{3.83}$$

Therefore, the RE is modified by inserting the boundary conditions set previously. Hence, the new velocity-based RE for the mobile region is given by:

$$v_i = \frac{dz_i}{dt} = \frac{1}{\theta_{mo}} \left\{ \gamma_i \left(K \left[\frac{\partial h_{mo}}{\partial z} + 1 \right]^b - q_a - S_{mo} - \Gamma_w \right) - K \left[\frac{\partial h_{mo}}{\partial z} + 1 \right]^{z_i(t)} + q_a + S_{mo} + \Gamma_w \right\} \tag{3.84}$$

Moreover, the discretization of the velocity based RE in the mobile region can be written as:

$$\frac{z_i^{n+1} - z_i^n}{\Delta t} = \frac{1}{\theta_{i,mo}} \left\{ \gamma_i \left(\overline{K_{i+1/2}^n} \left[\frac{h_{i+1}^n - h_i^n}{\Delta \overline{z_i^n}} + 1 \right]_b - q_0 - S_{mo} - \Gamma_w \right) - \overline{K_{i+1/2}^n} \left[\frac{h_{i+1}^n - h_i^n}{\Delta \overline{z_i^n}} + 1 \right] + q_0 + S_{mo} + \Gamma_w \right\} \tag{3.85}$$

where γ_i, $\Delta \overline{z_i^n}$, $\overline{K_{i+1/2}^n}$, S_{mo}, and Γ_w are given as follow:

$$\gamma_i = \frac{\int_a^{z_i(t)} \theta dz}{\int_a^b \theta dz} \tag{3.86}$$

$$\Delta \overline{z_i^n} = \frac{\Delta z_i^n + \Delta z_{i+1}^n}{2} \tag{3.87}$$

$$\overline{K_{i+1/2}^{n}} = \frac{\alpha K_i^n + \beta K_{i+1}^n}{\alpha + \beta} \tag{3.88}$$

$$\alpha = \frac{\Delta z_i^n}{2} \tag{3.89}$$

$$\beta = \frac{\Delta z_{i+1}^n}{2} \tag{3.90}$$

$$\Delta z_i^n = z_{i-1}^n - z_i^n \tag{3.91}$$

$$\Delta z_{i+1}^n = z_i^n - z_{i+1}^n \tag{3.92}$$

$$S_{mo} = max\left(\frac{\theta_{i,mo}^n}{\theta_{s,mo} - \theta_{wilt}}\right)\left(\frac{\theta_{i,mo}^n - \theta_{wilt}}{\theta_{s,mo}}\right)^{\frac{\gamma}{\theta_{i,mo}^n - \theta_{wilt}}} gT_p \tag{3.93}$$

$$\Gamma_w = \omega\left[\left(\frac{\theta_{i,mo}^n - \theta_{r,mo}}{\theta_{s,mo} - \theta_{r.mo}}\right) - \left(\frac{\theta_{i,im}^n - \theta_{r,im}}{\theta_{s,im} - \theta_{r,im}}\right)\right] \tag{3.94}$$

In addition, the change in amount of water in medium profile, (dW/dt) after each timestep, is known as:

$$\frac{dW}{dt} = \overline{K_{i+1/2}^n}\left[\frac{h_{i+1}^n - h_i^n}{\Delta \overline{z_i^n}} + 1\right]_b - q_0 - S_{mo} - \Gamma_w \tag{3.95}$$

Furthermore, to implement this moving boundary FD velocity-based RE, an initial profile of θ_i is known prior to the solution. In a time-loop, the values of h_i^n and $\overline{K_i^n}$ are then calculated, followed by dz_i/dt for the current time step, and the new values of z_i and W at the next step, by using Euler's first order explicit method. In the end, the value of θ_i^{n+1} is evaluated through the formula of discretized form below:

$$\theta_i^{n+1} = (\gamma_i - \gamma_{i-1})\frac{W}{\Delta z_i} \tag{3.96}$$

3.10.3 Fixed Mesh Layers for Hydraulic Module

In traditional ways, a mixed form of RE can be described explicitly by using the fixed mesh FD discretization, before plugging into a computational software (Lapidus & Pinder, 1982; Von Rosenberg, 1969). Thus, this method has led to a tridiagonal nonlinear set of equations, as given by (Celia *et al.*, 1987; Gottardi & Venutelli, 1993):

$$\alpha_i^m \, \delta_{i-1}^{m+1} + \beta_i^m \, \delta_i^{m+1} + \gamma_i^m \, \delta_{i+1}^{m+1} = R_i^m, \qquad i = 1, 2, 3, \dots, N \tag{3.97}$$

where α_i^m, β_i^m, γ_i^m, and R_i^m are the nonlinear functions of the independent variables h or θ and the dependent variables $\delta_j^{m+1} = h_j^{m+1} - h_j^m$ or $\delta_j^{m+1} = \theta_j^{m+1} - \theta_j^m$; $(j = i - 1,\ i,\ i + 1)$ are the increments of the variables h or θ for passing from iteration level m to iteration level $m + 1$; the superscripts $(m, m + 1, n)$ are referring to time hereafter; and N is the number of nodes. The terms with superscripts m and $m + 1$ would be calculated at two subsequent iterations at time $t = (n + 1)\Delta t$, while the terms with superscripts n would be evaluated at time $t = n\Delta t$, thus $\Delta t = t^{n+1} - t^n$. Then, this set of nonlinear algebraic equations would be solved through a standard implicit Picard iterative approach. In addition, the interblock terms, $K_{i\pm1/2}$ is estimated by the arithmetic means where $K_{i\pm1/2} = 0.5(K_i + K_{i\pm1})$.

Therefore, the numerical discretization for mixed form of partial differential RE in mobile region, obtained by a backward Euler approach, is presented as:

$$\begin{aligned} \frac{\theta_{i,mo}^{n+1,m+1} - \theta_{i,mo}^{n}}{\Delta t} &= \left[\frac{K_{i-\frac{1}{2}}^{n+1,m}}{(\Delta z)^2} \left(h_{i-1}^{n+1,m+1} - h_i^{n+1,m+1} \right) \right. \\ &\left. + \frac{K_{i+\frac{1}{2}}^{n+1,m}}{(\Delta z)^2} \left(h_{i+1}^{n+1,m+1} - h_i^{n+1,m+1} \right) \right] - \frac{K_{i+\frac{1}{2}}^{n+1,m} - K_{i-\frac{1}{2}}^{n+1,m}}{\Delta z} \\ &- S_{mo} - \Gamma_w \end{aligned} \tag{3.98}$$

where the sink term, S_{mo}, and water transfer rate, Γ_w, are found to be as follow:

$$S_{mo} = max\left(\frac{\theta_{i,mo}^{n}}{\theta_{s,mo} - \theta_{wilt}}\right)\left(\frac{\theta_{i,mo}^{n} - \theta_{wilt}}{\theta_{s,mo}}\right)^{\frac{\gamma}{\theta_{i,mo}^{n} - \theta_{wilt}}} gT_p \tag{3.99}$$

$$\Gamma_w = \omega\left[\left(\frac{\theta_{i,mo}^{n} - \theta_{r,mo}}{\theta_{s,mo} - \theta_{r.mo}}\right) - \left(\frac{\theta_{i,im}^{n} - \theta_{r,im}}{\theta_{s,im} - \theta_{r,im}}\right)\right] \tag{3.100}$$

On the other hand, the dependent variables, $\delta_i^{n+1,m+1} = h_i^{n+1,m+1} - h_i^{n+1,m}$ that are expressing $\theta_i^{n+1,m+1}$ in a truncated Taylor series with respect to h, is displayed as:

$$\begin{aligned}\theta_i^{n+1,m+1} &= \theta_i^{n+1,m} + \left.\frac{d\theta}{dh}\right|_i^{n+1,m}\left(h_i^{n+1,m+1} - h_i^{n+1,m}\right) \\ &= \theta_i^{n+1,m} + C_i^{n+1,m}\delta_i^{n+1,m+1}\end{aligned} \tag{3.101}$$

where C is the specific moisture capacity, $C(h)$. Thus, when substituting Equation (3.101) into Equation (3.98) and rearranged, the newly formed equation is given as:

$$\begin{aligned}&-\frac{K_{i-\frac{1}{2}}^{n+1,m}}{(\Delta z)^2}\left(\delta_{i-1}^{n+1,m+1}\right) + \left(\frac{C_i^{n+1,m}}{\Delta t} + \frac{K_{i-\frac{1}{2}}^{n+1,m}}{(\Delta z)^2} + \frac{K_{i+\frac{1}{2}}^{n+1,m}}{(\Delta z)^2}\right)\left(\delta_i^{n+1,m+1}\right) \\ &\quad - \frac{K_{i+\frac{1}{2}}^{n+1,m}}{(\Delta z)^2}\left(\delta_{i+1}^{n+1,m+1}\right) \\ &\quad = -\frac{\left(K_{i+\frac{1}{2}}^{n+1,m} - K_{i-\frac{1}{2}}^{n+1,m}\right)}{\Delta z} - \frac{\theta_{i,mo}^{n+1,m} - \theta_{i,mo}^{n}}{\Delta t} - S_{mo} - \Gamma_w\end{aligned} \tag{3.102}$$

Eventually, this tridiagonal nonlinear set of equations is inputted into MATLAB® as a tridiagonal nonlinear matrix for each time step, and solved by the tridiagonal matrix algorithm:

$$\begin{bmatrix} \beta_1^m & \gamma_1^m & 0 & 0 & 0 & \cdots & \cdots & 0 & 0 & 0 \\ \alpha_1^m & \beta_2^m & \gamma_2^m & 0 & 0 & \cdots & \cdots & 0 & 0 & 0 \\ 0 & \alpha_2^m & \beta_3^m & \gamma_3^m & 0 & \cdots & \cdots & 0 & 0 & 0 \\ 0 & 0 & \alpha_3^m & \beta_4^m & \gamma_4^m & \cdots & \cdots & 0 & 0 & 0 \\ 0 & 0 & 0 & \alpha_4^m & \beta_5^m & \cdots & \cdots & 0 & 0 & 0 \\ \vdots & \vdots & \vdots & \vdots & \vdots & \ddots & \ddots & \vdots & \vdots & \vdots \\ \vdots & \vdots & \vdots & \vdots & \vdots & \ddots & \ddots & \vdots & \vdots & \vdots \\ 0 & 0 & 0 & 0 & 0 & \cdots & \cdots & \beta_{N-2}^m & \gamma_{N-1}^m & 0 \\ 0 & 0 & 0 & 0 & 0 & \cdots & \cdots & \alpha_{N-2}^m & \beta_{N-1}^m & \gamma_N^m \\ 0 & 0 & 0 & 0 & 0 & \cdots & \cdots & 0 & \alpha_N^m & \beta_N^m \end{bmatrix} \begin{bmatrix} \delta_1^{m+1} \\ \delta_2^{m+1} \\ \delta_3^{m+1} \\ \delta_4^{m+1} \\ \delta_5^{m+1} \\ \vdots \\ \vdots \\ \delta_{N-2}^{m+1} \\ \delta_{N-1}^{m+1} \\ \delta_N^{m+1} \end{bmatrix} = \begin{bmatrix} R_1^m \\ R_2^m \\ R_3^m \\ R_4^m \\ R_5^m \\ \vdots \\ \vdots \\ R_{N-2}^m \\ R_{N-1}^m \\ R_N^m \end{bmatrix} \tag{3.103}$$

where

$$\alpha_i^{n+1,m} = -\frac{K_{i-\frac{1}{2}}^{n+1,m}}{(\Delta z)^2} \tag{3.104}$$

$$\beta_i^{n+1,m} = \frac{C_i^{n+1,m}}{\Delta t} + \frac{K_{i-\frac{1}{2}}^{n+1,m}}{(\Delta z)^2} + \frac{K_{i+\frac{1}{2}}^{n+1,m}}{(\Delta z)^2} \tag{3.105}$$

$$\gamma_i^{n+1,m} = -\frac{K_{i+\frac{1}{2}}^{n+1,m}}{(\Delta z)^2} \tag{3.106}$$

$$\begin{aligned} R_i^{n+1,m} = {} & \frac{K_{i-\frac{1}{2}}^{n+1,m}}{(\Delta z)^2}\left(h_{i-1}^{n+1,m} - h_i^{n+1,m}\right) + \frac{K_{i+\frac{1}{2}}^{n+1,m}}{(\Delta z)^2}\left(h_{i+1}^{n+1,m} - h_i^{n+1,m}\right) \\ & - \frac{K_{i+\frac{1}{2}}^{n+1,m} - K_{i-\frac{1}{2}}^{n+1,m}}{\Delta z} - \frac{\theta_{i,mo}^{n+1,m} - \theta_{i,mo}^{n}}{\Delta t} - S_{mo} - \Gamma_w \end{aligned} \tag{3.107}$$

The iterative process stops once the difference in pressure head computed between the two iterative levels at each spatial node for a specific temporal step is smaller than the prescribed tolerance, δ_a:

$$\delta_i^{m+1} = \left|h_i^{m+1} - h_i^m\right| \leq \delta_a \tag{3.108}$$

3.10.4 Initial and Boundary Conditions for Fixed Mesh–RE

In the fixed mesh approach, the initial and boundary conditions are set to be the same as those of MMM. Hence, the terms ($\alpha_i,\ \beta_i,\ \gamma_i,\ R_i$) in Equation (3.102) for the first block are found to be:

$$\alpha_1 = 0$$

$$\beta_1 \text{ from } \beta_i \text{ by putting } K^m_{i-\frac{1}{2}} = 0 \tag{3.109}$$

$$\gamma_1 \text{ from } \gamma_i$$

$$R_1 \text{ from } R_i \text{ by putting } \frac{K^m_{i-\frac{1}{2}}}{(\Delta z)^2}(h^m_0 - h^m_1) + \frac{K^m_{i-\frac{1}{2}}}{\Delta z} = 0$$

3.10.5 Nodal Fluxes

Generally, the components in Darcy's equation (flux) are computed at each time step for both water flow and solute transport equations, simultaneously, during the simulation. However, when only the flow equation is being solved alone, the flux components are computed at selected print times only. Thus, the z-components (space) of the nodal fluxes calculated for each node, *N* (Simunek *et al.*, 2008), are presented as:

$$q^{n+1}_1 = -K^{n+1}_{1+\frac{1}{2}}\left(\frac{h^{n+1}_2 - h^{n+1}_1}{\Delta z} + 1\right) \tag{3.110}$$

$$q^{n+1}_i = -\frac{K^{n+1}_{i+\frac{1}{2}}}{2}\left(\frac{h^{n+1}_{i+1} - h^{n+1}_i}{\Delta z} + 1\right) - \frac{K^{n+1}_{i-\frac{1}{2}}}{2}\left(\frac{h^{n+1}_i - h^{n+1}_{i+1}}{\Delta z} + 1\right) \tag{3.111}$$

$$q^{n+1}_N = -K^{n+1}_{1-\frac{1}{2}}\left(\frac{h^{n+1}_N - h^{n+1}_{N-1}}{\Delta z} + 1\right) - \frac{\Delta z}{2}\left(\frac{\theta^{n+1}_N - \theta^n_N}{\Delta t}\right) \tag{3.112}$$

3.10.6 Mass Balance Conservation

One of the measurements for a numerical simulation of a hydraulic model, is its ability to conserve global mass over the domain of interest (Celia & Bouloutas, 1990). However, it should be noted that the acceptability of a numerical simulator is necessary but insufficient to be based on the adequacy of the conservation of global mass. Thus, the measurement of the ability of a simulator to conserve mass is given by:

$$MB\ [t] = \frac{total\ additional\ mass\ in\ the\ domain}{total\ net\ flux\ into\ the\ domain} \tag{3.113}$$

Whereas, for the finite difference approximation with the implementation of first type boundary conditions, it is displayed by:

$$MB^{n+1} = \frac{\sum_{i=1}^{N}(\theta_i^{n+1} - \theta_i^0)(\Delta z)}{\sum_{i=1}^{N}\left[K_{N-\frac{1}{2}}^{n+1}\left(\frac{h_N^{n+1} - h_{N-1}^{n+1}}{\Delta z} + 1\right) - K_{\frac{1}{2}}^{n}\left(\frac{h_1^{n+1} - h_0^{n+1}}{\Delta z} + 1\right)\right]\Delta t} \tag{3.114}$$

3.10.7 Moving Mesh Layer for Solute Transport Module

Prior to numerically discretize the solute transport equation, the ADE is transformed by eliminating the water content, θ in the LHS of the equation, as well as neglecting the reaction and solute transfer terms. Hence, the ADE for the mobile region, is shown below:

$$\frac{\partial c_{mo}}{\partial t} + \frac{\rho f F_{mo} K_d}{\theta_{mo}}\frac{\partial c_{mo}}{\partial t} = \frac{\partial}{\partial z}\left(D_{mo}\frac{\partial c_{mo}}{\partial z}\right) - \frac{q_{mo}}{\theta_{mo}}\frac{\partial}{\partial z}\left(\frac{\partial c_{mo}}{\partial z}\right) \tag{3.115}$$

Similar to the hydraulic module of moving mesh method, the main concept in solute transport studies is to keep the fractional concentration between adjacent mesh points constant (Bruce, 2011). Thus, the formulation of the constant equation is given by:

$$\frac{\int_a^{z_i(t)} c dz}{\int_a^b c dz} = \gamma_i \tag{3.116}$$

where γ_i is constant in time. Thus, for a velocity-based moving boundary of ADE in mobile region for dual-porosity model, is displayed as:

$$v_i = \frac{dz_i}{dt} = \frac{1}{c_{mo}}\left\{\gamma_i\left(\left[\left(\frac{\theta_{mo}D_{mo}}{\theta_{mo}+\rho f F_{mo}K_d}\right)\left(\frac{\partial c_{mo}}{\partial z}\right)\right.\right.\right. \\ \left. - \left(\frac{q_{mo}}{\theta_{mo}+\rho f F_{mo}K_d}\right)\left(\frac{\partial c_{mo}}{\partial z}\right)\right]_a^b + \left[c_{mo}\frac{dz_i}{dt}\right]_a^b\Bigg) \\ - \left[\left(\frac{\theta_{mo}D_{mo}}{\theta_{mo}+\rho f F_{mo}K_d}\right)\left(\frac{\partial c_{mo}}{\partial z}\right)\right. \\ \left.\left. - \left(\frac{q_{mo}}{\theta_{mo}+\rho f F_{mo}K_d}\right)\left(\frac{\partial c_{mo}}{\partial z}\right)\right]_a^{z_i(t)} + \left[c_{mo}\frac{dz_i}{dt}\right]_a\right\} \tag{3.117}$$

where v_i is the solute velocity $[L/t]$; z_i is the vertical coordinate assumed positive downward; t is the time $[t]$; c_{mo} is the solute concentration at the mobile region $[M/L^3]$; γ_i is the fractional integral constant in time; θ_{mo} is the volumetric water content $[L^3/L^3]$; D_{mo} is the dispersion coefficient in the mobile region $[L^2/t]$; ρ is the soil bulk density $[M/L^3]$; f is the fraction of sorption sites in contact with the mobile region; F_{mo} is the mass fraction of all sites occupied in instantaneous equilibrium at the mobile region; K_d is the distribution coefficient obtained from the slope of the isotherm curve $[L^3/M]$; q_{mo} is the volumetric fluid flux in the mobile region $[L/t]$; a and b are the specific coordinates at two extreme locations $[L]$ depending on the boundary conditions, respectively; and $z_i(t) = dz_i/dt$ is the differential of vertical coordinate with respect to time $[L/t]$. A thorough derivation of Equation (3.117) is given in **Appendix G**.

Meanwhile, when the reaction term and solute transfer rates between the mobile and immobile regions are added into Equation (3.117), it gives:

$$\frac{dz_i}{dt} = \frac{1}{c_{mo}}\left\{\gamma_i\left(\left[\left(\frac{\theta_{mo}D_{mo}}{\theta_{mo}+\rho f F_{mo}K_d}\right)\left(\frac{\partial c_{mo}}{\partial z}\right) - \left(\frac{q_{mo}}{\theta_{mo}+\rho f F_{mo}K_d}\right)\left(\frac{\partial c_{mo}}{\partial z}\right)\right]_a^b + \left[c_{mo}\frac{q_{mo}}{\theta_{mo}}\right]_a^b - R_{mo} - \Gamma_{s1} - \Gamma_{s2}\right) - \left[\left(\frac{\theta_{mo}D_{mo}}{\theta_{mo}+\rho f F_{mo}K_d}\right)\left(\frac{\partial c_{mo}}{\partial z}\right) - \left(\frac{q_{mo}}{\theta_{mo}+\rho f F_{mo}K_d}\right)\left(\frac{\partial c_{mo}}{\partial z}\right)\right]_a^{z_i(t)} + \left[c_{mo}\frac{q_{mo}}{\theta_{mo}}\right]_a\right\} \quad (3.118)$$

where R_{mo} is the reaction term in mobile region $[M/L^3t]$, while Γ_{s1} and Γ_{s2} are the solute transfer rates $[M/L^3t]$ between the mobile and immobile regions for physical solute exchange and chemical kinetic sorption, respectively.

3.10.8 Initial and Boundary Conditions for MMM–ADE

The initial condition for the solute concentration is given as follow:

$$c(z,t) = c_0(z), \qquad t = t_0 \quad (3.119)$$

For the solute transport model, two types of boundary conditions (Dirichlet and Cauchy types) can be applied to the top and bottom boundaries. On the one hand, the first type of boundary condition (Dirichlet) prescribes the concentration at upper boundary, which display as:

$$\frac{dc}{da} = 0, \qquad t = t_0 \quad (3.120)$$

On the other hand, the third type of boundary condition (Cauchy) is employed to the lower boundary. However, the value is always equivalent to zero due to free drainage at the bottom of the bed, thus:

$$c_b\frac{db}{dt} = c_b\frac{q_b}{\theta_b} = 0 \quad (3.121)$$

Hence, by applying the stated boundaries conditions to the velocity-based ADE in the mobile region, the new equation is given as:

$$v_i = \frac{dz_i}{dt} = \frac{1}{c_{mo}}\left\{\gamma_i\left(\left[\left(\frac{\theta_{mo}D_{mo}}{\theta_{mo}+\rho f F_{mo}K_d}\right)\left(\frac{\partial c_{mo}}{\partial z}\right)\right]^b + \left[c_{mo}\frac{q_{mo}}{\theta_{mo}}\right]_a - R_{mo} - \Gamma_{s1} - \Gamma_{s2}\right)\right. \\ - \left[\left(\frac{\theta_{mo}D_{mo}}{\theta_{mo}+\rho f F_{mo}K_d}\right)\left(\frac{\partial c_{mo}}{\partial z}\right)\right. \\ \left.\left. - \left(\frac{q_{mo}}{\theta_{mo}+\rho f F_{mo}K_d}\right)\left(\frac{\partial c_{mo}}{\partial z}\right)\right]^{z_i(t)} + \left[c_{mo}\frac{q_{mo}}{\theta_{mo}}\right]_a\right\} \tag{3.122}$$

Therefore, the discretization of the velocity-based ADE in the mobile region can be written as:

$$\frac{z_i^{n+1}-z_i^n}{\Delta t} = \frac{1}{c_{i,mo}}\left\{\gamma_i\left(\left[\left(\frac{\theta_{i,mo}}{\theta_{i,mo}+\rho f F_{mo}K_d}\right)\left(\overline{D_{i+1/2}^n}\frac{c_{i+1}^n-c_i^n}{\Delta\overline{z_i^n}}\right)\right] + \left[c_0\frac{q_0}{\theta_0}\right] - R_{mo} - \Gamma_{s1} - \Gamma_{s2}\right)\right. \\ \left. - \left[\left(\frac{\theta_{i,mo}}{\theta_{i,mo}+\rho f F_{mo}K_d}\right)\left(\overline{D_{i+1/2}^n}\frac{c_{i+1}^n-c_i^n}{\Delta\overline{z_i^n}}\right)\right] + \left[c_0\frac{q_0}{\theta_0}\right]\right\} \tag{3.123}$$

where γ_i, $\Delta\overline{z_i^n}$, $\overline{D_{i+1/2}^n}$, R_{mo}, Γ_{s1}, and Γ_{s2} are given as follow:

$$\gamma_i = \frac{\int_a^{z_i(t)}\theta dz}{\int_a^b \theta dz} \tag{3.124}$$

$$\Delta\overline{z_i^n} = \frac{\Delta z_i^n + \Delta z_{i+1}^n}{2} \tag{3.125}$$

$$\overline{D_{i+1/2}^n} = \frac{\alpha D_i^n + \beta D_{i+1}^n}{\alpha+\beta} \tag{3.126}$$

$$\alpha = \frac{\Delta z_i^n}{2} \tag{3.127}$$

$$\beta = \frac{\Delta z_{i+1}^n}{2} \tag{3.128}$$

$$\Delta z_i^n = z_i^n - z_{i-1}^n \tag{3.129}$$

$$\Delta z_{i+1}^n = z_{i+1}^n - z_i^n \tag{3.130}$$

$$R = -\mu(\theta_{mo}^n c_{mo}^n + \rho s_{mo}^n) + \gamma(\theta_{mo}^n + \rho) \tag{3.131}$$

$$\Gamma_{i,s1} = \omega_{s1}(c_{mo}^n - c_{im}^n) \tag{3.132}$$

$$\Gamma_{i,s2} = \omega_{s2}\rho\left[(1 - F_{mo})K_d c_{mo}^n - s_{mo}^{n,k}\right] \tag{3.133}$$

In addition, the change in concentration of solutes in medium profile, (dM/dt) after each timestep, is known as:

$$\frac{dM}{dt} = \left[\left(\frac{\theta_{i,mo}}{\theta_{i,mo} + \rho f F_{mo} K_d}\right)\left(\overline{D_{i+1/2}^n}\frac{c_{i+1}^n - c_i^n}{\Delta\overline{z_i^n}}\right)\right] + \left[c_0\frac{q_0}{\theta_0}\right] - R_{mo} - \Gamma_{s1} - \Gamma_{s2} \tag{3.134}$$

3.10.9 Fixed Mesh Layers for Solute Transport Module

In fact, a fully implicit finite difference method with the implementation of Picard linearization is always the first choice in solving the RE, whereas a Crank-Nicolson finite difference method would be used for the solution of the ADE related problems. Generally, ADE involved primarily the first-order derivatives stemmed from another derivative, thus it needs at least second-order derivative approximations to describe and solve the ADE explicitly (Al-Niami & Rushton, 1978; Bresler, 1973). Therefore, by neglecting the adsorption and sink terms, a basic mass conservation for ADE can be presented as:

$$\Delta J = \frac{\partial \theta c}{\partial t} = \frac{\partial}{\partial z}\left(D\frac{\partial c}{\partial z}\right) - \frac{\partial qc}{\partial z} \tag{3.135}$$

where J is the total flux of solute $[M/L^3t]$.

Moreover, a thorough numerical implementation for solute transport scheme could be partitioned into three major terms: total flux $\left(\frac{\partial \theta c}{\partial t}\right)$, dispersion $\left[\frac{\partial}{\partial z}\left(D\frac{\partial c}{\partial z}\right)\right]$, and imposed flux, $\left(\frac{\partial qc}{\partial z}\right)$, respectively, as follows:

Total Flux:

$$\left(\frac{\partial \theta c}{\partial t}\right)_i^{n+\frac{1}{2}} = \frac{\theta_i^{n+1}c_i^{n+1} - \theta_i^n c_i^n}{\Delta t} - \frac{V_i^{n+\frac{1}{2}}\Delta t(\theta_i^{n+1} - \theta_i^n)}{16(\Delta z)^2}\left[V_{i-\frac{1}{2}}^{n+\frac{1}{2}}(c_{i-1}^{n+1} + c_{i-1}^n - c_i^{n+1} - c_i^n) - V_{i+\frac{1}{2}}^{n+\frac{1}{2}}(c_i^{n+1} + c_i^n - c_{i+1}^{n+1} - c_{i+1}^n)\right] \tag{3.136}$$

Dispersion:

$$\left[\frac{\partial}{\partial z}\left(D\frac{\partial c}{\partial z}\right)\right]_i^{n+\frac{1}{2}} = \frac{D_{i-\frac{1}{2}}^{n+\frac{1}{2}}(c_{i-1}^{n+1} + c_{i-1}^n - c_i^{n+1} - c_i^n)}{2(\Delta z)^2} - \frac{D_{i+\frac{1}{2}}^{n+\frac{1}{2}}(c_i^{n+1} + c_i^n - c_{i+1}^{n+1} - c_{i+1}^n)}{2(\Delta z)^2} \tag{3.137}$$

Imposed Flux:

$$\left(\frac{\partial qc}{\partial z}\right)_i^{n+\frac{1}{2}} = \frac{q_{i+\frac{1}{2}}^{n+\frac{1}{2}}(c_i^{n+1}+c_i^n) - q_{i-\frac{1}{2}}^{n+\frac{1}{2}}(c_{i-1}^{n+1}+c_{i-1}^n)}{2\Delta z} + \left[\frac{q_{i-\frac{1}{2}}^{n+\frac{1}{2}}(c_{i-1}^{n+1}+c_{i-1}^n-c_i^{n+1}-c_i^n)}{4\Delta z} - \frac{q_{i+\frac{1}{2}}^{n+\frac{1}{2}}(c_i^{n+1}+c_i^n-c_{i+1}^{n+1}-c_{i+1}^n)}{4\Delta z}\right] \quad (3.138)$$

where Δt is the temporal step and Δz is the spatial step assumed positive downward. A detailed derivation can be found in **Appendix H**.

Hence, the complete numerical discretization of ADE is obtained by substituting all the components, as presented in Equation (3.136), Equation (3.137), and Equation (3.138), into Equation (3.135), as follows:

$$\frac{\theta_i^{n+1}c_i^{n+1}-\theta_i^n c_i^n}{\Delta t} = \frac{\left(D_{i-\frac{1}{2}}^{n+\frac{1}{2}} - N_{i-\frac{1}{2}}^{n+\frac{1}{2}}\right)}{2(\Delta z)^2}(c_{i-1}^{n+1}+c_{i-1}^n-c_i^{n+1}-c_i^n) - \frac{\left(D_{i+\frac{1}{2}}^{n+\frac{1}{2}} - N_{i+\frac{1}{2}}^{n+\frac{1}{2}}\right)}{2(\Delta z)^2}(c_i^{n+1}+c_i^n-c_{i+1}^{n+1}-c_{i+1}^n) - \frac{\left[q_{i+\frac{1}{2}}^{n+\frac{1}{2}}(c_i^{n+1}+c_i^n) - q_{i-\frac{1}{2}}^{n+\frac{1}{2}}(c_{i-1}^{n+1}+c_{i-1}^n)\right]}{2\Delta z} \quad (3.139)$$

where N is the additional dispersion coefficient, when the second-order finite difference approximation is used, given as:

$$N_{i-\frac{1}{2}}^{n+\frac{1}{2}} = \frac{\Delta z}{2}\left(q_{i-\frac{1}{2}}^{n+\frac{1}{2}}\right) - \frac{V_i^{n+\frac{1}{2}} V_{i-\frac{1}{2}}^{n+\frac{1}{2}} \Delta t}{8}(\theta_i^{n+1} - \theta_i^n) \tag{3.140}$$

$$N_{i+\frac{1}{2}}^{n+\frac{1}{2}} = \frac{\Delta z}{2}\left(q_{i+\frac{1}{2}}^{n+\frac{1}{2}}\right) - \frac{V_i^{n+\frac{1}{2}} V_{i+\frac{1}{2}}^{n+\frac{1}{2}} \Delta t}{8}(\theta_i^{n+1} - \theta_i^n) \tag{3.141}$$

However, if the ADE model is differentiated based on the first-order approximation, the term *N* would no longer exist. Thus, the simplified ADE is displayed as:

$$\begin{aligned} &\frac{\theta_i^{n+1} c_i^{n+1} - \theta_i^n c_i^n}{\Delta t} \\ &= \frac{D_{i-\frac{1}{2}}^{n+\frac{1}{2}}(c_{i-1}^{n+1} + c_{i-1}^n - c_i^{n+1} - c_i^n)}{2(\Delta z)^2} \\ &- \frac{D_{i+\frac{1}{2}}^{n+\frac{1}{2}}(c_i^{n+1} + c_i^n - c_{i+1}^{n+1} - c_{i+1}^n)}{2(\Delta z)^2} \\ &- \frac{\left[q_{i+\frac{1}{2}}^{n+\frac{1}{2}}(c_i^{n+1} + c_i^n) - q_{i-\frac{1}{2}}^{n+\frac{1}{2}}(c_{i-1}^{n+1} + c_{i-1}^n)\right]}{2\Delta z} \end{aligned} \tag{3.142}$$

Furthermore, the basic ADE model obtained is required to include the adsorption and sink terms ignored earlier, as well as the mass transfer terms. Therefore, the overall ADE model with the inclusion of adsorption, sink, and mass transfer terms in the mobile region, is displayed as:

$$\frac{\theta_{i,mo}^{n+1}c_{i,mo}^{n+1}-\theta_{i,mo}^{n}c_{i,mo}^{n}}{\Delta t}+\rho f\frac{s_{i,mo}^{n+1,e}-s_{i.mo}^{n,e}}{\Delta t} \tag{3.143}$$

$$=\frac{D_{i-\frac{1}{2}}^{n+\frac{1}{2}}(c_{i-1}^{n+1}+c_{i-1}^{n}-c_{i}^{n+1}-c_{i}^{n})_{mo}}{2(\Delta z)^2}$$

$$-\frac{D_{i+\frac{1}{2}}^{n+\frac{1}{2}}(c_{i}^{n+1}+c_{i}^{n}-c_{i+1}^{n+1}-c_{i+1}^{n})_{mo}}{2(\Delta z)^2}$$

$$-\frac{\left[q_{i+\frac{1}{2}}^{n+\frac{1}{2}}(c_{i}^{n+1}+c_{i}^{n})_{mo}-q_{i-\frac{1}{2}}^{n+\frac{1}{2}}(c_{i-1}^{n+1}+c_{i-1}^{n})_{mo}\right]}{2\Delta z}-S_{mo}$$

$$-\Gamma_{s1}-\Gamma_{s2}$$

where the sink term, S_{mo} is given by:

$$S_{mo}=\mu_1\theta_{mo}^{n}c_{mo}^{n}+\mu_2\rho s_{mo}^{n}-\gamma_1\theta_{mo}^{n}-\gamma_2\rho \tag{3.144}$$

On the other hand, the adsorption term in considering both instantaneous and time-dependent processes in the mobile region, which can be formulated as follows:

$$\left(\rho f\frac{\partial s_{mo}^{e}}{\partial t}\right)_{i}^{n+\frac{1}{2}}=\rho f\frac{s_{i,mo}^{n+1,e}-s_{i.mo}^{n,e}}{\Delta t} \tag{3.145}$$

In addition, the terms for sink and mass transfer of solutes. are presented below:

Physical: $$\Gamma_{i,s1}=\omega_{s1}(c_{mo}^{n}-c_{im}^{n}) \tag{3.146}$$

Chemical: $$\Gamma_{i,s2}=\omega_{s2}\rho\left[(1-F_{mo})K_d c_{mo}^{n}-s_{mo}^{n,k}\right] \tag{3.147}$$

To present the system in the tridiagonal matrix, Equation (3.143) is rearranged to ease the computer work afterwards. The revised equation is shown below:

$$-\left(\frac{D_{i-\frac{1}{2}}^{n+1}}{4(\Delta z)^2}+\frac{D_{i-\frac{1}{2}}^{n}}{4(\Delta z)^2}-\frac{q_{i+\frac{1}{2}}^{n}}{4\Delta z}-\frac{q_{i-\frac{1}{2}}^{n}}{4\Delta z}\right)(\delta_{i-1}^{n+1}) \tag{3.148}$$

$$+\left(\frac{D_{i-\frac{1}{2}}^{n+1}}{4(\Delta z)^2}+\frac{D_{i-\frac{1}{2}}^{n}}{4(\Delta z)^2}+\frac{D_{i+\frac{1}{2}}^{n+1}}{4(\Delta z)^2}+\frac{D_{i+\frac{1}{2}}^{n}}{4(\Delta z)^2}+\frac{q_{i+\frac{1}{2}}^{n+1}}{4\Delta z}\right.$$

$$\left.+\frac{q_{i-\frac{1}{2}}^{n+1}}{4\Delta z}\right)(\delta_{i}^{n+1})-\left(\frac{D_{i+\frac{1}{2}}^{n+1}}{4(\Delta z)^2}+\frac{D_{i+\frac{1}{2}}^{n}}{4(\Delta z)^2}\right)(\delta_{i+1}^{n+1})$$

$$=\frac{D_{i-\frac{1}{2}}^{n+1}(\delta_{i-1}^{n+1}-\delta_{i}^{n+1})}{4(\Delta z)^2}+\frac{D_{i-\frac{1}{2}}^{n}(\delta_{i-1}^{n+1}-\delta_{i}^{n+1})}{4(\Delta z)^2}$$

$$-\frac{D_{i+\frac{1}{2}}^{n+1}(\delta_{i}^{n+1}-\delta_{i+1}^{n+1})}{4(\Delta z)^2}-\frac{D_{i+\frac{1}{2}}^{n}(\delta_{i}^{n+1}-\delta_{i+1}^{n+1})}{4(\Delta z)^2}$$

$$-\frac{\left[q_{i+\frac{1}{2}}^{n+1}(\delta_{i}^{n+1})-q_{i+\frac{1}{2}}^{n}(\delta_{i-1}^{n+1})\right]}{4\Delta z}$$

$$-\frac{\left[q_{i-\frac{1}{2}}^{n+1}(\delta_{i}^{n+1})-q_{i-\frac{1}{2}}^{n}(\delta_{i-1}^{n+1})\right]}{4\Delta z}-\frac{\theta_{i,mo}^{n+1}c_{i,mo}^{n+1}-\theta_{i,mo}^{n}c_{i,mo}^{n}}{\Delta t}-S_{mo}-\Gamma_{s1}-\Gamma_{s2}$$

where $\delta = c^{n+1} + c^{n}$ is a dependent variable. The complete working steps for the rearrangement is presented in **Appendix I**. The final tridiagonal nonlinear set of equations is inputted into MATLAB® as a tridiagonal nonlinear matrix for each time step and solved by the tridiagonal matrix algorithm:

$$\begin{bmatrix} \beta_1 & \gamma_1 & 0 & 0 & 0 & \cdots & \cdots & 0 & 0 & 0 \\ \alpha_1 & \beta_2 & \gamma_2 & 0 & 0 & \cdots & \cdots & 0 & 0 & 0 \\ 0 & \alpha_2 & \beta_3 & \gamma_3 & 0 & \cdots & \cdots & 0 & 0 & 0 \\ 0 & 0 & \alpha_3 & \beta_4 & \gamma_4 & \cdots & \cdots & 0 & 0 & 0 \\ 0 & 0 & 0 & \alpha_4 & \beta_5 & \cdots & \cdots & 0 & 0 & 0 \\ \vdots & \vdots & \vdots & \vdots & \vdots & \ddots & \ddots & \vdots & \vdots & \vdots \\ \vdots & \vdots & \vdots & \vdots & \vdots & \ddots & \ddots & \vdots & \vdots & \vdots \\ 0 & 0 & 0 & 0 & 0 & \cdots & \cdots & \beta_{N-2} & \gamma_{N-1} & 0 \\ 0 & 0 & 0 & 0 & 0 & \cdots & \cdots & \alpha_{N-1} & \beta_{N-1} & \gamma_N \\ 0 & 0 & 0 & 0 & 0 & \cdots & \cdots & 0 & \alpha_N & \beta_N \end{bmatrix} \begin{bmatrix} \delta_1^{n+1} \\ \delta_2^{n+1} \\ \delta_3^{n+1} \\ \delta_4^{n+1} \\ \delta_5^{n+1} \\ \vdots \\ \vdots \\ \delta_{N-2}^{n+1} \\ \delta_{N-1}^{n+1} \\ \delta_N^{n+1} \end{bmatrix} = \begin{bmatrix} R_1 \\ R_2 \\ R_3 \\ R_4 \\ R_5 \\ \vdots \\ \vdots \\ R_{N-2} \\ R_{N-1} \\ R_N \end{bmatrix} \tag{3.149}$$

where

$$\alpha_i = -\left(\frac{D_{i-\frac{1}{2}}^{n+1}}{4(\Delta z)^2} + \frac{D_{i-\frac{1}{2}}^{n}}{4(\Delta z)^2} - \frac{q_{i+\frac{1}{2}}^{n}}{4\Delta z} - \frac{q_{i-\frac{1}{2}}^{n}}{4\Delta z} \right) \tag{3.150}$$

$$\beta_i = \left(\frac{D_{i-\frac{1}{2}}^{n+1}}{4(\Delta z)^2} + \frac{D_{i-\frac{1}{2}}^{n}}{4(\Delta z)^2} + \frac{D_{i+\frac{1}{2}}^{n+1}}{4(\Delta z)^2} + \frac{D_{i+\frac{1}{2}}^{n}}{4(\Delta z)^2} + \frac{q_{i+\frac{1}{2}}^{n+1}}{4\Delta z} + \frac{q_{i-\frac{1}{2}}^{n+1}}{4\Delta z} \right) \tag{3.151}$$

$$\gamma_i = -\left(\frac{D_{i+\frac{1}{2}}^{n+1}}{4(\Delta z)^2} + \frac{D_{i+\frac{1}{2}}^{n}}{4(\Delta z)^2} \right) \tag{3.152}$$

$$\begin{aligned} R_i = {} & \frac{D_{i-\frac{1}{2}}^{n+1}(\delta_{i-1}^{n+1} - \delta_i^{n+1})}{4(\Delta z)^2} + \frac{D_{i-\frac{1}{2}}^{n}(\delta_{i-1}^{n+1} - \delta_i^{n+1})}{4(\Delta z)^2} - \frac{D_{i+\frac{1}{2}}^{n+1}(\delta_i^{n+1} - \delta_{i+1}^{n+1})}{4(\Delta z)^2} \\ & - \frac{D_{i+\frac{1}{2}}^{n}(\delta_i^{n+1} - \delta_{i+1}^{n+1})}{4(\Delta z)^2} - \frac{\left[q_{i+\frac{1}{2}}^{n+1}(\delta_i^{n+1}) - q_{i+\frac{1}{2}}^{n}(\delta_{i-1}^{n+1}) \right]}{4\Delta z} \\ & - \frac{\left[q_{i-\frac{1}{2}}^{n+1}(\delta_i^{n+1}) - q_{i-\frac{1}{2}}^{n}(\delta_{i-1}^{n+1}) \right]}{4\Delta z} - \frac{\theta_{i,mo}^{n+1} c_{i,mo}^{n+1} - \theta_{i,mo}^{n} c_{i,mo}^{n}}{\Delta t} \\ & - S_{mo} - \Gamma_{s1} - \Gamma_{s2} \end{aligned} \tag{3.153}$$

3.10.10 Initial and Boundary Conditions for Fixed Mesh–ADE

The solute concentrations in the mobile and immobile regions, as well as the adsorbed site for the initial conditions, are given as follow:

$$c_{mo}(z,0) = c_{mo_0}(z) \tag{3.154}$$

$$c_{im}(z,0) = c_{im_0}(z) \tag{3.155}$$

$$s^k_{mo}(z,0) = s^k_{mo_0}(z) \tag{3.156}$$

For the solute transport model, two types of boundary conditions (Dirichlet and Cauchy types) can be applied to the upper or lower boundaries. On the one hand, the first type of boundary condition (Dirichlet) prescribes the concentration at a boundary:

$$c(z,t) = c_0(z,t) \qquad \text{at } z = 0 \text{ or } z = L \tag{3.157}$$

On the other hand, the third type (Cauchy) boundary condition is used to prescribe the concentration flux at the upper or lower boundary conditions, given as:

$$-D\frac{\partial c}{\partial z} + qc = q_0 c_0 \qquad \text{at } z = 0 \text{ or } z = L \tag{3.158}$$

where q_0 is the upward liquid flux, and c_0 is the concentration of the influent liquid.

3.10.11 Stability Constraints

Numerical solutions for transport equations always come with the problems of undesired accuracy of the simulations. This particular circumstance is known as oscillatory behavior, where there is excessive numerical dispersion near the sharp concentration fronts (El-Kadi & Ling, 1993; Simunek *et al.*, 2008). In fact, the RE and the ADE are non-linear, especially when they involve the problems associated with convection and dispersion. According to past research, these unwanted oscillations can be avoided by selecting an appropriate combination of space and time discretization. Thus, two criteria are used for characterizing the space and time discretization, known as the Courant and

Peclet numbers. In addition, the Courant number is responsible for characterizing the convection process, whereas the Peclet number reflects the relative convection versus dispersion processes.

Therefore, the Courant number, Co and the grid Peclet number, Pe, are presented as:

$$Co = \frac{q\Delta t}{\theta \Delta z} \tag{3.159}$$

$$Pe = \frac{q\Delta z}{\theta D} \tag{3.160}$$

where Δt and Δz are referring to temporal and spatial discretization of a finite difference, respectively. The Peclet number tends to increase when the process of convection dominates over the dispersion for a particular solute transport model. Thus, it is recommended to keep the spatial discretization as small as possible, to achieve a desired numerical result. Additionally, it is also noted that the Courant number should be less than or equal to 1, and the Peclet number should not exceed 5 to ensure a robust simulation (Celia & Bouloutas, 1990).

3.10.12 Thickness of Sludge Deposit Layer

Similarly, the initial condition used for the hydraulic model is applied to the sludge deposit layer, at which the initial distribution of the pressure head, is given as follows:

$$h(z,t) = h_i(z), \qquad t = t_0 \tag{3.161}$$

where h_i is the prescribed pressure head at elevation, z, and t_0 is the time when simulation starts.

Therefore, the discretization of the thickness of sludge deposit layer can be written as:

$$\frac{L_i^{n+1} - L_i^n}{\Delta t} = \frac{\varepsilon_c}{\varepsilon_c - \varepsilon_s}\frac{k}{\mu}\left(\frac{h_i^{n+1} - h_i^n}{\Delta \overline{z_i^n}}\right)_L - q_0 \tag{3.162}$$

where $\Delta \overline{z_i^n}$ is given by:

$$\Delta \overline{z_i^n} = \frac{\Delta z_i^n + \Delta z_{i+1}^n}{2} \tag{3.163}$$

$$\Delta z_i^n = z_i^n - z_{i-1}^n \tag{3.164}$$

$$\Delta z_{i+1}^n = z_{i+1}^n - z_i^n \tag{3.165}$$

3.11 Summary of Model Development and Existing Limitations

In summary, the finalized equations, which are discretized via the MMM, are directly input into the MATLAB® program code to develop a process-based model that simulates the dewatering mechanisms in STRB under varying loading rates and resting periods. At the same time, the final discretized equations for the FMM are expected to be rearranged into a tridiagonal matrix form and plugged into MATLAB® for simulation purposes.

The hydraulic model for the STRB addresses the limitations of conventional models that assume fixed boundary conditions by incorporating dynamic aspects such as sludge deposition and surface ponding. Unlike traditional models, this approach accounts for changes in sludge deposit thickness, which influence hydraulic conductivity and permeability. The model integrates a variably saturated flow module to handle intermittent feeding and moving boundary conditions, incorporating various factors such as batch feeding, surface ponding, and free drainage. These elements are crucial for accurately simulating the complex interactions within the STRB system.

To ensure the accuracy of the model, a laboratory-scale STRB is constructed for calibration and validation. Key features of the model include a dual-porosity variably saturated flow model to describe hydraulic behavior, the CCF model to simulate sludge deposit dynamics, and a bio-kinetic module for modeling sludge mineralization. The

simulation process begins with initializing input files that contain data on geometry, time, hydraulic and solute transport modules sequentially, employing iterative procedures to achieve convergence.

The simulation employs a combination of moving and fixed mesh methods to model different layers of the STRB system effectively. Moving mesh methods are used for the sludge ponding and deposit layers are applied to the stationary reed bed substrate. Results are processed using MATLAB® for hydraulic and solute transport calculations, and the data are exported to Excel for analysis. This integrated approach allows for a comprehensive simulation of hydraulic flow and solute transport under dynamic conditions, ensuring that the model accurately reflects real-world scenarios.

3.12 Parametric Studies

In previous sections, the SLR and resting period have been determined to affect the STRB performance significantly. The variation in the SLRs and resting periods decides the hydraulic loading volume required, subsequently affecting the resultant flux peak and flow delay. An excessive hydraulic load is believed to cause waterlogging, while an insufficient load would result in cracks in the sludge deposit layer. Thus, the hydraulic load was analyzed for its sensitivity to the overall STRB profile.

Furthermore, the calibrations of the hydraulic head and saturated hydraulic conductivity were to match the flow-occurring delay and flux peak, respectively. An increased hydraulic head and saturated conductivity would result in a longer flow delay and a higher flux peak. The parametric study helps to determine an appropriate range of the hydraulic head and saturated conductivity, covering different types of flow cases. Hence, the parametric study also included their effects on the STRB efficiency.

Moreover, the continuous sludge accumulation increased the sludge deposit layer thickness while reducing the infiltration flux. The layer thickness increases its porosity, retaining more moisture and solid particles in the void space, thus resulting in a higher organic content. Further, the high sludge deposit organic content hinders the penetration of the liquid through the layer, reducing its MC. Hence, the sludge deposit thickness's sensitivity to the overall STRB performance was studied.

Table 3.7 shows the tested parameters range of the hydraulic load, hydraulic head, saturated hydraulic conductivity, and sludge deposit layer thickness, covering respective average values. Under a constant resting period of 6 days and SLR of 100 kg/m^2/year, the hydraulic loading volumes were calculated to be the same under a 50 kg/m^2/year SLR and a 3-day resting period increment, respectively. Hence, the same loading volume was used to analyze hydraulic load under varying SLRs and resting periods. The sensitivity analysis studies the importance of these parameters to the effluent flux, evapotranspiration, sludge accumulation, moisture, and organic contents of the sludge deposit layer.

Table 3.7: Tested parameters range of hydraulic load, head, conductivity, and sludge deposit thickness.

Tested parameters	Tested range	Increment	Average value
Hydraulic load (SLR @ resting period)	7,371 – 99,501 ml (50 – 450 kg/^{2}/year @ 6 days || 3 – 27 days)	7,370 ml (50 kg/^{2}/year @ 3 days)	14,741 ml (100 kg/^{2}/year @ 6 days)
Hydraulic head	-7 – -30 cm	-3 cm	-19 cm
Saturated hydraulic conductivity	0.0009 – 0.1269 cm/min	0.014 cm/min	0.0429 cm/min
Sludge deposit layer thickness	4 – 20 cm	2 cm	10 cm

CHAPTER 4: LABORATORY EXPERIMENTAL RESULTS

The laboratory experiment was carried out to calibrate and validate the formulated hydraulic model. The critical parameters determined in the experimental study were flux peak and flow-occurring delay. These two parameters were then compared with the saturated hydraulic conductivity and hydraulic head, respectively. Other information, such as water recovery, sludge characteristics, and water quality, are also collected for the simulation study.

The operational scheme of the constructed laboratory-scale STRB system was separated into two phases, namely the preliminary treatment (Phase 1) and main treatment (Phase 2), to identify the optimized SLR and better adjust the resting period before the main treatment. In Phase 1, the STRBs were acclimatized and operated under freshly acclimatized conditions, whereas the STRBs should be operated under the well-established conditions in Phase 2. The hydraulic behavior was assessed during the initial stage of the discharged flow to observe flux peak and flow-occurring delay. The complete loading schedule with respective dates is presented in **Appendix J**. The measurement of sludge deposit layer thickness and the sample of newly formed sludge deposits were taken daily to assess the moisture and total volatile solids content. The effluents from the discharge pipe were measured and collected in the BOD bottles daily to study water quality and STRB performance efficiency. The collected sludge deposits and effluents were sent to the laboratory for further analysis.

4.1 Quality of Raw Septage

The raw septage used in the experiment was retrieved from a household near the Curtin University Malaysia campus. The collected septage was then stored in a 400-gallon tank before loading onto the reed beds.

The TS concentrations for five batches of raw septage ranged between 17507 and 55780 mg/L. The variation of TS concentration was relatively high due to the different batches of septage used. The raw septage contained a high concentration of organic

materials with a relatively high COD. The COD of the raw septage fed in the reed bed ranged from 1980 to 6152 mg/L. Moreover, the NO_3 concentration was measured in the range of 162 to 433 mg/L. Meanwhile, the pH value was slightly alkaline, ranging from 7.44 to 8.45. Furthermore, the DO content in the raw septage was always below 1 mg/L, which is between 0.12 and 0.43 mg/L. The quality assessment showed that the DO concentrations are always inversely proportional to COD concentrations, as the increase in COD concentration increases oxygen consumption by biological process (Wang, Bengtsson, *et al.*, 2019; Wang *et al.*, 2020). The variations of the septage quality were high. Thus, the SLR is more efficient as the loading regime than the HLR (Tan *et al.*, 2020). The mean values of all the mentioned parameters and the respective standard deviations are presented in Table 4.1.

Table 4.1: Mean data of the raw septage used in the first month (n=5, which is the number of samples).

Parameter	1	2	3	4	5	Mean Value
TS (mg/L)	18780	55780	20365	10796	17507	24646 ± 17782
COD (mg/L)	6819	1980	6152	4724	4205	4776 ± 1885
NO_3 (mg/L)	394	361	162	354	433	341 ± 105
pH	7.96	8.45	7.44	8.09	7.75	-
DO (mg/L)	0.12	0.20	0.20	0.24	0.43	0.24 ± 0.12

4.2 Hydraulic Behavior in the STRBs

The experiments were conducted on a “feed-and-drain” basis through raw septage fed in batches according to the respective calculated volumes. The effluents were then discharged from the bottom of the bed as free drainage. The complete results of effluent flux are presented in **Appendix K**. Due to instrumental and safety limitations, the monitoring duration of the hydraulic dynamics with a short time interval was limited to the first 6 hours (360 mins) after the feeding, while continuous measurements of effluent volumes were made daily during the non-feeding period. Observations indicated that the hydraulic flow declined insignificantly after the initial six hours, with most water recovery occurring during this period.

There were five loading conditions in Phase 1 experiment: 50 kg SLR with a 6-day resting, 100 kg SLR with a 6-day resting, 150 kg SLR with a 6-day resting, 100 kg SLR with a 3-day resting, and 100 kg SLR with a 9-day resting. Each loading volume varied due to different TS concentrations of raw septage. The raw septage was expected to be more concentrated at the bottom of the sludge storage tank. Therefore, the TS concentration for the raw septage was tested and updated every 1 to 2 weeks.

According to the preliminary analysis, factors affecting the hydraulic dynamics and flux peaks of the draining dewatering in STRB included SLR, resting period, TS concentrations of raw septage, sludge deposit thickness, and sludge deposit condition before loading. A high SLR or longer resting period requires a larger hydraulic load, increasing the hydraulic head and consequently raising the overall infiltration flux and peak (Çakir *et al.*, 2015). Conversely, a high influent septage concentration reduces the percolation rate because high initial TS concentrations contain limited water, allowing more solids to accumulate and increase sludge deposit layer thickness (Tan *et al.*, 2020). The incremental thickness and reduced porosity retain more water in the layer, affecting the overall water recovery (Trein *et al.*, 2019). Continuous settling of solid particles on the sludge deposit layer fills the void spaces and clogs pores, leading to a substantial decrease in infiltration flux and peak. Additionally, cracks in the sludge deposit layer can allow influent septage to bypass it directly, significantly boosting effluent flux and impacting treatment performance (Khomenko *et al.*, 2019).

Uncontrollable external factors, such as climate conditions, also influence the dewatering and treatment performance of STRB. On hot and sunny days, high evapotranspiration rates lead to increased water loss to the atmosphere, decreasing total water recovery and enhancing the drying of the sludge deposit layer (Wanniarachchi & Sarukkalige, 2022). Conversely, high air humidity prolongs surface ponding during rainy days. Despite many fixed variables such as substrate layer, gravel size, and type and number of reeds, controllable variables remain SLR and resting period (Paredes *et al.*, 2020).

Several conditions of the reed bed were observed throughout the experiment, categorized as normal, ponding, and cracked conditions, as shown in Figure 4.1. The

respective cases of effluent flux development are presented in Figure 4.2, Figure 4.3, and Figure 4.4. It should be noted that the negative sign was used for the effluent flux, assuming positive elevation is upward.

(a) Normal condition

(b) Ponding condition

(c) Dry condition

(d) Cracked condition

Figure 4.1: Conditions of the reed bed.

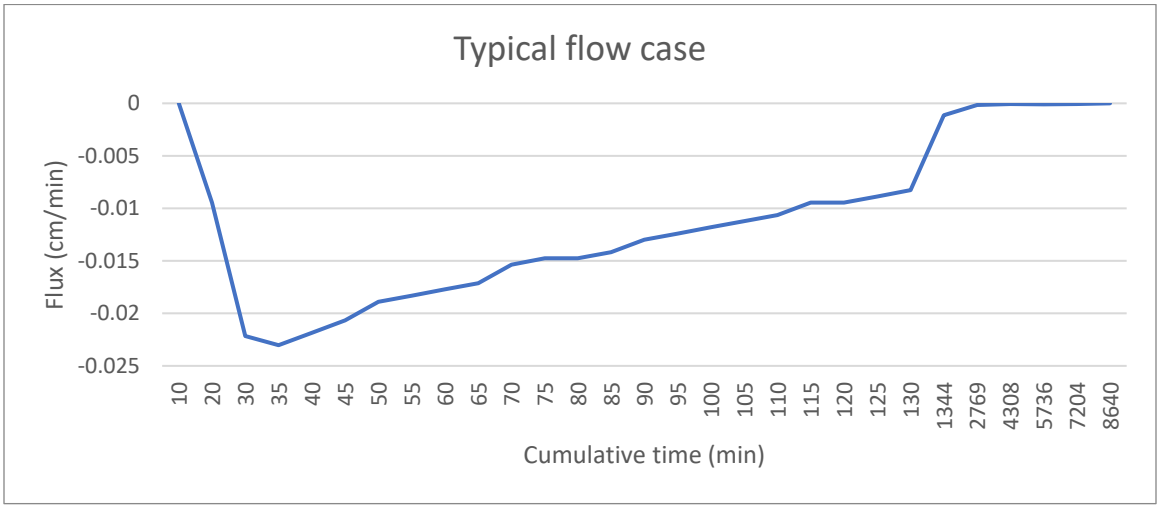

Figure 4.2: Typical flow case.

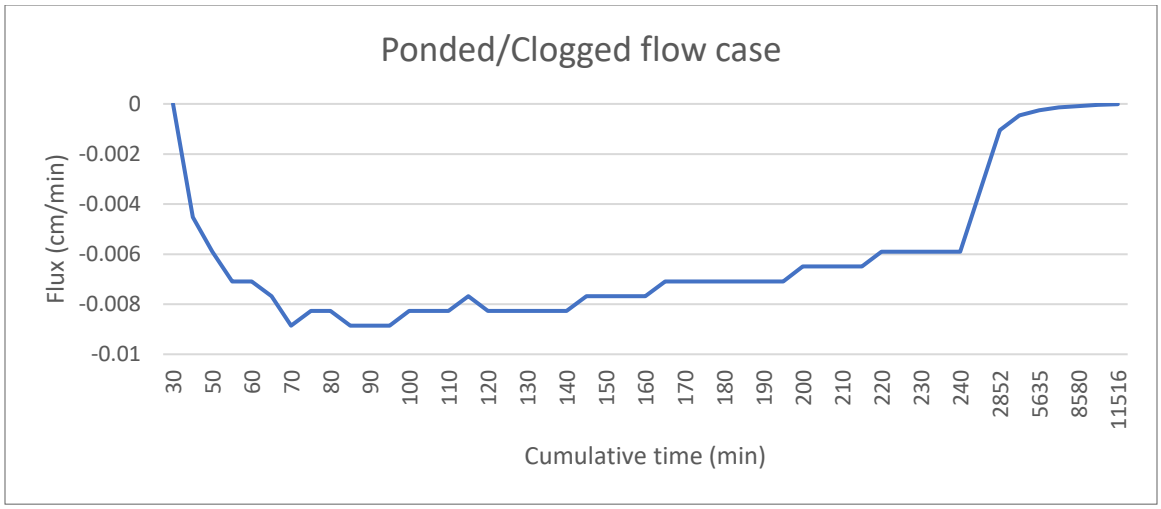

Figure 4.3: Ponded/clogged flow case.

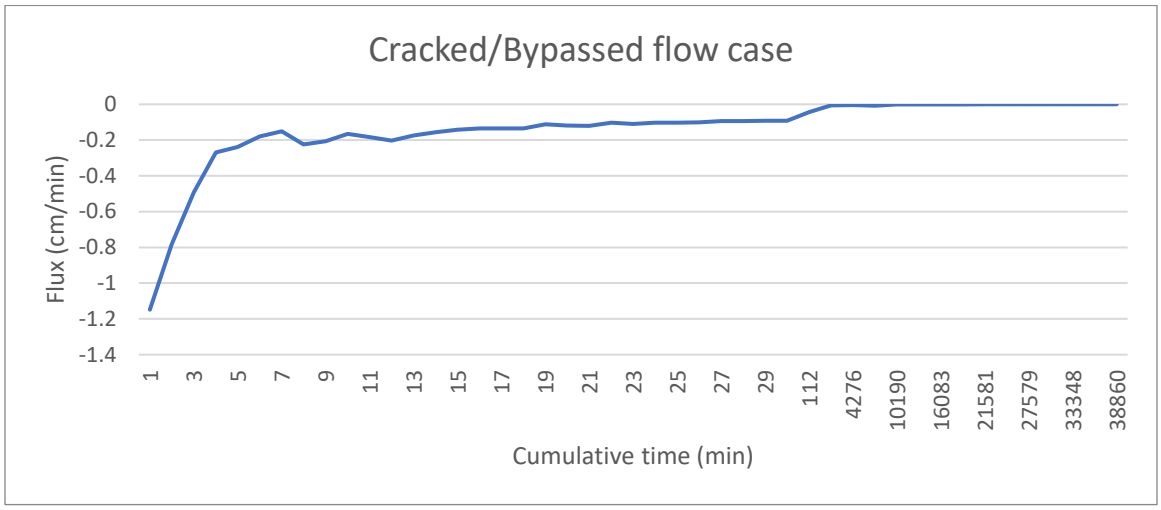

Figure 4.4: Cracked/bypassed flow case.

The typical hydraulic flux of the STRB system showed a trend where the fluxes increased rapidly from the beginning until the peak, and then gradually decreased until the end of the drainage. This behavior was primarily influenced by the pressure head difference, which directly affected the flux peak due to the maximum ponding depth as soon as the effluent was discharged (Ghanbarian, 2021). Over time, the continuous outflow reduced the head difference, thereby decelerating the percolation rate of the reed bed during the resting period.

Occasionally, the reed bed experienced ponding when the feeding volume of the raw septage exceeded infiltration capacity of the bed under high SLR or prolonged

resting periods. If the sludge deposits had not fully dried before the new feeding batch, the bed remained ponded, prolonging infiltration and causing waterlogging issues (Huong *et al.*, 2024a). In such cases, the flux peak was consistently lower compared to the other flow conditions, with a roughly linear reduction trend in flux due to minimal infiltration rates (Sheng *et al.*, 2019). Typically, the peak effluent flux was less than 0.01 cm/min for ponded conditions, where the pressure head difference had little effect on the effluent flux.

In case of bypassed flow, the sludge deposits within the reed bed were found to be over-dried or cracked, due to relatively low SLR and extended resting periods that increased dewatering via evapotranspiration. The effluent flow was significantly high, with no apparent increase in flux at the beginning of discharge. The flux peak was observed at the first minute, followed by a decreasing trend in overall effluent flux. This phenomenon was attributed to cracks in the sludge deposit caused by continuous moisture loss over the resting period (Khomenko *et al.*, 2019). Additionally, strong winds at the experimental site mechanically moved the reeds back and forth, creating numerous preferential flow paths (PFPs) due to reed stem movement. Consequently, the raw septage bypassed the low-permeable sludge deposit layer, resulting in a rapid increase in effluent flux at the start of the feeding cycle. Therefore, the situation was characterized by swift effluent discharge and extraordinarily high flux peaks (Dubash & Frigaard, 2007; Obour *et al.*, 2018).

4.2.1 Flux Peak

The flux peak of each bed decreased with the thickness of the accumulated sludge deposit layer along the treatment batches. The continuous deposition of solid sludge on the reed bed surface acted as a flow resistance layer that decreased the effluent and the flux peak. This is confirmed by observation in Beds 2 and 5. The overall flux peaks of Bed 2, which is twice as thick as the initial sludge deposit layer, were lower than Bed 5 in Phase 1 experiment. Figure 4.5 shows the overall flux peaks in Phase 1 and Phase 2 of experiments. The experiment's flux peaks were significantly higher in Phase 2 than in Phase 1. The continuous septage loading has increased the sludge deposit layer thickness

and led to waterlogging conditions. The filling of macropores in the sludge deposit layer decreased the layer permeability, which prolonged the surface ponding. Hence, the temporary ponding increased the hydraulic pressure acting on the bed surface, boosting the percolation rate.

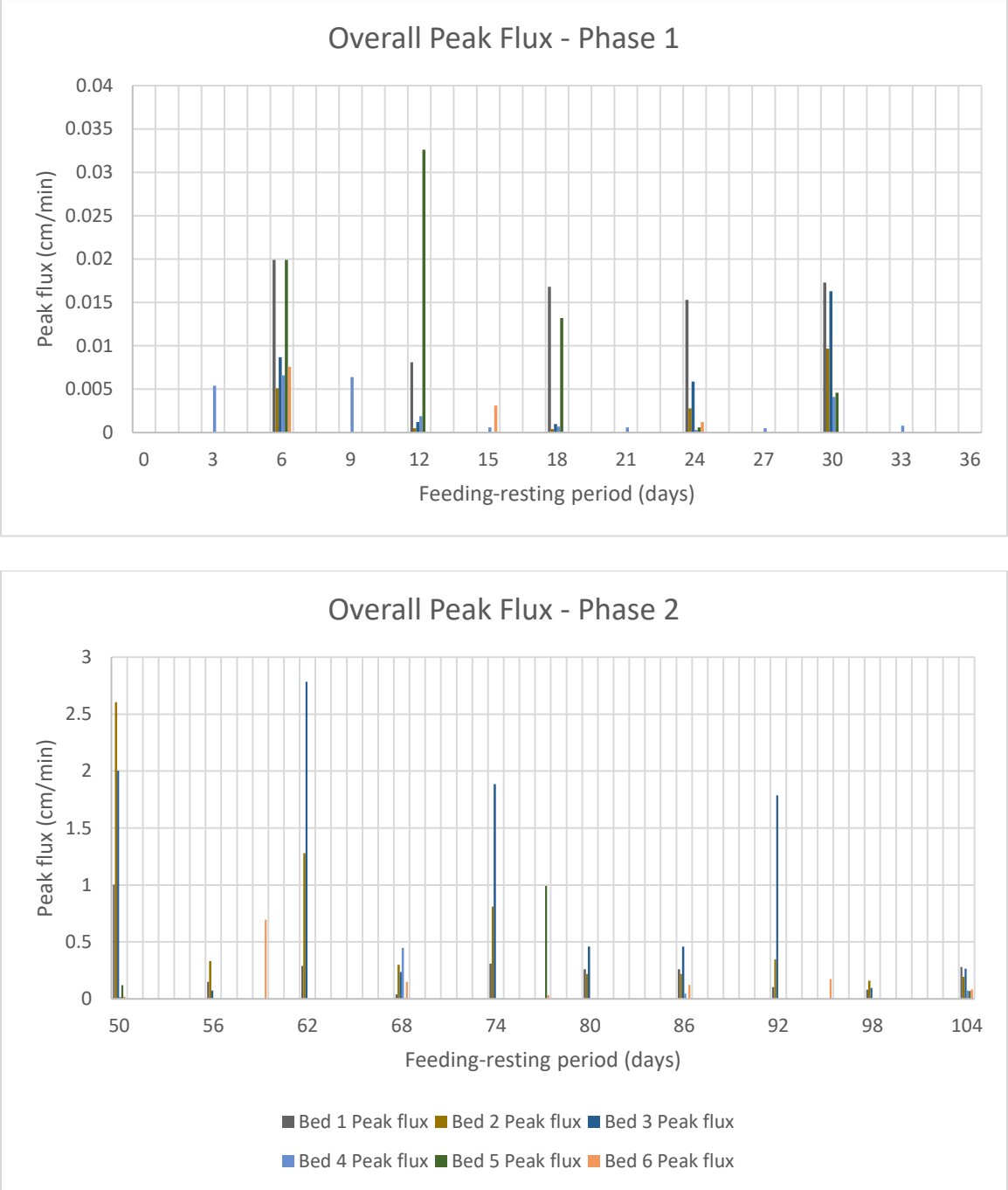

Figure 4.5: Flux peaks for each loading batch in Phases 1 and 2.

In STRB, the pressure head difference is the main driving force for the percolation process. Hence, the flux peak was proportionally increased with the sludge volume loaded, as shown in Figure 4.6. Using the generated trendline equations, it is then possible to estimate the flux peak from the known hydraulic load. However, further increment in hydraulic load did not significantly increase the effluent flux peak. The extra loads have suspended the effluent flow due to the clogging of the substrate layer upon particles settling on the thickened sludge deposit layer. In contrast, extraordinarily high fluxes were observed during an over-dried condition with crack occurrence on the sludge deposit layer (Khomenko *et al.*, 2019), as shown in Figure 4.1d. The cracks provide a PFP for the raw sludge to bypass the reed bed substrate filter, resulting in a high volume and instantaneous effluent discharge.

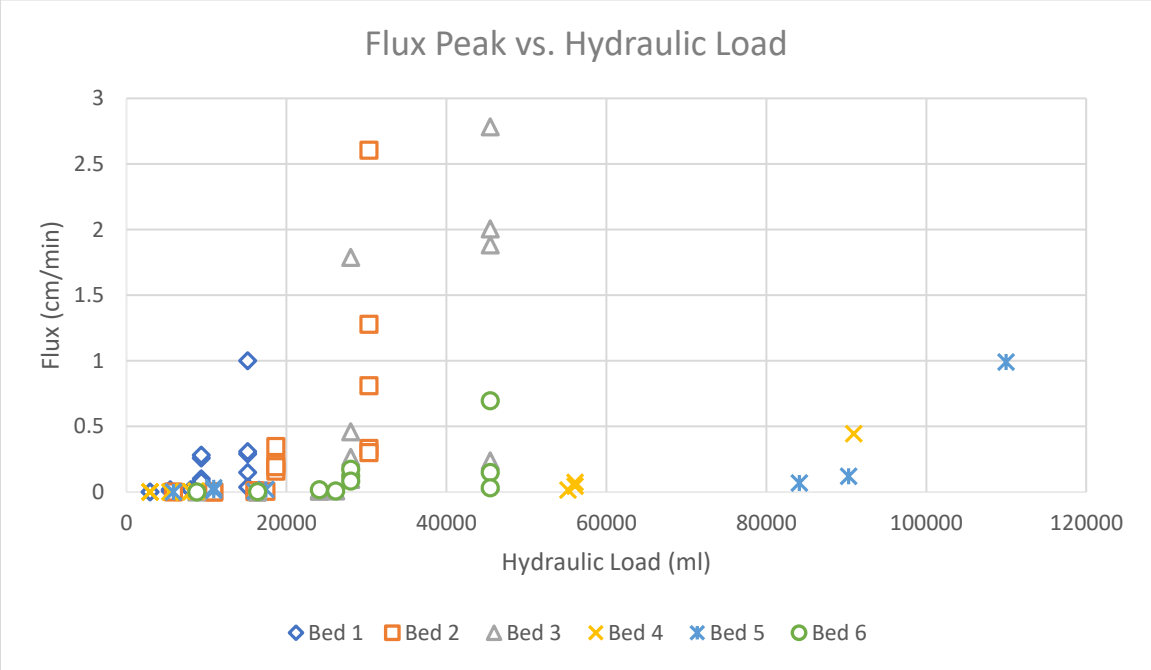

Figure 4.6: Graph of flux peaks versus hydraulic load.

4.2.2 Delay of Flow Occurrence

Generally, effluent discharge only occurs after the feeding in STRBs. It has been observed that there is always a delay between the time after loading and the start of discharge from the STRB outlet. This phenomenon is known as the delay of flow occurrence, depending on the reed bed's infiltration capacity. Also, the delay of effluent

flow can be used physically to estimate the bed's dryness, which indicates the reed bed's performance.

Furthermore, increasing the sludge deposit layer thickness could be another factor in the effluent flow delay. Typically, the delay in flow occurrence would present an increasing trend due to the continuous sludge accumulation, which inhibits the percolation process. The continuous sludge accumulation increases its thickness and specific resistance, whereas the incremental porosity allows more water to be detained within the layer. The newly loaded septage would then need to penetrate the less permeable sludge deposit layer before reaching the bottom of the bed, leading to longer flow delays. Figure 4.7 shows the overall flow delays in Phase 1 and Phase 2 experiments. In Phase 1 experiment, the overall flow delays in Bed 2 were longer than in Bed 5 due to the initial sludge deposit layer being twice thicker. Conclusively, the overall experimental results in Phase 1 showed an increasing trend of prolonged flow delays with the feeding-resting cycle.

However, the flow delays were significantly shorter in Phase 2 of the experiment. The flow delays of the first loading in Phase 2 of the experiment were comparable to those in Phase 1, where the beds rested for 2 weeks. The newly loaded septage required more time to fill up the dried reed bed and reach the bottom. Although continuous septage loading increased the sludge deposit thickness, the overall flow occurrence in Phase 2 was still swift (less than 10 mins). This was due to the waterlogging conditions of the prolonged resting period, where the septage retained from the previous loading batch increased the hydraulic pressure and enhanced the infiltration rate. On the other hand, cracks on the sludge deposit also boosted the discharge of flow-occurring where the influent septage directly bypassed the reed bed.

In addition, the flow delay can be analyzed through the initial TS concentration of the raw septage. A higher TS concentration of sludge would have a lesser water content. The low water content in the influent septage has lengthened the flow delay in the bed as less water percolated through the substrate medium. Inversely, the higher TS concentration would have led to more sludge deposited onto the bed surface, further

reducing the infiltration rate. Therefore, the higher the initial TS concentration of the septage, the longer the flow-occurring delay, as shown in Figure 4.8.

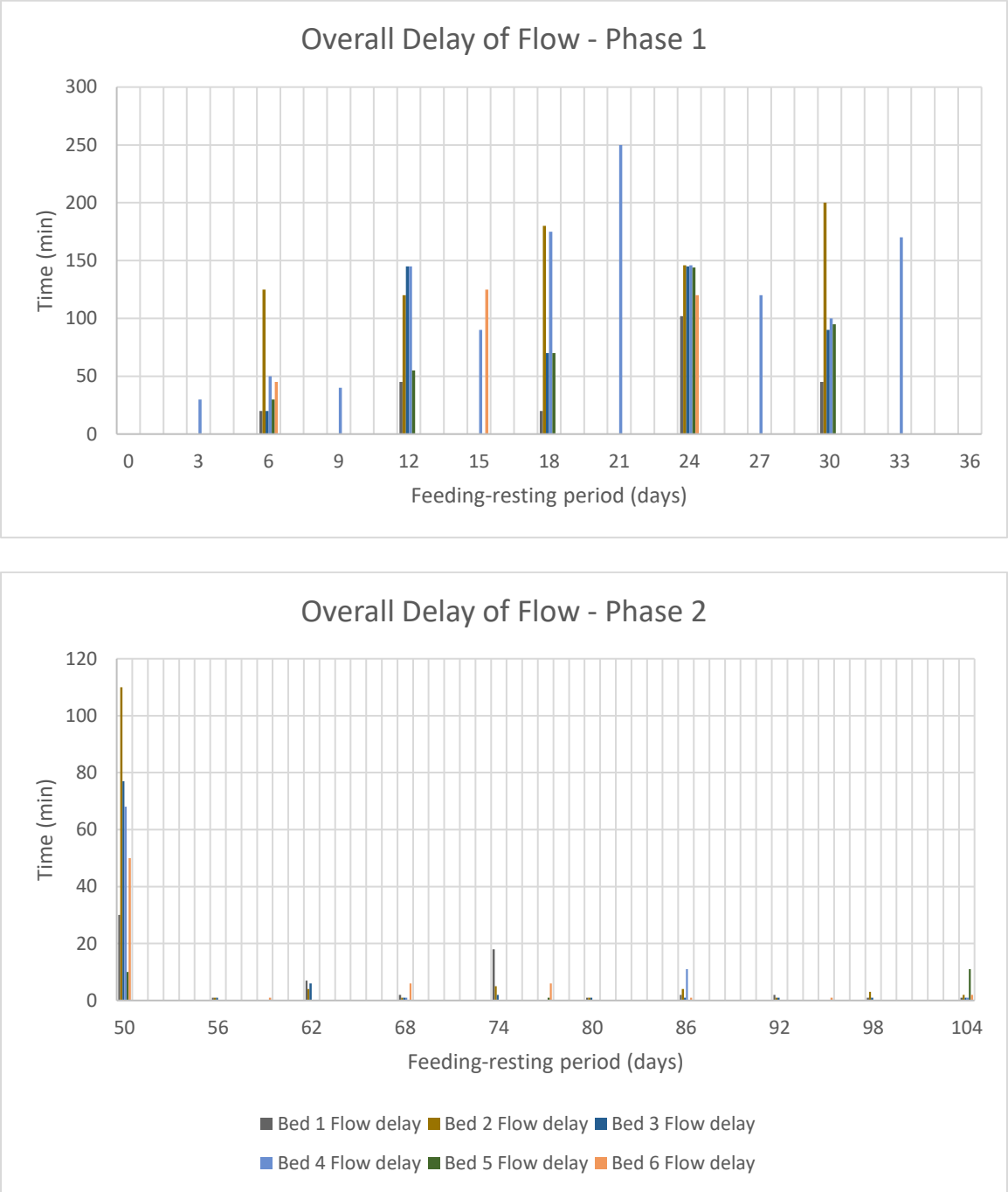

Figure 4.7: Delay of flow occurrence for each loading batch in Phases 1 and 2.

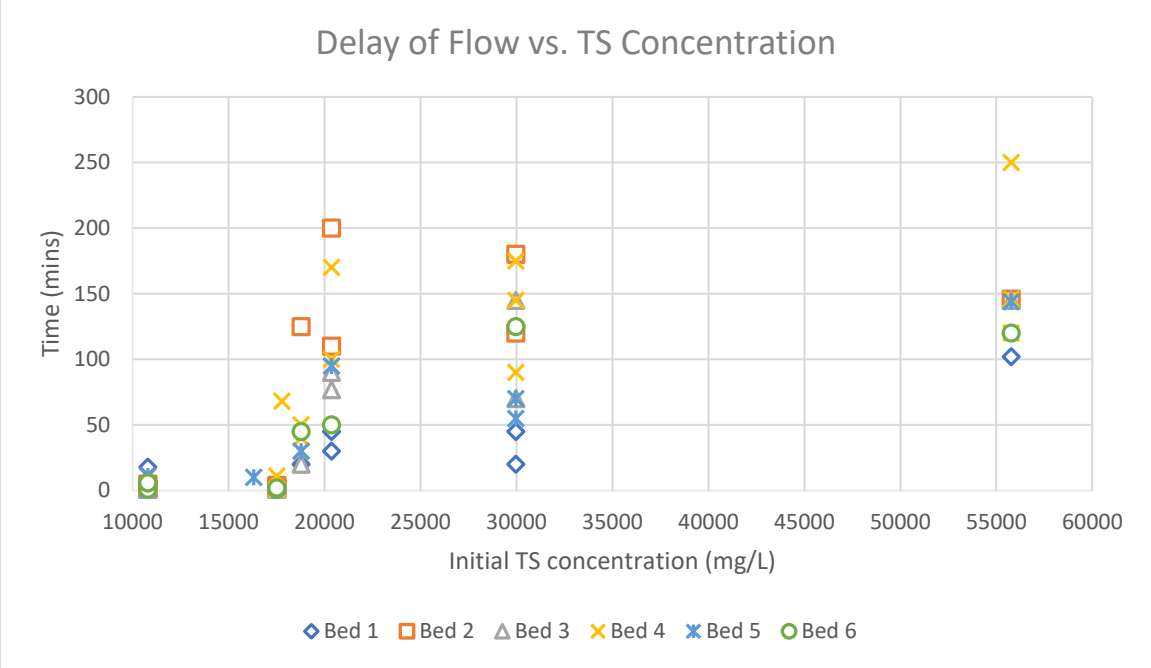

Figure 4.8: Graph of flow delay occurrence against influent solids concentration.

4.2.3 Water Recovery

Generally, the experimental results showed that the average water recovery from the outflow of the laboratory-scale STRBs was above 70%. The water recovery of the reed bed is believed to be related to the thickness of the sludge deposit layer. The increment of sludge deposit layer thickness would have retained more water, resulting in a lower recovery of effluent. Thus, the water recovery of each bed decreased with the incremental sludge deposit layer thickness in Phase 1 experiment, as shown in Figure 4.9.

Furthermore, Bed 2 was discovered to have a lower water recovery percentage compared to Bed 5 in Phase 1 experiment. This finding confirms that the bed with a thicker sludge deposit layer would have a lower water recovery. The best explanation is that the continuous sludge accumulation increased the sludge deposit layer thickness, thus retaining more water content. In other words, the high moisture content (MC) of the sludge deposit layer has greatly reduced the effluent volume, which further affected the total water recovery.

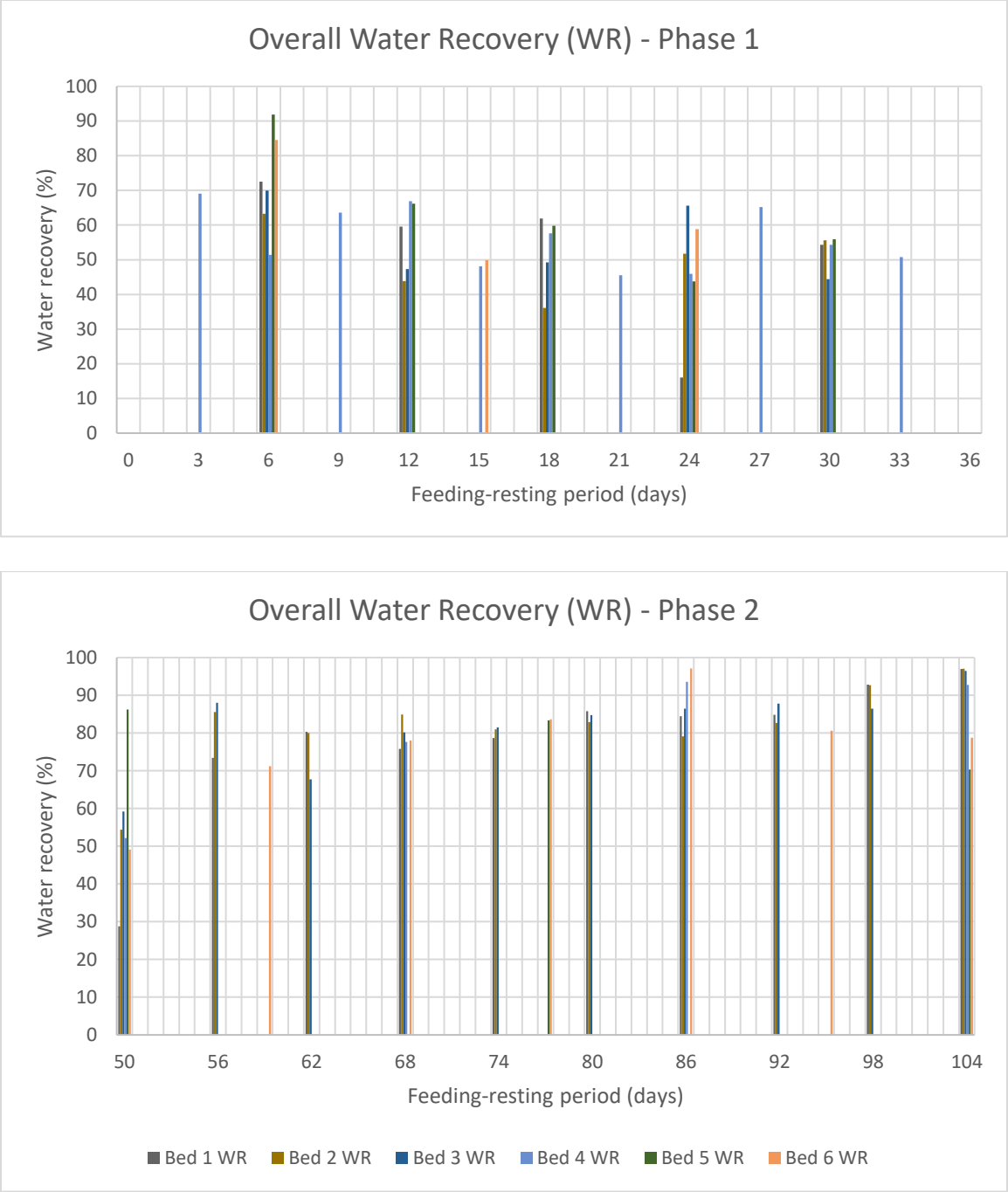

Figure 4.9: Water recovery for each loading batch in Phases 1 and 2.

However, the continuous feeding of septage in experiment Phase 2 led to an incremental water recovery over the experiments. The extensive increase in the sludge deposit layer thickness caused waterlogging conditions, thus retaining more water within the reed bed. Then, the retained water from the previous loading batch is drained together

with the new loading batch, thus improving the water recovery. Occasionally, the presence of cracks on the sludge deposit also increased the water recovery as the influent septage directly bypassed the reed bed.

Moreover, it has been determined that the percentage of water recovery was inversely proportional to the influent total solids content, as shown in Figure 4.10. The higher the influent TS, the lower the water recovery percentage at the end of each loading. The trending curve indicates a promising result, where a higher influent TS contained less water and led to a lesser amount of water being recovered. Hence, the water recovery from the STRB may be estimated using the known initial TS concentration of the septage.

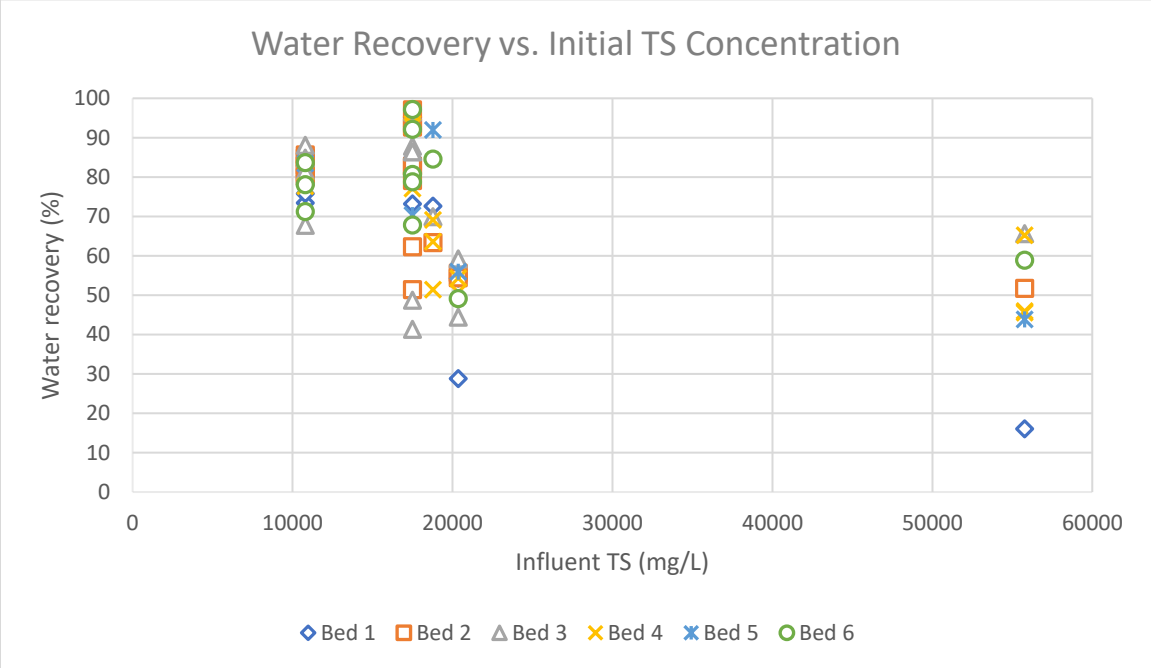

Figure 4.10: Graph of water recovery percentage versus influent total solids concentration.

Meanwhile, the optimum initial TS concentration of sludge for the water recovery was 15,000 to 20,000 mg/L. The highest water recovery percentage was 97.91%, via influent TS concentration of 18,780 mg/L. In comparison, the lowest was 16.04% when loaded with influent TS of 55,780 mg/L. It was unreasonable to have a full percentage recovery of water at the end of each loading, as there was always an occurrence of evapotranspiration by plants. The sludge deposit had removed some moisture through

instantaneous evaporation and leaf transpiration. The capillary action within the plant stem also aided the loss of water content. Additionally, the sludge deposit itself would have retained some of the moisture. In the case of a water recovery percentage beyond 100%, the incomplete drainage of the previous septage loaded is believed to have carried on to the subsequent treatment batch, leading to excessive water recovery.

4.3 Phase 1 Experiment

A one-month preliminary experiment (Phase 1) was carried out to determine the maturity of the newly operated laboratory-scale STRB-treating septage. Prior to the preliminary test, the reed beds were acclimatized for a month to ensure the adaptation of vegetation growth, as well as to develop a biofilm of bacteria in the sludge deposit and the substrate for better filtration capacity. After the acclimatization period, the sludge deposit layer and significant growth of reeds were observed. Figure 4.11 and Figure 4.12 show the reed growth before and after acclimatization, respectively.

Figure 4.11: The reed bed before acclimatization.

Figure 4.12: The reed bed after acclimatization.

After the acclimatization period, each bed was fed with a calculated volume of septage according to the SLR of its batch, where the TS concentration was determined through an oven test prior to the loading to calculate the sludge volume to be fed. This study focused on the effect of varying SLRs and resting periods on hydraulic dynamics, water recovery, effluent quality, and characteristics of sludge deposits. Generally, a waterlogging condition was observed on the bed surface upon feeding. Further, the

effluent discharge was assessed with flow-occurring delay, flux peak, and total water recovery. It is confirmed that the delay of flow occurrence is directly affected by the system maturity, where a thicker sludge deposit layer would have prolonged surface ponding, thus leading to a smaller flux peak and low water recovery (Khomenko *et al.*, 2019).

Moreover, raw septage contained high suspended solids and organic matter concentrations, but dissolved oxygen (DO) concentration was low. This study conducted a quality assessment of septage to evaluate the system maturity, including the influent and effluent concentrations of TS, chemical oxygen demand (COD), nitrate nitrogen (NO_3), pH, and DO. Figure 4.13 compares turbidity between the influent septage and effluent sample collected. The system's maturity can be observed from the turbidity removal in the effluent samples, where a significant purification was observed, representing the efficiency of physical treatment (S. Hu *et al.*, 2021). The filling of macropores in the substrate filter reduces the porosity and permeability of the STRB system, leading to better filtration efficiency. Another performance indicator is the reduction of organic matter in the effluent, demonstrating the efficiency of biological and chemical treatment mechanisms (Al Falahi *et al.*, 2021). The development of the bacteria enhances biological treatment as organic matter is extensively reduced upon consumption as food for growth. Furthermore, a continuous sampling approach was carried out to study the effect of hydraulic behavior and effluent quality, subsequently providing better insight into the overall performance of the proposed STRB system in treating septage.

Figure 4.13: Turbidity difference between raw septage (left) and effluent (right).

4.3.1 Thickness of Sludge Deposit Layer

The water lost to the atmosphere or percolated through the reed bed has reduced the thickness of the sludge deposit. Continuous loading of sludge onto the bed increased the actual thickness of the sludge deposit layer, forming a layer of film that hinders the percolation. Hence, it can be observed that the final layer thickness increased by roughly twice the initial thickness, as given in Table 4.2. It was noted that the attention that the initial thickness of each bed was fixed at 5 cm with 1 cm of allowance, and the thickness for Bed 2 would have doubled that of Bed 5. The increase in sludge deposit thickness reduced the system performance, as the percolation duration was lengthened due to the low infiltration rate.

Table 4.2: Thickness change of sludge deposit layer between initial and final of Phase 1 experiment.

Bed	SLR	Resting Period	Initial (cm)	Final (cm)	Difference (cm)
1	50 kg TS/m^2/year	6 days	5.33	7.50	2.17
2	100 kg TS/m^2/year		8.17	11.50	3.33
3	150 kg TS/m^2/year		4.50	11.33	6.83
4	100 kg TS/m^2/year	3 days	4.50	10.67	6.17
5		6 days	4.33	8.50	4.17
6		9 days	5.50	13.00	7.50

The main challenge in measuring the sludge deposit thickness is the exact sludge thickness during the ponding period. The dark color of the raw septage blurs the line between the ponding and the sludge deposit during the sedimentation of solids in raw septage. Ponding occurs on the surface of the reed bed after each loading, regardless of the initial sludge deposit thickness and SLRs. The ponding scenario is mainly due to the blockage of pores within the sludge deposit, which led to the temporary clogging in the bed. From observation, the reed bed was easily clogged when applying a larger volume of septage due to high SLR, where a significant volume of solids accumulates. However, this study also revealed that a prolonged ponding period on the bed surface was still observed when the raw septage had a high TS concentration, where the resulting hydraulic load based on the fixed SLR was small. This situation has negatively impacted the system performance, where the sludge dewatering relied more on evapotranspiration during the non-feeding period, leading to a longer time needed to reach desirable

dewatering efficiency. The effluent flow only occurred a few hours after feeding, exceeding the possible flow monitoring duration. Nonetheless, the subsequent effluents released were very clear in color, and contained lesser total solids and organic matter due to the slow effluent flux that resulted in a longer treatment duration in the bed.

The thickness of the sludge deposit layer decreased gradually with the ponding level after each loading batch due to drainage and evapotranspiration, as indicated in Figure 4.14. The detailed illustrations of the sludge deposit layer thickness for each bed are presented in **Appendix L**. The difference in sludge deposit layer thickness was in the range of 2 to 8 cm. The lowest final thickness was attributed to Bed 1, where the SLR was relatively small, yet the resting period was long enough to maintain the minimum moisture of the bed. In this case, cracks commonly happen due to dryness. The continuous loading of septage onto Bed 4, with the shortest resting period of 3 days, has increased much of the thickness and is comparable to that of Bed 6 with 9 days of resting period. In contrast, Bed 6 had the highest thickness difference of 7.5 cm, due to the higher SLR with the longer resting period of 9 days. The relatively higher SLR provided more septage to have retained on the bed surface, thus increasing the thickness significantly. In addition, the difference between the final thickness of Beds 2 and 5 was in an acceptable range of 1 cm.

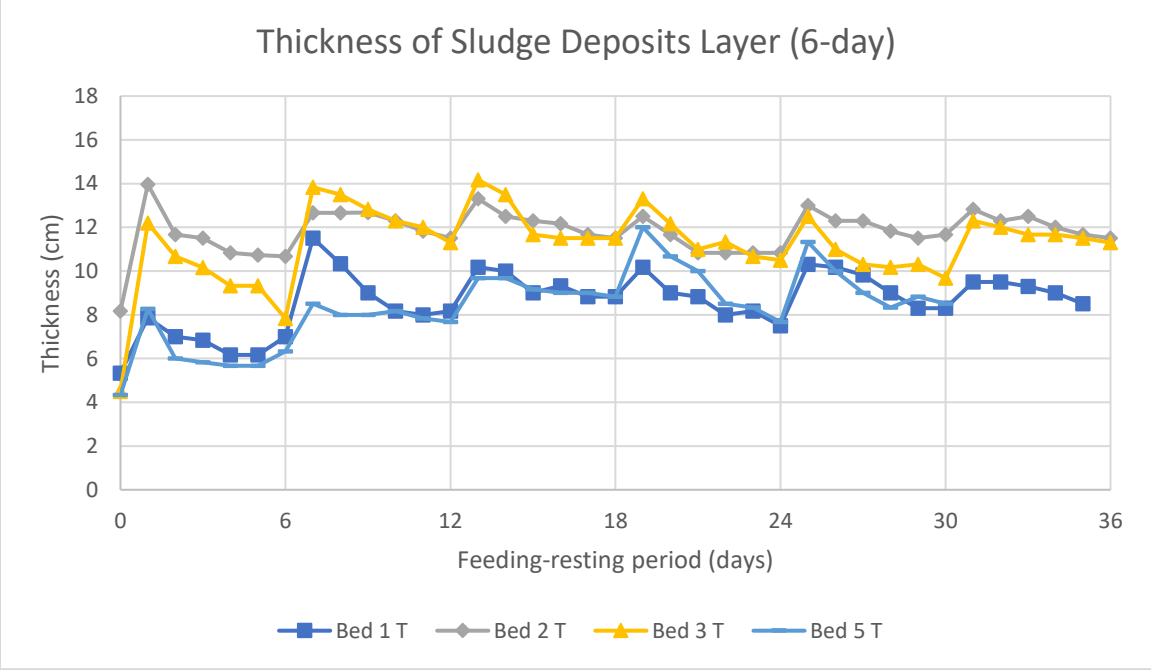

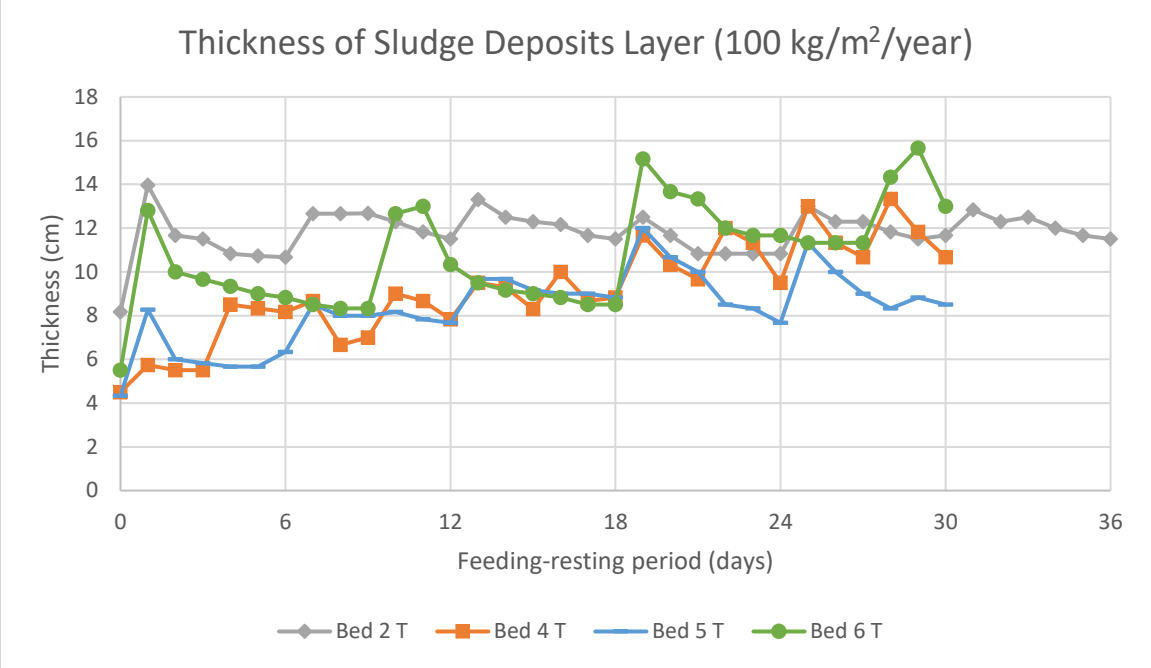

Figure 4.14: Thickness of sludge deposit layers in Phase 1 under varying SLRs and resting periods.

4.3.2 Moisture Content (MC) and Total Solids (TS) Content of Sludge Deposit

The sludge deposit's MC showed a gradual decline during the resting periods. The loss of MC in the sludge deposit directly increases the TS content. The TS content is the remaining portion of the MC in the sludge deposit. Thus, the MC of the sludge deposit is inversely proportional to the TS content, as illustrated in Figure 4.15 and Figure 4.16. Detailed illustrations of the MC and TS content of the sludge deposit for each bed are presented in **Appendix M** and **Appendix N**.

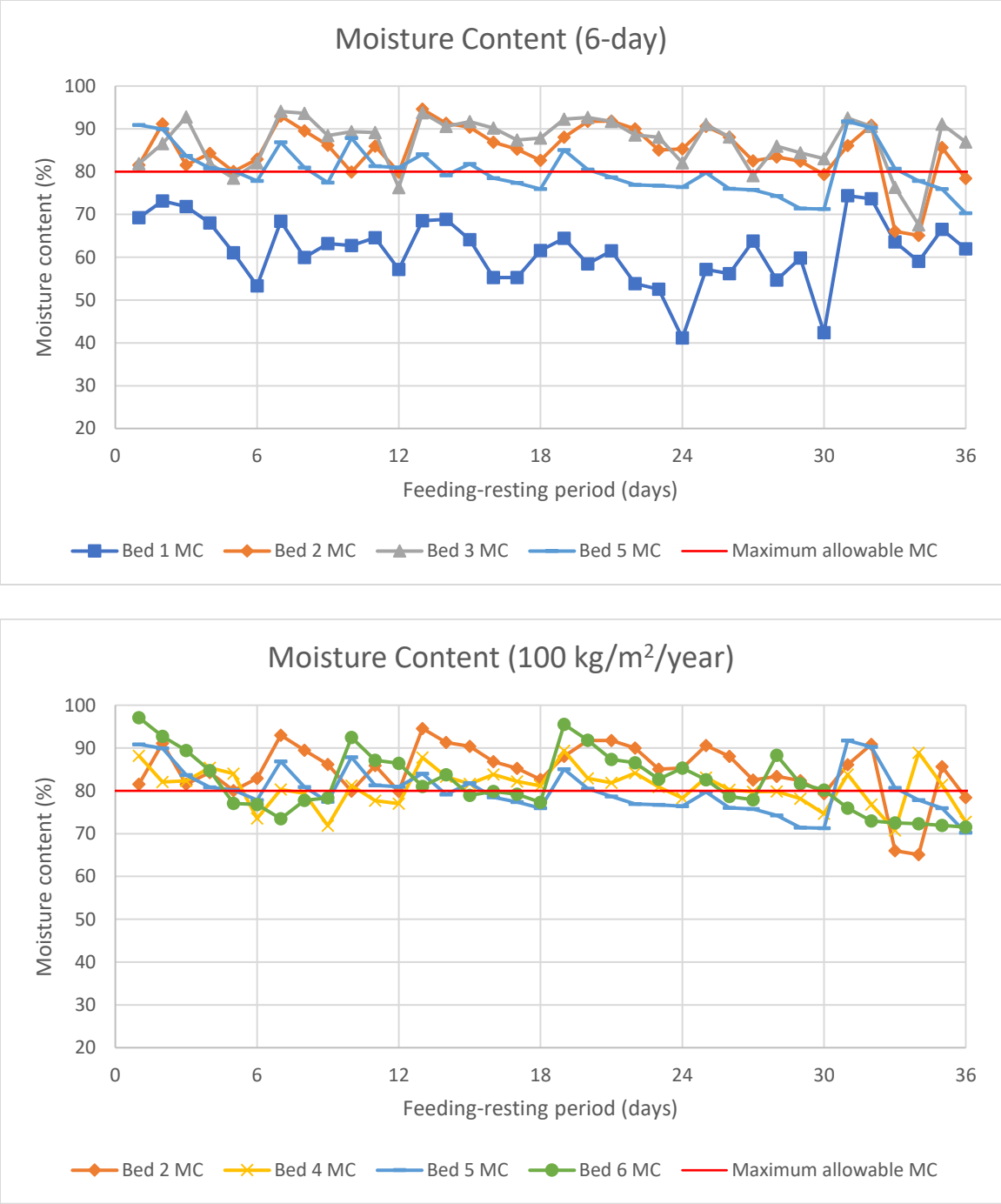

Figure 4.15: Moisture contents (MC) in Phase 1 under varying SLRs and resting periods.

Moreover, it was also observed that the MC directly relates to the thickness of the sludge deposit. The decrease in MC causes a reduction in sludge deposit thickness during the resting period. The decrease in the MC collapses layer pores, deforming the layer and shortening its thickness (Ghanbarian, 2021). The minimum TS content for final dried

solid sludge disposal is 20%, as determined by the Malaysian government (SPAN, 2008). Hence, this standard is crucial to describe the performance and reliability of the reed bed system. Based on the preliminary experimental results, only some of the TS content was found to obey the minimum requirement of 20%. Therefore, continuous analysis of the effect of variation in SLRs and resting periods on the MC and TS contents of the sludge deposit is critical for selecting an optimum operating regime.

Nevertheless, Bed 2 has a higher overall MC than Bed 5. Similarly, the total solids content of Bed 2 was lower than that of Bed 5. The difference in MC could be due to the different initial sludge deposit thicknesses used to operate the system. Regardless of the continuous deposition of sludge onto the sludge deposit layer, the thicker initial thickness layer would have provided more voids for water molecules to contain within the layer (Trein *et al.*, 2019). As a result, the MC for Bed 2 with the thicker initial thickness was high and comparable to that of the high SLR conditions of Beds 3 and 6. Further, the decrease in the MC also reduces the amount and development of bacteria due to dryness, increasing the organic content in the layer (Al Falahi *et al.*, 2021). As a result, the total volatile solids increased.

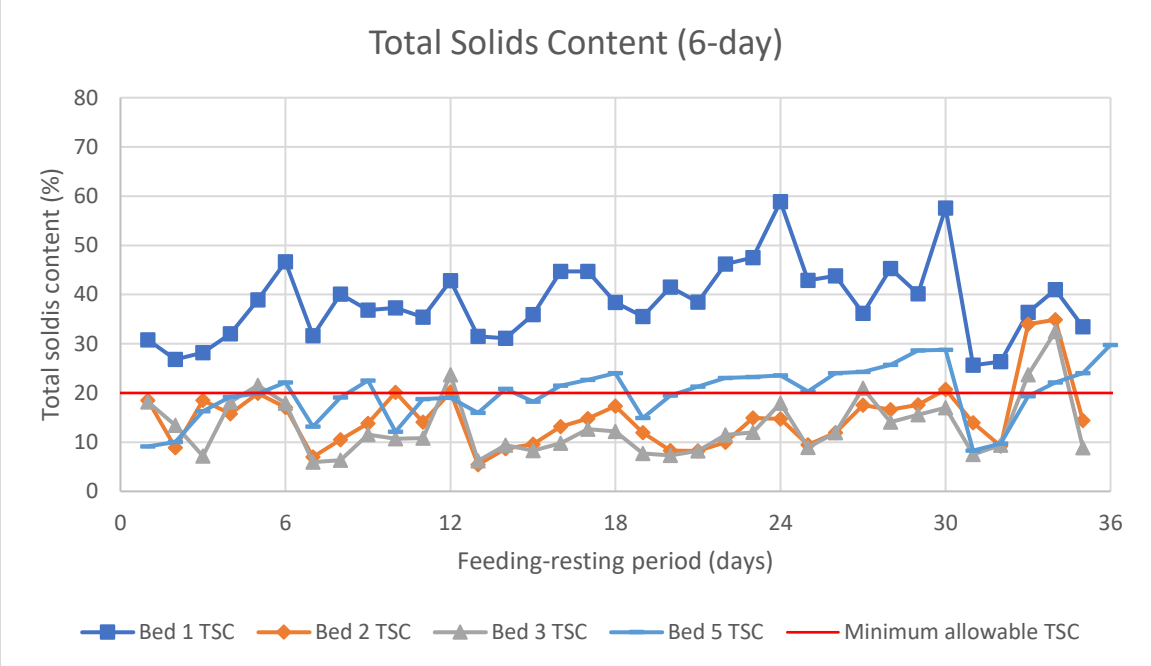

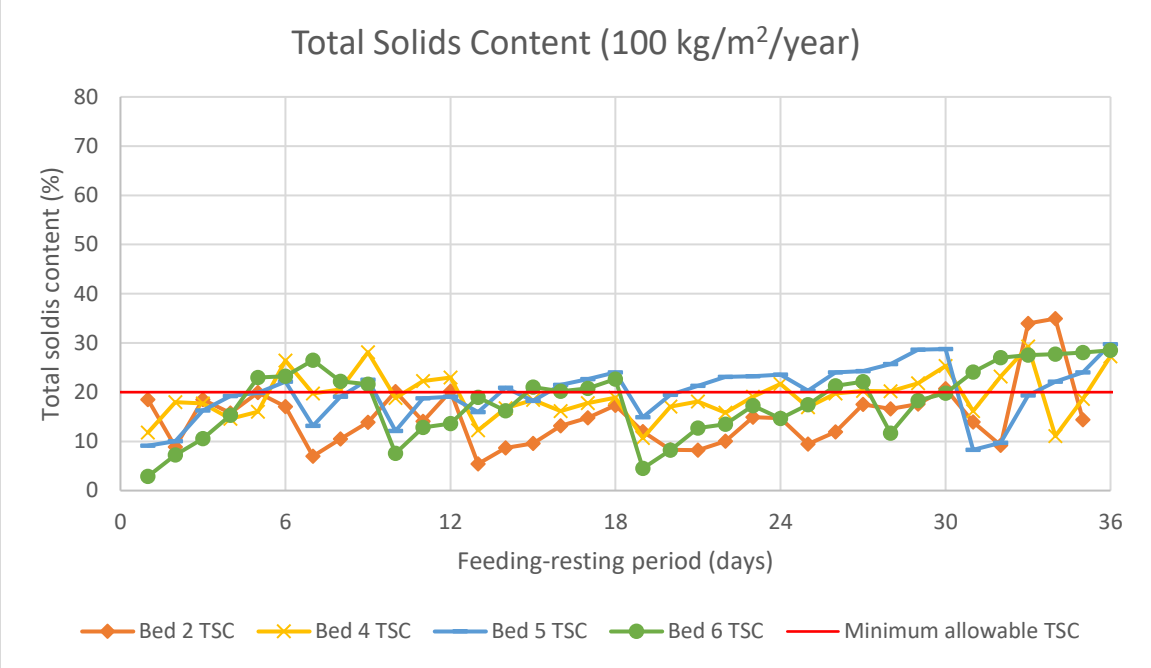

Figure 4.16: Total solids (TS) contents in Phase 1 under varying SLRs and resting periods.

4.3.3 Total Volatile Solids (TVS) Content of Sludge Deposit

The TVS content of the sludge deposit is organic matter deposited on the surface layer of the reed bed. The TVS contained in the sludge deposit were found to be much less than the total solids content. These semi-solids in the raw septage are deposited onto the sludge surface layer. Many microorganisms, especially bacteria, were growing in this layer and the substrate filter. These bacteria can decompose the organic components into finer products by consuming the essential nutrients for their growth (Pham *et al.*, 2021; Presti *et al.*, 2021; Wang *et al.*, 2018). Hence, the TVS content was observed to be directly proportional to the TS content in the sludge deposit. The TVS content gives a similar trend of gradual rise throughout the resting period, as shown in Figure 4.17. The detailed illustrations of the TVS content of the sludge deposit for each bed are presented in **Appendix O**. The increasing TVS content over the resting period was caused by the mineralization of nutrients in the sludge deposit. Thus, the sludge deposit layer has become more concentrated with organic matter.

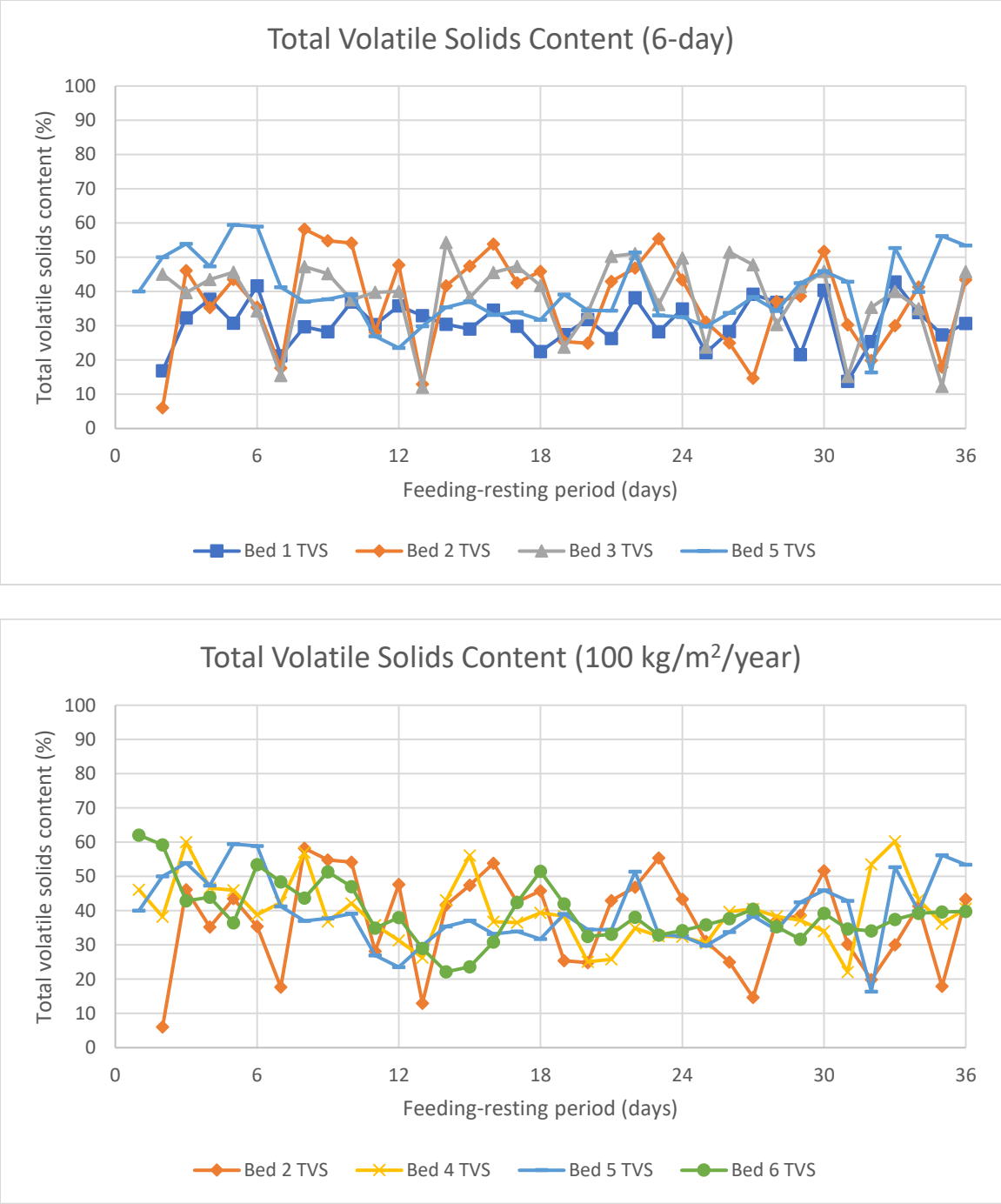

Figure 4.17: Total volatile solids (TVS) contents in Phase 1 under varying SLRs and resting periods.

Typically, continuous loading of raw septage keeps the bed in wet condition, at which the percentage of the TVS content should remain constant (Usman Khan & Kiaer Ahring, 2020). The TVS content is high under optimal SLR and resting period due to

sufficient moisture that maintains the entity of the sludge deposit layer. However, many factors affected the situation, such as the weather conditions, and sludge deposit layer cracks (Zhang *et al.*, 2020). For instance, the TVS content is low during rainy days due to high air humidity that decrease overall evapotranspiration rate, and under the presence of cracks in the sludge deposit layer where the influent septage bypasses the reed bed. In this case, the percentage of TVS content in the sludge deposit is a straightforward indicator of the organic matter removal, where a lower TVS content represents a better performance of the reed bed system, subject to initial TS concentration and quality of the raw septage used. This is because the highly concentrated septage is rich in organic matter and contains less moisture.

4.3.4 Chemical Oxygen Demand (COD) of Effluent

As a common indicator of water quality in wastewater treatment, the COD concentration directly represents water pollution by means of the organic matter contained in the wastewater. In this reed bed system, the COD concentration was measured to decrease daily and was expected to be constant at the end of the treatment, as shown in Figure 4.18. The substantial reduction of the COD in the first loading compared to the initial COD concentration indicates that the reed bed system was acclimatized well, where the bacteria have decomposed much of the organic matter. Detailed illustrations of the COD concentration of the effluent quality for each bed are presented in **Appendix P (a)**.

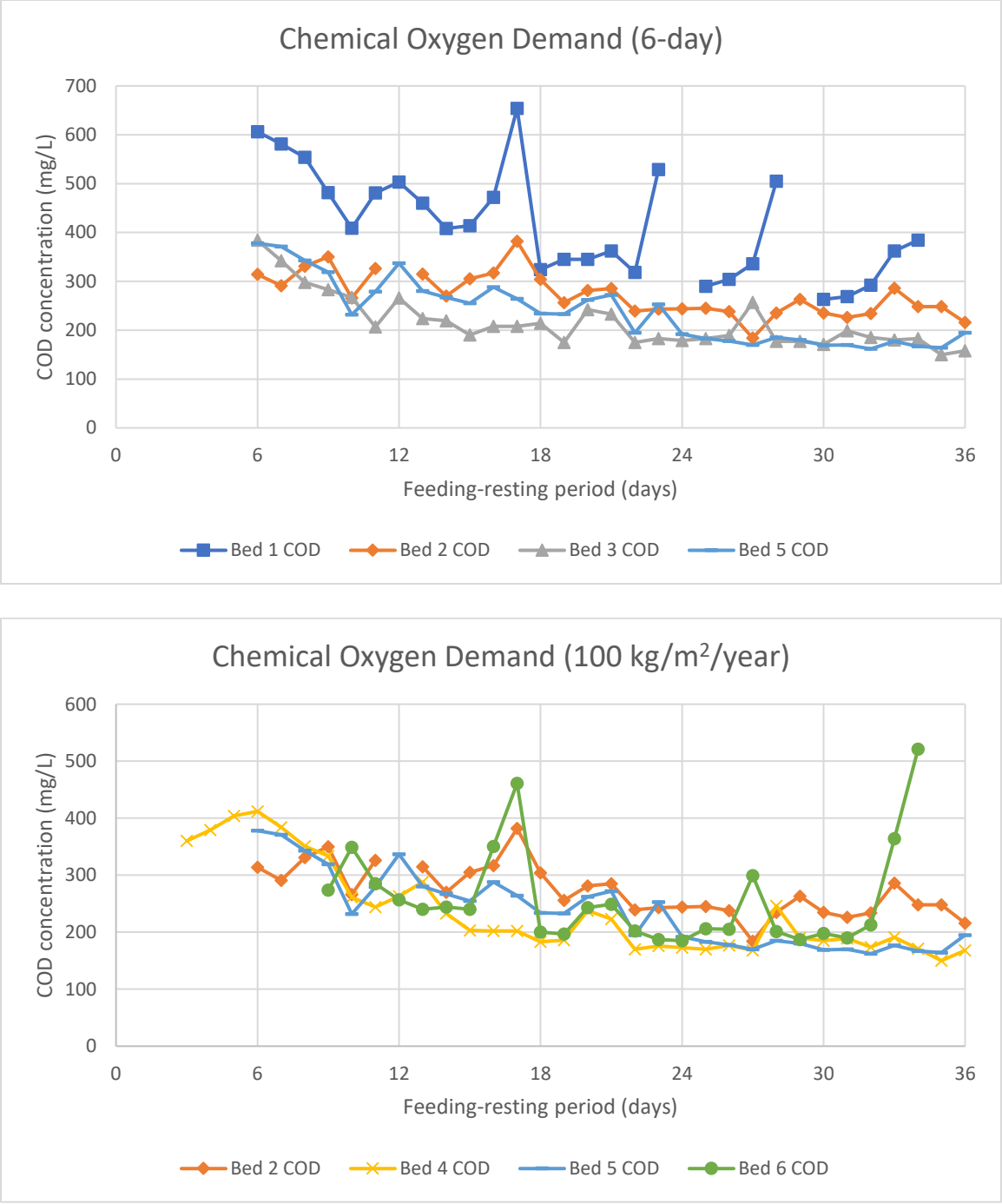

Figure 4.18: Chemical oxygen demand (COD) concentrations in Phase 1 under varying SLRs and resting periods.

In contrast, the first loading in Bed 4 produced a different trend, in which the COD increased to a constant state at around 400 mg/L. This is because the reed bed was very new and freshly loaded with the first batch of raw septage, where the essential

microorganisms had yet to be fully developed and covered the porous medium of the substrate filter. Hence, the thin sludge deposit contained less bacteria, producing poorer filtration efficiency. The growth of the bacteria in the substrate filter and sludge deposit is crucial to decomposing the organic matter. The COD decreased from batch to batch throughout the experiments and eventually remained at a concentration between 150 and 250 mg/L, except for Bed 1. Conclusively, the COD concentration has an inversed relationship with the sludge deposit layer thickness.

In addition, it was also noticed that the COD concentrations shot up to a significant value towards the end of some batches of loading. This situation was commonly found in Bed 1 due to the low SLR and insufficient MC. The bed could not maintain its overall moisture over a longer resting period. The bed was entirely drained before the given resting period, where the daily effluent collection could not be done continuously. In this case, the sludge deposit layer was found to be cracked for the subsequent loading. Thus, the revived COD concentration was mainly due to the untreated effluents that bypassed the system upon the occurrence of cracks. Also, the decline of effluent volumes towards the end of the resting period, at which the samples contained more organic matter than water content, aided the situation.

4.3.5 Nitrates (NO_3) of Effluent

The concentration of NO_3 is representative of organic nitrogen in the wastewater. The nitrogen source could be from ammonia, ammonium, and NO_3 itself. The nitrification and denitrification process in the nitrogen cycle has caused the amount of NO_3 to vary throughout the experiments (Bhattacharya & Mazumder, 2021; Jia *et al.*, 2020; Thakur & Medhi, 2019). However, the most reasonable tendency of the NO_3 concentration is described by a gradually increasing trend, as displayed in Figure 4.19. The detailed illustrations of the NO_3 concentration of the effluent quality for each bed are presented in **Appendix P (b)**.

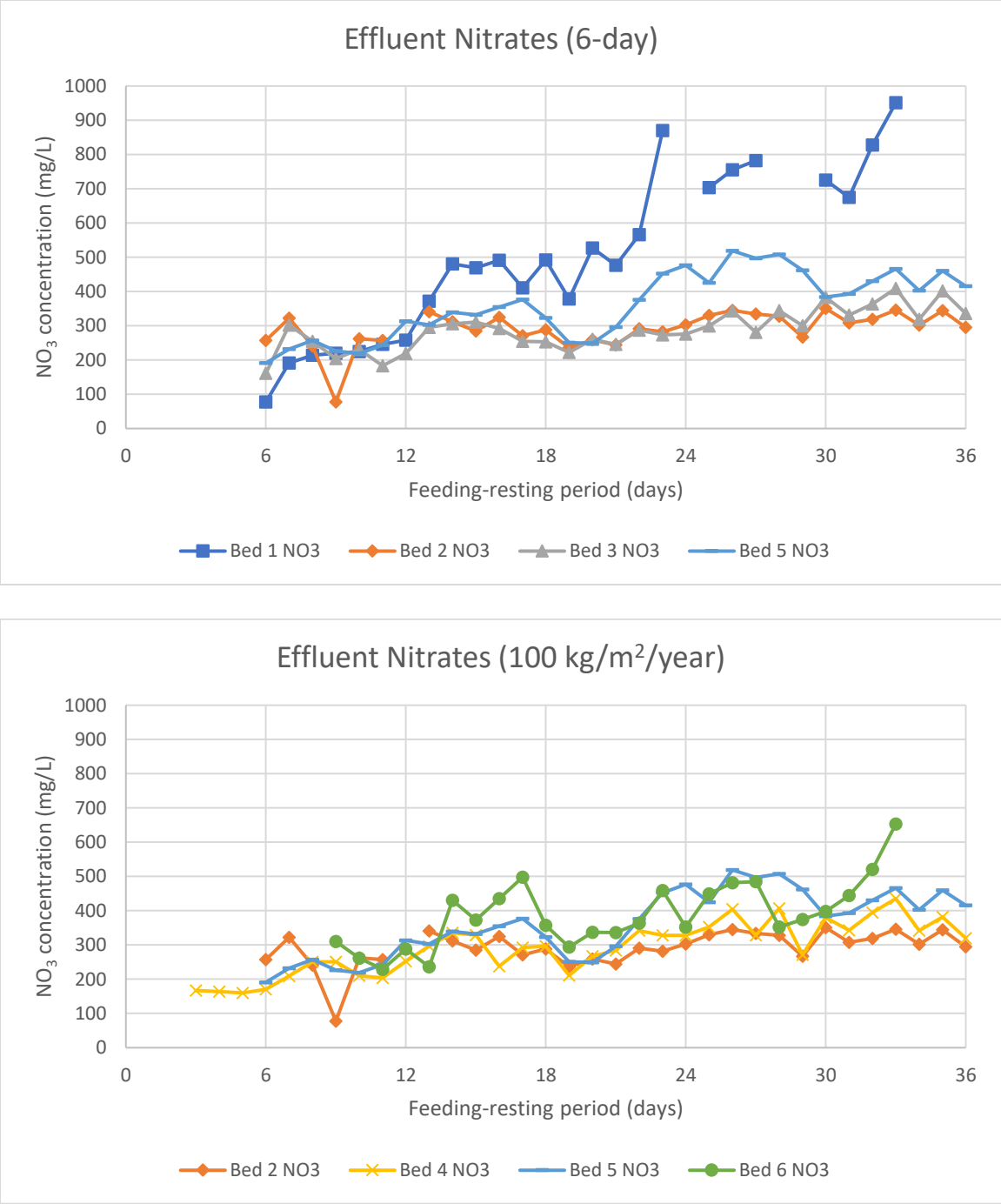

Figure 4.19: Nitrates (NO_3) concentrations in Phase 1 under varying SLRs and resting periods.

In contrast to COD, the amount of NO_3 concentration gradually increased. The main reason for the increment was the increase in the thickness of the sludge deposit layer. The thicker layer would have provided more bacteria to decompose the organic

matter in the sludge deposit, thus further decreasing the COD but boosting the NO_3 concentration in the meantime. The thick sludge deposit layer also detained the raw septage for a longer time. It allowed only a small amount of water to percolate through the biofilm slowly, further enhancing the treatment duration. From the observation, Bed 1 has the highest overall NO_3 concentration compared to the other beds. The relatively low SLR for Bed 1 ensured a thorough septage treatment, where the organic matter was mainly wholly treated. However, a lower NO_3 amount was observed in Bed 2 compared to Bed 5 despite its thicker sludge deposit layer. The possible explanation is that the nitrification and denitrification process was unbalanced, resulting in opposite outcomes of the experiment.

Moreover, it was also found that there was a direct inversed relationship between COD and NO_3 concentrations, where the lower the COD, the higher the amount of NO_3 (Ghasemi *et al.*, 2024). However, a similar trend was observed in the TVS content of the sludge deposit, at which the NO_3 concentration increased from batch to batch of feeding cycles until it settled on a constant concentration of about 350 mg/L, except for Bed 1. In this case, the reed bed has partially matured and developed, operating optimally.

4.3.6 pH of Effluent

The pH is one of the most common indicators to evaluate the strength of water quality. This study observed a consistent pH from 6 to 8, as illustrated in Figure 4.20. Detailed illustrations of the pH value of the effluent quality for each bed are presented in **Appendix P (c)**. The overall trend of the pH value was discovered to change from slightly acidic to slightly alkaline throughout the experiment. The neutral or somewhat alkaline circumstance is the most favorable to the denitrification of nitrate (Lei *et al.*, 2019).

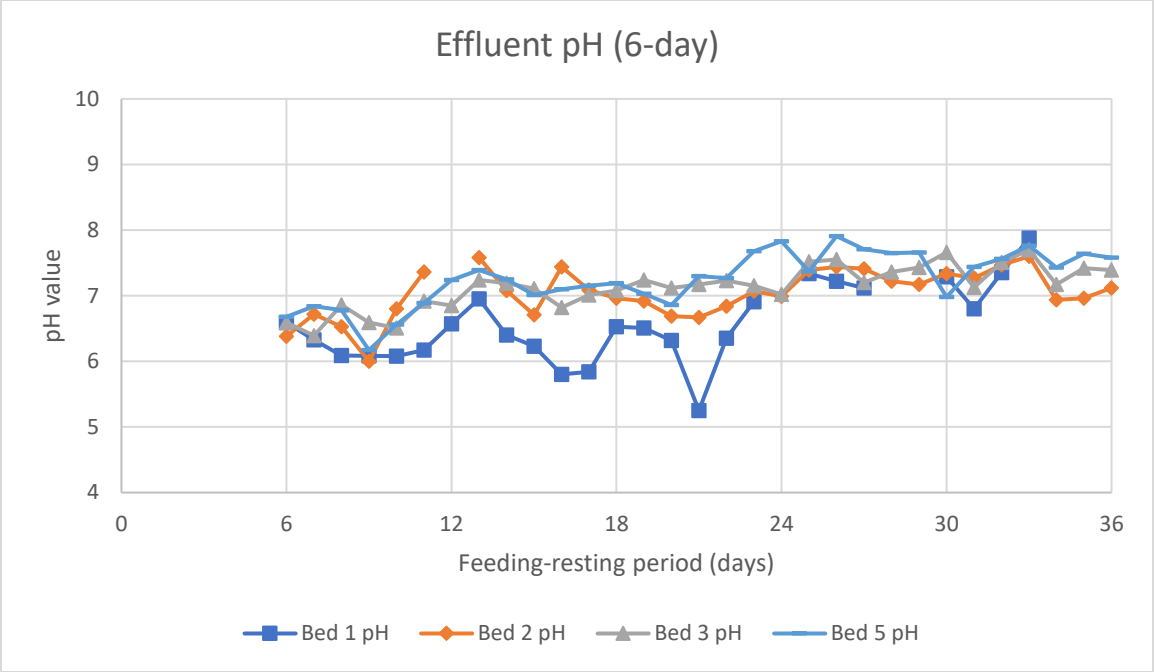

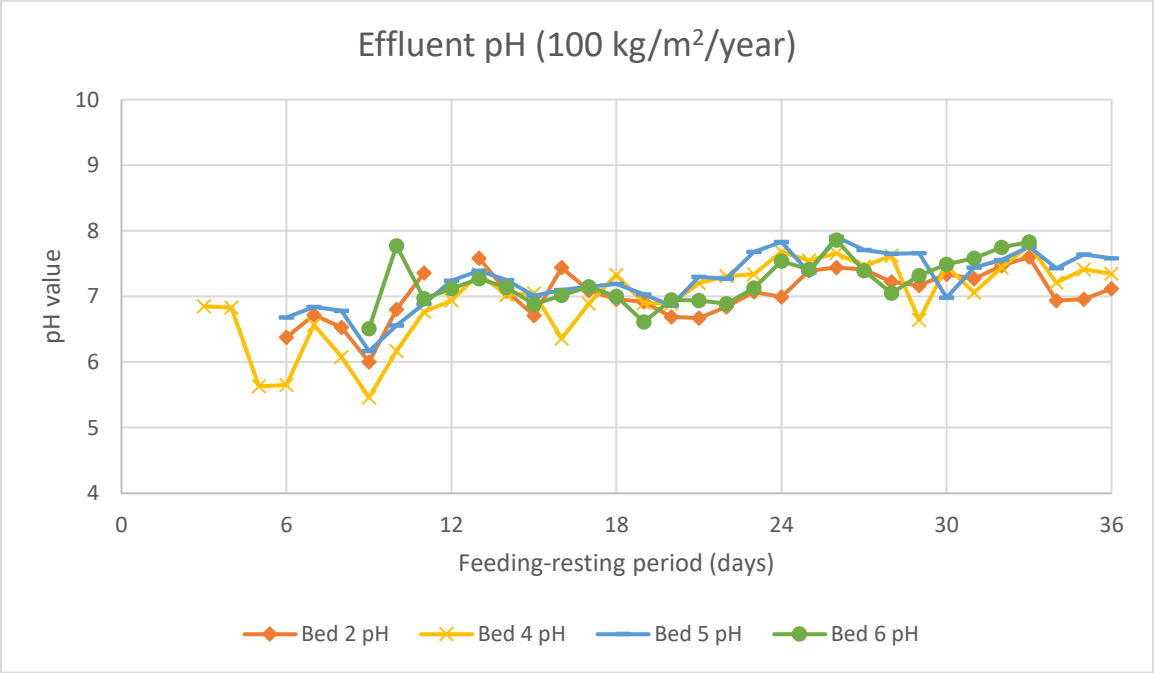

Figure 4.20: pH values in Phase 1 under varying SLRs and resting periods.

4.3.7 Dissolved Oxygen (DO) of Effluent

The DO is the oxygen contained in any water sample. It was observed that the DO concentration was initially around 0.5 mg/L. It increased to approximately 8.5 mg/L at

the end of Phase 1 experiment, as indicated in Figure 4.21. The high DO saturation concentration could be due to sufficient aeration pipe installation, optimal atmospheric pressure and temperature (Wang *et al.*, 2020). The detailed illustrations of the DO concentration of the effluent quality for each bed are presented in **Appendix P (d)**.

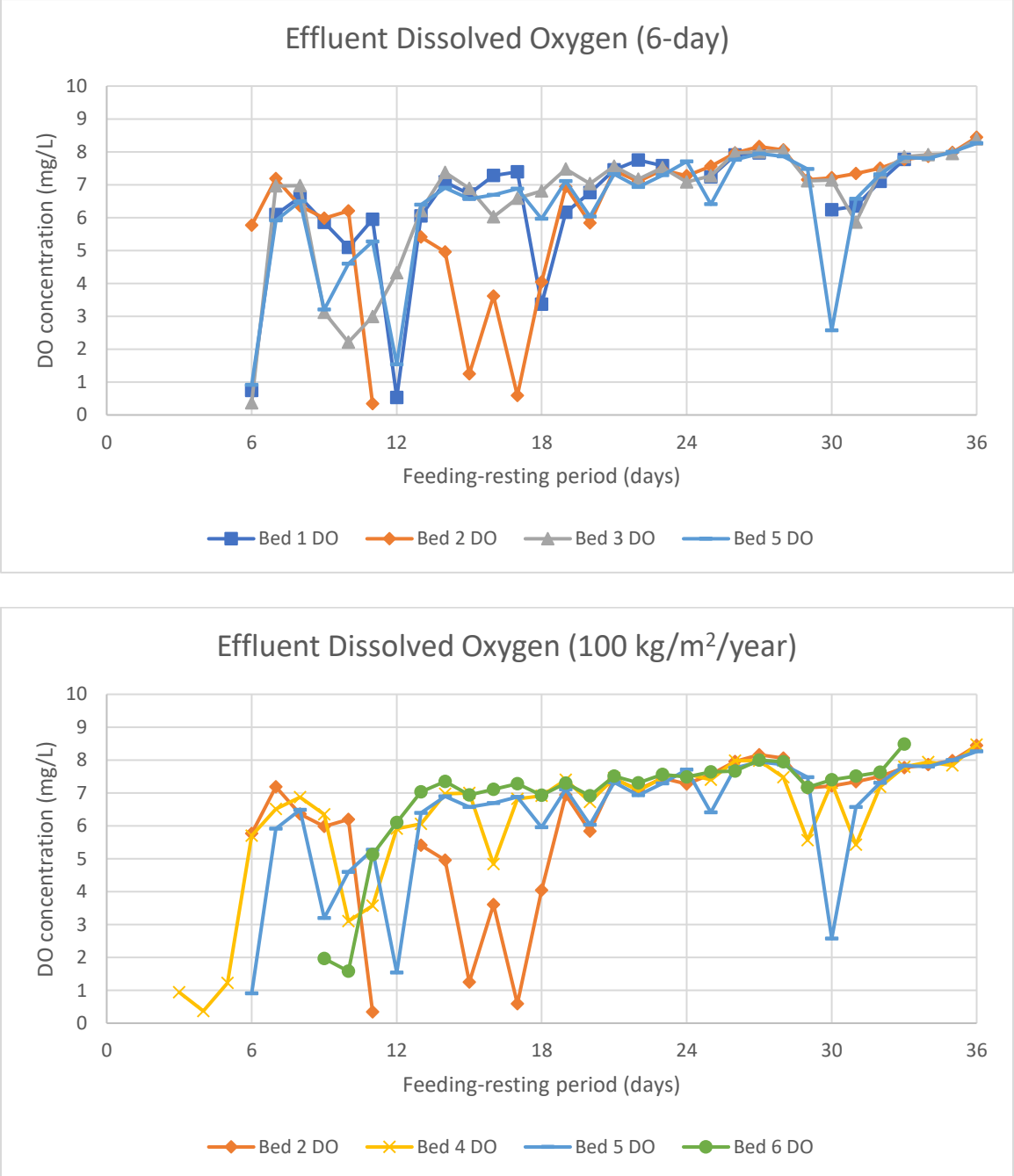

Figure 4.21: Dissolved oxygen (DO) concentrations in Phase 1 under varying SLRs and resting periods.

From the observation, the DO concentrations also increased from batch to batch, aligned with the increment of sludge deposit layer thickness. In this case, the difference in the initial thickness did not significantly affect the DO recovery, but the growth of bacteria in the sludge deposit layer played a crucial role. The growth of bacteria facilitates aerobic degradation of organic matter and nitrification of ammonium, resulting in an instantaneous reduction of oxygen demand in the upper layer of the treatment reed beds. Therefore, the treated leachate can percolate across the bed and dissolve the oxygen released from the aeration pipes, increasing the DO concentration in the effluent. Thus, the development of bacteria has only reached a maximum capacity towards the end of Phase 1 experiment. In such a scenario, the reed bed operates at its optimum performance.

The development and growth of nitrifying bacteria have yet to initially overcome the amount of DO produce (Guo *et al.*, 2019; Thakur & Medhi, 2019). In other words, denitrification theoretically overtakes the nitrification process at the early stage, resulting in a lower maximum DO concentration. Under aerobic respiration, where nitrification occurs, ammonia oxidizes to nitrate in the presence of oxygen. However, the excess amount of DO indicates that the nitrifying bacteria was the limiting factor to hinder the process from occurring (Raboni *et al.*, 2020; Wang, Bengtsson, *et al.*, 2019; Wang *et al.*, 2020).

Moreover, it was observed that the DO concentration was stabilized after the second batch of loadings. In this case, the production and aeration of DO has reached saturation, where the amount of DO was discovered to be within the range of 8 to 9 mg/L. Hence, the DO recovery and consumption for bacteria's growth have reached equilibrium.

4.3.8 Total Solids (TS) of Effluent

Throughout the treatment processes, the total solids collected from the effluent were measured to increase slowly before dropping significantly for each batch of loadings, as shown in Figure 4.22. The detailed illustrations of the TS concentration of the effluent quality for each bed are presented in **Appendix P (e)**.

In analyzing the effluent TS concentration, the change in thickness of the sludge deposit layer failed to show an effect on the removal efficiency. Typically, the TS concentration would decrease with incremental sludge deposit layer thickness. However, neither the initial thickness of the sludge deposit layer nor its increase as the experiment progressed impacted the effluent TS removal; the leading influencer was the climate effect on the sludge deposit. For instance, there were cases where the sludge deposit cracked under hot climates, and the influents bypassed the reed bed filter completely. Only some solid particles were detained on the sludge deposit and substrate filter, while the rest were discharged from the bottom of the bed. A possible trend for such a situation occurred for all beds during batches on days 30 to 36. Additionally, this situation was revealed to commonly happen for cases with low SLR and short resting periods, where the reed bed was loaded with a lesser amount of sludge, containing relatively small water content, leading to the possible crack on the sludge deposit due to dryness. The effluent TS concentration gradually reduced as the reed bed system pores were filled with these solids. The temporary clogging of pores in the sludge deposit and substrate filter has enhanced the treatment performance but lengthened the treatment duration. As a result, the TS concentration found in the effluent declined drastically.

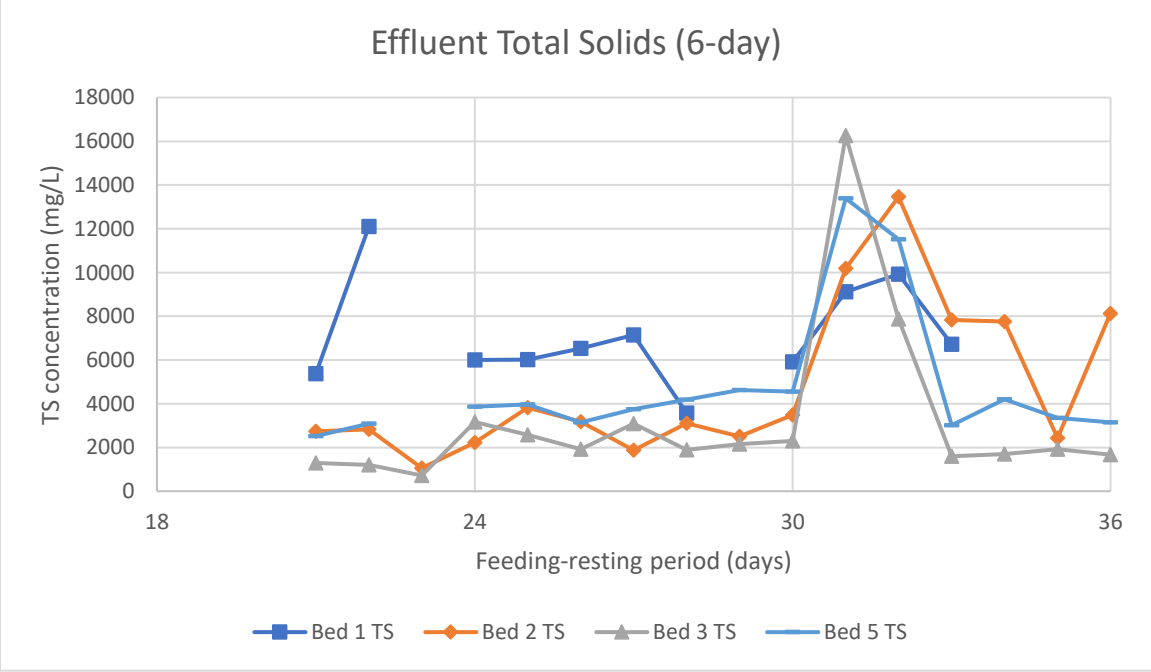

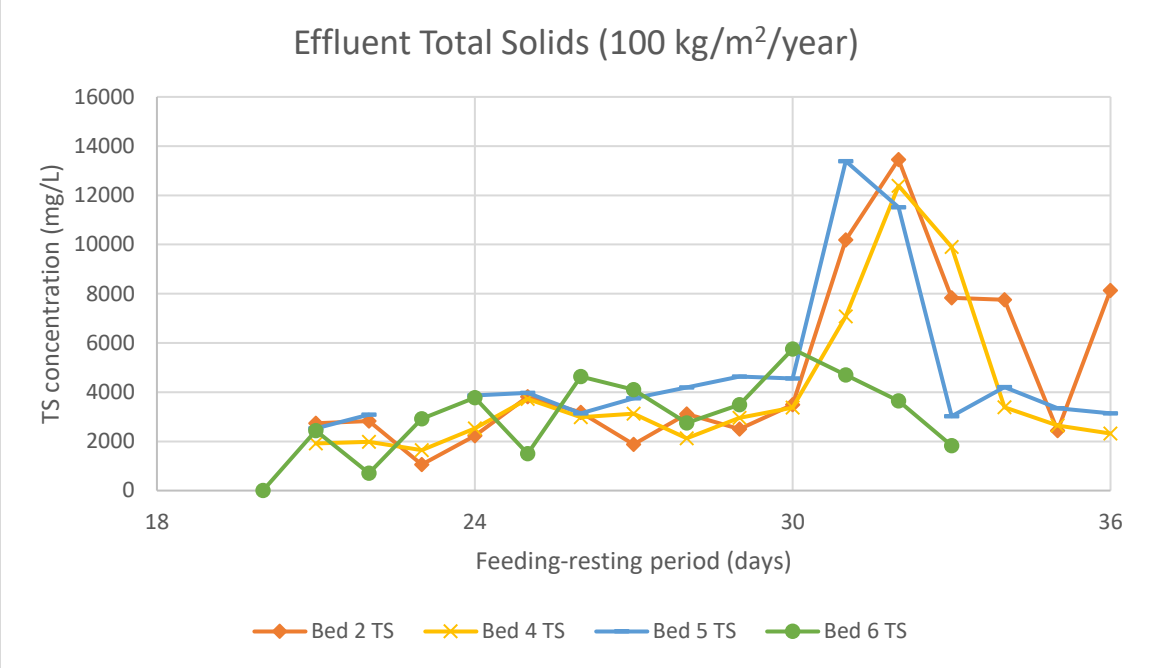

Figure 4.22: Total solids (TS) concentrations in Phase 1 under varying SLRs and resting periods.

Along the batches of loading, the possibly solid particles in the sludge have settled on top of the sludge deposit layer and substrate filter, potentially clogging the filter medium. The permanent blockage of the porous medium has reduced the percolation flow but enhanced the treatment efficiency of the reed bed system. Therefore, the TS removal efficiency improved throughout the treatment process.

4.3.9 Overall Treatment Performance

The physical treatment efficiency can be observed through the alteration in characteristics and properties of the sludge deposit. The MC and total solids (TS) content of the sludge deposit provided insight into the treatment performance of the bed. Table 4.3 shows each reed bed's average final MC and TS content.

Generally, the average final TS content in the sludge deposit was above 20%, except for Beds 2 and 3. Theoretically, the results for Beds 2 and 5 should be identical, as the SLR and resting period applied were the same. However, the difference in initial sludge deposit layer thickness has caused the average MC to differ. Certainly, Bed 2,

with a thicker initial thickness, would have a larger capacity to detain more water molecules within the bed. Thus, the average TS content was lower than that of Bed 5.

Table 4.3: Average final moisture content and total solids content for each reed bed in Phase 1 experiment.

Reed Beds	Initial Thickness (cm)	Average Moisture Content (%)	Average Total Solids Content (%)
Bed 1 (50@6)	5.33	51.12 ± 9.04	48.88 ± 9.04
Bed 2 (100@6)	8.17	82.00 ± 2.45	18.00 ± 2.45
Bed 3 (150@6)	4.50	82.26 ± 4.11	17.74 ± 4.11
Bed 4 (100@3)	4.50	78.48 ± 4.24	22.47 ± 4.24
Bed 5 (100@6)	4.33	77.53 ± 3.52	23.51 ± 3.52
Bed 6 (100@9)	5.50	77.86 ± 0.52	22.14 ± 0.52

In contrast, Bed 1 produced the best removal of water content in the sludge deposit, with 48.88% of TS content in the final solids. However, the exceptionally high quality of the solid produced indicates that the bed was yet to reach its optimum performance, as the productivity is low. Hence, this explains that the SLR of the raw septage should be increased to achieve its maximum possible loading capacity. Considering Beds 4, 5, and 6, the average TS content was above 20%, thus smaller standard deviation was considered. From the results, the operating conditions for Beds 5 and 6 were selected as the most optimal operating regime. The resting periods of 6 and 9 days of Beds 5 and 6, respectively, have revealed that the reed beds could treat the SLR of 100 kg/m^2/year from 6 days resting period and above.

Furthermore, the average total volatile solids (TVS) content for each bed was above 30%, as displayed in Table 4.4. In this case, Bed 1 showed the highest TVS content of 35.03% in the sludge deposit. This indicates that the bed was highly mineralized and contained abundant nutrients and microorganisms due to the longer resting period. A relatively low SLR shortens surface ponding, allowing more oxygen reaeration and leading to the development of bacteria for further decomposition of organic matter. Occasionally, Bed 2 had a relatively high TVS content compared to Bed 5 with the same loading regime. This was likely caused by the thicker initial sludge deposit layer in Bed 2, which contained more space and moisture for the growth of microorganisms. Hence, the experimental results indicate that the SLR of 100 kg/m^2/year,

with a resting period of 9 days and a 5.5 cm sludge deposit layer, was favorable for the mineralization process.

Table 4.4: Average final total volatile solids content for each reed bed in Phase 1 experiment.

Reed Beds	Initial Thickness (cm)	Average Total Volatile Solids Content (%)
Bed 1 (50@6)	5.33	35.03 ± 7.60
Bed 2 (100@6)	8.17	44.81 ± 6.07
Bed 3 (150@6)	4.50	42.35 ± 5.86
Bed 4 (100@3)	4.50	41.42 ± 11.97
Bed 5 (100@6)	4.33	38.56 ± 13.94
Bed 6 (100@9)	5.50	47.73 ± 6.33

The overall effluent treatment performances of COD removal, NO_3 recovered, pH value, DO recovered, and TS removal for three cases of initial TS concentration are presented in Figure 4.23 to Figure 4.27, respectively.

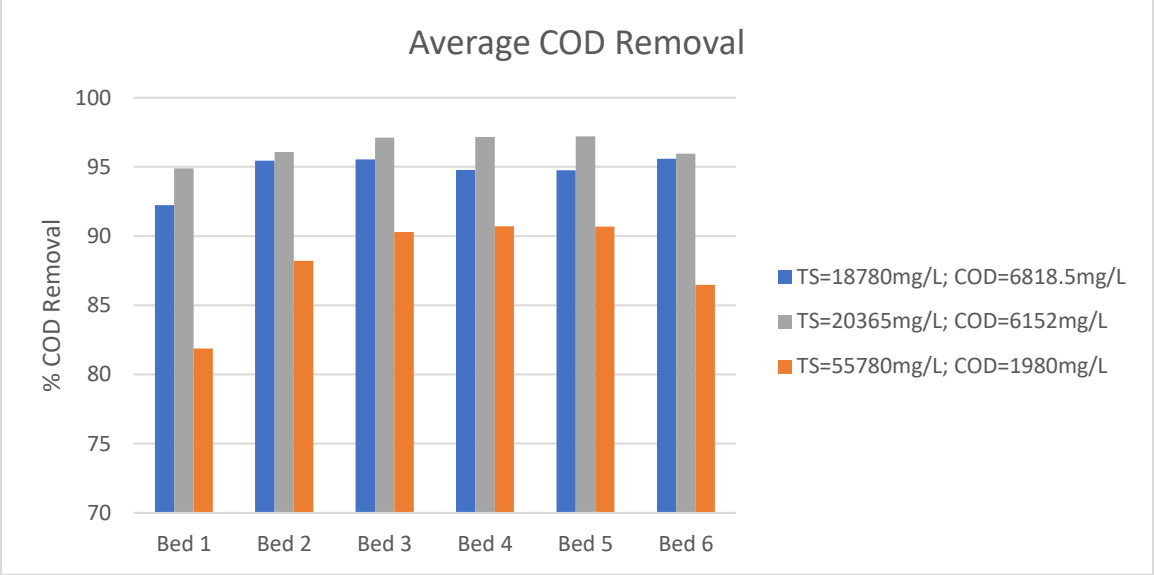

Figure 4.23: Average percentage of COD removal in Phase 1 experiment.

Generally, the overall COD removal percentage was above 80%, subjected to the initial TS concentration. It is believed that the higher the initial TS concentration, the higher the treatment performance. However, a roughly 5 to 15% reduction in COD removal was observed when the initial TS concentration was increased from approximately 20000 to 55000 mg/L. Hence, the raw sludge quality greatly affected the

COD removal compared to the initial TS concentration. By observing the reed bed system's different conditions, Beds 3, 4, and 5 produced the most optimum bed performance. The average COD removal for the mentioned beds was beyond 90% for all three cases of initial TS concentration.

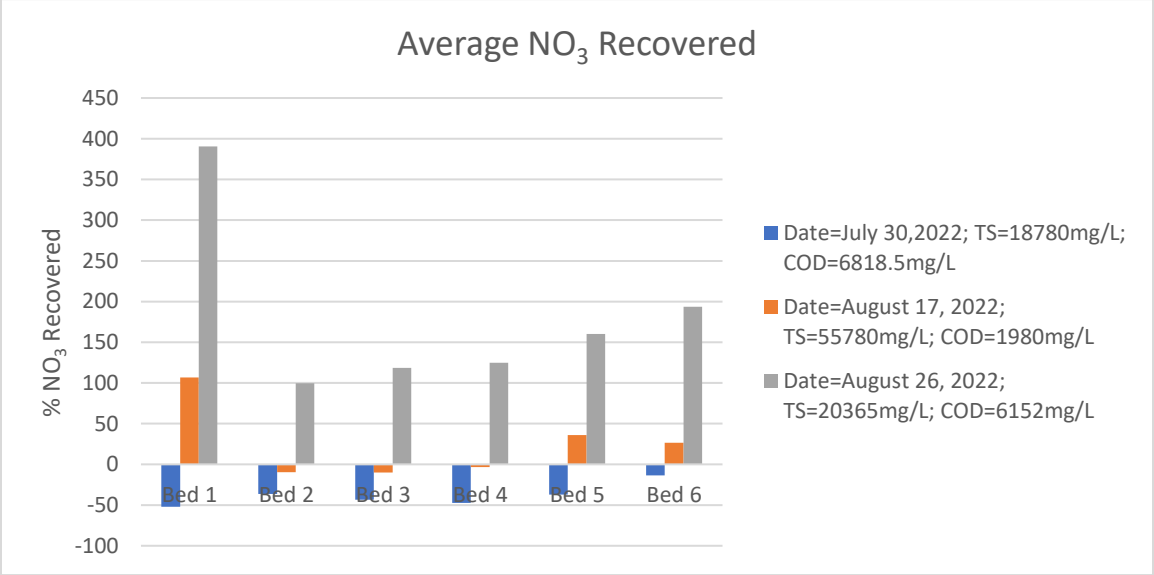

Figure 4.24: Average percentage of NO_3 recovery in Phase 1 experiment.

Further, the overall NO_3 recovered percentage was found to be unclear. Some of the percentage recoveries of NO_3 were calculated to be in terms of negative values. In this case, the NO_3 was removed instead of recovered due to the insufficient development of nitrifying bacteria. Typically, nitrification oxidizes ammonia to nitrate, positively increasing the NO_3 content. However, denitrification and ammonification processes dominated the nitrification. Under anaerobic conditions where denitrification occurs, nitrate reduces to molecular nitrogen without oxygen (Thakur & Medhi, 2019). The denitrification process reduces the amount of NO_3 content drastically. Thus, the amount of NO_3 produced was reasonably low enough to recover the consumption of NO_3 by denitrifying bacteria. Therefore, it can be observed that all the percentages of NO_3 recovery for each bed indicated a negative value in the first few batches of loading. As the experiment progressed, the NO_3 recovery improved to a positive value in the effluent. These positive values indicated that the conditions were favorable for the growth of bacteria, and septage treatment performed well in the reed beds.

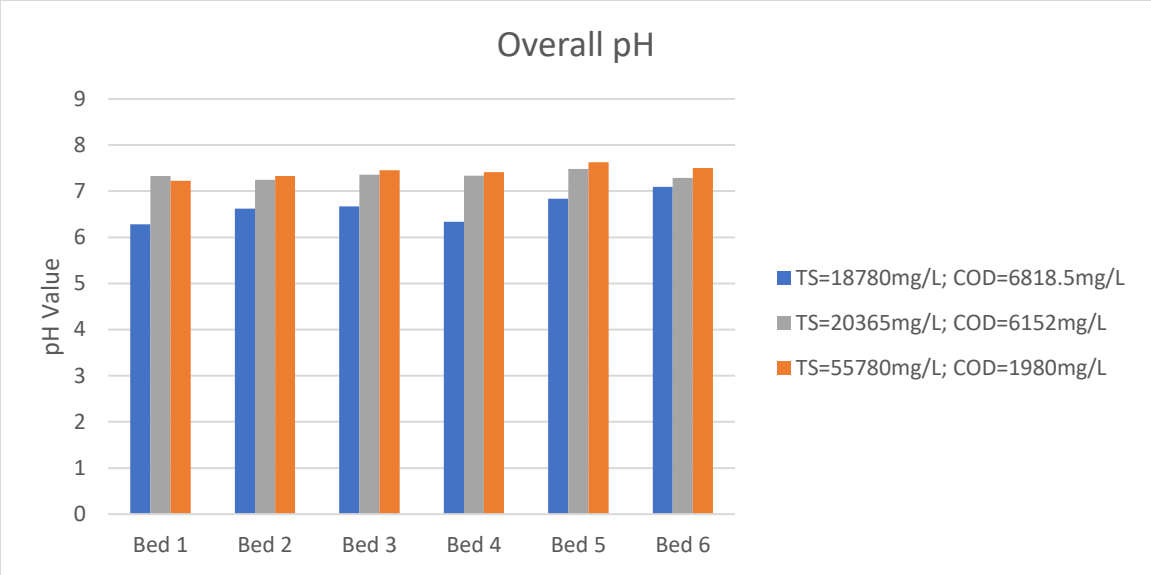

Figure 4.25: Overall pH value in Phase 1 experiment.

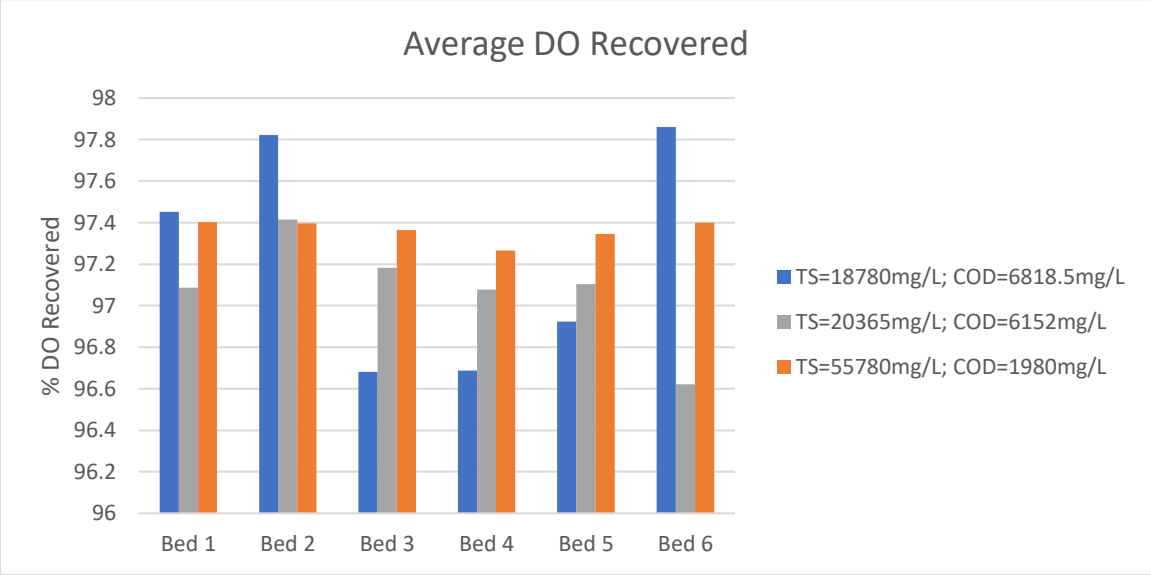

Figure 4.26: Average percentage of DO recovery in Phase 1 experiment.

The average pH values in the range of 6 to 7.5 described the effluent as neither acidic nor alkaline. Therefore, the results suggest that wastewater treatment by the reed bed has no apparent effect on the pH value of the treated effluent, as this is a chemical-free treatment process.

Moreover, the average percentage of DO recovery for all three initial TS cases was above 96.6%. A very high percentage of DO recovery indicated that the reed bed

was sufficiently aerated, where the development of bacteria within the system managed to decompose the nutrients. Nitrifying and denitrifying bacteria that have broken down the NH_3 and NO_3 compounds has directly led to decreased DO concentration. However, the sufficiently aerated oxygen has recovered its level to a saturation concentration under optimal atmospheric pressure and temperature. Hence, the average DO recovery percentage for all the beds has revealed that the reed bed system was favored for septage treatment, regardless of the SLR and resting period.

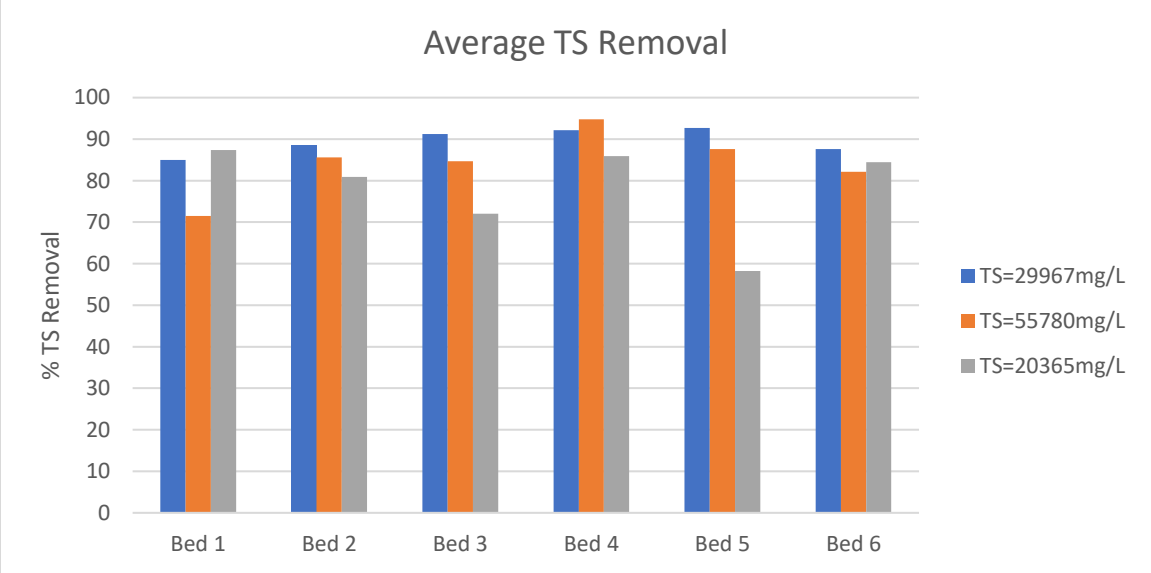

Figure 4.27: Average percentage of TS removal in Phase 1 experiment.

Lastly, the average TS removal in the effluent was above 70% in general. Some TS removal was revealed to be beyond 90%, as the bed was ponded with loaded sludge. Hence, the infiltration duration was extended, which enhanced the treatment performance accordingly. However, this condition has also prolonged the overall treatment process and affected the time efficiency. The experiments showed that the TS removal percentage could be as low as 58.23%, indicating that the effluent has bypassed the filter medium and weakened the reed bed's treatment performance due to cracks in the sludge deposit layer of the bed.

4.4 Phase 2 Experiment

The procedure for the main treatment (Phase 2) of the reed bed system in this project study was identical to Phase 1 experiment. In this stage, the reed bed has fully developed, and the reed bed system could treat the septage robustly and reliably. In Phase 2 experiment, the SLR and resting period were revised further to investigate the effects on the reed bed system. Hence, the updated loading conditions for the reed beds, subjected to the initial TS concentration, are listed in Table 4.5. Some of the necessary data for Phase 2 experiment, identical to Phase 1 experiment, are presented in **Appendix Q**. The initial sludge deposit layer thickness was kept constant at 11 ± 1 cm for each bed, except for Beds 1 and 5. In this part of the experiment, the initial thickness of Beds 1 and 5 did not play an essential role in assessing SLRs and resting periods as the small and large hydraulic loads in Beds 1 and 5 would always cause cracks on sludge deposit layer or lead to waterlogging condition, respectively.

Table 4.5: Main treatment loading regime.

Reed Beds	Initial Thickness (cm)	SLR	Resting Period
Bed 1	7.50	50 kg TS/m^2/year	6 days
Bed 2	11.50	100 kg TS/m^2/year	
Bed 3	11.33	150 kg TS/m^2/year	
Bed 4	10.67	100 kg TS/m^2/year	18 days
Bed 5	8.33		27 days
Bed 6	11.33		9 days

4.4.1 Effluent Flux

Typically, a large hydraulic load creates a high-pressure head difference for infiltration. This pressure head is the main driving force for the “feed-and-drain” in the porous medium, so the hydraulic load should be large enough to sustain the infiltration capacity. However, an excessive load of sludge leads to a clogging situation. Thus, the infiltration rate is retarded, as indicated in Figure 4.28. It can be observed that the flux peak increased from approximately 0.12 to 0.35 cm/min when an additional 50 kg/m^2/year SLR was loaded. Meanwhile, the flux peak showed the lowest value of around 0.09 cm/min when applying the SLR of 150 kg/m^2/year. The results further confirmed that the

reed bed was only operational for a SLR of 100 kg/m^2/year but not with higher SLRs. According to Gholipour *et al.* (2022), the optimal operating regime is also 100 kg/m^2/year in tropical climate countries. Additionally, it was confirmed that SLRs higher than 100 kg/m^2/year would be inappropriate as the loading regime for STRB (Tan *et al.*, 2020).

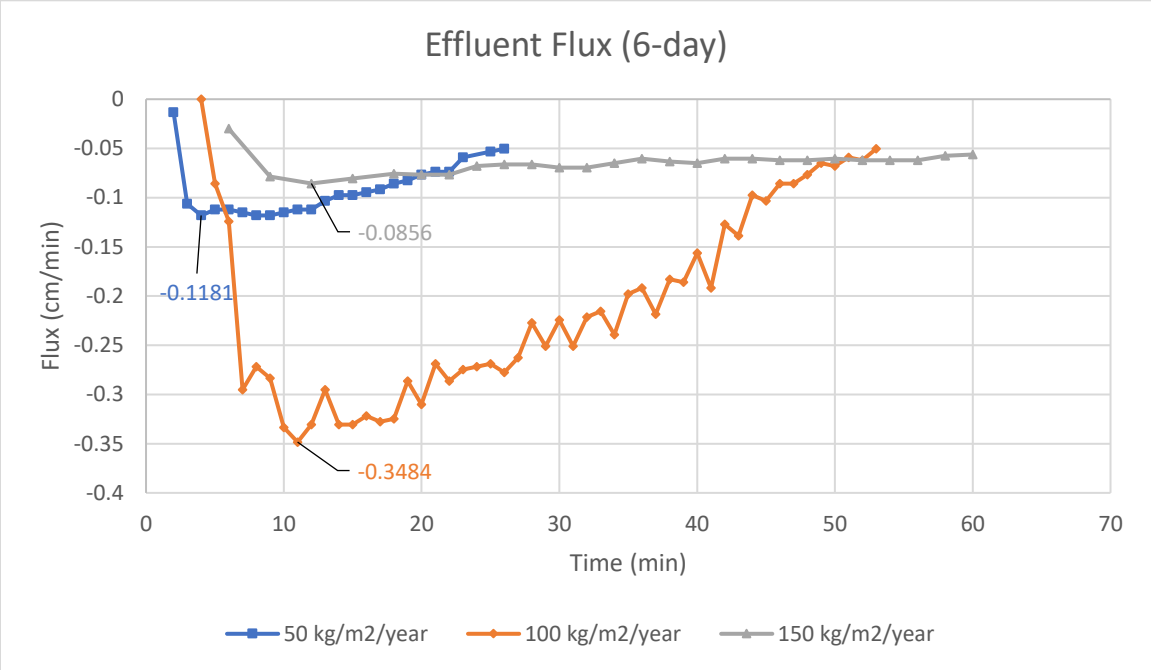

Figure 4.28: Effluent fluxes for 50, 100, and 150 kg/m^2/year SLRs under 6-day resting period.

Moreover, a relationship was presented between the same SLR of 100 kg/m^2/year and a resting period of 6, 9, 18, and 27 days, as displayed in Figure 4.29. A longer resting period required a higher volume of sludge to be loaded, which needed more time for the percolation process. Although prolonging the retention time would lead to better removal efficiency, the waiting period is not conducive towards treatment efficiency. The prolonged waterlogging condition requires a larger storage capacity, leading to an extensive increase in the capital cost of STRB. Therefore, a critical point between the SLR and resting period is crucial for a reed bed system to achieve the best efficiency in operation.

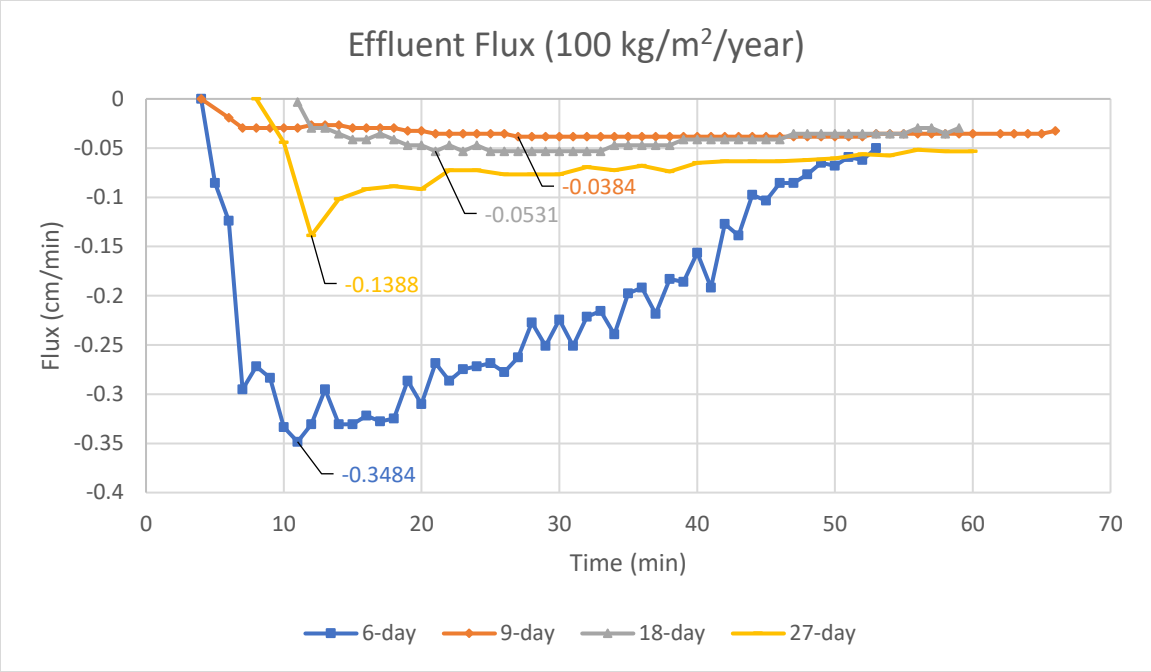

Figure 4.29: Effluent fluxes for 6-, 9-, 18-, and 27-day resting periods under 100 kg/m^2/year SLR.

Similarly, the longer resting period has decreased the effluent flux and the flux peak. The flux peak was the highest at around 0.35 cm/min for 6 days resting period. However, the flux peak has dropped to 0.04 cm/min for 9 days of the resting period. The low permeability of the sludge deposit layer was the main reason for the ponding condition, causing the reduction in effluent flux as less water can infiltrate through the bed. In the 6-day resting period, the hydraulic load sufficiently sustained the wetness of the bed without extending the ponding condition. The pressure difference in the hydraulic load was adequate to act as the driving force to enhance the percolation rate, subsequently increasing the effluent flow rate.

Nonetheless, it was observed that the peak of the fluxes increased with a longer resting period (Leite *et al.*, 2023). The increase in resting periods from 9- to 27-day showed a slight increment in the flux peaks. In this case, the pressure head difference increased upon the increasing hydraulic loads. Initially, the ponding condition clogged the substrate layers, reducing the infiltration to a reasonably low rate. As soon as the hydraulic difference increased, the weight of loaded sludge enhanced the percolation rate

by squashing and pushing the influent to enable it to penetrate the substrate layers, resulting in a higher flux peak (Çakir *et al.*, 2015; Gill *et al.*, 2023).

4.4.2 Sludge Deposit Thickness Layer

In Phase 2 experiment, the change in sludge deposit thickness was more stable upon continuous accumulation and compression than that in Phase 1 experiment. The thickness of the overall sludge deposit increased incrementally as per Phase 1 experiment. However, the increments of the sludge deposit layer showed a declining trend after each loading batch due to the moisture loss to the atmosphere and drainage through percolation, as indicated in Figure 4.30. The extremely high thickness of the sludge deposit layer under 100 kg/m^2/year SLR and 18-day resting period was caused by the ponded condition, where the bed has been clogged due to the continuous loading of septage for a month, which partially reduced the infiltration rate due to the extensive growth of microorganisms. In addition, the large volume of septage loaded due to the relatively long resting period required has increased the possibility of clogging.

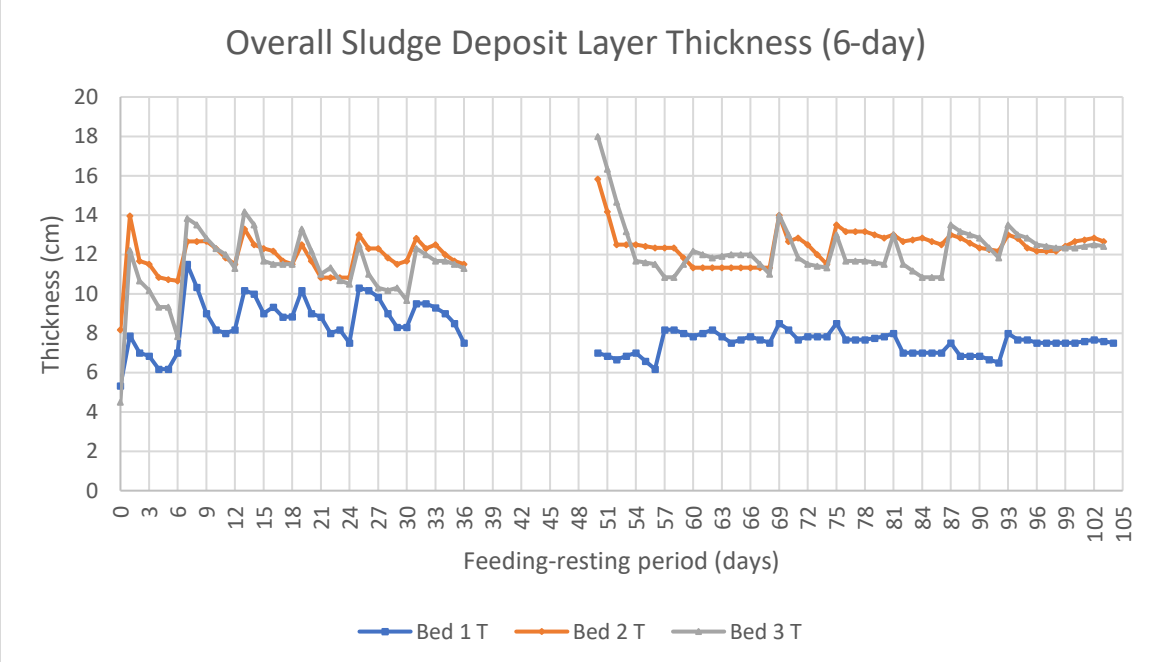

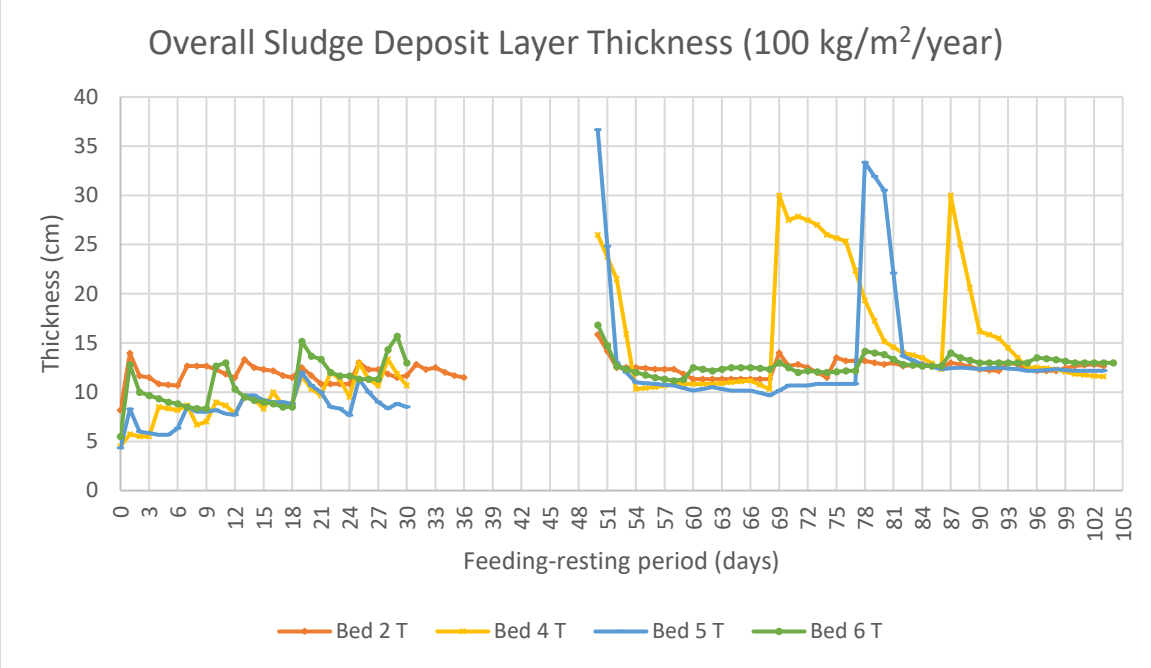

Figure 4.30: Overall thickness of sludge deposit layer under varying SLRs and resting periods.

4.4.3 Moisture Content (MC) and Total Solids (TS) Content

Generally, the MC of the sludge deposit always decreases with time, regardless of the drainage efficiency. The moisture loss to the atmosphere could be via evaporation or transpiration by plants. The MC directly relates to the TS content, as illustrated in Figure 4.31. In other words, the increase in TS content can acknowledge the decrease in MC.

Therefore, it can be observed that the MC increased throughout 50 kg/m^2/year SLRs, while it declined for 150 kg/m^2/year SLRs, and vice versa for the TS content. However, the MC for 100 kg/m^2/year SLR showed a relatively stable and constant trend at approximately 70% throughout the treatment. The final TS content of the dried solid sludge has reached about 30%, confirming the efficiency and performance of the reed bed system.

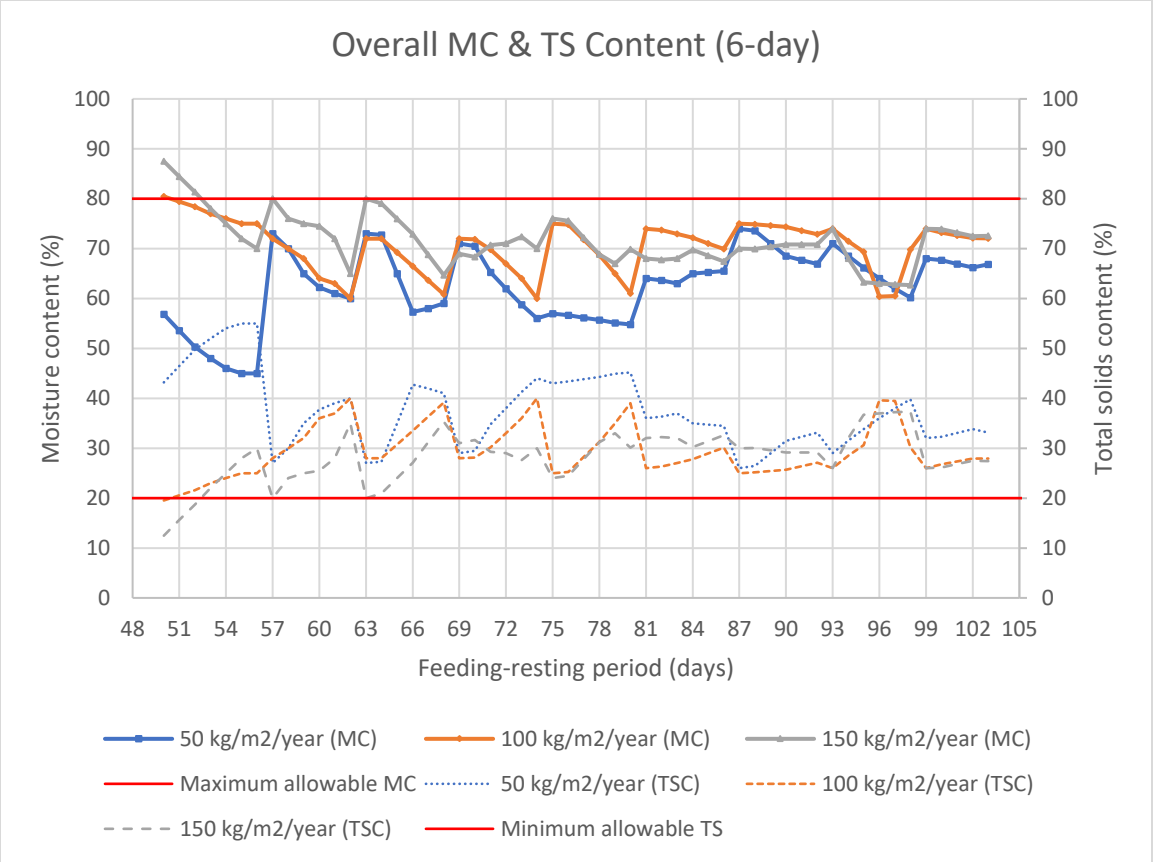

Figure 4.31: Moisture and total solids contents for 50, 100, and 150 kg/m^2/year SLRs under 6-day resting period.

Furthermore, the increasing TS content trend shown by the 150 kg/m^2/year SLR described that the bed adapted to the large hydraulic load. The larger hydraulic load initially caused an over-wetted bed condition, but the bed dried sufficiently during the prolonged resting period (Hua *et al.*, 2018). Inversely, the TS content of the 50 kg/m^2/year SLR was getting lower, indicating that the bed was adapting to the small hydraulic load. The over-dried condition of the bed led to a very high TS content initially, but the bed's wetness increased upon the continuous feeding of raw septage throughout the experiment. The incremental sludge deposit thickness increased its porosity, causing more water to be retained in the bed (Trein *et al.*, 2019). This is proven by the slight increase in the overall MC throughout the entire treatment period.

The reed bed's most favored resting period was 6 days, as shown in Figure 4.32. The bed was maintained with sufficient moisture at around 70% of MC throughout the

treatment. Meanwhile, the other reed beds have presented a relatively unstable and unfavorable trend.

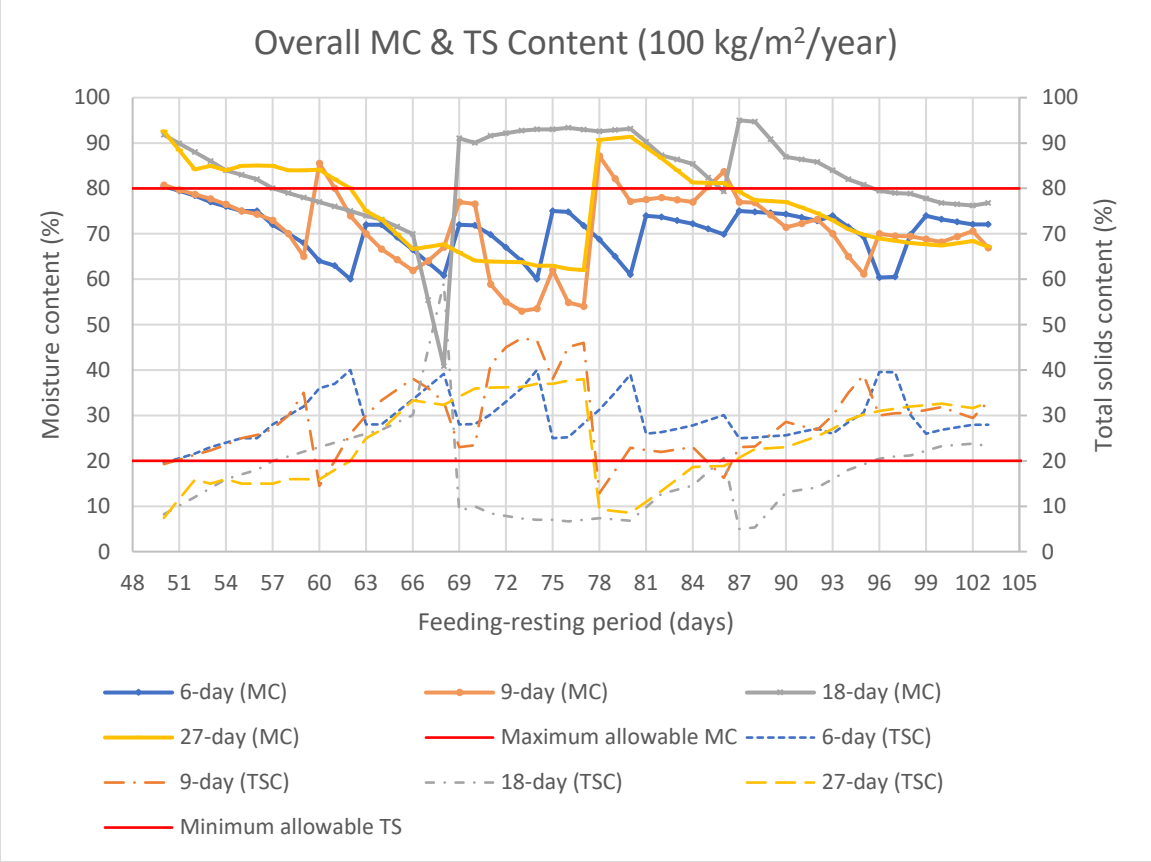

Figure 4.32: Moisture and total solids contents for 6-, 9-, 18-, and 27-day resting periods under 100 kg/m²/year SLR.

4.4.4 Total Volatile Solids (TVS) Content

In contrast to Phase 1 experiment, the TVS content of the sludge deposit stabilized at the end of Phase 2 experiment. Figure 4.33 illustrates the TVS content in the sludge deposit with respect to SLR and resting period. The overall TVS contents for each bed ranged from 20% to 50%, showing a gradual reduction in the TVS contents across the feeding-resting cycle. In this case, the mineralization of nutrients within the sludge deposit was at optimum condition, as the sludge deposit was maintained with sufficient porosity for oxygen aeration (Bui *et al.*, 2019). The best example can be seen through the loading condition of 100 kg/m²/year SLR with 18-day resting period, where the TVS content

decreased gradually due to sludge ponding and shot up towards the end of treatment after infiltration. However, the TVS content of 100 kg/m^2/year SLR with 6-day resting period was the most stable. As the bed was consistently maintained in wet conditions, the nutrient mineralization in the sludge deposit reached equilibrium (Huong *et al.*, 2023a).

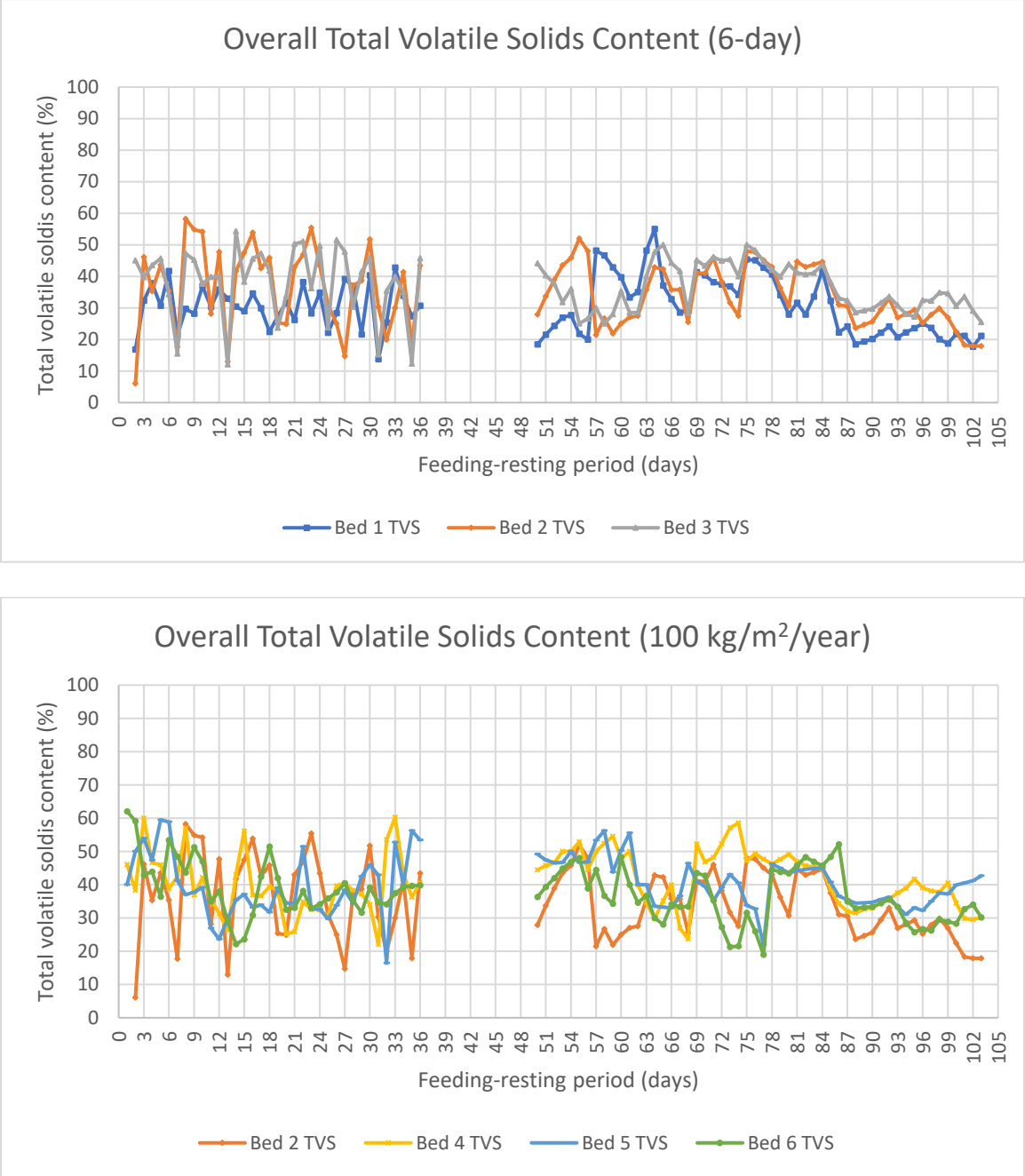

Figure 4.33: Overall total volatile solids content under varying SLRs and resting periods.

In addition, the graph of TVS contents with respect to resting periods has confirmed that the dryness of the bed was the main reason for the changes in TVS content. The ponding condition has hindered the oxygen from aerating in the sludge deposit. Thus, the mineralization only occurred after the ponding level started to decrease. Therefore, the overall TVS content decreased with prolonged resting periods. The excessive loss of water content has eventually led to an over-dried bed condition. The insufficient MC has led to the bacteria's inadequacy in mineralizing the existing nutrients effectively. The over-dried condition, with possible cracks in the sludge deposit layer, has allowed some of the influent sludge that contained organic matter to bypass the reed bed. This has been proven by low TVS content tested in the sludge deposit.

4.4.5 Shrinkage Limit (SL)

The shrinkage limit (SL) of the sludge deposit determines its ability to maintain the shape prior to deformation and possible cracks due to water loss by drainage or evapotranspiration during the resting period. The deformation of the sludge deposit layer is highly unwanted, especially the formation of cracks, as this would deteriorate the dewatering and treatment efficiency of the STRB system. The average MCs (MCs) throughout the experiment and the respective SLs are given in Table 4.6.

Table 4.6: Average overall percentage of moisture contents and respective shrinkage limits.

Bed	Average overall moisture content (%)	Shrinkage limit (%)
1	62.14 ± 7.52	76.20
2	76.28 ± 9.02	74.78
3	77.76 ± 9.22	72.89
4	82.09 ± 8.17	77.03
5	77.38 ± 8.24	73.87
6	75.34 ± 9.46	77.12
Mean	**75.17 ± 8.61**	**75.32 ± 1.89**

The total average MC throughout the experiment was determined to be 75.17 ± 8.61%, close to the SL of 75.32 ± 1.89%. This indicates that the beds were primarily maintained with sufficient moisture throughout treatment. The SL with a standard deviation of 1.89% suggests the sludge deposits had similar characteristics. The

difference in the SLs was mainly due to the organic content in the sludge deposits. A low SL represents a low organic content in the sludge deposit and vice versa (Mohajerani *et al.*, 2019). However, the corresponding sludge mineralization and stabilization varied the organic content in the sludge deposits, subject to the bed conditions. Figure 4.34 shows the relationship between each bed's MC and SL of the sludge deposit layers. Perhaps the ponding condition would have low sludge mineralization and stabilization due to low oxygen reaeration, thus resulting in high final organic content (Huong *et al.*, 2024a). Whereas the organic content is low upon the crack occurrence on the sludge deposit with sufficient oxygen supply, as shown in Bed 1.

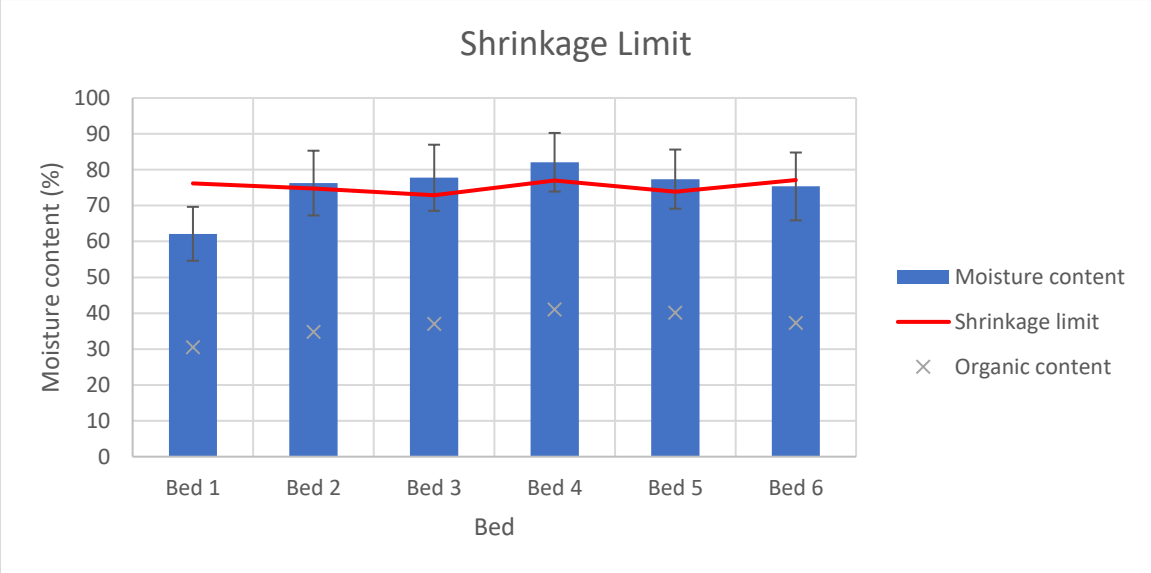

Figure 4.34: Shrinkage limit of the sludge deposit layers.

Results showed that the MCs of Beds 1 and 6 could not meet the SLs of the sludge deposits. Bed 1 has the lowest average MC of 62.14% compared to its SL of 76.20%, with a roughly 14% difference. The significant difference in the percentage reveals the sludge deposit had excessive organic content but insufficient MC due to low SLR and a relatively long resting period. Further, a longer resting period for Bed 6 has dried the sludge deposit layer and possibly led to the occurrence of cracks. The relatively low MC in the bed might not be sufficient for the bacteria to decompose the organic matter; thus, the MC was slightly lower than its SL.

Meanwhile, the MCs of Bed 2 to 5 were beyond the SLs, indicating the moisture of the sludge deposits sufficiently stabilized the organic matter. Bed 4 has the highest MC due to clogging conditions, leading to high SL. The excessive hydraulic loads containing more volatile solids have directly increased the total organic content. Moreover, the prolonged ponding condition that leads to low sludge mineralization and stabilization also causes the high organic matter content in the sludge deposit layer.

Conclusively, the loading condition of more than 100 kg/m^2/year SLR with an appropriate resting period would have sufficient MC of the sludge deposits to achieve its SL, thus preventing the effluent from bypassing the sludge deposit layer upon the crack occurrence.

4.4.6 Overall Treatment Efficiency

The effluent quality of Phase 2 experiment was observed to conform to a similar trend to Phase 1 experiment. In this part of the experiment, the effluent quality was better than that in Phase 1 due to the growth and development of bacteria within the substrate medium. Additionally, the thickened sludge deposit layer upon continuous sludge accumulation has reduced the layer permeability, thus increasing the interaction between bacteria and contaminants by retarding the percolation rate. Hence, the lowest COD concentration was 74 mg/L, while the highest NO_3 concentration reached 2623 mg/L. The pH value remained in the range of 6 to 8. Meanwhile, the highest DO concentration was determined to be 8.28 mg/L. Figure 4.35 to Figure 4.39 show the overall removal or recovery behaviors of the tested effluent quality for COD, NO_3, pH, DO, and TS throughout the experiment, respectively.

The minimum, average, and maximum concentrations of the overall Phase 2 experiment performance for all beds are presented in Table 4.7. In addition, Table 4.8 shows the removal percentage for COD and TS. These concentration values indicated that the reed bed system was treating septage well. In this stage, the reed beds have thoroughly developed and operated optimally.

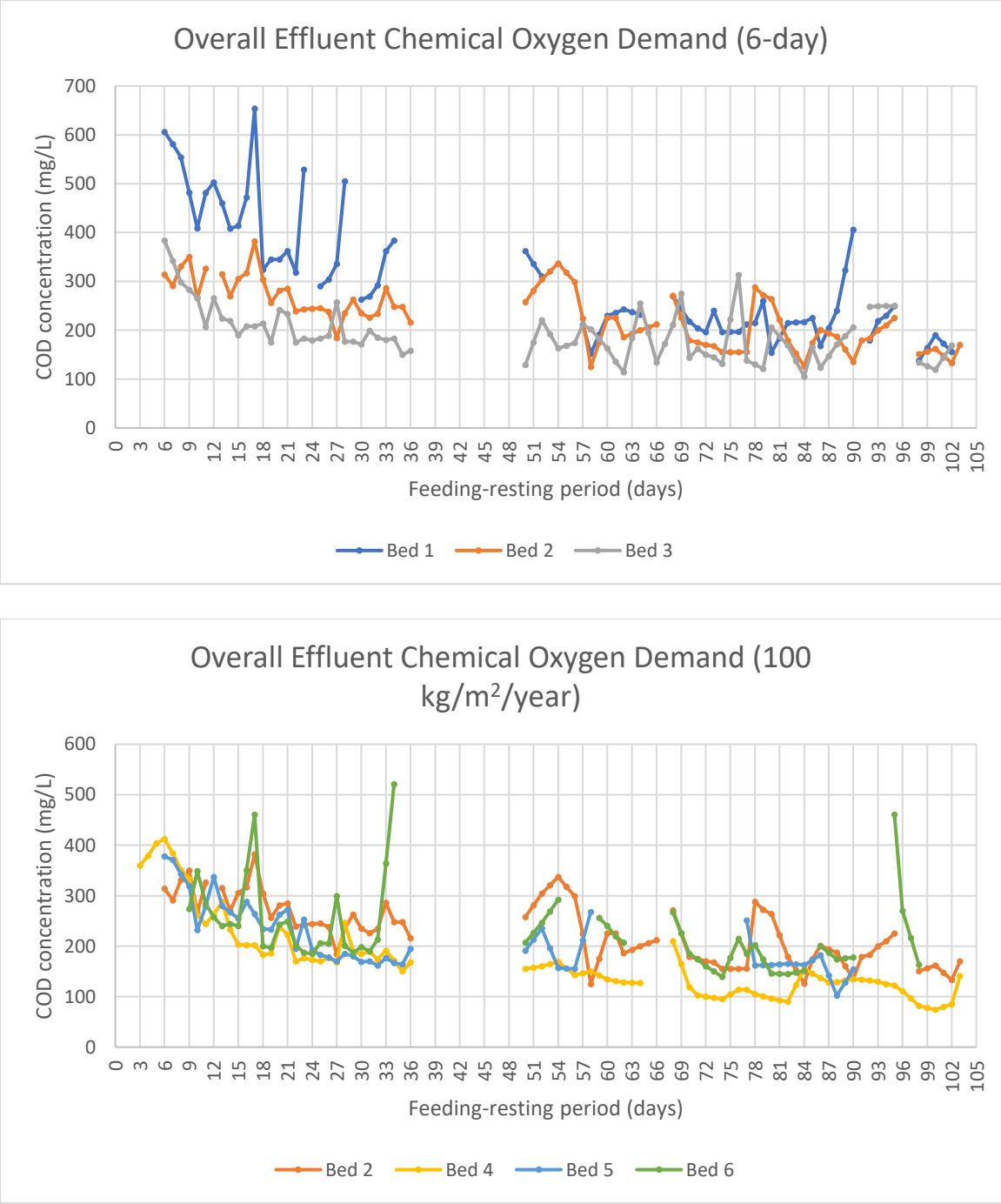

Figure 4.35: Overall chemical oxygen demand concentration under varying SLRs and resting periods.

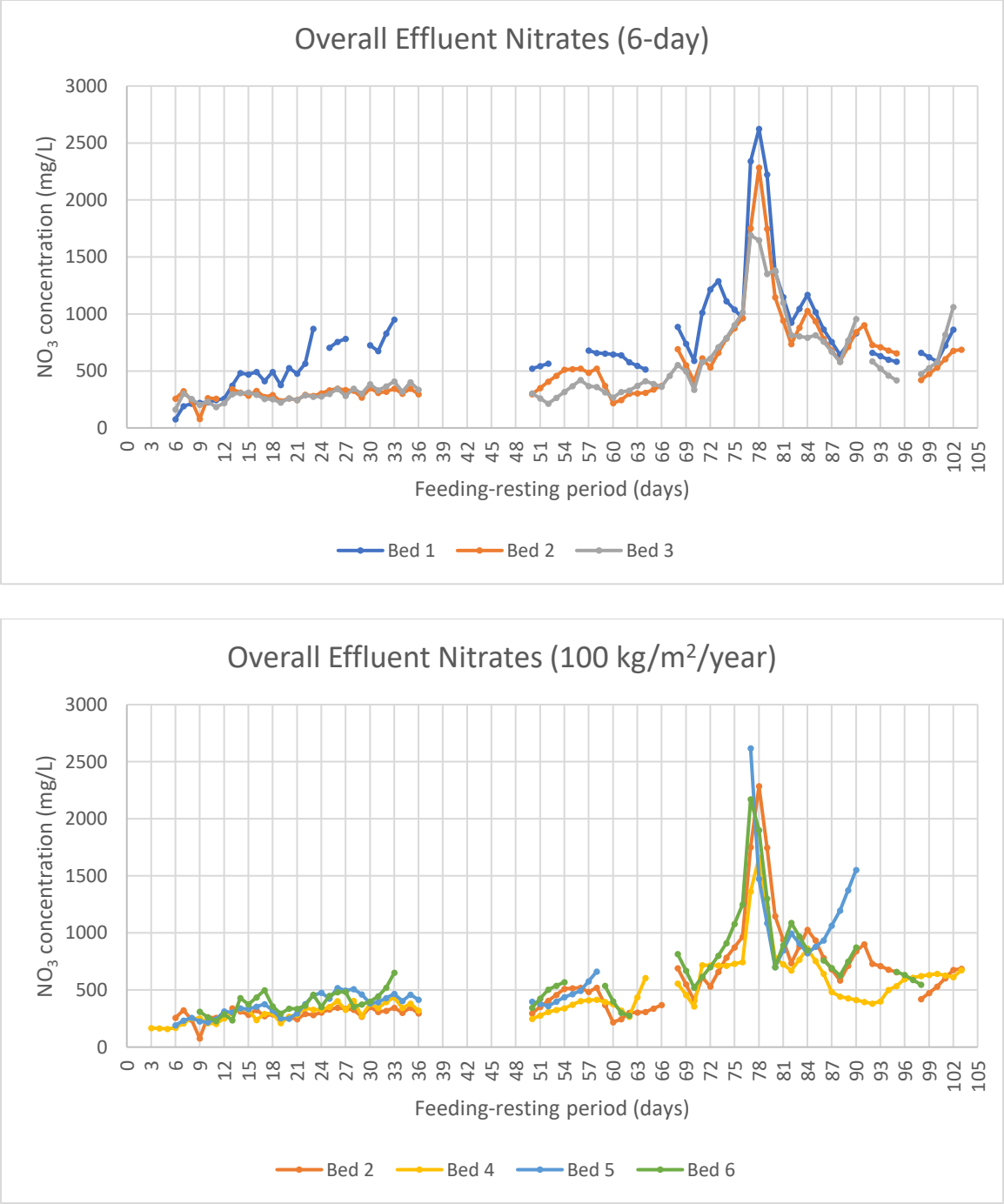

Figure 4.36: Overall nitrates concentration under varying SLRs and resting periods.

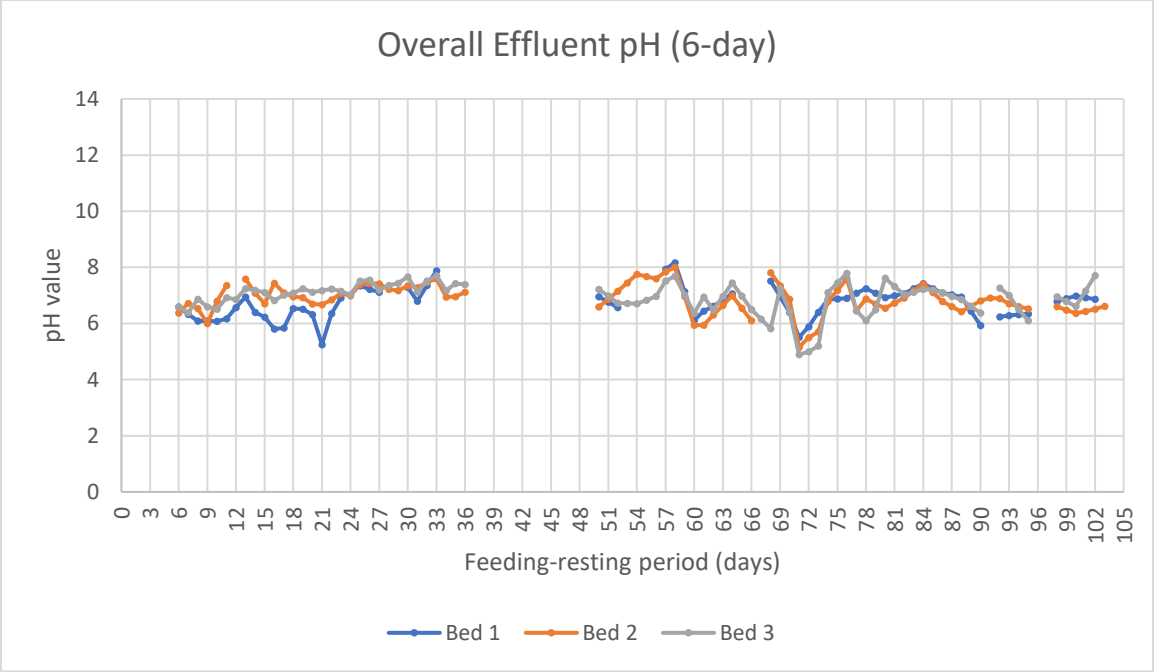

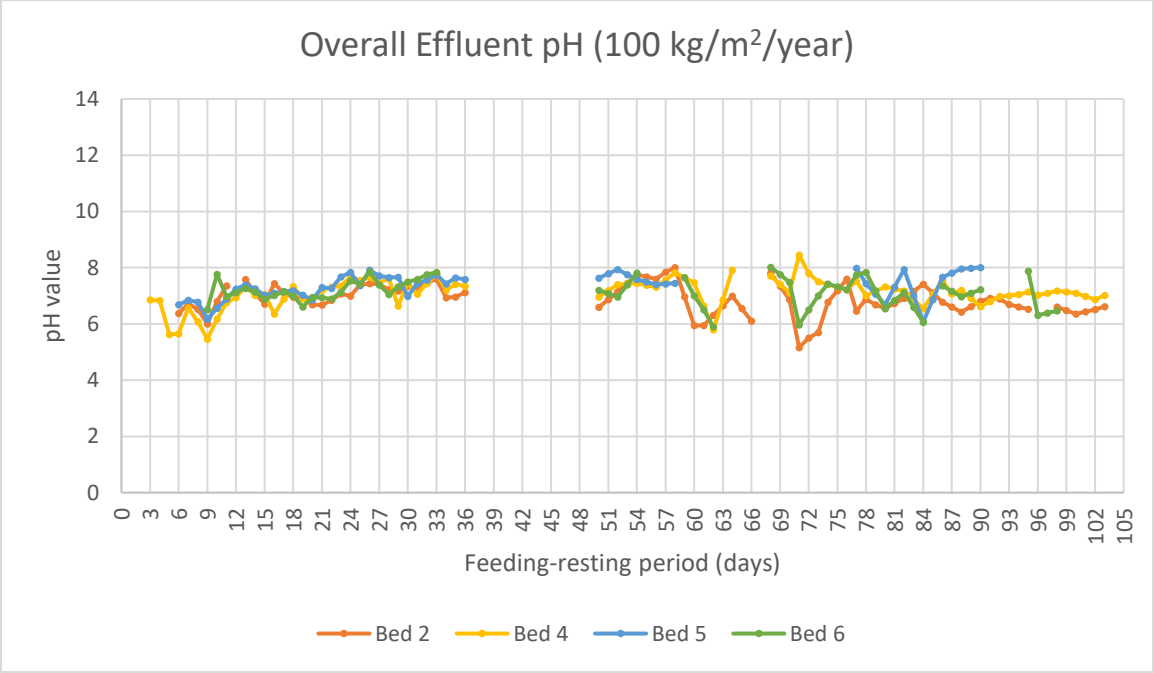

Figure 4.37: Overall pH value under varying SLRs and resting periods.

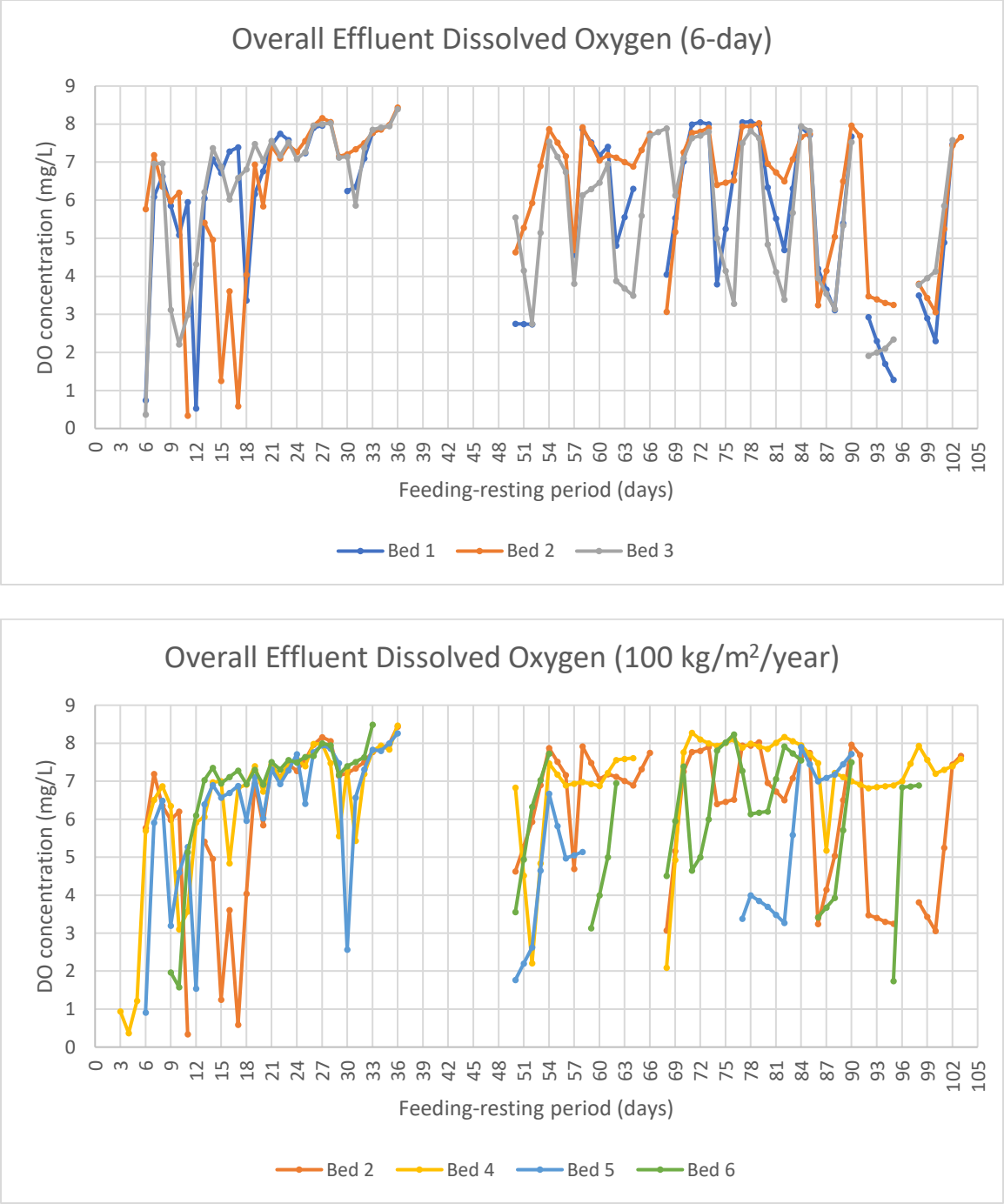

Figure 4.38: Overall dissolved oxygen concentration under varying SLRs and resting periods.

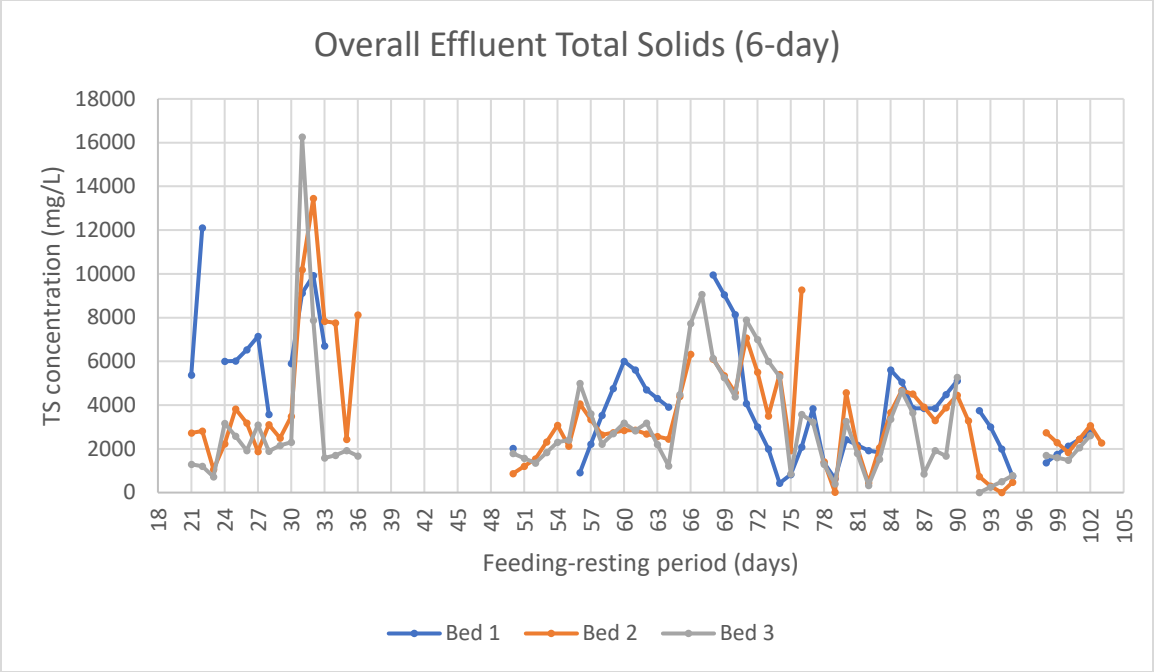

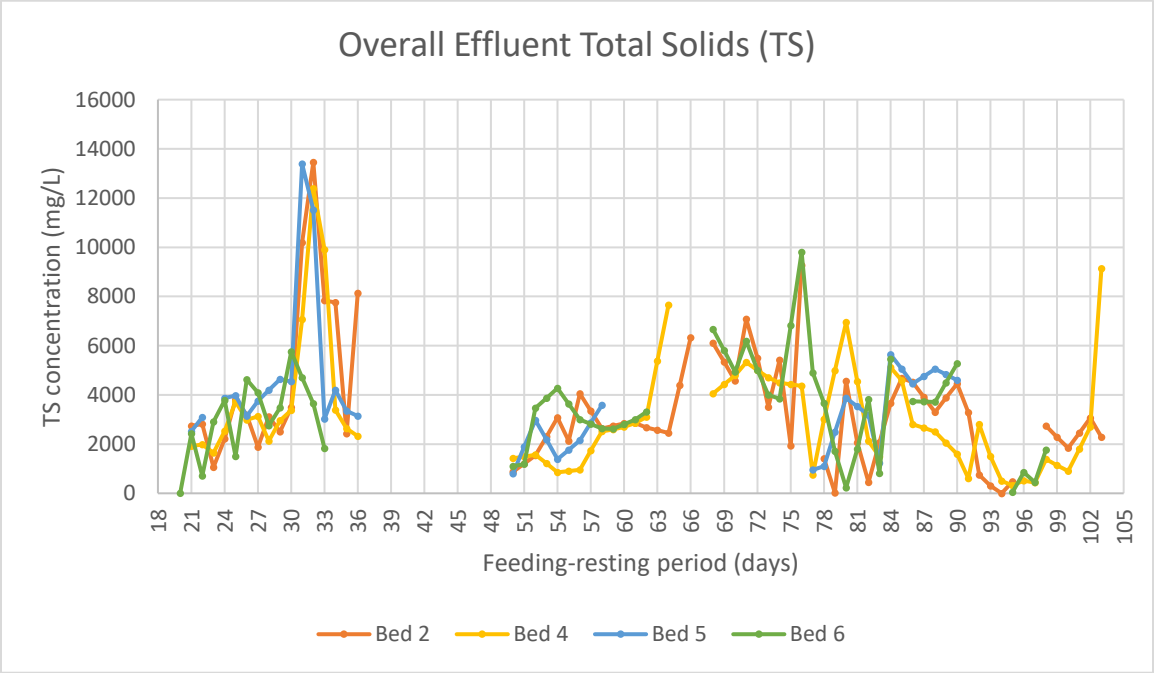

Figure 4.39: Overall total solids concentration under varying SLRs and resting periods.

Table 4.7: The minimum, average, and maximum concentration of effluent quality for the main treatment.

Bed	Conditions (kg/m^2/year | day]		COD (mg/L)			NO_3 (mg/L)			pH			DO (mg/L)			TS (mg/L)		
	SLR	Resting period	Min	Average	Max	Min	Average	Max	Min	Average	Max	Min	Average	Max	Min	Average	Max
1	50	6	138	229.29 ± 55.64	406	513	923.82 ± 473.51	2623	5.51	-	8.17	1.26	5.50 ± 2.21	8.06	429	3415.77 ± 2172.39	9960
2	100	6	125	206.75 ± 54.45	337	217	686.69 ± 377.73	2285	5.16	-	8.00	1.46	6.33 ± 1.76	8.12	0	3102.88 ± 1888.39	9265
3	150	6	105	178.95 ± 56.18	406	214	637.42 ± 341.79	1690	4.89	-	8.05	1.49	5.51 ± 1.98	7.95	0	2983.64 ± 2147.07	9065
4	100	3	74	126.33 ± 29.19	210	247	583.34 ± 264.03	1659	5.80	-	8.45	2.09	7.00 ± 1.39	8.28	322	2891.50 ± 2005.61	9137
5	100	6	102	176.41 ± 38.50	268	359	896.59 ± 519.29	2617	6.07	-	8.01	1.77	5.13 ± 1.91	7.90	803	3058.11 ± 1515.94	5640
6	100	9	139	204.96 ± 60.12	461	277	804.75 ± 422.57	2171	5.90	-	8.02	1.74	6.02 ± 1.68	8.23	49	3519.81 ± 2041.45	9806
Ave	-	-	**114**	**187.12 ± 49.01**	**348**	**305**	**755.44 ± 399.82**	**2174**	**5.56**	-	**8.12**	**1.64**	**5.92 ± 1.82**	**8.09**	267	3161.95 ± 241.30	8812

Table 4.8: Removal percentage of COD and TS.

Parameter	COD						TS					
	Bed 1	**Bed 2**	**Bed 3**	**Bed 4**	**Bed 5**	**Bed 6**	**Bed 1**	**Bed 2**	**Bed 3**	**Bed 4**	**Bed 5**	**Bed 6**
Average Initial Quality (mg/L)	5026.97						16222.60					
Average Effluent Quality (mg/L)	229.29	206.75	178.95	126.33	176.41	204.96	3415.77	3102.88	2983.64	2891.50	3058.11	3519.81
Removal Percentage (%)	95.44	95.89	96.44	97.49	96.49	95.92	78.94	80.87	81.61	82.18	81.15	78.30
Overall Removal Percentage (%)	**96.28**						**82.14**					

Regarding efficiency in Phase 2 experiment, the overall removal of COD reached 94.5% for all three different initial TS conditions, as shown in Figure 4.40. The best performance regarding the removal efficiency was observed to be Bed 4, with a COD removal efficiency of approximately 97%. This is reasonable because the prolonged resting period of 18 days required a relatively large hydraulic load, thus creating a ponding condition and enhancing the infiltration efficiency (Khomenko *et al.*, 2019).

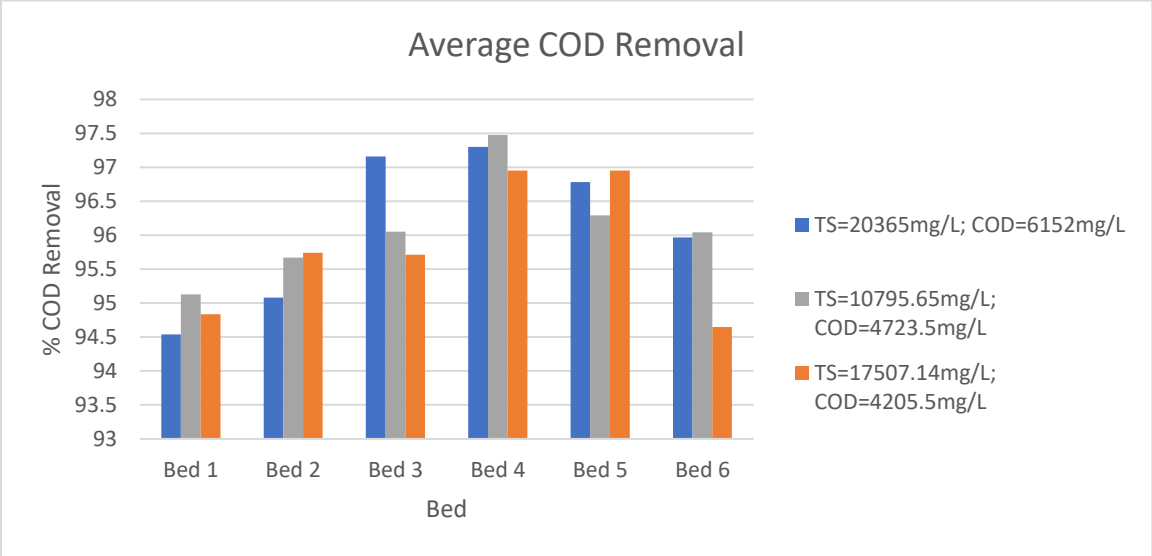

Figure 4.40: Average percentage of COD removal in Phase 2 experiment.

However, a further increase in hydraulic loads upon lengthening the resting periods to 27 days did not show a significant increase in the elimination of COD. This is believed to be caused by the insufficient DO for bacteria decomposition due to the extended ponding period that hindered oxygen aeration (Raboni *et al.*, 2020). Additionally, the bed, which had a longer resting period, had caused cracks on the sludge deposit, where the influent sludge bypassed the substrate filter before the ponding occurred, affecting the overall efficiency of COD removal. For the same reason, the NO_3 recovered percentage was significantly high in Bed 5, as displayed in Figure 4.41. Moreover, the lower SLR for Bed 1 produced the same outcome: the NO_3 concentration was high.

In such a situation, denitrification is unlikely due to high DO concentration, as shown in Figure 4.42. Typically, a robust and reliable reed bed system should have a

relatively high concentration of NO_3 in the effluent (Yan *et al.*, 2019). However, an optimum condition is achieved when the nitrification and denitrification are maintained at an equilibrium state, where the amount of DO aerated is correspondingly sufficient for the utility of nitrifying bacteria in the reactions (J. Hu *et al.*, 2021).

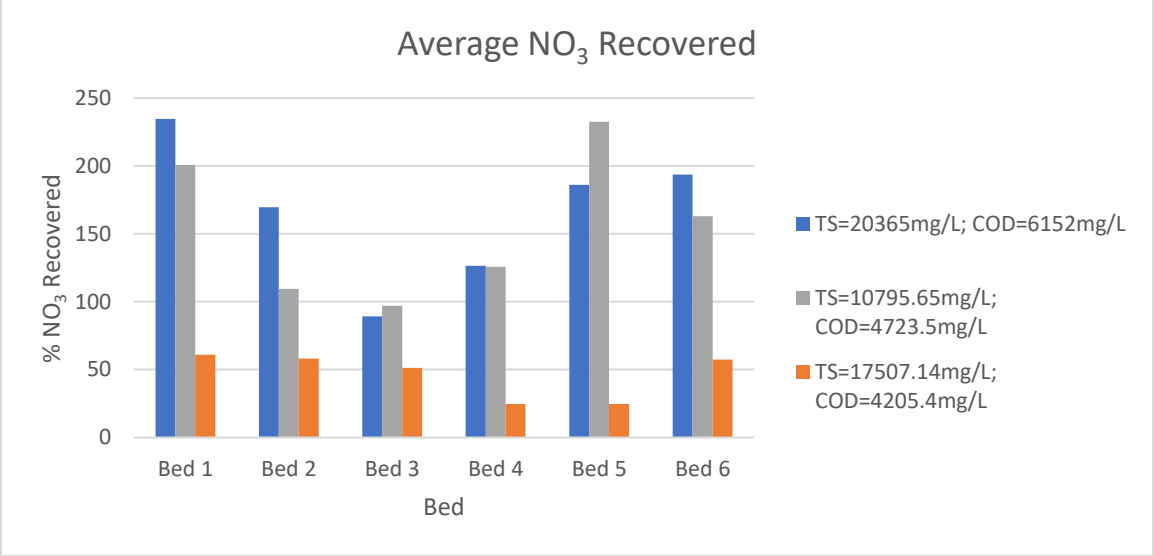

Figure 4.41: Average percentage of NO_3 recovery in Phase 2 experiment.

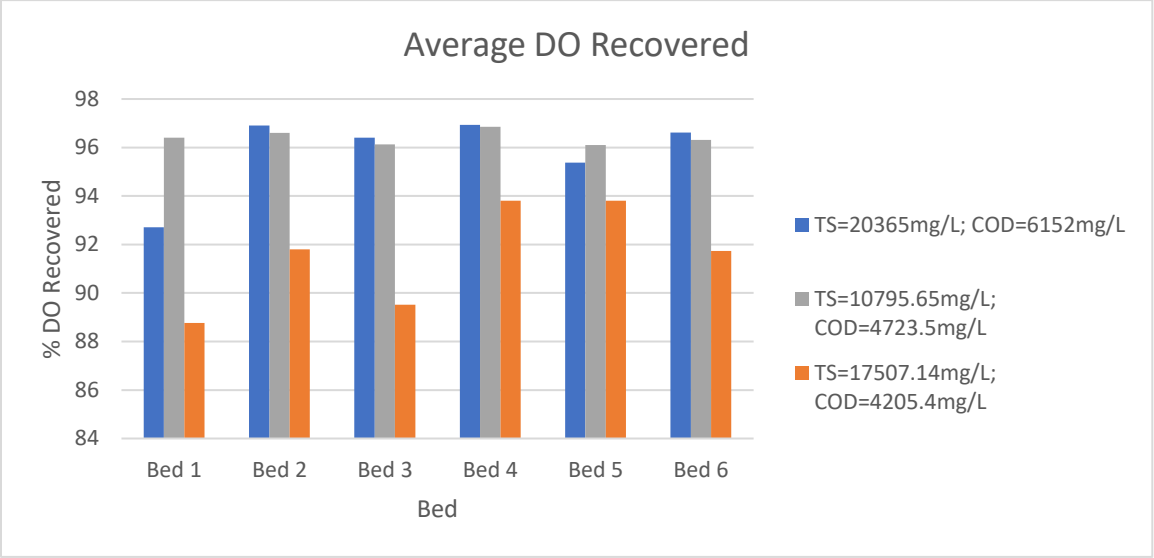

Figure 4.42: Average percentage of DO recovery in Phase 2 experiment.

On the other hand, the pH value was slightly alkaline whenever the resting period was prolonged, as shown in Bed 4, 5, and 6 of Figure 4.43. The results indicated that the bed with the ponding condition treated the effluents well, thus subtly increasing the pH

value. Moreover, the effluent TS removal was very subjective to the condition of the bed. The higher TS removal percentage indicated that the bed was ponded, whereas the significantly lower TS removal percentage was due to cracks on the sludge deposit. The highest removal percentage of TS was revealed to be 100%, as indicated in Figure 4.44. However, such a situation has described the effluent's TS content as low enough to be significantly measured. These results have further confirmed that the reed bed system was fully developed and met the objectives for its existence.

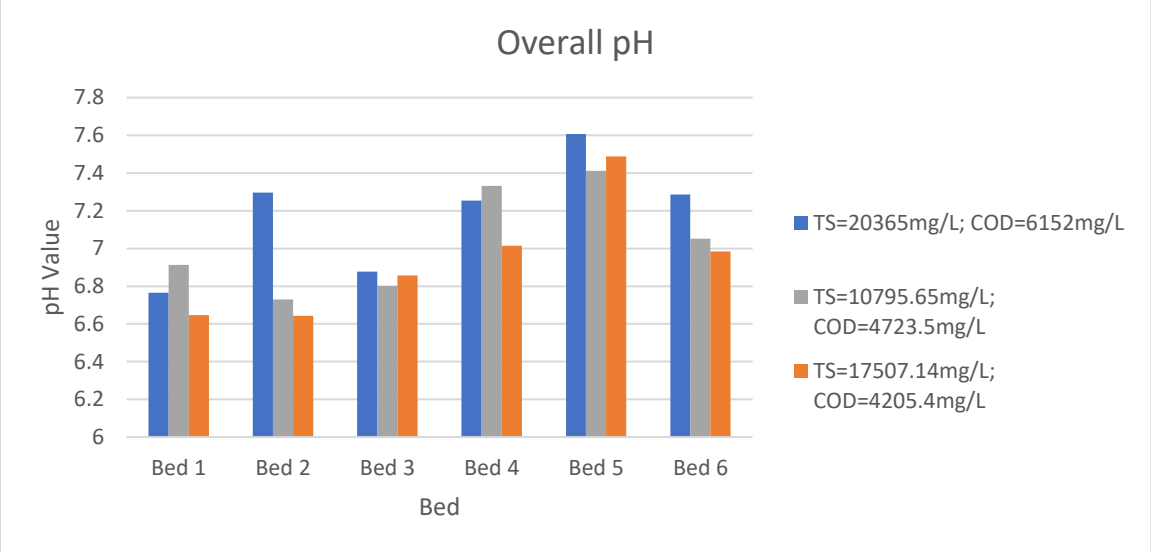

Figure 4.43: Overall pH value in Phase 2 experiment.

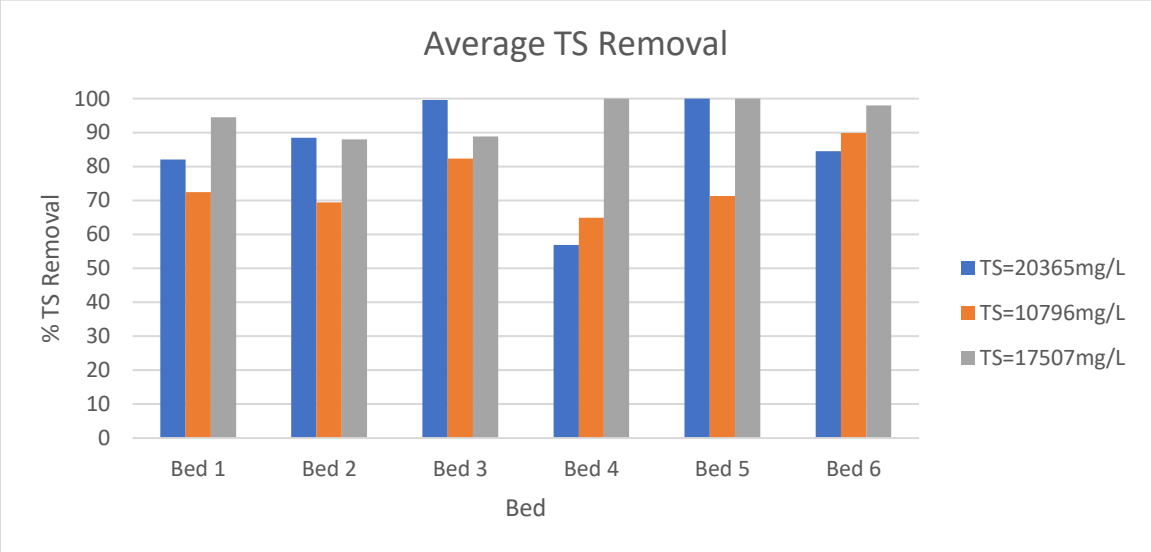

Figure 4.44: Average percentage of TS removal for the main treatment.

4.5 Analysis of Variance (ANOVA)

The experimental data was interpreted to determine the significance of dependent variables such as flow characteristics, sludge deposit layer properties, and water quality parameters against the independent variables of SLRs and resting periods using the analysis of variance (ANOVA). The application of ANOVA allows variance with a 95% confidence level, thus making dependent variables of less than 0.05 p-value significantly responsive to the independent variables.

The significances of water recovery, flow delay, and flux peaks of flow characteristics, thickness, MC, and total volatile solids of sludge deposit layer, and water quality parameters – effluent COD, NO_3, pH, DO, and TS are summarized in Table 4.9. These metrices were evaluated with respect to SLRs and resting periods across Phase 1 and Phase 2 experiments. A detailed ANOVA is shown in **Appendix R**.

Table 4.9: Significance of flow characteristics, sludge deposit layer, and water quality parameters.

Parameter	Groups	Phase	Significance (p-value)	Status
Water recovery	SLRs	1	0.8693	Not significant
	Resting periods		0.4602	Not significant
	SLRs	2	0.7902	Not significant
	Resting periods		0.8961	Not significant
	Beds	Overall	0.6265	Not significant
Flow delay	SLRs	1	0.0050	Significant
	Resting periods		0.4431	Not significant
	SLRs	2	0.8307	Not significant
	Resting periods		0.9185	Not significant
	Beds	Overall	0.0245	Significant
Flux peaks	SLRs	1	0.0194	Significant
	Resting periods		0.0182	Significant
	SLRs	2	0.1394	Not significant
	Resting periods		0.3685	Not significant
	Beds	Overall	0.0463	Significant
Sludge deposit layer thickness	SLRs	1	2.28E-17	Significant
	Resting periods		7.14E-05	Significant
	SLRs	2	2.83E-71	Significant
	Resting periods		4.21E-05	Significant
	Beds	Overall	6.12E-24	Significant
Moisture content	SLRs	1	1.90E-32	Significant
	Resting periods		0.4128	Not significant

	SLRs	2	2.76E-14	Significant
	Resting periods		2.97E-14	Significant
	Beds	Overall	4.38E-47	Significant
Total volatile solids	SLRs	1	0.0090	Significant
	Resting periods		0.9930	Not significant
	SLRs	2	0.0042	Significant
	Resting periods		5.09E-08	Significant
	Beds	Overall	1.43E-14	Significant
Effluent COD	SLRs	1	2.38E-16	Significant
	Resting periods		0.4525	Not significant
	SLRs	2	0.0006	Significant
	Resting periods		4.57E-14	Significant
	Beds	Overall	2.93E-20	Significant
Effluent NO_3	SLRs	1	1.01E-07	Significant
	Resting periods		0.0002	Significant
	SLRs	2	0.0030	Significant
	Resting periods		0.0056	Significant
	Beds	Overall	2.15E-05	Significant
Effluent pH	SLRs	1	1.02E-05	Significant
	Resting periods		0.0381	Significant
	SLRs	2	0.9512	Not significant
	Resting periods		1.00E-06	Significant
	Beds	Overall	2.43E-10	Significant
Effluent DO	SLRs	1	0.8196	Not significant
	Resting periods		0.4237	Not significant
	SLRs	2	0.0515	Not significant
	Resting periods		5.62E-05	Significant
	Beds	Overall	0.0073	Significant
Effluent TS	SLRs		0.0205	Significant
	Resting periods		0.2204	Not significant
	SLRs		0.5803	Not significant
	Resting periods		0.2402	Not significant
	Beds		0.0861	Not significant

4.5.1 Significance of Flow Characteristics

In terms of water recovery, the average was approximately 55 ± 5% for Phase 1 and 80 ± 4% for Phase 2. The p-values for water recovery suggest that neither SLRs nor resting periods significantly affected the water recovery rates. The water recovery percentage is potentially affected by the sludge deposit layer thickness and weather condition instead of the loading regime.

For flow delay, the average delay ranged from 45 to 155 minutes in Phase 1, showing a significant effect of SLRs, while resting periods had an insignificant impact. Initially, the thin sludge deposit layer has a higher permeability for infiltration. However, its permeability reduces across time throughout continuous septage loading due to incremental solids retained on the surface. Conversely, in Phase 2, no significant effects of SLRs or resting periods on flow delay were observed. The thickened sludge deposit layer has noticeably reduced its permeability to a significant level, resulting in a small infiltration flux. The overall p-value for flow delay, calculated with respect to reed beds, was 0.0245. indicating a significant influence of SLRs and resting periods.

Regarding flux peaks, Phase 1 exhibited average peaks below 0.02 cm/min, with significant effects from both SLRs and resting periods due to thin sludge deposit layer. In Phase 2, flux peaks varied more, reaching up to approximately 1 cm/min with continuous feeding and draining for 10 cycles due to thickened sludge deposit layer and possible cracks. The thickened sludge deposit layer was found to decrease infiltration flux while the possible crack occurrence has substantially increased the flux peaks. The average flux peaks for different resting periods ranged between 0.1454 and 0.6255 cm/min. Although the difference in flux peaks due to varied resting periods resulted in a higher p-value compared to SLRs, the overall significance of SLRs and resting periods on flux peaks remained noticeable, with a p-value less than 0.05.

4.5.2 Significance of Sludge Deposit Layer Properties

The very low p-values in Table 4.9 highlight the significant impact of SLRs and resting periods on the thickness of the sludge deposit layer. The incremental thickness was certainly caused by the continuous loading. However, a higher SLR or a longer resting period would increase the sludge deposit layer thickness significantly, leading to a remarkably flux reduction and ponding condition. Also, an excessively thickened sludge deposit layer due to high SLRs or prolonged resting periods would eventually result in the formation of cracks, causing extraordinarily high flux peaks. This indicates that variations in SLRs and resting periods significantly affect the sludge deposit thickness.

For MC, significant effects were observed except for variations in resting periods during Phase 1. Initially, the thin sludge deposit layer was not affected by the variation in resting periods, as the thin layer would always be in cracked condition. Along the treatment, the incremental solids accumulation maintained the sludge deposit layer from cracking, ensuring the entity of the layer for successful filtration. As a result, the average MC was 81 ± 1%, attributed to the long resting periods and the short resting periods did not cause significant changes in MC.

Similarly, total volatile solids exhibited a trend like that of MC. The p-values were generally low, except for the varied resting periods in Phase 1. The short resting periods resulted in minimal changes in sludge stabilization, with an average total volatile solid of 39 ± 1% due to crack occurrence. Influent septage bypassed the reed bed directly and discharged as untreated effluent, resulting in incomplete biological treatment within the sludge deposit layer and substrate medium. This suggests that longer resting periods contribute to greater sludge stabilization, which was reflected in a lower p-value in Phase 2.

In conclusion, the consistently low p-values across these parameters demonstrate the significant influence of SLRs and resting periods on sludge deposit layer properties. These findings underscore the importance of incorporating these parameters into simulations for a more comprehensive understanding.

4.5.3 Significance of Water Quality Parameters

The p-values in Table 4.9 for effluent COD were generally low, indicating that both SLRs and resting periods significantly impact effluent COD. However, in Phase 1, resting periods did not show a significant effect on effluent COD, as well as the observations for MC and total volatile solids in the sludge deposit layer. The short resting periods in this phase led to insufficient drying of the sludge deposit layer via evapotranspiration, minimizing differences in MCs and resulting in higher p-values.

For effluent NO_3, both phases showed low p-values, reflecting significant effects of SLRs and resting periods. The presence and activity of nitrifying and denitrifying

bacteria were key factors influencing the concentration of the effluent NO_3. Mineralization by plants was through denitrification under anaerobic conditions and nitrification under aerobic conditions. Higher variance in effluent NO_3 between different beds contributed to the lower p-values observed.

The p-value for effluent pH was also low, indicating significant effects of SLRs and resting periods, apart from varied SLRs in Phase 2. The effluent pH typically decreased slightly compared to the influent pH after treatment. However, the consistency of effluent pH was affected by the influent septage concentration.

Regarding effluent DO, the average concentration was consistently around 6 ± 1 mg/L. In Phase 2, prolonged resting periods resulted in increased surface ponding, which led to a low p-value and highlighted the significance of resting periods on the effluent DO. The lower p-values in Phase 2 compared to Phase 1 were attributed to higher SLRs and longer resting periods, which reduced the infiltration rate and increased surface ponding. Consequently, septage retention time within the bed created larger differences in effluent DO between beds.

Finally, the significant of SLRs and resting periods on effluent TS was relatively low. Effluent TS primarily dependent on the concentration of the influent septage. Variations in influent septage concentration led to increased variability in effluent TS, resulting in an overall p-value above 0.05 and indicating lesser significance of SLRs and resting periods on this parameter.

4.6 Summary of Experimental Result

In summary, the overall performance of the laboratory-scale STRB-based septage treatment system was excellent. The average COD and TS removal percentage was high, at 96% and 82%, respectively. Meanwhile, the average pH value of 7.03 decreased slightly compared to the untreated raw septage. The relatively high DO concentration of approximately 6 mg/L was found to be very favorable, where it indicated that the reed bed system was aerated well and well-developed with sufficient nitrifying bacteria for

mineralization. The treatment performance was comparable to the other existing wastewater treatment systems.

In Phase 1 experiment, the flux peak and the flow-occurring delay regarding the effluent fluxes were analyzed. The flux peak was determined to increase with the hydraulic load, while the flow-occurring delay increased with the initial TS concentration of the loaded septage. Also, water recovery was discovered to decrease with the increasing initial TS concentration of the loaded septage. In Phase 2 of the experiment, the overall shrinkage limits of the sludge deposit layers were determined for each bed. Generally, the MC of the sludge deposit layer was able to maintain above the SL, preventing liquid from bypassing the STRB. The final organic content of the sludge deposit in Phase 2 was measured to be lower than that in Phase 1 experiment upon sludge stabilization. The growth and development of bacteria decomposed most of the nutrients and transformed them into biodegradable components, leading to a substantial decrease in TVS.

Conclusively, the optimum SLR and resting period were 100 kg/m^2/year and 6 days, respectively. The reed beds with the mentioned conditions showed a very stable trend of sludge deposit moisturizing, solids dewatering, nutrient mineralizing, organic stabilizing, and effluent contaminants removal. The temporary ponding condition allowed the bed to maintain sufficient moisture to prevent cracks yet produce a high-quality dried solid with at least 20% TS content. Further, the reasonable dryness of the bed provided adequate oxygen aeration in the sludge deposit layer, mineralizing the nutrients sufficiently and resulting in high sludge mineralization. Moreover, forming the sludge deposit layer without cracking has further enhanced infiltration capacity to remove effluent contaminants.

In addition, the ANOVA has revealed that all the variables tested in the laboratory experiments were remarkably significant, except for water recovery. Under varying SLRs, the flow delays and flux peaks increased with hydraulic loads due to prolonged surface ponding. The initial sludge deposit layer thickness played an important role in limiting the infiltration flux of the STRB, where a thicker layer would result in a slower flow due to higher resistance. Hence, the SLRs greatly affected the moisture and organic contents

of the layer. A high SLR substantially increases sludge deposit layer thickness, further capturing more moisture with incremented porosity and enhancing sludge mineralization and stabilization. This improves the COD, NO_3, and TS removals of the effluent quality. However, the DO concentration was not affected much under varying SLRs, as it depends more on the growth and development of bacteria during resting periods.

In contrast, the resting periods less influenced the flow delays and flux peaks. A longer resting period required a larger hydraulic load, increasing flow delays and flux peaks. However, a sufficiently prolonged resting period allowed a complete drainage of effluent and dewatered the sludge deposit to a minimum MC. The large hydraulic load upon an extended resting period greatly affected the thickness of the sludge deposit layer. The substantial increase in the layer thickness led to waterlogging conditions, decreasing the layer permeability, and causing high final moisture and organic contents. This reduces the sludge mineralization and stabilization, resulting in poorer dewatering efficiency of the sludge deposit layer. Moreover, the extended resting period would also result in an over-drying of the sludge deposit after the drainage. The possible crack on the sludge deposit layer allowed the influent septage to bypass the reed bed directly, leading to a lower effluent quality. Hence, the extended resting period affected the effluent COD and TS concentrations significantly, while the effluent DO concentration improved remarkably due to sufficient oxygen reaeration.

CHAPTER 5: SIMULATION RESULTS

This section analyzes the process-based numerical model formulated in Chapter 3 by calibrating the model with the experimental data collected, as explained in Chapter 4. The hydraulic model simulation is used to understand the dewatering phenomenon in STRBs. At the same time, the incorporated compressible cake filtration is simulated using the moving mesh method to improve the model robustness in predicting the influence of the sludge deposit layer on dewatering efficiency.

5.1 Assumptions

The objective of the hydraulic simulation is to match the simulated results with the measured data of effluent flux obtained from the laboratory-scale STRB for septage treatment. As not all the factors were able to be measured in this study, several assumptions were made in the simulations:

- The modeling was a one-dimensional simulation as the imposed flux was distributed evenly on the reed bed and infiltrated vertically through the filter medium without any significant flow divergence. Thus, the substantial turbulence of the flow was neglected.
- The hydraulic properties of the reed bed and the associated hydraulic behavior (e.g., infiltration flux and evapotranspiration rate) were assumed to be horizontally homogenous over the reed bed. All the simulated results were presented as per unit area [L^{-2}].
- The initial pressure distribution was assumed to be under the equilibrium state, where the initial pressure was equivalent along the substrate profile before the operation.
- The effect of vegetation was only considered in terms of the root water uptake, while its influence on the hydraulic performance (e.g., change of hydraulic properties due to the cracking around the stem and root penetration) was assumed to be lumped with the hydraulic properties of the substrate profile.

- The ET rate was assumed to be constant throughout the simulation.
- The hydraulic properties of the newly formed sludge deposit were assumed to be equivalent to the existing sludge deposit.
- The hysteresis effect was not considered in the hydraulic simulation.
- The sink term considered in the proposed model only included the water loss from the ET and the water content retained in the immobile region. Therefore, the associated water recovery was theoretically conservative with the amount of the influent.

5.2 Simulation Set-Up

The substrate profile in the STRB simulation for hydraulic dynamics consists of three layers: the small-size gravel layer, the medium-size gravel layer, and the drainage layer, which aligns with the laboratory-scale STRB system, as illustrated in Figure 5.1. The sludge deposit found on top of the reed bed surface, which has been identified as a crucial factor in the hydraulic performance, was also included in the simulation as the top layer. Meanwhile, the drainage layer was excluded from the simulation profile, as its influence on the overall hydraulic retention time was negligibly small in the system.

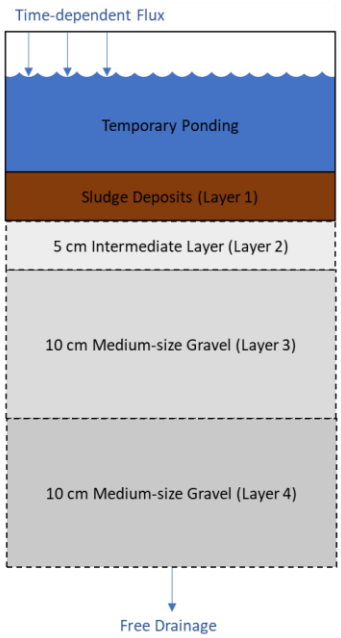

Figure 5.1: Substrate profile in the simulation.

Apart from the particulate constituents that are retained on the bed surface and form the sludge deposit layer, a certain amount of solid that passes through the surface layer and is deposited at the upper zone of the main layer increases the total thickness. Consequently, the hydraulic properties of this zone changed with time due to the reduction of porosity (Kim & Forquet, 2016). Therefore, considering a 5 cm intermediate layer was necessary to describe this transition interface at the top of the main layer. As a result, the thickness of the small-size gravel layer was reduced to 10 cm, while the thickness of the medium-size gravel remained at 10 cm.

As for the upper boundary condition, the sludge loading time was fixed to be three minutes. The feeding flux was calculated based on the hydraulic load [L^3] with respect to the reed bed surface area [L^2]. Free drainage was assumed at the lower boundary condition, which did not require any prescribed fluxes or conditions. On the other hand, the other necessary information for the hydraulic simulation is given in Table 5.1.

Table 5.1: Information on geometry, time, and iteration criteria in hydraulic simulation.

Information in the hydraulic simulation	Values
Spatial discretization [L]	1.00 cm
Temporal discretization [T]	1/360 minutes
Minimum tolerance for pressure head [L]	0.01 cm
Minimum tolerance for pressure head [L]	1.00 cm
Maximum allowable number of iterations	30.00

The spatial discretization (*dz*) was set to 1 cm in the hydraulic simulation. Certainly, a finer discretization improves the resolution and accuracy of the results. However, the computation duration has increased substantially, which is not beneficial regarding time efficiency. Further, the standard unit for the time used in the simulation was set in minutes. The time frame for the simulation was defined from the measured data, with a maximum time frame of 600 minutes (10 hours) due to the limitation of data storage in the simulation software. The default temporal discretization was set to be 1/360 minute to ensure a robust simulation. Moreover, the tolerance range for the pressure head in the iterative computation was set to be 0.01 and 1.00 cm, as a larger pressure head would lead to an error in water content (Huang *et al.*, 1996). In fact,

the convergence limit in this study was 0.001 cm. Further, the mass balance analysis was then used to evaluate the reliability of the time discretization and iteration criteria in the hydraulic simulation with mass balance error < 10^{-14}.

5.3 Review of Calibration Procedure and Establishment of Hydraulic Properties

This study comprehensively described the hydraulic behavior using the modified Richards' equation discretized by the moving mesh method. The main input parameters were initial water content, hydraulic head, and sludge thickness, whereas the main output parameters were flux, hydraulic head, and sludge accumulation. The flux, hydraulic head, and sludge thickness were expected to increase extensively upon septage loading and decrease gradually due to drainage dewatering and evapotranspiration. However, the sludge accumulation was always incremental during the feeding and settling.

One of the main challenges in the calibration was the lack of standard hydraulic parameters for granular porous medium. The variably saturated hydraulic properties of the porous medium in the reed bed could be determined through direct laboratory and indirect modeling methods. Generally, the porosity (θ), saturated hydraulic conductivity (K_s), and hydraulic retention curve (HRC) of the porous medium are the main concerns for the hydraulic simulation, which are evaluated by porosity test, constant head test, and hanging column test, respectively. In addition, the VGM parameters are estimated via the application of RETC software (van Genuchten *et al.*, 1991). However, the outcomes obtained from the experiments were statistically insufficient to provide a reliable result due to instrumental constraints (Khaleel & Relyea, 1997; Morvannou *et al.*, 2013).

Moreover, the indirect method of hydraulic parameters determination is accessed through the inversed modeling of the measured data or via calibration using a mathematical model to fit the measured data. In inversed modeling, the main limitation is insufficient data to conduct adequate analysis, especially in event-based simulation (Dittmer *et al.*, 2005). In contrast, collecting enormous amounts of data would be very time consuming and costly to satisfy the requirement of inverse modeling. Therefore, a relatively more budget-friendly alternative is calibrating the hydraulic parameters by

fitting the simulated results obtained from the mathematical model with the measured data (Toscano *et al.*, 2009).

Table 5.2 displays the literature on equilibrium hydraulic flow parameters for gravel used in simulating the hydraulic behavior of STRB or similar systems such as subsurface constructed wetlands. It was found that even though the particle size used was identical in the simulation, the hydraulic parameters varied from case to case, where there was no general trend to be observed. The saturated hydraulic conductivity ranged from 0.5 to 1000 cm/min, giving a large standard deviation of 327.75 cm/min. Such deviations were believed to be attributed to the difference in the purpose and calibration procedure of the studies. Therefore, these hydraulic parameters were only reliable in a specific condition and could not be used as global parameters. Furthermore, Morvannou *et al.* (2012) proposed the only calibrated hydraulic parameters for the dual-porosity model, as summarized in Table 5.3, where the hydraulic parameters were inversely modeled using an in-situ assessment based on the water content along the reed bed.

Table 5.2: Hydraulic parameters of gravel used in the literature for equilibrium hydraulic flow simulation of STRB.

Reference	Particle size *(mm)*	θ_r *(-)*	θ_s *(-)*	α *(cm^{-1})*	n *(-)*	K_s *($cm\ min^{-1}$)*
Carsel and Parrish (1988)	-	0.045	0.430	0.145	2.68	0.50
Langergraber and Šimůnek (2005)	4-8	0.045	0.410	0.145	5.00	1000.00
	16-32	0.056	0.150	0.145	1.92	1000.00
Langergraber and Šimůnek (2006)	2-8	0.050	0.370	0.050	2.80	600.00
Toscano *et al.* (2009)	16-32	0.050	0.190	0.028	4.00	8.30
Maier *et al.* (2009)	4-8	-	0.350	0.085	9.80	7.80
	8-16	-	-	0.097	8.60	258.00
Giraldi *et al.* (2010)	5-10	0.036	0.483	0.145	2.68	23.88
	20-30	0.035	0.483	0.145	2.68	120.00
	50-60	0.035	0.480	0.145	2.68	120.00
Morvannou *et al.* (2013)	-	0.310	0.406	2.860	1.35	6.60
	-	0.220	0.406	2.770	1.30	6.60
	30-60	0.230	0.440	2.720	1.47	71.40
Fournel *et al.* (2013)	10-20	0.040	0.430	0.180	3.30	70.00

Samsó *et al.* (2016)	2-44	0.010	0.390	0.145	2.68	6.94
Moezzibadi *et al.* (2019)	-	0.102	0.520	0.217	2.61	0.544
	-	0.154	0.630	0.161	3.03	0.620
Thazhathu Veetil and Thampi (2021)	1-4	0.056	0.310	0.154	1.62	162.00
	Mean	0.095	0.405	0.574	3.34	192.40
	SD	0.090	0.114	1.018	2.33	327.75
	Min	0.010	0.150	0.028	1.30	0.50
	Max	0.310	0.630	2.860	9.80	1000.00

Table 5.3: Hydraulic parameters of gravel used in the literature for preferential hydraulic flow simulation of STRB.

Reference	θ_r^m (-)	θ_s^m (-)	α (cm^{-1})	n (-)	K_s ($cm\ min^{-1}$)	θ_r^{im} (-)	θ_s^{im} (-)	ω (min^{-1})
Morvannou *et al.* (2012)	0.0	0.02	0.145	5.00	1500.00	0.38	0.39	0.30
	0.0	0.05	0.145	1.92	1500.00	0.34	0.36	0.30

In most cases, the gravel was seldom used as the main layer, while it acted as the intermediate layer or drainage layer in the substrate profile (Fournel *et al.*, 2013; Langergraber & Šimůnek, 2005; Langergraber & Šimůnek, 2006; Morvannou *et al.*, 2012; Toscano *et al.*, 2009). The drainage layer was assumed to be saturated in the simulation. Hence, its effect on the overall calibration was minor. Therefore, the values of VGM parameters always referred to the standard of sand (Langergraber & Šimůnek, 2005). It has been highlighted that the sludge deposit layer's characteristics are crucial to the overall hydraulic performance. Hence, Morvannou *et al.* (2013) have developed a set of hydraulic parameters for the sludge deposit, as presented in Table 5.4.

Table 5.4: Hydraulic parameters of sludge deposit used in the literature for equilibrium hydraulic flow simulation of STRB.

Reference	θ_r (-)	θ_s (-)	α (cm^{-1})	n (-)	K_s ($cm\ min^{-1}$)
Morvannou *et al.* (2013)	0.65	0.84	0.15	1.80	0.45

However, the θ_r and θ_s values of the sludge deposit layer used in the research were extremely high compared to the standard hydraulic parameters of loam and slit, as shown in Table 5.5. The values of α and K_s were comparable to the standard value of sand, whereas the value of *n* was close to the standard value of loam. Therefore, the range

of the hydraulic parameters of the sludge deposit was obtained by interpolating data between the standard parameters of sand and loam.

Table 5.5: Standard equilibrium hydraulic flow parameters of loam and slit.

Reference	Soil Catalogue	θ_r (-)	θ_s (-)	α (cm^{-1})	n (-)	K_s ($cm\ min^{-1}$)
Carsel and Parrish (1988)	Loam	0.078	0.430	0.036	1.56	0.017
	Slit	0.034	0.460	0.016	1.370	0.004

Meanwhile, determining specific cake resistance and viscosity for the sludge deposit was also an issue in the hydraulic simulation. The limited instrumental equipment has hindered the evaluation of specific cake resistance and viscosity of the septage used in this study. Hence, the specific cake resistance and viscosity values were retrieved from the literature for different types of sludge used in the simulation, as indicated in Table 5.6 and Table 5.7, respectively. Particularly in sludge treatment, the values of the specific cake resistance were revealed to be significantly high, with a power of 10 to 13, due to its non-conditioned sludge characteristics and lack of any chemical additive. The specific cake resistance and viscosity values used in this study were 30×10^{13} m/kg and 0.015 kg/ms, respectively, per the non-conditioned biodigester sludge. Since septic sludge contains abundant solids and organic matter, the resultant layer permeability is always low, leading to a high specific cake resistance (Reichert *et al.*, 2018), as shown in domestic sludge. These values were then included in the compressible cake filtration model to estimate the sludge accumulation.

Table 5.6: Specific cake resistance used in the literature for sludge accumulation.

Reference	Source of wastewater	Type of sludge	α (m/kg)
Eden (1983)	Domestic	Activated sludge	$(4\text{-}12) \times 10^{13}$
		Biodigester sludge	$(3\text{-}30) \times 10^{13}$
		Conditioned digested sludge	$(2\text{-}20) \times 10^{11}$
		Conditioned primary sludge	$(3\text{-}10) \times 10^{11}$
Mahesh *et al.* (2006)	Pulp and paper	Without any additive	6.80×10^{11}
		With NaCl as additive	3.20×10^{11}
		With PAA as additive	4.60×10^{11}
Garg *et al.* (2005)		Thermochemical and	102.80-272.20

		Electrochemical sludge	
Verma *et al.* (2010)	Petrochemical	$FeCl_3$	2.49×10^{11}
		$FeCl_3$ + C-PAA	1.14×10^{10}
Ramavandi (2014)	Textile	FCE	1.75×10^{11}

Table 5.7: Viscosity used in the literature for sludge accumulation.

Reference	Type of sludge	*μ (kg/ms)*
Wolski (2021)	Non-conditioned digested sludge	0.015
	Non-conditioned excess sludge	0.009
	Conditioned digested sludge	0.020
	Conditioned excess sludge	0.011
Goel *et al.* (2004)	Digested sludge	0.200 - 0.400
Brar *et al.* (2005)	Fermented sludge	≤ 0.150
Bhaga and Weber (1981)	Liquid manure	0.006 - 0.008 for TS of 25% 0.010 - 0.030 for TS of 5.4% 0.250 - 2.93 for TS of 12.1%
Dubash and Frigaard (2007)	Anaerobically digested sludge	0.037 - 0.406
USEPA (1979)	Anaerobically digested sludge	≤ 0.310 for TS ≤ 4% 0.310 - 0.625 for TS of 4 - 5%
Eshtiaghi *et al.* (2012)	Thickened digested sludge	0.050 - 1.000

In summary, the optimal hydraulic parameters were calibrated through visual evaluation and error analysis, such as mean absolute error MAE, to fit the measured effluent flux from the conducted experiments. The hydraulic parameter for gravel was elaborated from the standard parameters of sand, while the hydraulic parameter for sludge deposit was interpolated between the standard parameters of sand and loam. Finally, the specific cake resistance of the sludge deposit was estimated to be identical to that of the biodigester sludge.

5.4 Inputs for Evapotranspiration (ET)

Based on the historical weather data in Miri, Sarawak, from July to November 2022, the average daily air temperature was 26.8 ℃, ranging from 21.6 to 33.7 ℃. Due to the frequent rains, the average daily humidity was relatively high throughout the experimental period, at around 87 %. The average wind velocity was recorded to be 3.3

ms^{-1}. In addition, Julian Day determined the potential solar radiation due to the absence of solar radiation data. The other essential data for the ET simulation is presented in Table 5.8 (Paredes *et al.*, 2020).

Table 5.8: Inputs for evapotranspiration.

Parameters	Values
Height of crop, h_c (m)	1.00
Height of wind measurement, z_w (m)	2.00
Height of humidity measurement, z_h (m)	2.00
LAI_{active} coefficient, α (-)	0.50
Empirical coefficient in Beer-lambert law, a_{bl} (-)	0.50
Maximum root depth, z_R (cm)	30.00
Fraction of the roof length density in the top 10% of the root zone, F_{10} (-)	0.40
Wilting point, $\Theta_{wilting}$ (-)	0.10
Functional parameter for water stress distribution, γ_α (-)	0.23
Root length density, g_0 (g/cm^3)	0.01

5.5 Inputs for Sludge Accumulation

The fraction of particles retained on the reed bed surface estimated the sludge accumulation rate. Considering the different types of initial TS concentration used for the raw septage, the density and porosity of the sludge varied along the batches of loading. Hence, the inputs of sludge accumulation based on the initial TS concentration for sludge and sludge deposit were calculated and summarized in Table 5.9 and Table 5.10, respectively. The sludge density and porosity were determined from the septage's initial TS concentration and solids content, respectively. In contrast, the sludge deposit porosity was obtained from the solids content of the sludge deposit layer. These data were essential in calculating sludge cake/deposit permeability for the respective reed bed.

Table 5.9: Inputs of sludge properties for sludge accumulation.

Initial TS Concentration (mg/L)	Density, ρ (kg/m^3)	Sludge Porosity, ε_s (-)
18780	18.78	0.0094
29967	29.97	0.0150
55780	55.78	0.0279
20365	20.37	0.0102

10796	10.80	0.0054
17507	17.51	0.0088

Table 5.10: Inputs of cake/sludge deposit properties for sludge accumulation.

Initial TS Concentration (mg/L)	Sludge Deposit Porosity, ε_c (-)					
	Bed 1	**Bed 2**	**Bed 3**	**Bed 4**	**Bed 5**	**Bed 6**
18780	0.47	0.17	0.18	0.18	0.22	0.22
29967	0.43	0.20	0.24	0.23	0.19	0.23
55780	0.59	0.15	0.18	0.18	0.25	0.22
20365	0.58	0.21	0.17	0.08	0.07	0.19
10796	0.29	0.15	0.14	0.59	0.18	0.14
17507	0.34	0.30	0.32	0.21	0.34	0.16

The porosity of the sludge was parallel to its density. The higher sludge density indicates higher solids concentration in a specific sludge volume. Due to different loading conditions, the sludge deposit porosity varied across the reed beds. The beds with shorter resting periods and lower SLRs would have higher porosity upon extensive water loss by drainage and evapotranspiration. Therefore, settling solid particles on the sludge deposit layer requires known initial sludge and sludge deposit porosity to estimate the filling of these voids and further sludge accumulation (Huong *et al.*, 2024b).

5.6 Procedure for Calibration of Hydraulic Parameters to Fit the Measured Data

Typically, the variably saturated flow model simulates an effluent flux proportional to the surface ponding level. Since the ponding is temporary, the pressure difference varies throughout the simulation. However, in the cases of 'bypassed' and 'clogged', the ponding level either dropped drastically or remained static for a long time, thus affecting the overall hydraulic performance. Therefore, these cases were not considered in the scope of this simulation. In the calibration, two major concerns were the fit of the measured peak effluent flux and the start of effluent discharge to the simulated flux. Hence, the main goal of this simulation was to fit all sets of the measured effluent flux with the same set of hydraulic parameters to verify its reliability.

Since the variably saturated flow is a function of water content, the portion between the mobile and immobile regions is essential to the hydraulic simulation. Giraldi

and Iannelli (2009) confirmed that most dead zones were found in the bed's upper layers. This assumption is valid due to the presence of micropores capable of retaining stagnant water. Hence, the immobile regions in the sludge deposit and intermediate layer are more significant than the gravel layers.

Generally, the sludge deposit layer was assumed to mainly consist of an immobile region, which saturated the layer throughout the operation. In the simulation for septage treatment, the values of the VGM parameters were typically too low to describe the high inherent water content before the reed bed was loaded. However, the water migration between the mobile and immobile regions has always reached equilibrium in the simulation. Further, the saturated hydraulic conductivity was revealed to be the most sensitive parameter to match the maximum effluent flux, which has dominated the flux across this low permeability layer. Therefore, the hydraulic parameters in this simulation match the measured effluent flux obtained in the laboratory-scale STRB system and are displayed in Table 5.11 (Tan *et al.*, 2017).

Table 5.11: Values of hydraulic parameters used in the hydraulic simulation.

Hydraulic Parameters	**Layer 1 – Sludge deposit layer**	**Layer 2 – Intermediate layer (5 cm)**	**Layer 3 – Small-size gravel layer (10 cm)**	**Layer 4 – Medium-size gravel layer (10 cm)**
$\boldsymbol{\theta_r^m}$	0.08	0.06	0.04	0.04
$\boldsymbol{\theta_s^m}$	0.22	0.28	0.32	0.36
$\boldsymbol{\alpha}$ $(\boldsymbol{cm^{-1}})$	0.07	0.18	0.29	0.36
$\boldsymbol{n}$	1.80	2.70	3.50	4.00
$\boldsymbol{K_s}$ $(\boldsymbol{cm\ min^{-1}})$	-	10.00	1300.00	1500.00
$\boldsymbol{l}$	0.50	0.50	0.50	.050
$\boldsymbol{\theta_r^{im}}$	0.10	0.03	0	0
$\boldsymbol{\theta_s^{im}}$	0.20	0.18	0.14	0.12
$\boldsymbol{\omega}$ $(\boldsymbol{min^{-1}})$	0.002	0.007	0.02	0.04

The sludge deposit layer has the most apparent impact on the hydraulic flux in the substrate profile. Therefore, the effect of the intermediate and gravel layers was considered minor, and the hydraulic properties of these layers were fixed as constant in the calibration. There are several guidelines found for the calibration process:

- Generally, the intermediate and grave layers are unsaturated due to the limited amount of sludge percolation through the sludge deposit layer.
- The effective saturation in the mobile region was a function of the saturated water content (θ_s^m). In unsaturated flow, the unsaturated hydraulic conductivity is greatly reduced by the low effective saturation due to the high θ_s^m. Therefore, these parameters' values must be weighed carefully during calibration.
- The VGM parameters, α and n are typically governed by the amount of water retained in the substrate, corresponding to the pressure head. If the values of these parameters used in the gravel are as low as those used for sand or silt, the inherent water content and flux estimated from the initial pressure distribution would be unreasonable and eventually fail to converge during the iterative computation.
- The amount of water exchange between the mobile and immobile regions was insignificant due to the low effective saturation in both regions.

In addition, the initial water content in the reed bed is another crucial factor in the hydraulic simulation. The flow of water was discovered to be less smooth when the bed was in dry condition. Therefore, the initial water content, the proposed model's initial pressure head, was optimized to match the flow-occurring delay.

5.7 Results and Discussions

The hydraulic module has successfully simulated the flux behavior in line with the Richards equation theory. Out of 78 sets of flux data obtained throughout the experiments, 25 were ponded cases, 9 were bypassed cases, and the remaining 44 were considered normal cases. Most promising simulations were normal cases without ponding and cracks on the sludge deposit layer.

Generally, the degree of freedom in the model simulation is better kept to a small number as more degrees of freedom increase the difficulty of calibration. Hence, the degrees of freedom in the conventional hydraulic simulation are limited to the saturated conductivity of the sludge deposit layer, K_s and the initial pressure distribution, h. These two variables manipulated the flux peaks and the flow-occurring delays, which governed the main mechanism of the hydraulic simulation. This study also tested the model with

different variables, including the sludge deposit thickness and the hydraulic load. Therefore, 10 sets of flux data were selected for the presentation, mostly referring to the typical cases, and some of the minor ponding cases. The overall trend of the preliminary simulated results is shown in **Appendix S**.

The simulated results were analyzed using the mean absolute error (MAE), mean absolute error percentage (MAE%), root mean square error (RMSE), and regression analysis to verify the accuracy of the proposed model. The RMSE is a statistical calculation to quantify the deviation between the actual and the predicted data, where a lower value indicates a better simulation performance. Hence, the MAE, MAE%, and RMSE are calculated as shown in Equations (5.1) to (5.3).

$$MAE = \frac{1}{n}\sum_{i=1}^{n}|A_t - P_t| \tag{5.1}$$

$$MAE\% = \frac{1}{n}\sum_{i=1}^{n}\left|\frac{A_t - P_t}{A_t}\right| \times 100\% \tag{5.2}$$

$$RMSE = \sqrt{\frac{1}{n}\sum_{i=1}^{n}(A_t - P_t)^2} \tag{5.3}$$

where A_t is the actual flow rate in the experiment, P_t is the simulated flow rate of the simulation, and n is the number of the data set.

On the other hand, a linear regression analysis was conducted between the measured and simulated fluxes to determine the coefficient of determination (R^2). The values of R^2 ranged from 0 to 1, describing the similarity of the overall flow trends between the actual and the predicted data. However, the values of R^2 were unable to be an indicator of accuracy in the hydraulic simulation but represented the consistency of variation between the measured and simulated data. The values of R^2 were obtained from the regression analysis function in Microsoft Excel.

5.7.1 Hydraulic Behavior

In this study, the modified Richards' equation with velocity-based finite difference discretization has successfully described the hydraulic dynamics in the STRBs. The observed flow trends are categorized as normal, ponding, and cracked cases. Under normal flow cases, the effluent flux increases rapidly to the peak before gradually decreasing upon drainage dewatering and evapotranspiration. In contrast, the dewatering process is extensively lengthened in ponding cases due to the large hydraulic load applied. Further, the flux peak under the cracked flow case is extraordinarily high without visible increment during the feeding stage. The effluent instantly dashed out from the bottom of the bed after septage loading, and the drainage flow decreased significantly after the peak.

In the hydraulic simulation, the modified Richards' equation using the moving-mesh method describes the changes in sludge ponding level and sludge deposit layer thickness. The main driving force is the hydraulic head, *h*, and the saturated hydraulic conductivity, *Ks* of the sludge deposit layer, which limits the maximum allowable infiltration rate of the overall effluent flux. During the temporary ponding condition, the top boundary is set to be a head-controlled dewatering. In contrast, flux-controlled drainage dewatering during the resting period and the bottom boundary are always free drainage conditions. Thus, the proposed model simulates the moving boundary of the sludge ponding level and the sludge deposit thickness simultaneously with the resulting infiltration flux, evapotranspiration rate, and organic content.

Calibrating as low as two degrees of freedom delivered a simple approach to match the measured data with simulated outcomes. The K_s values were calibrated in advance to match the peak effluent flux, followed by the values of *h* to be adjusted to fit the flow delay occurrence. Both parameters were weighted simultaneously, where the K_s values significantly impacted the delay of flow occurrence, but the values of *h* had a minor influence on the flux peak. The summary of the calibrated parameters and the error analysis is displayed in **Appendix T**. Figure 5.4 to Figure 5.7 illustrate the successful simulations of the calibrated flux and cumulative discharge results for each bed. The overall simulated effluent flux and cumulative effluent results have effectively matched

the experimental measurements of the selected cases regardless of the SLRs and resting periods, indicating the robustness of the model in simulating the effluent flow.

Richards' equation describes the hydraulic head difference as the driving force for the infiltration flow in the STRB (Huong *et al.*, 2024b). By means, a larger head difference due to high loading results in a faster hydraulic flow. For instance, the highest effluent flux was noticed in case AY with the hydraulic load of 90940 ml, presenting a flux peak of 0.4456 cm/min. In contrast, case A has the lowest flux peak of 0.0054 cm/min upon the smallest hydraulic load of 8710 ml. Occasionally, there were cases where the flow pattern did not obey the typical flow trend, and it could be attributed to cracked, ponding, and clogging conditions.

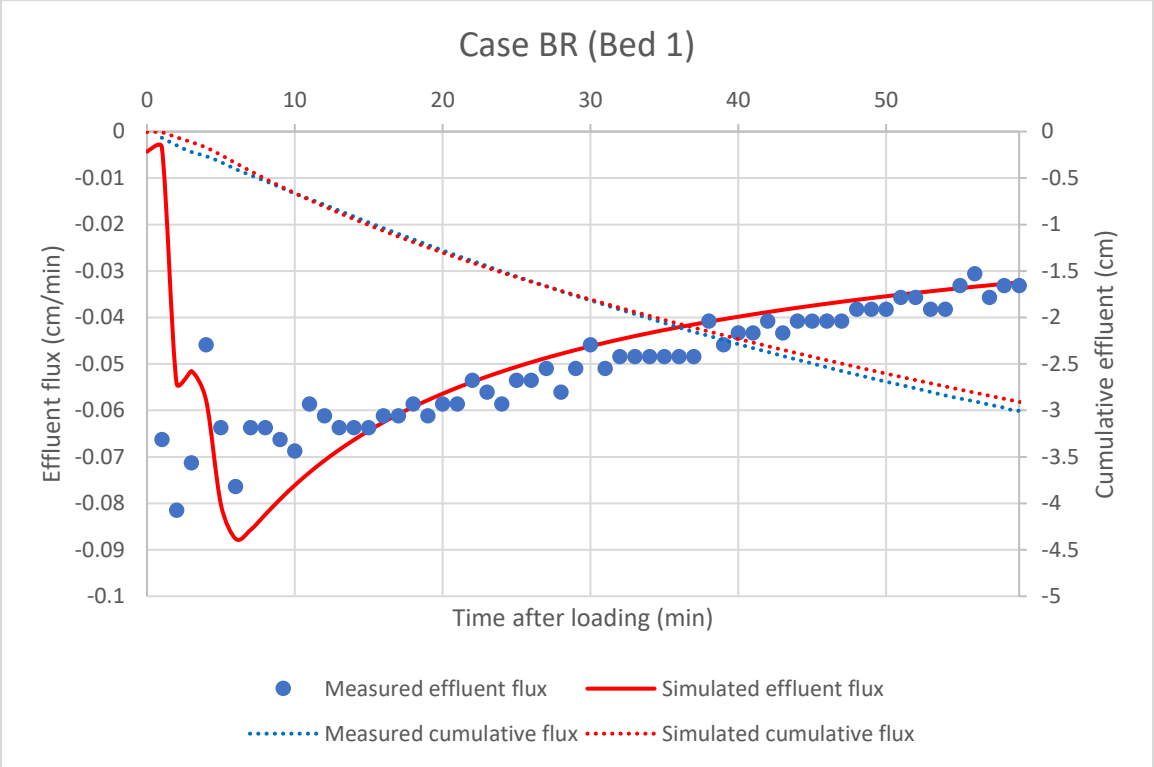

Figure 5.2: Simulated flux of case BR (Bed 1 | 9345 ml | 7.50 cm).

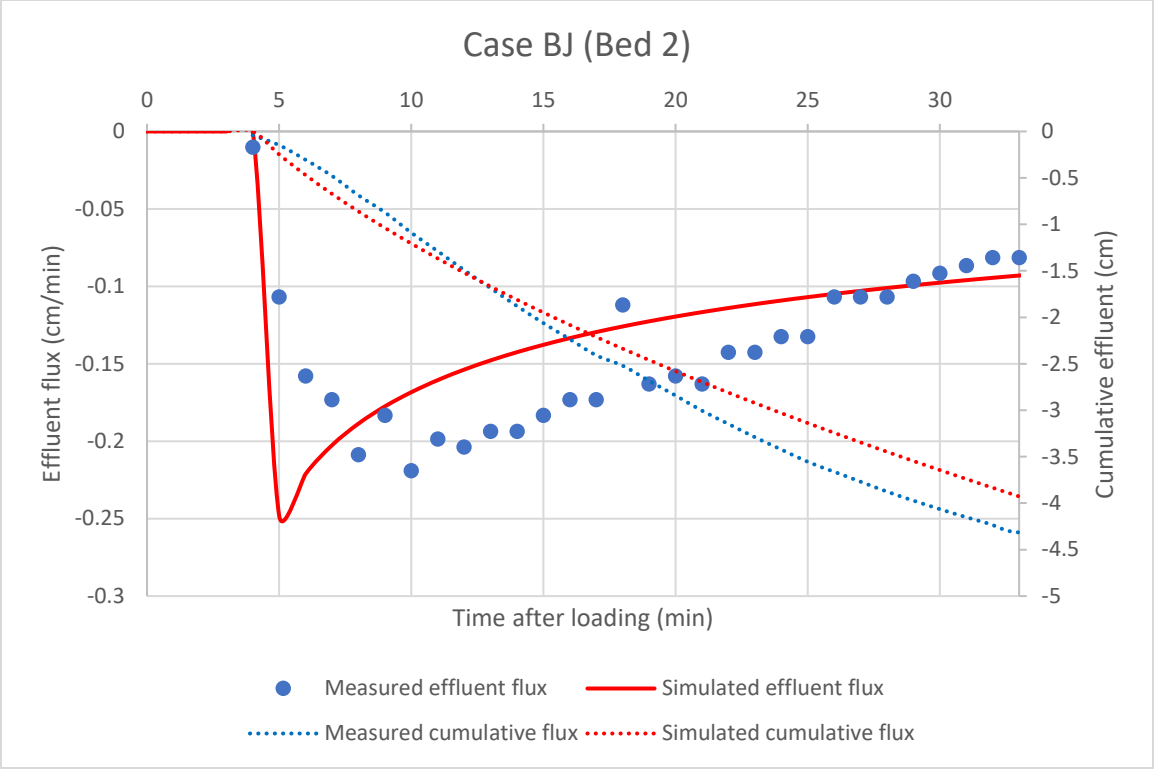

Figure 5.3: Simulated flux of case BJ (Bed 2 | 18690 ml | 12.50 cm).

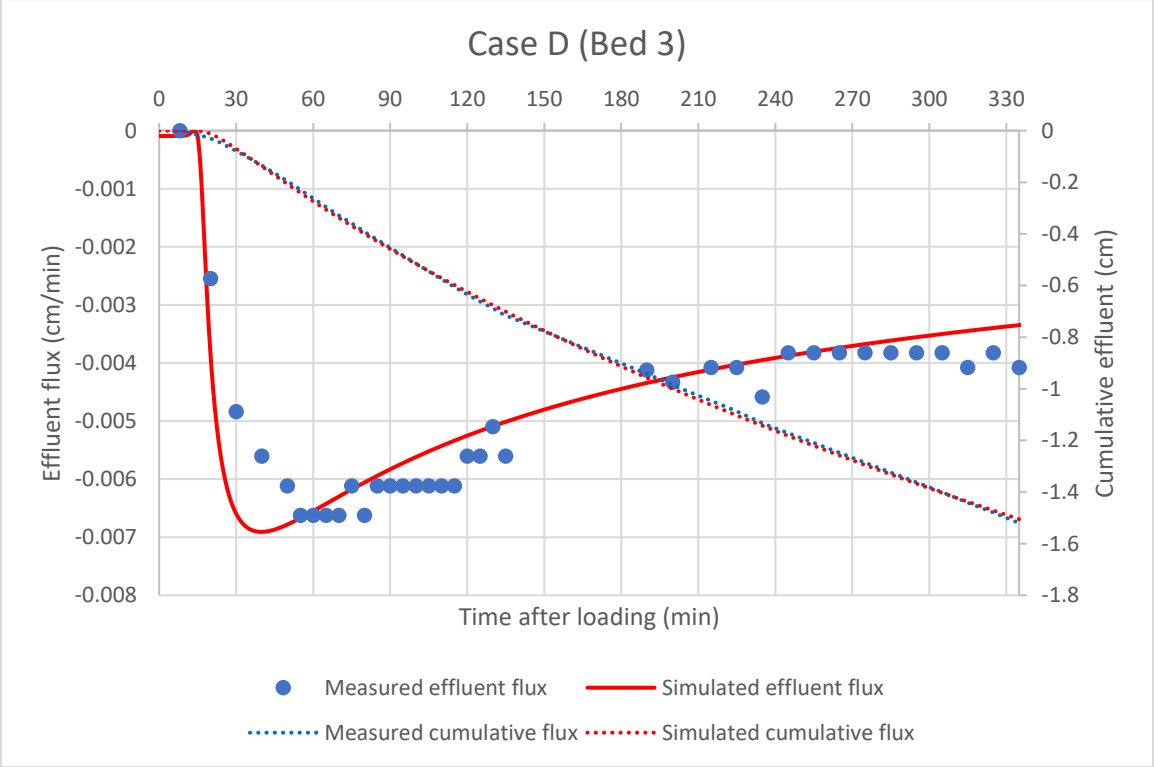

Figure 5.4: Simulated flux of case D (Bed 3 | 8710 ml | 7.83 cm).

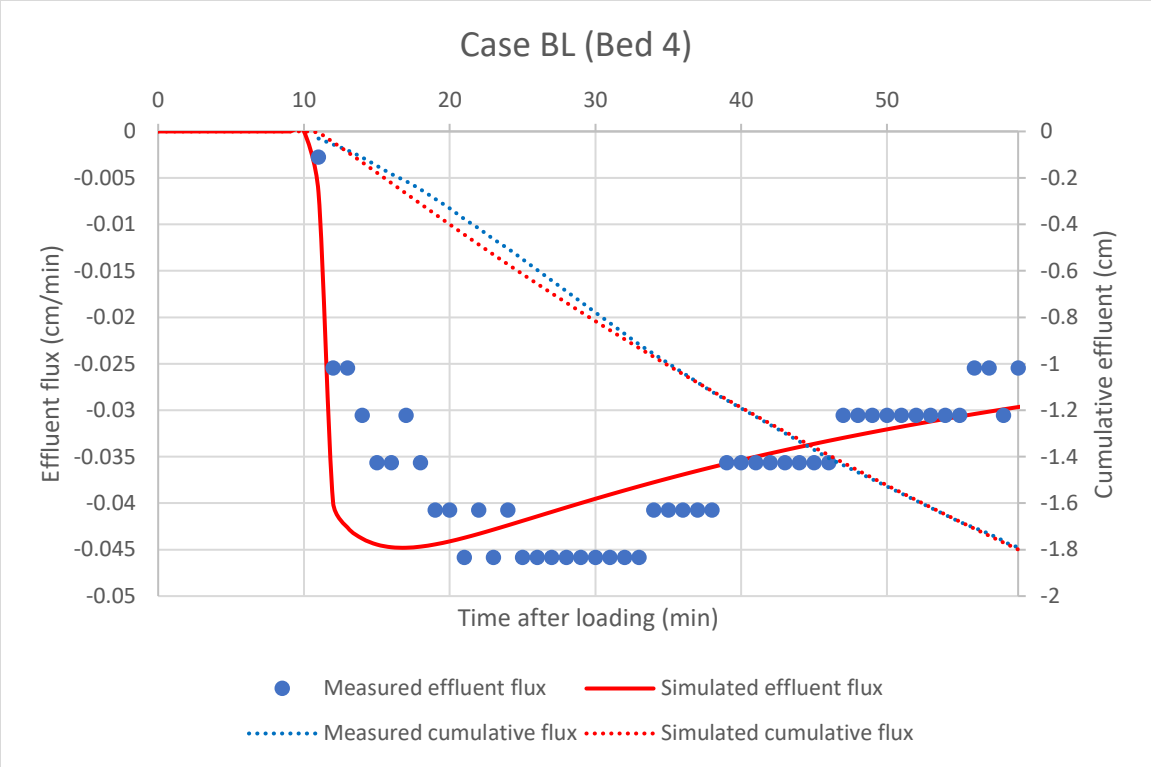

Figure 5.5: Simulated flux of case BL (Bed 4 | 56080 ml | 12.33 cm).

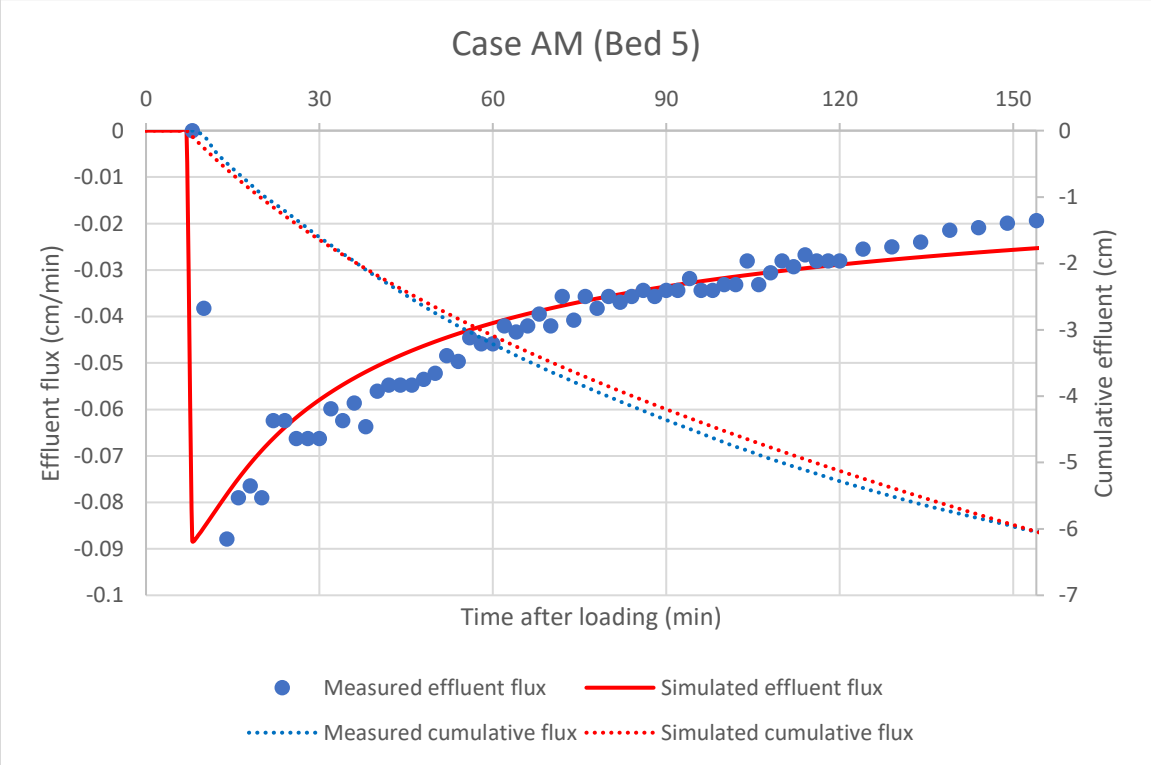

Figure 5.6: Simulated flux of case AM (Bed 5 | 90315 ml | 8.00 cm).

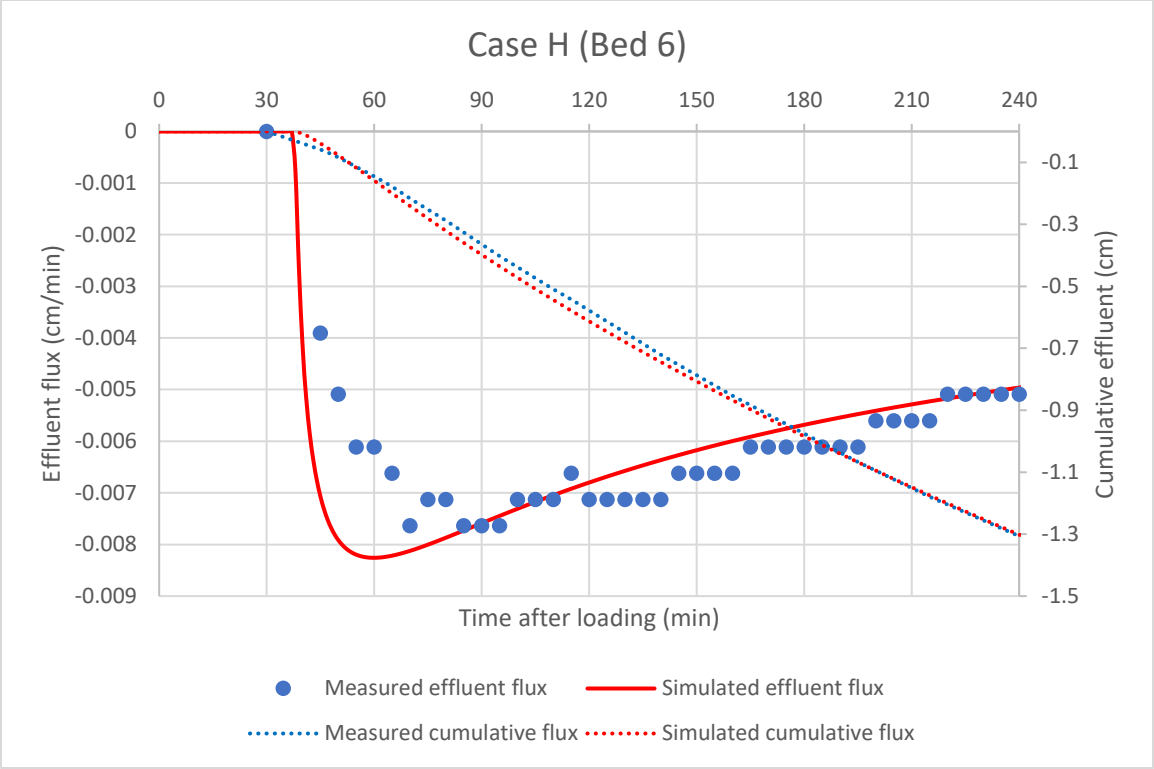

Figure 5.7: Simulated flux of case H (Bed 6 | 26140 ml | 8.33 cm).

In cracked conditions, the predicted pressure head failed to match the measured data due to instant effluent discharge but showed a good match with the flux peak in cracked conditions, as shown in Figure 5.8 (case AP). Although the sludge deposit was considered thick at 12.33 cm, cracks were still found on the sludge deposit layer. The influent sludge penetrated through the sludge deposit layer and directly bypassed the reed bed, leading to a significant increase in the effluent flux at the early stage of treatment (Huong *et al.*, 2024a). Subsequently, the effluent flux declined drastically after the extraordinarily high flux peak at 2.6050 cm/min. This condition has caused a large deviation between the measured and predicted cumulative effluents.

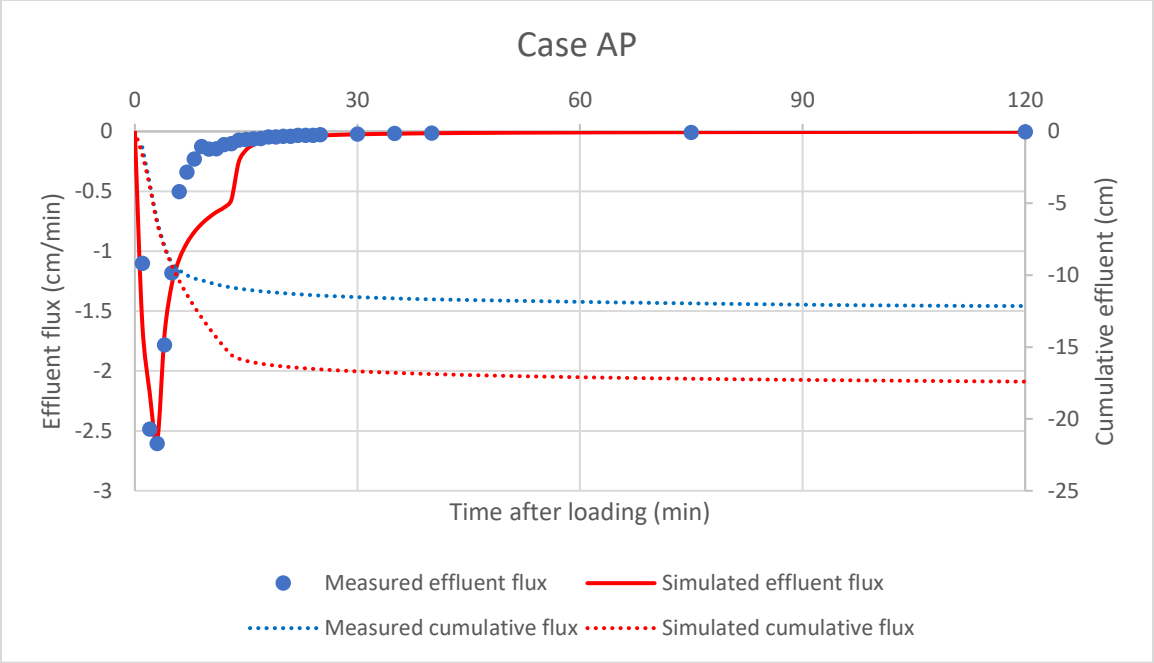

Figure 5.8: Simulated flux of case AP (30310 ml | 12.33 cm).

In contrast, the predicted initial pressure head failed to simulate the actual flow occurrence delay and flux peak due to the severity of ponding. Figure 5.9 (case AY) shows the minor ponding condition with 90940 ml of hydraulic load and 10.33 cm of sludge deposit layer. Although the proposed model could describe the overall trend of effluent flux drainage, the predicted effluent flux peak was higher in the feeding stage, thus leading to higher cumulative effluent. The ponding condition is believed to be caused by the continuous accumulation of the sludge deposit layer, which acted as a film that reduced the layer permeability (Tan *et al.*, 2023). A similar outcome of the clogging condition can be seen in Figure 5.10 (case BZ). In this case, the hydraulic load was 28040 ml with a sludge deposit layer thickness of 13 cm. In such a condition, the measured effluent flux presented a relatively constant discharge after the peak at 0.0840 cm/min. The model simulation failed to match the actual flow occurrence delay and flux peak, as well as the constant effluent flux during the drainage. The thicker sludge deposit layer is believed to be the leading cause of the severity of the ponding, where the duration of constant effluent discharge was prolonged to economically unprofitable. Hence, extensively prolonged surface ponding leading to waterlogging would always result in a typically low hydraulic conductivity.

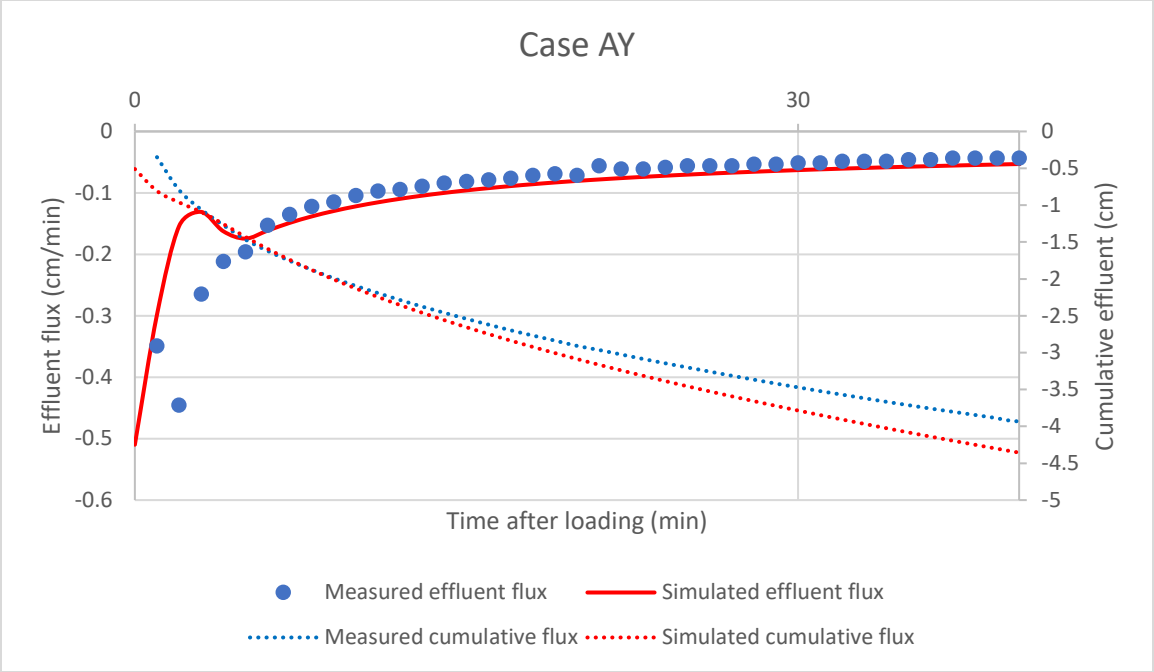

Figure 5.9: Simulated flux of case AY (90940 ml | 10.33 cm).

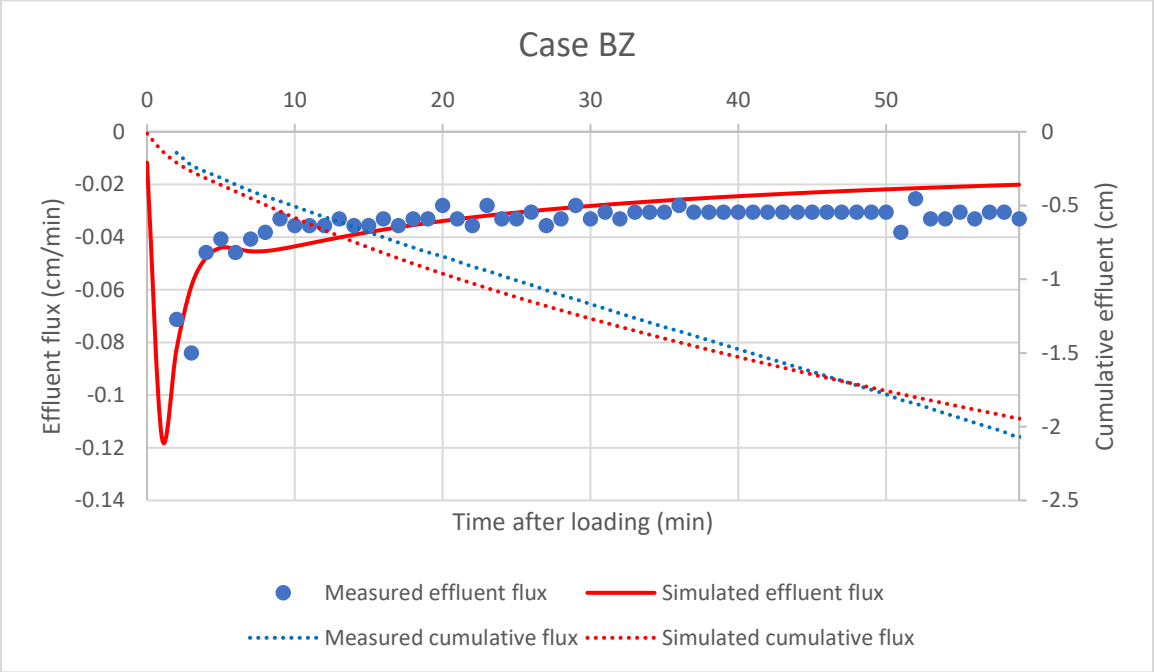

Figure 5.10: Simulated flux of case BZ (28040 ml | 13.00 cm).

In most cases, the effluent flux was generally over-predicted by the proposed model, as shown in Figure 5.11 (case B). The proposed hydraulic module is theoretically mass conservative because Richards' equation is derived using the water balanced in the

porous medium (Celia & Bouloutas, 1990). Hence, the compressible cake filtration theory and the influence of evapotranspiration have been applied to the model to account for the water balance, yet the simulated results were still over-predicted. The main reason is believed to be caused by the temporary retention of water inside the reed bed system, especially the sludge deposit (Obour *et al.*, 2018). The relatively high porosity of the sludge deposit and the substrate mediums have retained and stored some of the water within the bed, thus reducing the water recovery. The average water recovery for 78 cases at approximately 70% further supported the influence of water retention in the sludge deposits on the simulation accuracy.

Further, another possibility of flux overprediction could be due to the underestimation of the exchange rate. Since a dual-porosity variably saturated flow has been considered in this study, the water exchange between the mobile and immobile zones should always be in equilibrium (Ghanbarian, 2021). However, a lower water exchange rate would lead to a slower infiltration process, retaining more water inside the reed bed profile and affecting the overall water recovery.

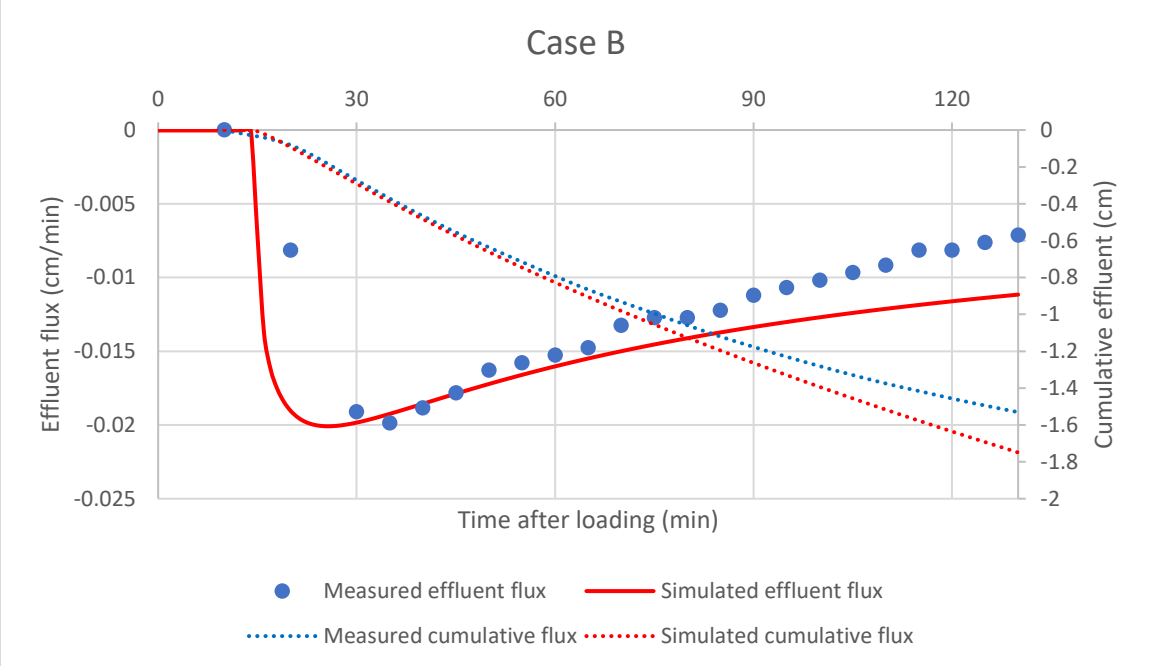

Figure 5.11: Simulated flux of case B (8710 ml | 7.00 cm).

Generally, the initial pressure head was calibrated to match the occurring time delay of effluent flux. This value implies the initial MC of the bed before new loading. Hence, a lower pressure head would result in longer flow delays due to the low MC in porous media, as it takes longer to reach saturation (Huong *et al.*, 2024b). Since the effluent flux is determined by the difference in the hydraulic head across the spatial discretion, the continuous effluent discharge would reduce the pressure difference upon the shallower ponding depth, subsequently decelerating the infiltration rate to an insignificant level (Ghanbarian, 2021).

However, a higher initial head distribution in the STRB of more than -10 cm usually presents a distinct effluent discharge curve. The sufficiently short pressure difference creates a shorter spatial path for the imposed flux to reach the bottom of the bed, reducing the flow-occurring delays to even below 1st minute. Hence, this situation has incidentally described the cracked sludge deposit layer that provides "preferential flow pathways" for the influent septage to bypass the substrate medium directly, leading to shorter infiltration across the STRB profile (Khomenko *et al.*, 2019). In contrast, when the hydraulic load reached the maximum capacity of the bed, the clogging condition retarded the bed and extensively prolonged the flow-occurring delay. However, the proposed model simulated the hydraulic flux with insignificant changes in the flux peak and flow-occurring delay for initial head distribution lower than -29 cm. Therefore, the optimal hydraulic head in the simulation should be kept in the range of -10 to -29 cm to avoid major deviations in the outcome. In other words, the hydraulic load must be kept to an allowable treatment capacity of the bed to prevent clogging.

Figure 5.12 shows the relationship between the pressure head and flow-occurring delay. The calibrated pressure heads decreased with the flow-occurring delays, which means the lower pressure head describes the longer flow-occurring delay. The calibrated pressure heads distribution ranged from -6 to -29 cm with an average value of approximately -19 ± 8 cm, regardless of the cracked and ponding cases. Since the influent septage bypassed the filter medium upon the cracked sludge deposit layer, instantaneous effluent discharge would lead to pressure heads larger than -10 cm. In other words, the

moisture content (MC) of the bed is considered low enough when the calibrated pressure heads are larger than -10 cm.

In contrast, the calibrated pressure head is at -11 to -28 cm when the bed is wet due to higher initial MC. Further, the pressure head lower than -29 cm is deemed a clogging condition, requiring a longer duration to overcome the wetness of the bed. In this case, the hydraulic load exceeded the maximum infiltration capacity of the bed, subsequently affecting the overall system performance due to the prolonged temporary ponding condition (Huong *et al.*, 2024a).

Since the ponding depth determines the hydraulic pressure acted on the reed bed, the maximum infiltration capacity is always limited to the hydraulic conductivity of the sludge deposit layer (Tan *et al.*, 2023). The sludge deposit layer has the lowest hydraulic conductivity across the reed bed profile and acts as a semi-permeable biofilm to filter the incoming septage (Trein *et al.*, 2019). Hence, the saturated hydraulic conductivity values of the sludge deposit layer were calibrated to fit the flux effluent peak of the gravity drainage.

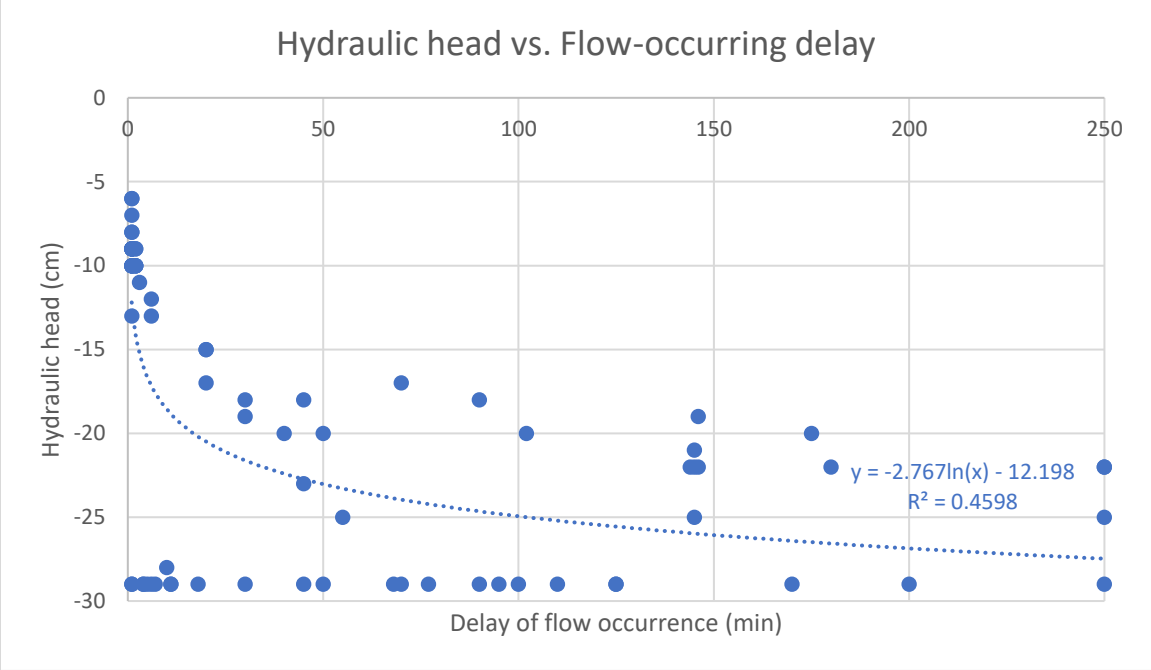

Figure 5.12: Relationship between hydraulic head and delay of flow occurrence.

Figure 5.13 shows the relationship between the saturated hydraulic conductivity of the sludge deposit layer and the flux peak. A relatively promising linear regression curve with the value of 0.8906 indicated that the calibrated saturated hydraulic conductivity always increased with the saturated hydraulic conductivity of the sludge deposit layer (Huong *et al.*, 2024b). The average saturated hydraulic conductivity was 0.0429 ± 0.1003 cm/min. The standard deviation was higher than the average value due to the cracked and ponding cases. The minimum and maximum saturated hydraulic conductivities were 0.0001 and 0.6000 cm/min, respectively. This finding reveals that a constant value of saturated hydraulic conductivity is unlikely to match all instances. Thus, the calibration of this parameter is essential (Huong *et al.*, 2023a). However, the overall calibrated saturated hydraulic conductivities were lower than 0.1 cm/min for cases without cracked and ponding conditions.

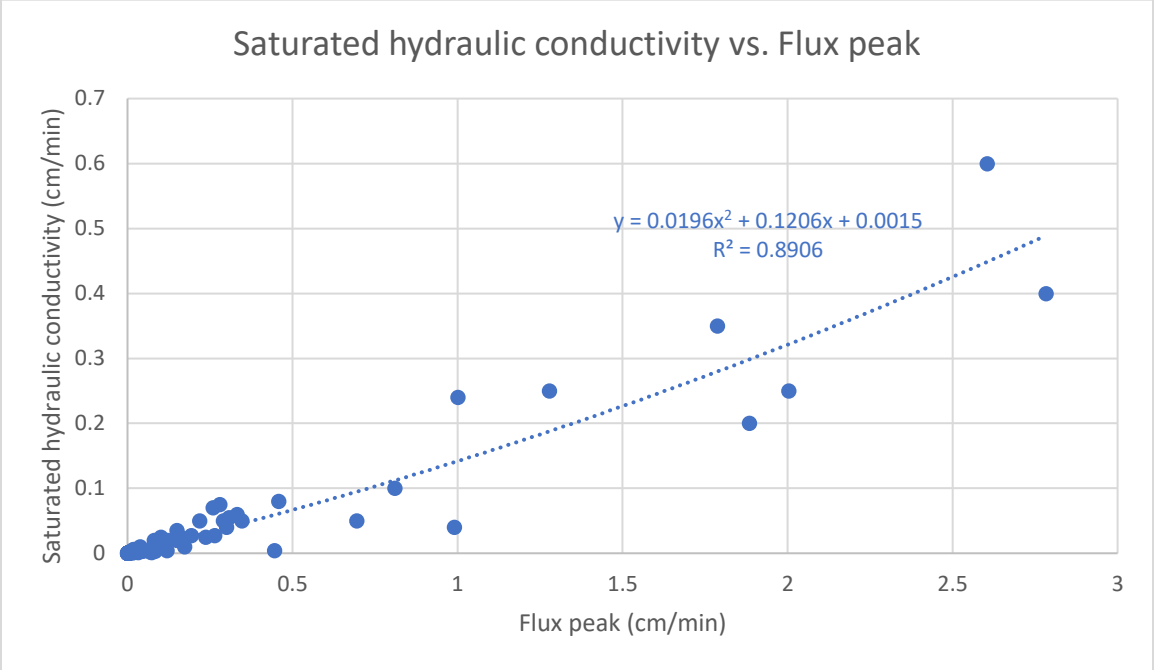

Figure 5.13: Relationship between flux peak and saturated hydraulic conductivity.

It has been determined that the saturated hydraulic conductivity of the sludge deposit layer always increases with the flux peak as it gives a relatively high R^2 value. However, the clogging of the substrates, which led to severe ponding conditions, deteriorates the overall predicted hydraulic heads of the simulation results. Since the simulation could not match the flow-occurring delays of the ponding conditions, the

predicted hydraulic head of -29 cm was assumed to be the clogging conditions. It was excluded when analyzing loading conditions (solids loading rates and resting periods). Figure 5.14 shows the relationship between the hydraulic head and flow delay under varying SLRs with a constant 6-day resting period. In contrast, these normal cases showed a significantly strong R^2 value of 0.9763, 0.9641, and 0.8743 for the 50, 100, and 150 kg/m^2/year SLRs, respectively. Hence, the generated trendline equations of $y = -2.364\ln(x) - 8.9074$, $y = -2.118\ln(x) - 9.5821$, and $y = -2.532\ln(x) - 9.0139$ can be used to estimate the hydraulic heads using the measured flow delays. The R^2 values also revealed that the proposed model is stable in predicting the hydraulic heads of the STRBs, where the results consistency declined with incremental SLRs. Further, the overall calibrated hydraulic heads for 100 kg/m^2/year SLR were higher than the other loading conditions, indicating the sustainability of the initial bed MC.

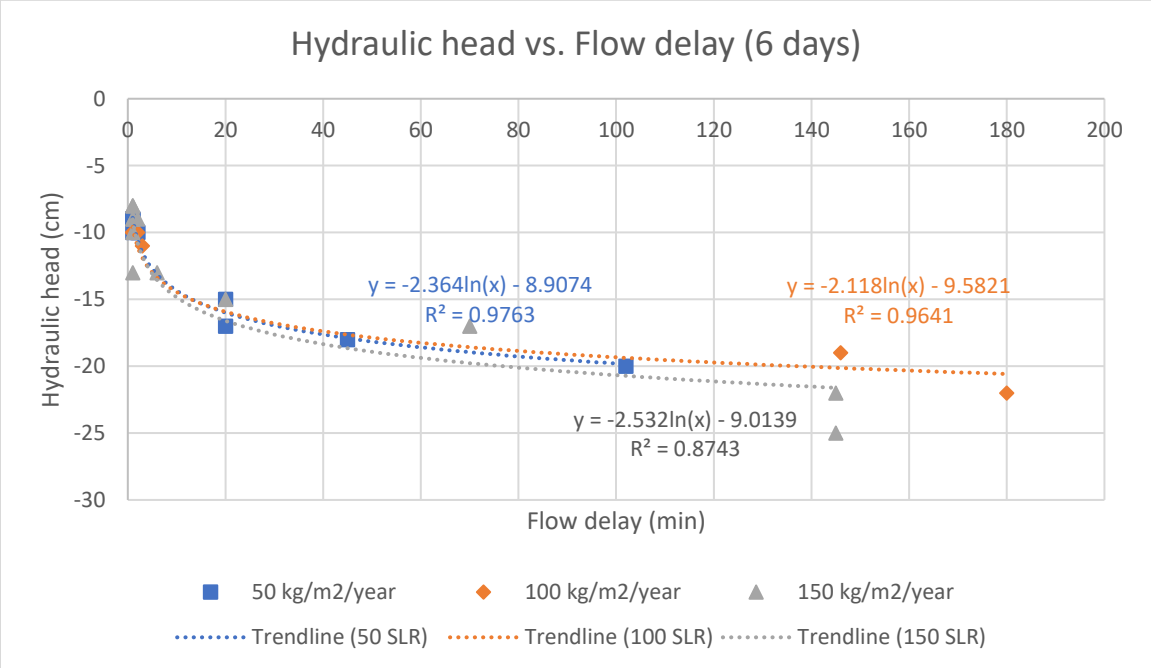

Figure 5.14: Graph of hydraulic head versus flow delay under varying SLRs.

On the other hand, the saturated hydraulic conductivity of the sludge deposit layer can be estimated through the generated trendline equations using the measured flux peak under different SLRs, as shown in Figure 5.15. The generated trendline equations are $y = 0.0344x^2 + 0.2033x + 0.0018$, $y = 0.0400x^2 + 0.1274x + 0.0006$, and $y =$

$0.0032x^2 + 0.1494x + 0.0017$ for the 50, 100, and 150 kg/m^2/year SLRs, respectively. The exclusion of the clogging conditions further reduced the deviation between the experimental and simulation results, leading to higher R^2 values of 0.9849, 0.9954, and 0.9367 for the respective SLRs compared to the overall R^2 value of 0.8906 with all cases included. The strong R^2 values for different loading conditions indicated the robustness of the proposed model in predicting the saturated hydraulic conductivity of the sludge deposit layer. Further, the highest R^2 value was seen in the 100 kg/m^2/year SLR and a 6-day resting period of the loading regime, proving the STRB is best operated with such a condition. In addition, the highest possible saturated hydraulic conductivity of 0.6 cm/min under such a condition also revealed the flexibility of the STRB in treating the septage in a wide range of infiltration flux.

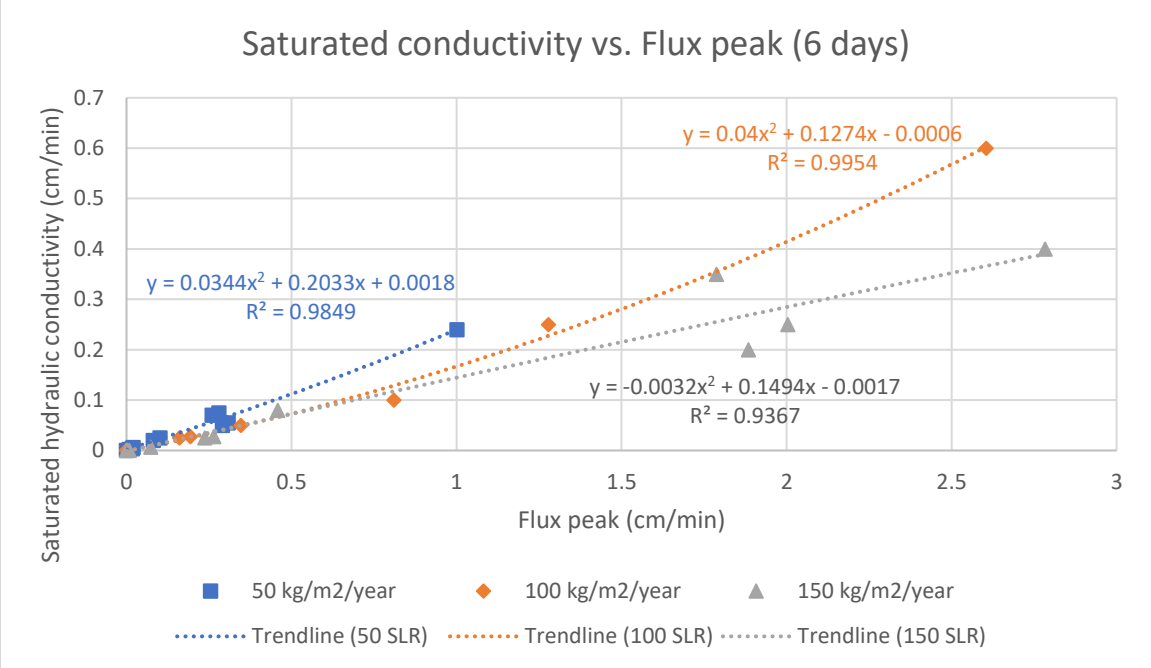

Figure 5.15: Graph of saturated hydraulic conductivity versus flux peak under varying SLRs.

Moreover, the hydraulic heads and the saturated hydraulic conductivities without the clogging conditions under varying resting periods also showed a similar result. The results for 18- and 27-day resting periods were excluded from the data analysis as these prolonged resting periods led to clogging conditions, and the hydraulic heads were mostly below -29 cm. Figure 5.16 and Figure 5.17 show the graphs of the hydraulic head

against flow delay and saturated hydraulic conductivity against flux peak under varying resting periods, respectively. The generated trendline equations were $y = -1.9831\ln(x) - 11.485$, $y = -2.118\ln(x) - 9.5821$, and $y = -2.964\ln(x) - 7.8307$ for the 3-, 6-, and 9-day resting periods, respectively. The R^2 values of 0.5225, 0.9641, and 0.9027 for the 3-, 6-, and 9-day resting periods, respectively, indicated that the proposed model has robustly calibrated the hydraulic heads to match with the measured flow delays under loading conditions of 100 kg/m^2/year SLR and 6-day resting period. The lowest hydraulic head range of approximately -10 to -20 cm confirmed the optimal resting period of 6 days, where the low hydraulic head indicates the low MC in the bed. Thus, the drainage process can be completed in time without prolonged ponding conditions (9-day resting period) or insufficient water to act as the driving force for dewatering (3-day resting period).

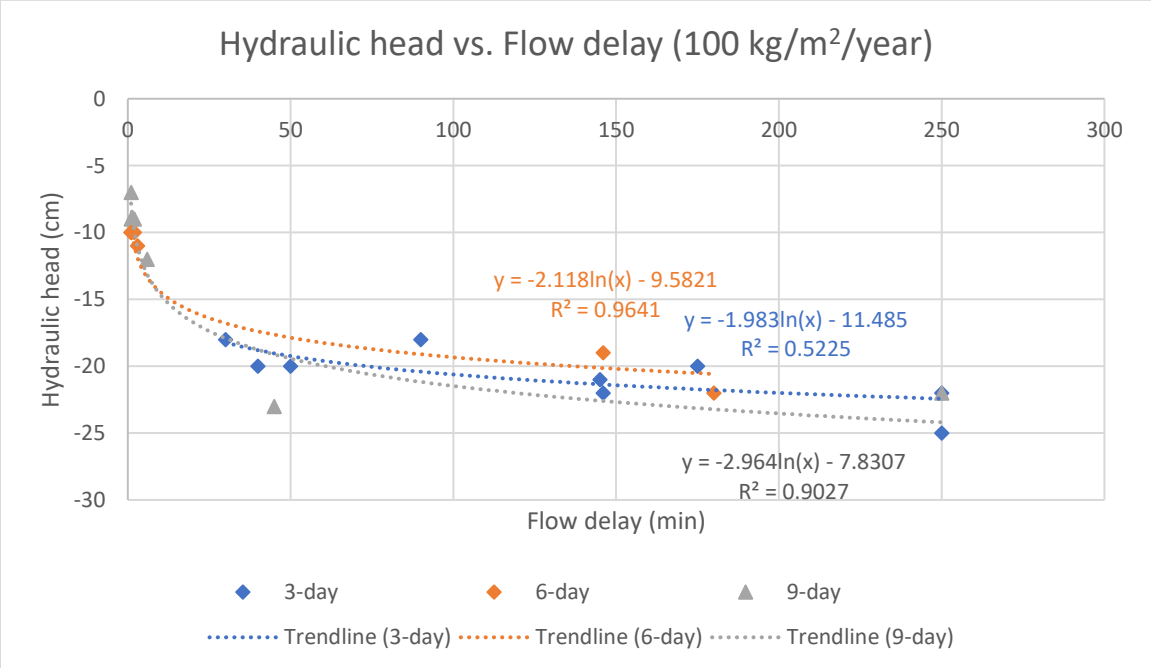

Figure 5.16: Graph of hydraulic head versus flow delay under varying resting periods.

In contrast, the generated trendline equations of $y = -32.299x^2 + 0.4000x + 7E^{-5}$, $y = 0.0400x^2 + 0.1274x + 0.0006$, and $y = 0.0391x^2 + 0.0442x + 0.0004$ with the R^2 values of 0.8840, 0.9954, and 0.9985 for the 3-, 6-, and 9-day resting periods, respectively, were determined for the relationship between the saturated hydraulic

conductivity and the flux peak under the constant 100 kg/m^2/year SLR. Since the drainage dewatering depends on the hydraulic head and saturated hydraulic conductivity of the sludge deposit layer, a higher hydraulic head and saturated conductivity would result in a faster draining rate. The loading condition of a 6-day resting period and 100 kg/m^2/year SLR presents a broader range of saturated conductivity from 0.0001 to 0.6 cm/min, ensuring a faster drainage and is time efficient.

In error analysis, the overall MAE and RMSE were calculated to be 0.039022 and 0.055862, respectively, indicating the robustness of the proposed model in simulating the effluent flow in STRB-treating septage. Meanwhile, the MAE% for 78 cases ranged from 4.94% to 331.72%. The extraordinarily high error percentage beyond 100% indicates that the MAE% is less appropriate for the flux data analysis. This is mostly due to the flux values of less than 1.0 cm/min, as they involved many decimals that have led to extremely high deviations (Armstrong & Collopy, 1992). Hence, the average MAE% of approximately 48% was considered high due to the incapability of the proposed model to describe the cracked and clogging cases with a simple calibration. However, the MAE% for 57 out of 78 cases was below average, which confirmed the reliability of the proposed model. Additionally, an average water recovery of approximately 70% upon incomplete drainage and evapotranspiration also contributed to the high MAE%, leading to a relatively low R^2 value of 0.5898 ± 0.2208.

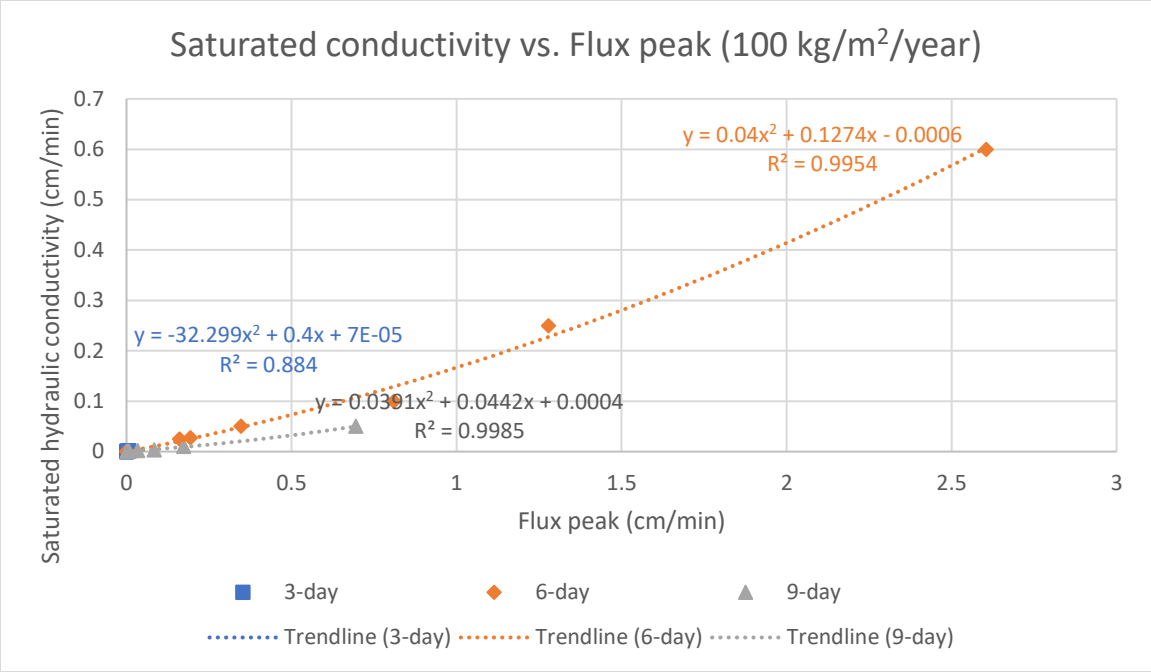

Figure 5.17: Graph of saturated hydraulic conductivity versus flux peak under varying resting periods.

Moreover, the average MAE and RMSE were always low for all loading conditions. However, the average MAE% was high due to flux overprediction towards the end of the treatment period, leading to a relatively low R^2 value. The average MAE% increased with SLRs (47.77% > 54.54% > 81.10%) of 50, 100, and 150 kg/m^2/year. In contrast, the lowest MAE% of 17.03% was found in the resting period of 18 days under varying resting periods, while the highest MAE% was attributed to a 6-day resting period with 81.10%. The high error percentage was caused by the high number of feeding-resting cycles, where the continuous sludge accumulation causes prolonged surface ponding and results in deviations. Hence, the standard deviations of the MAE, MAE%, and RMSE between the measured and predicted flux data were always larger than the average values due to the highly inconsistent results of the flow cases. These major errors were attributed to the cracked and clogging cases, where the predicted hydraulic heads and saturated conductivities always failed to match the flow-occurring delays and flux peaks, respectively.

5.7.2 Evapotranspiration (ET)

The potential evapotranspiration (ET) rate was estimated using the Penmen Monteith equation based on the weather data. The weather data, such as air temperature, wind speed, and relative humidity across the experimental period (July to November 2022), are shown in **Appendix U**. The minimum and maximum air temperatures were 21.6 and 33.7°C, respectively. The maximum wind speed was 7.9 m/s. At the same time, the minimum and maximum relative humidities were 47 and 100%, respectively. Certainly, considering evaporation and transpiration by vegetation has improved the accuracy of the hydraulic simulation based on the water balances. However, factors such as weather and climate conditions always affect the efficiency of ET. The Penman-Monteith equation has successfully described the water loss via the vegetation but is significantly dependent on the weather conditions as the equation is employed with climatic data (Dlouhá *et al.*, 2021). In Malaysia, the weather conditions are always high in temperature and windy, which causes a high ET rate. In return, the humidity and total rainfall are high, which potentially limits its efficiency.

Particularly in this study, the average crop height was assumed to be 1 m, with the empirical factor of *LAI* equivalent to 4. The index of *LAI* was used to represent the ET rate, which has shown a dependency on vegetation growth in the hydraulic simulation. The common reeds used in the study were one of the most seen vegetation applied to the reed bed system. These reeds are remarkable with their transpiration capability, rapid growth rate, impressive contaminants tolerance, and ponding condition (Abideen *et al.*, 2020; Abideen *et al.*, 2022; Mazumder *et al.*, 2021).

The simulation of water loss through evapotranspiration (ET) was included as a sink term of Richards' equation that involved the upper layer of the sludge deposit layer. With the inclusion of the ET mechanism in the proposed model, the estimation of water loss to the atmosphere could simulate the actual water uptake by plants. However, it is determined that the influence of water removal by the ET is generally less influential, bringing a significant figure in the overall hydraulic module, and is only remarkable when a long resting period is implemented in STRB (Cascone *et al.*, 2019; Wanniarachchi & Sarukkalige, 2022).

The potential ET rate was estimated according to the parameters given in Table 5.8. However, the average simulated ET rate of 0.0051 cm/day was significantly low enough to represent the water loss via the ET due to the small size of the reed bed. Further, the reed beds with shorter resting periods also resulted in a lower ET rate. By means, the insufficient resting period, which results in the cracks on the sludge deposits, would have a higher ET rate initially due to larger surface area exposure. Still, the consistently dried and cracked conditions of the sludge deposits have caused the influent to bypass the reed bed, eventually leading to a lower ET rate (Tan *et al.,* 2023). Conclusively, a longer resting period is always required for the respective hydraulic load to prolong the temporary ponding condition for the ET process.

Figure 5.18 shows the simulated MCs under varying resting periods with a constant 100 kg/m^2/year SLR. The results indicated that the simulated MC for the 27-day resting period has the lowest percentage at the end of treatment, which further confirmed the importance of ET in drying the sludge deposit during the non-feeding period. However, the prolonged resting period would increase the actual operational cost, burdening a developing country (Krzyk & Drev, 2023). Therefore, the treatment duration is only extended to meet the final disposal of 20% solids which complies with the government standard.

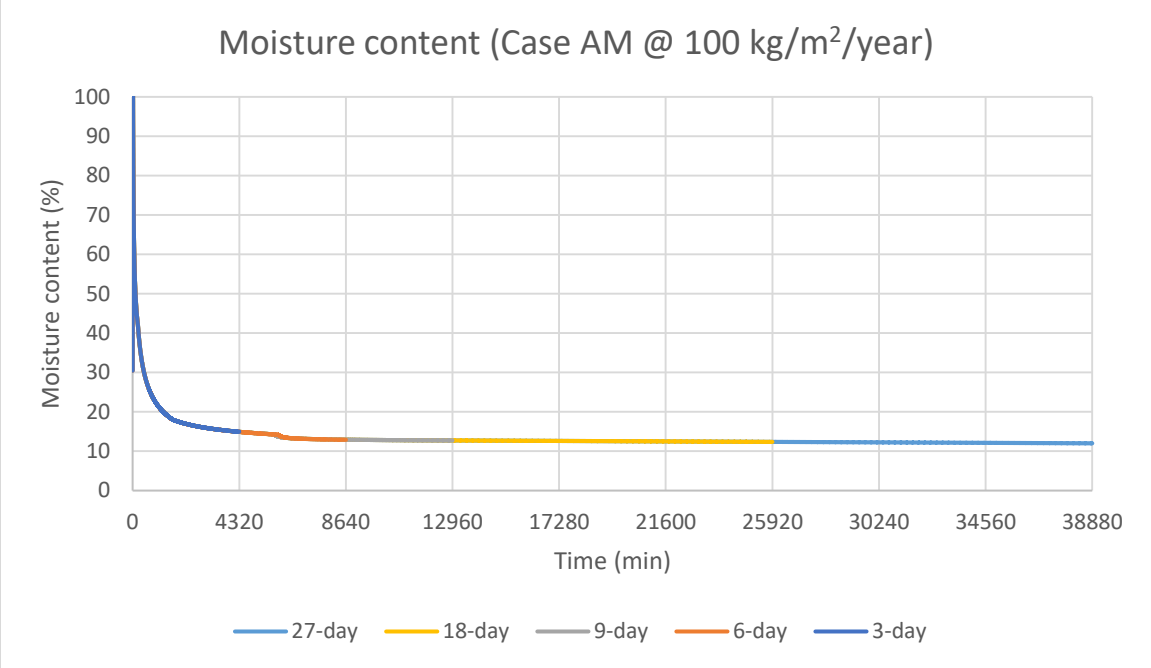

Figure 5.18: Simulated moisture content with a constant 100 kg/m^2/year SLR under varying resting periods of case AM (90315 ml | 8.00 cm).

5.7.3 Sludge Accumulation

The proposed model has considered sludge accumulation's influence on hydraulic dynamics. The accumulated sludge deposit is believed to have reduced the infiltration rate. The current approach simulated the sludge accumulation as a function of time with the variation of thickness in the moving-mesh layer. At the same time, its hydraulic properties complied with the saturated conductivity. The sludge deposit accumulation was estimated by applying compressible cake filtration theory, where the changes in sludge thickness were based on the imposed flux with respective sludge and sludge deposit porosity (Höfgen *et al.*, 2019). Since the sludge porosity coefficients are always small, the governing parameter for the sludge model is the infiltration flux.

The average simulated sludge accumulation for 78 cases was 0.22 cm/day, much higher than the measured sludge accumulation of 0.05 cm/day, as indicated in Table 5.12. The standard deviations of the sludge thickness increments were high due to different numbers of experimental runs. The TS loads for each loading ranged from 0.16 to 1.47 kg, directly increasing the sludge deposit layer thickness.

Figure 5.19 compares the average measured and simulated sludge deposit increments with respect to the TS loads under different loading conditions. It shows that average measured sludge increments were the highest under 100 kg/m^2/year SLR and 3-day resting period loading conditions. The continuous septage loading with a shorter resting period sustained the bed moisture, ensuring the entity of the sludge deposit layer and accumulating more solids on the layer surface. The lowest possible total solids loads of 1.76 kg but recorded with the highest sludge deposit layer thickness of 0.16 cm has confirmed the situation.

Moreover, the difference between the average sludge deposit increments and the total solid loads increases with the prolonged resting periods. Typically, an extended resting period requires larger hydraulic loads to support the drainage capacity, thus accumulating more solids on the sludge deposit layer. However, the extensive drying of the sludge deposit layer during the resting period would lead to crack occurrence, further reducing the sludge deposit thickness with solids bypassing the filter medium (Huong *et al.*, 2024a).

Table 5.12: Average measured and simulated sludge deposit increments.

SLR (kg/m^2/year) | Resting period (day)	**50 | 6**	**100 | 6**	**150 | 6**	**100 | 3**	**100 | 9**	**100 | 18**	**100 | 27**	**Mean**
Number of treatments	15	15	15	11	10	4	3	-
TS loads (kg/loading)	0.16	0.33	0.49	0.16	0.49	0.98	1.47	0.58 ± 0.48
Total solid loads (kg)	2.40	4.95	7.35	1.76	4.90	3.92	4.41	4.24 ± 1.84
Total increments (cm)	0.50	1.83	4.50	5.17	4.67	1.50	4.17	3.19 ± 1.86
Average measured increments per day (cm/day)	0.01	0.02	0.05	0.16	0.05	0.02	0.05	0.05 ± 0.05
Average simulated increments (cm/day)	0.08	0.25	0.50	0.39	0.19	0.11	0.04	0.22 ± 0.17

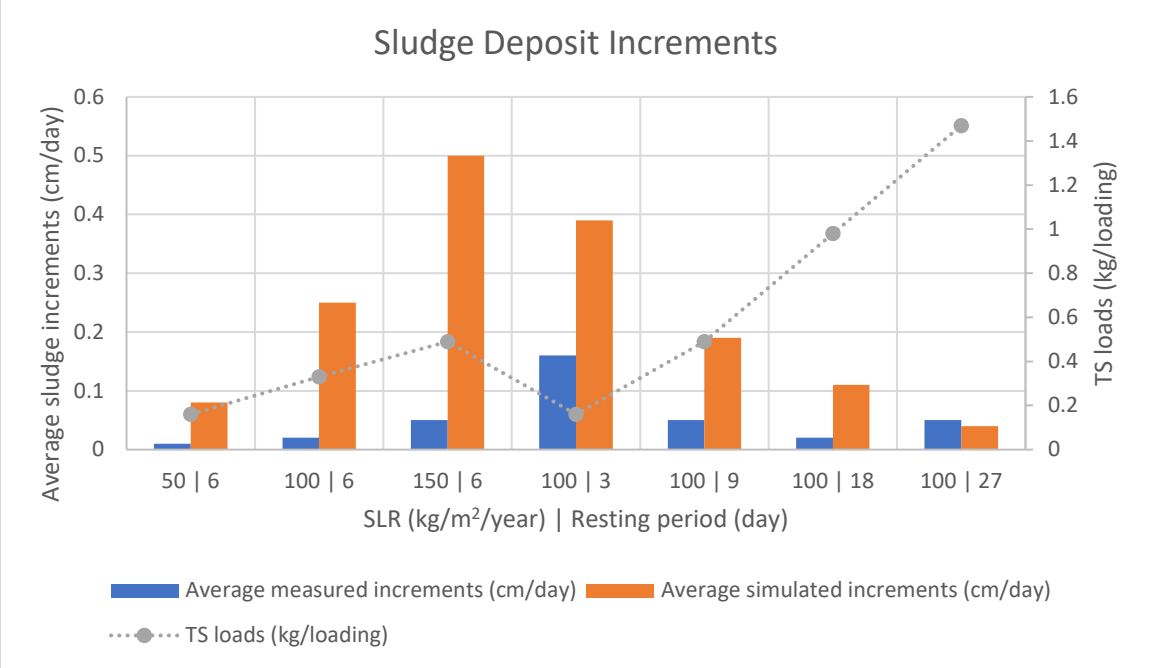

Figure 5.19: Sludge deposit increments under different loading regimes.

In contrast, the highest average simulated sludge deposit increments were under loading conditions of 150 kg/m^2/year SLR and a 6-day resting period. Since the numerical model simulation uses mathematical calculations to estimate the sludge thickness based on the imposed flux, the higher SLRs provide more hydraulic loads to boost the infiltration flux further, leading to higher sludge accumulation (Sørensen *et al.*, 1996). Such an outcome was mainly caused by the large hydraulic loads, as the sludge equation used in the proposed model depends on the imposed flux. In other words, the difference between the predicted and measured results is minimal when the hydraulic load is small. Hence, the simulated sludge accumulation matched the trend of the measured result for cases with smaller hydraulic loads, as shown in Figure 5.20.

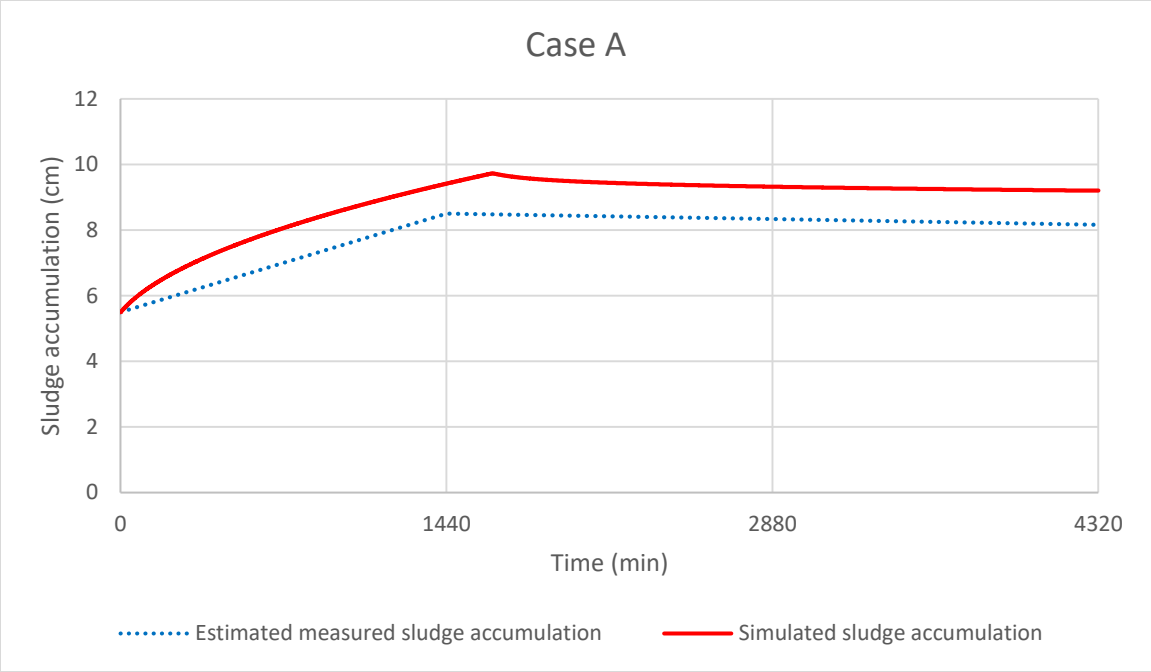

Figure 5.20: Simulated sludge accumulation of case A (8710 ml | 5.50 cm).

Certainly, the larger hydraulic load, by means of higher SLR, would lead to more sludge accumulation on top of the sludge deposit layer (Tan *et al.*, 2023). However, the difference between the simulated and measured sludge accumulation increases with the increasing hydraulic load, as shown in Figure 5.21. Upon feeding, the settlement of solid particles is rapid in the early stage of treatment and starts to decelerate gradually during the ponding when there is no external disturbance. However, this statement is only valid without the cracks on the sludge deposit layer. Upon the crack occurrence, the measured sludge accumulation is highly affected due to some of the influent septage bypassing the substrate filter directly, leading to lower measured sludge accumulation.

Moreover, the high MC in the sludge deposit layer also caused the deviation in the simulated results with increased sludge deposit thickness. Since the thicker sludge deposit layer has lower permeability, the simulated sludge accumulation rate was slower than the measured thickness due to the thicker initial sludge deposit input in the simulation. Further, the proposed sludge model uses compressible cake filtration theory, including sludge accumulation and compression, deteriorating the results (Friedrich *et al.*, 2022). The proposed sludge model describes the newly loaded sludge accumulating onto

the existing compressed sludge deposit layer. Hence, the reduced infiltration flux due to the compressed layer decelerated the subsequent sludge accumulation rate.

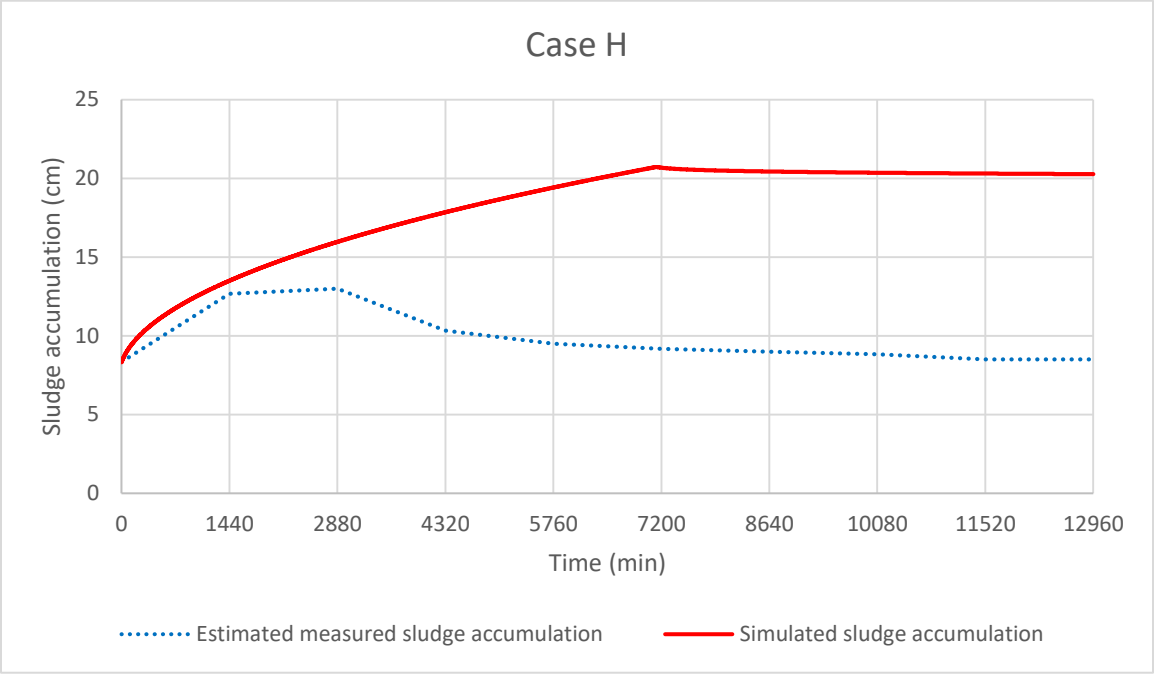

Figure 5.21: Simulated sludge accumulation of case H (26140 ml | 8.33 cm).

In addition, the manual measurement of thickness using a ruler also decreased the accuracy of the results. Although the thickness measurements were taken averagely from three points of the sludge deposits, the unsmooth surface of the gravel layer below the sludge deposits has led to inaccuracies in the results. Also, the mixture of septage has blurred the line between the solid sludge and wastewater, making it difficult to measure the actual sludge deposit layer thickness. As a result, the simulated sludge accumulation was overpredicted.

5.7.4 Sludge Stabilization

The growth and decay of microorganisms in the sludge deposit define sludge stabilization. The development of bacteria consumes organic matter as food for growth and production, while the decay of bacteria has indirectly provided additional organic content in the sludge deposit layer (Wang, Jiang, *et al.*, 2022). As discussed in Chapter 3, the organic content includes biodegradable and inert substances that undergo biological processes.

The biodegradable substances can be degraded into finer components such as nitrates and phosphorus. In contrast, the inert particles are undegradable in the biological process, remaining unchanged throughout the biological process.

According to the results and discussions in Chapter 4, the overall TVS content decreased with lower SLRs and shorter resting periods. In such a circumstance, the sludge deposit layer deforms and finally cracks upon extensive moisture loss. Further, the sludge deposit is reaerated with sufficient oxygen for sludge mineralization and stabilization. The significantly low TVS content for the case of 50 kg/m^2/year SLR with a 6-day resting period has confirmed the scenario. However, the incremental SLRs and prolonged resting periods up to 150 kg/m^2/year and 27 days showed a distinct outcome. The large hydraulic load has created a waterlogging condition where the oxygen is hindered from entering the sludge deposit layer, thus reducing the sludge stabilization.

During the sludge stabilization, the TVS content was determined to decrease throughout the resting period. The TVS content decreased with TS content, where the removal of TS was slightly higher than the TVS (Le Pera *et al.*, 2021). Since the overall organic content measures the growth and decay of microorganisms, the changes in the organic concentration in the sludge deposit layer can be described through biokinetic simulation. The sludge stabilization determines the breaking down of organic matter into nutrients, thus allowing it to be absorbed by plants or involved in biochemical processes (ammonification, nitrification, and denitrification). The modeling of sludge stabilization in the sludge deposit layer would monitor the possible organic changes in the reed bed system and estimate the final organic content of the stabilized sludge (Cramer & Tränckner, 2020).

The sludge stabilization in the sludge deposit layer was modeled according to the ASM3 (Gujer *et al.*, 1999), which involves both production and decaying of the organic matter. The reaction term in the solute transport module was extracted to simulate the sludge stabilization individually. Then, the initial concentrations of the nutrients, such as dissolved oxygen, bicarbonate, and nitrates, were prescribed in the proposed model. In addition, the COD concentration was obtained experimentally and inputted into the model to initiate the biokinetic simulation. Since COD concentration is the primary

variable in sludge stabilization, it dominates the organic content in the sludge deposit layer. Hence, the biokinetic model was added after the hydraulic simulation as it involves the changes in volumetric water content.

The ASM3 involves several biological processes: hydrolysis, aerobic and anoxic growth of heterotrophs, growth of autotrophs, and lysis (Simon-Várhelyi *et al.*, 2020). The growth of the heterotrophs and autotrophs mainly contributed to the overall decrease in the organic content by consuming soluble, biodegradable organic materials and nutrients for development. At the same time, lysis increases the overall organic content due to the breakdown of the biomass and microorganisms. Hence, the COD concentration is best for monitoring the changes in the organic content of the sludge deposit layer, presenting a gradual decreasing curve along the resting period as the growth of the microorganisms always dominates the lysis.

The average measured and simulated organic concentrations for 78 cases were 849.65 mg/L and 464.77 mg/L, respectively. The average TVS removal for the predicted organic content was 92.58%, higher than the actual removal of 83.09%. Figure 5.22 shows a promising simulation of sludge stabilization with only a 6.57% difference in the final organic content. The difference is believed to be caused by the inconsistency of the measured TVS contents, which varied across the treatment duration due to varying MCs. The highly moisturized sludge deposit would have lower organic content due to lesser organic matter retrieved for laboratory tests (Osei *et al.*, 2019). Further, the ponding condition also hindered the oxygen from entering the sludge deposit, leading to insufficient growth of bacteria and, thus, a lower final organic content.

In contrast, the increase in the measured organic content was due to the occurrence of cracks on the sludge deposit layer, which increases the total surface area for bacteria respiration. The large exposure of the sludge deposits to the atmosphere allowed a higher oxygen exchange rate, providing favorable environment for the development of bacteria (Wang *et al.*, 2020). Hence, the regrowth of the microorganisms has led to a larger deviation in the measured and simulated organic contents, as shown in Figure 5.23.

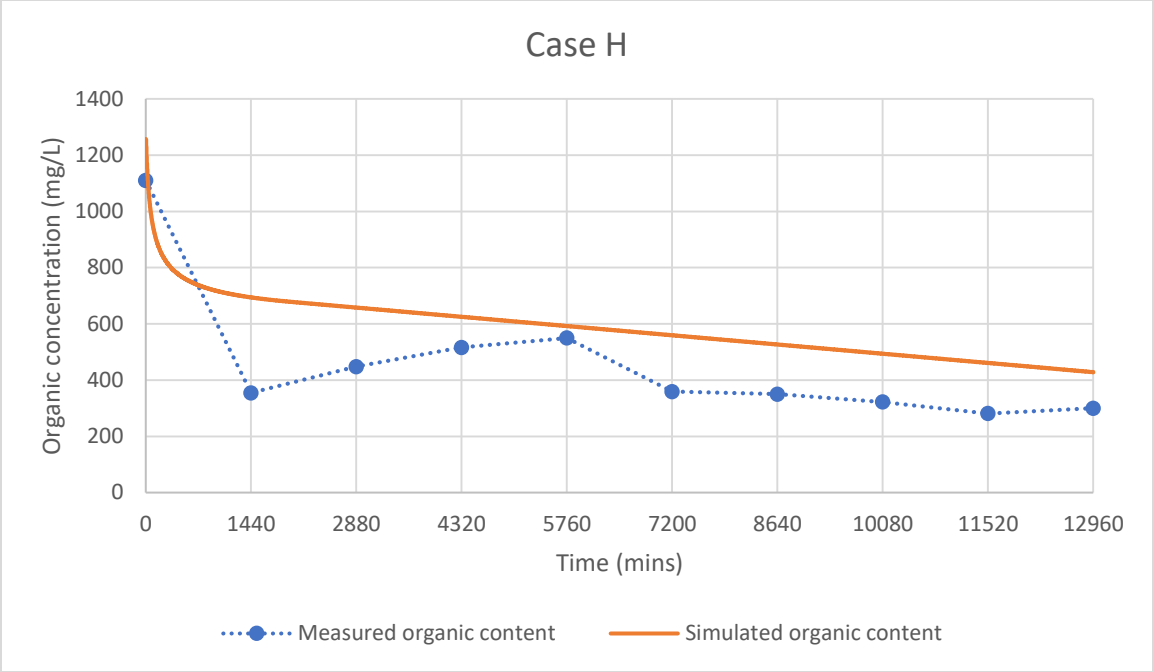

Figure 5.22: Simulated organic content of case H (26140 ml | 8.33 cm | 6818.5 mg/L).

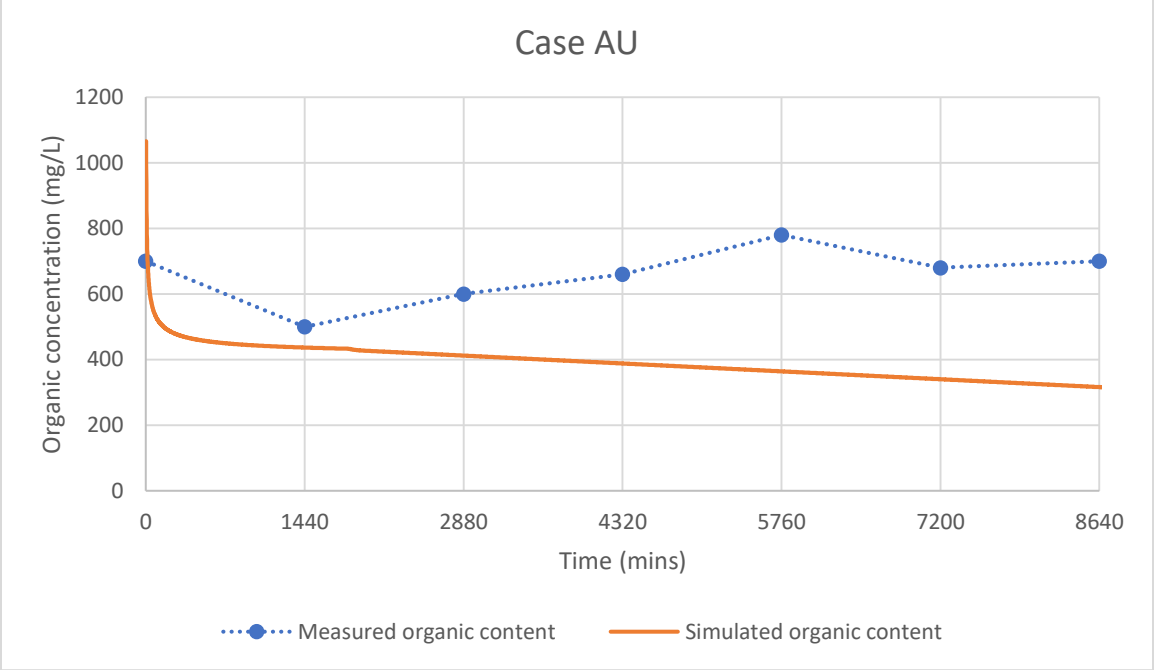

Figure 5.23: Simulated organic content of case AU (27/09/2022 | Bed 3 | 45470ml).

The overall measured results were found to fluctuate throughout the resting period. However, the simulated organic contents were smoother, presenting a gradual reclining curve. The main reason for high error deviations was the waterlogging and crack

conditions on the sludge deposit layer. Under normal flow case conditions where the ponding was temporary, the measured organic content decreased with the resting period. However, there were cases where the organic content shot up to extremely high concentrations, indicating the occurrence of cracks in the sludge deposit layer. The crack occurrence would have boosted the effluent flux and lengthened the sludge deposit drying period. The sufficient oxygen reaeration in the sludge deposit allowed for extensive decomposition, resulting in higher microorganism production and final organic content (Wang, Bengtsson, *et al.*, 2019). In contrast, the cases with higher SLRs and prolonged resting periods would have led to ponding conditions. The severity of the ponding situation hindered the oxygen exchange between the atmosphere and the sludge deposit, leading to low final organic content in the sludge deposit. The decomposition of nutrients only starts after the surface ponding disappears, thus presenting a U- or V-shape curve throughout the resting period.

The highest organic content was observed during the loading period of the simulated results. The biodegradation process occurs whenever the sludge is loaded. Thus, nutrient decomposition directly decreases the organic content in the sludge deposit layer. Since biodegradation is slow, the organic content tends to decrease gradually throughout the resting period (Wang, Jiang, *et al.*, 2022). The proposed model could not simulate the results incorporating unique flow cases such as waterlogging and cracked conditions. However, the ideal case of organic matter decomposition has been excellently simulated through the proposed model. Conclusively, the changes in organic content should be seen in a long-term vision as the decomposition of nutrients is a slow process.

5.7.5 Comparison Between FMM and MMM

A comparison between fixed-mesh and moving-mesh methods of discretization was performed in the simulation of the hydraulic results. The conventional method of discretization was performed by Picard's iteration, where the solution nodes are solved using the old meshes (Tang, 2005). This method has been widely used in modeling the hydraulic flux in sludge treatment areas, especially with the HYDRUS software (Grecco *et al.*, 2019). However, as the adaptive mesh refinement scheme was discovered, the

results improved from the fixed-mesh method (Bruce, 2011; Lee *et al.*, 2015). The moving-boundary condition due to ponding and sludge accumulation can then be modeled through the simulation, thus enhancing the robustness of the proposed model. In contrast to the conventional method, the equation and solution nodes are solved simultaneously to generate a new solution node in the next step.

Especially for the hydraulic simulation in the sludge treatment reed bed, the moving-mesh method can simulate the ideal cases of temporary ponding on top of the bed surface. The boundaries are always changing upon different infiltration rates due to drainage and evapotranspiration. Hence, these changes could be ideally simulated through the application of MMM. Figure 5.24 shows the comparison between the simulated cases using the FMM of HYDRUS and the MMM of the proposed model. The same initial condition of -15 cm hydraulic head and saturated hydraulic flux of 0.015 cm/min under the imposed flux of 1.5 cm/min was used to simulate the effluent fluxes through the FMM and MMM of discretization. From the results, the flux peaks were matched nicely at around 0.024 cm/min, but the delay of flow occurrence was slightly slower in the FMM. Further, the higher infiltration rate during the resting period extensively increased the cumulative effluent at the end of treatment. Such a condition is believed to be caused by the overprediction in effluent flux due to the thinner sludge deposit layer, thus reducing the layer permeability and allowing more water to pass through.

In the MMM application, considering the sludge deposit accumulation increased the thickness of the top simulation mesh, further reducing the infiltration rate and providing a better result. The meshes are always moving with the equation nodes, thus controlling the effluent flux by limiting the infiltration rate through the saturated hydraulic conductivity of the sludge surface layer. This has further confirmed that the MMM simulation is promising and trustworthy in modeling the hydraulic flow in STRB.

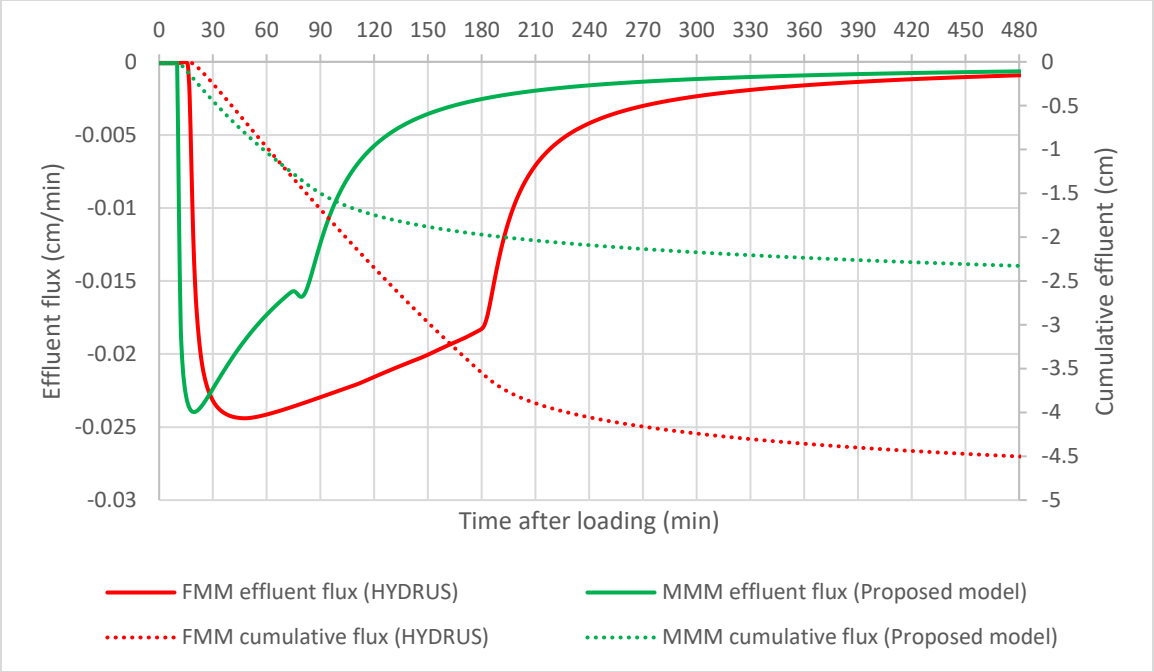

Figure 5.24: Comparison between FMM and MMM.

5.8 Summary of Simulation Results

In summary, the proposed hydraulic module worked well in simulating the effluent flux of the laboratory-scale STRB. The substrate medium was partitioned into the sludge deposit layer (measured thickness from experimental), intermediate layer (5 cm), small-sized gravel layer (10 cm), and medium-sized gravel layer (10 cm). The drainage layer was excluded in the domain of interest of the simulation model as its influence was significantly minor. The top boundary condition was switched between temporal flux-controlled and head-controlled driving forces to describe the draining and temporary ponding scenario. Additionally, the bottom boundary condition was set to be a free drainage condition.

In the hydraulic simulation, the initial condition of the hydraulic head in the reed bed was calibrated to match the delay of flow occurrence. In contrast, the saturated hydraulic conductivity of the sludge deposit layer was based on the flux peak. The proposed model was promising in simulating the effluent flux of the STRB with respect to different SLRs, resting periods, sludge quality, and sludge thickness. Regarding the error analysis conducted, the proposed model was found to have successfully matched the

hydraulic flows in many cases, excluding the “bypassed” and “clogged” cases. The low average MAE and RMSE values of 0.039022 and 0.055862 indicated that the proposed model was theoretically and technically stable and reliable in simulating the hydraulic flow for septage treatment. Moreover, the highest R2 value can reach up to 0.9620, further confirming the proposed model's consistency and robustness.

In addition to the prescribed pressure head and the delay of flow occurrence, the current findings revealed a possible proportional relationship between the two parameters. The increase in the pressure head would have caused an increase in the duration of the flow occurrence. This is explained by the large hydraulic load, resulting in high pressure, and prolonging the ponding condition. Furthermore, the saturated hydraulic conductivity of the sludge deposit layer was discovered to increase with the flux peak due to the improving permeability of the layer. Certainly, saturated conductivity dominates the maximum hydraulic conductivity, limiting the infiltration flux through the layer. Hence, the incremental sludge deposit layer thickness due to continuous sludge accumulation would decrease the flux percolation rate upon the reduction in layer permeability. In addition, the research findings for the conventional simulation method were believed to have over-predicted the effluent flux when the accumulation of the sludge deposit layer was disregarded.

Moreover, the ET rate was considered insignificant to the hydraulic simulation. However, including the ET sub-model was necessary to illustrate the possible water loss via the vegetation. The resulting ET rate was minor in this study due to the small surface area of the reed bed, but it might be meaningful in other research to better explain the water loss to the atmosphere.

Sludge accumulation has a major impact on hydraulic simulation, especially in the formation of a sludge deposit layer. This layer formation is crucial to enhance the contaminant removal by prolonging the ponding duration, thus allowing sufficient biochemical interaction due to a slower infiltration rate. The predicted sludge accumulation matched the trend of measured results with rapid initial sludge accumulation before decelerating gradually. The predicted sludge accumulation rate can estimate the possible sludge deposited onto the reed bed, providing additional

information about the relationship between the sludge deposit layer thickness and respective effluent flux. Conclusively, the proposed model managed to describe the moving boundary condition due to the sludge accumulation and the shrinkage upon evaporation and drainage effect.

Furthermore, sludge stabilization has been successfully simulated through the application of ASM3, where the biokinetic model involved the growth and decay of organic matter. The overall simulated organic content matched the decreasing trend of the measured data, indicating a robust simulation in the biokinetic model. Upon ponding condition, the measured organic content was slightly lower than the measured results due to the inactivity of microorganisms. The waterlogging hindered oxygen exchange between the sludge deposit and the atmosphere, leading to insufficient growth of microorganisms, thus lowering the organic content in the sludge deposit layer. However, the deviations between the simulated and measured organic contents were fatal under the cracked sludge deposit layer. The crack occurrence on the sludge deposit layer has allowed more oxygen reaeration in the sludge deposit, causing an extensive development of microorganisms and, eventually, higher organic content. Conclusively, the biokinetic model simulated the possible sludge stabilization in the sludge deposit layer without ponding conditions and cracked sludge deposits.

In addition, a comparison between the FMM and MMM simulations in hydraulic flow was made to enhance the significance of this project study. The results showed that the MMM of discretization has generated better results in the hydraulics of STRB. The MMM complies with the moving boundary condition, which accommodates the sludge accumulation based on the saturated hydraulic conductivity of the sludge deposit layer, thus preventing overprediction in the flux peaks. As a result, the overall effluent and cumulative flux matched the measured data promisingly.

To conclude, the proposed model has successfully simulated the desired results. Yet, it has proven its robustness and reliability by implementing moving boundary conditions due to surface ponding and sludge deposit accumulation.

CHAPTER 6: PARAMETRIC STUDIES

6.1 Determination of Sensitivity Parameters

The SLR and resting period are the main operating regime for the STRB. These parameters control the volume of sludge loaded to the reed bed, affecting subsequent discharge behaviors and sludge deposit characteristics. In hydraulic simulation, the hydraulic head and saturated hydraulic conductivity are the controlled parameters of the overall simulation results. The hydraulic head relates to the delay in the flow occurrence. In contrast, the saturated hydraulic conductivity of the sludge deposit layer controls the maximum infiltration flux through the reed bed, also known as the flux peak during the feeding-resting cycle.

Previous chapters of this study focus on the known factors influencing the STRB performance, mainly weighted on the dewatering efficiency of the system. Hence, further study of the effect of controlled parameters on the STRB performance is discussed in this chapter. The tested parameters include hydraulic head and saturated conductivity corresponding to the sludge deposit layer thickness and SLR and resting period with the respective loading volumes. These parameters are investigated to study the effect on sludge dewatering, including effluent flux, moisture content (MCs), sludge accumulation, organic content, and evapotranspiration. In short, the effluent flux is the draining rate of the STRB system, where the hydraulic load directly affects the MC, sludge accumulation, and organic content of the sludge deposit layer, as well as the overall evapotranspiration of water loss to the atmosphere.

Table 6.1 summarizes the total 78 sets of experimental runs for the STRBs in septage treatment, categorized according to the type of flow cases. The average water recovery of 70.33 ± 18.62% implied that the STRB efficiently dewatered sludge via drainage. The remaining moisture was assumed to either have been lost through evapotranspiration or retained in the pores of the sludge deposit layer and substrate bed, leading to incomplete drainage and water recovery. Essential data from the simulation data, including hydraulic head and conductivity, were compiled for parametric study. The hydraulic pressure indicates the dryness of the bed, while a higher pressure (closer to zero)

indicates the bed is highly moisturized. An average hydraulic pressure of -19 ± 8 cm has been determined for simulating the effluent flux in the STRB. The initial pressure is relatively consistent across the beds due to the same types of sludge and gravel used (Huong *et al.*, 2024b). Although the hydraulic loads varied in different loading conditions, the applied sludges were infiltrated through the same substrate thickness, and the only changes in the layer thickness were the sludge deposits.

Moreover, the saturated hydraulic conductivity, *Ks*, is crucial to the dewatering efficiency. According to the calibrated values, the saturated hydraulic conductivity of the sludge deposit layer used in matching the drainage flow pattern ranged from 0.0001 to 0.600 cm/min, indicating a varying characteristic of the sludge deposit layer. On the one hand, a low *Ks* value resulted in a prolonged ponding condition, leading to a slow flux peak and low water recovery over the feeding-resting cycle. On the other hand, a relatively high *Ks* value represents the bypassed condition in the bed, where the cracks in the sludge deposit layer result in a faster infiltration rate and flux peak.

On average, the initial thickness of the sludge deposit layer was 10.00 ± 2.03 cm, and the average sludge density, porosity, and sludge deposit porosity were 22.20 kg/m^3, 0.24, and 0.0111, respectively. Since the sludge deposit thickness has the lowest hydraulic conductivity, the incremental sludge deposit thickness directly reduces the resultant flux. The continuous sludge accumulation increases the amount of solids deposited on the existing layer, causing possible blockage of pores, and leading to longer surface ponding. Hence, this information on the sludge deposit layer was then used as the constant variables in the parametric study.

In addition, the sensitivity analysis of the sludge stabilization was also included. The average initial COD concentration of 4763.32 ± 1384.20 mg/L was fixed at constant to simulate the outflow dynamics of the organic content. The MC of the sludge deposit layer would affect its organic content (Saeed *et al.*, 2022). The moisturized sludge deposit layer sustains the bacteria growth, allowing continuous sludge mineralization and stabilization. Hence, the hydraulic load controls the moisture and organic contents, while the hydraulic head and saturated hydraulic conductivity regulate the infiltration flux and dryness of the sludge deposit layer.

Table 6.1: Loading conditions and parameters based on flow cases (D=sludge deposit density, E_C=sludge deposit porosity, E_S=sludge porosity).

Loading Batch | RP (days) | SLR ($kg/m^2/year$)			HL (cm^3)	T (cm)	WR (%)	D (g/cm^3)	E_C	E_S	FD (min)	FP (cm/min)	Calibrated h (cm)	Calibrated K_s (cm/min)	Condition
Normal flow cases													
A	3	100	8,710	5.50	69.06	18.78	0.18	0.0094	30	0.0054	-18	0.0015	-
B	6	50	8,710	7.00	72.56	18.78	0.47	0.0094	20	0.0199	-17	0.0060	-
D	6	150	26,140	7.83	69.93	18.78	0.18	0.0094	20	0.0087	-15	0.0006	-
E	3	100	8,710	8.17	51.38	18.78	0.18	0.0094	50	0.0066	-20	0.0010	-
G	3	100	8,710	7.00	113.61	18.78	0.18	0.0094	40	0.0064	-20	0.0015	-
H	9	100	26,140	8.33	84.56	18.78	0.22	0.0094	45	0.0076	-23	0.0009	-
I	6	50	5,460	8.17	59.52	29.97	0.43	0.0150	45	0.0081	-18	0.0025	-
O	6	50	5,460	8.83	61.90	29.97	0.43	0.0150	20	0.0168	-15	0.0035	-
AR	9	100	45,470	11.33	71.23	10.80	0.14	0.0054	1	0.6952	-7	0.0500	-
AU	6	150	45,470	11.83	67.75	10.80	0.14	0.0054	6	0.0738	-13	0.0065	-
AV	6	50	15,150	7.50	75.76	10.80	0.29	0.0054	2	0.2903	-10	0.0500	-
AY	18	100	90,940	10.33	77.64	10.80	0.59	0.0054	1	0.4456	-6	0.0040	-
BC	6	150	45,470	11.33	81.49	10.80	0.14	0.0054	2	0.2368	-9	0.0250	-
BE	9	100	45,470	12.17	83.63	10.80	0.14	0.0054	6	0.0331	-12	0.0020	-
BF	6	50	15,150	7.83	85.81	10.80	0.29	0.0054	1	0.3081	-9	0.0550	-
BG	6	100	30,310	12.83	82.93	10.80	0.15	0.0054	1	0.8098	-10	0.1000	-
BH	6	150	45,470	11.50	84.76	10.80	0.14	0.0054	1	1.8844	-9	0.2000	-
BI	6	50	9,345	7.00	84.43	17.51	0.34	0.0088	2	0.2597	-10	0.0700	-
BK	6	150	28,040	10.83	86.45	17.51	0.32	0.0088	1	0.4584	-10	0.0800	-
BN	6	50	9,345	6.50	84.43	17.51	0.34	0.0088	2	0.1019	-10	0.0250	-
BO	6	100	18,690	12.17	82.72	17.51	0.30	0.0088	1	0.3463	-10	0.0500	-
BP	6	150	28,040	11.83	87.82	17.51	0.32	0.0088	1	1.7876	-8	0.3500	-

BQ	9	100	28,040	13.00	80.60	17.51	0.14	0.0088	1	0.1732	-9	0.0100	-
BR	6	50	9,345	7.50	92.83	17.51	0.34	0.0088	1	0.0815	-10	0.0200	-
BS	6	100	18,690	12.17	92.70	17.51	0.30	0.0088	3	0.1604	-11	0.0250	-
BU	6	50	9,345	7.50	96.95	17.51	0.34	0.0088	1	0.2801	-9	0.0750	-
BV	6	100	18,690	12.50	97.03	17.51	0.30	0.0088	2	0.1935	-10	0.0275	-
BX	18	100	56,080	11.50	92.80	17.51	0.21	0.0088	1	0.0738	-9	0.0010	-
BZ	9	100	28,040	13.00	78.78	17.51	0.16	0.0088	2	0.0840	-9	0.0030	-
Mean			**25,470**	**9.76**	**81.07**	**16.55**	**0.27**	**0.0083**	**11**	**0.3054**	**-12**	**0.0430**	**-**
Std Deviation			**19,447**	**2.38**	**12.69**	**5.00**	**0.12**	**0.0025**	**16**	**0.4713**	**4**	**0.0731**	**-**
Minimum			**5,460**	**5.50**	**51.38**	**10.80**	**0.14**	**0.0054**	**1**	**0.0054**	**-23**	**0.0006**	**-**
Maximum			**90,940**	**13.00**	**113.61**	**29.97**	**0.59**	**0.0150**	**50**	**1.8844**	**-6**	**0.3500**	**-**
Cracked flow case													
F	6	100	17,420	6.33	91.91	18.78	0.22	0.0094	30	0.0199	-19	0.0015	Cracked
M	6	100	10,917	7.67	66.18	29.97	0.19	0.0150	55	0.0326	-25	0.0014	Cracked
AO	6	50	15,150	6.17	73.43	10.80	0.29	0.0054	1	1.0008	-9	0.2400	Cracked
AP	6	100	30,310	12.33	85.60	10.80	0.15	0.0054	1	2.6050	-10	0.6000	Cracked
AQ	6	150	45,470	11.50	88.04	10.80	0.14	0.0054	1	2.0041	-9	0.2500	Cracked
AW	6	100	30,310	11.33	84.87	10.80	0.15	0.0054	1	1.2783	-10	0.2500	Cracked
AX	6	150	45,470	11.00	80.16	10.80	0.14	0.0054	1	2.7833	-13	0.4000	Cracked
BD	27	100	110,000	10.83	83.39	10.80	0.18	0.0054	1	0.9906	-6	0.0400	Cracked
Mean			**38,131**	**9.65**	**81.70**	**14.19**	**0.18**	**0.0071**	**11**	**1.3393**	**-13**	**0.2229**	**-**
Std Deviation			**31,832**	**2.50**	**8.32**	**6.96**	**0.05**	**0.0035**	**20**	**1.0568**	**6**	**0.2094**	**-**
Minimum			**10,917**	**6.17**	**66.18**	**10.80**	**0.14**	**0.0054**	**1**	**0.0199**	**-25**	**0.0014**	**-**
Maximum			**110,000**	**12.33**	**91.91**	**29.97**	**0.29**	**0.0150**	**55**	**2.7833**	**-6**	**0.6000**	**-**
Ponded flow case													
K	6	150	16,380	11.33	47.31	29.97	0.24	0.0150	145	0.0012	-25	0.0002	Ponded
L	3	100	5,460	7.83	66.85	29.97	0.23	0.0150	145	0.0019	-21	0.0005	Ponded
N	3	100	5,460	8.33	48.08	29.97	0.23	0.0150	90	0.0006	-18	0.0002	Ponded
P	6	100	10,917	11.50	36.14	29.97	0.20	0.0150	180	0.0004	-22	0.0001	Ponded

Q	6	150	16,380	11.50	49.27	29.97	0.24	0.0150	70	0.0010	-17	0.0001	Ponded
R	3	100	5,460	8.83	57.60	29.97	0.23	0.0150	175	0.0007	-20	0.0003	Ponded
U	3	100	2,930	9.67	45.56	55.78	0.18	0.0279	250	0.0006	-25	0.0004	Ponded
V	6	50	2,930	7.50	16.04	55.78	0.59	0.0279	102	0.0001	-20	0.0001	Ponded
W	6	100	5,870	10.83	51.70	55.78	0.15	0.0279	146	0.0003	-19	0.0001	Ponded
X	6	150	8,800	10.50	65.57	55.78	0.18	0.0279	145	0.0006	-22	0.0002	Ponded
Y	3	100	2,930	9.50	45.90	55.78	0.18	0.0279	146	0.0003	-22	0.0002	Ponded
Z	6	100	5,870	7.67	43.78	55.78	0.25	0.0279	144	0.0006	-22	0.0003	Ponded
AA	3	100	2,930	10.67	65.19	55.78	0.18	0.0279	250	0.0005	-22	0.0004	Ponded
AB	9	100	8,800	11.33	58.86	55.78	0.22	0.0279	250	0.0012	-22	0.0009	Ponded
BW	6	150	28,040	12.33	96.47	17.51	0.32	0.0088	1	0.2648	-8	0.0275	Ponded
Mean			**8,610**	**9.95**	**52.95**	**42.90**	**0.24**	**0.0215**	**149**	**0.0183**	**-20**	**0.0021**	**-**
Std Deviation			**6,956**	**1.60**	**17.64**	**14.58**	**0.10**	**0.0073**	**69**	**0.0682**	**4**	**0.0070**	**-**
Minimum			**2,930**	**7.50**	**16.04**	**17.51**	**0.15**	**0.0088**	**1**	**0.0001**	**-25**	**0.0001**	**-**
Maximum			**28,040**	**12.33**	**96.47**	**55.78**	**0.59**	**0.0279**	**250**	**0.2648**	**-8**	**0.0275**	**-**
Clogged flow case (Simulated hydraulic heads failed to match flux peaks)													
C	6	100	17,420	10.67	63.29	18.78	0.17	0.0094	125	0.0051	-29	0.0004	-
J	6	100	10,917	11.50	43.83	29.97	0.20	0.0150	250	0.0005	-29	0.0001	Ponded
S	6	100	10,917	8.83	59.77	29.97	0.19	0.0150	70	0.0132	-29	0.0018	Cracked
T	9	100	16,380	8.50	49.91	29.97	0.23	0.0150	125	0.0031	-29	0.0004	Ponded
AC	6	50	8,030	8.33	54.30	20.37	0.58	0.0102	45	0.0153	-29	0.0030	-
AD	6	100	16,070	11.67	55.57	20.37	0.21	0.0102	200	0.0028	-29	0.0005	Ponded
AE	6	150	24,110	9.67	44.38	20.37	0.17	0.0102	90	0.0059	-29	0.0007	-
AF	3	100	8,030	10.67	54.30	20.37	0.08	0.0102	100	0.0041	-29	0.0008	-
AG	6	100	16,070	8.50	55.91	20.37	0.07	0.0102	95	0.0046	-29	0.0006	Ponded
AH	3	100	8,030	10.67	50.75	20.37	0.08	0.0102	170	0.0008	-29	0.0004	Ponded
AI	6	50	8,030	7.00	28.77	20.37	0.58	0.0102	30	0.0173	-29	0.0055	-
AJ	6	100	16,070	11.00	54.39	20.37	0.21	0.0102	110	0.0097	-29	0.0025	Ponded
AK	6	150	24,110	11.00	59.21	20.37	0.17	0.0102	77	0.0163	-29	0.0018	Ponded

AL	18	100	55,210	10.00	52.20	20.37	0.08	0.0102	68	0.0163	-29	0.0008	Ponded
AM	27	100	90,315	8.00	86.25	20.37	0.07	0.0102	10	0.1197	-28	0.0040	-
AN	9	100	24,110	11.00	49.13	20.37	0.19	0.0102	50	0.0188	-29	0.0030	Ponded
AS	6	50	15,150	8.17	80.33	10.80	0.29	0.0054	7	0.1502	-29	0.0350	-
AT	6	100	30,310	11.33	79.99	10.80	0.15	0.0054	4	0.3323	-29	0.0600	-
AZ	9	100	45,470	12.33	78.02	10.80	0.14	0.0054	6	0.1502	-29	0.0200	-
BA	6	50	15,150	7.83	78.68	10.80	0.29	0.0054	18	0.0382	-29	0.0100	Ponded
BB	6	100	30,310	11.50	80.96	10.80	0.15	0.0054	5	0.3005	-29	0.0400	-
BJ	6	100	18,690	12.50	79.11	17.51	0.30	0.0088	4	0.2190	-29	0.0500	-
BL	18	100	56,080	12.33	93.59	17.51	0.21	0.0088	11	0.0458	-29	0.0033	-
BM	9	100	28,040	12.67	97.11	17.51	0.16	0.0088	1	0.1222	-29	0.0200	-
BT	6	150	28,040	12.33	86.45	17.51	0.32	0.0088	1	0.0968	-29	0.0175	-
BY	27	100	84,120	12.17	70.30	17.51	0.34	0.0088	11	0.0688	-29	0.0023	-
Mean			**27,122**	**10.39**	**64.87**	**19.03**	**0.22**	**0.0095**	**65**	**0.0684**	**-29**	**0.0109**	**-**
Std Deviation			**22,066**	**1.72**	**17.51**	**5.41**	**0.13**	**0.0027**	**68**	**0.0940**	**0**	**0.0169**	**-**
Minimum			**8,030**	**7.00**	**28.77**	**10.80**	**0.07**	**0.0054**	**1**	**0.0005**	**-29**	**0.0001**	**-**
Maximum			**90,315**	**12.67**	**97.11**	**29.97**	**0.58**	**0.0150**	**250**	**0.3323**	**-28**	**0.0600**	**-**

Among 78 cases of hydraulic dynamics in the laboratory-scale STRB, 9 cases were found in cracked sludge deposit condition, 25 in ponding condition, and the remaining 45 as normal flows. In the simulation, the hydraulic pressure of smaller than -28 cm failed to match the flow-occurring delay; thus, those cases are not presented. Also, it is noted that hydraulic pressure larger than -10 cm often causes cracks in the sludge deposit, which leads to effluents bypassing the substrate filter. The average hydraulic heads were determined to be -12 ± 4 cm, -13 ± 6 cm, and -20 ± 4 cm, and the average saturated hydraulic conductivities were 0.0430 ± 0.0731 cm/min, 0.2229 ± 0.2094 cm/min, and 0.0021 ± 0.0070 cm/min, respectively, under normal, cracked, and ponded flow cases.

Figure 6.1 shows the relationship between the hydraulic pressure and flow-occurring delay for different flow cases. Based on the trendlines, the hydraulic head showed a logarithmic relationship with the flow delay. The cracked flow cases were often calibrated with a hydraulic head larger than -10 cm, presenting a trendline equation of $y = -3.432\ln(x) - 9.4466$ with a relatively low R^2 value of 0.8803. Meanwhile, the calibrated hydraulic heads for ponded cases were mostly below -20 cm, giving a trendline equation of $y = -2.757\ln(x) - 7.4393$ with the lowest R^2 value of 0.8304. In contrast, the trendline equation of $y = -2.821\ln(x) - 8.3854$ could be used for possible hydraulic head or flow delay estimation in normal flow cases. The highest R^2 value of 0.9043 further supported the results consistency of the normal case, where most hydraulic heads ranged from -6 to -23 cm within the first hour of flow delay.

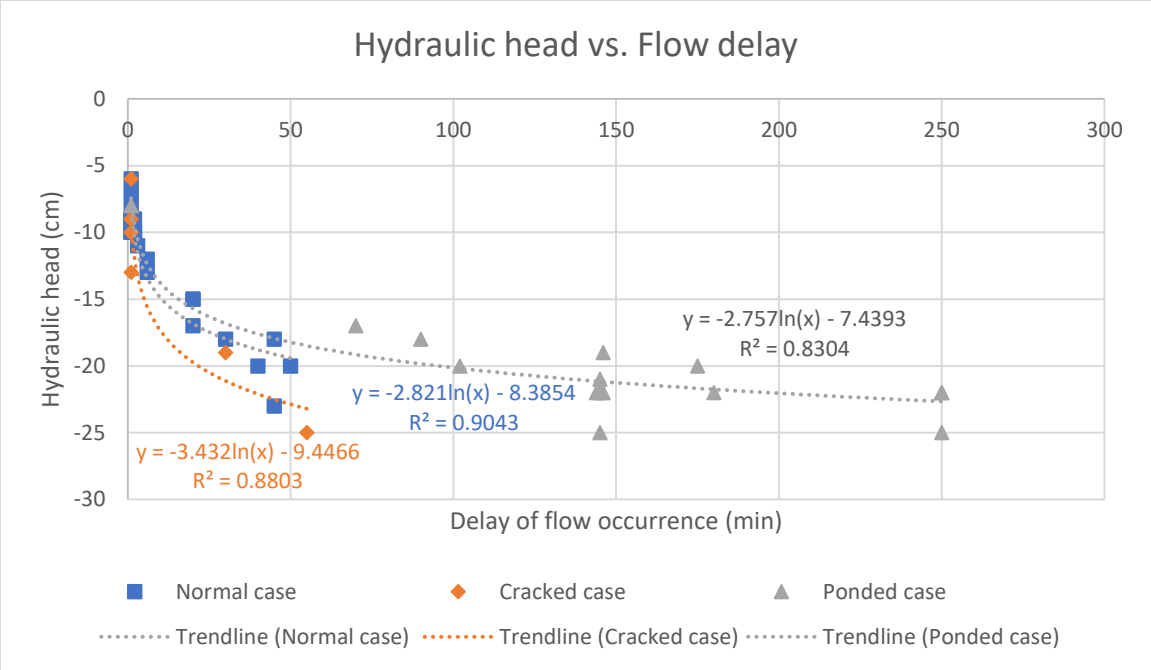

Figure 6.1: Graph of hydraulic head versus delay of flow occurrence (Normal, cracked, and ponded cases).

A similar result was seen in the relationship between the saturated hydraulic conductivity and the flux peak, as shown in Figure 6.2. The generated trendline equations for the normal, cracked, and ponded cases are $y = 0.0167x^2 + 0.1133x + 0.0033$, $y = 0.0137x^2 + 0.1398x + 0.0023$, and $y = -0.5627x^2 + 0.2525x + 0.0001$ with R^2 values of 0.8471, 0.8075, and 0.9994, respectively. The ponded flow case has the highest R^2 value due to lesser calibrated conductivities. The cracked flow case has the lowest R^2 value due to highly varying flux peaks. In contrast, most normal cases have a flux peak and saturated conductivity lower than 1 cm/min and 0.1 cm/min, respectively, leading to a relatively consistent polynomial relationship. However, the standard deviations were high, revealing that the saturated conductivity always varied with flow cases. Thus, the saturated conductivity of the sludge deposit layer is less likely to be used as a global factor in hydraulic dynamic simulation for STRB, particularly for the cracked cases, where the hydraulic conductivity could be random. Generally, the saturated conductivity was controlled within 0.001 to 0.1 cm/min, with the flux peak ranging from 0.005 to 0.5 cm/min; thus, the values smaller or larger than this range are regarded as ponded or cracked flow case, respectively.

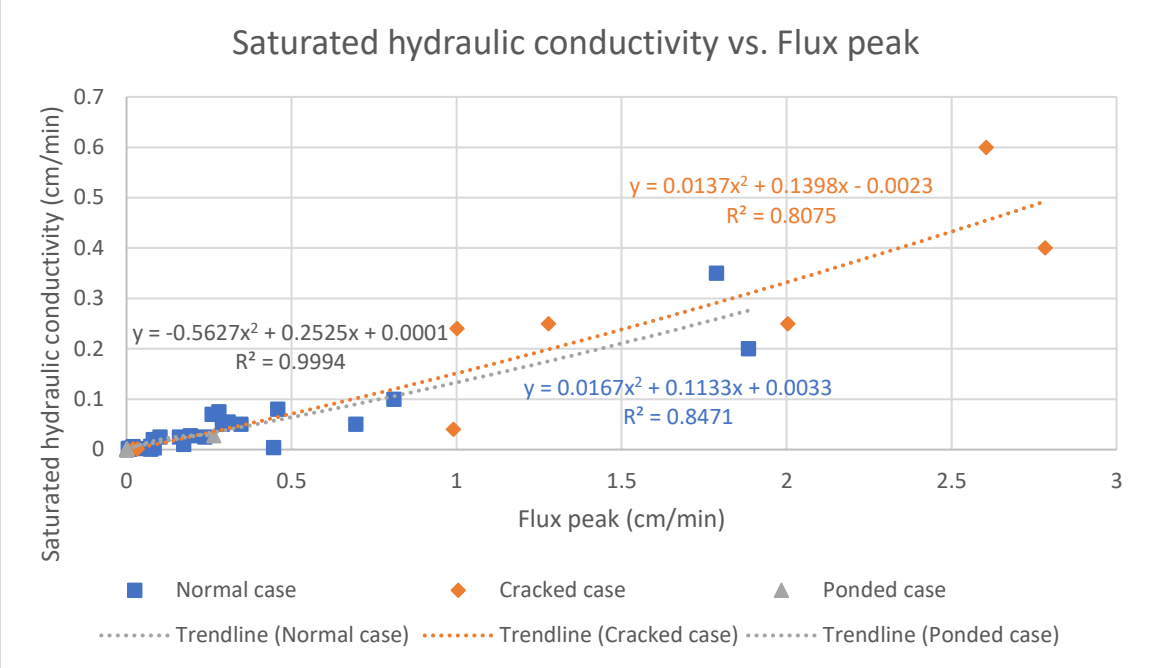

Figure 6.2: Graph of flux peak versus saturated hydraulic conductivity (Normal, cracked, and ponded cases).

Furthermore, the relationship between the hydraulic head and saturated conductivity was studied by categorizing the average hydraulic heads according to the average saturated hydraulic conductivities. As a result, the average saturated conductivity increased with the average hydraulic head, as shown in Figure 6.3. The resulting logarithmic trendline equation of $y = 1.5398\ln(x) - 7.6186$ can then estimate the possible hydraulic head with the known saturated hydraulic conductivity or vice versa. The hydraulic head increment was the highest for saturated conductivity below 0.05 cm/min and increased gradually to 0.60 cm/min. Hence, the expected appropriate hydraulic head would be at -10 to -20 cm to avoid a cracked or ponded flow case. The generated trendline equation can be used as a reference for the hydraulic head or conductivity estimation, subject to factors such as weather conditions, sludge deposit layer thickness, and initial sludge concentration.

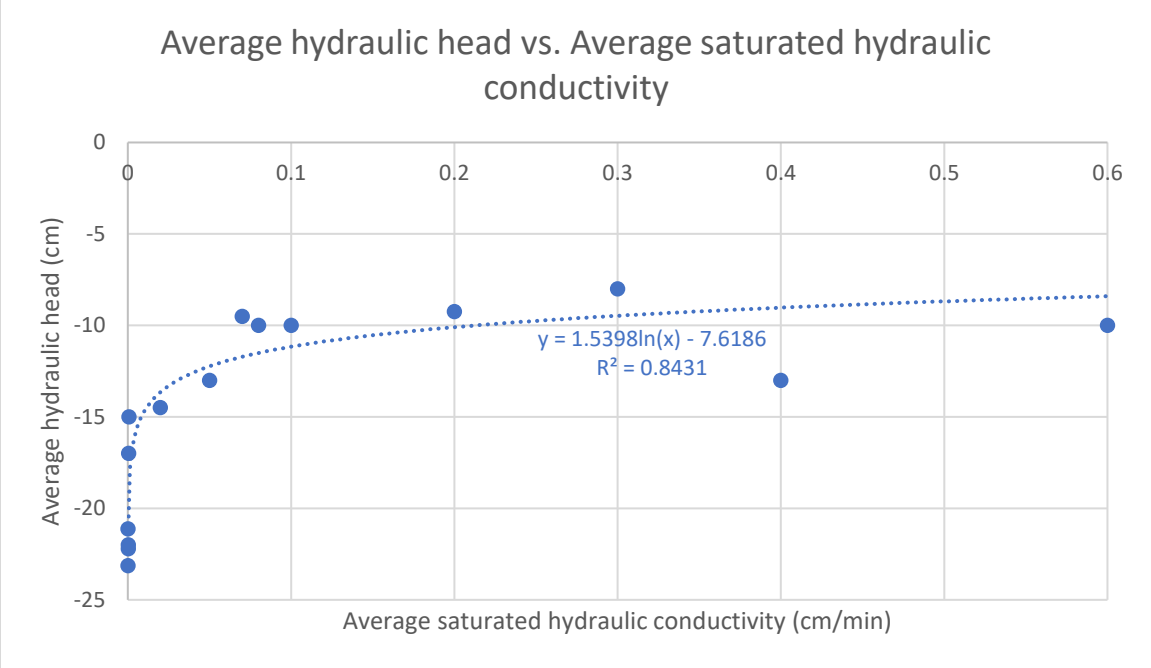

Figure 6.3: Graph of average hydraulic head versus average saturated hydraulic conductivity.

Figure 6.4 shows a graph of the average hydraulic heads and average saturated hydraulic conductivities against a range of the average initial sludge deposit layer thicknesses. Both hydraulic head and saturated hydraulic conductivity presented a "U-shaped" curve across the sludge deposit thickness with the lowest values of -25 cm and 0.0004 cm/min, respectively, as the sludge deposit layer thickness ranged from 9 to 10 cm. Hence, the optimum initial sludge deposit layer thickness ranged from 7 to 11 cm, with the hydraulic head from -18 to -25 cm and the saturated hydraulic conductivity from 0.0004 to 0.0211 cm/min. The hydraulic head and conductivity above this range are then regarded as cracked flow cases, where the influent sludge bypassed the reed bed directly, thus resulting in shorter flow delays and higher flux peaks. Inversely, the hydraulic head and conductivity below this range are then considered to be ponded flow cases, where the prolonged retention time extensively detained the influent sludge on the sludge deposit layer, leading to slower flow delays and lower flux peaks. The polynomial trendline equations of $y = 0.6162x2 - 5.8479x - 8.5204$ and $y = 0.0002x2 - 0.0008x + 0.0283$ are then possible to estimate the hydraulic head and saturated hydraulic conductivity, respectively, using the known initial sludge deposit layer thickness.

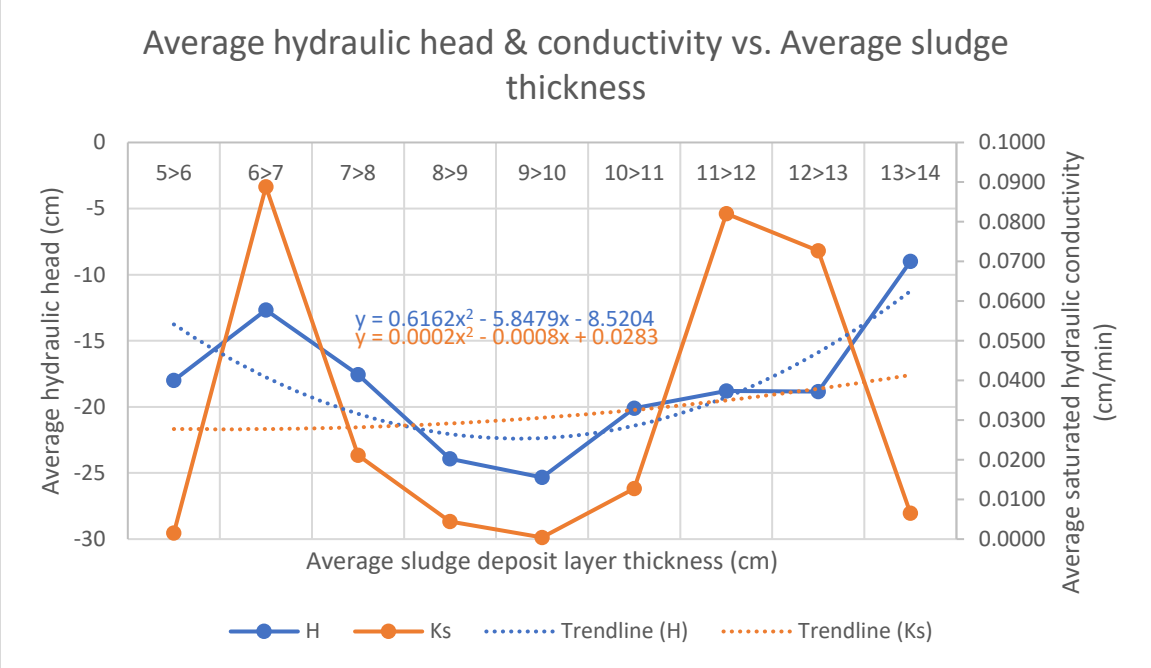

Figure 6.4: Graph of average hydraulic head and saturated hydraulic conductivity versus average sludge deposit layer thickness.

Moreover, the average hydraulic head and saturated hydraulic conductivity were classified according to a range of water recoveries, as shown in Figure 6.5. The generated polynomial trendline equations of $y = 0.0033x2 - 0.2023x - 21.26$ and $y = 0.00001x2 - 0.0003x - 0.001$ can estimate the hydraulic head and saturated conductivity using the known water recovery. Both hydraulic head and saturated conductivity were found to increase with the water recovery, where the best STRB performance is under a hydraulic head of -14 cm and a saturated conductivity of 0.124 cm/min, which has 80% water recovery. The relatively high hydraulic head and saturated conductivity shortened the retention time, while high water recovery ensures a continuous loading of septage, making the STRB economically beneficial. However, increasing the water recovery to 90% does not lead to a higher hydraulic head, and the saturated conductivity drops significantly due to clogging conditions. The influent septage retained on the sludge deposit layer reduces the water recovery percentage, affecting the overall STRB performance despite a higher contaminant removal in the effluents.

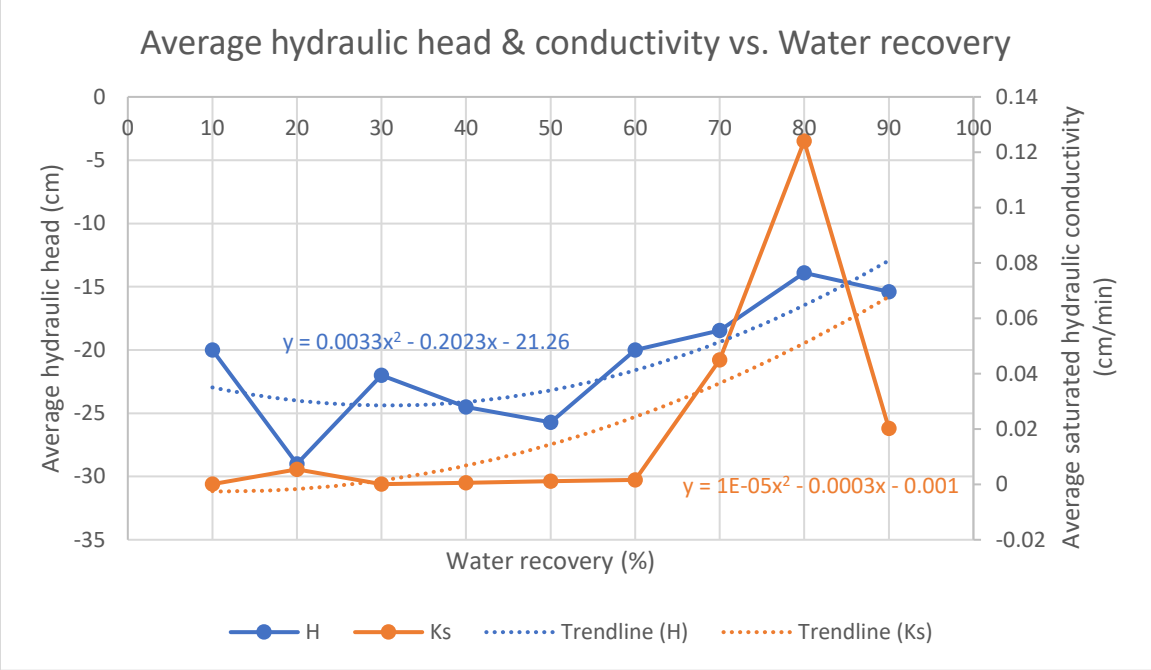

Figure 6.5: Graph of average hydraulic head and saturated hydraulic conductivity versus average water recovery.

Conclusively, the hydraulic head decreased with an increasing flow delay, where the generated logarithmic trendline equation of $y = -2.821\ln(x) - 8.3854$ showed the best fit under normal flow case, with the hydraulic head range of -6 to -23 cm and below 60 minutes flow delay. In contrast, the saturated hydraulic conductivity showed a polynomial relationship with the flux peak, where the saturated conductivity increased with the flux peak. The generated trendline equation of $y = 0.0167x^2 + 0.1133x + 0.0033$ can be used to estimate the saturated conductivity below 0.35 cm/min or flux peak below 1.9 cm/min under the normal. Further, the hydraulic head and saturated conductivity also showed a logarithmic relationship with a trendline equation of $y = 1.5398\ln(x) - 7.618$, where the hydraulic head increased with the saturated conductivity, in the range of -8 to -24 cm and 0.0004 to 0.6 cm/min, respectively. Moreover, the hydraulic head and saturated conductivity were found to have the lowest values of -25 cm and 0.0001 cm/min, respectively, through a 9 to 10 cm sludge deposit layer. In addition, the hydraulic head and saturated conductivity also increased with the water recovery. The hydraulic head of -14 cm and the saturated conductivity of 0.124 cm/min were determined to have the highest water recovery of 80%.

6.2 Sensitivity Analysis

The sensitivity test analyzed the effects of hydraulic load, head, conductivity, and thickness on the sludge deposit and effluent behaviors. The hydraulic load volume was calculated according to the SLRs and resting periods. The simulation ran for 60 minutes, covering the initial effluent flux, MC, sludge accumulation, organic content, and evapotranspiration profiles. The tested parameter values covered the hydraulic load of the optimal loading condition, the overall average calibrated hydraulic head, saturated hydraulic conductivity, and sludge deposit layer thickness. The initial sludge concentration, porosity, and deposit porosity values were kept constant at 22.2 kg/m^3, 0.24, and 0.0111, respectively.

6.2.1 SLR and Resting Period

The loading volume of 50 kg/m^2/year SLR with a 6-day resting period is equivalent to 100 kg/m^2/year SLR with a 3-day resting period in a feeding-resting cycle. The SLRs and resting periods with the respective hydraulic loads are calculated in Table 6.2. The tested SLRs ranged from 50 to 450 kg/m^2/year SLR with 6-day resting period, equivalent to 3 to 27 days resting periods with 100 kg/m^2/year SLR. Hence, the calculated loading volumes were 7371 to 99501 ml, with constant values of 10 cm initial sludge deposit layer thickness, 4763.32 mg/L COD concentration, -19 cm hydraulic head, and 0.0429 cm/min saturated conductivity. The constant values were obtained from the average of 78 cases, covering different flow cases of the sludge deposit and bed conditions.

Table 6.2: Hydraulic loads under a constant 6-day resting period and varying SLRs.

SLR (kg/m^2/year) @ 6-day resting period	Sludge thickness (cm)	COD concentration (mg/L)	Hydraulic head (cm)	Saturated conductivity (cm/min)	Hydraulic load (ml)
50	10	4763.32	-19	0.0429	7,371
100	10	4763.32	-19	0.0429	14,741
150	10	4763.32	-19	0.0429	22,111
200	10	4763.32	-19	0.0429	29,481
250	10	4763.32	-19	0.0429	36,852
300	10	4763.32	-19	0.0429	44,223

350	10	4763.32	-19	0.0429	60,192
400	10	4763.32	-19	0.0429	78,618
450	10	4763.32	-19	0.0429	99,501

The simulated effluent fluxes under varying hydraulic loads with the respective SLRs and resting periods are shown in Figure 6.6. From the observation, the flux peak increased with the hydraulic load. The highest flux peak is approximately 1.0 cm/min, and the lowest is 0.1 cm/min. Further, the delay of flow occurrence was shortened from around 6 to 3 minutes. The changes in flow delays were most apparent during hydraulic loads less than 45L while insignificant for larger hydraulic loads. Typically, larger hydraulic loads shorten the flow delays to less than a minute. Still, the three-minute prescribed feeding duration in the simulation limits the fastest flow-occurring delay at the 3rd minute. In addition, the duration of drainage dewatering is also prolonged with incremental hydraulic loads. The larger hydraulic loads lengthened the surface ponding, slowly dewatering the sludge through the low permeable sludge deposit layer, leading to a slower treatment process, and improving effluent quality. Therefore, the hydraulic load should be kept within 45 L, i.e. 300 kg/m^2/year SLR, to avoid an extensive, prolonged waiting period, negatively impacting the STRB efficiency.

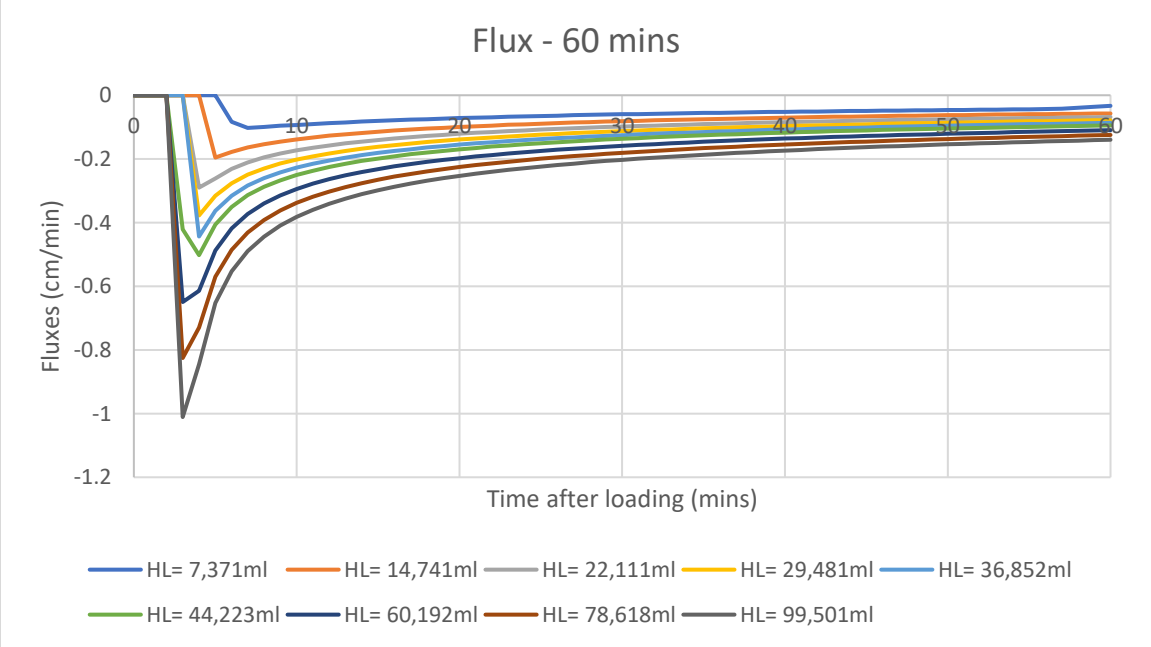

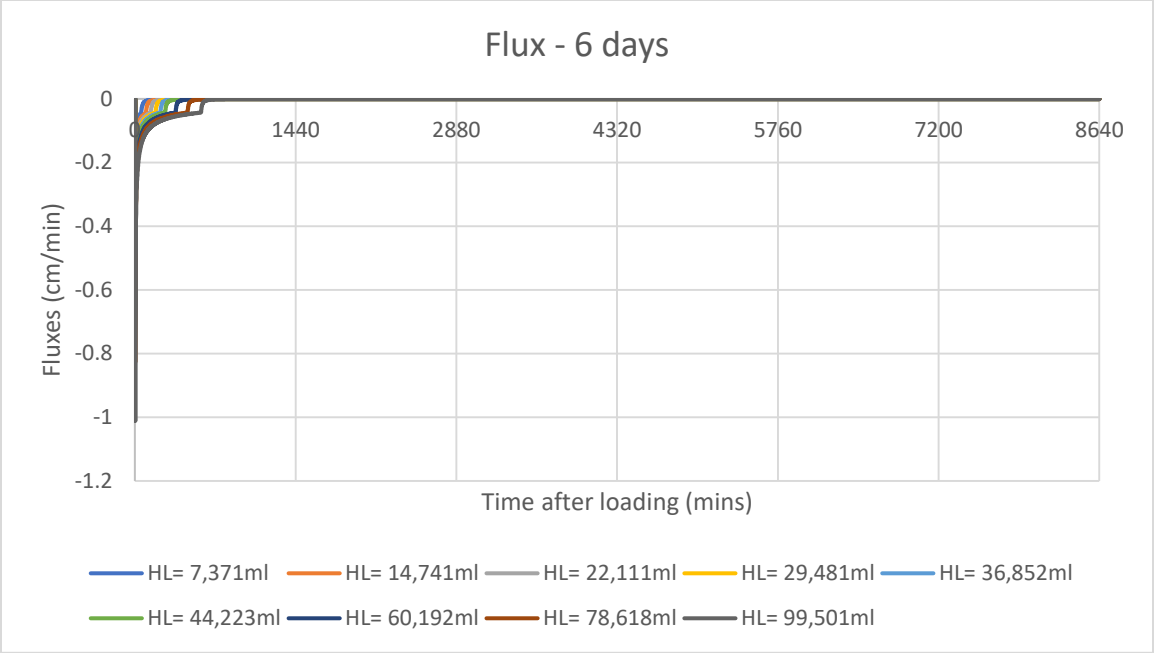

Figure 6.6: Sensitivity analysis of effluent fluxes under varying hydraulic loads for the first hour and 6 days.

Furthermore, the MCs of the sludge deposit layer increased with the hydraulic loads, as shown in Figure 6.7. The larger hydraulic loads lengthened the surface ponding duration, moisturizing the sludge deposit layer and preventing the layer from deformation and cracks. Moreover, the larger hydraulic loads would also enhance the infiltration flux, allowing more effluent to drain through the reed bed. In other words, a sufficiently high infiltration rate fastened the drainage dewatering process, leading to a high final solids content of the sludge deposit layer (Trein *et al.*, 2019). Further, the lowest MC peak at 20% under the hydraulic loads below 10 L, i.e. 50 kg/m^2/year SLR, showed that the STRB was underperformed. Such a loading condition limited the overall performance, where the bed could treat larger hydraulic loads before exceeding its maximum loading capacity. Therefore, the optimal SLR should be above 50 kg/m^2/year to prevent the occurrence of cracks.

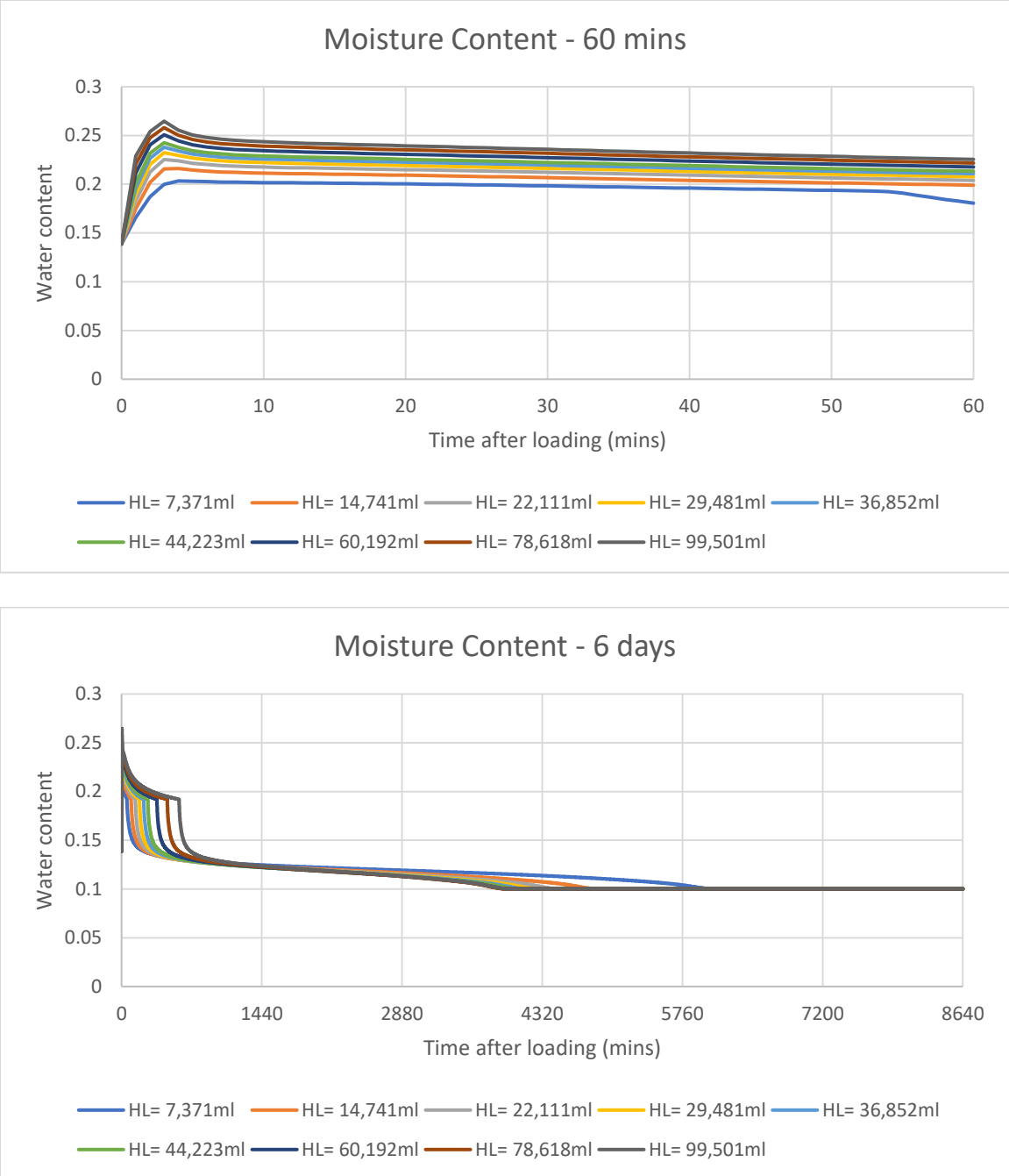

Figure 6.7: Sensitivity analysis of moisture content under varying hydraulic loads for the first hour and 6 days.

Similarly, the sludge accumulation on the sludge deposit layer also increased with the hydraulic loads, as indicated in Figure 6.8. The sludge accumulation peaks ranged from 14 to 60 cm under the hydraulic load in the range of 7371 to 99501 ml. The significantly high sludge thickness was due to the application of the compressible cake

filtration model, which describes the overall sludge level as the imposed flux (Pergam & Briesen, 2023). The sludge accumulation was the highest in the first three minutes of the feeding process, followed by a slower incremental sludge accumulation due to particle settling, and finally reached a constant thickness upon draining completion. Then, the sludge deposit layer thickness is expected to decrease gradually during the resting period due to evapotranspiration. Thus, the simulation duration of 60 minutes needs to be increased to profile the sludge accumulation behaviors due to the large hydraulic loads, as settling solid particles is a slow process. Further, the difference in the sludge accumulations increased substantially above hydraulic load of 45 L. Therefore, the hydraulic load is preferred to keep within 45 L to prevent overprediction in MC.

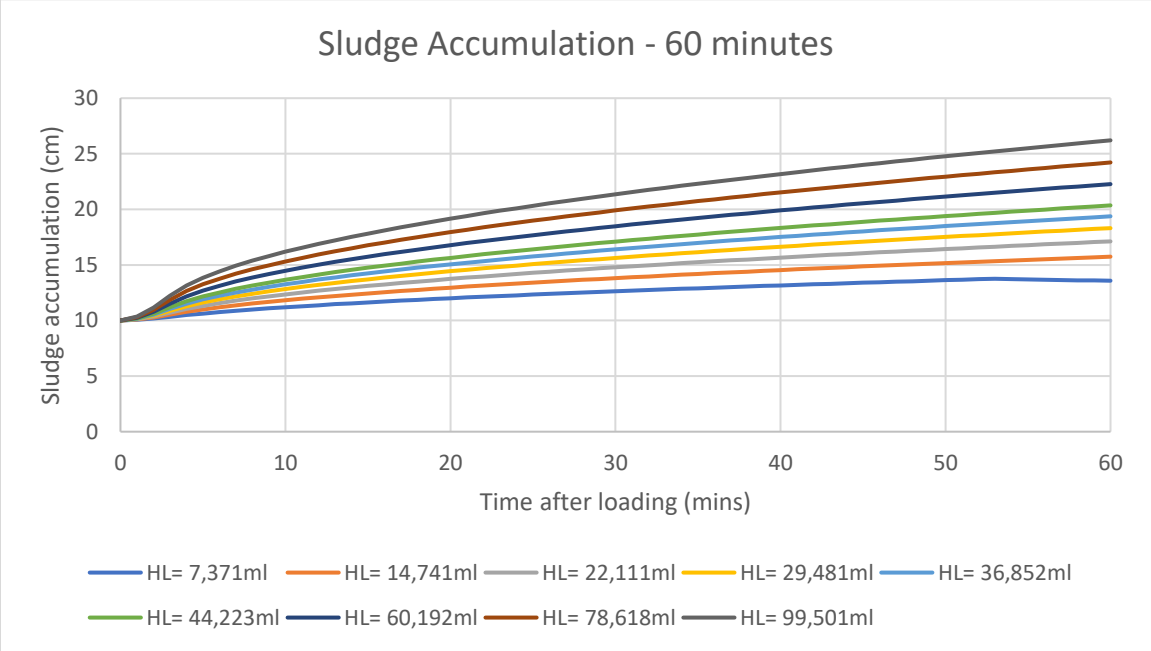

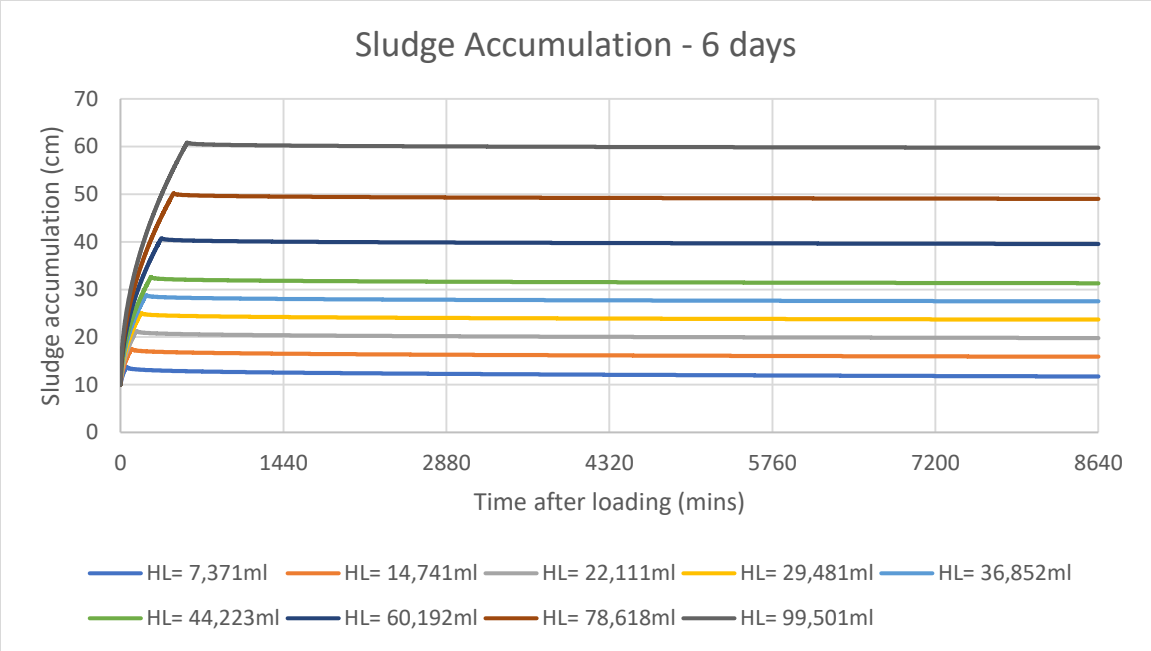

Figure 6.8: Sensitivity analysis of sludge accumulation under varying hydraulic loads for the first hour and 6 days.

In contrast, the overall simulated organic concentration of the sludge deposit layer has the opposite trend compared to the MC, as shown in Figure 6.9. The overall organic concentrations decreased with larger hydraulic loads due to prolonged surface ponding, where the microorganisms have limited oxygen for further growth and development. However, the sludge stabilization was still significant. The ASM3 describes the sludge mineralization and stabilization using the production and decay of microorganisms (Simon-Várhelyi *et al.*, 2020). Hence, the simulation instantaneously computes the resultant organic content of the sludge deposit during the feeding phase, resulting in an 80% reduction of the initial COD concentration. Additionally, the sludge deposit organic concentration after the 3rd minute was around 960 mg/L and reduced to a final concentration of approximately 450 mg/L.

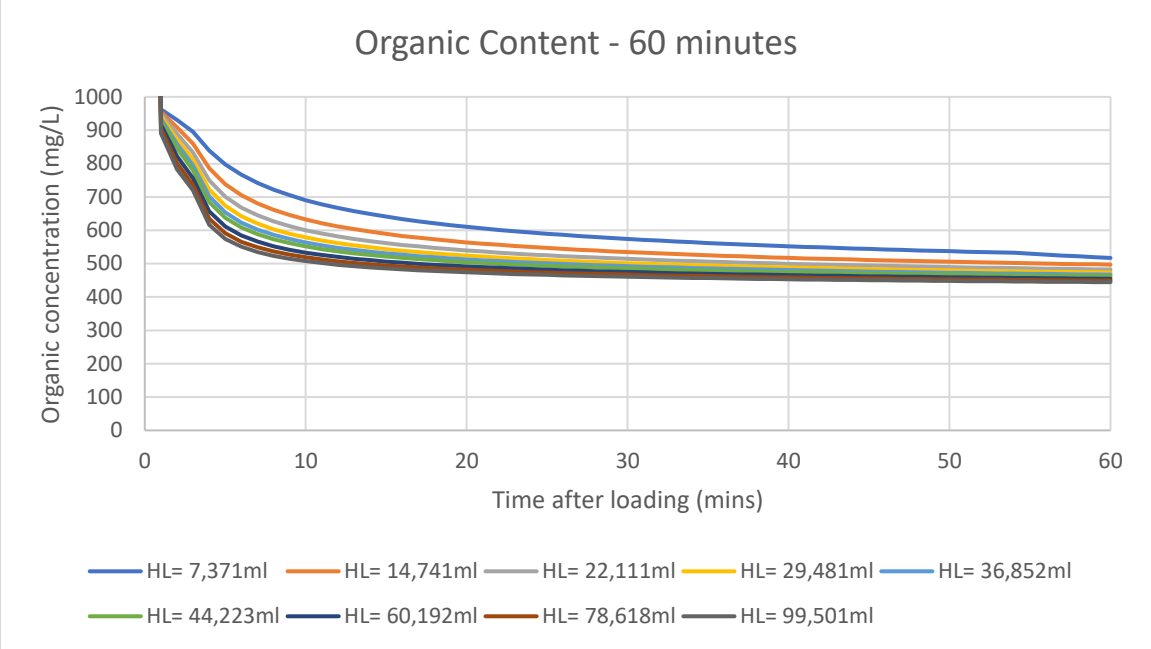

Figure 6.9: Sensitivity analysis of organic content under varying hydraulic loads for the first hour.

In addition, the evapotranspiration rates increased with the hydraulic loads, as shown in Figure 6.10. The increment in the evapotranspiration rates was roughly consistent with the incremental hydraulic loads due to the same MC loss to the atmosphere. However, the larger hydraulic loads create a longer surface ponding, lengthening the plant transpiration and water evaporation. Moreover, the evapotranspiration on the top surface layer showed a relatively small dewatering rate. The evapotranspiration rate is mainly dependent on the reed coverage on the bed surface (Abeysiriwardana *et al.*, 2022). Thus, a relatively small STRB scale at roughly 0.2 m^2 surface area would result in an insignificant evapotranspiration rate.

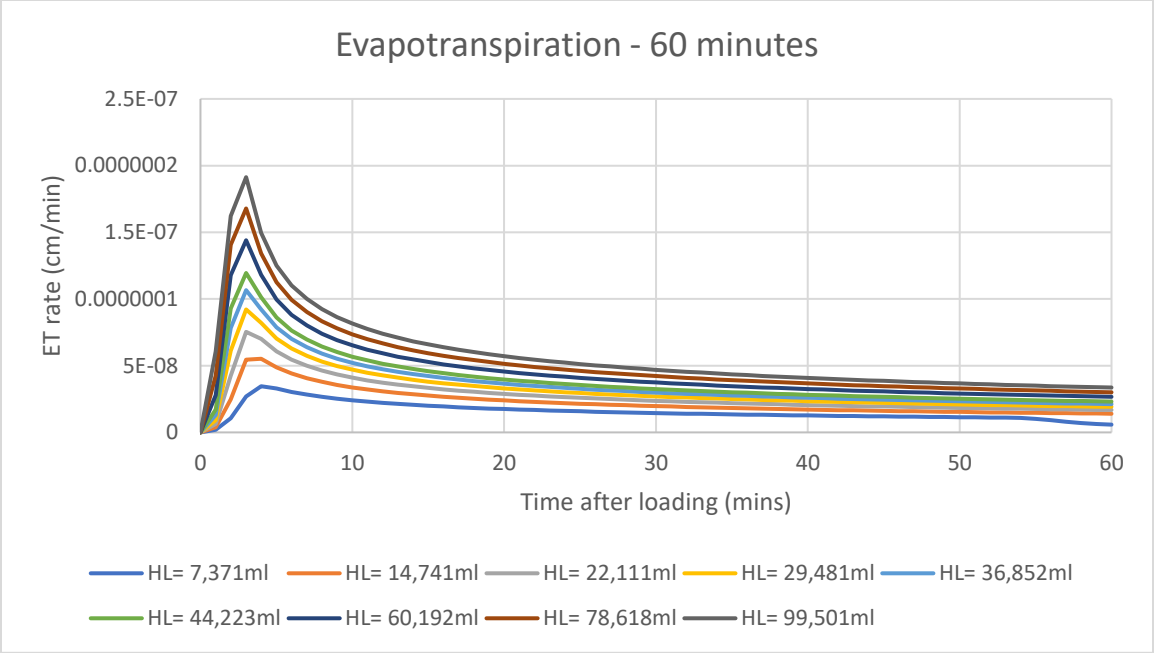

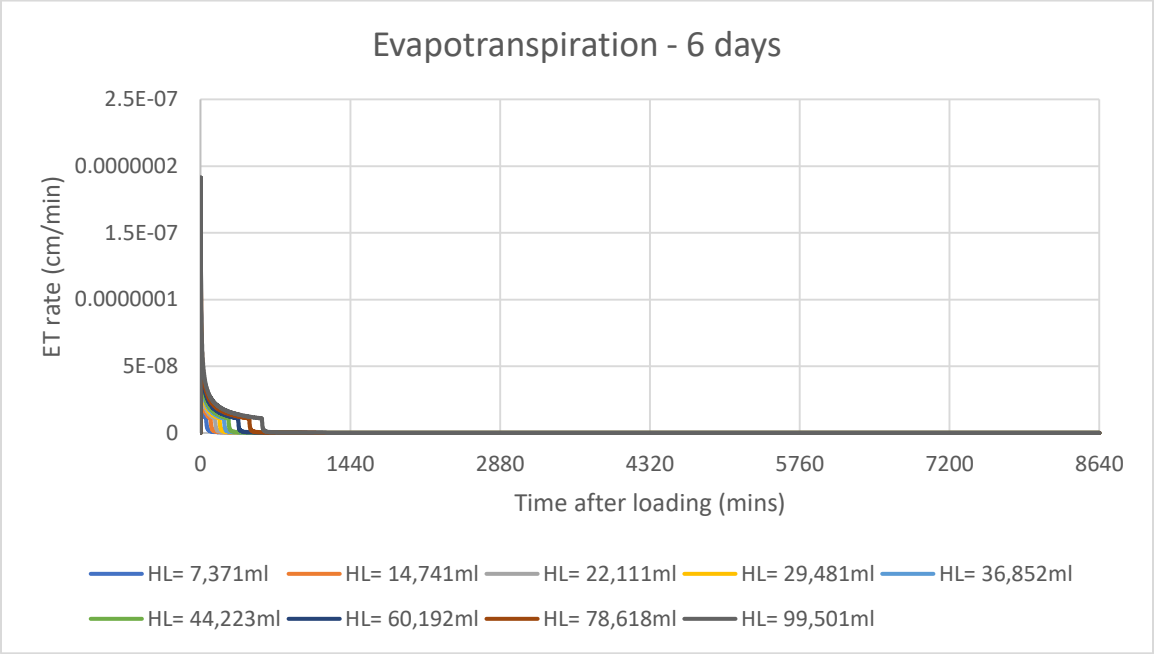

Figure 6.10: Sensitivity analysis of evapotranspiration under varying hydraulic loads for the first hour and 6 days.

6.2.2 Hydraulic Head

The hydraulic head of the normal flow case ranged from -10 to -28 cm, with an average head of -19 cm. Thus, the tested head range was extended from -7 to -30 cm to analyze the parameter sensitivity. Table 6.3 shows the input parameters according to the hydraulic head difference. The other parameters, such as the initial sludge thickness, saturated hydraulic conductivity, and hydraulic load, were fixed at the average values in the simulation. As discussed earlier, a hydraulic head larger than -10 cm would result in a bypassed flow case, whereas the pressure below -28 cm shows a clogged flow case. Figure 6.11 to Figure 6.15 shows the effects of varying hydraulic heads on the effluent flux, MC, sludge accumulation, organic content, and evapotranspiration, respectively.

Table 6.3: Variation in hydraulic heads.

Hydraulic head (cm)	SLR (kg/m^2/year) @ 6-day resting period	Sludge thickness (cm)	COD concentration (mg/L)	Saturated conductivity (cm/min)	Hydraulic load (ml)
-7	100	10	4763.32	0.0429	14,741
-10	100	10	4763.32	0.0429	14,741
-13	100	10	4763.32	0.0429	14,741
-16	100	10	4763.32	0.0429	14,741
-19	100	10	4763.32	0.0429	14,741
-21	100	10	4763.32	0.0429	14,741
-24	100	10	4763.32	0.0429	14,741
-27	100	10	4763.32	0.0429	14,741
-30	100	10	4763.32	0.0429	14,741

From the observation, the hydraulic heads increased with the flux peaks and decreased with the flow delays. The initial head distribution describes the MC in the bed simulation profile, where a dryer of the initial bed condition would result in a lower hydraulic head (Huong *et al.*, 2023b). Thus, the simulation requires overcoming the high initial head difference before the imposed hydraulic load, resulting in a longer flow delay. However, the 0.0429 cm/min saturated hydraulic conductivity of the sludge deposit limited the flow delay from extending more than 4 minutes, leading to insignificant differences in the hydraulic heads below -16 cm. Hence, the hydraulic heads increased with the flux peaks due to the incremental bed MC under the same hydraulic load. In

addition, the hydraulic head larger than -10 cm was found to present a distinct effluent flux. The instantaneous flow discharge with a relatively high flux peak could describe the cracked condition of the bed, where the effluent directly bypasses the sludge deposit layer. Therefore, the hydraulic head should be kept below -10 cm to avoid such an inconsistent flow.

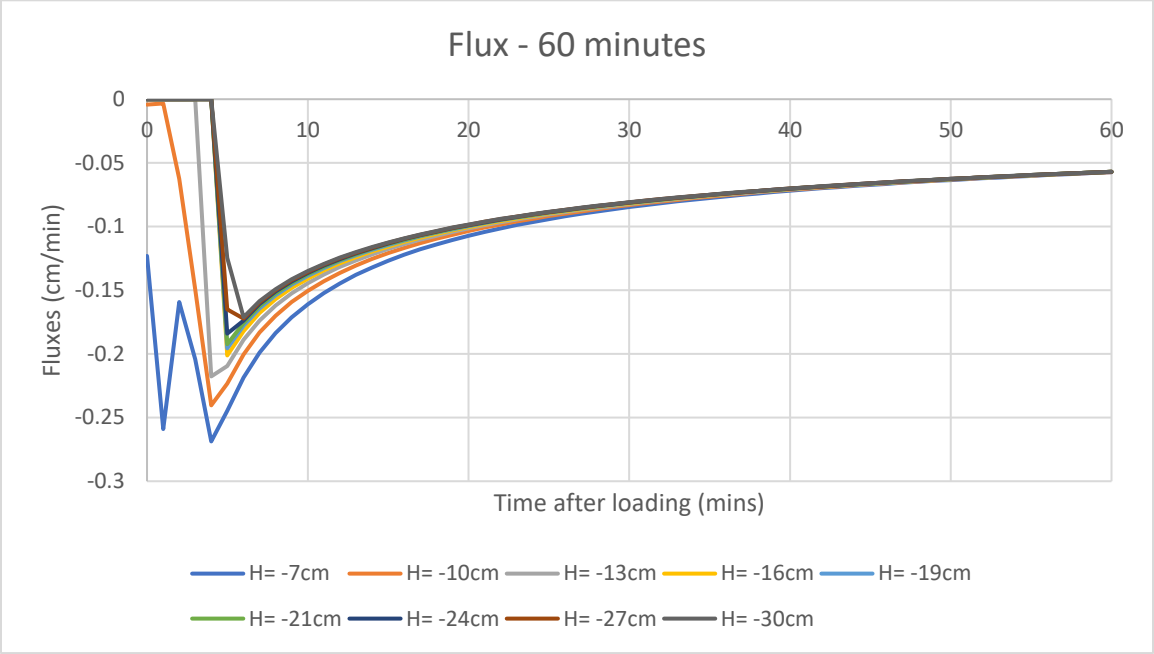

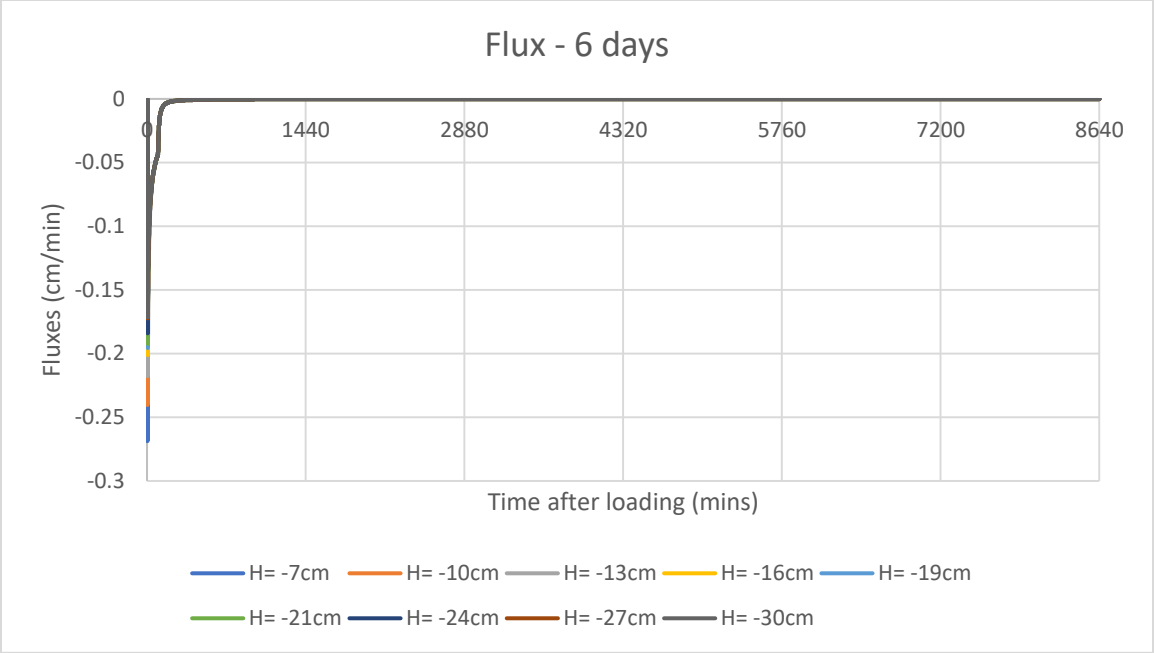

Figure 6.11: Sensitivity analysis of effluent flux under varying hydraulic heads for the first hour and 6 days.

Moreover, the MC peaks of the sludge deposit layer decreased with the hydraulic heads. Certainly, the hydraulic head describes the bed condition, whereas a lower hydraulic head indicates a lower bed MC. The hydraulic head ranged from -7 to -30 cm, providing an initial MC of 12 to 26%. The hydraulic head above -13 cm has the most significant difference in the MCs, while insignificant below -16 cm. The MC increased substantially upon feeding, followed by settling solid particles on the sludge deposit layer, which caused a noticeable reduction in the MC. Due to water loss in the sludge deposit via evapotranspiration during the resting period, the MCs gradually decreased to around 20%.

In contrast, the sludge accumulations on the sludge deposit layer were comparatively similar under varying hydraulic heads, as the sludge deposit thickness is mainly affected by the hydraulic loads. Meanwhile, the organic contents of the sludge deposit layer were also analyzed to be relatively similar under varying hydraulic heads. The organic content was reduced due to the moisture loss, where the decay of microorganisms dominated the growth. Thus, it can be concluded that the hydraulic heads less influenced the sludge accumulation and organic content.

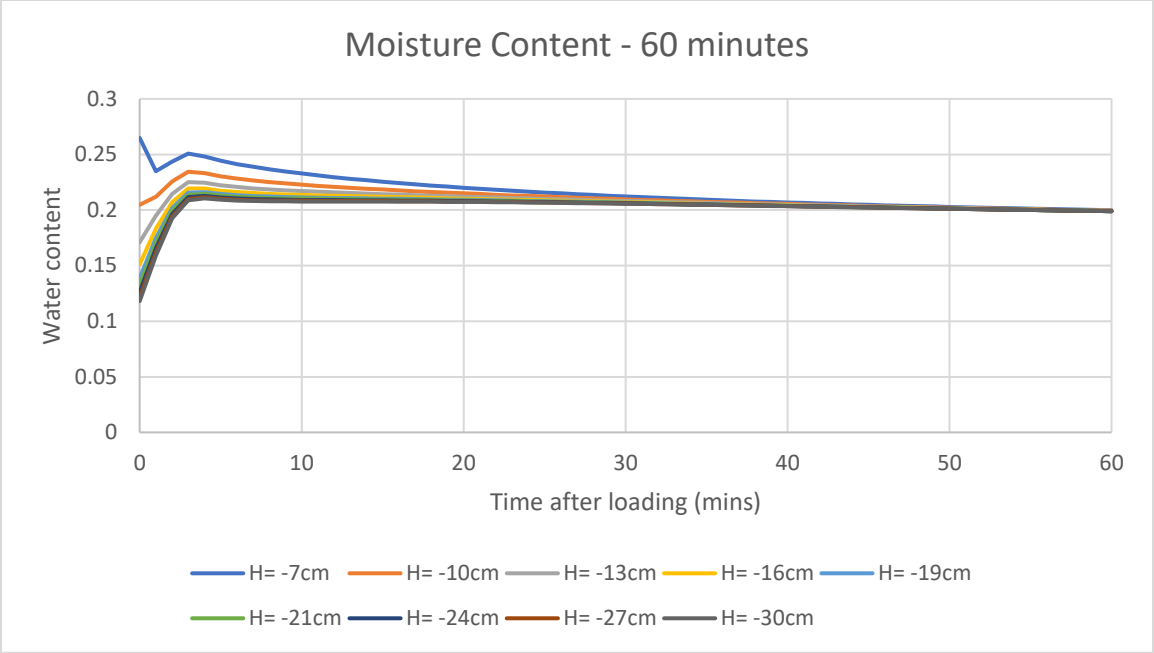

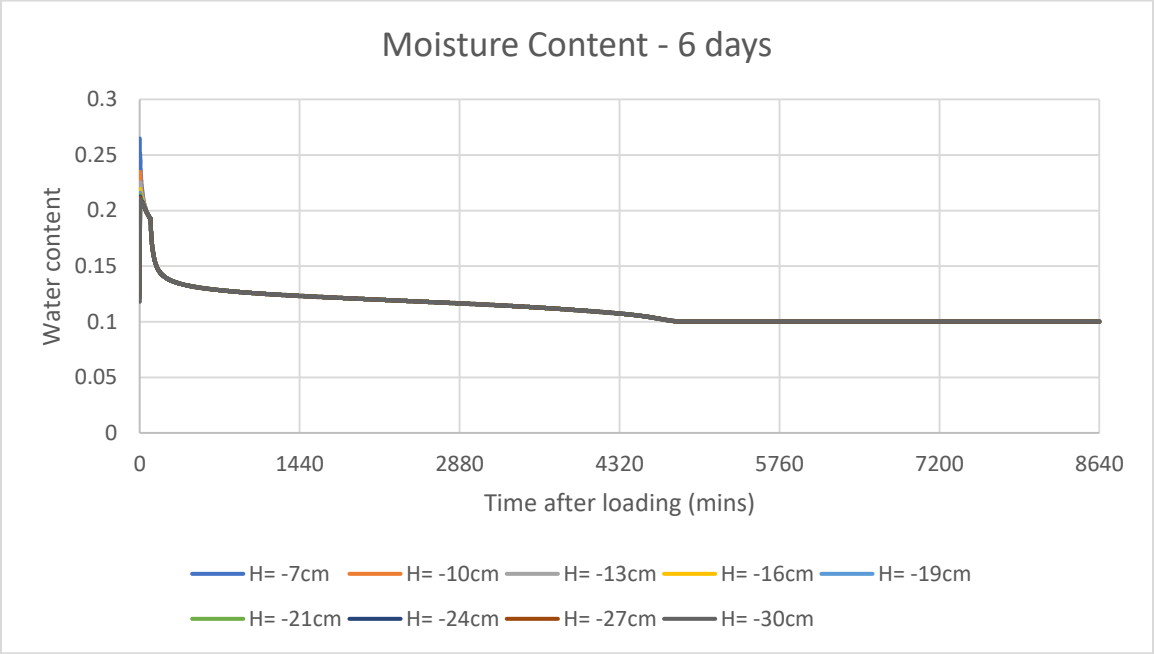

Figure 6.12: Sensitivity analysis of moisture content under varying hydraulic heads for the first hour and 6 days.

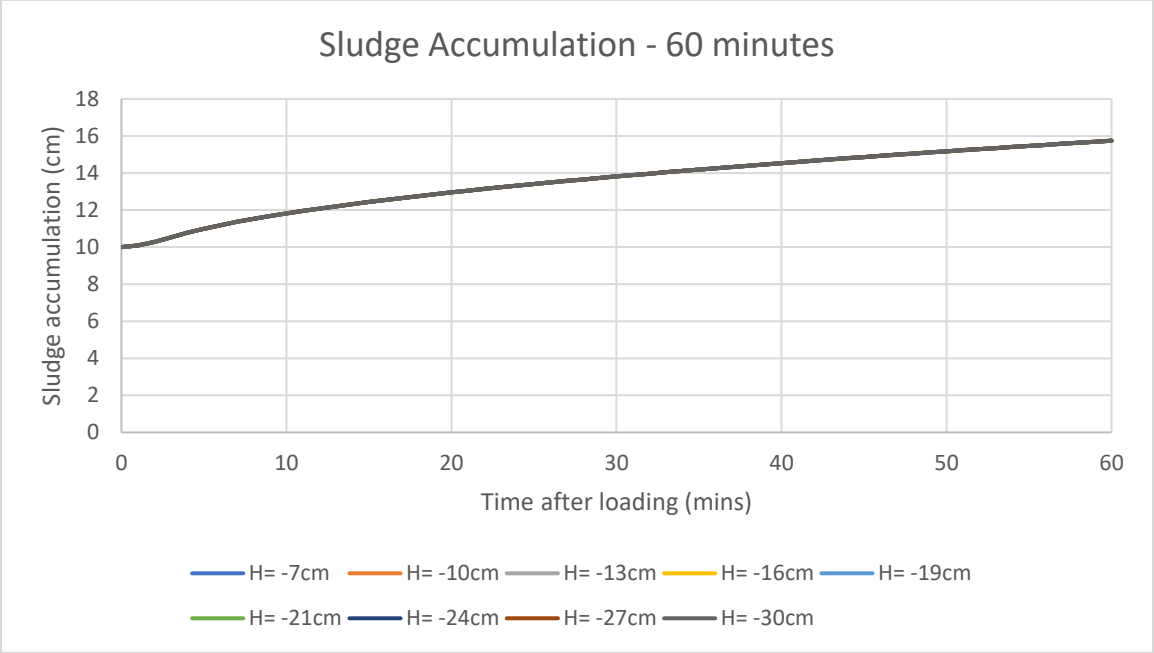

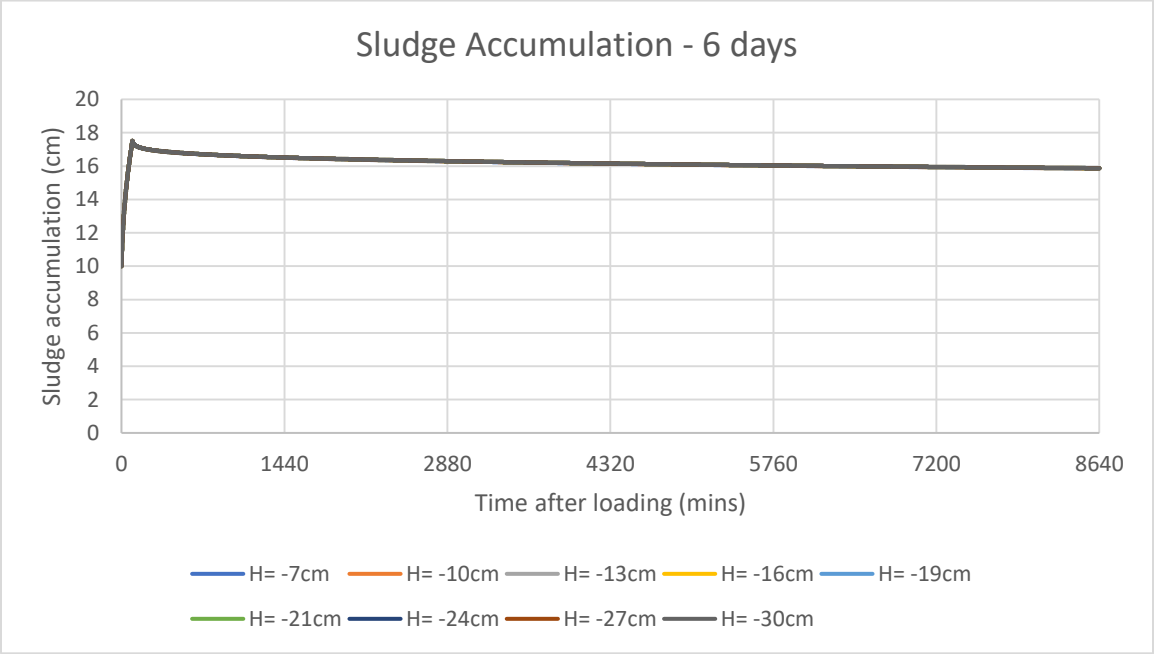

Figure 6.13: Sensitivity analysis of sludge accumulation under varying hydraulic heads for the first hour and 6 days.

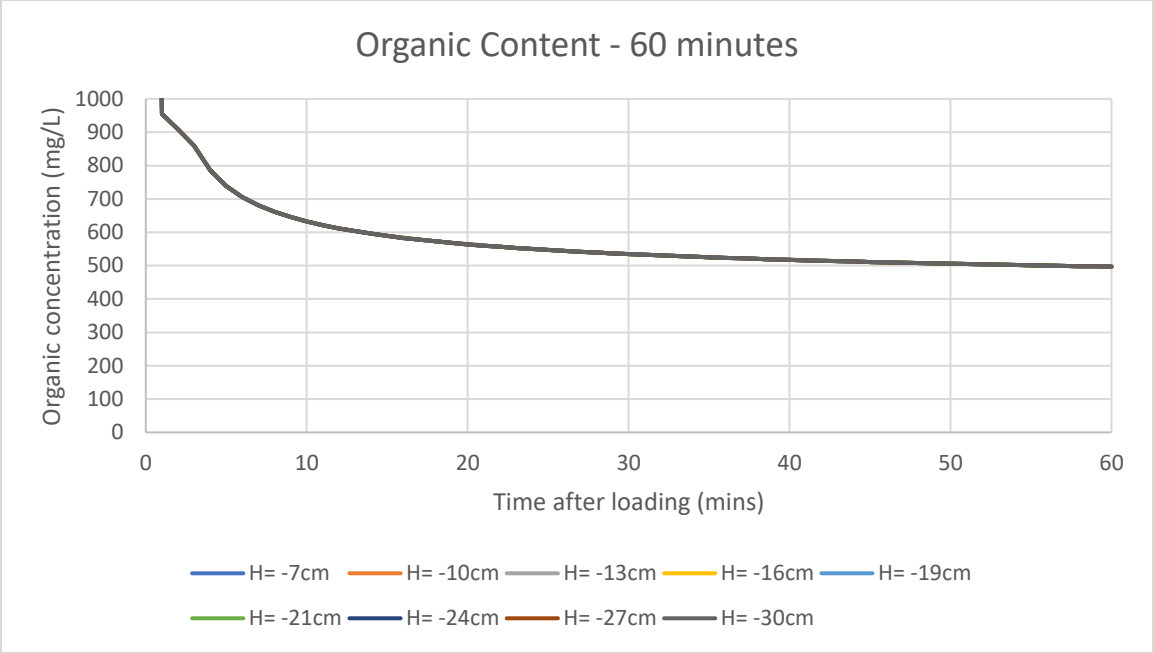

Figure 6.14: Sensitivity analysis of organic content under varying hydraulic heads for the first hour.

Furthermore, the evapotranspiration peaks decreased with the hydraulic heads, especially during the feeding phase. The higher initial bed MC, attributed to the higher hydraulic head, has boosted the evapotranspiration rate at the early stage. Then, the gradual reduction in the MC decreased the water loss to the atmosphere, slowly decreasing the evapotranspiration rate. The simulation of a -7 cm hydraulic head describes the cracked flow case condition, where the sudden evapotranspiration rate increment was due to the crack occurrence on the sludge deposit layer, creating a larger surface area for extensive oxygen exchange, which directly increased the evapotranspiration rate.

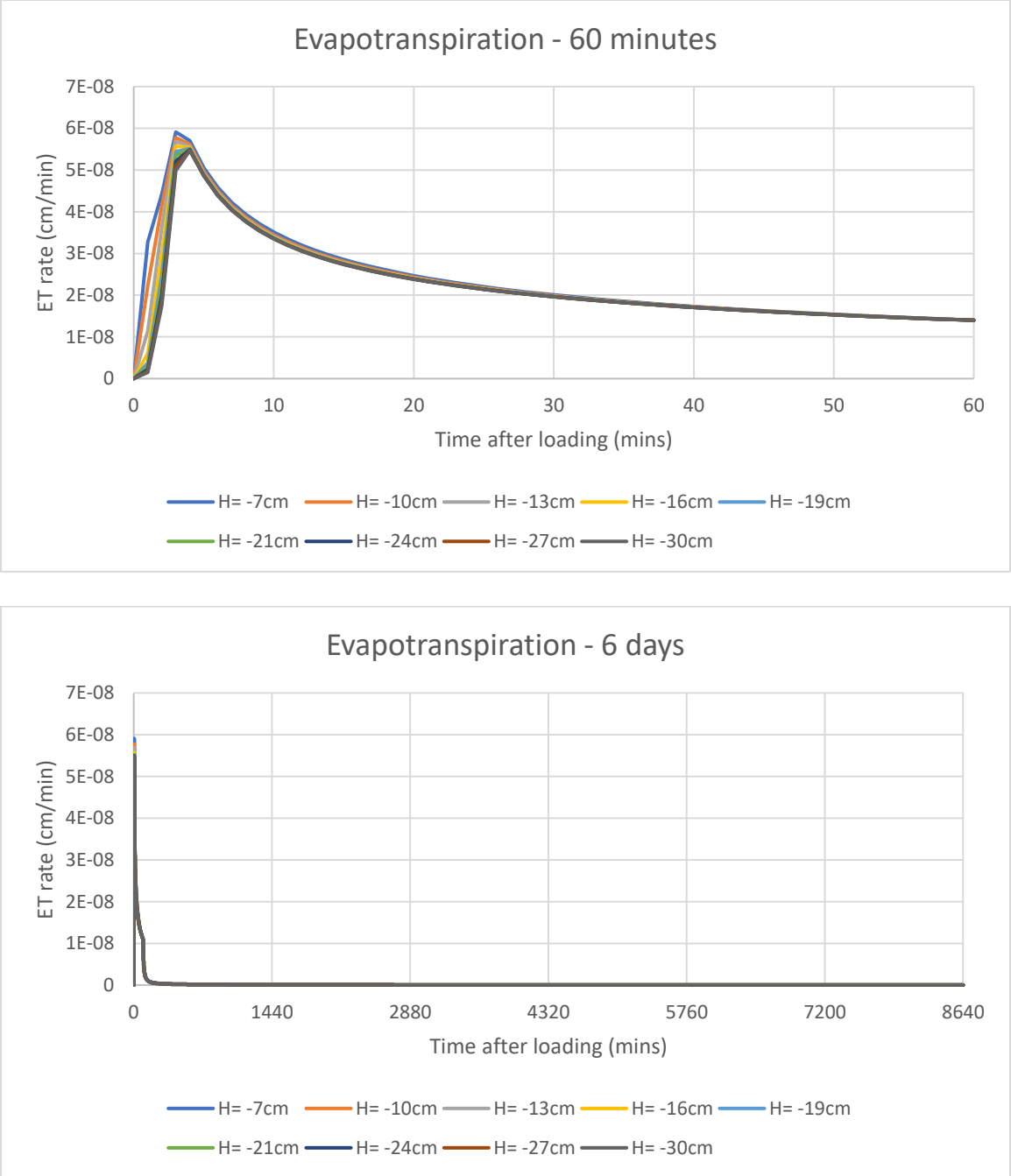

Figure 6.15: Sensitivity analysis of evapotranspiration under varying hydraulic heads for the first hour and 6 days.

6.2.3 Saturated Hydraulic Conductivity

The saturated hydraulic conductivity of the sludge deposit layer increases with the hydraulic load. However, the effect of the saturated hydraulic conductivity under a constant hydraulic load is unknown. Hence, the values of the hydraulic load, head, and sludge deposit layer thickness were fixed constantly. At the same time, the saturated conductivity was manipulated to analyze its sensitivity over the outflow dynamics. Table 6.4 shows the variation in the saturated hydraulic conductivity used in the sensitivity analysis, covering from 0.0009 to 0.1269 cm/min with an increment conductivity of 0.0140 cm/min.

Table 6.4: Variation in saturated hydraulic conductivities.

Saturated conductivity (cm/min)	SLR (kg/m^2/year) @ 6-day resting period	Sludge thickness (cm)	COD concentration (mg/L)	Hydraulic head (cm)	Hydraulic load (ml)
0.0009	100	10	4763.32	-19	14,741
0.0149	100	10	4763.32	-19	14,741
0.0289	100	10	4763.32	-19	14,741
0.0429	100	10	4763.32	-19	14,741
0.0569	100	10	4763.32	-19	14,741
0.0709	100	10	4763.32	-19	14,741
0.0849	100	10	4763.32	-19	14,741
0.0989	100	10	4763.32	-19	14,741
0.1129	100	10	4763.32	-19	14,741
0.1269	100	10	4763.32	-19	14,741

Figure 6.16 shows the effluent flux dynamics under varying saturated hydraulic conductivities. The flux peaks were found to increase with the saturated conductivities. The saturated conductivity relates to the permeability of the sludge deposit layer, where the saturated conductivity increases with the layer permeability. By means, the sludge deposit controls the overall percolation rate through the STRB substrate filters. Several factors control the sludge deposit layer permeability, such as its layer thickness, moisture, and organic contents. Indeed, the sludge deposit with a higher organic content ensures a higher shrinkage limit, sustaining more moisture within the bed, thus reducing the effluent flux (Mohajerani *et al.*, 2019). The flux peaks increased significantly with

incremental conductivities from 0.0009 to 0.0149 cm/min, while the changes were less visible with higher conductivities. Further, the saturated conductivity increments also shortened the flow-occurring delay, accelerating the effluent flux and boosting the drainage dewatering. Similarly, the difference in the flow delays was significant in lower conductivities, especially below 0.001 cm/min. The significantly low conductivity extensively prolongs the flow delay, affecting the overall STRB efficiency.

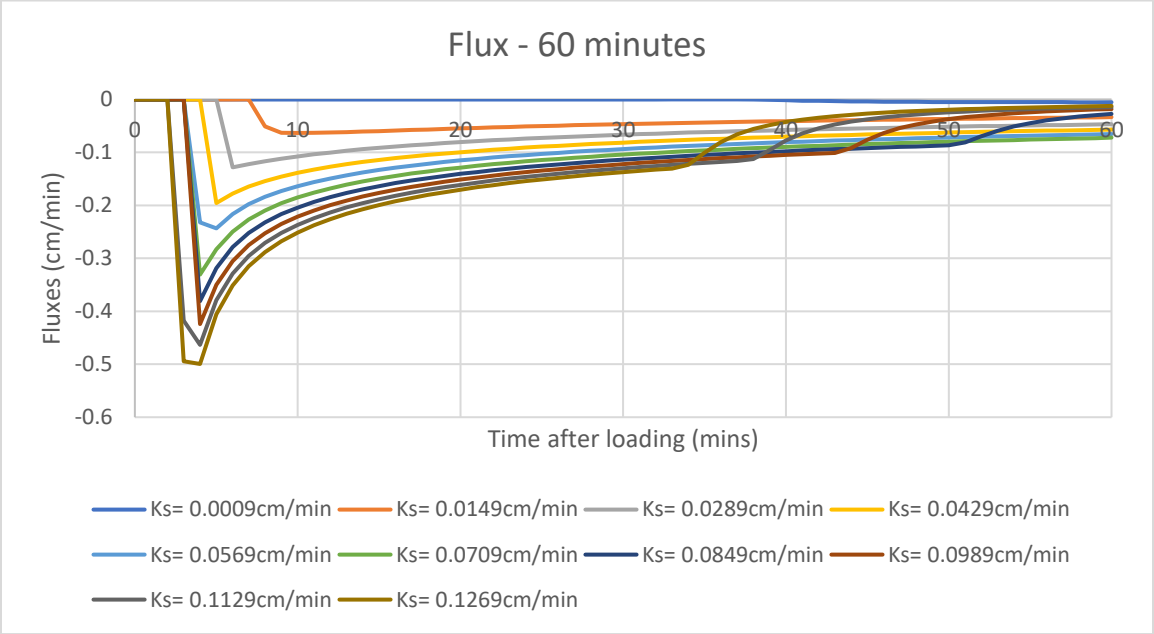

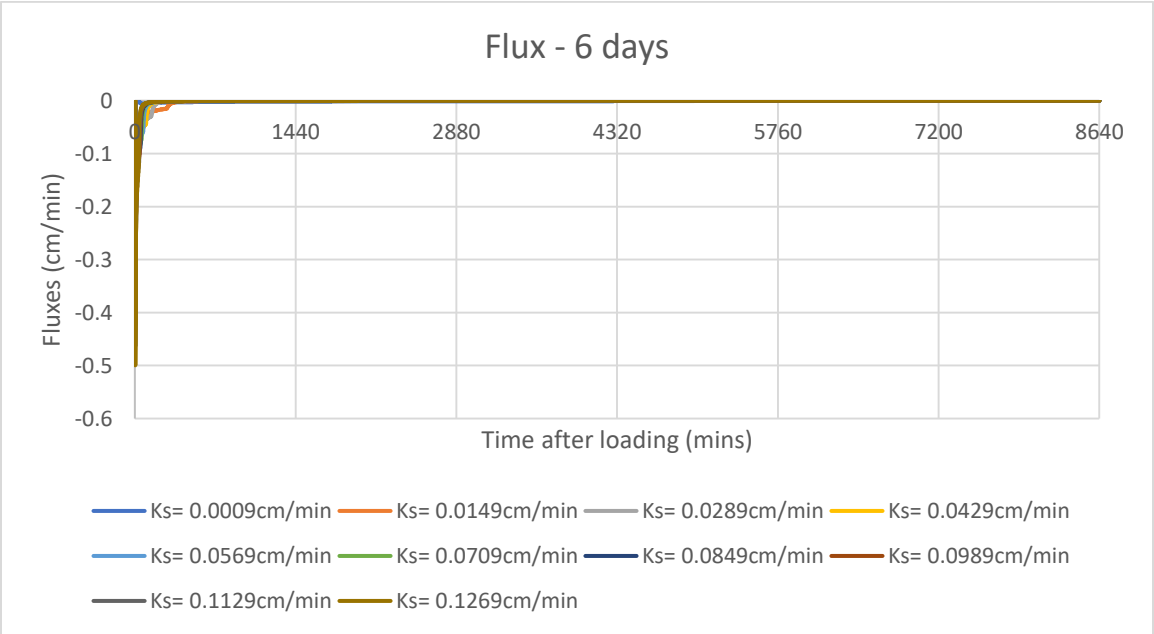

Figure 6.16: Sensitivity analysis of effluent flux under varying saturated conductivities for the first hour and 6 days.

Figure 6.17 shows the changes in MC under varying saturated conductivities. The MCs increased with the saturated conductivities. However, the MC peaks were relatively similar with saturated conductivities higher than 0.07 cm/min, as the constant hydraulic load of 14741 ml maximized the MC at around 25%. The higher saturated conductivity ensures a higher maximum percolation rate through the sludge deposit layer, resulting in a faster drainage. Further, the hydraulic conductivity of 0.0009 cm/min showed a distinct MC curve, where the MC tends to continue increasing for the first 60 minutes. The insufficient saturated conductivity extensively retarded the infiltration process, leading to prolonged drainage dewatering and higher final MC. Therefore, the saturated conductivity should be maintained above 0.001 cm/min to boost the infiltration rate and time efficiency.

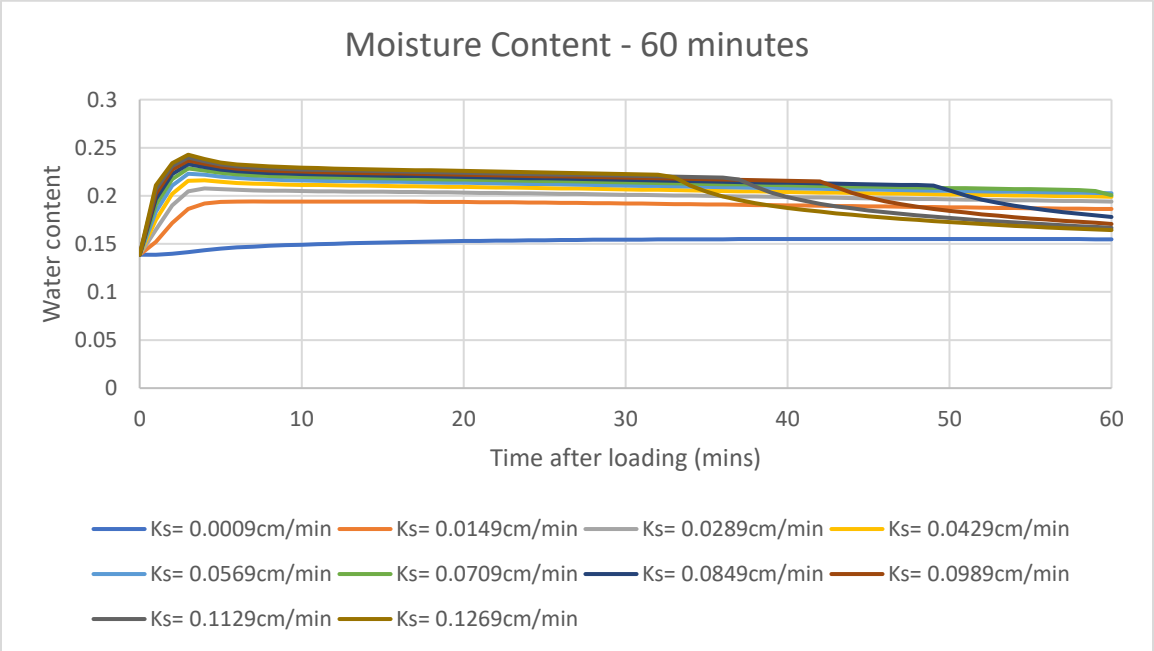

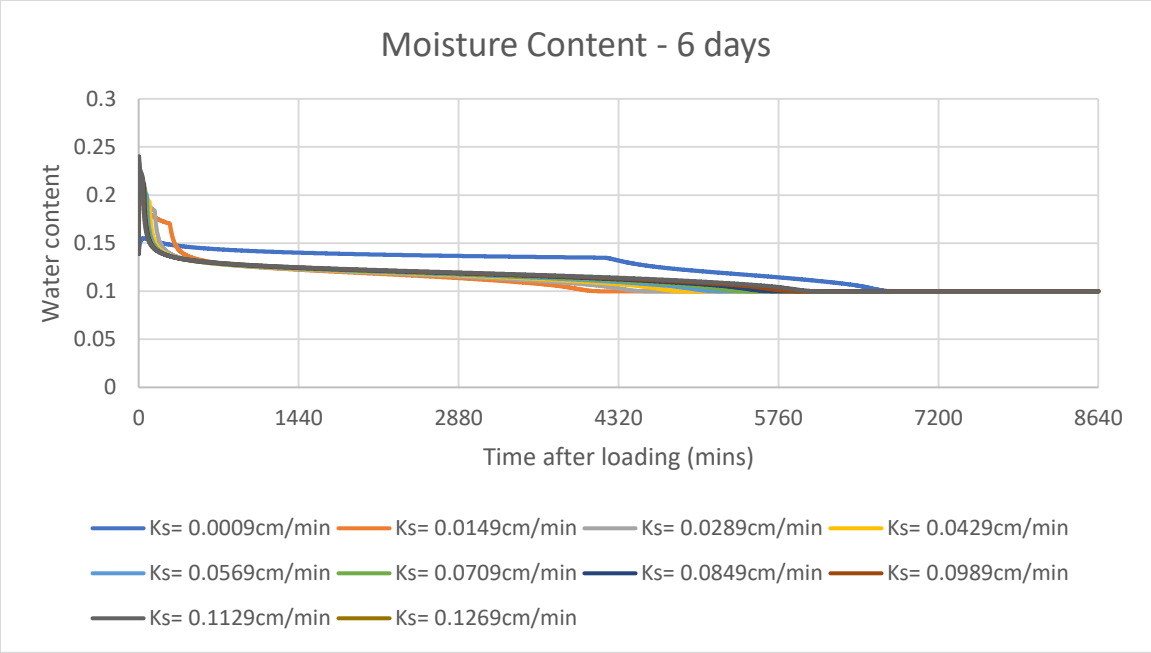

Figure 6.17: Sensitivity analysis of moisture content under varying saturated conductivities for the first hour and 6 days.

Moreover, the sludge deposit layer showed an incremental sludge accumulation with the saturated hydraulic conductivity, as shown in Figure 6.18. Due to higher draining and particle settling rates, the sludge accumulation peak durations decreased from approximately 60 to 35 minutes, increasing conductivities from 0.0709 to 0.1269 cm/min. Moreover, the reduction in the final sludge deposit thickness was significant, with higher conductivity. A quicker drainage completion increased the sludge deposit exposure to the atmosphere, allowing a longer contact duration for water loss via evapotranspiration. Therefore, reducing sludge deposits should be considered a long-term effect, as a longer resting period would result in a dryer sludge deposit.

An opposite trend in the MC was observed for the sludge stabilization, as displayed in Figure 6.19. The organic content stabilized quicker under a higher saturated conductivity. A longer ponding duration, upon a lower hydraulic load and MC, would result in sludge deposit deformation and, eventually, cracks. In such a condition, the microorganisms in the sludge deposit layer receive excessive oxygen for growth and development, leading to a high final organic content, as indicated in the case with 0.0009 cm/min saturated conductivity.

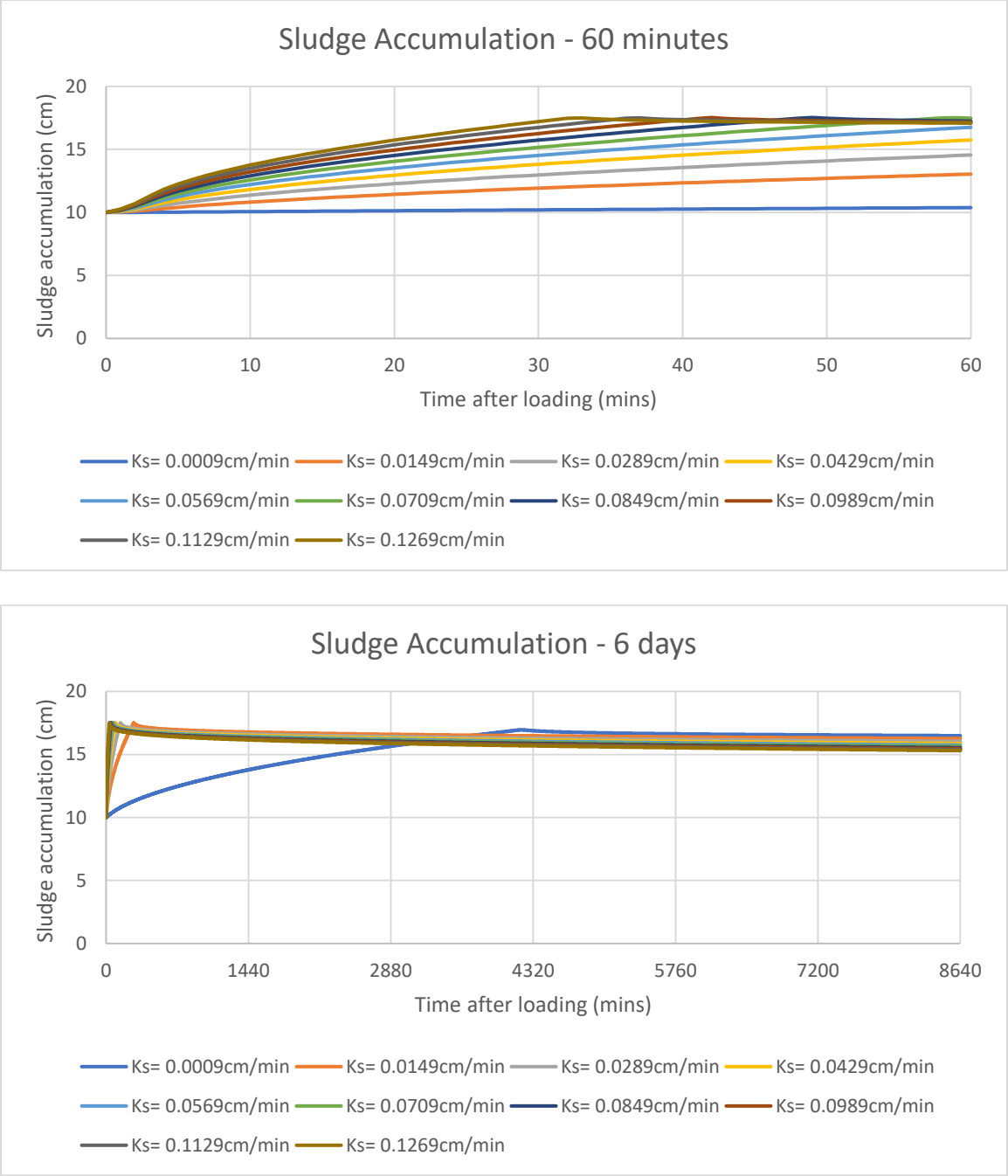

Figure 6.18: Sensitivity analysis of sludge accumulation under varying saturated conductivities for the first hour and 6 days.

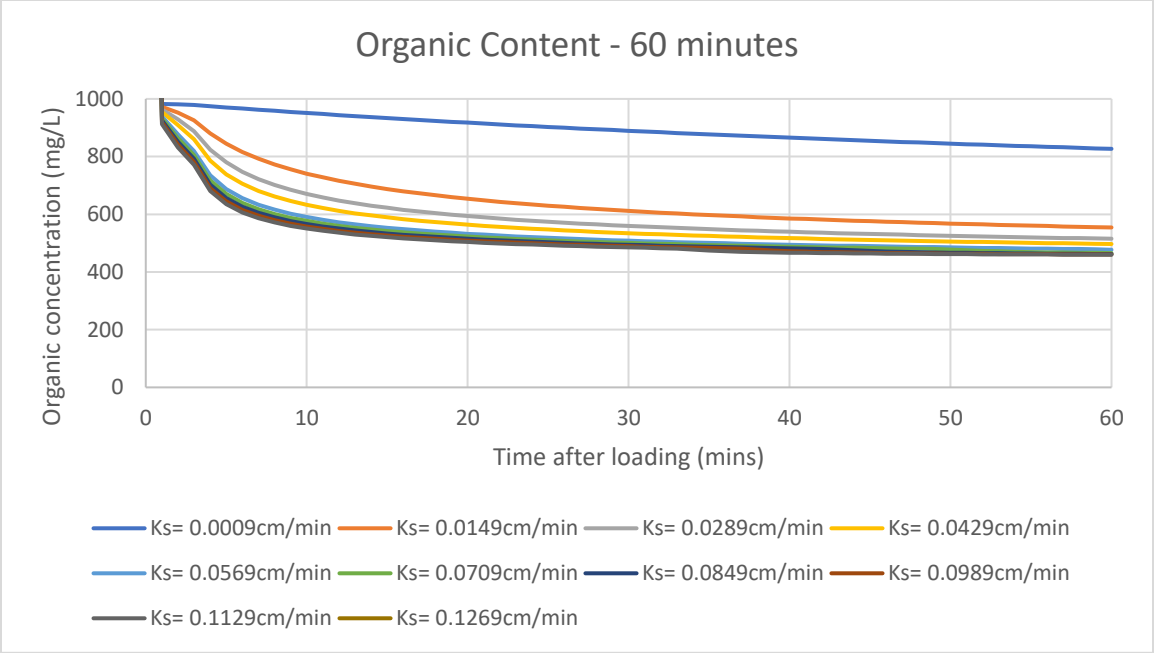

Figure 6.19: Sensitivity analysis of organic content under varying saturated conductivities for the first hour.

In addition, the simulated evapotranspiration rates under varying hydraulic conductivity are shown in Figure 6.20. The overall evapotranspiration rates increased with the saturated hydraulic conductivities over the feeding-resting period. The higher hydraulic conductivity extends the infiltration rate limit, leading to faster drainage dewatering. As a result, the sludge deposit MC decreases extensively, shortening the overall treatment duration. The Penman-Monteith equation describes the evapotranspiration rate using the sludge deposit MC (Abeysiriwardana *et al.*, 2022). Thus, higher saturated conductivity shortens the drainage process, prolonging the drying of the sludge deposit and resulting in a higher evapotranspiration rate.

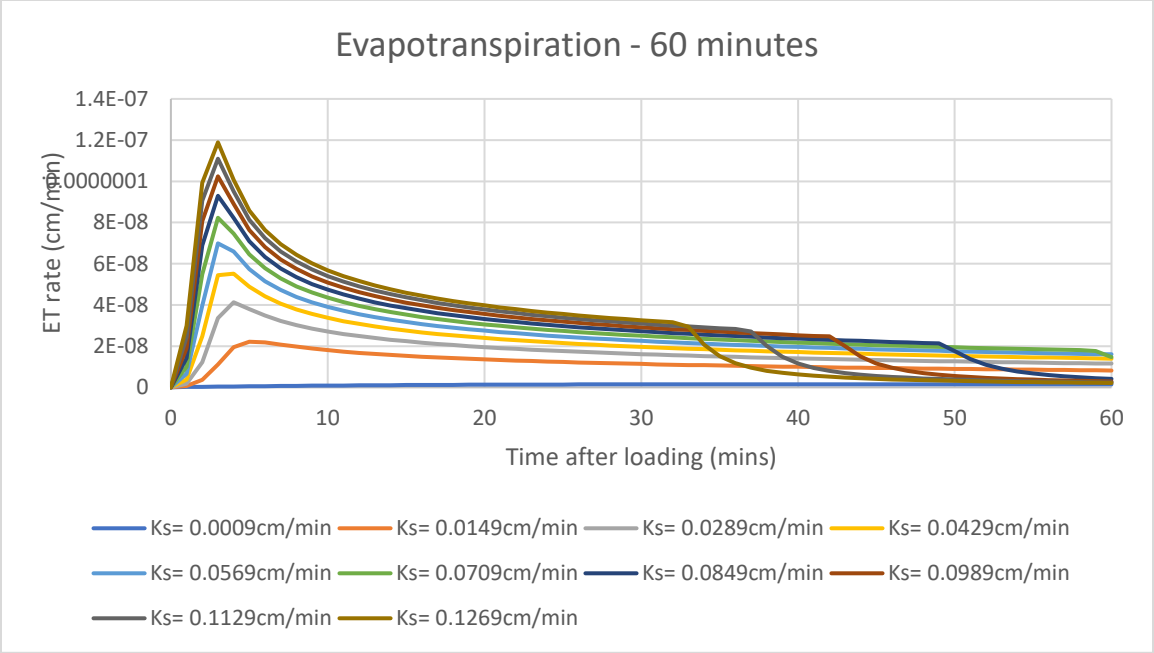

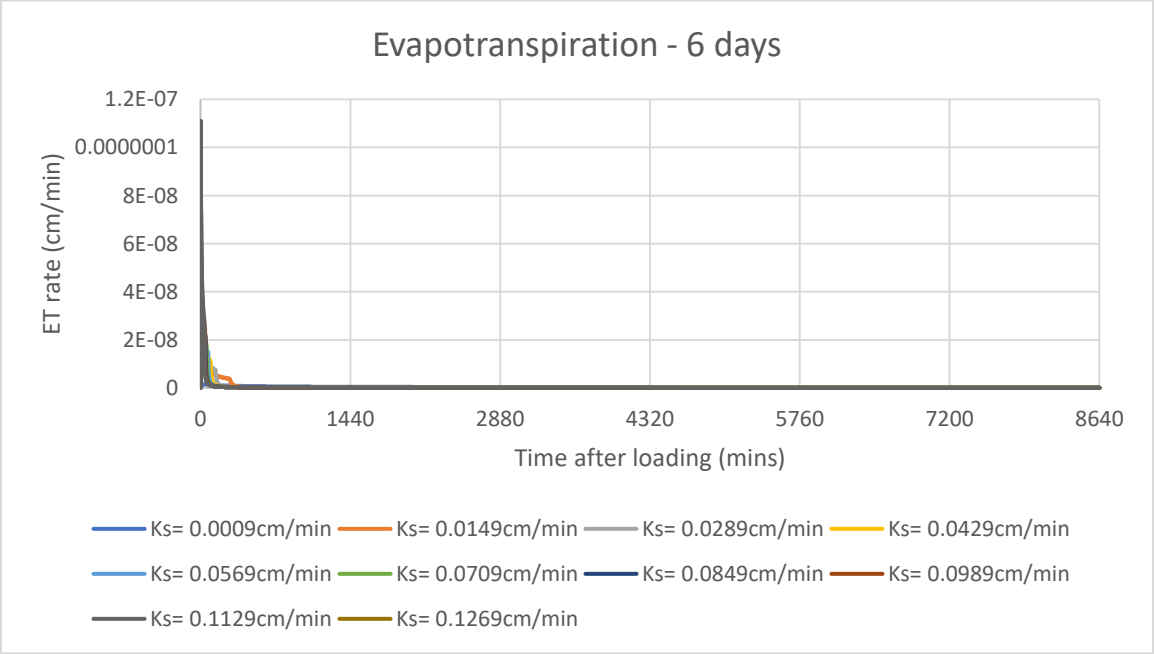

Figure 6.20: Sensitivity analysis of evapotranspiration under varying saturated conductivities for the first hour and 6 days.

6.2.4 Sludge Deposit Layer Thickness

The increase in the thickness of the sludge deposit layer reduced the subsequent infiltration and effluent flux. The thicker sludge deposit would increase the specific resistance of the layer, decreasing its permeability and resulting in a lower flux peak. The effect of the incremental sludge deposit thickness on the effluent flux, MC, sludge accumulation, organic content, and evapotranspiration was studied according to Table 6.5. The sensitivity analysis of the sludge deposit layer thickness covered the overall average measured sludge deposit thickness, ranging from 4 to 20 cm with a 2 cm increment.

Table 6.5: Variation in sludge deposit layer thickness.

Sludge thickness (cm)	SLR (kg/m^2/year) @ 6-day resting period	COD concentration (mg/L)	Hydraulic head (cm)	Saturated conductivity (cm/min)	Hydraulic load (ml)
4	100	4763.32	-19	0.0429	14,741
6	100	4763.32	-19	0.0429	14,741
8	100	4763.32	-19	0.0429	14,741
10	100	4763.32	-19	0.0429	14,741
12	100	4763.32	-19	0.0429	14,741
14	100	4763.32	-19	0.0429	14,741
16	100	4763.32	-19	0.0429	14,741
18	100	4763.32	-19	0.0429	14,741
20	100	4763.32	-19	0.0429	14,741

Figure 6.21 shows the effect of effluent flux under varying sludge deposit layer thickness. The flux peaks decreased from approximately 0.22 to 0.18 cm/min, with an incremental sludge deposit thickness from 4 to 20 cm. An incremental sludge thickness represents an increase in the mesh length. In the simulation, the increased spatial length, *dz* prolongs the travel distance for the imposed flux to infiltrate the substrate medium before discharging from the bottom of the bed (Huong *et al.*, 2024b). The reduction in the flux peaks nicely described the actual sludge deposit condition, where the sludge deposit layer thickness increases with its specific resistance, resulting in a lower flux peak.

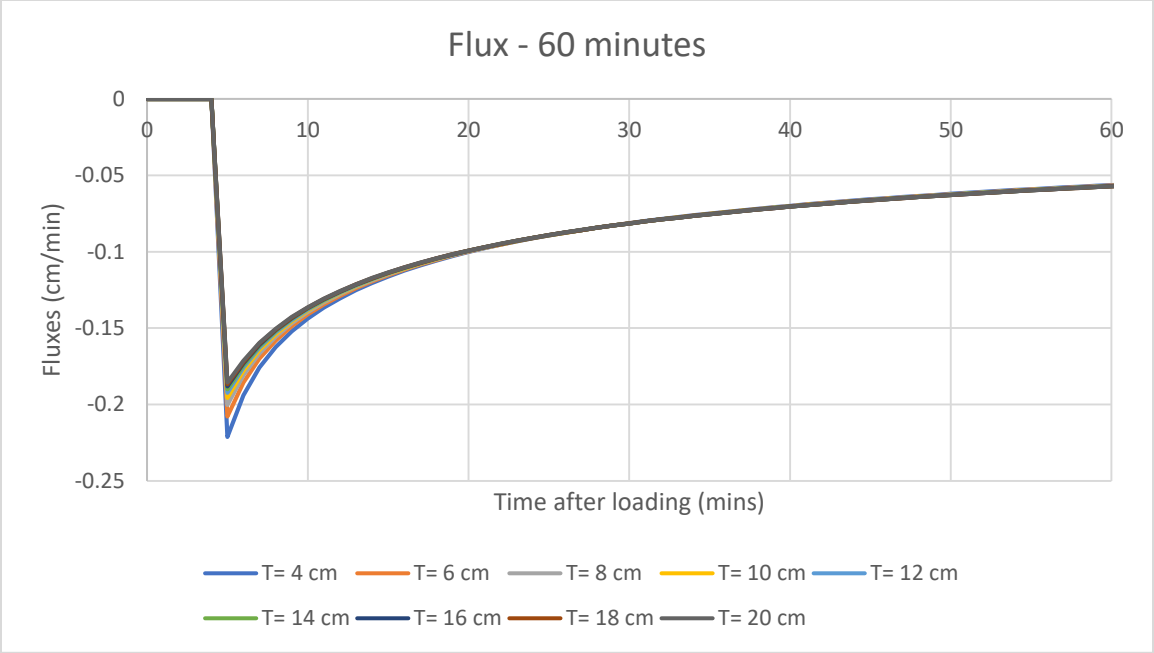

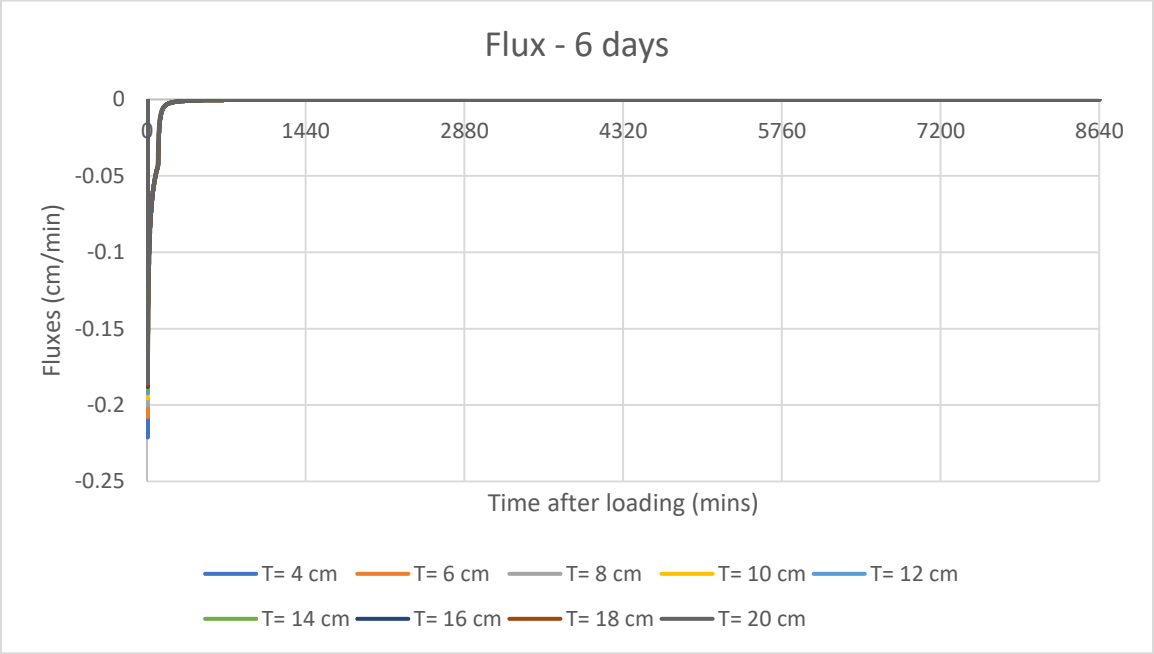

Figure 6.21: Sensitivity analysis of effluent flux under varying sludge thickness for the first hour and 6 days.

Figure 6.22 shows the effect of MC under varying sludge deposit layer thickness. The MC peaks decreased slightly from 22 to 21% with the incremental sludge deposit layer thickness from 4 to 20 cm. Typically, a thicker sludge deposit layer would have a higher porosity, retaining more moisture within the layer. However, the compressible

cake filtration model describes the specific resistance as always changing with the infiltration flux. The increase in the specific resistance decreases the infiltration rate, directly reducing the amount of water penetrating the sludge deposit layer. Conclusively, the effect of sludge thickness on the MC is considered minimal, as the MC peaks reduced slightly upon continuous sludge accumulation up to 20 cm.

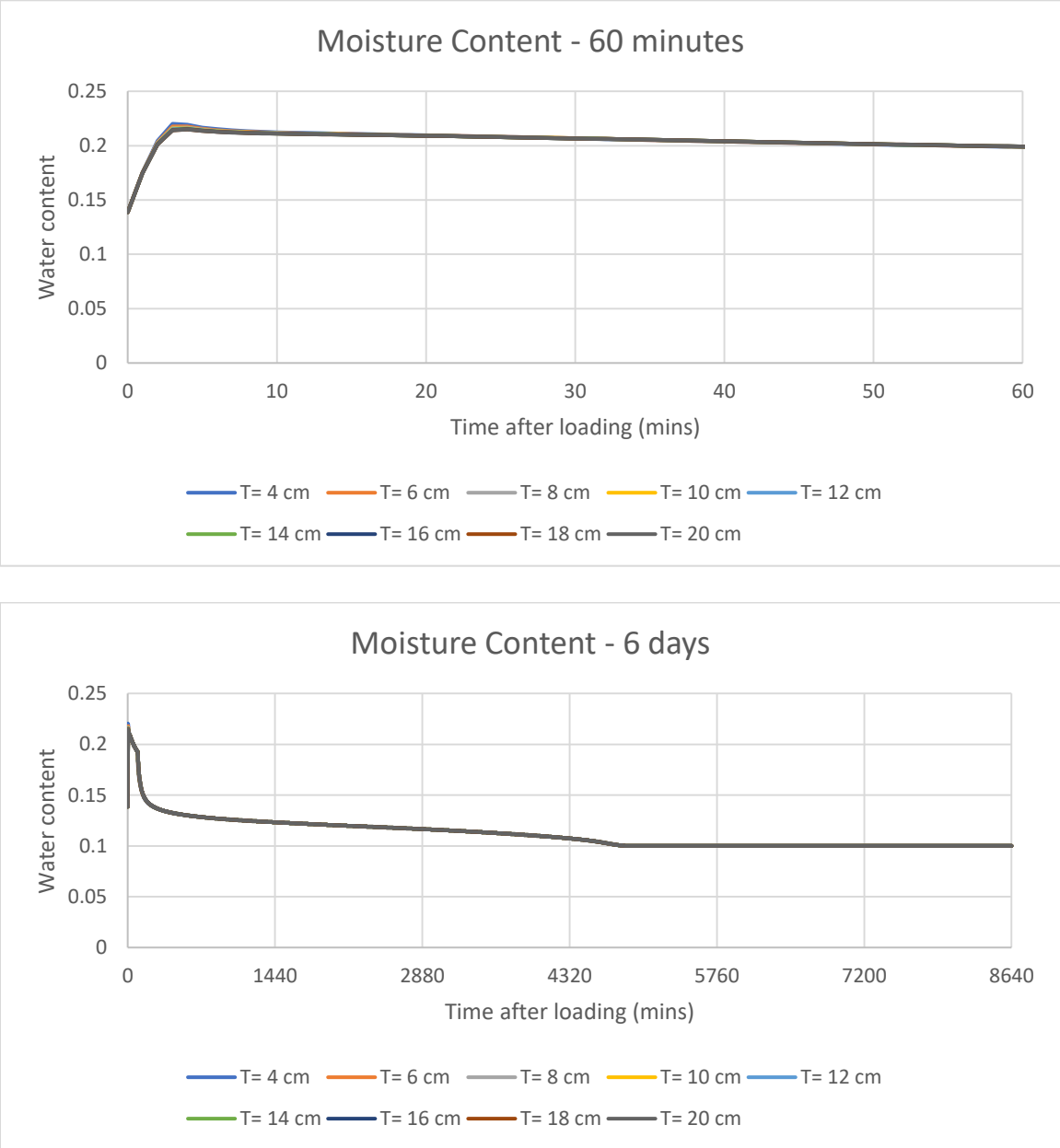

Figure 6.22: Sensitivity analysis of moisture content under varying sludge thickness for the first hour and 6 days.

Figure 6.23 shows the effect of sludge accumulation under varying sludge deposit layer thickness. Due to the same sludge accumulation rate, the incremental sludge deposit thickness consistently increased the sludge accumulation thickness by 2 cm. Hence, varying sludge deposit layer thickness does not affect the sludge accumulation rate.

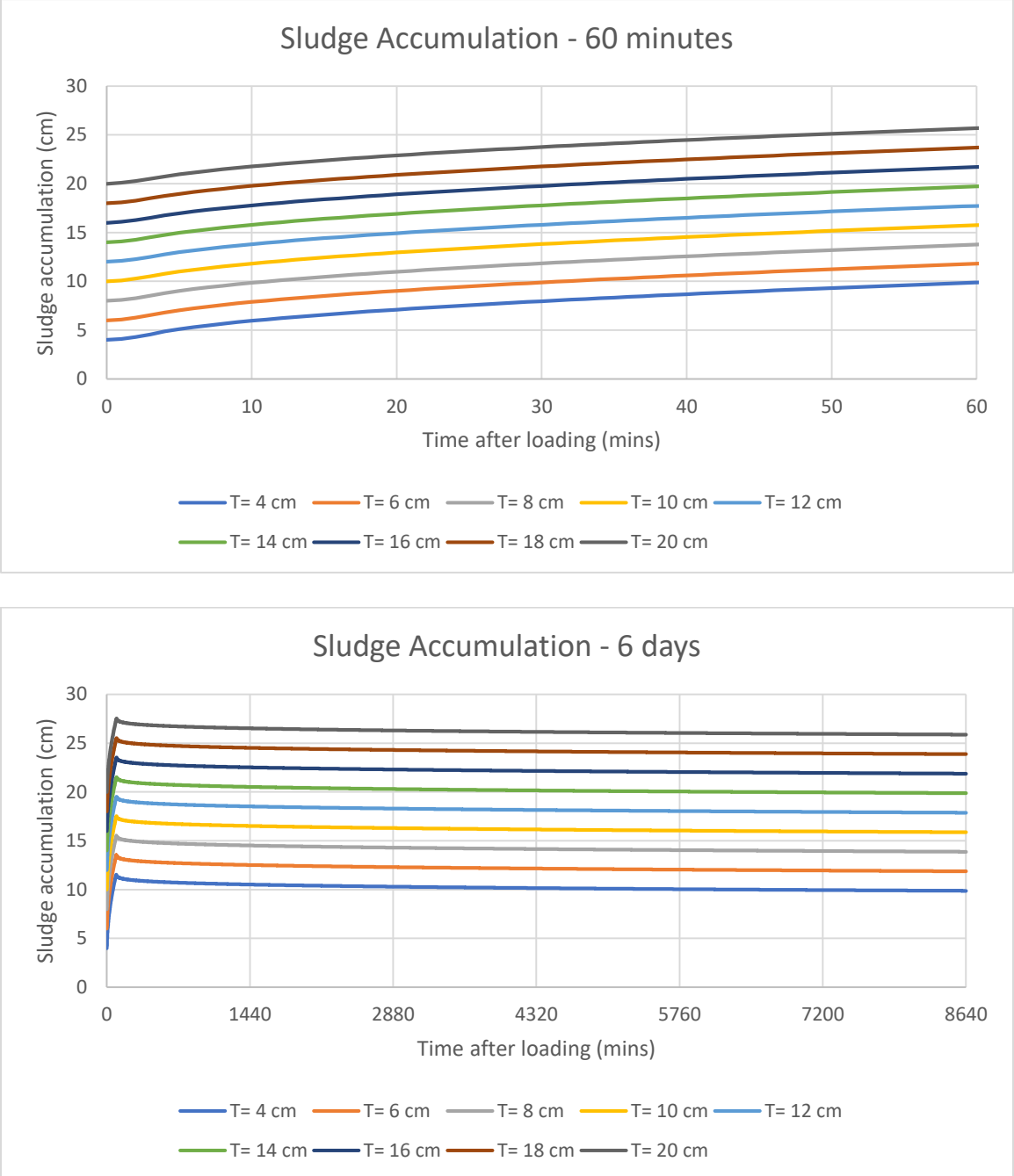

Figure 6.23: Sensitivity analysis of sludge accumulation under varying sludge thickness for the first hour and 6 days.

Figure 6.24 shows the effect of organic content under varying sludge deposit layer thickness. The organic contents increased with the sludge deposit layer thicknesses. The incremental sludge deposit thickness contains more nutrients for bacteria growth and development, directly increasing the organic content. However, the organic content in the sludge deposit layer slowly decreases upon sludge mineralization and stabilization.

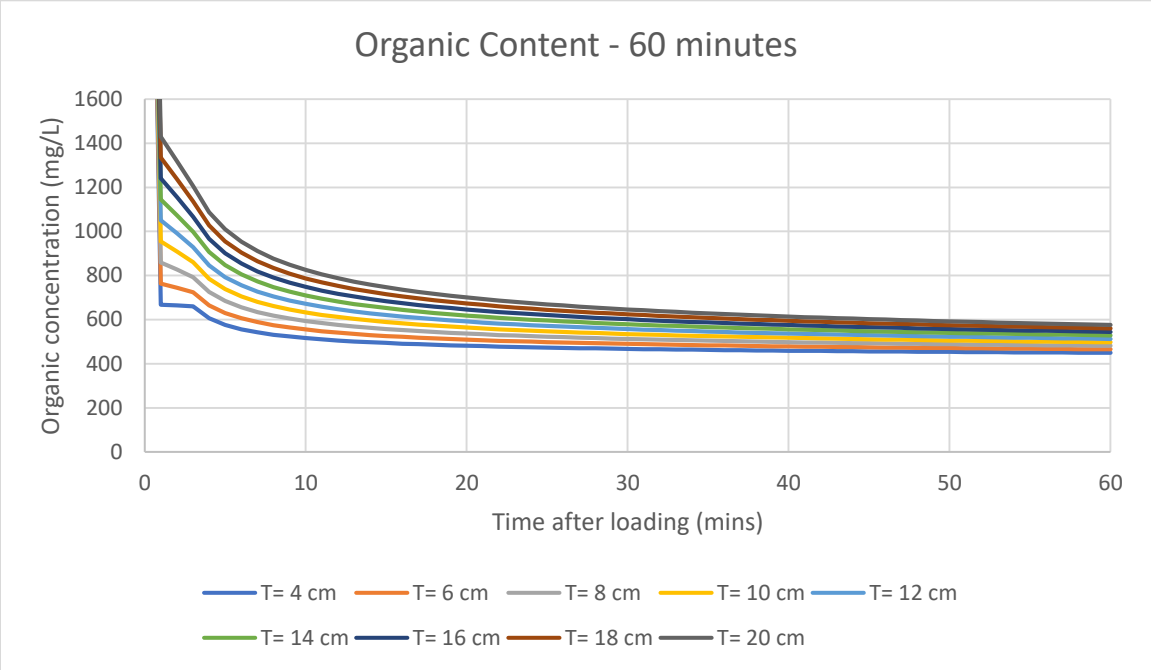

Figure 6.24: Sensitivity analysis of organic content under varying sludge thickness for the first hour.

Figure 6.25 shows the effect of evapotranspiration under varying sludge deposit layer thickness. The increase in the sludge deposit thickness decreased the evapotranspiration peak. A thicker sludge deposit would have a higher porosity, filling with moisture or solid particles. However, moisture filling in the void space would reduce the layer porosity and the contact opportunity with the atmosphere. As a result, the evapotranspiration rate was reduced, leading to drainage dewatering, which dominated the drying of sludge deposits via the evapotranspiration. Therefore, a thinner sludge deposit layer is determined to have a higher evapotranspiration rate.

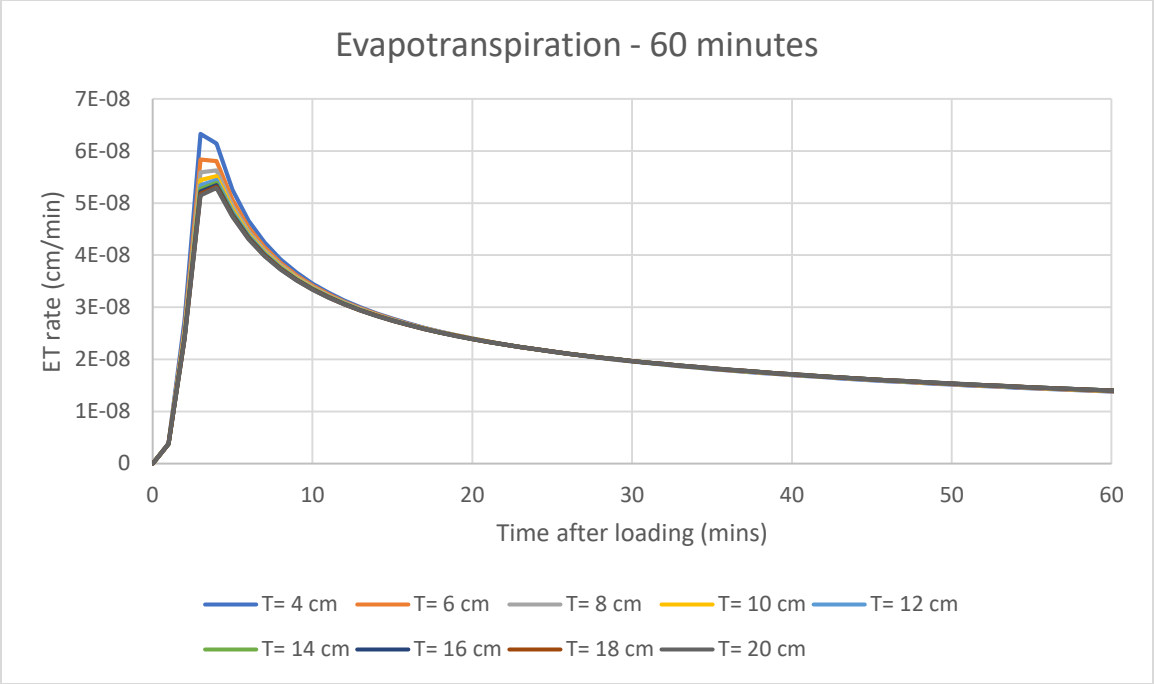

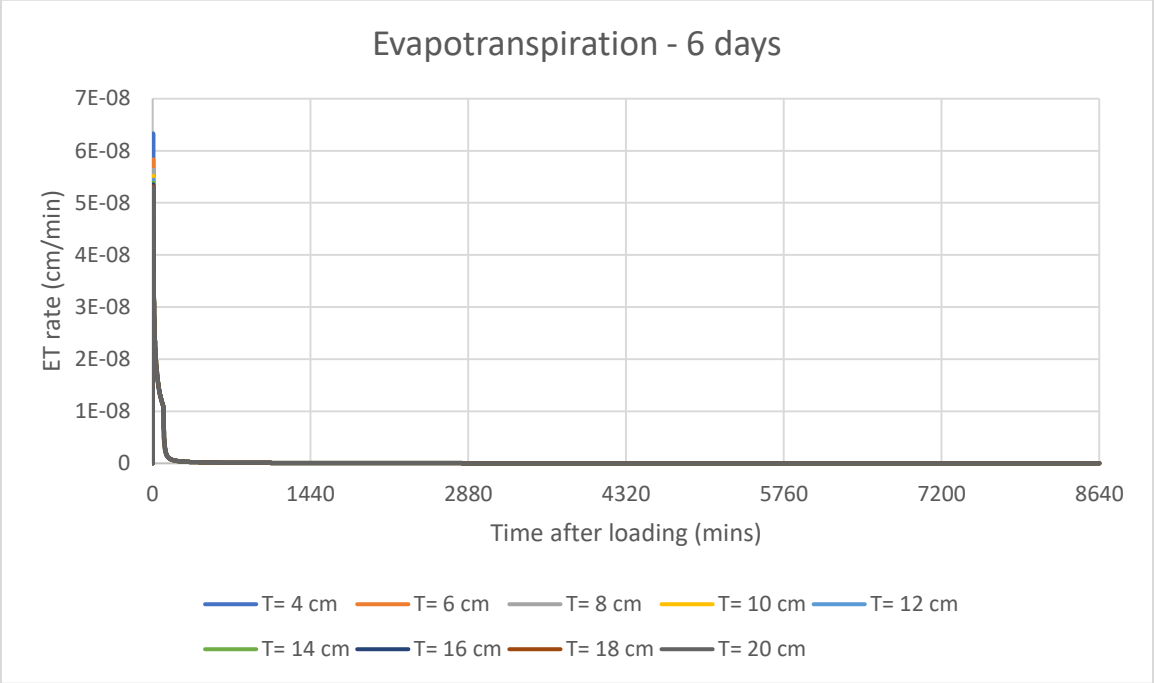

Figure 6.25: Sensitivity analysis of evapotranspiration under varying sludge thickness for the first hour and 6 days.

6.3 Summary of Parametric Studies

In the parametric study, the parameters of hydraulic loads, heads, saturated conductivities, and sludge deposit thickness were tested for sensitivity over the effluent discharge dynamics, MCs of the sludge deposit, and overall evapotranspiration rate. To determine the average hydraulic head and saturated conductivity, 78 experimental data sets were analyzed and interpreted. The average hydraulic head and saturated conductivity were determined to be -19.29 ± 8.39 cm and 0.0429 ± 0.1003 cm/min, respectively. Meanwhile, the hydraulic loads for different SLRs and resting periods were determined according to the respective TS loads. Hence, the parameters were analyzed for the sensitivities in the covered range over the first 60-minute and 6-day simulation periods.

Under varying SLRs and resting periods, the loading volumes were determined to be equivalent for SLRs and resting periods ranging from 50 to 450 kg/m^2/year and 3 to 30 days, respectively. The effluent flux peak and MC were simulated to increase with the hydraulic load. Further, the sludge deposit layer showed an incremental sludge accumulation upon larger hydraulic loads. In contrast, the organic content showed a trend opposite to the MC. In addition, the simulated ET rate was relatively low and increased with the hydraulic load. The hydraulic load should be kept in the range of 15 to 45 L, i.e. 100 to 300 kg/m^2/year SLR, to avoid an extensively prolonged waiting period, negatively impacting the STRB efficiency. The SLR below 50 kg/m^2/year and above 300 kg/m^2/year would lead to crack occurrence and MC overprediction, respectively.

On the other hand, the sensitivity test of the variation in hydraulic heads covered ideal, ponded, and bypassed flow cases. The tested hydraulic pressure ranged from -7 to -30 cm, where the average experimental hydraulic head was -19 cm. The results revealed that the effluent flux presents a bypassed flow case with a pressure larger than -10 cm and a ponding condition with a pressure smaller than -28 cm. In the bypassed flow case, the effluent flux presented a distinct outflow dynamic where the flux peak was significantly high. Moreover, the delay of flow occurrence increases with the hydraulic head due to possible clogging of void space in the sludge deposit. Hence, the MCs also increased with the hydraulic heads. However, the sludge accumulation and stabilization showed a similar trend under varying hydraulic loads, with the most apparent changes during the

loading period. Further, the ET rate for pressure above -10 cm was occasionally high upon crack occurrence on the sludge deposit layer, thus providing additional surface area for water loss via the ET. Conclusively, the sludge accumulation and organic content are less influenced by the hydraulic heads, and the hydraulic head should be kept below -10 cm to avoid inconsistent flow.

Furthermore, the variation in saturated hydraulic conductivities controlled the sludge deposit layer permeability. The tested conductivities ranged from 0.0009 to 0.1269 cm/min, showing an incremental flux peak and reduced flow-occurring delay. The higher the saturated conductivity, the higher the layer permeability, creating a higher flux peak and reducing the delay of flow occurrence. The changes in the MC were most visible with saturated conductivity less than 0.06 cm/min, where the MC peaks decreased with the conductivities. Similarly, the sludge accumulation reached a maximum thickness at around 17.8 cm with saturated conductivities above 0.06 cm/min, followed by gradual reduction due to evapotranspiration. At the same time, the organic content showed a trend opposite to that of the MC. In addition, the ET rate increased significantly with the saturated conductivity but dropped drastically with higher conductivities during the resting period. Therefore, higher saturated conductivity shortens the drainage process, prolonging the drying of the sludge deposit and resulting in a higher evapotranspiration rate.

Moreover, the variation in sludge deposit layer thicknesses has a smaller effect than the saturated conductivity. The flux peaks were reduced with the incremental sludge deposit thickness. The reduction in the flux peaks describes the sludge accumulation, where the thickness increases with its specific resistance, resulting in a lower flux peak. Hence, continuous sludge accumulation from 4 to 20 cm reduced the MC peaks slightly. However, the organic contents increased with the sludge deposit layer thicknesses. In addition, a thinner sludge deposit layer is determined to have a higher evapotranspiration rate.

CHAPTER 7: CONCLUSION

7.1 Conclusion

In conclusion, the formulated numerical model successfully simulated the hydraulic dynamics in the STRB under a moving-boundary condition due to sludge ponding and sludge accumulation. The combination of moving- and fixed-mesh discretization methods allowed the newly loaded septage to be treated as the moving-boundary condition while the substrate medium remained stationary. The moving-mesh discretization method efficiently describes the changes in the mesh size upon drainage dewatering and sludge deposit drying. Sludge feeding would increase the spatial distance between the meshes, reducing the infiltration and effluent flux. This is allied with the lower sludge deposit layer permeability reported in other research, where continuous sludge accumulation increases its specific resistance, leading to a lower discharge flux.

The laboratory-scale STRB has successfully operated and produced a desirable result. The optimal loading conditions of 100 kg/m^2/year SLR and 6-day resting period attributed the best results. The overall average effluent COD and TS removals were 96% and 82%, respectively, comparable to the other research findings. Further, the continuous sludge loading increased the sludge deposit layer thickness. A thicker sludge deposit layer retained more moisture, sustaining the entity of the sludge deposit and prolonging the hydraulic retention time. Hence, the resultant water recovery was lower in the thicker sludge deposit, with an average overall percentage of 70%. The remaining moisture was lost via evapotranspiration or retained in the bed. Further, the incremental sludge deposit thickness increases its specific cake resistance, leading to a lower permeability and, eventually, a longer flow delay and a lower flux peak. The final sludge deposit TS content ranged from 18 to 49%, which complies with the standard disposal requirement of 20%. The sludge deposit MC was within its average shrinkage limit of 75%, preventing the semi-permeable sludge deposit layer from deformation and cracks. Moreover, the sludge stabilization was favorable under an increasing TVS removal trend and the sludge deposit development. The average overall TVS content ranged from 30 to

41%, indicating the rich organic matter in the raw sludge. Indeed, a higher organic content would result in a higher shrinkage limit, directly increasing its elasticity and sustainability. In addition, the ANOVA revealed that the flow delays and flux peaks are highly affected by the SLRs and resting periods. A larger hydraulic load required by the higher SLR or longer resting period would result in a prolonged surface ponding condition. In contrast, an insufficient hydraulic load would directly lead to influent sludge bypassing the reed bed, influencing overall STRB performance efficiency. Therefore, an appropriate loading regime is required to control the moisture and organic contents of the sludge deposit layer, subsequently affecting the sludge mineralization and stabilization.

In the simulation study, the proposed model worked robustly in simulating the hydraulic dynamics of the laboratory-scale STRB under moving boundary conditions. The overall average MAE and RMSE of the flux data were 0.03902 and 0.05586, respectively, indicating a relatively low error distribution compared to the average flux. However, the standard deviations were always larger than the respective average errors. The result deviations were mainly attributed to the flux overprediction in the late phase of effluent discharge. Hence, the resultant average MAE% was 48%, with 32 out of 78 cases below 20% error. The low effluent flux below 1.0 cm/min deteriorates the overall error percentage, making the MAE% less appropriate for flux analysis. A relatively low overall average R^2 value of 0.5898 confirmed the situation. Nonetheless, the calibrated hydraulic head, h and saturated hydraulic conductivity, Ks matched the flow delay and flux peak, respectively, in most cases. Further, the average overall simulated evapotranspiration (ET) rate of 0.0051 cm/day revealed that the potential ET rate is insignificant in a short-term effect.

Moreover, the average overall simulated and measured sludge accumulation rates were 0.22 cm/day and 0.05 cm/day, respectively. The simulated sludge accumulation matched the measured results of rapid thickness increment at the early phase due to solids settling on the sludge deposit layer, followed by a gradual reduction upon draining and evapotranspiration processes. The proposed model considers the compressible cake filtration theory, where the sludge deposit layer changes its thickness upon feeding and resting. The increment in sludge deposit thickness increases the spatial length of the

simulation nodes, reducing the infiltration and effluent fluxes. Hence, the overall cumulative effluent was reduced by nearly 50% using the moving-mesh method (MMM) of discretization, confirming that a thicker sludge deposit layer would result in a lower infiltration rate and water recovery. Although applying the MMM improved the flux results upon incremental sludge deposit thickness, the simulated sludge accumulation rate was still higher due to occasional cracks on the sludge deposit layer, which provide "preferential flow pathways" for infiltration. Further, the measured sludge accumulation rate was underestimated due to the sludge mixture turbulence upon feeding, blurring the lines between the sludge and sludge deposit.

Meanwhile, the simulation of organic dynamics finely matched the decreasing trend of the measured sludge deposit TVS content over the resting period. The application of ASM3 describes the changes in the organic content due to bacteria growth and decay throughout the feeding-resting cycle. The bacteria growth and development consume nutrients, directly improving the effluent quality and reducing the organic content of the sludge deposit. However, the measured organic content fluctuated throughout the resting period. The organic content decreased extensively during the early phase of the treatment due to temporary surface ponding, hindering the oxygen from entering the sludge deposit layer. Meanwhile, the organic content increased towards the end of the treatment due to cracks on the sludge deposit layer, enhancing the oxygen exchange in the atmosphere and promoting bacterial regrowth. Hence, the sludge stabilization requires an appropriate loading regime, such as a 100 kg/m^2/year SLR with a 6-day resting period, where the temporary surface ponding ensures the sludge deposits moisture within its shrinkage limit for bacteria growth and avoids the occurrence of cracks.

The laboratory-scale STRB-treating septage performed best under a 100 kg/m^2/year SLR and a 6-day resting period under moving-boundary conditions. The final solids content of the sludge deposit could reach beyond 20% while complying with its shrinkage limit under such a loading condition. The resultant effluent flux and flow-occurring delay could sustain a complete drainage dewatering, ensuring low operational and maintenance costs. Applying the MMM simulated the effluent flux, ET, sludge

accumulation, and stabilization dynamics smoothly. The parametric study also showed the importance of the hydraulic load, head, saturated conductivity, and sludge deposit thickness to the overall STRB performance.

7.2 Recommendations and Future Works

The optimal loading condition is 100 kg/m^2/year with a 6-day resting period. The moving-mesh method efficiently described the moving boundary conditions of the sludge ponding and sludge deposit accumulation. Subsequently, the resultant infiltration and effluent flux determined the evapotranspiration, thickness, moisture, and organic contents of the sludge deposit layer.

However, the flux overprediction during the late phase of the treatment deteriorated the overall STRB simulation efficiency. The incomplete drainage dewatering is believed to cause the underestimation in overall effluent flux, retaining some of the moisture in the sludge deposit and bed substrate. In recommendation, an overall scaling/correction factor related to the water recovery can be introduced to reduce the error deviations between the measured and simulated flux results in the simulation.

Further, applying compressible cake filtration theory (CCF) overestimated the overall sludge accumulation due to the assumption of sludge loading volume as the dominating factor. The CCF model describes the sludge accumulation dependent mainly on the imposed flux, where a higher hydraulic load leads to a higher sludge accumulation. However, the sludge accumulation should be entirely based on the solid particle settling rate on the sludge deposit layer. Hence, the CCF model can be modified to accommodate the ideal sludge accumulation process.

Moreover, an excessive hydraulic load leads to a waterlogging condition, and an insufficient hydraulic load causes cracks in sludge deposits. In waterlogging conditions, the continuous sludge accumulation on the sludge deposit layer permanently clogs the bed, leading to prolonged surface ponding. Whereas the sludge deposit layer cracks during prolonged resting period. In such circumstances, an additional sub-model

regarding the clogging and crack occurrence, associated with sludge deposit shrinkage limit, can be included in the simulation to describe the clogged and cracked flow cases.

In addition, the organic content fluctuated during the resting period, especially the bacteria regrowth towards the end of the treatment, deteriorating the simulation result. The simulated trend of the organic content describes the overall sludge stabilization, where the organic matter reduces gradually throughout the resting period. However, the sludge ponding and crack in the sludge deposit caused the denitrification to dominate over nitrification and vice versa. The reduction in oxygen exchange rate decreases the amount of bacteria for nitrification during the ponding condition. Under waterlogging conditions, the prolonged surface ponding significantly hindered the sludge deposit layer from contacting with the atmosphere, leading to bacteria decay extensively in the end of the treatment. In contrast, the bacteria nitrifies the organic matter aerobically under excessive oxygen condition due to the cracks in the sludge deposit, leading to bacteria regrowth towards the end of the treatment. Therefore, the kinetic model can be improved by monitoring the microorganism growth and decay to accommodate the fluctuation and regrowth of the bacteria.

REFERENCES

Abeysiriwardana, H. D., Muttil, N., & Rathnayake, U. (2022). A Comparative Study of Potential Evapotranspiration Estimation by Three Methods with FAO Penman–Monteith Method across Sri Lanka. *Hydrology*, *9*(11), 206. https://doi.org/10.3390/hydrology9110206

Abideen, Z., Koyro, H.-W., Huchzermeyer, B., Ansari, R., Zulfiqar, F., & Gul, B. (2020). Ameliorating effects of biochar on photosynthetic efficiency and antioxidant defence of Phragmites karka under drought stress. *Plant Biology*, *22*(2), 259-266. https://doi.org/10.1111/plb.13054

Abideen, Z., Koyro, H. W., Hussain, T., Rasheed, A., Alwahibi, M. S., Elshikh, M. S., Hussain, M. I., Zulfiqar, F., Mansoor, S., & Abbas, Z. (2022). Biomass Production and Predicted Ethanol Yield Are Linked with Optimum Photosynthesis in Phragmites karka under Salinity and Drought Conditions. *Plants*, *11*(13), 1657. https://doi.org/10.3390/plants11131657

Adwet, W. M., Pant, H. J., Mangala, M. J., & Masinza, S. A. (2019). Evaluation of hydraulic performance of an anaerobic pond using radiotracer technique. *Applied Radiation and Isotopes*, *145*, 101-105. https://doi.org/10.1016/j.apradiso.2018.12.017

Afifi, S., Alnahhal, S., & Abdelall, S. (2015, 2015/01/01/). Developing an Integrated Sustainable Sanitation System for Urban Areas: Gaza Strip Case study. *Procedia CIRP*, *26*, 767-774. https://doi.org/https://doi.org/10.1016/j.procir.2014.07.158

Al-Ajalin, F., Abdullah, S., Idris, M., Kurniawan, S., Ramli, N., & Imron, M. (2022). Removal of ammonium, phosphate, and COD by bacteria isolated from Lepironia articulata and Scirpus grossus root system. *International Journal of Environmental Science and Technology*, *19*(12), 11893-11904.

Al-Ajalin, F. A. H., Idris, M., Abdullah, S., Kurniawan, S. B., & Imron, M. (2020a). Effect of wastewater depth to the performance of short-term batching-experiments horizontal flow constructed wetland system in treating domestic wastewater. *Environmental Technology & Innovation*, *20*, 101106. https://doi.org/10.1016/j.eti.2020.101106

Al-Ajalin, F. A. H., Idris, M., Abdullah, S. R. S., Kurniawan, S. B., & Imron, M. F. (2020b). Evaluation of short-term pilot reed bed performance for real domestic wastewater treatment. *Environmental Technology & Innovation, 20*, 101110. https://doi.org/10.1016/j.eti.2020.101110

Al-Niami, A. N. S., & Rushton, K. R. (1978). Finite-difference solutions for one-dimensional dispersion using an improved mesh design. *Journal of Hydrology, 39*(3), 301-310. https://doi.org/10.1016/0022-1694(78)90007-0

Al-Rashdi, T. T., Ahmed, M., Stefanakis, A., Al-Wardy, M., & Al-Haddabi, M. (2024). A study of pilot sludge treatment reed beds for sludge dewatering and treatment under a hot and arid climate. *Environmental Science and Pollution Research, 31*(8), 12467-12482. https://doi.org/10.1007/s11356-023-31804-x

Al Falahi, O. A., Abdullah, S. R. S., Hasan, H. A., Othman, A. R., Ewadh, H. M., Al-Baldawi, I. A., Kurniawan, S. B., Imron, M. F., & Ismail, N. I. (2021). Simultaneous removal of ibuprofen, organic material, and nutrients from domestic wastewater through a pilot-scale vertical sub-surface flow constructed wetland with aeration system. *Journal of Water Process Engineering, 43*, 102214. https://doi.org/10.1016/j.jwpe.2021.102214

Allen, R. G., Pereira, L. S., Raes, D., & Smith, M. (1998). *Crop evapotranspiration - Guidelines for computing crop water requirements - FAO Irrigation and drainage paper 56*.

Amatya, D. M., Muwamba, A., Panda, S., Callahan, T., Harder, S., & Pellett, C. (2018). Assessment of Spatial and Temporal Variation of Potential Evapotranspiration Estimated by Four Methods for South Carolina. Journal of South Carolina Water Resources 5(1): 3-24. *5*, 3-24. https://doi.org/10.34068/JSCWR.05.01

Arbogast, T. (1992). The existence of weak solutions to single porosity and simple dual-porosity models of two-phase incompressible flow. *Nonlinear Analysis: Theory, Methods & Applications, 19*(11), 1009-1031. https://doi.org/10.1016/0362-546X(92)90121-T

Armstrong, J. S., & Collopy, F. (1992, 1992/06/01/). Error measures for generalizing about forecasting methods: Empirical comparisons. *International Journal of Forecasting, 8*(1), 69-80. https://doi.org/https://doi.org/10.1016/0169-2070(92)90008-W

Ashkanani, A., Almomani, F., Khraisheh, M., Bhosale, R., Tawalbeh, M., & AlJaml, K. (2019). Bio-carrier and operating temperature effect on ammonia removal from secondary wastewater effluents using moving bed biofilm reactor (MBBR). *Science of The Total Environment, 693*, 133425.

Bandelt Riess, P. M., Kuhn, M., Först, P., & Briesen, H. (2021). Investigating the Effect of Packed Structures on Filter Cake Compressibility. *Chemical Engineering & Technology*, *44*(4), 661-669. https://doi.org/10.1002/CEAT.202000451

Bashir, A., Malik, L. A., Ahad, S., Manzoor, T., Bhat, M. A., Dar, G. N., & Pandith, A. H. (2019). Removal of heavy metal ions from aqueous system by ion-exchange and biosorption methods. *Environmental Chemistry Letters*, *17*(2), 729-754. https://doi.org/10.1007/s10311-018-00828-y

Bassetto, S., Cancès, C., Enchéry, G., & Tran, Q.-H. (2022). On several numerical strategies to solve Richards' equation in heterogeneous media with finite volumes. *Computational Geosciences*, *26*(5), 1297-1322. https://doi.org/10.1007/s10596-022-10150-w

Bazilevs, Y., Takizawa, K., Tezduyar, T. E., Korobenko, A., Kuraishi, T., & Otoguro, Y. (2023). Computational aerodynamics with isogeometric analysis. *Journal of Mechanics*, *39*, 24-39. https://doi.org/10.1093/jom/ufad002

Beulke, S., Renaud, F., & Brown, C. (2002). Development of guidance on parameter estimation for the preferential flow model MACRO 4.2.

Bhaga, D., & Weber, M. E. (1981). Bubbles in viscous liquids: shapes, wakes and velocities. *Journal of Fluid Mechanics*, *105*, 61-85. https://doi.org/10.1017/S002211208100311X

Bhattacharya, R., & Mazumder, D. (2021). Simultaneous nitrification and denitrification in moving bed bioreactor and other biological systems. *Bioprocess and Biosystems Engineering*, *44*(4), 635-652. https://doi.org/10.1007/s00449-020-02475-6

Bień, B., & Bień, J. D. (2022). Analysis of Reject Water Formed in the Mechanical Dewatering Process of Digested Sludge Conditioned by Physical and Chemical Methods. *Energies, 15*(5). https://doi.org/10.3390/en15051678

Bisheh-Niasar, M., & Ameri, M. A. (2018). Moving Mesh Non-standard Finite Difference Method for Non-linear Heat Transfer in a Thin Finite Rod. *Applied and Computational Mechanics, 4*, 161-166.

Blaney, H. F., & Criddle, W. D. (1962). *Determining consumptive use and irrigation water requirements*. Technical Bulletins No.1275.

Blomberg, K., Kosse, P., Mikola, A., Kuokkanen, A., Fred, T., Heinonen, M., Mulas, M., Lübken, M., Wichern, M., & Vahala, R. (2018). Development of an extended ASM3 model for predicting the nitrous oxide emissions in a full-scale wastewater treatment plant. *Environmental science & technology, 52*(10), 5803-5811.

Brar, S. K., Verma, M., Tyagi, R. D., Valéro, J. R., & Surampalli, R. Y. (2005). Sludge based Bacillus thuringiensis biopesticides: Viscosity impacts. *Water research, 39*(13), 3001-3011. https://doi.org/10.1016/j.watres.2005.04.072

Bresler, E. (1973). Simultaneous transport of solutes and water under transient unsaturated flow conditions. *Water Resources Research, 9*(4), 975-986. https://doi.org/10.1029/WR009i004p00975

Brindt, N., & Wallach, R. (2020). The moving‐boundary approach for modeling 2‐D gravity‐driven stable and unstable flow in partially wettable soils. *Water Resources Research, 56*(5), e2019WR025772.

Brix, H. (2017). Sludge Dewatering and Mineralization in Sludge Treatment Reed Beds. *Water, 9*(3). https://doi.org/10.3390/w9030160

Bruce, M. (2011). *Solving Richards' equation using fixed and moving mesh schemes* The University of Reading].

Brunone, B., Ferrante, M., Romano, N., & Santini, A. (2003). Numerical Simulations of One-Dimensional Infiltration into Layered Soils with the Richards Equation

Using Different Estimates of the Interlayer Conductivity. *Vadoese Zone, 2*, 193-200.

Bui, J. J. X., Tan, Y. Y., Tang, F. E., & Ho, C. (2018). A tracer study in a vertical flow constructed wetland treating septage. *World Journal of Engineering, 15*(3), 345-353. https://doi.org/10.1108/wje-09-2017-0306

Bui, J. J. X., Tang, F. E., Tan, Y. Y., Wong, K. S., & Saptoro, A. (2019). Dewatering and Mineralization of Sludge in Vertical Flow Constructed Wetlands: A Review. *IOP Conference Series: Materials Science and Engineering, 495*. https://doi.org/10.1088/1757-899x/495/1/012069

Burger, T. (2023). Controlling for false discoveries subsequently to large scale one‐way ANOVA testing in proteomics: Practical considerations. *Proteomics*, 2200406.

Çakir, R., Gidirislioglu, A., & Çebi, U. (2015, 2015/12/01/). A study on the effects of different hydraulic loading rates (HLR) on pollutant removal efficiency of subsurface horizontal-flow constructed wetlands used for treatment of domestic wastewaters. *Journal of Environmental Management, 164*, 121-128. https://doi.org/https://doi.org/10.1016/j.jenvman.2015.08.037

Capodaglio, A. G., Callegari, A., Cecconet, D., & Molognoni, D. (2017). Sustainability of decentralized wastewater treatment technologies. *Water Practice and Technology, 12*(2), 463-477. https://doi.org/10.2166/wpt.2017.055

Cardiff, P., & Demirdžić, I. (2021). Thirty Years of the Finite Volume Method for Solid Mechanics. *Archives of Computational Methods in Engineering, 28*(5), 3721-3780. https://doi.org/10.1007/s11831-020-09523-0

Carneiro, M. A., Athayde Junior, G. B., Sena, R. F., Porto, C. A., & Kohlgrüber, V. (2022). Raw sewage treatment by a single-stage vertical flow constructed wetland: a case study in Brazil. *Journal of Water, Sanitation and Hygiene for Development, 12*(5), 443-453. https://doi.org/10.2166/washdev.2022.038

Carsel, R. F., & Parrish, R. S. (1988). Developing joint probability distributions of soil water retention characteristics. *Water Resources Research, 24*(5), 755-769.

Carvalho, P. N., Arias, C. A., & Brix, H. (2017). Constructed Wetlands for Water Treatment: New Developments. *Water*, *9*(6). https://doi.org/10.3390/w9060397

Cascone, S., Coma, J., Gagliano, A., & Pérez, G. (2019). The evapotranspiration process in green roofs: A review. *Building and Environment*, *147*, 337-355. https://doi.org/10.1016/j.buildenv.2018.10.024

Casulli, V., & Zanolli, P. (2010). A Nested Newton-Type Algorithm for Finite Volume Methods Solving Richards' Equation in Mixed Form. *SIAM Journal on Scientific Computing*, *32*(4), 2255-2273. https://doi.org/10.1137/100786320

Celia, M. A., Ahuja, L. R., & Pinder, G. F. (1987). Orthogonal collocation and alternating-direction procedures for unsaturated flow problems. *Advances in Water Resources*, *10*(4), 178-187. https://doi.org/10.1016/0309-1708(87)90027-3

Celia, M. A., & Bouloutas, E. T. (1990). General Mass-Conservative Numerical Solution for the Unsaturated Flow Equation. *Water Resources Research*, *26*, 483-496.

Chai, W. S., Cheun, J. Y., Kumar, P. S., Mubashir, M., Majeed, Z., Banat, F., Ho, S.-H., & Show, P. L. (2021). A review on conventional and novel materials towards heavy metal adsorption in wastewater treatment application. *Journal of Cleaner Production*, *296*, 126589. https://doi.org/10.1016/j.jclepro.2021.126589

Chandana, N., & Rao, B. (2022, 2022/01/01/). A critical review on sludge management from onsite sanitation systems: A knowledge to be revised in the current situation. *Environmental Research*, *203*, 111812. https://doi.org/https://doi.org/10.1016/j.envres.2021.111812

Chen, J., Bu, J., Su, Y., Yuan, M., Cao, K., & Gao, Y. (2022). Urban evapotranspiration estimation based on anthropogenic activities and modified Penman-Monteith model. *Journal of Hydrology*, *610*, 127879.

Christiansen Jerald, E. (1968). Pan Evaporation and Evapotranspiration from Climatic Data. *Journal of the Irrigation and Drainage Division*, *94*(2), 243-266. https://doi.org/10.1061/JRCEA4.0000568

Conaway, K., Lebu, S., Heilferty, K., Salzberg, A., & Manga, M. (2023, 2023/06/01/). On-site sanitation system emptying practices and influential factors in Asian low- and middle-income countries: A systematic review. *Hygiene and Environmental Health Advances, 6*, 100050. https://doi.org/10.1016/j.heha.2023.100050

Cramer, M., & Tränckner, J. (2020). Development of Decay in Biofilms under Starvation Conditions—Rethinking of the Biomass Model. *Water, 12*(5), 1249. https://doi.org/10.3390/w12051249

Cui, Y., Zhang, W., Sun, H., Wu, W., & Zou, X. (2015, 10/01). Polycyclic Aromatic Hydrocarbon Accumulation in Phragmites australis Grown on Constructed Wetland for Sludge Stabilization. *Journal of Residuals Science and Technology, 12*, 215-220. https://doi.org/10.12783/issn.1544-8053/12/4/4

Das, T., Usher, S. P., Batstone, D. J., Othman, M., Rees, C. A., Stickland, A. D., & Eshtiaghi, N. (2023). Impact of volatile solids destruction on the shear and solid-liquid separation behaviour of anaerobic digested sludge. *Science of The Total Environment, 894*, 164546.

de Rozari, P., Greenway, M., & El Hanandeh, A. (2018). Nitrogen removal from sewage and septage in constructed wetland mesocosms using sand media amended with biochar. *Ecological Engineering, 111*, 1-10. https://doi.org/10.1016/j.ecoleng.2017.11.002

Dehghan, M., & Shirilord, A. (2020). Matrix multisplitting Picard-iterative method for solving generalized absolute value matrix equation. *Applied Numerical Mathematics, 158*, 425-438. https://doi.org/10.1016/j.apnum.2020.08.001

Dittmer, U., Meyer, D., & Langergraber, G. (2005). Simulation of a subsurface vertical flow constructed wetland for CSO treatment. *Water Science and Technology, 51*(9), 225-232.

Dlouhá, D., Dubovský, V., & Pospíšil, L. (2021). Optimal Calibration of Evaporation Models against Penman–Monteith Equation. *Water, 13*(11), 1484. https://doi.org/10.3390/w13111484

Dorfi, E., & Drury, L. (1987). Simple Adaptive Grids for 1D Initial Value Problems. *Journal of Computational Physics - J COMPUT PHYS, 69*, 175-195. https://doi.org/10.1016/0021-9991(87)90161-6

Duan, X., Qin, L., & Lu, J. (2020). A novel moving mesh method for solving fluid dynamic equations. *AIP Advances, 10*(8), 085120. https://doi.org/10.1063/5.0014413

Dubash, N., & Frigaard, I. A. (2007). Propagation and stopping of air bubbles in Carbopol solutions. *Journal of Non-Newtonian Fluid Mechanics, 142*(1), 123-134. https://doi.org/10.1016/j.jnnfm.2006.06.006

Eden, G. E. (1983). Modern Trends in Sludge Management: Sludge Conditioning. *Water Science and Technology, 15*(1), 37-48. https://doi.org/10.2166/wst.1983.0005

Efome, J. E., Rana, D., Matsuura, T., & Lan, C. Q. (2019). Effects of operating parameters and coexisting ions on the efficiency of heavy metal ions removal by nano-fibrous metal-organic framework membrane filtration process. *Science of The Total Environment, 674*, 355-362. https://doi.org/10.1016/j.scitotenv.2019.04.187

El-Kadi, A. I., & Ling, G. (1993). The Courant and Peclet Number criteria for the numerical solution of the Richards Equation. *Water Resources Research, 29*(10), 3485-3494. https://doi.org/10.1029/93WR00929

Elbaza, A., Aboulfotoha, A., ElGoharya, E., & Rehamb, M. (2021). Evaluation of the use of modified paved drying beds compared to the conventional sand drying beds. *Desalination and Water Treatment, 213*, 148-158.

Eshtiaghi, N., Yap, S. D., Markis, F., Baudez, J. C., & Slatter, P. (2012). Clear model fluids to emulate the rheological properties of thickened digested sludge. *Water Res, 46*(9), 3014-3022. https://doi.org/10.1016/j.watres.2012.03.003

Farthing, M. W., & Ogden, F. L. (2017). Numerical Solution of Richards' Equation: A Review of Advances and Challenges. *Soil Science Society of America Journal, 81*(6), 1257-1269. https://doi.org/10.2136/sssaj2017.02.0058

Fawell, P. D., Nguyen, T. V., Solnordal, C. B., & Stephens, D. W. (2021). Enhancing Gravity Thickener Feedwell Design and Operation for Optimal Flocculation through the Application of Computational Fluid Dynamics. *Mineral Processing and Extractive Metallurgy Review*, *42*(7), 496-510. https://doi.org/10.1080/08827508.2019.1678156

Feng, L., Liu, Y., Zhang, J., Li, C., & Wu, H. (2020). Dynamic variation in nitrogen removal of constructed wetlands modified by biochar for treating secondary livestock effluent under varying oxygen supplying conditions. *Journal of Environmental Management*, *260*, 110152. https://doi.org/10.1016/j.jenvman.2020.110152

Fetter Jr, C. (2000). *Applied Hydrogeology* (Fourth ed.). Pearson New International Edition.

Fournel, J., Forquet, N., Molle, P., & Grasmick, A. (2013). Modeling constructed wetlands with variably saturated vertical subsurface-flow for urban stormwater treatment. *Ecological Engineering*, *55*, 1-8.

Friedrich, T., Kuhn, M., Nasato, D. S., & Briesen, H. (2022). Material Properties in Cake Filtration – Discrete Element Simulation of Compression - Permeability Cells. *Chemical Engineering & Technology*, *45*(5), 898-906.

Fu, G., Wu, J., Han, J., Zhao, L., Chan, G., & Leong, K. (2020). Effects of substrate type on denitrification efficiency and microbial community structure in constructed wetlands. *Bioresource technology*, *307*, 123222. https://doi.org/10.1016/j.biortech.2020.123222

Gabr, M. E. (2022). Design methodology for sewage water treatment system comprised of Imhoff ‘s tank and a subsurface horizontal flow constructed wetland: a case study Dakhla Oasis, Egypt. *Journal of Environmental Science and Health, Part A*, *57*(1), 52-64. https://doi.org/10.1080/10934529.2022.2026735

Garg, A., Mishra, I., & Chand, S. (2005). Thermochemical precipitation as a pretreatment step for the chemical oxygen demand and color removal from pulp and paper mill effluent. *Industrial & Engineering Chemistry Research*, *44*(7), 2016-2026.

Gentilucci, M., Bufalini, M., Materazzi, M., Barbieri, M., Aringoli, D., Farabollini, P., & Pambianchi, G. (2021). Calculation of Potential Evapotranspiration and Calibration of the Hargreaves Equation Using Geostatistical Methods over the Last 10 Years in Central Italy. *Geosciences, 11*(8), 348. https://doi.org/10.3390/geosciences11080348

Gerke, H. H., & van Genuchten, M. T. (1993a). A dual-porosity model for simulating the preferential movement of water and solutes in structured porous media. *Water Resources Research, 29*(2), 305-319. https://doi.org/10.1029/92wr02339

Gerke, H. H., & van Genuchten, M. T. (1993b). Evaluation of a first-order water transfer term for variably saturated dual-porosity flow models. *Water Resources Research, 29*(4), 1225-1238. https://doi.org/10.1029/92wr02467

Ghanbarian, B. (2021). Unsaturated hydraulic conductivity in dual-porosity soils: Percolation theory. *Soil and Tillage Research, 212*, 105061. https://doi.org/10.1016/j.still.2021.105061

Ghanbarian, B., Hunt, A. G., & Daigle, H. (2016). Fluid flow in porous media with rough pore-solid interface. *Water Resources Research, 52*(3), 2045-2058. https://doi.org/10.1002/2015WR017857

Ghasemi, M., Hasani Zonoozi, M., & Hoseini Shamsabadi, M. J. (2024). Simultaneous nitrification and denitrification pattern in aerated moving-bed sequencing batch reactor: Choosing appropriate SRT for different COD/N ratios. *Water Practice and Technology*, wpt2024124. https://doi.org/10.2166/wpt.2024.124

Gholipour, A., Fragoso, R., Duarte, E., & Galvão, A. (2022). Sludge Treatment Reed Bed under different climates: A review using meta-analysis. *Science of The Total Environment, 843*, 156953. https://doi.org/10.1016/j.scitotenv.2022.156953

Gholipour, A., Fragoso, R., Galvão, A., & Duarte, E. (2024). Evaluating drained water quality in a pilot worm-sludge treatment reed bed planted with Arundo donnas in the Mediterranean climate. *Science of The Total Environment, 928*, 172587. https://doi.org/10.1016/j.scitotenv.2024.172587

Gill, L. W., Mac Mahon, J., Knappe, J., & Morrissey, P. (2023, 2023/06/01/). Hydraulic conductivity assessment of falling head percolation tests used for the design of

on-site wastewater treatment systems. *Water research, 236*, 119968. https://doi.org/https://doi.org/10.1016/j.watres.2023.119968

Giraldi, D., de Michieli Vitturi, M., & Iannelli, R. (2010). FITOVERT: A dynamic numerical model of subsurface vertical flow constructed wetlands. *Environmental Modelling & Software, 25*(5), 633-640. https://doi.org/10.1016/j.envsoft.2009.05.007

Giraldi, D., & Iannelli, R. (2009). Short-term water content analysis for the optimization of sludge dewatering in dedicated constructed wetlands (reed bed systems). *Desalination, 246*(1), 92-99. https://doi.org/10.1016/j.desal.2008.02.038

Goel, R., Komatsu, K., Yasui, H., & Harada, H. (2004). Process performance and change in sludge characteristics during anaerobic digestion of sewage sludge with ozonation. *Water Science and Technology, 49*(10), 105-113. https://doi.org/10.2166/wst.2004.0620

Gottardi, G., & Venutelli, M. (1993). Richards: Computer program for the numerical simulation of one-dimensional infiltration into unsaturated soil. *Computers & Geosciences, 19*(9), 1239-1266. https://doi.org/10.1016/0098-3004(93)90028-4

Grecco, K. L., de Miranda, J. H., Silveira, L. K., & van Genuchten, M. T. (2019). HYDRUS-2D simulations of water and potassium movement in drip irrigated tropical soil container cultivated with sugarcane. *Agricultural Water Management, 221*, 334-347.

Greenway, M., de Rozari, P., & El Hanandeh, A. (2022, 2022/07/01/). Plant growth and nutrient accumulation in Melaleuca quinquenervia and Cymbopogon citratus treating high strength sewage effluent in constructed wetland systems with biochar media. *Ecological Engineering, 180*, 106667. https://doi.org/https://doi.org/10.1016/j.ecoleng.2022.106667

Gujer, W., Henze, M., Mino, T., & Loosdrecht, M. v. (1999). Activated sludge model No. 3. *Water Science and Technology, 39*(1), 183-193. https://doi.org/10.1016/S0273-1223(98)00785-9

Gujer, W., Henze, M., Mino, T., Matsuo, T., Wentzel, M. C., & Marais, G. v. R. (1995). The Activated Sludge Model No. 2: Biological phosphorus removal. *Water*

Science and Technology, 31(2), 1-11. https://doi.org/10.1016/0273-1223(95)00175-M

Guo, J., Cheng, J., Li, B., Wang, J., & Chu, P. (2019). Performance and microbial community in the biocathode of microbial fuel cells under different dissolved oxygen concentrations. *Journal of Electroanalytical Chemistry*, *833*, 433-440. https://doi.org/10.1016/j.jelechem.2018.12.015

Gupta, S., Kushwaha, P., Chauhan, A. S., & Badhotiya, G. K. (2023). Desludging and sanitation service models in sanitation value chain: Emerging opportunities and challenges. *AIP Conference Proceedings, 2521*(1). https://doi.org/10.1063/5.0113975

Haddis, A., Van der Bruggen, B., & Smets, I. (2020). Constructed wetlands as nature based solutions in removing organic pollutants from wastewater under irregular flow conditions in a tropical climate. *Ecohydrology & Hydrobiology*, *20*(1), 38-47. https://doi.org/10.1016/j.ecohyd.2019.03.001

Han, S., Tian, F., Wang, W., & Wang, L. (2021). Sigmoid Generalized Complementary Equation for Evaporation Over Wet Surfaces: A Nonlinear Modification of the Priestley-Taylor Equation. *Water Resources Research, 57*(9), e2020WR028737. https://doi.org/10.1029/2020WR028737

Haydar, S., Anis, M., & Afaq, M. (2020). Performance evaluation of hybrid constructed wetlands for the treatment of municipal wastewater in developing countries. *Chinese Journal of Chemical Engineering*, *28*(6), 1717-1724.

Healy, R. W. (1990). *Simulation of Solute Transport Invariably Saturated Porous Media with Supplemental Information on Modifications to the U.S. Geological Survey's Computer Program VS2D* (Vol. 90). Diffusion in hydrology.

Henze, M., Grady Jr, L., Gujer, W., Marais, G., & Matsuo, T. (1987). Activated Sludge Model No 1. *Wat Sci Technol, 29*.

Henze, M., Gujer, W., Mino, T., Matsuo, T., Wentzel, M. C., Marais, G. v. R., & Van Loosdrecht, M. C. M. (1999). Activated sludge model No.2D, ASM2D. *Water Science and Technology, 39*(1), 165-182. https://doi.org/10.1016/S0273-1223(98)00829-4

Ho, L. T., Alvarado, A., Larriva, J., Pompeu, C., & Goethals, P. (2019). An integrated mechanistic modeling of a facultative pond: Parameter estimation and uncertainty analysis. *Water research, 151*, 170-182.

Höfgen, E., Kühne, S., Peuker, U. A., & Stickland, A. D. (2019). A comparison of filtration characterisation devices for compressible suspensions using conventional filtration theory and compressional rheology. *Powder Technology, 346*, 49-56. https://doi.org/10.1016/j.powtec.2019.01.056

Hu, J., Yan, J., Wu, L., Bao, Y., Yu, D., & Li, J. (2021). Simultaneous nitrification and denitrification of hypersaline wastewater by a robust bacterium Halomonas salifodinae from a repeated-batch acclimation. *Bioresource technology, 341*, 125818. https://doi.org/10.1016/j.biortech.2021.125818

Hu, S., Chen, H., & Chen, Z. (2021). Performance of sludge drying reed beds for the leachate purification: Effects of sludge loading frequencies and plant species. *Environ Res, 194*, 110452. https://doi.org/10.1016/j.envres.2020.110452

Hu, S., Zuo, X., Lv, Z., He, J., Wu, Y., Liu, H., & Chen, Z. (2020). Drained water quality in sludge treatment wetlands: Effects of earthworm densities and plant species. *Journal of Cleaner Production, 247*, 119128. https://doi.org/10.1016/j.jclepro.2019.119128

Hua, G., Kong, J., Ji, Y., & Li, M. (2018). Influence of clogging and resting processes on flow patterns in vertical flow constructed wetlands. *Science of The Total Environment, 621*, 1142-1150. https://doi.org/10.1016/j.scitotenv.2017.10.113

Huang, C., Liu, Q., Li, Z.-L., Ma, X.-d., Hou, Y.-N., Ren, N.-Q., & Wang, A.-J. (2021). Relationship between functional bacteria in a denitrification desulfurization system under autotrophic, heterotrophic, and mixotrophic conditions. *Water research, 188*, 116526.

Huang, K., Mohanty, B., & Van Genuchten, M. T. (1996). A new convergence criterion for the modified Picard iteration method to solve the variably saturated flow equation. *Journal of Hydrology, 178*(1-4), 69-91.

Hube, S., & Wu, B. (2021). Mitigation of emerging pollutants and pathogens in decentralized wastewater treatment processes: A review. *Science of The Total Environment*, *779*, 146545.

Huong, Y. Z., Tan, Y. Y., Tang, F. E., & Saptoro, A. (2023a). DEWATERING AND STABILIZATION OF SLUDGE RESIDUE IN SLUDGE TREATMENT REED BEDS TREATING SEPTAGE. *Science International*.

Huong, Y. Z., Tan, Y. Y., Tang, F. E., & Saptoro, A. (2023b). Modelling of Hydraulic Dynamics in Sludge Treatment Reed Beds with Moving Boundary Condition. MATEC Web of Conferences, EDP Sciences.

Huong, Y. Z., Tan, Y. Y., Tang, F. E., & Saptoro, A. (2024a). Influence of sludge deposit layer on sludge treatment reed beds treating septage. *Journal of Water, Sanitation and Hygiene for Development*, washdev2024162. https://doi.org/10.2166/washdev.2024.162

Huong, Y. Z., Tan, Y. Y., Tang, F. E., & Saptoro, A. (2024b). Modelling sludge dewatering in treatment reed bed considering sludge deposit formation. *Modeling Earth Systems and Environment*. https://doi.org/10.1007/s40808-023-01930-z

Jafari, M., Derlon, N., Desmond, P., van Loosdrecht, M. C. M., Morgenroth, E., & Picioreanu, C. (2019). Biofilm compressibility in ultrafiltration: A relation between biofilm morphology, mechanics and hydraulic resistance. *Water research*, *157*, 335-345. https://doi.org/10.1016/j.watres.2019.03.073

Jain, M., Upadhyay, M., Gupta, A. K., & Ghosal, P. S. (2022). A review on the treatment of septage and faecal sludge management: A special emphasis on constructed wetlands. *Journal of Environmental Management*, *315*, 115143. https://doi.org/10.1016/j.jenvman.2022.115143

Jayswal, N., & Rodríguez, J. (2021). Effect of temperature and loading frequency on the performance of vertical subsurface flow constructed wetlands: Modelling study using HYDRUS. https://doi.org/10.1101/2021.03.25.436912

Jehawi, O. H., Abdullah, S. R. S., Kurniawan, S. B., Ismail, N. I., Idris, M., Al Sbani, N. H., Muhamad, M. H., & Hasan, H. A. (2020). Performance of pilot Hybrid Reed Bed constructed wetland with aeration system on nutrient removal for domestic

wastewater treatment. *Environmental Technology & Innovation, 19*. https://doi.org/10.1016/j.eti.2020.100891

Jensen, M. E., Burman, R. D., & Allen, R. G. (1990). Evapotranspiration and irrigation water requirements: A manual. *American Society of Civil Engineers (USA): Committee on Irrigation Water Requirements*.

Ji, M., Hu, Z., Hou, C., Liu, H., Ngo, H. H., Guo, W., Lu, S., & Zhang, J. (2020). New insights for enhancing the performance of constructed wetlands at low temperatures. *Bioresour Technol, 301*, 122722. https://doi.org/10.1016/j.biortech.2019.122722

Jia, Y., Zhou, M., Chen, Y., Hu, Y., & Luo, J. (2020). Insight into short-cut of simultaneous nitrification and denitrification process in moving bed biofilm reactor: Effects of carbon to nitrogen ratio. *Chemical Engineering Journal, 400*, 125905. https://doi.org/10.1016/j.cej.2020.125905

Joshi, S. S., Shivapur, A., Karjinni, V., Patil⁴, M., Jadhav, M. P., & Patil, M. A. M. (2020). A Research Paper on Treatment of Domestic Wastewater using Vertical Flow Constructed Wetland (VFCW).

Jóźwiakowska, K., & Bugajski, P. (2023). Influence of the Bed Temperature on the Operational Reliability of a Hybrid Constructed Wetland Wastewater Treatment Plant in South-Western Poland—A Case Study. *Sustainability, 15*(15), 11790. https://www.mdpi.com/2071-1050/15/15/11790

Jóźwiakowski, K., Marzec, M., Kowalczyk-Juśko, A., Gizińska-Górna, M., Pytka-Woszczyło, A., Malik, A., Listosz, A., & Gajewska, M. (2019). 25 years of research and experiences about the application of constructed wetlands in southeastern Poland. *Ecological Engineering, 127*, 440-453. https://doi.org/10.1016/j.ecoleng.2018.12.013

Jung, Y. T., Narayanan, N. C., & Cheng, Y.-L. (2018). Cost comparison of centralized and decentralized wastewater management systems using optimization model. *Journal of Environmental Management, 213*, 90-97. https://doi.org/10.1016/j.jenvman.2018.01.081

Kabir, M. I., Hoque, M. A., & Banik, B. K. (2020). Performance of a reed bed system for faecal wastewater treatment: case study. *Water Practice and Technology*, *15*(4), 993-998. https://doi.org/10.2166/wpt.2020.077

Kannan, R., Vogelsberger, M., Marinacci, F., McKinnon, R., Pakmor, R., & Springel, V. (2019). arepo-rt: radiation hydrodynamics on a moving mesh. *Monthly Notices of the Royal Astronomical Society*, *485*(1), 117-149. https://doi.org/10.1093/mnras/stz287

Kapumbe, D., Min, L., Zhang, X., Kisoholo, M., & Yongfeng, L. (2019). Modeling and simulation of membrane bioreactor model based on ASM3 for domestic wastewater treatment. *Applied Ecology and Environmental Research*, *17*(5), 11395-11407.

Karia, G., Christian, R., & JARIWALA, N. D. (2023). *Wastewater treatment: Concepts and design approach*. PHI Learning Pvt. Ltd.

Karolinczak, B., & Dąbrowski, W. (2017). Effectiveness of septage pre-treatment in vertical flow constructed wetlands. *Water Sci Technol*, *76*(9-10), 2544-2553. https://doi.org/10.2166/wst.2017.398

Khaleel, R., & Relyea, J. (1997). Correcting laboratory-measured moisture retention data for gravels. *Water Resources Research*, *33*(8), 1875-1878.

Khalekuzzaman, M., Alamgir, M., Islam, M. B., & Hasan, M. (2019). A simplistic approach of algal biofuels production from wastewater using a Hybrid Anaerobic Baffled Reactor and Photobioreactor (HABR-PBR) System. *PloS one*, *14*(12), e0225458.

Khalifa, M. E., El-Reash, Y. G. A., Ahmed, M. I., & Rizk, F. W. (2020). Effect of media variation on the removal efficiency of pollutants from domestic wastewater in constructed wetland systems. *Ecological Engineering*, *143*. https://doi.org/10.1016/j.ecoleng.2019.105668

Khan, N. A., El Morabet, R., Khan, R. A., Ahmed, S., Dhingra, A., Alsubih, M., & Khan, A. R. (2020). Horizontal sub surface flow Constructed Wetlands coupled with tubesettler for hospital wastewater treatment. *Journal of Environmental Management*, *267*, 110627. https://doi.org/10.1016/j.jenvman.2020.110627

Khomenko, O., Dotro, G., Jefferson, B., Coulon, F., & Bajón Fernández, Y. (2019). Influence of sludge layer properties on the hydraulic behaviour of gravel-based vertical flow constructed wetlands for primary treatment of sewage. *Science of The Total Environment, 691*, 1137-1143. https://doi.org/10.1016/j.scitotenv.2019.07.121

Kim, B., Bel, T., Bourdoncle, P., Dimare, J., Troesch, S., & Molle, P. (2017). Septage unit treatment by sludge treatment reed beds for easy management and reuse: performance and design considerations. *Water Science and Technology, 77*(2), 279-285. https://doi.org/10.2166/wst.2017.461

Kim, B., & Forquet, N. (2016). Pore-scale observation of deposit within the gravel matrix of a vertical flow constructed wetland. *Environmental technology, 37*(24), 3146-3150. https://doi.org/10.1080/09593330.2016.1178334

Kołecka, K., Obarska-Pempkowiak, H., & Gajewska, M. (2016). Sludge Treatment Reed Beds (STRBs) as a Eco-solution of Sludge Utilization for Local Wastewater Treatment Plants. In J. Vymazal (Ed.), *Natural and Constructed Wetlands: Nutrients, heavy metals and energy cycling, and flow* (pp. 119-130). Springer International Publishing. https://doi.org/10.1007/978-3-319-38927-1_9

Kołecka, K., Obarska-Pempkowiak, H., & Gajewska, M. (2018). Polish experience in operation of sludge treatment reed beds. *Ecological Engineering, 120*, 405-410. https://doi.org/10.1016/j.ecoleng.2018.06.022

Koncz, V., Izsák, F., Noszticzius, Z., & Kály-Kullai, K. (2021). Adaptive moving mesh algorithm based on local reaction rate. *Heliyon, 7*(1), e05842. https://doi.org/10.1016/j.heliyon.2020.e05842

Krzyk, M., & Drev, D. (2023). Septic Tanks as Small Municipal Sewage Treatment Plants. Advanced Technologies, Systems, and Applications VII, Cham.

Lai, C.-T., & Katul, G. (2000). The dynamic role of root-water uptake in coupling potential to actual transpiration. *Advances in Water Resources, 23*(4), 427-439. https://doi.org/10.1016/S0309-1708(99)00023-8

Langergraber, G., Rousseau, D. P. L., García, J., & Mena, J. (2009). CWM1: a general model to describe biokinetic processes in subsurface flow constructed wetlands. *Water Science and Technology, 59*(9), 1687-1697. https://doi.org/10.2166/wst.2009.131

Langergraber, G., & Šimůnek, J. (2005). Modeling Variably Saturated Water Flow and Multicomponent Reactive Transport in Constructed Wetlands. *Vadose Zone Journal, 4*(4), 924-938. https://doi.org/10.2136/vzj2004.0166

Langergraber, G., & Šimůnek, J. (2006). The multi-component reactive transport module CW2D for constructed wetlands for the HYDRUS software package. *Hydrus Software Ser, 2*.

Lapidus, L., & Pinder, G. F. (1982). *Numerical Solution of Partial Differential Equations in Science and Engineering*. John Wiley and Sons, New York.

Le Pera, A., Sellaro, M., Migliori, M., Bianco, M., & Zanardi, G. (2021). Dry Mesophilic Anaerobic Digestion of Separately Collected Organic Fraction of Municipal Solid Waste: Two-Year Experience in an Industrial-Scale Plant. *Processes, 9*(2), 213. https://www.mdpi.com/2227-9717/9/2/213

Lee, T. E., Baines, M. J., & Langdon, S. (2015). A finite difference moving mesh method based on conservation for moving boundary problems. *Journal of Computational and Applied Mathematics, 288,* 1-17. https://doi.org/10.1016/j.cam.2015.03.032

Lei, X., Jia, Y., Chen, Y., & Hu, Y. (2019). Simultaneous nitrification and denitrification without nitrite accumulation by a novel isolated Ochrobactrum anthropic LJ81. *Bioresource technology, 272*, 442-450. https://doi.org/10.1016/j.biortech.2018.10.060

Leite, W. R. M., Magnus, B. S., de Moraes, B. A. B., Kato, M. T., Florencio, L., da Costa, R. H. R., & Belli Filho, P. (2023). Mesophilic anaerobic digestion of waste activated sludge in an intermittent mixing reactor: Effect of hydraulic retention time and organic loading rate. *Journal of Environmental Management, 338*, 117839.

Li, C., Liu, S., Ma, T., Zheng, M., & Ni, J. (2019). Simultaneous nitrification, denitrification and phosphorus removal in a sequencing batch reactor (SBR) under low temperature. *Chemosphere*, *229*, 132-141.

Li, H. (2022). The Finite Element Method. In H. Li (Ed.), *Graded Finite Element Methods for Elliptic Problems in Nonsmooth Domains* (pp. 1-12). Springer International Publishing. https://doi.org/10.1007/978-3-031-05821-9_1

Li, K. Y., De Jong, R., & Boisvert, J. B. (2001). An exponential root-water-uptake model with water stress compensation. *Journal of Hydrology*, *252*(1), 189-204. https://doi.org/10.1016/S0022-1694(01)00456-5

Li, X., Ding, A., Zheng, L., Anderson, B. C., Kong, L., Wu, A., & Xing, L. (2018). Relationship between design parameters and removal efficiency for constructed wetlands in China. *Ecological Engineering*, *123*, 135-140. https://doi.org/10.1016/j.ecoleng.2018.08.005

Li, X., Wu, S., Yang, C., & Zeng, G. (2020). Microalgal and duckweed based constructed wetlands for swine wastewater treatment: A review. *Bioresource technology*, *318*, 123858.

Li, Z., & Hodges, B. R. (2021). Revisiting Surface-Subsurface Exchange at Intertidal Zone with a Coupled 2D Hydrodynamic and 3D Variably-Saturated Groundwater Model. *Water*, *13*(7), 902. https://doi.org/10.3390/w13070902

List, F., & Radu, F. A. (2016). A study on iterative methods for solving Richards' equation. *Computational Geosciences*, *20*(2), 341-353. https://doi.org/10.1007/s10596-016-9566-3

Llorens, E., Saaltink, M. W., & García, J. (2011). CWM1 implementation in RetrasoCodeBright: First results using horizontal subsurface flow constructed wetland data. *Chemical Engineering Journal*, *166*(1), 224-232. https://doi.org/10.1016/j.cej.2010.10.065

Lu, R., Nagel, T., Poonoosamy, J., Naumov, D., Fischer, T., Montoya, V., Kolditz, O., & Shao, H. (2022). A new operator-splitting finite element scheme for reactive transport modeling in saturated porous media. *Computers & Geosciences*, *163*, 105106. https://doi.org/10.1016/j.cageo.2022.105106

Luo, L., Yao, J., Liu, W., Yang, L., Li, H., Liang, M., Ma, H., Liu, Z., & Chen, Y. (2021). Comparison of bacterial communities and antibiotic resistance genes in oxidation ditches and membrane bioreactors. *Scientific Reports, 11*(1), 1-10.

Ma, J., Cui, Y., Li, A., Zhang, W., Ma, C., & Chen, Z. (2020, 2020/11/15/). Occurrence and distribution of five antibiotic resistance genes during the loading period in sludge treatment wetlands. *Journal of Environmental Management, 274*, 111190. https://doi.org/https://doi.org/10.1016/j.jenvman.2020.111190

Ma, J., Cui, Y., Li, A., Zhang, W., Ma, C., Luosang, Z., Chen, Z., & Zhao, K. (2021, 2021/12/15/). Tracking macrolides, sulfonamides, fluoroquinolones, and tetracyclines in sludge treatment wetlands during loading and resting periods. *Separation and Purification Technology, 279*, 119599. https://doi.org/https://doi.org/10.1016/j.seppur.2021.119599

Magri, M. E., Francisco, J. G. Z., Sezerino, P. H., & Philippi, L. S. (2016, 2016/10/01/). Constructed wetlands for sludge dewatering with high solids loading rate and effluent recirculation: Characteristics of effluent produced and accumulated sludge. *Ecological Engineering, 95*, 316-323. https://doi.org/https://doi.org/10.1016/j.ecoleng.2016.06.085

Mahesh, S., Prasad, B., Mall, I. D., & Mishra, I. M. (2006). Electrochemical Degradation of Pulp and Paper Mill Wastewater. Part 2. Characterization and Analysis of Sludge. *Industrial & Engineering Chemistry Research, 45*(16), 5766-5774. https://doi.org/10.1021/ie0603969

Maier, U., DeBiase, C., Baeder-Bederski, O., & Bayer, P. (2009). Calibration of hydraulic parameters for large-scale vertical flow constructed wetlands. *Journal of Hydrology, 369*(3-4), 260-273.

Malovanyy, M., Zhuk, V., Sliusar, V., & Sereda, A. (2018). Two-stage treatment of solid waste leachates in aerated lagoons and at municipal wastewater treatment plants. *Восточно-Европейский журнал передовых технологий*(1 (10)), 23-30.

Mancuso, M., & Fioreze, M. (2018). Numerical Simulation of Flow and Biokinetic Processes in Subsurface Flow Constructed Wetlands: A Systematic Review. *Journal of Urban and Environmental Engineering, 12*(1), 120-127. https://doi.org/10.4090/juee.2018.v12n1.120127

May Cua, E. R. (2019). A Cylindrical-Conical Photobioreactor and a Sludge Drying Bed as as Efficient System for Cultivation of the Green Microalgae Coelastrum sp. and Dry Biomass Recovery. *Revista Mexicana de Ingeniería Química, 18*(1), 1-11. https://doi.org/10.24275/uam/izt/dcbi/revmexingquim/2019v18n1/May

Mazumder, K., Sumi, T. S., Golder, M., Biswas, B., Maknoon, & Kerr, P. G. (2021). Antidiabetic profiling, cytotoxicity and acute toxicity evaluation of aerial parts of Phragmites karka (Retz.). *Journal of Ethnopharmacology*, *270*, 113781. https://doi.org/10.1016/j.jep.2021.113781

McCarter, C. P. R., Rezanezhad, F., Gharedaghloo, B., Price, J. S., & Van Cappellen, P. (2019). Transport of chloride and deuterated water in peat: The role of anion exclusion, diffusion, and anion adsorption in a dual porosity organic media. *Journal of Contaminant Hydrology*, *225*, 103497. https://doi.org/10.1016/j.jconhyd.2019.103497

Mellbye, B. L., Giguere, A. T., Murthy, G. S., Bottomley, P. J., Sayavedra-Soto, L. A., & Chaplen, F. W. (2018). Genome-scale, constraint-based modeling of nitrogen oxide fluxes during coculture of Nitrosomonas europaea and Nitrobacter winogradskyi. *Msystems*, *3*(3), e00170-00117.

Mladenov, N., Dodder, N. G., Steinberg, L., Richardot, W., Johnson, J., Martincigh, B. S., Buckley, C., Lawrence, T., & Hoh, E. (2022). Persistence and removal of trace organic compounds in centralized and decentralized wastewater treatment systems. *Chemosphere*, *286*, 131621.

Moezzibadi, M., Charpentier, I., Wanko, A., & Mosé, R. (2019). Temporal estimation of hydrodynamic parameter variability in stormwater constructed wetlands–The hysteresis effect during multi-rainfall events. *Ecological Engineering*, *127*, 1-10.

Mohajerani, A., Ukwatta, A., Jeffrey-Bailey, T., Swaney, M., Ahmed, M., Rodwell, G., Bartolo, S., Eshtiaghi, N., & Setunge, S. (2019). A proposal for recycling the world's unused stockpiles of treated wastewater sludge (biosolids) in fired-clay bricks. *Buildings*, *9*(1), 14.

Monteith, J. L. (1965). Evaporation and environment. *Symposia of the Society for Experimental Biology*, *19*, 205-234.

Moreira, F. D., & Dias, E. H. O. (2020). Constructed wetlands applied in rural sanitation: A review. *Environ Res*, *190*, 110016. https://doi.org/10.1016/j.envres.2020.110016

Morvannou, A., Forquet, N., Vanclooster, M., & Molle, P. (2012). Which hydraulic model to use in vertical flow constructed wetlands? 13th International Conference on Wetland Systems for Water Pollution Control,

Morvannou, A., Forquet, N., Vanclooster, M., & Molle, P. (2013). Characterizing hydraulic properties of filter material of a vertical flow constructed wetland. *Ecological Engineering*, *60*, 325-335.

Mostafa, R. R., Kisi, O., Adnan, R. M., Sadeghifar, T., & Kuriqi, A. (2023). Modeling potential evapotranspiration by improved machine learning methods using limited climatic data. *Water*, *15*(3), 486.

Mpongwana, N., Ntwampe, S. K. O., Omodanisi, E. I., Chidi, B. S., & Razanamahandry, L. C. (2019). Sustainable Approach to Eradicate the Inhibitory Effect of Free-Cyanide on Simultaneous Nitrification and Aerobic Denitrification during Wastewater Treatment. *Sustainability*, *11*(21), 6180. https://www.mdpi.com/2071-1050/11/21/6180

Mualem, Y. (1976). A new model for predicting the hydraulic conductivity of unsaturated porous media. *Water Resources Research*, *12*(3), 513-522. https://doi.org/10.1029/WR012i003p00513

Mustafa, A., & Ali, M. (2019). Waste materials as substrates in vertical flow constructed wetlands treating domestic wastewater. *WIT Transactions on Ecology and the Environment*, *231*, 339-346.

Nawaz, M. I., Yi, C. W., Ni, L. X., Zhao, H., Wang, H. J., Yi, R. J., Yin, L. L., Aleem, M., & Zaman, M. (2019). Removal of nitrobenzene from wastewater by vertical flow constructed wetland and optimizing substrate composition using Hydrus-1D: optimizing substrate composition of vertical flow constructed wetland for removing nitrobenzene from wastewater. *International Journal of Environmental Science and Technology*, *16*(12), 8005-8014. https://doi.org/10.1007/s13762-019-02217-6

Ni, Q., Wang, T., Liao, J., Shi, W., Huang, Z., Miao, H., Wu, P., & Ruan, W. (2020). Operational performances and enzymatic activities for eutrophic water treatment by vertical-flow and horizontal-flow constructed wetlands. *Water, 12*(7), 2007.

Nielsen, D. R., Th. Van Genuchten, M., & Biggar, J. W. (1986). Water flow and solute transport processes in the unsaturated zone. *Water Resources Research, 22*(9S), 89S-108S. https://doi.org/10.1029/WR022i09Sp0089S

Nielsen, S. (2023). Combined treatment of sludge from a wastewater treatment plant and wastewater from a stormwater basin in a Sludge Treatment Reed Bed System during >25 years. *Ecological Engineering, 194*, 107020. https://doi.org/10.1016/j.ecoleng.2023.107020

Nielsen, S., & Larsen, J. D. (2016). Operational strategy, economic and environmental performance of sludge treatment reed bed systems - based on 28 years of experience. *Water Sci Technol, 74*(8), 1793-1799. https://doi.org/10.2166/wst.2016.295

Nielsen, S., & Stefanakis, A. I. (2020). Sustainable Dewatering of Industrial Sludges in Sludge Treatment Reed Beds: Experiences from Pilot and Full-Scale Studies under Different Climates. *Applied Sciences, 10*(21). https://doi.org/10.3390/app10217446

Obour, P. B., Jensen, J. L., Lamandé, M., Watts, C. W., & Munkholm, L. J. (2018). Soil organic matter widens the range of water contents for tillage. *Soil and Tillage Research, 182*, 57-65. https://doi.org/10.1016/j.still.2018.05.001

Odusanya, A., Mehdi-Schulz, B., Schürz, C., Adebayo Olubukola, O., Awokola, O., Awomeso, A., Adejuwon, J., & Karsten, S. (2018). Multi-site calibration and validation of SWAT with satellite-based evapotranspiration in a data sparse catchment in southwestern Nigeria. *Hydrology and Earth System Sciences Discussions*, 1-37. https://doi.org/10.5194/hess-2018-170

Ooi, E. H., J. Y. Chia, N., Ooi, E. T., Foo, J. J., Liao, I. Y., R. Nair, S., & Mohd Ali, A. F. (2018). Comparison between single- and dual-porosity models for fluid transport in predicting lesion volume following saline-infused radiofrequency ablation. *International Journal of Hyperthermia, 34*(8), 1142-1156. https://doi.org/10.1080/02656736.2018.1437282

Osei, A. R., Konate, Y., & Abagale, F. K. (2019). Pollutant removal and growth dynamics of macrophyte species for faecal sludge treatment with constructed wetland technology. *Water Sci Technol, 80*(6), 1145-1154. https://doi.org/10.2166/wst.2019.354

Owusu-Twum, M. Y., & Sharara, M. A. (2020). Sludge management in anaerobic swine lagoons: A review. *Journal of Environmental Management, 271*, 110949. https://doi.org/10.1016/j.jenvman.2020.110949

Panuvatvanich, A., Koottatep, T., & Kone, D. (2009, 2009/06/01/). Influence of sand layer depth and percolate impounding regime on nitrogen transformation in vertical-flow constructed wetlands treating faecal sludge. *Water research, 43*(10), 2623-2630. https://doi.org/https://doi.org/10.1016/j.watres.2009.03.029

Panwar, R. S., & Makvana, K. S. (2017). <panwar 2017.pdf>. *Reed- Phragmitis Karka based constructed wetland for the treatment of domestic wastewater in Ujjain city of central India, 4*(4), 1-5.

Parde, D., Patwa, A., Shukla, A., Vijay, R., Killedar, D. J., & Kumar, R. (2021). A review of constructed wetland on type, treatment and technology of wastewater. *Environmental Technology & Innovation, 21*, 101261. https://doi.org/10.1016/j.eti.2020.101261

Paredes, P., Pereira, L. S., Almorox, J., & Darouich, H. (2020). Reference grass evapotranspiration with reduced data sets: Parameterization of the FAO Penman-Monteith temperature approach and the Hargeaves-Samani equation using local climatic variables. *Agricultural Water Management, 240*, 106210. https://doi.org/10.1016/j.agwat.2020.106210

Penman, H. L. (1948). Natural evaporation from open water, bare soil and grass. *Proc. R. Soc. Lond.* , 120-145.

Pergam, P., & Briesen, H. (2023). Reduced order modeling for compressible cake filtration processes using proper orthogonal decomposition. *Computers & Chemical Engineering, 171*, 108165. https://doi.org/10.1016/j.compchemeng.2023.108165

Pham, V. H. T., Ahn, J., Kim, J., Lee, S., Lee, I., Kim, S., Chang, S., & Chung, W. (2021). Volatile Fatty Acid Production from Food Waste Leachate Using Enriched Bacterial Culture and Soil Bacteria as Co-Digester. *Sustainability, 13*(17), 9606. https://doi.org/10.3390/su13179606

Presti, D., Cosenza, A., Capri, F. C., Gallo, G., Alduina, R., & Mannina, G. (2021). Influence of volatile solids and pH for the production of volatile fatty acids: Batch fermentation tests using sewage sludge. *Bioresource technology*, *342*, 125853. https://doi.org/10.1016/j.biortech.2021.125853

Priestley, C. H. B., & Taylor, R. J. (1972). On the Assessment of Surface Heat Flux and Evaporation Using Large-Scale Parameters. *Monthly Weather Review, 100*(2), 81-92. https://doi.org/10.1175/1520-0493(1972)100<0081:OTAOSH>2.3.CO;2

Prost-Boucle, S., Pelus, L., Becheau, E., Cervoise, L., Troesch, S., & Molle, P. (2023). Combination of sequencing batch reactor and vertical flow treatment wetlands: A full-scale experience for rum distillery wastewater treatment in a tropical climate. *Nature-Based Solutions, 3*, 100056. https://doi.org/10.1016/j.nbsj.2023.100056

Przydatek, G., & Wota, A. K. (2020). Analysis of the comprehensive management of sewage sludge in Poland. *Journal of Material Cycles and Waste Management, 22*(1), 80-88. https://doi.org/10.1007/s10163-019-00937-y

Pucher, B., & Langergraber, G. (2018). Simulating vertical flow wetlands using filter media with different grain sizes with the HYDRUS Wetland Module. *Journal of Hydrology and Hydromechanics*, *66*(2), 227-231. https://doi.org/10.1515/johh-2017-0053

Putro, L. H. S., Budianta, D., Rohendi, D., & Rejo, A. (2020). Modeling methane emission of wastewater anaerobic pond at palm oil mill using radial basis function neural network. *International Journal on Advanced Science, Engineering and Information Technology, 10*(1), 260-268.

Raboni, M., Viotti, P., Rada, E. C., Conti, F., & Boni, M. R. (2020). The sensitivity of a specific denitrification rate under the dissolved oxygen pressure. *International Journal of Environmental Research and Public Health, 17*(24), 9366.

Rajabzadeh, A. R., Legge, R. L., & Weber, K. P. (2015). Multiphysics modelling of flow dynamics, biofilm development and wastewater treatment in a subsurface vertical flow constructed wetland mesocosm. *Ecological Engineering, 74*, 107-116. https://doi.org/10.1016/j.ecoleng.2014.09.122

Ramavandi, B. (2014). Removal of chemical oxygen demand from textile wastewater using a natural coagulant. *Korean Journal of Chemical Engineering, 31*. https://doi.org/10.1007/s11814-013-0197-2

Reichert, J. M., Mentges, M. I., Rodrigues, M. F., Cavalli, J. P., Awe, G. O., & Mentges, L. R. (2018). Compressibility and elasticity of subtropical no-till soils varying in granulometry organic matter, bulk density and moisture. *CATENA, 165*, 345-357. https://doi.org/10.1016/j.catena.2018.02.014

Richards, L. A. (1931). Capillary Conduction of Liquids through Porous Mediums. *Physics, 1*(5), 318-333. https://doi.org/10.1063/1.1745010

Saeed, T., Majed, N., Kumar Yadav, A., Hasan, A., & Jihad Miah, M. (2022). Constructed wetlands for drained wastewater treatment and sludge stabilization: Role of plants, microbial fuel cell and earthworm assistance. *Chemical Engineering Journal, 430*, 132907. https://doi.org/10.1016/j.cej.2021.132907

Salem, M., Mohamed, E., Mossad, M., & Mahanna, H. (2022). Random Forest modelling and evaluation of the performance of a full-scale subsurface constructed wetland plant in Egypt. *Ain Shams Engineering Journal, 13*(6), 101778.

Samsó, R., & Garcia, J. (2013). BIO_PORE, a mathematical model to simulate biofilm growth and water quality improvement in porous media: Application and calibration for constructed wetlands. *Ecological Engineering, 54*, 116-127. https://doi.org/10.1016/j.ecoleng.2013.01.021

Samsó, R., García, J., Molle, P., & Forquet, N. (2016). Modelling bioclogging in variably saturated porous media and the interactions between surface/subsurface flows: Application to Constructed Wetlands. *Journal of Environmental Management, 165*, 271-279.

Sánchez, F., Rey, H., Viedma, A., Nicolás-Pérez, F., Kaiser, A., & Martínez, M. (2018). CFD simulation of fluid dynamic and biokinetic processes within activated sludge reactors under intermittent aeration regime. *Water research, 139*, 47-57.

Sánchez, M., Gonzalo, O. G., Yáñez, S., Ruiz, I., & Soto, M. (2021). Influence of nutrients and pH on the efficiency of vertical flow constructed wetlands treating winery wastewater. *Journal of Water Process Engineering, 42*, 102103.

Shahid, M. A., Maqbool, N., & Khan, S. J. (2022). An integrated investigation on anaerobic membrane-based thickening of fecal sludge and the role of extracellular polymeric substances (EPS) in solid-liquid separation. *Journal of Environmental Management, 305*, 114350. https://doi.org/10.1016/j.jenvman.2021.114350

Sharma, C., & Sharma, S. (2018). *Centralized Versus Decentralized Wastewater Treatment and Reuse: A Feasibility Study for NITTTR Campus, Chandigarh*.

Shen, Y., Zhuang, L., Zhang, J., Fan, J., Yang, T., & Sun, S. (2019). A study of ferric-carbon micro-electrolysis process to enhance nitrogen and phosphorus removal efficiency in subsurface flow constructed wetlands. *Chemical Engineering Journal, 359*, 706-712. https://doi.org/10.1016/j.cej.2018.11.152

Sheng, J., Huang, T., Ye, Z., Hu, B., Liu, Y., & Fan, Q. (2019). Evaluation of van Genuchten-Mualem model on the relative permeability for unsaturated flow in aperture-based fractures. *Journal of Hydrology, 576*, 315-324. https://doi.org/10.1016/j.jhydrol.2019.06.047

Sierra, J. D. M., Oosterkamp, M. J., Wang, W., Spanjers, H., & van Lier, J. B. (2019). Comparative performance of upflow anaerobic sludge blanket reactor and anaerobic membrane bioreactor treating phenolic wastewater: Overcoming high salinity. *Chemical Engineering Journal, 366*, 480-490.

Simon-Várhelyi, M., Cristea, V.-M., & Brehar, M. A. (2020). Efficient calibration methodology of the wastewater treatment plant model based on ASM3 and application to municipal wastewater. *Desalination and Water Treatment, 189*, 108-118.

Šimůnek, J., Jarvis, N. J., van Genuchten, M. T., & Gärdenäs, A. (2003). Review and comparison of models for describing non-equilibrium and preferential flow and

transport in the vadose zone. *Journal of Hydrology, 272*(1), 14-35. https://doi.org/10.1016/S0022-1694(02)00252-4

Šimůnek, J., & van Genuchten, M. T. (2008). Modeling Nonequilibrium Flow and Transport Processes Using HYDRUS. *Vadose Zone Journal, 7*(2), 782-797. https://doi.org/10.2136/vzj2007.0074

Šimůnek, J., Wendroth, O., Wypler, N., & Van Genuchten, M. T. (2001). Non-equilibrium water flow characterized by means of upward infiltration experiments. *European Journal of Soil Science, 52*(1), 13-24. https://doi.org/10.1046/j.1365-2389.2001.00361.x

Simunek, J. J., Saito, H., Sakai, M., & Van Genuchten, M. (2008). *The HYDRUS-1D Software Package for Simulating the One-Dimensional Movement of Water, Heat, and Multiple Solutes in Variably-Saturated Media*.

Singh, D., & Gurjar, B. R. (2023, 2023/02/03). Recent innovation and impacts of nano-based technologies for wastewater treatment on humans: a review. *Environmental Monitoring and Assessment, 195*(3), 357. https://doi.org/10.1007/s10661-022-10790-6

Singh, S., Upadhyay, S., Rani, A., Sharma, P. K., Rawat, J. M., Rawat, B., Prashant, & Bhattacharya, P. (2023). Assessment of pathogen removal efficiency of vertical flow constructed wetland treating septage. *Scientific Reports*, *13*(1), 18703.

Sørensen, P. B., Moldrup, P., & Hansen, J. (1996). Filtration and expression of compressible cakes. *Chemical Engineering Science, 51*(6), 967-979. https://doi.org/10.1016/0009-2509(95)00339-8

SPAN. (2008). *Malaysian Sewerage Industry Guidelines - Sewage Treatment Plants* (Vol. IV). National Water Services Commission, Ministry of Energy, Water and Communications.

Stamatakis, K., & Tien, C. (1991). Cake formation and growth in cake filtration. *Chemical Engineering Science, 46*(8), 1917-1933. https://doi.org/10.1016/0009-2509(91)80153-P

Stefanakis, A. (2020). Constructed Wetlands for Sustainable Wastewater Treatment in Hot and Arid Climates: Opportunities, Challenges and Case Studies in the Middle East. *Water, 12*(6). https://doi.org/10.3390/w12061665

Tan, Y. Y., Huong, Y. Z., Tang, F. E., & Saptoro, A. (2023). A review of sewage sludge dewatering and stabilisation in reed bed system: towards the process-based modelling. *International Journal of Environmental Science and Technology*. https://doi.org/10.1007/s13762-023-05063-9

Tan, Y. Y., Tang, F. E., Ho, C. L. I., & Jong, V. (2017). Dewatering and Treatment of Septage Using Vertical Flow Constructed Wetlands. *Technologies, 5*(4). https://doi.org/10.3390/technologies5040070

Tan, Y. Y., Tang, F. E., & Saptoro, A. (2021). Process-based models for nitrogen dynamics in subsurface flow constructed wetlands: A state-of-the-art review. *Environmental Reviews*. https://doi.org/10.1139/er-2021-0001

Tan, Y. Y., Tang, F. E., Saptoro, A., & Khor, E. H. (2020). Effect of loading rate and sludge deposit on a VFCW treating septage. *Journal of Applied Water Engineering and Research, 8*(1), 1-14. https://doi.org/10.1080/23249676.2020.1719217

Tang, T. (2005). Moving mesh methods for computational fluid dynamics. *Contemp. Math., 383*. https://doi.org/10.1090/conm/383/07162

Tayler, K. (2018). *Faecal Sludge and Septage Treatment - A guide for low- and middle-income countries*. Practical Action Publishing. https://doi.org/10.3362/9781780449869

Thakur, I. S., & Medhi, K. (2019). Nitrification and denitrification processes for mitigation of nitrous oxide from waste water treatment plants for biovalorization: Challenges and opportunities. *Bioresource technology, 282*, 502-513. https://doi.org/10.1016/j.biortech.2019.03.069

Thazhathu Veetil, S., & Thampi, S. G. (2021). Performance evaluation and numerical simulation of vertical subsurface flow constructed wetlands in wastewater treatment. *Advances in Environmental Technology*, *7*(1), 37-46.

Tien, C., Bai, R., & Ramarao, B. V. (1997). Analysis of cake growth in cake filtration: Effect of fine particle retention. *AIChE Journal*, *43*(1), 33-44. https://doi.org/10.1002/aic.690430106

Tiller, F. M., & Yeh, C. S. (1987). The role of porosity in filtration. Part XI: Filtration followed by expression. *AIChE Journal*, *33*(8), 1241-1256. https://doi.org/10.1002/aic.690330803

Tisdell, C. C. (2019). On Picard's iteration method to solve differential equations and a pedagogical space for otherness. *International Journal of Mathematical Education in Science and Technology*, *50*(5), 788-799. https://doi.org/10.1080/0020739X.2018.1507051

Torrens, A., Folch, M., & Salgot, M. (2021). Design and Performance of an Innovative Hybrid Constructed Wetland for Sustainable Pig Slurry Treatment in Small Farms. *Frontiers in Environmental Science*, *8*. https://doi.org/10.3389/fenvs.2020.577186

Toscano, A., Langergraber, G., Consoli, S., & Cirelli, G. L. (2009). Modelling pollutant removal in a pilot-scale two-stage subsurface flow constructed wetlands. *Ecological Engineering*, *35*(2), 281-289.

Trein, C. M., Zumalacarregui, J. A. G., Moraes, M. A. d. A., & von Sperling, M. (2019). Reduction of area and influence of the deposit layer in the first stage of a full-scale French system of vertical flow constructed wetlands in a tropical area. *Water Science and Technology*, *80*(2), 347-356. https://doi.org/10.2166/wst.2019.278

Turc, L. (1961). Water requirements assessment of irrigation, potential evapotranspiration: Simplified and updated climatic formula. *Annales Agronomiques*, *12*, 13-49.

Uggetti, E., Ferrer, I., Llorens, E., & García, J. (2010, 2010/05/01/). Sludge treatment wetlands: A review on the state of the art. *Bioresource technology*, *101*(9), 2905-2912. https://doi.org/https://doi.org/10.1016/j.biortech.2009.11.102

USEPA. (1979). *Process Design Manual for Sludge Treatment and Disposal*. Environmental Research Information Center. Technology Transfer, Center for

Environmental Research Information, Brown and Caldwell. https://books.google.com.my/books?id=soBAngAACAAJ

Usman Khan, M., & Kiaer Ahring, B. (2020). Anaerobic digestion of biorefinery lignin: Effect of different wet explosion pretreatment conditions. *Bioresource technology*, *298*, 122537. https://doi.org/10.1016/j.biortech.2019.122537

van Genuchten, M. T. (1980). A Closed-form Equation for Predicting the Hydraulic Conductivity of Unsaturated Soils. *Soil Science Society of America Journal*, *44*(5), 892-898. https://doi.org/10.2136/sssaj1980.03615995004400050002x

van Genuchten, M. T., Leij, F. J., & Yates, S. R. (1991). The RETC Code for Quantifying the Hydraulic Functions of Unsaturated Solids. *U.S. Salinity Laboratory U.S. Department of Agriculture, Agricultural Research Service Riverside, California 9250 1*.

van Genuchten, M. T., & Wierenga, P. J. (1976). Mass Transfer Studies in Sorbing Porous Media I. Analytical Solutions. *Soil Science Society of America Journal*, *40*(4), 473-480. https://doi.org/10.2136/sssaj1976.03615995004000040011x

Varado, N., Braud, I., & Ross, P. J. (2006). Development and assessment of an efficient vadose zone module solving the 1D Richards' equation and including root extraction by plants. *Journal of Hydrology*, *323*(1-4), 258-275. https://doi.org/10.1016/j.jhydrol.2005.09.015

Varma, M., Gupta, A. K., Ghosal, P. S., & Majumder, A. (2021). A review on performance of constructed wetlands in tropical and cold climate: Insights of mechanism, role of influencing factors, and system modification in low temperature. *Sci Total Environ*, *755*(Pt 2), 142540. https://doi.org/10.1016/j.scitotenv.2020.142540

Vasconcellos, C. A. B. d., & Amorim, J. C. C. (2001). Numerical Simulation of Unsaturated Flow in Porous Media using a Mass-Conservation Model. *XVI Congresso Brasileiro De Engenharia Mecanica 16th Brazilian Congress of Mechanical Engineering*.

Veernapu, S. K., & Cherukuri, N. (2023). Effect of Shaft Speed, Crack Depth and L/D Ratio in Rotor Bearing System: using Taguchi method and ANOVA. *Research and Development in Machine Design, 6*(2), 13-25.

Verma, S., Prasad, B., & Mishra, I. M. (2010). Pretreatment of petrochemical wastewater by coagulation and flocculation and the sludge characteristics. *J Hazard Mater*, *178*(1-3), 1055-1064. https://doi.org/10.1016/j.jhazmat.2010.02.047

Von Rosenberg, D. U. (1969). *Methods for the numerical solution of partial differential equations, by Dale U. von Rosenberg*. American Elsevier Pub. Co.

Wang, Bengtsson, S., Oehmen, A., Carvalho, G., Werker, A., & Reis, M. A. (2019). Application of dissolved oxygen (DO) level control for polyhydroxyalkanoate (PHA) accumulation with concurrent nitrification in surplus municipal activated sludge. *New biotechnology*, *50*, 37-43.

Wang, Jiang, J., Zhao, Q., & Wang, K. (2022). Effects of substrate type on variation of sludge organic compounds, bioelectric production and microbial community structure in bioelectrochemically-assisted sludge treatment wetland. *Journal of Environmental Management*, *307*, 114548. https://doi.org/10.1016/j.jenvman.2022.114548

Wang, Liu, Y., Wang, J., Luo, T., Zhang, R., Sun, J., Zheng, Q., & Jiao, N. (2019, 2019/05/01/). Seasonal dynamics of bacterial communities in the surface seawater around subtropical Xiamen Island, China, as determined by 16S rRNA gene profiling. *Marine Pollution Bulletin*, *142*, 135-144. https://doi.org/https://doi.org/10.1016/j.marpolbul.2019.03.035

Wang, Zhao, Q., Jiang, J., & Wang, K. (2022, 2022/03/01/). Insight into the organic matter degradation enhancement in the bioelectrochemically-assisted sludge treatment wetland: Transformation of the organic matter and microbial community evolution. *Chemosphere*, *290*, 133259. https://doi.org/https://doi.org/10.1016/j.chemosphere.2021.133259

Wang, G., Dai, X., Zhang, D., He, Q., Dong, B., Li, N., & Ye, N. (2018). Two-phase high solid anaerobic digestion with dewatered sludge: Improved volatile solid degradation and specific methane generation by temperature and pH regulation. *Bioresource technology*, *259*, 253-258. https://doi.org/10.1016/j.biortech.2018.03.074

Wang, J., Yang, H., Liu, X., & Chang, J. (2020). The impact of temperature and dissolved oxygen (DO) on the partial nitrification of immobilized fillers, and application in municipal wastewater. *RSC advances*, *10*(61), 37194-37201.

Wanniarachchi, S., & Sarukkalige, R. (2022). A Review on Evapotranspiration Estimation in Agricultural Water Management: Past, Present, and Future. *Hydrology*, *9*(7), 123. https://www.mdpi.com/2306-5338/9/7/123

Waqas, S., & Bilad, M. R. (2019). A review on rotating biological contactors. *Indonesian Journal of Science and Technology*, *4*(2), 241-256.

Wolski, P. (2021). Analysis of rheological properties of thickened sewage sludge. *Desalination and Water Treatment*, *232*, 331-338. https://doi.org/10.5004/dwt.2021.27517

Xiang, K., Li, Y., Horton, R., & Feng, H. (2020). Similarity and difference of potential evapotranspiration and reference crop evapotranspiration – a review. *Agricultural Water Management*, *232*. https://doi.org/10.1016/j.agwat.2020.106043

Xing, B.-S., Han, Y., Wang, X. C., Cao, S., Wen, J., & Zhang, K. (2020). Acclimatization of anaerobic sludge with cow manure and realization of high-rate food waste digestion for biogas production. *Bioresource technology*, *315*, 123830. https://doi.org/10.1016/j.biortech.2020.123830

Yan, L., Liu, S., Liu, Q., Zhang, M., Liu, Y., Wen, Y., Chen, Z., Zhang, Y., & Yang, Q. (2019). Improved performance of simultaneous nitrification and denitrification via nitrite in an oxygen-limited SBR by alternating the DO. *Bioresource technology*, *275*, 153-162. https://doi.org/10.1016/j.biortech.2018.12.054

Yang, F., Zhang, H., Zhang, X., Zhang, Y., Li, J., Jin, F., & Zhou, B. (2021). Performance analysis and evaluation of the 146 rural decentralized wastewater treatment facilities surrounding the Erhai Lake. *Journal of Cleaner Production*, *315*, 128159.

Yang, Z., Li, J., Liu, J., Cao, J., Sheng, D., & Cai, T. (2019). Evaluation of a pilot-scale bio-trickling filter as a VOCs control technology for the chemical fibre wastewater treatment plant. *Journal of Environmental Management*, *246*, 71-76.

Yu, W., Yang, J., Tao, S., Shi, Y., Yu, J., Lv, Y., Liang, S., Xiao, K., Liu, B., Hou, H., Hu, J., & Wu, X. (2017). A comparatively optimization of dosages of oxidation agents based on volatile solids and dry solids content in dewatering of sewage sludge. *Water research*, *126*, 342-350. https://doi.org/10.1016/j.watres.2017.09.044

Yuan, C., Huang, T., Zhao, X., & Zhao, Y. (2020). Numerical Models of Subsurface Flow Constructed Wetlands: Review and Future Development. *Sustainability*, *12*(8). https://doi.org/10.3390/su12083498

Zahermand, S., Vafaeian, M., & Bazyar, M. H. (2020). Analysis of the physical and chemical properties of soil contaminated with oily (petroleum) hydrocarbons. *Earth Sciences Research Journal*, *24*(2), 163-168. https://doi.org/10.15446/esrj.v24n2.76217

Zhang, X.-Y., Li, Q.-W., Gao, J.-Q., Hu, Y.-H., Song, M.-H., & Yue, Y. (2020). Effects of rainfall amount and frequency on soil nitrogen mineralization in Zoigê alpine wetland. *European Journal of Soil Biology*, *97*, 103170. https://doi.org/10.1016/j.ejsobi.2020.103170

Zhang, Y., & Duan, X. (2020). Chemical precipitation of heavy metals from wastewater by using the synthetical magnesium hydroxy carbonate. *Water Science and Technology*, *81*(6), 1130-1136. https://doi.org/10.2166/wst.2020.208

Zhong, H., Liu, X., Tian, Y., Zhang, Y., & Liu, C. (2021, 2021/07/01/). Biological power generation and earthworm assisted sludge treatment wetland to remove organic matter in sludge and synchronous power generation. *Science of The Total Environment*, *776*, 145909. https://doi.org/https://doi.org/10.1016/j.scitotenv.2021.145909

Note: Every reasonable effort has been made to acknowledge the owners of copyright material. I would be pleased to hear from any copyright owner who has been omitted or incorrectly acknowledged.

APPENDICES

Appendix A: Richards' Equations – Detailed derivation (Celia & Bouloutas, 1990)

Mixed form: $$\frac{\partial \theta}{\partial t} = \frac{\partial}{\partial z}\left[K(h)\left(\frac{\partial h}{\partial z} + 1\right)\right]$$

h-based: $$C(h)\frac{\partial h}{\partial t} = \frac{\partial}{\partial z}\left[K(h)\left(\frac{\partial h}{\partial z} + 1\right)\right]$$

θ-based: $$\frac{\partial \theta}{\partial t} = \frac{\partial}{\partial z}\left[D(\theta)\left(\frac{\partial h}{\partial z} + 1\right)\right]$$

where θ = volumetric water content $[L^3/L^3]$,
$K(h)$ = unsaturated hydraulic conductivity $[L/t]$,
$C(h)$ = $d\theta/dh$ is the specific moisture capacity $[L^{-1}]$,
$D(\theta)$ = $K(h)/C(h)$ is the water diffusivity $[L^2/t]$,
h = pressure head $[L]$,
t = time $[t]$,
z = vertical coordinate assumed positive upward $[L]$.

1. **Darcy's law:**

$$q = -K(h)\frac{\partial H}{\partial z} = -K(h)\frac{\partial (h+z)}{\partial z} = -K(h)\left(\frac{\partial h}{\partial z} + 1\right)$$

where q = flux density $[L/t]$,
H = $(h + z)$ is the head equivalent of hydraulic potential $[L]$.

2. **Continuity equation:**

$$\frac{\partial \theta}{\partial t} = -\frac{\partial q}{\partial z}$$

$$\frac{\partial \theta}{\partial t} = \frac{\partial}{\partial z}\left[K(h)\left(\frac{\partial h}{\partial z} + 1\right)\right]$$

Appendix B: Penman-Monteith Equation – Detailed steps and calculations (Allen *et al.*, 1998)

$$ET_0 = \frac{1}{\lambda}\left[\frac{\Delta(R_n - G) + \rho_a c_p \frac{(e_s - e_a)}{r_a}}{\Delta + \gamma\left(1 + \frac{r_s}{r_a}\right)}\right]$$

where ET_0 = potential evapotranspiration rate (mm/d),
λ = latent heat of vaporization $(2.45\ MJ/kg)$,
Δ = slope of the vapor pressure curve $(kPa/°C)$,
R_n = net radiation at surface (MJ/m^2d),
G = soil heat flux (MJ/m^2d),
ρ_a = atmospheric density (kg/m^{-3}),
c_p = specific heat of dry air $(1.013 \times 10^{-3}\ MJ/kg°C)$,
e_s = saturation vapor pressure (kPa),
e_a = actual vapor pressure (kPa),
r_a = aerodynamic resistance (s/m),
r_s = surface resistance (s/m),
γ = psychrometric constant $(kPa/°C)$.

Step 1: Determining the net radiation at surface, R_n:

$$R_n = R_{ns} - R_{nl}$$

where R_{ns} = net solar or short-wave radiation (MJ/m^2d),
R_{nl} = net outgoing long-wave radiation (MJ/m^2d).

For the net solar or short-wave radiation, R_{ns}:

$$R_{ns} = (1 - \alpha)R_s$$

where α = albedo or the canopy reflection coefficient (0.23),
R_s = incoming solar radiation (MJ/m^2d).

For the incoming solar radiation, R_s:

$$R_s = (a_s + \frac{n}{N} b_s) R_a$$

where a_s, b_s = regression constants ($a_s = 0.25,\ b_s = 0.5$),
n = actual sunshine duration ($12\ hours$),
N = maximum possible duration of sunshine or daylight hours ($hour$),
R_a = extraterrestrial radiation (MJ/m^2d),
n/N = relative sunshine duration.

For the maximum possible duration of sunshine or daylight hours, N:

$$N = \frac{24}{\pi} \omega_s$$

where ω_s = sunset hour angle (rad).

For the sunset hour angle, ω_s:

$$\omega_s = \cos^{-1}(-\tan\varphi \tan\delta)$$

For the extraterrestrial radiation, R_a:

$$R_a = \frac{24(60)}{\pi} G_{sc} d_r (\omega_s \sin\varphi \sin\delta + \cos\varphi \cos\delta \sin\omega_s)$$

where G_{sc} = solar constant ($0.0820\ MJ/m^2min$),
d_r = inverse relative distance between the Earth and the Sun,
φ = site latitude (rad) [$Miri = 4.3995°N$],

δ = solar declination (rad).

For the relative distance between the Earth and the Sun, d_r:

$$d_r = 1 + 0.033 \cos \frac{2\pi J}{365}$$

where J = number of the day in the year.

For the solar declination, δ:

$$\delta = 0.409 \sin \left(\frac{2\pi J}{365} - 1.39 \right)$$

Thus, for the net outgoing long-wave radiation, R_{nl}:

$$R_{nl} = \sigma \left[\frac{T_{max,K}^4 + T_{min,K}^4}{2} \right] \left(0.34 - 0.14 \sqrt{e_a} \right) \left(1.35 \frac{R_s}{R_{so}} - 0.35 \right)$$

where σ = Stefan-Boltzmann constant ($4.903 \times 10^{-9}\ MJ/K^4 m^2 d$),
$T_{max,K}$ = maximum absolute temperature during the 24-hour period (℃ + 273.15),
$T_{min,K}$ = minimum absolute temperature during the 24-hour period (℃ + 273.15),
e_a = actual vapor pressure (kPa),
R_{so} = clear sky radiation ($MJ/m^2 d$),
R_s/R_{so} = relative short-wave radiation (≤ 1).

For the actual vapor pressure, e_a:

$$e_a = \frac{e^0(T_{min}) \frac{RH_{max}}{100} + e^0(T_{max}) \frac{RH_{min}}{100}}{2}$$

where $e^0(T_{min})$ = saturation vapor pressure at daily minimum temperature (kPa),
$e^0(T_{max})$ = saturation vapor pressure at daily maximum temperature (kPa),
RH_{max} = maximum relative humidity (%),
RH_{min} = minimum relative humidity (%).

For the saturation vapor pressure at minimum temperature, $e^0(T_{min})$ and maximum temperature, $e^0(T_{max})$:

$$e^0(T_{min}) = 0.6108\ exp\left[\frac{17.27\ T_{min}}{T_{min} + 237.3}\right]$$
$$e^0(T_{max}) = 0.6108\ exp\left[\frac{17.27\ T_{max}}{T_{max} + 237.3}\right]$$

where T_{min} = minimum daily air temperature (°C),
T_{max} = maximum daily air temperature (°C).

For the clear sky radiation, R_{so}:

$$R_{so} = (a_s + b_s)R_a$$

where a_s, b_s = regression constants ($a_s = 0.25,\ b_s = 0.5$),
R_a = extraterrestrial radiation (MJ/m^2d).
$a_s + b_s$ = fraction of extraterrestrial radiation reaching the earth on clear-sky days ($n = N$).

Step 2: Determining the saturation vapor pressure, e_s.

$$e_s = \frac{e^0(T_{min}) + e^0(T_{max})}{2}$$

where $e^0(T_{min})$ = saturation vapor pressure at minimum temperature (kPa),
$e^0(T_{max})$ = saturation vapor pressure at maximum temperature (kPa).

Step 3: Determining the soil heat flux, G.

For hourly or shorter period: during daytime: $G_{hr} = 0.1R_n$

during nighttime: $G_{hr} = 0.5R_n$

For 1-10 days period: $G_{day} \approx 0$

For monthly period: $G_{month,i} = 0.07(T_{month,i+1} - T_{month,i-1})$

where $T_{month,i+1}$ = mean air temperature of next month (℃),
$T_{month,i-1}$ = mean air temperature of previous month (℃).

Step 4: Determining the atmospheric density, ρ_a.

$$\rho_a = \frac{1000P}{R(273.15 + T_{mean})}$$

where P = actual atmospheric pressure (kPa),
R = specific gas constant $(287.05\ J/kgK)$,
T_{mean} = mean air temperature (℃).

For the actual atmospheric pressure, P:

$$P = 101.3\left[\frac{293 - 0.0065z}{293}\right]^{5.26}$$

where z = elevation above sea level (m) $[Miri = 8\ m]$.

For the mean air temperature, T_{mean}:

$$T_{mean} = \frac{T_{min} + T_{max}}{2}$$

where T_{min} = minimum daily air temperature (℃),
T_{max} = maximum daily air temperature (℃).

Step 5: Determining the slope of the vapor pressure curve, Δ.

$$\Delta = \frac{4098\left[0.6108\ exp\left(\frac{17.27\ T_{mean}}{T_{mean}+237.3}\right)\right]}{(T_{mean}+237.3)^2}$$

where T_{mean} = mean air temperature (℃).

Step 6: Determining the aerodynamic resistance, r_a.

$$r_a = \frac{\ln\left[\frac{z_w - d}{z_{mt}}\right]\ln\left[\frac{z_h - d}{z_{hvt}}\right]}{k^2 u_z}$$

where z_w = measurement of wind height (m),
z_{mt} = roughness length of momentum transfer (m),
d = zero plane displacement height (m),
z_h = measurement of humidity height (m),
z_{hvt} = roughness length of heat and vapor transfer (m),
k = von Karman's constant (0.41),
u_z = wind speed at heigh z (m/s).

For the roughness length of momentum transfer, z_{mt}, zero-plane displacement height, d, and roughness length of heat and vapor transfer, z_{hvt}:

$$z_{mt} = 0.123\ h$$
$$d = \frac{2}{3}\ h$$
$$z_{hvt} = 0.1\ z_{mt}$$

where h = crop height (m).

Step 7: Determining the surface resistance, r_s.

$$r_s = \frac{r_l}{LAI_{active}}$$

where r_l = bulk stomatal resistance of the well-illuminated leaf $(100\ s/m)$,
LAI_{active} = active leaf area index.

For the active leaf area index, LAI_{active}:

$$LAI_{active} = 0.5\ LAI$$

where $LAI = 24\ h$,
h = crop height (m).

Step 8: Determining the psychrometric constant, γ.

$$\gamma = \frac{c_p P}{\varepsilon \lambda}$$

where c_p = specific heat of dry air $(1.013 \times 10^{-3}\ MJ/kg℃)$,
P = actual atmospheric pressure, (kPa),
ε = ratio of molecular weight of water vapor to dry air (0.622),
λ = latent heat of vaporization $(2.45\ MJ/kg)$.

Appendix C: Cake Filtration Thickness Layer – Detailed derivation (Tien *et al.*, 1997)

$$\frac{dL}{dt} = \frac{\varepsilon_c}{\varepsilon_c - \varepsilon_s}\left(\frac{k}{\mu}\frac{\partial p}{\partial z}\right)_L - q_{l,m}$$

where L = thickness of cake layer $[L]$,
t = time $[t]$,
$\varepsilon_c \& \varepsilon_s$ = particle volume fractions on the cake and sludge side of the interface,
k = permeability coefficient $[L^2]$,
μ = liquid viscosity $[M/Lt]$,
p = pressure $[M/Lt^2]$,
z = vertical coordinate assumed positive upward $[L]$,
$q_{l,m}$ = permeation flux of filtrate through the medium (filtrate flux) $[L^3/L^2t]$.

1. **Darcy's law:**

$$\frac{q_{l,c}}{1-\varepsilon_c} - \frac{q_{s,c}}{\varepsilon_c} = \frac{k}{(1-\varepsilon_c)\mu}\left(\frac{\partial p}{\partial z}\right)$$

where $q_{l,c} \& q_{s,c}$ are the liquid and solid fluxes on the cake side at the interface $[L^3/L^2t]$.

When the boundary conditions are set to be as follow:

At medium surface $(z = 0)$: $$q_{l,m} = \left(\frac{k}{\mu}\frac{\partial p}{\partial z}\right)_0$$

At cake-sludge interface $(z = L)$: $$q_{s,c} = \frac{\varepsilon_c}{1-\varepsilon_c}\left[q_{l,c} - \left(\frac{k}{\mu}\frac{\partial p}{\partial z}\right)_L\right]$$

On the other hand, it is determined that the liquid and solid fluxes are constant throughout the sludge phase, thus:

$$\frac{q_{s,s}}{q_{l,s}} = \frac{\varepsilon_s}{1-\varepsilon_s}$$
$$q_{s,s} = q_{l,s}\left(\frac{\varepsilon_s}{1-\varepsilon_s}\right)$$

where $q_{s,c}$ and $q_{l,s}$ are the solid and liquid fluxes on the cake and sludge side at the interface $[L^3/L^2t]$, respectively.

2. Mass conservation:

For the determination of liquid flux on the cake side at the interface $q_{l,c}$ $[L^3/L^2t]$:

$$q_{l,c} + q_{s,c} = q_{l,m}$$
$$q_{l,c} + \frac{\varepsilon_c}{1-\varepsilon_c}\left[q_{l,c} - \left(\frac{k}{\mu}\frac{\partial p}{\partial z}\right)_L\right] = -\left(\frac{k}{\mu}\frac{\partial p}{\partial z}\right)_0$$
$$q_{l,c}\left(\frac{1}{1-\varepsilon_c}\right) = -\frac{\varepsilon_c}{1-\varepsilon_c}\left(\frac{k}{\mu}\frac{\partial p}{\partial z}\right)_L - \left(\frac{k}{\mu}\frac{\partial p}{\partial z}\right)_0$$
$$q_{l,c} = -\varepsilon_c\left(\frac{k}{\mu}\frac{\partial p}{\partial z}\right)_L - (1-\varepsilon_c)\left(\frac{k}{\mu}\frac{\partial p}{\partial z}\right)_0$$

For the determination of liquid flux on the sludge side at the interface $q_{l,s}$ $[L^3/L^2t]$:

$$q_{l,s} + q_{s,s} = q_{l,m}$$
$$q_{l,s} + q_{l,s}\left(\frac{\varepsilon_s}{1-\varepsilon_s}\right) = -\left(\frac{k}{\mu}\frac{\partial p}{\partial z}\right)_0$$
$$q_{l,s}\left(\frac{1}{1-\varepsilon_s}\right) = -\left(\frac{k}{\mu}\frac{\partial p}{\partial z}\right)_0$$
$$q_{l,s} = -(1-\varepsilon_s)\left(\frac{k}{\mu}\frac{\partial p}{\partial z}\right)_0$$

Thus, the change in cake filtration thickness layer over the specific time is given as:

$$\frac{dL}{dt} = \frac{q_{l,c} - q_{l,s}}{\varepsilon_s - \varepsilon_c}$$

$$\frac{dL}{dt} = \left(\frac{1}{\varepsilon_s - \varepsilon_c}\right)\left\{\left[-\varepsilon_c\left(\frac{k}{\mu}\frac{\partial p}{\partial z}\right)_L - (1-\varepsilon_c)\left(\frac{k}{\mu}\frac{\partial p}{\partial z}\right)_0\right] - \left[-(1-\varepsilon_s)\left(\frac{k}{\mu}\frac{\partial p}{\partial z}\right)_0\right]\right\}$$

$$\frac{dL}{dt} = \frac{\varepsilon_c}{\varepsilon_c - \varepsilon_s}\left(\frac{k}{\mu}\frac{\partial p}{\partial z}\right)_L - \left(\frac{k}{\mu}\frac{\partial p}{\partial z}\right)_0$$

Appendix D: Typical values of kinetic parameters and the units (Gujer *et al.*, 1999; Gujer *et al.*, 1995)

Parameter	Description	Temperature		Units
		10℃	**20**℃	
$\boldsymbol{k_H}$	Hydrolysis rate constant	2	3	g X_S g^{-1} X_H d^{-1}
$\boldsymbol{K_X}$	Hydrolysis saturation constant	1	1	g X_S g^{-1} X_H
Heterotrophs (Denitrification), $\boldsymbol{X_H}$				
$\boldsymbol{\mu_H}$	Heterotrophic maximum growth rate	1	2	d^{-1}
$\boldsymbol{K_O}$	Saturation constant for S_O	0.2	0.2	g O_2 m^{-3}
$\boldsymbol{K_S}$	Saturation constant for S_S	2	2	g COD m^{-3}
$\boldsymbol{K_{NH}}$	Saturation constant for S_{NH}	0.01	0.01	g N m^{-3}
$\boldsymbol{K_{HCO}}$	Bicarbonate saturation constant of X_H	0.1	0.1	mole HCO_3^- m^{-3}
$\boldsymbol{K_{PO}}$	Saturation constant for S_{PO}	0.01	0.01	g P m^{-3}
$\boldsymbol{\eta_{NO}}$	Anoxic reduction factor	0.6	0.6	-
$\boldsymbol{K_{NO}}$	Saturation constant for S_{NO}	0.5	0.5	g S_{NO} m^{-3}
$\boldsymbol{b_H}$	Rate constant for lysis of X_H	0.2	0.4	d^{-1}
Autotrophs (Nitrification), $\boldsymbol{X_A}$				
$\boldsymbol{\mu_A}$	Autotrophic maximum growth rate	0.35	1	d^{-1}
$\boldsymbol{K_{A,O}}$	Saturation constant for S_O of X_A	0.5	0.5	g O_2 m^{-3}
$\boldsymbol{K_{A,NH}}$	Saturation constant for S_{NH} of X_A	1	1	g N m^{-3}
$\boldsymbol{K_{A,HCO}}$	Bicarbonate saturation constant of X_A	0.5	0.5	mole HCO_3^- m^{-3}
$\boldsymbol{K_{A,PO}}$	Saturation constant for S_{PO} of X_A	0.01	0.01	g P m^{-3}
$\boldsymbol{b_A}$	Rate constant for lysis of X_A	0.05	0.15	d^{-1}

For any other temperature circumstances:

$$k(T) = k(20℃) \cdot \exp[\theta_T \cdot (T - 20℃)]$$

where θ_T [$℃^{-1}$] is obtained from:

$$\theta_T = \frac{\ln\left[\frac{k(T_1)}{k(T_2)}\right]}{T_1 - T_2}$$

Appendix E: Model Components and Typical Wastewater Composition (Primary Effluent (Gujer *et al.*, 1999; Gujer *et al.*, 1995)

$COD_{Total} = 260\ g\ COD\ m^{-3}$; $TKN = 25\ g\ N\ m^{-3}$; $TP = 6\ g\ P\ m^{-3}$		
Soluble Components		
Parameter	**Description**	**Concentration Units**
S_O	Dissolved oxygen	0 g O_2 m^{-3}
S_I	Soluble inert organics	30 g COD m^{-3}
S_S	Readily biodegradable substrates	100 g COD m^{-3}
S_{NH}	Ammonium	16 g N m^{-3}
S_N	Dinitrogen (Denitrification)	0 g N m^{-3}
S_{NO}	Nitrite	0 g N m^{-3}
S_{HCO}	Bicarbonate (Alkalinity)	5 mole HCO_3^- m^{-3}
S_{PO}	Phosphate	3.6 g P m^{-3}
Particulate Components		
X_I	Inert particulate organics	25 g COD m^{-3}
X_S	Slowly biodegradable substrates	75 g COD m^{-3}
X_H	Heterotrophic biomass	30 g COD m^{-3}
X_A	Autotrophic, nitrifying biomass	0 g COD m^{-3}

Appendix F: Velocity-based RE – Detailed derivation (Bruce, 2011)

$$v_i = \frac{dz_i}{dt} = \frac{1}{\theta}\left\{\gamma_i\left(K\left[\frac{\partial h}{\partial z}+1\right]_a^b + \left[\theta\frac{dz_i}{dt}\right]_a^b\right) - K\left[\frac{\partial h}{\partial z}+1\right]_a^{z_i(t)} + \left[\theta\frac{dz_i}{dt}\right]_a\right\}$$

where
- v_i = hydraulic velocity $[L/t]$,
- z_i = vertical coordinate assumed positive downward $[L]$,
- t = time $[t]$,
- θ = volumetric water content $[L^3/L^3]$,
- γ_i = fractional integral constant in time,
- K = hydraulic conductivity $[L/t]$,
- h = pressure head $[L]$,
- $a\&b$ = specific coordinates at two extreme locations $[L]$ depending on the boundary conditions, respectively,
- $z_i(t)$ = dz_i/dt is the differential of vertical coordinate with respect to time $[L/t]$.

From the time constant equation, γ_i based on the fractional integral of θ with respect to space coordinate, z:

$$\frac{\int_a^{z_i(t)}\theta dz}{\int_a^b \theta dz} = \gamma_i$$

By differentiating the equation using Quotient rule with respect to time, t and substituting in γ_i:

$$\frac{\frac{d}{dt}\int_a^{z_i(t)}\theta dz \int_a^b \theta dz}{\left[\int_a^b \theta dz\right]^2} - \frac{\frac{d}{dt}\int_a^b \theta dz \int_a^{z_i(t)}\theta dz}{\left[\int_a^b \theta dz\right]^2} = 0$$

$$\frac{\frac{d}{dt}\int_a^{z_i(t)}\theta dz}{\int_a^b \theta dz} - \frac{\frac{d}{dt}\int_a^b \theta dz \cdot \gamma_i}{\int_a^b \theta dz} = 0$$

$$\gamma_i \frac{d}{dt}\int_a^b \theta dz = \frac{d}{dt}\int_a^{z_i(t)} \theta dz$$

Meanwhile, by using Leibniz rule:

$$\frac{d}{dt}\int \theta dz = \int \left[\frac{\partial \theta}{\partial t} + \frac{\partial}{\partial z}\left(\theta \frac{dz}{dt}\right)\right] dz$$

Thus, when substituting the equation obtained by Leibniz rule into the previous equation:

$$\gamma_i \int_a^b \left[\frac{\partial \theta}{\partial t} + \frac{\partial}{\partial z}\left(\theta \frac{dz_i}{dt}\right)\right] dz = \int_a^{z_i(t)} \left[\frac{\partial \theta}{\partial t} + \frac{\partial}{\partial z}\left(\theta \frac{dz_i}{dt}\right)\right] dz$$

Since we are dealing with mixed form of RE, hence:

$$\gamma_i \int_a^b \left\{\frac{\partial}{\partial z}\left[K\frac{\partial h}{\partial z} + 1\right] + \frac{\partial}{\partial z}\left(\theta \frac{dz_i}{dt}\right)\right\} dz = \int_a^{z_i(t)} \frac{\partial}{\partial z}\left[K\frac{\partial h}{\partial z} + 1\right] + \frac{\partial}{\partial z}\left(\theta \frac{dz_i}{dt}\right) dz$$

When we intended to transform the equation into velocity-based, the equation is rearranged by expanding the integrals:

$$\left[K\frac{\partial h}{\partial z} + 1\right]_a^b \gamma_i + \left[\theta \frac{dz_i}{dt}\right]_a^b \gamma_i = \left[K\frac{\partial h}{\partial z} + 1\right]_a^{z_i(t)} + \left[\theta \frac{dz_i}{dt}\right]_a^{z_i(t)}$$

$$\left[K\frac{\partial h}{\partial z} + 1\right]_a^b \gamma_i + \left[\theta \frac{dz_i}{dt}\right]_a^b \gamma_i = \left[K\frac{\partial h}{\partial z} + 1\right]_a^{z_i(t)} + \left[\theta \frac{dz_i}{dt}\right]^{z_i(t)} - \left[\theta \frac{dz_i}{dt}\right]_a$$

Therefore, the final expression of velocity based RE is presented as:

$$\frac{dz_i}{dt} = \frac{1}{\theta}\left\{\gamma_i\left(\left[K\frac{\partial h}{\partial z} + 1\right]_a^b + \left[\theta \frac{dz_i}{dt}\right]_a^b\right) - \left[K\frac{\partial h}{\partial z} + 1\right]_a^{z_i(t)} + \left[\theta \frac{dz_i}{dt}\right]_a\right\}$$

Appendix G: Velocity-based ADE – Detailed derivation

$$v_i = \frac{dz_i}{dt} = \frac{1}{c_{mo}}\left\{\gamma_i\left(\left[\left(\frac{\theta_{mo}D_{mo}}{\theta_{mo}+\rho f F_{mo}K_d}\right)\left(\frac{\partial c_{mo}}{\partial z}\right)-\left(\frac{q_{mo}}{\theta_{mo}+\rho f F_{mo}K_d}\right)\left(\frac{\partial c_{mo}}{\partial z}\right)\right]_a^b + \left[c_{mo}\frac{dz_i}{dt}\right]_a^b\right) - \left[\left(\frac{\theta_{mo}D_{mo}}{\theta_{mo}+\rho f F_{mo}K_d}\right)\left(\frac{\partial c_{mo}}{\partial z}\right)-\left(\frac{q_{mo}}{\theta_{mo}+\rho f F_{mo}K_d}\right)\left(\frac{\partial c_{mo}}{\partial z}\right)\right]_a^{z_i(t)} + \left[c_{mo}\frac{dz_i}{dt}\right]_a\right\}$$

where v_i = solute velocity $[L/t]$,
z_i = vertical coordinate assumed positive downward $[L]$,
t = time $[t]$,
c_{mo} = solute concentration at mobile region $[M/L^3]$,
γ_i = fractional integral constant in time,
θ_{mo} = volumetric water content in mobile region $[L^3/L^3]$,
D_{mo} = dispersion coefficient in mobile region $[L^2/t]$,
ρ = soil bulk density $[M/L^3]$,
f = fraction of sorption sites in contact with mobile region,
F_{mo} = the mass fraction of all sites occupied in instantaneous equilibrium at the mobile region,
K_d = distribution coefficient obtained from the slope of isotherm curve $[L^3/M]$,
q_{mo} = volumetric fluid flux in mobile region $[L/t]$,
$a\&b$ = specific coordinates at two extreme locations $[L]$ depending on the boundary conditions, respectively,
$z_i(t)$ = dz_i/dt is the differential of vertical coordinate with respect to time $[L/t]$.

By rearranging the ADE:

$$\frac{\partial c_{mo}}{\partial t} + \frac{\rho f F_{mo} K_d}{\theta_{mo}} \frac{\partial c_{mo}}{\partial t} = \frac{\partial}{\partial z}\left(D_{mo} \frac{\partial c_{mo}}{\partial z}\right) - \frac{q_{mo}}{\theta_{mo}} \frac{\partial}{\partial z}\left(\frac{\partial c_{mo}}{\partial z}\right)$$

$$\left(1 + \frac{\rho f F_{mo} K_d}{\theta_{mo}}\right) \frac{\partial c_{mo}}{\partial t} = \frac{\partial}{\partial z}\left(D_{mo} \frac{\partial c_{mo}}{\partial z}\right) - \frac{q_{mo}}{\theta_{mo}} \frac{\partial}{\partial z}\left(\frac{\partial c_{mo}}{\partial z}\right)$$

$$\frac{\partial c_{mo}}{\partial t} = \left(\frac{\theta_{mo}}{\theta_{mo} + \rho f F_{mo} K_d}\right)\left[\frac{\partial}{\partial z}\left(D_{mo} \frac{\partial c_{mo}}{\partial z}\right) - \frac{q_{mo}}{\theta_{mo}} \frac{\partial}{\partial z}\left(\frac{\partial c_{mo}}{\partial z}\right)\right]$$

$$\frac{\partial c_{mo}}{\partial t} = \left(\frac{\theta_{mo}}{\theta_{mo} + \rho f F_{mo} K_d}\right) \frac{\partial}{\partial z}\left(D_{mo} \frac{\partial c_{mo}}{\partial z}\right) - \left(\frac{q_{mo}}{\theta_{mo} + \rho f F_{mo} K_d}\right) \frac{\partial}{\partial z}\left(\frac{\partial c_{mo}}{\partial z}\right)$$

From the time constant equation, γ_i based on the fractional integral of c with respect to space coordinate, z:

$$\frac{\int_a^{z_i(t)} c dz}{\int_a^b c dz} = \gamma_i$$

By differentiating the equation using Quotient rule with respect to time, t and substituting in γ_i:

$$\frac{\frac{d}{dt}\int_a^{z_i(t)} c dz \int_a^b c dz}{\left[\int_a^b c dz\right]^2} - \frac{\frac{d}{dt}\int_a^b c dz \int_a^{z_i(t)} c dz}{\left[\int_a^b c dz\right]^2} = 0$$

$$\frac{\frac{d}{dt}\int_a^{z_i(t)} c dz}{\int_a^b c dz} - \frac{\frac{d}{dt}\int_a^b c dz \cdot \gamma_i}{\int_a^b c dz} = 0$$

$$\gamma_i \frac{d}{dt}\int_a^b c dz = \frac{d}{dt}\int_a^{z_i(t)} c dz$$

Meanwhile, by using Leibniz rule:

$$\frac{d}{dt}\int c dz = \int \left[\frac{\partial c}{\partial t} + \frac{\partial}{\partial z}\left(c \frac{dz}{dt}\right)\right] dz$$

Thus, when substituting the equation obtained by Leibniz rule into the previous equation:

$$\gamma_i \int_a^b \left[\frac{\partial c}{\partial t} + \frac{\partial}{\partial z}\left(c\frac{dz_i}{dt}\right)\right] dz = \int_a^{z_i(t)} \left[\frac{\partial c}{\partial t} + \frac{\partial}{\partial z}\left(c\frac{dz_i}{dt}\right)\right] dz$$

Since we are dealing with ADE in this case, hence:

$$\begin{aligned}\gamma_i \int_a^b \Bigg\{ &\left(\frac{\theta_{mo}}{\theta_{mo} + \rho f F_{mo} K_d}\right)\frac{\partial}{\partial z}\left(D_{mo}\frac{\partial c_{mo}}{\partial z}\right) - \left(\frac{q_{mo}}{\theta_{mo} + \rho f F_{mo} K_d}\right)\frac{\partial}{\partial z}\left(\frac{\partial c_{mo}}{\partial z}\right) \\ &+ \frac{\partial}{\partial z}\left(c_{mo}\frac{dz_i}{dt}\right)\Bigg\} dz \\ &= \int_a^{z_i(t)} \left(\frac{\theta_{mo}}{\theta_{mo} + \rho f F_{mo} K_d}\right)\frac{\partial}{\partial z}\left(D_{mo}\frac{\partial c_{mo}}{\partial z}\right) \\ &- \left(\frac{q_{mo}}{\theta_{mo} + \rho f F_{mo} K_d}\right)\frac{\partial}{\partial z}\left(\frac{\partial c_{mo}}{\partial z}\right) + \frac{\partial}{\partial z}\left(c_{mo}\frac{dz_i}{dt}\right) dz\end{aligned}$$

When we intended to transform the equation into velocity-based, the equation is rearranged by expanding the integrals:

$$\begin{aligned}&\left[\left(\frac{\theta_{mo} D_{mo}}{\theta_{mo} + \rho f F_{mo} K_d}\right)\left(\frac{\partial c_{mo}}{\partial z}\right) - \left(\frac{q_{mo}}{\theta_{mo} + \rho f F_{mo} K_d}\right)\left(\frac{\partial c_{mo}}{\partial z}\right)\right]_a^b \gamma_i + \left[c_{mo}\frac{dz_i}{dt}\right]_a^b \gamma_i \\ &\quad = \left[\left(\frac{\theta_{mo} D_{mo}}{\theta_{mo} + \rho f F_{mo} K_d}\right)\left(\frac{\partial c_{mo}}{\partial z}\right) - \left(\frac{q_{mo}}{\theta_{mo} + \rho f F_{mo} K_d}\right)\left(\frac{\partial c_{mo}}{\partial z}\right)\right]_a^{z_i(t)} \\ &\quad + \left[c_{mo}\frac{dz_i}{dt}\right]_a^{z_i(t)} \\ &\left[\left(\frac{\theta_{mo} D_{mo}}{\theta_{mo} + \rho f F_{mo} K_d}\right)\left(\frac{\partial c_{mo}}{\partial z}\right) - \left(\frac{q_{mo}}{\theta_{mo} + \rho f F_{mo} K_d}\right)\left(\frac{\partial c_{mo}}{\partial z}\right)\right]_a^b \gamma_i + \left[c_{mo}\frac{dz_i}{dt}\right]_a^b \gamma_i \\ &\quad = \left[\left(\frac{\theta_{mo} D_{mo}}{\theta_{mo} + \rho f F_{mo} K_d}\right)\left(\frac{\partial c_{mo}}{\partial z}\right) - \left(\frac{q_{mo}}{\theta_{mo} + \rho f F_{mo} K_d}\right)\left(\frac{\partial c_{mo}}{\partial z}\right)\right]_a^{z_i(t)} \\ &\quad + \left[c_{mo}\frac{dz_i}{dt}\right]^{z_i(t)} - \left[c_{mo}\frac{dz_i}{dt}\right]_a\end{aligned}$$

Therefore, by rearranging and substituting the term ($dz_i/dt = q/\theta$), the final expression of the velocity-based ADE is presented as:

$$\frac{dz_i}{dt} = \frac{1}{c_{mo}}\left\{\gamma_i\left(\left[\left(\frac{\theta_{mo}D_{mo}}{\theta_{mo}+\rho f F_{mo}K_d}\right)\left(\frac{\partial c_{mo}}{\partial z}\right) - \left(\frac{q_{mo}}{\theta_{mo}+\rho f F_{mo}K_d}\right)\left(\frac{\partial c_{mo}}{\partial z}\right)\right]_a^b + \left[c_{mo}\frac{q_{mo}}{\theta_{mo}}\right]_a^b\right) - \left[\left(\frac{\theta_{mo}D_{mo}}{\theta_{mo}+\rho f F_{mo}K_d}\right)\left(\frac{\partial c_{mo}}{\partial z}\right) - \left(\frac{q_{mo}}{\theta_{mo}+\rho f F_{mo}K_d}\right)\left(\frac{\partial c_{mo}}{\partial z}\right)\right]_a^{z_i(t)} + \left[c_{mo}\frac{q_{mo}}{\theta_{mo}}\right]_a\right\}$$

Appendix H: Fixed Mesh ADE – Detailed derivation (Bresler, 1973)

$$\frac{\partial \theta c}{\partial t} = \frac{\partial}{\partial z}\left(D\frac{\partial c}{\partial z} - qc\right) \tag{1}$$

Determination of the time derivative function, $\frac{\partial \theta c}{\partial t}$ on the LHS of Equation (1):

Generally, the time derivative partial differential equation, $\frac{\partial \theta c}{\partial t}$ can be written in the following form as shown in Equation (2) and each of the terms are put in Taylor's series expansion, as follows:

$$\left(\frac{\partial \theta c}{\partial t}\right)_i^{n+\frac{1}{2}} = \theta_i^{n+\frac{1}{2}}\left(\frac{\partial c}{\partial t}\right)_i^{n+\frac{1}{2}} + c_i^{n+\frac{1}{2}}\left(\frac{\partial \theta}{\partial t}\right)_i^{n+\frac{1}{2}} \tag{2}$$

where

$$\theta_i^{n+\frac{1}{2}} = \frac{\theta_i^{n+1} - \theta_i^n}{2} - \left[\frac{(\Delta t)^2}{8}\frac{\partial^2 \theta}{\partial t^2}\right]_i^{n+\frac{1}{2}} + O(\Delta t)^3 \tag{3}$$

$$\left(\frac{\partial c}{\partial t}\right)_i^{n+\frac{1}{2}} = \frac{c_i^{n+1} - c_i^n}{\Delta t} + O(\Delta t)^2 \tag{4}$$

$$c_i^{n+\frac{1}{2}} = \frac{c_i^{n+1} - c_i^n}{2} - \left[\frac{(\Delta t)^2}{8}\frac{\partial^2 c}{\partial t^2}\right]_i^{n+\frac{1}{2}} + O(\Delta t)^3 \tag{5}$$

$$\left(\frac{\partial \theta}{\partial t}\right)_i^{n+\frac{1}{2}} = \frac{\theta_i^{n+1} - \theta_i^n}{\Delta t} + O(\Delta t)^2 \tag{6}$$

and $O(\Delta t)$ is the truncation error. Thus, by substituting Equations (3), (4), (5), and (6) into Equation (2), we have:

$$\left(\frac{\partial \theta c}{\partial t}\right)_i^{n+\frac{1}{2}} = \frac{\theta_i^{n+1} c_i^{n+1} - \theta_i^n c_i^n}{\Delta t} - \frac{\Delta t}{8}\left[\frac{\partial^2 \theta}{\partial t^2}(c_i^{n+1} - c_i^n) + \left(\frac{\partial^2 c}{\partial t^2}\right)_i^{n+\frac{1}{2}}(\theta_i^{n+1} - \theta_i^n)\right] + O(\Delta t)^2 \quad (7)$$

When the term, $\frac{\partial^2 \theta}{\partial t^2}$ and truncation error, $O(\Delta t)^2$ is neglected, we can simplify Equation (7) becomes:

$$\left(\frac{\partial \theta c}{\partial t}\right)_i^{n+\frac{1}{2}} = \frac{\theta_i^{n+1} c_i^{n+1} - \theta_i^n c_i^n}{\Delta t} - \frac{\Delta t}{8}\left[(c_i^{n+1} - c_i^n) + \left(\frac{\partial^2 c}{\partial t^2}\right)_i^{n+\frac{1}{2}}(\theta_i^{n+1} - \theta_i^n)\right] \quad (8)$$

On the other hand, by ignoring the dispersion term, $D\frac{\partial c}{\partial z}$ on the LHS of Equation (1), we get:

$$\left(\frac{\partial \theta c}{\partial t}\right)_i^{n+\frac{1}{2}} = -\left(\frac{\partial q c}{\partial z}\right)_i^{n+\frac{1}{2}} \quad (9)$$

When the entire Equation (9) is divided by θ on both sides where it is determined that $\theta = q/V$, the equation becomes:

$$\left(\frac{\partial c}{\partial t}\right)_i^{n+\frac{1}{2}} = -\left(V\frac{\partial c}{\partial z}\right)_i^{n+\frac{1}{2}} \quad (10)$$

Then, by taking the second derivative on Equation (10) with respect to time and space, respectively, we obtain:

$$\left(\frac{\partial^2 c}{\partial t^2}\right)_i^{n+\frac{1}{2}} = -\left(\frac{\partial V}{\partial t}\frac{\partial c}{\partial z} + V\frac{\partial^2 c}{\partial t \partial z}\right)_i^{n+\frac{1}{2}} \quad (11)$$

$$\left(\frac{\partial^2 c}{\partial t \partial z}\right)_i^{n+\frac{1}{2}} = -\frac{\partial}{\partial z}\left(V\frac{\partial c}{\partial z}\right)_i^{n+\frac{1}{2}} \tag{12}$$

Thus, by substituting Equation (12) into Equation (11), it gives:

$$\left(\frac{\partial^2 c}{\partial t^2}\right)_i^{n+\frac{1}{2}} = V_i^{n+\frac{1}{2}}\frac{\partial}{\partial z}\left(V_i^{n+\frac{1}{2}}\frac{\partial c_i^{n+\frac{1}{2}}}{\partial z}\right) - \frac{\partial V}{\partial t}\frac{\partial c}{\partial z} \tag{13}$$

Meanwhile, by solving the term, $\frac{\partial}{\partial z}\left(V_i^{n+\frac{1}{2}}\frac{\partial c_i^{n+\frac{1}{2}}}{\partial z}\right)$ and when the last term, $\frac{\partial V}{\partial t}\frac{\partial c}{\partial z}$ on the RHS of Equation (13) is negligible, the equation is displayed as:

$$\left(\frac{\partial^2 c}{\partial t^2}\right)_i^{n+\frac{1}{2}} = V_i^{n+\frac{1}{2}}\left[\frac{V_{i-\frac{1}{2}}^{n+\frac{1}{2}}\left(c_{i-1}^{n+\frac{1}{2}} - c_i^{n+\frac{1}{2}}\right)}{(\Delta z)^2} - \frac{V_{i+\frac{1}{2}}^{n+\frac{1}{2}}\left(c_i^{n+\frac{1}{2}} - c_{i+1}^{n+\frac{1}{2}}\right)}{(\Delta z)^2}\right] \tag{14}$$

Therefore, by substituting Equation (14) into Equation (8), we have:

$$\begin{aligned}\left(\frac{\partial \theta c}{\partial t}\right)_i^{n+\frac{1}{2}} = {} & \frac{\theta_i^{n+1}c_i^{n+1} - \theta_i^n c_i^n}{\Delta t} \\ & - \frac{V_i^{n+\frac{1}{2}}\Delta t(\theta_i^{n+1} - \theta_i^n)}{8(\Delta z)^2}\left[V_{i-\frac{1}{2}}^{n+\frac{1}{2}}\left(c_{i-1}^{n+\frac{1}{2}} - c_i^{n+\frac{1}{2}}\right)\right. \\ & \left. - V_{i+\frac{1}{2}}^{n+\frac{1}{2}}\left(c_i^{n+\frac{1}{2}} - c_{i+1}^{n+\frac{1}{2}}\right)\right]\end{aligned} \tag{15}$$

where

$$c_{i-1}^{n+\frac{1}{2}} = \frac{c_{i-1}^{n+1} + c_{i-1}^n}{2} \tag{16}$$

$$c_i^{n+\frac{1}{2}} = \frac{c_i^{n+1} + c_i^n}{2} \tag{17}$$

$$c_{i+1}^{n+\frac{1}{2}} = \frac{c_{i+1}^{n+1} + c_{i+1}^n}{2} \tag{18}$$

Lastly, by substituting Equation (16), (17), and (18) into Equation (15), we would get:

$$\left(\frac{\partial \theta c}{\partial t}\right)_i^{n+\frac{1}{2}} = \frac{\theta_i^{n+1} c_i^{n+1} - \theta_i^n c_i^n}{\Delta t} - \frac{V_i^{n+\frac{1}{2}} \Delta t(\theta_i^{n+1} - \theta_i^n)}{16(\Delta z)^2} \left[V_{i-\frac{1}{2}}^{n+\frac{1}{2}} (c_{i-1}^{n+1} + c_{i-1}^n - c_i^{n+1} - c_i^n) - V_{i+\frac{1}{2}}^{n+\frac{1}{2}} (c_i^{n+1} + c_i^n - c_{i+1}^{n+1} - c_{i+1}^n) \right] \tag{19}$$

Determination of the dispersion term, $\frac{\partial}{\partial z}\left(D\frac{\partial c}{\partial z}\right)$ on the RHS of the Equation (1):

By referring to the Equation (14), the newly formed equation is given as:

$$\left[\frac{\partial}{\partial z}\left(D\frac{\partial c}{\partial z}\right)\right]_i^{n+\frac{1}{2}} = \frac{D_{i-\frac{1}{2}}^{n+\frac{1}{2}} \left(c_{i-1}^{n+\frac{1}{2}} - c_i^{n+\frac{1}{2}}\right)}{(\Delta z)^2} - \frac{D_{i+\frac{1}{2}}^{n+\frac{1}{2}} \left(c_i^{n+\frac{1}{2}} - c_{i+1}^{n+\frac{1}{2}}\right)}{(\Delta z)^2} \tag{20}$$

In the end, by substituting Equation (16), (17), and (18) into Equation (20), we would get:

$$\left[\frac{\partial}{\partial z}\left(D\frac{\partial c}{\partial z}\right)\right]_i^{n+\frac{1}{2}} = \frac{D_{i-\frac{1}{2}}^{n+\frac{1}{2}} (c_{i-1}^{n+1} + c_{i-1}^n - c_i^{n+1} - c_i^n)}{2(\Delta z)^2} - \frac{D_{i+\frac{1}{2}}^{n+\frac{1}{2}} (c_i^{n+1} + c_i^n - c_{i+1}^{n+1} - c_{i+1}^n)}{2(\Delta z)^2} \tag{21}$$

Determination of the last term, $\frac{\partial qc}{\partial z}$ on the RHS of the Equation (1):

Firstly, by expressing the components, $\left(q_{i+\frac{1}{2}}^{n+\frac{1}{2}},\ q_{i-\frac{1}{2}}^{n+\frac{1}{2}},\ c_{i-1}^{n+\frac{1}{2}}\right)$ in Taylor's series expansion, we have:

$$q_{i+\frac{1}{2}}^{n+\frac{1}{2}} = q_i^{n+\frac{1}{2}} + \frac{\Delta z}{2}\left(\frac{\partial q}{\partial z}\right)_i^{n+\frac{1}{2}} + \frac{(\Delta z)^2}{8}\left(\frac{\partial^2 q}{\partial t^2}\right)_i^{n+\frac{1}{2}} + O(\Delta z)^3 \tag{22}$$

$$q_{i-\frac{1}{2}}^{n+\frac{1}{2}} = q_i^{n+\frac{1}{2}} - \frac{\Delta z}{2}\left(\frac{\partial q}{\partial z}\right)_i^{n+\frac{1}{2}} + \frac{(\Delta z)^2}{8}\left(\frac{\partial^2 q}{\partial t^2}\right)_i^{n+\frac{1}{2}} - O(\Delta z)^3 \tag{23}$$

$$c_{i-1}^{n+\frac{1}{2}} = c_i^{n+\frac{1}{2}} + \Delta z\left(\frac{\partial c}{\partial z}\right)_i^{n+\frac{1}{2}} + \frac{(\Delta z)^2}{2}\left(\frac{\partial^2 c}{\partial t^2}\right)_i^{n+\frac{1}{2}} - O(\Delta z)^3 \tag{24}$$

Then, by subtracting the products of $\frac{q_{i+\frac{1}{2}}^{n+\frac{1}{2}} c_i^{n+\frac{1}{2}}}{\Delta z}$ and $\frac{q_{i-\frac{1}{2}}^{n+\frac{1}{2}} c_{i-1}^{n+\frac{1}{2}}}{\Delta z}$, the residue of the equation is shown below:

$$\left(\frac{\partial qc}{\partial z}\right)_i^{n+\frac{1}{2}} = \frac{q_{i+\frac{1}{2}}^{n+\frac{1}{2}} c_i^{n+\frac{1}{2}} - q_{i-\frac{1}{2}}^{n+\frac{1}{2}} c_{i-1}^{n+\frac{1}{2}}}{\Delta z} + \frac{\Delta z}{2}\frac{\partial}{\partial z}\left(q\frac{\partial c}{\partial z}\right)_i^{n+\frac{1}{2}} + O(\Delta z)^2 \tag{25}$$

Thus, the term, $\frac{\partial}{\partial z}\left(q\frac{\partial c}{\partial z}\right)_i^{n+\frac{1}{2}}$ is solved by second-order finite difference approximation, as follow:

$$\frac{\partial}{\partial z}\left(q\frac{\partial c}{\partial z}\right)_i^{n+\frac{1}{2}} = \frac{q_{i-\frac{1}{2}}^{n+\frac{1}{2}}\left(c_{i-1}^{n+\frac{1}{2}} - c_i^{n+\frac{1}{2}}\right)}{(\Delta z)^2} - \frac{q_{i+\frac{1}{2}}^{n+\frac{1}{2}}\left(c_i^{n+\frac{1}{2}} - c_{i+1}^{n+\frac{1}{2}}\right)}{(\Delta z)^2} \tag{26}$$

By substituting Equation (26) into Equation (25) and ignore the truncation error, $O(\Delta z)^2$, the new equation is given as:

$$\left(\frac{\partial qc}{\partial z}\right)_i^{n+\frac{1}{2}} = \frac{q_{i+\frac{1}{2}}^{n+\frac{1}{2}} c_i^{n+\frac{1}{2}} - q_{i-\frac{1}{2}}^{n+\frac{1}{2}} c_{i-1}^{n+\frac{1}{2}}}{\Delta z} + \left[\frac{q_{i-\frac{1}{2}}^{n+\frac{1}{2}}\left(c_{i-1}^{n+\frac{1}{2}} - c_i^{n+\frac{1}{2}}\right)}{2\Delta z} - \frac{q_{i+\frac{1}{2}}^{n+\frac{1}{2}}\left(c_i^{n+\frac{1}{2}} - c_{i+1}^{n+\frac{1}{2}}\right)}{2\Delta z}\right] \quad (27)$$

Finally, by inserting the Equations (16), (17), and (18) into Equation (27), we would get:

$$\left(\frac{\partial qc}{\partial z}\right)_i^{n+\frac{1}{2}} = \frac{q_{i+\frac{1}{2}}^{n+\frac{1}{2}}(c_i^{n+1} + c_i^n) - q_{i-\frac{1}{2}}^{n+\frac{1}{2}}(c_{i-1}^{n+1} + c_{i-1}^n)}{2\Delta z} + \left[\frac{q_{i-\frac{1}{2}}^{n+\frac{1}{2}}(c_{i-1}^{n+1} + c_{i-1}^n - c_i^{n+1} - c_i^n)}{4\Delta z} - \frac{q_{i+\frac{1}{2}}^{n+\frac{1}{2}}(c_i^{n+1} + c_i^n - c_{i+1}^{n+1} - c_{i+1}^n)}{4\Delta z}\right] \quad (28)$$

Appendix I: Rearrangement of the Advective-Dispersion Equation (ADE) – Detailed steps

$$\frac{\theta_i^{n+1}c_i^{n+1} - \theta_i^n c_i^n}{\Delta t} = \frac{D_{i-\frac{1}{2}}^{n+\frac{1}{2}}(c_{i-1}^{n+1} + c_{i-1}^n - c_i^{n+1} - c_i^n)}{2(\Delta z)^2} - \frac{D_{i+\frac{1}{2}}^{n+\frac{1}{2}}(c_i^{n+1} + c_i^n - c_{i+1}^{n+1} - c_{i+1}^n)}{2(\Delta z)^2} - \frac{\left[q_{i+\frac{1}{2}}^{n+\frac{1}{2}}(c_i^{n+1} + c_i^n) - q_{i-\frac{1}{2}}^{n+\frac{1}{2}}(c_{i-1}^{n+1} + c_{i-1}^n)\right]}{2\Delta z} \quad (1)$$

where

$$D_{i-\frac{1}{2}}^{n+\frac{1}{2}} = \frac{D_{i-\frac{1}{2}}^{n+1} + D_{i-\frac{1}{2}}^n}{2} \quad (2)$$

$$D_{i+\frac{1}{2}}^{n+\frac{1}{2}} = \frac{D_{i+\frac{1}{2}}^{n+1} + D_{i+\frac{1}{2}}^n}{2} \quad (3)$$

$$q_{i+\frac{1}{2}}^{n+\frac{1}{2}} = \frac{q_{i+\frac{1}{2}}^{n+1} + q_{i+\frac{1}{2}}^n}{2} \quad (4)$$

$$q_{i-\frac{1}{2}}^{n+\frac{1}{2}} = \frac{q_{i-\frac{1}{2}}^{n+1} + q_{i-\frac{1}{2}}^n}{2} \quad (5)$$

When substituting Equation (2), (3), (4), and (5) into Equation (1), we get:

$$\frac{\theta_i^{n+1}c_i^{n+1} - \theta_i^n c_i^n}{\Delta t} \tag{6}$$
$$= \frac{D_{i-\frac{1}{2}}^{n+1}(c_{i-1}^{n+1} + c_{i-1}^n - c_i^{n+1} - c_i^n)}{4(\Delta z)^2}$$
$$+ \frac{D_{i-\frac{1}{2}}^{n}(c_{i-1}^{n+1} + c_{i-1}^n - c_i^{n+1} - c_i^n)}{4(\Delta z)^2}$$
$$- \frac{D_{i+\frac{1}{2}}^{n+1}(c_i^{n+1} + c_i^n - c_{i+1}^{n+1} - c_{i+1}^n)}{4(\Delta z)^2}$$
$$- \frac{D_{i+\frac{1}{2}}^{n}(c_i^{n+1} + c_i^n - c_{i+1}^{n+1} - c_{i+1}^n)}{4(\Delta z)^2}$$
$$- \frac{\left[q_{i+\frac{1}{2}}^{n+1}(c_i^{n+1} + c_i^n) + q_{i+\frac{1}{2}}^{n}(c_i^{n+1} + c_i^n)\right]}{4\Delta z}$$
$$+ \frac{\left[q_{i-\frac{1}{2}}^{n+1}(c_{i-1}^{n+1} + c_{i-1}^n) + q_{i-\frac{1}{2}}^{n}(c_{i-1}^{n+1} + c_{i-1}^n)\right]}{4\Delta z}$$

Then, Equation (6) is expanded and plugged in the following equations:

$$D_{i-\frac{1}{2}}^{n+1}c_{i-1}^n + D_{i+\frac{1}{2}}^{n+1}c_{i+1}^n = 2D_i^{n+1}c_i^n \tag{7}$$
$$D_{i-\frac{1}{2}}^{n+1}c_i^n + D_{i+\frac{1}{2}}^{n+1}c_i^n = 2D_i^{n+1}c_i^n \tag{8}$$
$$D_{i-\frac{1}{2}}^{n}c_{i-1}^{n+1} + D_{i+\frac{1}{2}}^{n}c_{i+1}^{n+1} = 2D_i^{n+1}c_i^n \tag{9}$$
$$D_{i-\frac{1}{2}}^{n}c_i^{n+1} + D_{i+\frac{1}{2}}^{n}c_i^{n+1} = 2D_i^{n+1}c_i^n \tag{10}$$

Hence, when Equation (8 – 7) and Equation (10 – 9), the residual of the solution is equivalent to zero. Therefore, the new equation becomes:

$$\frac{\theta_i^{n+1}c_i^{n+1}-\theta_i^{n}c_i^{n}}{\Delta t} \tag{11}$$
$$= \frac{D^{n+1}_{i-\frac{1}{2}}(c^{n+1}_{i-1}-c_i^{n+1})}{4(\Delta z)^2}+\frac{D^{n}_{i-\frac{1}{2}}(c^{n}_{i-1}-c_i^{n})}{4(\Delta z)^2}-\frac{D^{n+1}_{i+\frac{1}{2}}(c_i^{n+1}-c^{n+1}_{i+1})}{4(\Delta z)^2}$$
$$-\frac{D^{n}_{i+\frac{1}{2}}(c_i^{n}-c^{n}_{i+1})}{4(\Delta z)^2}-\frac{\left[q^{n+1}_{i+\frac{1}{2}}(c_i^{n+1})+q^{n}_{i+\frac{1}{2}}(c_i^{n})\right]}{4\Delta z}$$
$$+\frac{\left[q^{n+1}_{i-\frac{1}{2}}(c^{n+1}_{i-1})+q^{n}_{i-\frac{1}{2}}(c^{n}_{i-1})\right]}{4\Delta z}$$

Eventually, when Equation (11) is arranged according to the tridiagonal matrix system, the final equation gives:

$$-\left(\frac{D^{n+1}_{i-\frac{1}{2}}}{4(\Delta z)^2}+\frac{q^{n+1}_{i-\frac{1}{2}}}{4\Delta z}\right)(c^{n+1}_{i-1})+\left(\frac{\theta_i^{n+1}}{\Delta t}+\frac{D^{n+1}_{i-\frac{1}{2}}}{4(\Delta z)^2}+\frac{D^{n+1}_{i+\frac{1}{2}}}{4(\Delta z)^2}+\frac{q^{n+1}_{i+\frac{1}{2}}}{4\Delta z}\right)(c_i^{n+1}) \tag{12}$$
$$-\left(\frac{D^{n+1}_{i+\frac{1}{2}}}{4(\Delta z)^2}\right)(c^{n+1}_{i+1})$$
$$=\frac{D^{n}_{i-\frac{1}{2}}(c^{n}_{i-1}-c_i^{n})}{4(\Delta z)^2}-\frac{D^{n}_{i+\frac{1}{2}}(c_i^{n}-c^{n}_{i+1})}{4(\Delta z)^2}-\frac{q^{n}_{i+\frac{1}{2}}(c_i^{n})}{4\Delta z}+\frac{q^{n}_{i-\frac{1}{2}}(c^{n}_{i-1})}{4\Delta z}$$
$$+\frac{\theta_i^{n}c_i^{n}}{\Delta t}$$

Appendix J: Experimental Loading Scheme

Week	Date	Bed 1	Bed 2	Bed 3	Bed 4	Bed 5	Bed 6
Week 1	Wednesday, July 27, 2022						
	Thursday, July 28, 2022						
	Friday, July 29, 2022						
	Saturday, July 30, 2022				A		
	Sunday, July 31, 2022						
Week 2	Monday, August 1, 2022						
	Tuesday, August 2, 2022	B	C	D	E	F	
	Wednesday, August 3, 2022						
	Thursday, August 4, 2022						
	Friday, August 5, 2022				G		H
	Saturday, August 6, 2022						
	Sunday, August 7, 2022						
Week 3	Monday, August 8, 2022	I	J	K	L	M	
	Tuesday, August 9, 2022						
	Wednesday, August 10, 2022						
	Thursday, August 11, 2022				N		
	Friday, August 12, 2022						
	Saturday, August 13, 2022						
	Sunday, August 14, 2022	O	P	Q	R	S	T
Week 4	Monday, August 15, 2022						
	Tuesday, August 16, 2022						
	Wednesday, August 17, 2022				U		
	Thursday, August 18, 2022						
	Friday, August 19, 2022						
	Saturday, August 20, 2022	V	W	X	Y	Z	
	Sunday, August 21, 2022						
Week 5	Monday, August 22, 2022						
	Tuesday, August 23, 2022				AA		AB
	Wednesday, August 24, 2022						
	Thursday, August 25, 2022						
	Friday, August 26, 2022	AC	AD	AE	AF	AG	
	Saturday, August 27, 2022						
	Sunday, August 28, 2022						
Week 6	Monday, August 29, 2022				AH		
	Tuesday, August 30, 2022						
	Wednesday, August 31, 2022						
	Thursday, September 1, 2022						
	Friday, September 2, 2022						
	Saturday, September 3, 2022						
	Sunday, September 4, 2022						
Week 7	Monday, September 5, 2022						
	Tuesday, September 6, 2022						
	Wednesday, September 7, 2022						
	Thursday, September 8, 2022						
	Friday, September 9, 2022						
	Saturday, September 10, 2022						
	Sunday, September 11, 2022						
Week 8	Monday, September 12, 2022						

	Tuesday, September 13, 2022						
	Wednesday, September 14, 2022						
	Thursday, September 15, 2022	AI	AJ	AK	AL	AM	AN
	Friday, September 16, 2022						
	Saturday, September 17, 2022						
	Sunday, September 18, 2022						
Week 9	Monday, September 19, 2022						
	Tuesday, September 20, 2022						
	Wednesday, September 21, 2022	AO	AP	AQ			
	Thursday, September 22, 2022						
	Friday, September 23, 2022						
	Saturday, September 24, 2022						AR
	Sunday, September 25, 2022						
Week 10	Monday, September 26, 2022						
	Tuesday, September 27, 2022	AS	AT	AU			
	Wednesday, September 28, 2022						
	Thursday, September 29, 2022						
	Friday, September 30, 2022						
	Saturday, October 1, 2022						
	Sunday, October 2, 2022						
Week 11	Monday, October 3, 2022	AV	AW	AX	AY		AZ
	Tuesday, October 4, 2022						
	Wednesday, October 5, 2022						
	Thursday, October 6, 2022						
	Friday, October 7, 2022						
	Saturday, October 8, 2022						
	Sunday, October 9, 2022	BA	BB	BC			
Week 12	Monday, October 10, 2022						
	Tuesday, October 11, 2022						
	Wednesday, October 12, 2022					BD	BE
	Thursday, October 13, 2022						
	Friday, October 14, 2022						
	Saturday, October 15, 2022	BF	BG	BH			
	Sunday, October 16, 2022						
Week 13	Monday, October 17, 2022						
	Tuesday, October 18, 2022						
	Wednesday, October 19, 2022						
	Thursday, October 20, 2022						
	Friday, October 21, 2022	BI	BJ	BK	BL		BM
	Saturday, October 22, 2022						
	Sunday, October 23, 2022						
Week 14	Monday, October 24, 2022						
	Tuesday, October 25, 2022						
	Wednesday, October 26, 2022						
	Thursday, October 27, 2022	BN	BO	BP			
	Friday, October 28, 2022						
	Saturday, October 29, 2022						
	Sunday, October 30, 2022						BQ
Week 15	Monday, October 31, 2022						
	Tuesday, November 1, 2022						
	Wednesday, November 2, 2022	BR	BS	BT			

	Thursday, November 3, 2022						
	Friday, November 4, 2022						
	Saturday, November 5, 2022						
	Sunday, November 6, 2022						
Week 16	Monday, November 7, 2022						
	Tuesday, November 8, 2022						

Legend:

	Feeding / loading period
	Non-feeding / resting period
	Idle period

Appendix K: Experimental Results of Hydraulic Behavior and Treatment Performance

(a) Batch A – Bed 4 (Saturday, July 30, 2022)

Time Intervals (min)	Cumulative Time (min)	Collected Volume (ml)	Effluent Flux (cm/min)	Sludge Deposit Layer (cm)	TS (mg/L)	COD (mg/L)	NO_3 (mg/L)	pH	DO (mg/L)
Influent	**-**	**8710**	**-**	**5.5**	**18780**	**5911-7726**	**394**	**7.96**	**0.12**
15	15	0	0	8.5	-	-	-	-	-
15	30	20	-0.000787324	-	-	360	167	6.85	0.94
15	45	80	-0.003149296	-	-	-	-	-	-
15	60	100	-0.00393662	-	-	-	-	-	-
15	75	125	-0.004920776	-	-	-	-	-	-
15	90	160	-0.006298593	-	-	-	-	-	-
15	105	160	-0.006298593	-	-	-	-	-	-
15	120	155	-0.006101762	-	-	-	-	-	-
15	135	155	-0.006101762	-	-	-	-	-	-
15	150	160	-0.006298593	-	-	-	-	-	-
15	165	160	-0.006298593	-	-	-	-	-	-
60	225	575	-0.005658892	-	-	-	-	-	-
15	240	140	-0.005511269	-	-	-	-	-	-
15	255	140	-0.005511269	-	-	-	-	-	-
15	270	130	-0.005117607	-	-	-	-	-	-
15	285	130	-0.005117607	-	-	-	-	-	-
15	300	125	-0.004920776	-	-	379	164	6.83	0.37
1416	1716	2950	-0.001230194	8.333333333	-	404	160	5.63	1.22
1132	2848	550	-0.0002869	8.166666667	-	412	170	5.65	5.7
	Total	**6015**							

(b) Batch B – Bed 1 (Tuesday, August 2, 2022)

Time Intervals (min)	Cumulative Time (min)	Collected Volume (ml)	Effluent Flux (cm/min)	Sludge Deposit Layer (cm)	TS (mg/L)	COD (mg/L)	NO_3 (mg/L)	pH	DO (mg/L)
Influent	**-**	**8710**	**-**	**7**	**18780**	**5911-7726**	**394**	**7.96**	**0.12**
10	10	0	0	-	-	-	-	-	-
10	20	160	-0.009447889	-	-	606	77.5	6.59	0.74
10	30	375	-0.02214349	-	-	-	-	-	-
5	35	195	-0.023029229	-	-	-	-	-	-
5	40	185	-0.021848243	-	-	-	-	-	-
5	45	175	-0.020667257	-	-	-	-	-	-
5	50	160	-0.018895778	-	-	-	-	-	-
5	55	155	-0.018305285	-	-	-	-	-	-
5	60	150	-0.017714792	-	-	-	-	-	-
5	65	145	-0.017124299	-	-	-	-	-	-
5	70	130	-0.01535282	-	-	-	-	-	-
5	75	125	-0.014762327	-	-	-	-	-	-
5	80	125	-0.014762327	-	-	-	-	-	-
5	85	120	-0.014171833	-	-	-	-	-	-
5	90	110	-0.012990847	-	-	-	-	-	-
5	95	105	-0.012400354	-	-	-	-	-	-
5	100	100	-0.011809861	-	-	-	-	-	-
5	105	95	-0.011219368	-	-	-	-	-	-
5	110	90	-0.010628875	-	-	-	-	-	-
5	115	80	-0.009447889	-	-	-	-	-	-
5	120	80	-0.009447889	-	-	-	-	-	-
5	125	75	-0.008857396	-	-	-	-	-	-
5	130	70	-0.008266903	-	-	595	148	6.62	2.63
1214	1344	2310	-0.001123591	11.5	-	581	191	6.33	6.09
1425	2769	415	-0.000171968	10.33333333	-	554	214	6.09	6.62

1539	4308	165	-6.33082E-05	9	-	481.5	219.5	6.085	5.855
1428	5736	250	-0.000103378	8.17	-	409	225	6.08	5.09
1468	7204	175	-7.03926E-05	8	-	481	246	6.17	5.95
1436	8640	0	0	8.17	-	-	-	-	-
	Total	**6320**							

(c) Batch C – Bed 2 (Tuesday, August 2, 2022)

Time Intervals (min)	Cumulative Time (min)	Collected Volume (ml)	Effluent Flux (cm/min)	Sludge Deposit Layer (cm)	TS (mg/L)	COD (mg/L)	NO_3 (mg/L)	pH	DO (mg/L)
Influent	**-**	**17420**	**-**	**10.66666667**	**18780**	**5911-7726**	**394**	**7.96**	**0.12**
100	100	0	0	-	-	-	-	-	-
25	125	90	-0.002125775	-	-	314	257	6.38	5.77
5	130	50	-0.005904931	-	-	-	-	-	-
5	135	35	-0.004133451	-	-	-	-	-	-
5	140	40	-0.004723944	-	-	-	-	-	-
60	200	300	-0.002952465	-	-	-	-	-	-
5	205	30	-0.003542958	-	-	-	-	-	-
15	220	60	-0.002361972	-	-	-	-	-	-
10	230	50	-0.002952465	-	-	-	-	-	-
10	240	50	-0.002952465	-	-	291	342	6.56	6.72
10	250	50	-0.002952465	-	-	-	-	-	-
10	260	50	-0.002952465	-	-	-	-	-	-
10	270	50	-0.002952465	-	-	-	-	-	-
10	280	45	-0.002657219	-	-	-	-	-	-
10	290	45	-0.002657219	-	-	-	-	-	-
10	300	30	-0.001771479	-	-	-	-	-	-
10	310	50	-0.002952465	-	-	-	-	-	-
10	320	50	-0.002952465	-	-	-	-	-	-
10	330	55	-0.003247712	-	-	-	-	-	-

10	340	50	-0.002952465	-	-	-	-	-	-
1005	1345	2390	-0.001404257	12.66666667	-	291	322	6.72	7.19
1426	2771	3685	-0.001525924	12.66666667	-	331	241	6.53	6.36
1544	4315	555	-0.000212256	12.67	-	350	77.6	6	5.98
1422	5737	2370	-0.000246194	12.3	-	266	262	6.8	6.2
1465	7202	695	-0.000280132	11.83	-	326	257	7.36	0.34
1431	8633	190	-7.84023E-05	11.5	-	-	-	-	-
	Total	**11065**							

(d) Batch D – Bed 3 (Tuesday, August 2, 2022)

Time Intervals (min)	Cumulative Time (min)	Collected Volume (ml)	Effluent Flux (cm/min)	Sludge Deposit Layer (cm)	TS (mg/L)	COD (mg/L)	NO_3 (mg/L)	pH	DO (mg/L)
Influent	**-**	**26140**	**-**	**7.833333333**	**18780**	**5911-7726**	**394**	**7.96**	**0.12**
8	8	0	0	-	-	-	-	-	-
12	20	60	-0.002952465	-	-	384	161	6.59	0.37
10	30	95	-0.005609684	-	-	-	-	-	-
10	40	110	-0.006495424	-	-	-	-	-	-
10	50	120	-0.007085917	-	-	-	-	-	-
5	55	65	-0.00767641	-	-	-	-	-	-
5	60	65	-0.00767641	-	-	-	-	-	-
5	65	65	-0.00767641	-	-	-	-	-	-
5	70	65	-0.00767641	-	-	-	-	-	-
5	75	60	-0.007085917	-	-	-	-	-	-
5	80	65	-0.00767641	-	-	-	-	-	-
5	85	60	-0.007085917	-	-	-	-	-	-
5	90	60	-0.007085917	-	-	-	-	-	-
5	95	60	-0.007085917	-	-	-	-	-	-
5	100	70	-0.008266903	-	-	-	-	-	-
5	105	60	-0.007085917	-	-	-	-	-	-

5	110	60	-0.007085917	-	-	-	-	-	-
5	115	60	-0.007085917	-	-	-	-	-	-
5	120	55	-0.006495424	-	-	-	-	-	-
5	125	55	-0.006495424	-	-	-	-	-	-
5	130	50	-0.005904931	-	-	-	-	-	-
5	135	55	-0.006495424	-	-	-	-	-	-
55	190	445	-0.008266903	-	-	-	-	-	-
5	195	85	-0.010038382	-	-	-	-	-	-
20	215	120	-0.003542958	-	-	-	-	-	-
10	225	80	-0.004723944	-	-	-	-	-	-
10	235	90	-0.005314438	-	-	-	-	-	-
10	245	75	-0.004428698	-	-	385	223	6.63	1.99
10	255	75	-0.004428698	-	-	-	-	-	-
10	265	75	-0.004428698	-	-	-	-	-	-
10	275	75	-0.004428698	-	-	-	-	-	-
10	285	75	-0.004428698	-	-	-	-	-	-
10	295	75	-0.004428698	-	-	-	-	-	-
10	305	75	-0.004428698	-	-	-	-	-	-
10	315	80	-0.004723944	-	-	-	-	-	-
10	325	75	-0.004428698	-	-	-	-	-	-
10	335	80	-0.004723944	-	-	-	-	-	-
1013	1348	3900	-0.002273369	13.83	-	342	302	6.39	6.96
1424	2772	3350	-0.001389152	13.5	-	298	255	6.86	6.97
1404	4176	3045	-0.001280663	12.83	-	283	204	6.59	3.12
1386	5562	2820	-0.001201436	12.3	-	267	231	6.51	2.21
1468	7030	1375	-0.000553084	12	-	207	183	6.92	2.99
1426	8456	795	-0.000329202	11.3	-	266	219	6.85	4.32
	Total	**18280**							

(e) Batch E – Bed 4 (Tuesday, August 2, 2022)

Time Intervals (min)	Cumulative Time (min)	Collected Volume (ml)	Effluent Flux (cm/min)	Sludge Deposit Layer (cm)	TS (mg/L)	COD (mg/L)	NO_3 (mg/L)	pH	DO (mg/L)
Influent	**-**	**8710**	**-**	**8.166666667**	**18780**	**5911-7726**	**394**	**7.96**	**0.12**
30	30	0	0	-	-	-	-	-	-
20	50	30	-0.00088574	-	-	436	209	6.67	2.74
10	60	30	-0.001771479	-	-	-	-	-	-
10	70	60	-0.003542958	-	-	-	-	-	-
10	80	75	-0.004428698	-	-	-	-	-	-
10	90	105	-0.006200177	-	-	-	-	-	-
5	95	55	-0.006495424	-	-	-	-	-	-
5	100	55	-0.006495424	-	-	-	-	-	-
5	105	65	-0.00767641	-	-	-	-	-	-
5	110	65	-0.00767641	-	-	-	-	-	-
5	115	55	-0.006495424	-	-	-	-	-	-
5	120	60	-0.007085917	-	-	-	-	-	-
5	125	55	-0.006495424	-	-	-	-	-	-
5	130	60	-0.007085917	-	-	-	-	-	-
60	190	410	-0.00679067	-	-	-	-	-	-
5	195	55	-0.006495424	-	-	-	-	-	-
10	205	80	-0.004723944	-	-	-	-	-	-
10	215	65	-0.003838205	-	-	-	-	-	-
10	225	65	-0.003838205	-	-	-	-	-	-
10	235	60	-0.003542958	-	-	-	-	-	-
10	245	55	-0.003247712	-	-	-	-	-	-
10	255	55	-0.003247712	-	-	-	-	-	-
15	270	75	-0.002952465	-	-	-	-	-	-
15	285	75	-0.002952465	-	-	-	-	-	-
15	300	70	-0.002755634	-	-	-	-	-	-
15	315	70	-0.002755634	-	-	-	-	-	-

15	330	70	-0.002755634	-	-	-	-	-	-
5	335	20	-0.002361972	-	-	-	-	-	-
1016	1351	1605	-0.000932816	8.666666667	-	384	209	6.57	6.51
1423	2774	605	-0.000251053	6.666666667	-	351	251	6.08	6.87
1530	4304	270	-0.000104205	7	-	334	251	5.46	6.35
	Total	**4475**							

(f) Batch F – Bed 5 (Tuesday, August 2, 2022)

Time Intervals (min)	Cumulative Time (min)	Collected Volume (ml)	Effluent Flux (cm/min)	Sludge Deposit Layer (cm)	TS (mg/L)	COD (mg/L)	NO_3 (mg/L)	pH	DO (mg/L)
Influent	**-**	**17420**	**-**	**6.333333333**	**18780**	**5911-7726**	**394**	**7.96**	**0.12**
20	20	0	0	-	-	-	-	-	-
10	30	70	-0.004133451	-	-	378	191	6.68	0.91
10	40	110	-0.006495424	-	-	-	-	-	-
5	45	70	-0.008266903	-	-	-	-	-	-
5	50	65	-0.00767641	-	-	-	-	-	-
5	55	75	-0.008857396	-	-	-	-	-	-
5	60	70	-0.008266903	-	-	-	-	-	-
5	65	85	-0.010038382	-	-	-	-	-	-
5	70	75	-0.008857396	-	-	-	-	-	-
5	75	85	-0.010038382	-	-	-	-	-	-
5	80	75	-0.008857396	-	-	-	-	-	-
5	85	80	-0.009447889	-	-	-	-	-	-
5	90	85	-0.010038382	-	-	-	-	-	-
5	95	85	-0.010038382	-	-	-	-	-	-
5	100	80	-0.009447889	-	-	-	-	-	-
5	105	85	-0.010038382	-	-	-	-	-	-
5	110	85	-0.010038382	-	-	-	-	-	-
5	115	85	-0.010038382	-	-	-	-	-	-

5	120	80	-0.009447889	-	-	-	-	-	-
5	125	75	-0.008857396	-	-	-	-	-	-
5	130	80	-0.009447889	-	-	-	-	-	-
60	190	405	-0.012105108	-	-	-	-	-	-
5	195	125	-0.014762327	-	-	-	-	-	-
15	210	240	-0.009447889	-	-	-	-	-	-
10	220	190	-0.011219368	-	-	-	-	-	-
10	230	290	-0.017124299	-	-	-	-	-	-
5	235	195	-0.023029229	-	-	-	-	-	-
5	240	175	-0.020667257	-	-	639	326	7.76	0.51
5	245	165	-0.019486271	-	-	-	-	-	-
5	250	165	-0.019486271	-	-	-	-	-	-
5	255	170	-0.020076764	-	-	-	-	-	-
5	260	165	-0.019486271	-	-	-	-	-	-
5	265	125	-0.014762327	-	-	-	-	-	-
5	270	125	-0.014762327	-	-	-	-	-	-
5	275	130	-0.01535282	-	-	-	-	-	-
5	280	140	-0.016533806	-	-	-	-	-	-
5	285	110	-0.012990847	-	-	-	-	-	-
5	290	135	-0.015943313	-	-	-	-	-	-
5	295	90	-0.010628875	-	-	-	-	-	-
5	300	80	-0.009447889	-	-	-	-	-	-
5	305	70	-0.008266903	-	-	-	-	-	-
5	310	60	-0.007085917	-	-	-	-	-	-
5	315	65	-0.00767641	-	-	-	-	-	-
5	320	65	-0.00767641	-	-	-	-	-	-
5	325	65	-0.00767641	-	-	-	-	-	-
5	330	70	-0.008266903	-	-	-	-	-	-
1022	1352	4205	-0.002429573	8.5	-	371	232	6.84	5.91
1420	2772	1140	-0.000474058	8	-	343	257	6.78	6.49
1515	4287	525	-0.000204626	8	-	319	226	6.17	3.2

1452	5739	4035	-0.000218216	8.17	-	232	219	6.56	4.6
1452	7191	570	-0.000231805	7.83	-	279	243	6.89	5.27
1430	8621	320	-0.000132138	7.67	-	303	293	7	4.31
	Total	**16010**							

(g) Batch G – Bed 4 (Friday, August 5, 2022)

Time Intervals (min)	Cumulative Time (min)	Collected Volume (ml)	Effluent Flux (cm/min)	Sludge Deposit Layer (cm)	TS (mg/L)	COD (mg/L)	NO_3 (mg/L)	pH	DO (mg/L)
Influent	**-**	**8710**	**-**	**7**	**18780**	**5911-7726**	**394**	**7.96**	**0.12**
10	10	0	0	-	-	-	-	-	-
30	40	105	-0.002066726	-	-	341	252	6.15	1.41
10	50	50	-0.002952465	-	-	-	-	-	-
10	60	50	-0.002952465	-	-	-	-	-	-
10	70	60	-0.003542958	-	-	-	-	-	-
10	80	75	-0.004428698	-	-	-	-	-	-
10	90	85	-0.005019191	-	-	-	-	-	-
10	100	90	-0.005314438	-	-	-	-	-	-
10	110	95	-0.005609684	-	-	-	-	-	-
10	120	105	-0.006200177	-	-	-	-	-	-
10	130	115	-0.00679067	-	-	-	-	-	-
10	140	125	-0.007381163	-	-	-	-	-	-
10	150	115	-0.00679067	-	-	-	-	-	-
10	160	110	-0.006495424	-	-	-	-	-	-
10	170	115	-0.00679067	-	-	-	-	-	-
10	180	100	-0.005904931	-	-	-	-	-	-
10	190	85	-0.005019191	-	-	-	-	-	-
10	200	75	-0.004428698	-	-	-	-	-	-
1163	1363	5000	-0.002538663	9	-	261	210	6.17	3.1
1460	2823	2460	-0.00099494	8.666666667	-	244	204	6.77	3.57

1429	4252	880	-0.000363635	7.833333333	-	263	252	6.94	5.91
	Total	**9895**							

(h) Batch H – Bed 6 (Friday, August 5, 2022)

Time Intervals (min)	Cumulative Time (min)	Collected Volume (ml)	Effluent Flux (cm/min)	Sludge Deposit Layer (cm)	TS (mg/L)	COD (mg/L)	NO_3 (mg/L)	pH	DO (mg/L)
Influent	**-**	**26140**	**-**	**8.333333333**	**18780**	**5911-7726**	**394**	**7.96**	**0.12**
30	30	0	0	12.66666667	-	-	-	-	-
15	45	115	-0.004527113	-	-	274	310	6.51	1.97
5	50	50	-0.005904931	-	-	-	-	-	-
5	55	60	-0.007085917	-	-	-	-	-	-
5	60	60	-0.007085917	-	-	-	-	-	-
5	65	65	-0.00767641	-	-	-	-	-	-
5	70	75	-0.008857396	-	-	-	-	-	-
5	75	70	-0.008266903	-	-	-	-	-	-
5	80	70	-0.008266903	-	-	-	-	-	-
5	85	75	-0.008857396	-	-	-	-	-	-
5	90	75	-0.008857396	-	-	-	-	-	-
5	95	75	-0.008857396	-	-	-	-	-	-
5	100	70	-0.008266903	-	-	-	-	-	-
5	105	70	-0.008266903	-	-	-	-	-	-
5	110	70	-0.008266903	-	-	-	-	-	-
5	115	65	-0.00767641	-	-	-	-	-	-
5	120	70	-0.008266903	-	-	-	-	-	-
5	125	70	-0.008266903	-	-	-	-	-	-
5	130	70	-0.008266903	-	-	-	-	-	-
5	135	70	-0.008266903	-	-	-	-	-	-
5	140	70	-0.008266903	-	-	-	-	-	-
5	145	65	-0.00767641	-	-	-	-	-	-

5	150	65	-0.00767641	-	-	-	-	-	-
5	155	65	-0.00767641	-	-	-	-	-	-
5	160	65	-0.00767641	-	-	-	-	-	-
5	165	60	-0.007085917	-	-	-	-	-	-
5	170	60	-0.007085917	-	-	-	-	-	-
5	175	60	-0.007085917	-	-	-	-	-	-
5	180	60	-0.007085917	-	-	-	-	-	-
5	185	60	-0.007085917	-	-	-	-	-	-
5	190	60	-0.007085917	-	-	-	-	-	-
5	195	60	-0.007085917	-	-	-	-	-	-
5	200	55	-0.006495424	-	-	-	-	-	-
5	205	55	-0.006495424	-	-	-	-	-	-
5	210	55	-0.006495424	-	-	-	-	-	-
5	215	55	-0.006495424	-	-	-	-	-	-
5	220	50	-0.005904931	-	-	-	-	-	-
5	225	50	-0.005904931	-	-	-	-	-	-
5	230	50	-0.005904931	-	-	-	-	-	-
5	235	50	-0.005904931	-	-	-	-	-	-
5	240	50	-0.005904931	-	-	-	-	-	-
1164	1404	14590	-0.003474448	13	-	349	261	7.77	1.58
1448	2852	2560	-0.001043966	10.33333333	-	285	229	6.97	5.13
1431	4283	1110	-0.000458034	9.5	-	257	288	7.12	6.1
1352	5635	585	-0.000255502	9.166666667	-	240	236	7.27	7.03
1482	7117	350	-0.000139455	9	-	244	430	7.14	7.35
1463	8580	230	-9.28321E-05	8.833333333	-	240	373	6.88	6.94
1421	10001	95	-3.9477E-05	8.5	-	350.5	435.5	7.015	7.11
1515	11516	20	-7.79529E-06	8.5	-	461	498	7.15	7.28
	Total	**22015**							

(i) Batch I – Bed 1 (Monday, August 8, 2022)

Time Intervals (min)	Cumulative Time (min)	Collected Volume (ml)	Effluent Flux (cm/min)	Sludge Deposit Layer (cm)	TS (mg/L)	COD (mg/L)	NO_3 (mg/L)	pH	DO (mg/L)
Influent	**-**	**5460**	**-**	**8.17**	**29967**	**5911-7726**	**394**	**7.96**	**0.12**
30	30	0	0	-	-	-	-	-	-
15	45	55	-0.002165141	-	-	503	258	6.57	0.53
20	65	200	-0.005904931	-	-	-	-	-	-
10	75	160	-0.009447889	-	-	-	-	-	-
10	85	155	-0.009152642	-	-	-	-	-	-
5	90	75	-0.008857396	-	-	-	-	-	-
5	95	75	-0.008857396	-	-	-	-	-	-
5	100	75	-0.008857396	-	-	-	-	-	-
5	105	70	-0.008266903	-	-	-	-	-	-
5	110	65	-0.00767641	-	-	-	-	-	-
5	115	65	-0.00767641	-	-	-	-	-	-
5	120	60	-0.007085917	-	-	-	-	-	-
5	125	60	-0.007085917	-	-	-	-	-	-
5	130	60	-0.007085917	-	-	-	-	-	-
5	135	55	-0.006495424	-	-	-	-	-	-
5	140	50	-0.005904931	-	-	-	-	-	-
5	145	50	-0.005904931	-	-	-	-	-	-
5	150	50	-0.005904931	-	-	-	-	-	-
50	200	300	-0.003542958	-	-	-	-	-	-
40	240	165	-0.002435784	-	-	-	-	-	-
50	290	155	-0.001830528	-	-	-	-	-	-
1055	1345	785	-0.000439372	10.17	-	460	372	6.95	6.05
1470	2815	260	-0.000104441	10	-	408	481	6.4	7.08
1470	4285	125	-5.0212E-05	9	-	414	469	6.23	6.72
1427	5712	50	-2.069E-05	9.333333333	-	472	491	5.8	7.28
1506	7218	20	-7.84187E-06	8.83	-	654	411	5.84	7.39

1253	8471	10	-4.71263E-06	8.833333333	-	-	-	-	-
	Total	**3250**							

(j) Batch J – Bed 2 (Monday, August 8, 2022)

Time Intervals (min)	Cumulative Time (min)	Collected Volume (ml)	Effluent Flux (cm/min)	Sludge Deposit Layer (cm)	TS (mg/L)	COD (mg/L)	NO_3 (mg/L)	pH	DO (mg/L)
Influent	**-**	**10917**	**-**	**11.5**	**29967**	**5911-7726**	**394**	**7.96**	**0.12**
720	720	0	0	-	-	-	-	-	-
720	1440	265	-0.000217334	13.3	-	315	341	7.58	5.41
1478	2918	980	-0.000391531	12.5	-	270	312	7.08	4.96
1477	4395	1465	-0.000585696	12.3	-	305	285	6.71	1.25
1418	5813	555	-0.000508477	12.17	-	317	325	7.44	3.61
1513	7326	1105	-0.000431259	11.67	-	382	271	7.09	0.59
1247	8573	415	-0.000196515	11.5	-	304	288	6.96	4.04
	Total	**4785**							

(k) Batch K – Bed 3 (Monday, August 8, 2022)

Time Intervals (min)	Cumulative Time (min)	Collected Volume (ml)	Effluent Flux (cm/min)	Sludge Deposit Layer (cm)	TS (mg/L)	COD (mg/L)	NO_3 (mg/L)	pH	DO (mg/L)
Influent	**-**	**16380**	**-**	**11.3**	**29967**	**5911-7726**	**394**	**7.96**	**0.12**
50	50	0	0	-	-	-	-	-	-
95	145	105	-0.00065265	-	-	254	267	6.96	3.11
50	195	60	-0.000708592	-	-	-	-	-	-
40	235	80	-0.001180986	-	-	-	-	-	-
25	260	60	-0.001417183	-	-	-	-	-	-
25	285	60	-0.001417183	-	-	-	-	-	-

1050	1335	1560	-0.000877304	14.17	-	224	295	7.24	6.21
1477	2812	1390	-0.000555711	13.5	-	219	306	7.19	7.37
1473	4285	1460	-0.000585282	11.67	-	190	311	7.11	6.89
227	4512	230	-0.000598297	-	-	-	-	-	-
1194	5706	985	-0.000487132	11.5	-	208	292	6.82	6.02
1511	7217	1035	-0.000404474	11.5	-	208	255	7.01	6.59
1255	8472	725	-0.000341121	11.3	-	214	253	7.08	6.81
	Total	**7750**							

(l) Batch L – Bed 4 (Monday, August 8, 2022)

Time Intervals (min)	Cumulative Time (min)	Collected Volume (ml)	Effluent Flux (cm/min)	Sludge Deposit Layer (cm)	TS (mg/L)	COD (mg/L)	NO_3 (mg/L)	pH	DO (mg/L)
Influent	**-**	**5460**	**-**	**7.833333333**	**29967**	**5911-7726**	**394**	**7.96**	**0.12**
90	90	0	0	-	-	-	-	-	-
55	145	90	-0.000966261	-	-	380	289	7.24	0.3
50	195	120	-0.001417183	-	-	-	-	-	-
40	235	80	-0.001476233	-	-	-	-	-	-
25	260	65	-0.001535282	-	-	-	-	-	-
20	280	75	-0.002214349	-	-	-	-	-	-
1047	1327	1275	-0.000719082	9.5	-	380	289	7.24	0.3
1482	2809	1000	-0.000398443	9.3	-	288	296	7.35	6.06
1468	4277	590	-0.000237324	8.3	-	233	335	7.02	6.97
1247	5524	355	-0.000168103	-	-	203	329	7.05	7
	Total	**3650**							

(m) Batch M – Bed 5 (Monday, August 8, 2022)

Time Intervals	Cumulative Time	Collected	Effluent Flux	Sludge Deposit	TS	COD	NO_3	pH	DO

(min)	(min)	Volume (ml)	(cm/min)	Layer (cm)	(mg/L)	(mg/L)	(mg/L)		(mg/L)
Influent	**-**	**10917**	**-**	**7.67**	**29967**	**5911-7726**	**394**	**7.96**	**0.12**
45	45	0	0	-	-	-	-	-	-
10	55	55	-0.003247712	-	-	337	313	7.24	1.54
10	65	65	-0.003838205	-	-	-	-	-	-
10	75	100	-0.005904931	-	-	-	-	-	-
5	80	95	-0.011219368	-	-	-	-	-	-
5	85	70	-0.008266903	-	-	-	-	-	-
5	90	90	-0.010628875	-	-	-	-	-	-
5	95	320	-0.037791556	-	-	-	-	-	-
5	100	290	-0.034248598	-	-	-	-	-	-
5	105	235	-0.027753174	-	-	-	-	-	-
5	110	205	-0.024210216	-	-	-	-	-	-
5	115	185	-0.021848243	-	-	-	-	-	-
5	120	140	-0.016533806	-	-	-	-	-	-
5	125	105	-0.012400354	-	-	-	-	-	-
5	130	70	-0.008266903	-	-	-	-	-	-
5	135	65	-0.00767641	-	-	-	-	-	-
5	140	60	-0.007085917	-	-	-	-	-	-
5	145	60	-0.007085917	-	-	-	-	-	-
45	190	360	-0.004723944	-	-	-	-	-	-
40	230	270	-0.003985828	-	-	-	-	-	-
50	280	285	-0.00336581	-	-	-	-	-	-
1057	1337	2375	-0.001326794	9.67	-	280	303	7.39	6.39
1478	2815	950	-0.000379546	9.67	-	267	339	7.25	6.9
1464	4279	425	-0.00017142	9.17	-	255	332	7.01	6.57
1422	5701	205	-8.51273E-05	9	-	288	355	7.1	6.69
1515	7216	100	-3.89764E-05	9	-	264	377	7.15	6.88
1243	8459	45	-2.13775E-05	8.83	-	-	-	-	-
	Total	**22015**							

(n) Batch N – Bed 4 (Thursday, August 11, 2022)

Time Intervals (min)	Cumulative Time (min)	Collected Volume (ml)	Effluent Flux (cm/min)	Sludge Deposit Layer (cm)	TS (mg/L)	COD (mg/L)	NO_3 (mg/L)	pH	DO (mg/L)
Influent	**-**	**5460**	**-**	**8.3**	**29967**	**5911-7726**	**394**	**7.96**	**0.12**
25	25	0	0	-	-	-	-	-	-
65	90	60	-0.000545071	-	-	239	258	6.56	3.62
90	180	90	-0.000590493	-	-	-	-	-	-
1197	1377	1300	-0.000641304	10	-	202	238	6.36	4.84
1513	2890	820	-0.000320029	8.666666667	-	202	292	6.89	6.82
1247	4137	355	-0.000168103	8.833333333	-	183	296	7.33	6.91
	Total	**2625**							

(o) Batch O – Bed 1 (Sunday, August 14, 2022)

Time Intervals (min)	Cumulative Time (min)	Collected Volume (ml)	Effluent Flux (cm/min)	Sludge Deposit Layer (cm)	TS (mg/L)	COD (mg/L)	NO_3 (mg/L)	pH	DO (mg/L)
Influent	**-**	**5460**	**-**	**8.833333333**	**29967**	**5911-7726**	**394**	**7.96**	**0.12**
15	15	0	0	-	-	-	-	-	-
5	20	125	-0.014762327	-	-	324	492	6.53	3.37
5	25	165	-0.019486271	-	-	-	-	-	-
5	30	125	-0.014762327	-	-	-	-	-	-
5	35	120	-0.014171833	-	-	-	-	-	-
5	40	110	-0.012990847	-	-	-	-	-	-
5	45	90	-0.010628875	-	-	-	-	-	-
5	50	85	-0.010038382	-	-	-	-	-	-
5	55	80	-0.009447889	-	-	-	-	-	-
5	60	80	-0.009447889	-	-	-	-	-	-
5	65	75	-0.008857396	-	-	-	-	-	-

5	70	65	-0.00767641	-	-	-	-	-	-
5	75	65	-0.00767641	-	-	-	-	-	-
5	80	60	-0.007085917	-	-	-	-	-	-
5	85	60	-0.007085917	-	-	-	-	-	-
5	90	60	-0.007085917	-	-	-	-	-	-
5	95	55	-0.006495424	-	-	-	-	-	-
5	100	50	-0.005904931	-	-	-	-	-	-
5	105	50	-0.005904931	-	-	-	-	-	-
5	110	40	-0.004723944	-	-	-	-	-	-
5	115	40	-0.004723944	-	-	-	-	-	-
5	120	40	-0.004723944	-	-	-	-	-	-
5	125	30	-0.003542958	-	-	-	-	-	-
5	130	30	-0.003542958	-	-	-	-	-	-
5	135	30	-0.003542958	-	-	-	-	-	-
5	140	25	-0.002952465	-	-	-	-	-	-
46	186	160	-0.002053889	-	-	-	-	-	-
64	250	185	-0.001706894	-	-	-	-	-	-
53	303	155	-0.001726914	-	-	-	-	-	-
1176	1479	690	-0.000346463	10.17	-	345	378	6.51	6.16
219	1698	50	-0.000134816	9	-	-	-	-	-
1283	2981	185	-8.51451E-05	8.83	5379.710145	345	527	6.32	6.76
1355	4336	110	-4.79367E-05	8	12109.9006	362	477	5.25	7.45
1549	5885	70	-2.66846E-05	8.17	-	318	566	6.35	7.75
1335	7220	20	-8.84634E-06	7.5	-	529	870	6.91	7.58
	Total	**3380**							

(p) Batch P – Bed 2 (Sunday, August 14, 2022)

Time Intervals (min)	Cumulative Time (min)	Collected Volume (ml)	Effluent Flux (cm/min)	Sludge Deposit Layer (cm)	TS (mg/L)	COD (mg/L)	NO_3 (mg/L)	pH	DO (mg/L)
Influent	**-**	**10917**	**-**	**11.5**	**29967**	**5911-**	**394**	**7.96**	**0.12**

						7726			
10	10	0	0	-	-	-	-	-	-
170	180	50	-0.000173674	-	-	291	299	7.41	7.18
115	295	35	-0.000179715	-	-	-	-	-	-
1180	1475	520	-0.000260217	12.5	-	256	236	6.92	6.94
222	1697	195	-0.000518676	-	-	-	-	-	-
1287	2984	805	-0.000369345	11.67	-	281	259	6.69	5.84
1352	4336	845	-0.000369058	10.83	2732.951588	285	244	6.67	7.43
124	4460	100	-0.000346479	-	-	-	-	-	-
237	4697	130	-0.000323899	10.83	2820.467265	239	291	6.84	7.1
1188	5885	650	-0.000323081	10.83	1063.952816	243	282	7.07	7.45
1335	7220	615	-0.000272025	10.83	2222.870871	244	303	6.99	7.27
	Total	**3945**							

(q) Batch Q – Bed 3 (Sunday, August 14, 2022)

Time Intervals (min)	Cumulative Time (min)	Collected Volume (ml)	Effluent Flux (cm/min)	Sludge Deposit Layer (cm)	TS (mg/L)	COD (mg/L)	NO_3 (mg/L)	pH	DO (mg/L)
Influent	**-**	**16380**	**-**	**11.5**	**29967**	**5911-7726**	**394**	**7.96**	**0.12**
30	30	0	0	-	-	-	-	-	-
40	70	60	-0.00088574	-	-	198	159	7.02	6.6
95	165	170	-0.001056672	-	-	-	-	-	-
80	245	85	-0.001089304	-	-	-	-	-	-
50	295	95	-0.001121937	-	-	-	-	-	-
1180	1475	1875	-0.000938283	13.3	-	175	222	7.24	7.48
215	1690	270	-0.000741549	-	-	-	-	-	-
1287	2977	1455	-0.000667574	12.17	-	242	260	7.12	7.03
1356	4333	1395	-0.000607476	11	1294.189769	233	246	7.17	7.56
120	4453	125	-0.000615097	-	-	-	-	-	-
239	4692	285	-0.000605777	11.3	1210.626611	175	287	7.23	7.17

1188	5880	1200	-0.000596458	10.67	717.7421222	183	273	7.15	7.52
1336	7216	1055	-0.000466295	10.5	3169.403557	179	276	7.02	7.08
	Total	**8070**							

(r) Batch R – Bed 4 (Sunday, August 14, 2022)

Time Intervals (min)	Cumulative Time (min)	Collected Volume (ml)	Effluent Flux (cm/min)	Sludge Deposit Layer (cm)	TS (mg/L)	COD (mg/L)	NO_3 (mg/L)	pH	DO (mg/L)
Influent	**-**	**5460**	**-**	**8.833333333**	**29967**	**5911-7726**	**394**	**7.96**	**0.12**
80	80	0	0	-	-	-	-	-	-
95	175	80	-0.000497257	-	-	178	289	6.97	7.05
80	255	75	-0.000553587	-	-	-	-	-	-
50	305	55	-0.000649542	-	-	-	-	-	-
1182	1487	1595	-0.000796816	11.66666667	-	186	211	6.9	7.4
212	1699	170	-0.000473509	-	-	-	-	-	-
1283	2982	650	-0.000299159	10.33333333	-	238	267	6.89	6.73
1362	4344	490	-0.000212439	9.666666667	1921.615945	223	284	7.2	7.45
118	4462	30	-0.000150125	-	-	-	-	-	-
	Total	**3145**							

(s) Batch S – Bed 5 (Sunday, August 14, 2022)

Time Intervals (min)	Cumulative Time (min)	Collected Volume (ml)	Effluent Flux (cm/min)	Sludge Deposit Layer (cm)	TS (mg/L)	COD (mg/L)	NO_3 (mg/L)	pH	DO (mg/L)
Influent	**-**	**10917**	**-**	**8.83**	**29967**	**5911-7726**	**394**	**7.96**	**0.12**
50	50	0	0	-	-	-	-	-	-
20	70	55	-0.001623856	-	-	234	323	7.19	5.96
10	80	40	-0.002361972	-	-	-	-	-	-

10	90	50	-0.002952465	-	-	-	-	-	-
5	95	60	-0.004723944	-	-	-	-	-	-
5	100	55	-0.006495424	-	-	-	-	-	-
5	105	50	-0.005904931	-	-	-	-	-	-
5	110	50	-0.005904931	-	-	-	-	-	-
5	115	55	-0.006495424	-	-	-	-	-	-
5	120	75	-0.008857396	-	-	-	-	-	-
5	125	65	-0.00767641	-	-	-	-	-	-
5	130	75	-0.008857396	-	-	-	-	-	-
5	135	55	-0.006495424	-	-	-	-	-	-
5	140	75	-0.008857396	-	-	-	-	-	-
5	145	70	-0.008266903	-	-	-	-	-	-
5	150	90	-0.010628875	-	-	-	-	-	-
5	155	75	-0.008857396	-	-	-	-	-	-
5	160	110	-0.012990847	-	-	-	-	-	-
5	165	110	-0.012990847	-	-	-	-	-	-
5	170	130	-0.01535282	-	-	-	-	-	-
5	175	95	-0.011219368	-	-	-	-	-	-
5	180	110	-0.012990847	-	-	-	-	-	-
5	185	85	-0.010038382	-	-	-	-	-	-
5	190	70	-0.008266903	-	-	-	-	-	-
5	195	80	-0.009447889	-	-	-	-	-	-
55	250	495	-0.008562149	-	-	-	-	-	-
5	255	65	-0.00767641	-	-	-	-	-	-
5	260	50	-0.005904931	-	-	-	-	-	-
5	265	60	-0.007085917	-	-	-	-	-	-
5	270	35	-0.004133451	-	-	-	-	-	-
5	275	50	-0.005904931	-	-	-	-	-	-
5	280	70	-0.005314438	-	-	-	-	-	-
5	285	40	-0.004723944	-	-	-	-	-	-
10	295	30	-0.001771479	-	-	-	-	-	-

1183	1478	1960	-0.000978332	12	-	233	251	7.03	7.11
218	1696	150	-0.000406303	-	-	-	-	-	-
1279	2975	600	-0.00027701	10.66666667	-	262	249	6.86	6.03
1365	4340	390	-0.000168712	10	2521.547772	272	296	7.3	7.32
360	4700	75	-0.000123019	8.5	3085.714286	195	376	7.27	6.93
1188	5888	200	-9.94096E-05	8.333333333	-	253	452	7.68	7.29
1340	7228	470	-4.97048E-05	7.666666667	-	192	477	7.83	7.71
	Total	**6525**							

(t) Batch T – Bed 6 (Sunday, August 14, 2022)

Time Intervals (min)	Cumulative Time (min)	Collected Volume (ml)	Effluent Flux (cm/min)	Sludge Deposit Layer (cm)	TS (mg/L)	COD (mg/L)	NO_3 (mg/L)	pH	DO (mg/L)
Influent	**-**	**16380**	**-**	**8.5**	**29967**	**5911-7726**	**394**	**7.96**	**0.12**
60	60	0	0	-	-	-	-	-	-
65	125	65	-0.000590493	-	-	200	357	7	6.93
15	140	50	-0.00196831	-	-	-	-	-	-
15	155	60	-0.002361972	-	-	-	-	-	-
10	165	50	-0.002952465	-	-	-	-	-	-
10	175	50	-0.002952465	-	-	-	-	-	-
10	185	50	-0.002952465	-	-	-	-	-	-
55	240	260	-0.003247712	-	-	-	-	-	-
10	250	60	-0.003542958	-	-	-	-	-	-
10	260	55	-0.003247712	-	-	-	-	-	-
10	270	55	-0.003247712	-	-	-	-	-	-
10	280	55	-0.003247712	-	-	-	-	-	-
10	290	55	-0.003247712	-	-	-	-	-	-
1177	1467	2370	-0.001189013	15.16666667	-	197	294	6.61	7.3
222	1689	275	-0.000731467	-	-	-	-	-	-
1283	2972	1710	-0.000615024	13.66666667	2425.074354	243	337	6.95	6.91

1362	4334	1150	-0.000498581	13.33333333	2431.265621	249	336	6.94	7.51
114	4448	85	-0.00044028	-	-	-	-	-	-
244	4692	175	-0.000423509	-	-	-	-	-	-
1189	5881	670	-0.000332742	12	704.6388726	202	364	6.89	7.31
1340	7221	105	-0.000235227	11.66666667	2911.272358	187	459	7.13	7.56
1415	8636	330	-0.000137712	11.66666667	3777.128102	185	352	7.54	7.49
1556	10192	280	-0.000106258	11.33333333	1505.25934	206	449	7.41	7.64
1336	11528	100	-4.41986E-05	11.33333333	4629.728861	205	482	7.86	7.67
1420	12948	60	-2.49504E-05	11.33333333	4095.398699	299	485	7.39	8
	Total	**8175**							

(u) Batch U – Bed 4 (Wednesday, August 17, 2022)

Time Intervals (min)	Cumulative Time (min)	Collected Volume (ml)	Effluent Flux (cm/min)	Sludge Deposit Layer (cm)	TS (mg/L)	COD (mg/L)	NO_3 (mg/L)	pH	DO (mg/L)
Influent	**-**	**2930**	**-**	**9.666666667**	**55780**	**1980**	**361**	**8.45**	**0.2**
200	200	0	0	-	-	-	-	-	-
50	250	60	-0.000708592	-	-	-	-	-	-
1186	1436	555	-0.000276327	12	1980.509981	170	342	7.31	7.07
1340	2776	465	-0.00020491	11.33333333	1647.967131	176	328	7.34	7.46
1415	4191	255	-0.000106414	9.5	2533.619178	173	328	7.68	7.58
	Total	**1335**							

(v) Batch V – Bed 1 (Saturday, August 20, 2022)

Time Intervals (min)	Cumulative Time (min)	Collected Volume (ml)	Effluent Flux (cm/min)	Sludge Deposit Layer (cm)	TS (mg/L)	COD (mg/L)	NO_3 (mg/L)	pH	DO (mg/L)
Influent	-	**2930**	-	7.5	**55780**	1980	361	8.45	0.2
102	102	0	0	10.3	-	-	-	-	-
1440	1542	300	-0.000123019	10.17	6019.633265	290	703	7.34	7.24

1342	2884	100	-4.4001E-05	9.83	6533.368412	304	755	7.22	7.9
1424	4308	50	-2.07336E-05	9	7147.624875	336	782	7.12	7.96
1452	5760	20	-8.13351E-06	8.3	3573.812437	505	-	-	-
1481	7241	0	0	8.3	-	-	-	-	-
	Total	**470**							

(w) Batch W – Bed 2 (Saturday, August 20, 2022)

Time Intervals (min)	Cumulative Time (min)	Collected Volume (ml)	Effluent Flux (cm/min)	Sludge Deposit Layer (cm)	TS (mg/L)	COD (mg/L)	NO_3 (mg/L)	pH	DO (mg/L)
Influent	**-**	**5870**	**-**	**10.83**	**55780**	**1980**	**361**	**8.45**	**0.2**
0	0	0	0	-	-	-	-	-	-
146	146	100	-0.000404447	13	3816.793893	245	330	7.39	7.56
1396	1542	715	-0.000302437	12.3	3178.928247	238	345	7.44	7.96
1345	2887	695	-0.000305125	12.3	1877.682403	184	334	7.41	8.16
1418	4305	585	-0.00024361	11.83	3108.429329	235	328	7.22	8.06
1454	5759	530	-0.000215242	11.5	2498.825339	263	267	7.17	7.15
1481	7240	410	-0.000163472	11.67	3486.055777	235	351	7.34	7.21
	Total	**3035**							

(x) Batch X – Bed 3 (Saturday, August 20, 2022)

Time Intervals (min)	Cumulative Time (min)	Collected Volume (ml)	Effluent Flux (cm/min)	Sludge Deposit Layer (cm)	TS (mg/L)	COD (mg/L)	NO_3 (mg/L)	pH	DO (mg/L)
Influent	**-**	**8800**	**-**	**10.5**	**55780**	**1980**	**361**	**8.45**	**0.2**
0	0	0	0	-	-	-	-	-	-
145	145	115	-0.000468322	12.5	2582.138723	183	299	7.52	7.27
1398	1543	1640	-0.00069271	11	1917.118081	189	343	7.55	7.96
1341	2884	1280	-0.000563632	10.3	3092.616954	257	281	7.2	8
1422	4306	1140	-0.000473391	10.17	1891.222121	177	344	7.36	8.03

1454	5760	885	-0.000359413	10.3	2157.802964	177	300	7.43	7.12
1481	7241	710	-0.000283086	9.67	2306.881097	171	383	7.66	7.14
	Total	**5770**							

(y) Batch Y – Bed 4 (Saturday, August 20, 2022)

Time Intervals (min)	Cumulative Time (min)	Collected Volume (ml)	Effluent Flux (cm/min)	Sludge Deposit Layer (cm)	TS (mg/L)	COD (mg/L)	NO_3 (mg/L)	pH	DO (mg/L)
Influent	**-**	**2930**	**-**	**9.5**	**55780**	**5911-7726**	**394**	**7.96**	**0.12**
0	0	0	0	-	-	-	-	-	-
146	146	20	-8.08895E-05	-	-	-	-	-	-
1399	1545	750	-0.000316562	13	3720.302846	170	352	7.55	7.4
1341	2886	385	-0.00016953	11.33333333	2984.190624	177	404	7.66	7.98
1418	4304	190	-7.91211E-05	10.66666667	3123.605533	168	328	7.46	7.98
	Total	**1345**							

(z) Batch Z – Bed 5 (Saturday, August 20, 2022)

Time Intervals (min)	Cumulative Time (min)	Collected Volume (ml)	Effluent Flux (cm/min)	Sludge Deposit Layer (cm)	TS (mg/L)	COD (mg/L)	NO_3 (mg/L)	pH	DO (mg/L)
Influent	**-**	**5870**	**-**	**7.666666667**	**55780**	**1980**	**361**	**8.45**	**0.2**
0	0	0	0	-	-	-	-	-	-
144	144	70	-0.000287045	11.33333333	3968.338632	183	425	7.37	6.41
1402	1546	1785	-0.000751805	10	3142.298248	178	519	7.91	7.76
1339	2885	365	-0.000160963	9	3755.154699	170	497	7.71	7.95
1417	4302	150	-6.25081E-05	8.333333333	4194.397027	185	508	7.65	7.86
1459	5761	125	-5.05906E-05	8.833333333	4633.639356	180	462	7.66	7.48
1489	7250	75	-2.97428E-05	8.5	4551.243241	210	531	7.45	7.76
	Total	**2570**							

(aa) Batch AA – Bed 4 (Tuesday, August 23, 2022)

Time Intervals (min)	Cumulative Time (min)	Collected Volume (ml)	Effluent Flux (cm/min)	Sludge Deposit Layer (cm)	TS (mg/L)	COD (mg/L)	NO_3 (mg/L)	pH	DO (mg/L)
Influent	**-**	**2930**	**-**	**10.66666667**	**55780**	**1980**	**361**	**8.45**	**0.2**
0	0	0	0	-	-	-	-	-	-
1441	1441	1515	-0.000620817	10.33333333	2124.50911	246	407	7.62	7.48
1476	2917	275	-0.000110017	9.83	2953.835767	190	271	6.64	5.56
1501	4418	120	-4.7208E-05	9.666666667	3374.770387	185	380	7.46	7.31
	Total	**1910**							

(ab) Batch AB – Bed 6 (Tuesday, August 23, 2022)

Time Intervals (min)	Cumulative Time (min)	Collected Volume (ml)	Effluent Flux (cm/min)	Sludge Deposit Layer (cm)	TS (mg/L)	COD (mg/L)	NO_3 (mg/L)	pH	DO (mg/L)
Influent	**-**	**8800**	**-**	**-**	**55780**	**1980**	**361**	**8.45**	**0.2**
0	0	0	0	-	-	-	-	-	-
1448	1448	3485	-0.00142118	-	2746.61427	201	352	7.05	7.95
1474	2922	920	-0.000368557	-	3484.733548	187	374	7.32	7.17
1502	4424	465	-0.000182809	-	5749.213	198	398	7.49	7.4
1505	5929	185	-7.25855E-05	-	4696.417171	190	444	7.58	7.51
1430	7359	90	-3.71639E-05	-	3643.621342	213	521	7.75	7.63
1286	8645	20	-9.18341E-06	-	1821.810671	364	653	7.83	8.49
1477	10122	15	-5.99688E-06	-	-	521	-	-	-
1438	11560	0	0	-	-	-	-	-	-
1414	12974	0	0	-	-	-	-	-	-
	Total	**5180**							

(ac) Batch AC – Bed 1 (Friday, August 26, 2022)

Time Intervals	Cumulative Time	Collected	Effluent Flux	Sludge Deposit	TS (mg/L)	COD	NO_3	pH	DO

(min)	(min)	Volume (ml)	(cm/min)	Layer (cm)		(mg/L)	(mg/L)		(mg/L)
Influent	**-**	**8030**	**-**	**8.3**	**20365**	**6152**	**162**	**7.44**	**0.2**
30	30	0	0	-	-	-	-	-	-
15	45	20	-0.000787324	-	-	263	725	7.29	6.24
10	55	110	-0.006495424	-	-	-	-	-	-
5	60	150	-0.017714792	-	-	-	-	-	-
5	65	125	-0.014762327	-	-	-	-	-	-
5	70	120	-0.014171833	-	-	-	-	-	-
5	75	110	-0.012990847	-	-	-	-	-	-
5	80	110	-0.012990847	-	-	-	-	-	-
5	85	110	-0.012990847	-	-	-	-	-	-
5	90	100	-0.011809861	-	-	-	-	-	-
5	95	100	-0.011809861	-	-	-	-	-	-
5	100	90	-0.010628875	-	-	-	-	-	-
5	105	90	-0.010628875	-	-	-	-	-	-
5	110	85	-0.010038382	-	-	-	-	-	-
5	115	85	-0.010038382	-	-	-	-	-	-
5	120	85	-0.010038382	-	-	-	-	-	-
5	125	75	-0.008857396	-	-	-	-	-	-
5	130	75	-0.008857396	-	-	-	-	-	-
5	135	75	-0.008857396	-	-	-	-	-	-
5	140	70	-0.008266903	-	-	-	-	-	-
5	145	80	-0.009447889	-	-	-	-	-	-
5	150	70	-0.008266903	-	-	-	-	-	-
5	155	70	-0.008266903	-	-	-	-	-	-
5	160	70	-0.008266903	-	-	-	-	-	-
5	165	65	-0.00767641	-	-	-	-	-	-
5	170	60	-0.007085917	-	-	-	-	-	-
5	175	60	-0.007085917	-	-	-	-	-	-
5	180	60	-0.007085917	-	-	-	-	-	-
5	185	55	-0.006495424	-	-	-	-	-	-

5	190	55	-0.006495424	-	-	-	-	-	-
5	195	50	-0.005904931	-	-	-	-	-	-
5	200	50	-0.005904931	-	-	-	-	-	-
5	205	50	-0.005904931	-	-	-	-	-	-
33	238	225	-0.004026089	-	-	-	-	-	-
1265	1503	1285	-0.000599829	9.5	5908.419498	269	675	6.8	3.36
1428	2931	180	-7.44319E-05	9.5	9125.969774	292	828	7.35	7.1
1286	4217	65	-2.98461E-05	9.3	9929.113049	362	951	7.88	7.77
1477	5694	25	-9.9948E-06	9	6712.478384	384	-	-	-
1437	7131	0	0	8.5	-	-	-	-	-
1414	8545	0	0	7.5	-	-	-	-	-
	Total	**4360**							

(ad) Batch AD – Bed 2 (Friday, August 26, 2022)

Time Intervals (min)	Cumulative Time (min)	Collected Volume (ml)	Effluent Flux (cm/min)	Sludge Deposit Layer (cm)	TS (mg/L)	COD (mg/L)	NO_3 (mg/L)	pH	DO (mg/L)
Influent	**-**	**16070**	**-**	**11.67**	**20365**	**6152**	**162**	**7.44**	**0.2**
0	0	0	0	-	-	-	-	-	-
200	200	155	-0.000457632	12.83		235	349	7.37	7.28
20	220	70	-0.002066726	-	-	-	-	-	-
10	230	55	-0.003247712	-	-	-	-	-	-
1282	1512	3270	-0.001506172	12.3	10183.39116	226	308	7.27	7.34
1419	2931	2050	-0.000853073	12.5	13458.23067	234	319	7.47	7.5
1291	4222	1155	-0.000528288	12	7835.500846	286	346	7.6	7.77
170	4392	135	-0.000468921	-	-	-	-	-	-
1300	5692	880	-0.000399718	12	7762.025432	248	302	6.94	7.86
1428	7120	690	-0.000285322	11.67	2431.750401	248	344	6.96	7.98
1411	8531	470	-0.000196692	11.5	8128.759551	216	295	7.12	8.44
	Total	**8930**							

(ae) Batch AE – Bed 3 (Friday, August 26, 2022)

Time Intervals (min)	Cumulative Time (min)	Collected Volume (ml)	Effluent Flux (cm/min)	Sludge Deposit Layer (cm)	TS (mg/L)	COD (mg/L)	NO_3 (mg/L)	pH	DO (mg/L)
Influent	**-**	**24110**	**-**	**9.67**	**20365**	**6152**	**162**	**7.44**	**0.2**
0	0	0	0	-	-	-	-	-	-
90	90	35	-0.000229636	-	-	183	319	7.17	4.34
20	110	30	-0.00088574	-	-	-	-	-	-
10	120	60	-0.003542958	-	-	-	-	-	-
10	130	70	-0.004133451	-	-	-	-	-	-
10	140	75	-0.004428698	-	-	-	-	-	-
10	150	85	-0.005019191	-	-	-	-	-	-
10	160	95	-0.005609684	-	-	-	-	-	-
10	170	110	-0.006495424	-	-	-	-	-	-
10	180	115	-0.00679067	-	-	-	-	-	-
10	190	110	-0.006495424	-	-	-	-	-	-
10	200	100	-0.005904931	-	-	-	-	-	-
10	210	100	-0.005904931	-	-	-	-	-	-
10	220	90	-0.005314438	-	-	-	-	-	-
10	230	90	-0.005314438	-	-	-	-	-	-
1270	1500	3350	-0.0015576	12.3	16260.92021	199	331	7.13	5.86
1429	2929	1770	-0.000731401	12	7872.461734	185	364	7.51	7.38
1286	4215	1010	-0.000463762	11.67	1591.560184	180	409	7.7	7.85
172	4387	140	-0.000480634	-	-	-	-	-	-
1302	5689	1115	-0.000505683	11.67	1698.180159	183	319	7.17	7.91
1437	7126	1245	-0.000511596	11.5	1924.8592	150	402	7.42	7.95
1410	8536	905	-0.000379004	11.3	1678.853078	158	336	7.39	8.39
	Total	**10700**							

(af) Batch AF – Bed 4 (Friday, August 26, 2022)

Time Intervals (min)	Cumulative Time (min)	Collected Volume (ml)	Effluent Flux (cm/min)	Sludge Deposit Layer (cm)	TS (mg/L)	COD (mg/L)	NO_3 (mg/L)	pH	DO (mg/L)
Influent	**-**	**8030**	**-**	**-**	**20365**	**6152**	**162**	**7.44**	**0.2**
0	0	0	0	-	-	-	-	-	-
100	100	20	-0.000118099	-	-	179	332	7.09	3.25
15	115	55	-0.002165141	-	-	-	-	-	-
10	125	70	-0.004133451	-	-	-	-	-	-
10	135	70	-0.004133451	-	-	-	-	-	-
10	145	80	-0.004723944	-	-	-	-	-	-
10	155	55	-0.003247712	-	-	-	-	-	-
10	165	50	-0.002952465	-	-	-	-	-	-
10	175	50	-0.002952465	-	-	-	-	-	-
10	185	50	-0.002952465	-	-	-	-	-	-
10	195	50	-0.002952465	-	-	-	-	-	-
10	205	50	-0.002952465	-	-	-	-	-	-
10	215	50	-0.002952465	-	-	-	-	-	-
10	225	45	-0.002657219	-	-	-	-	-	-
10	235	50	-0.002952465	-	-	-	-	-	-
1275	1510	2520	-0.001167092	-	7073.715562	189	343	7.06	5.43
1427	2937	850	-0.00035173	-	12391.48531	174	395	7.44	7.19
1279	4216	245	-0.000113112	-	9902.880187	191	435	7.78	7.79
	Total	**4360**							

(ag) Batch AG – Bed 5 (Friday, August 26, 2022)

Time Intervals (min)	Cumulative Time (min)	Collected Volume (ml)	Effluent Flux (cm/min)	Sludge Deposit Layer (cm)	TS (mg/L)	COD (mg/L)	NO_3 (mg/L)	pH	DO (mg/L)
Influent	**-**	**16070**	**-**	**-**	**20365**	**6152**	**162**	**7.44**	**0.2**
0	0	0	0	-	-	-	-	-	-

95	95	35	-0.00021755	-	-	169	384	6.98	2.57
15	110	65	-0.002558803	-	-	-	-	-	-
10	120	60	-0.003542958	-	-	-	-	-	-
10	130	70	-0.004133451	-	-	-	-	-	-
10	140	70	-0.004133451	-	-	-	-	-	-
10	150	80	-0.004723944	-	-	-	-	-	-
10	160	75	-0.004428698	-	-	-	-	-	-
10	170	70	-0.004133451	-	-	-	-	-	-
10	180	75	-0.004428698	-	-	-	-	-	-
10	190	90	-0.005314438	-	-	-	-	-	-
10	200	75	-0.004428698	-	-	-	-	-	-
10	210	75	-0.004428698	-	-	-	-	-	-
10	220	70	-0.004133451	-	-	-	-	-	-
10	230	65	-0.003838205	-	-	-	-	-	-
1269	1499	4260	-0.00198227	-	13390.42797	170	393	7.44	6.57
1438	2937	2110	-0.00086644	-	11511.89563	162	430	7.56	7.31
1286	4223	790	-0.000362745	-	3023.998452	177	466	7.76	7.83
169	4392	70	-0.000244583	-	-	-	-	-	-
1307	5699	430	-0.000194271	-	4199.202623	167	403	7.43	7.8
1428	7127	245	-0.00010131	-	3352.261066	164	460	7.64	8
1416	8543	105	-4.37866E-05	-	3143.613501	195	416	7.58	8.26
	Total	**8985**							

(ah) Batch AH – Bed 4 (Monday, August 29, 2022)

Time Intervals (min)	Cumulative Time (min)	Collected Volume (ml)	Effluent Flux (cm/min)	Sludge Deposit Layer (cm)	TS (mg/L)	COD (mg/L)	NO_3 (mg/L)	pH	DO (mg/L)
Influent	**-**	**8030**	**-**	**-**	**20365**	**6152**	**162**	**7.44**	**0.2**
0	0	0	0	-	-	-	-	-	-
170	170	45	-0.000156307	-	-	-	-	-	-
1308	1478	2170	-0.000979641	-	3389.674176	171	342	7.21	7.94

1431	2909	1315	-0.000542626	-	2639.509051	150	382	7.41	7.84
1415	4324	545	-0.000227434	-	2316.960148	168	320	7.35	8.47
	Total	**4075**							

(ai) Batch AI – Bed 1 (Thursday, September 15, 2022)

Time Intervals (min)	Cumulative Time (min)	Collected Volume (ml)	Effluent Flux (cm/min)	Sludge Deposit Layer (cm)	TS (mg/L)	COD (mg/L)	NO_3 (mg/L)	pH	DO (mg/L)
Influent	**-**	**8030**	**-**	**7**	**20365**	**6152**	**162**	**7.44**	**0.2**
25	25	0	0	-	-	-	-	-	-
5	30	90	-0.010628875	-	-	362	520	6.96	2.75
5	35	170	-0.020076764	-	-	-	-	-	-
5	40	150	-0.017714792	-	-	-	-	-	-
5	45	135	-0.015943313	-	-	-	-	-	-
5	50	110	-0.012990847	-	-	-	-	-	-
5	55	105	-0.012400354	-	-	-	-	-	-
5	60	95	-0.011219368	-	-	-	-	-	-
5	65	90	-0.010628875	-	-	-	-	-	-
5	70	80	-0.009447889	-	-	-	-	-	-
5	75	65	-0.00767641	-	-	-	-	-	-
5	80	60	-0.007085917	-	-	-	-	-	-
5	85	65	-0.00767641	-	-	-	-	-	-
5	90	50	-0.005904931	-	-	-	-	-	-
5	95	50	-0.005904931	-	-	-	-	-	-
5	100	50	-0.005904931	-	-	-	-	-	-
5	105	45	-0.005314438	-	-	-	-	-	-
5	110	40	-0.004723944	-	-	-	-	-	-
2170	2280	835	-0.000227217	6.666666667	-	336	542	6.77	2.745
2440	4720	25	-6.05013E-06	7	-	310	564	6.57	2.74

2917	7637	0	0	6.166666667	-	-	-	-	-
	Total	**2310**							

(aj) Batch AJ – Bed 2 (Thursday, September 15, 2022)

Time Intervals (min)	Cumulative Time (min)	Collected Volume (ml)	Effluent Flux (cm/min)	Sludge Deposit Layer (cm)	TS (mg/L)	COD (mg/L)	NO_3 (mg/L)	pH	DO (mg/L)
Influent	**-**	**16070**	**-**	**15.83333333**	**20365**	**6152**	**162**	**7.44**	**0.2**
100	100	0	0	-	-	-	-	-	-
10	110	80	-0.004723944	-	873.6924	258	297	6.59	4.63
5	115	95	-0.011219368	-	-	-	-	-	-
5	120	90	-0.010628875	-	-	-	-	-	-
5	125	80	-0.009447889	-	-	-	-	-	-
5	130	70	-0.008266903	-	-	-	-	-	-
5	135	75	-0.008857396	-	-	-	-	-	-
5	140	90	-0.010628875	-	-	-	-	-	-
5	145	85	-0.010038382	-	-	-	-	-	-
5	150	80	-0.009447889	-	-	-	-	-	-
5	155	80	-0.009447889	-	-	-	-	-	-
5	160	80	-0.009447889	-	-	-	-	-	-
5	165	75	-0.008857396	-	-	-	-	-	-
5	170	75	-0.008857396	-	-	-	-	-	-
5	175	75	-0.008857396	-	-	-	-	-	-
5	180	75	-0.008857396	-	-	-	-	-	-
5	185	75	-0.008857396	-	-	-	-	-	-
5	190	75	-0.008857396	-	-	-	-	-	-
5	195	75	-0.008857396	-	-	-	-	-	-
5	200	70	-0.008266903	-	-	-	-	-	-
5	205	75	-0.008857396	-	-	-	-	-	-
5	210	60	-0.007085917	-	-	-	-	-	-
5	215	75	-0.008857396	-	-	-	-	-	-

5	220	75	-0.008857396	-	-	-	-	-	-
5	225	75	-0.008857396	-	-	-	-	-	-
5	230	80	-0.009447889	-	-	-	-	-	-
5	235	75	-0.008857396	-	-	-	-	-	-
2762	2997	6635	-0.001418509	12.5	1545.469	304	405	7.15	5.93
2821	5818	615	-0.000128732	12.5	3081.986	337	511	7.75	7.87
2918	8736	140	-2.83307E-05	12.33333333	1173.885	299	520	7.59	7.16
	Total	**8740**							

(ak) Batch AK – Bed 3 (Thursday, September 15, 2022)

Time Intervals (min)	Cumulative Time (min)	Collected Volume (ml)	Effluent Flux (cm/min)	Sludge Deposit Layer (cm)	TS (mg/L)	COD (mg/L)	NO_3 (mg/L)	pH	DO (mg/L)
Influent	**-**	**24110**	**-**	**18**	**20365**	**6152**	**162**	**7.44**	**0.2**
65	65	0	0	-	-	-	-	-	-
12	77	115	-0.005658892	-	-1790.1	129	304	7.22	5.55
3	80	55	-0.010825706	-	-	-	-	-	-
5	85	90	-0.010628875	-	-	-	-	-	-
5	90	100	-0.011809861	-	-	-	-	-	-
5	95	110	-0.012990847	-	-	-	-	-	-
5	100	105	-0.012400354	-	-	-	-	-	-
5	105	115	-0.01358134	-	-	-	-	-	-
5	110	120	-0.014171833	-	-	-	-	-	-
5	115	125	-0.014762327	-	-	-	-	-	-
5	120	125	-0.014762327	-	-	-	-	-	-
5	125	125	-0.014762327	-	-	-	-	-	-
5	130	135	-0.015943313	-	-	-	-	-	-
5	135	150	-0.017714792	-	-	-	-	-	-
5	140	135	-0.015943313	-	-	-	-	-	-
5	145	130	-0.01535282	-	-	-	-	-	-
5	150	130	-0.01535282	-	-	-	-	-	-

5	155	130	-0.01535282	-	-	-	-	-	-
5	160	135	-0.015943313	-	-	-	-	-	-
5	165	100	-0.017419545	-	-	-	-	-	-
5	170	160	-0.018895778	-	-	-	-	-	-
5	175	160	-0.018895778	-	-	-	-	-	-
5	180	130	-0.01535282	-	-	-	-	-	-
5	185	125	-0.014762327	-	-	-	-	-	-
5	190	125	-0.014762327	-	-	-	-	-	-
5	195	115	-0.01358134	-	-	-	-	-	-
5	200	110	-0.012990847	-	-	-	-	-	-
5	205	100	-0.011809861	-	-	-	-	-	-
5	210	100	-0.011809861	-	-	-	-	-	-
5	215	100	-0.011809861	-	-	-	-	-	-
5	220	105	-0.012400354	-	-	-	-	-	-
5	225	105	-0.012400354	-	-	-	-	-	-
5	230	105	-0.012400354	-	-	-	-	-	-
2764	2994	9900	-0.002115008	14.66666667	1348.290368	221	214	6.73	2.75
2819	5813	1630	-0.000341434	11.66666667	2305.58494	163	316	6.7	7.54
2920	8733	580	-0.00011729	11.5	2510.544286	174	420	6.97	6.74
	Total	**14275**							

(al) Batch AL – Bed 4 (Thursday, September 15, 2022)

Time Intervals (min)	Cumulative Time (min)	Collected Volume (ml)	Effluent Flux (cm/min)	Sludge Deposit Layer (cm)	TS (mg/L)	COD (mg/L)	NO_3 (mg/L)	pH	DO (mg/L)
Influent	**-**	**55210**	**-**	**26**	**20365**	**6152**	**162**	**7.44**	**0.2**
55	55	0	0	-	-	-	-	-	-
13	68	170	-0.007721832	-	1421.185465	155	247	6.96	6.83
7	75	165	-0.013918765	-	-	-	-	-	-
5	80	120	-0.014171833	-	-	-	-	-	-
5	85	115	-0.01358134	-	-	-	-	-	-

5	90	125	-0.014762327	-	-	-	-	-	-
5	95	115	-0.01358134	-	-	-	-	-	-
5	100	115	-0.01358134	-	-	-	-	-	-
5	105	110	-0.012990847	-	-	-	-	-	-
5	110	115	-0.01358134	-	-	-	-	-	-
5	115	115	-0.01358134	-	-	-	-	-	-
5	120	110	-0.012990847	-	-	-	-	-	-
5	125	110	-0.012990847	-	-	-	-	-	-
5	130	110	-0.012990847	-	-	-	-	-	-
5	135	110	-0.012990847	-	-	-	-	-	-
5	140	115	-0.01358134	-	-	-	-	-	-
5	145	105	-0.012400354	-	-	-	-	-	-
5	150	110	-0.012990847	-	-	-	-	-	-
5	155	100	-0.011809861	-	-	-	-	-	-
5	160	105	-0.012400354	-	-	-	-	-	-
5	165	95	-0.011219368	-	-	-	-	-	-
5	170	95	-0.011219368	-	-	-	-	-	-
5	175	95	-0.011219368	-	-	-	-	-	-
5	180	95	-0.011219368	-	-	-	-	-	-
5	185	90	-0.010628875	-	-	-	-	-	-
5	190	90	-0.010628875	-	-	-	-	-	-
5	195	160	-0.010038382	-	-	-	-	-	-
5	200	80	-0.009447889	-	-	-	-	-	-
5	205	80	-0.009447889	-	-	-	-	-	-
5	210	80	-0.009447889	-	-	-	-	-	-
2771	2981	17800	-0.003793135	21.5	1566.389751	225	308	7.4	2.21
2820	5801	4100	-0.000858518	10.33333333	856.2621304	169	341	7.45	7.47
2922	8723	1850	-0.000373858	10.5	955.2141044	143	404	7.31	6.89
2896	11619	730	-0.000148847	10.83333333	2518.834009	235	416	7.82	6.98
3009	14628	320	-6.27975E-05	10.83333333	2853.611954	134	376	7.47	6.88
2605	17233	560	-5.81832E-05	10.83333333	3102.218086	128	267	5.8	7.56

2866	20099	260	-5.35688E-05	11	7654.43	127	606	7.91	7.61
3052	23151	0	0	11.16666667	-	-	-	-	-
2838	25989	0	0	10.33333333	-	-	-	-	-
	Total	**28820**							

(am) Batch AM – Bed 5 (Thursday, September 15, 2022)

Time Intervals (min)	Cumulative Time (min)	Collected Volume (ml)	Effluent Flux (cm/min)	Sludge Deposit Layer (cm)	TS (mg/L)	COD (mg/L)	NO_3 (mg/L)	pH	DO (mg/L)
Influent	**-**	**90315**	**-**	**36.66666667**	**20365**	**6152**	**162**	**7.44**	**0.2**
8	8	0	0	-	-	-	-	-	-
2	10	150	-0.04428698	-	802.8025106	191	399	7.63	1.77
2	12	470	-0.13876587	-	-	-	-	-	-
2	14	345	-0.101860053	-	-	-	-	-	-
2	16	310	-0.091526425	-	-	-	-	-	-
2	18	300	-0.088573959	-	-	-	-	-	-
2	20	310	-0.091526425	-	-	-	-	-	-
2	22	245	-0.0723354	-	-	-	-	-	-
2	24	245	-0.0723354	-	-	-	-	-	-
2	26	260	-0.076764098	-	-	-	-	-	-
2	28	260	-0.076764098	-	-	-	-	-	-
2	30	260	-0.076764098	-	-	-	-	-	-
2	32	235	-0.069382935	-	-	-	-	-	-
2	34	245	-0.0723354	-	-	-	-	-	-
2	36	230	-0.067906702	-	-	-	-	-	-
2	38	250	-0.073811633	-	-	-	-	-	-
2	40	220	-0.064954237	-	-	-	-	-	-
2	42	215	-0.063478004	-	-	-	-	-	-
2	44	215	-0.063478004	-	-	-	-	-	-
2	46	215	-0.063478004	-	-	-	-	-	-
2	48	210	-0.062001771	-	-	-	-	-	-

2	50	205	-0.060525539	-	-	-	-	-	-
2	52	190	-0.056096841	-	-	-	-	-	-
2	54	195	-0.057573074	-	-	-	-	-	-
2	56	175	-0.051668143	-	-	-	-	-	-
2	58	180	-0.053144376	-	-	-	-	-	-
2	60	180	-0.053144376	-	-	-	-	-	-
2	62	165	-0.048715678	-	-	-	-	-	-
2	64	170	-0.05019191	-	-	-	-	-	-
2	66	165	-0.048715678	-	-	-	-	-	-
2	68	155	-0.045763212	-	-	-	-	-	-
2	70	165	-0.048715678	-	-	-	-	-	-
2	72	140	-0.041334514	-	-	-	-	-	-
2	74	160	-0.047239445	-	-	-	-	-	-
2	76	140	-0.041334514	-	-	-	-	-	-
2	78	150	-0.04428698	-	-	-	-	-	-
2	80	140	-0.041334514	-	-	-	-	-	-
2	82	145	-0.042810747	-	-	-	-	-	-
2	84	140	-0.041334514	-	-	-	-	-	-
2	86	135	-0.039858282	-	-	-	-	-	-
2	88	140	-0.041334514	-	-	-	-	-	-
2	90	135	-0.039858282	-	-	-	-	-	-
2	92	135	-0.039858282	-	-	-	-	-	-
2	94	125	-0.036905816	-	-	-	-	-	-
2	96	135	-0.039858282	-	-	-	-	-	-
2	98	135	-0.039858282	-	-	-	-	-	-
2	100	130	-0.038382049	-	-	-	-	-	-
2	102	130	-0.038382049	-	-	-	-	-	-
2	104	110	-0.032477118	-	-	-	-	-	-
2	106	130	-0.038382049	-	-	-	-	-	-
2	108	120	-0.035429584	-	-	-	-	-	-
2	110	110	-0.032477118	-	-	-	-	-	-

2	112	115	-0.033953351	-	-	-	-	-	-
2	114	105	-0.031000886	-	-	-	-	-	-
2	116	110	-0.032477118	-	-	-	-	-	-
2	118	110	-0.032477118	-	-	-	-	-	-
2	120	110	-0.032477118	-	-	-	-	-	-
4	124	200	-0.029524653	-	-	-	-	-	-
5	129	245	-0.02893416	-	-	-	-	-	-
5	134	235	-0.027753174	-	-	-	-	-	-
5	139	210	-0.024800709	-	-	-	-	-	-
5	144	205	-0.024210216	-	-	-	-	-	-
5	149	195	-0.023029229	-	-	-	-	-	-
5	154	190	-0.022438736	-	-	-	-	-	-
2737	2891	49400	-0.010657785	13	2972.599111	235	359	7.94	2.63
2851	5742	15790	-0.003270391	11	1384.4024	157	437	7.58	6.67
2907	8649	680	-0.000138127	10.83333333	2149.510389	155	493	7.4	4.97
2723	11372	160	-3.46966E-05	10.66666667	3587.694423	268	662	7.45	5.14
3192	14564	15	-2.77487E-06	10.16666667	-	-	-	-	-
2608	17172	0	0	10.5	-	-	-	-	-
2864	20036	0	0	10.16666667	-	-	-	-	-
3052	23088	0	0	10.16666667	-	-	-	-	-
2838	25926	0	0	9.666666667	-	-	-	-	-
3005	28931	0	0	10.66666667	-	-	-	-	-
1674	30605	0	0	10.66666667	-	-	-	-	-
3885	34490	0	0	10.83333333	-	-	-	-	-
2949	37439	0	0	10.83	-	-	-	-	-
1392	38831	0	0	-	-	-	-	-	-
	Total	**77895**							

(an) Batch AN – Bed 6 (Thursday, September 15, 2022)

Time Intervals	Cumulative Time	Collected	Effluent Flux	Sludge Deposit	TS (mg/L)	COD	NO_3	pH	DO

(min)	(min)	Volume (ml)	(cm/min)	Layer (cm)		(mg/L)	(mg/L)		(mg/L)
Influent	**-**	**24110**	**-**	**16.83333333**	**20365**	**6152**	**162**	**7.44**	**0.2**
45	45	0	0	-	-	-	-	-	-
5	50	65	-0.00767641	-	1103.270738	207	345	7.2	3.56
5	55	165	-0.019486271	-	-	-	-	-	-
5	60	140	-0.016533806	-	-	-	-	-	-
5	65	135	-0.015943313	-	-	-	-	-	-
5	70	140	-0.016533806	-	-	-	-	-	-
5	75	130	-0.01535282	-	-	-	-	-	-
5	80	135	-0.015943313	-	-	-	-	-	-
5	85	185	-0.021848243	-	-	-	-	-	-
5	90	140	-0.016533806	-	-	-	-	-	-
5	95	145	-0.017124299	-	-	-	-	-	-
5	100	150	-0.017714792	-	-	-	-	-	-
5	105	145	-0.017124299	-	-	-	-	-	-
5	110	185	-0.021848243	-	-	-	-	-	-
5	115	145	-0.017124299	-	-	-	-	-	-
5	120	140	-0.016533806	-	-	-	-	-	-
5	125	140	-0.016533806	-	-	-	-	-	-
5	130	145	-0.017124299	-	-	-	-	-	-
5	135	145	-0.017124299	-	-	-	-	-	-
5	140	140	-0.016533806	-	-	-	-	-	-
5	145	120	-0.014171833	-	-	-	-	-	-
5	150	135	-0.015943313	-	-	-	-	-	-
5	155	125	-0.014762327	-	-	-	-	-	-
5	160	130	-0.01535282	-	-	-	-	-	-
5	165	130	-0.01535282	-	-	-	-	-	-
5	170	120	-0.014171833	-	-	-	-	-	-
5	175	120	-0.014171833	-	-	-	-	-	-
5	180	125	-0.014762327	-	-	-	-	-	-
5	185	120	-0.014171833	-	-	-	-	-	-

5	190	140	-0.016533806	-	-	-	-	-	-
5	195	115	-0.01358134	-	-	-	-	-	-
5	200	120	-0.014171833	-	-	-	-	-	-
5	205	120	-0.014171833	-	-	-	-	-	-
5	210	120	-0.014171833	-	-	-	-	-	-
5	215	120	-0.014171833	-	-	-	-	-	-
2768	2983	9500	-0.00202662	12.66666667	4277.538498	246	504	6.96	6.33
2824	5807	200	-4.18196E-05	12	2637.141841	292	569	7.81	7.73
2921	8728	0	0	11.5	-	-	-	-	-
2896	11624	0	0	11.16666667	-	-	-	-	-
	Total	**11845**							

(ao) Batch AO – Bed 1 (Wednesday, September 21, 2022)

Time Intervals (min)	Cumulative Time (min)	Collected Volume (ml)	Effluent Flux (cm/min)	Sludge Deposit Layer (cm)	TS (mg/L)	COD (mg/L)	NO_3 (mg/L)	pH	DO (mg/L)
Influent	**-**	**15150**	**-**	**6.166666667**	**10795.65**	**5802**	**308**	**8.23**	**0.21**
1	1	1465	-0.865072335	-	910.3810212	271	703	7.7	1.26
1	2	1965	-1.160318866	-	-	-	-	-	-
1	3	1280	-0.755831119	-	-	-	-	-	-
1	4	820	-0.484204311	-	-	-	-	-	-
1	5	690	-0.407440213	-	-	-	-	-	-
1	6	470	-0.277531739	-	-	-	-	-	-
1	7	500	-0.295246531	-	-	-	-	-	-
1	8	345	-0.203720106	-	-	-	-	-	-
1	9	235	-0.13876587	-	-	-	-	-	-
1	10	230	-0.135813404	-	-	-	-	-	-
1	11	170	-0.10038382	-	-	-	-	-	-
1	12	160	-0.09447889	-	-	-	-	-	-
1	13	130	-0.076764098	-	-	-	-	-	-
1	14	115	-0.067906702	-	-	-	-	-	-

1	15	105	-0.062001771	-	-	-	-	-	-
5	20	300	-0.035429584	-	-	-	-	-	-
5	25	195	-0.023029229	-	-	-	-	-	-
5	30	140	-0.016533806	-	-	-	-	-	-
5	35	110	-0.012990847	-	-	-	-	-	-
5	40	95	-0.011219368	-	-	-	-	-	-
5	45	85	-0.010038382	-	-	-	-	-	-
30	75	275	-0.005412853	-	-	-	-	-	-
40	115	205	-0.003026277	-	-	-	-	-	-
45	160	150	-0.00196831	-	-	-	-	-	-
2727	2887	745	-0.000161319	8.166666667	3528.962215	152	658	8.17	7.87
3010	5897	75	-1.47133E-05	7.833333333	6003.295042	319	646	6.11	7.17
2677	8574	70	-1.54406E-05	8.166666667	5212.180042	241	628	6.78	7.64
	Total	**11125**							

(ap) Batch AP – Bed 2 (Wednesday, September 21, 2022)

Time Intervals (min)	Cumulative Time (min)	Collected Volume (ml)	Effluent Flux (cm/min)	Sludge Deposit Layer (cm)	TS (mg/L)	COD (mg/L)	NO_3 (mg/L)	pH	DO (mg/L)
Influent	**-**	**30310**	**-**	**12.33333333**	**10795.65**	**5802**	**308**	**8.23**	**0.21**
1	1	2160	-1.275465013	-	4051.05303	323	446	7.69	1.46
1	2	4880	-2.881606141	-	-	-	-	-	-
1	3	5115	-3.020372011	-	-	-	-	-	-
1	4	3500	-2.066725716	-	-	-	-	-	-
1	5	2320	-1.369943903	-	-	-	-	-	-
1	6	985	-0.581635666	-	-	-	-	-	-
1	7	670	-0.395630351	-	-	-	-	-	-
1	8	450	-0.265721878	-	-	-	-	-	-
1	9	250	-0.147623265	-	-	-	-	-	-
1	10	290	-0.171242988	-	-	-	-	-	-
1	11	285	-0.168290523	-	-	-	-	-	-

1	12	215	-0.126956008	-	-	-	-	-	-
1	13	200	-0.118098612	-	-	-	-	-	-
1	14	145	-0.085621494	-	-	-	-	-	-
1	15	135	-0.079716563	-	-	-	-	-	-
1	16	120	-0.070859167	-	-	-	-	-	-
1	17	115	-0.067906702	-	-	-	-	-	-
1	18	90	-0.053144376	-	-	-	-	-	-
1	19	90	-0.053144376	-	-	-	-	-	-
1	20	80	-0.047239445	-	-	-	-	-	-
1	21	80	-0.047239445	-	-	-	-	-	-
1	22	65	-0.038382049	-	-	-	-	-	-
1	23	65	-0.038382049	-	-	-	-	-	-
1	24	65	-0.038382049	-	-	-	-	-	-
1	25	55	-0.032477118	-	-	-	-	-	-
5	30	210	-0.024800709	-	-	-	-	-	-
5	35	170	-0.020076764	-	-	-	-	-	-
5	40	135	-0.015943313	-	-	-	-	-	-
35	75	550	-0.009279177	-	-	-	-	-	-
45	120	360	-0.004723944	-	-	-	-	-	-
2726	2846	1755	-0.00038016	12.33333333	2635.222654	125	521	8	7.92
3011	5857	225	-4.41252E-05	11.33333333	2837.189	225	217	5.94	7.05
2678	8535	115	-2.53572E-05	11.33333333	2865.984092	225	271	5.94	7.32
	Total	**25945**							

(aq) Batch AQ – Bed 3 (Wednesday, September 21, 2022)

Time Intervals (min)	Cumulative Time (min)	Collected Volume (ml)	Effluent Flux (cm/min)	Sludge Deposit Layer (cm)	TS (mg/L)	COD (mg/L)	NO_3 (mg/L)	pH	DO (mg/L)
Influent	**-**	**45470**	**-**	**11.5**	**10795.65**	**5802**	**308**	**8.23**	**0.21**
1	1	1380	-0.814880425	-	4992.920486	221	377	7.34	1.49
1	2	3860	-2.279303218	-	-	-	-	-	-

1	3	3730	-2.20253912	-	-	-	-	-	-
1	4	3935	-2.323590198	-	-	-	-	-	-
1	5	3555	-2.099202834	-	-	-	-	-	-
1	6	3470	-2.049010924	-	-	-	-	-	-
1	7	3115	-1.839385887	-	-	-	-	-	-
1	8	2660	-1.570711544	-	-	-	-	-	-
1	9	2345	-1.38470623	-	-	-	-	-	-
1	10	1915	-1.130794213	-	-	-	-	-	-
1	11	1490	-0.879834662	-	-	-	-	-	-
1	12	1020	-0.602302923	-	-	-	-	-	-
1	13	470	-0.277531739	-	-	-	-	-	-
1	14	485	-0.286389135	-	-	-	-	-	-
1	15	385	-0.227339829	-	-	-	-	-	-
1	16	310	-0.183052849	-	-	-	-	-	-
1	17	205	-0.121051078	-	-	-	-	-	-
1	18	180	-0.106288751	-	-	-	-	-	-
1	19	150	-0.088573959	-	-	-	-	-	-
1	20	130	-0.076764098	-	-	-	-	-	-
1	21	115	-0.067906702	-	-	-	-	-	-
1	22	100	-0.059049306	-	-	-	-	-	-
1	23	95	-0.056096841	-	-	-	-	-	-
1	24	85	-0.05019191	-	-	-	-	-	-
1	25	80	-0.047239445	-	-	-	-	-	-
5	30	285	-0.033658105	-	-	-	-	-	-
5	35	225	-0.026572188	-	-	-	-	-	-
5	40	190	-0.022438736	-	-	-	-	-	-
5	45	155	-0.018305285	-	-	-	-	-	-
5	50	130	-0.01535282	-	-	-	-	-	-
5	55	115	-0.01358134	-	-	-	-	-	-
5	60	105	-0.012400354	-	-	-	-	-	-
5	65	95	-0.011219368	-	-	-	-	-	-

5	70	85	-0.010038382	-	-	-	-	-	-
2728	2798	2435	-0.000527071	10.83333333	2208.945176	202	359	7.69	6.13
3010	5808	425	-8.33753E-05	12.16666667	3175.624933	163	268	6.36	6.46
2678	8486	520	-0.000114659	11.83333333	2496.600158	109	364	7.52	7.45
	Total	**40030**							

(ar) Batch AR – Bed 6 (Saturday, September 24, 2022)

Time Intervals (min)	Cumulative Time (min)	Collected Volume (ml)	Effluent Flux (cm/min)	Sludge Deposit Layer (cm)	TS (mg/L)	COD (mg/L)	NO_3 (mg/L)	pH	DO (mg/L)
Influent	**-**	**45470**	**-**	**11.3**	**10795.65**	**5802**	**308**	**8.23**	**0.21**
1	1	825	-0.487156776	-	2620.15464	256	538	7.65	3.13
1	2	1365	-0.806023029	-	-	-	-	-	-
1	3	780	-0.460584588	-	-	-	-	-	-
1	4	785	-0.463537053	-	-	-	-	-	-
1	5	820	-0.484204311	-	-	-	-	-	-
1	6	795	-0.469441984	-	-	-	-	-	-
1	7	930	-0.549158547	-	-	-	-	-	-
1	8	850	-0.501919102	-	-	-	-	-	-
1	9	740	-0.436964866	-	-	-	-	-	-
1	10	765	-0.451727192	-	-	-	-	-	-
1	11	775	-0.457632123	-	-	-	-	-	-
1	12	860	-0.507824033	-	-	-	-	-	-
1	13	745	-0.439917331	-	-	-	-	-	-
1	14	765	-0.451727192	-	-	-	-	-	-
1	15	800	-0.472394449	-	-	-	-	-	-
1	16	685	-0.485680543	-	-	-	-	-	-
1	17	845	-0.498966637	-	-	-	-	-	-
1	18	600	-0.354295837	-	-	-	-	-	-
1	19	660	-0.389725421	-	-	-	-	-	-
1	20	765	-0.451727192	-	-	-	-	-	-

2	22	1185	-0.349867139	-	-	-	-	-	-
2	24	1280	-0.377915559	-	-	-	-	-	-
2	26	1140	-0.336581045	-	-	-	-	-	-
2	28	1090	-0.321818719	-	-	-	-	-	-
2	30	980	-0.2893416	-	-	-	-	-	-
2	32	915	-0.270150576	-	-	-	-	-	-
2	34	915	-0.270150576	-	-	-	-	-	-
2	36	895	-0.264245645	-	-	-	-	-	-
2	38	755	-0.222911131	-	-	-	-	-	-
2	40	570	-0.168290523	-	-	-	-	-	-
2	42	475	-0.140242102	-	-	-	-	-	-
2	44	385	-0.113669914	-	-	-	-	-	-
2	46	315	-0.093002657	-	-	-	-	-	-
2	48	300	-0.088573959	-	-	-	-	-	-
2	50	250	-0.073811633	-	-	-	-	-	-
2	52	235	-0.069382935	-	-	-	-	-	-
2	54	205	-0.060525539	-	-	-	-	-	-
2	56	185	-0.054620608	-	-	-	-	-	-
2	58	155	-0.045763212	-	-	-	-	-	-
2	60	155	-0.045763212	-	-	-	-	-	-
2	62	150	-0.04428698	-	-	-	-	-	-
2	64	135	-0.039858282	-	-	-	-	-	-
2	66	140	-0.041334514	-	-	-	-	-	-
2	68	125	-0.036905816	12.5	-	-	-	-	-
3089	3157	3200	-0.000611712	12.16666667	-	240	400	7	4
2610	5767	100	-2.26243E-05	12.16666667	3306.617615	207	277	5.9	6.95
2861	8628	0	0	12.5	-	-	-	-	-
3052	11680	0	0	12.5	-	-	-	-	-
2838	14518	0	0	12.33333333	-	-	-	-	-
	Total	**32390**							

(as) Batch AS – Bed 1 (Tuesday, September 27, 2022)

Time Intervals (min)	Cumulative Time (min)	Collected Volume (ml)	Effluent Flux (cm/min)	Sludge Deposit Layer (cm)	TS (mg/L)	COD (mg/L)	NO_3 (mg/L)	pH	DO (mg/L)
Influent	**-**	**15150**	**-**	**8.166666667**	**10795.65**	**5802**	**308**	**8.23**	**0.21**
7	7	185	-0.015605888	-	4704.315988	243	577	6.62	4.81
1	8	130	-0.076764098	-	-	-	-	-	-
1	9	190	-0.112193682	-	-	-	-	-	-
1	10	235	-0.13876587	-	-	-	-	-	-
1	11	245	-0.1446708	-	-	-	-	-	-
1	12	240	-0.141718335	-	-	-	-	-	-
1	13	260	-0.153528196	-	-	-	-	-	-
1	14	295	-0.174195453	-	-	-	-	-	-
1	15	280	-0.165338057	-	-	-	-	-	-
1	16	295	-0.174195453	-	-	-	-	-	-
1	17	265	-0.156480661	-	-	-	-	-	-
1	18	260	-0.153528196	-	-	-	-	-	-
1	19	260	-0.153528196	-	-	-	-	-	-
1	20	260	-0.153528196	-	-	-	-	-	-
1	21	245	-0.1446708	-	-	-	-	-	-
1	22	280	-0.165338057	-	-	-	-	-	-
1	23	215	-0.126956008	-	-	-	-	-	-
1	24	240	-0.141718335	-	-	-	-	-	-
1	25	235	-0.13876587	-	-	-	-	-	-
1	26	230	-0.135813404	-	-	-	-	-	-
1	27	220	-0.129908474	-	-	-	-	-	-
2	29	415	-0.12252731	-	-	-	-	-	-
1	30	205	-0.121051078	-	-	-	-	-	-
1	31	190	-0.112193682	-	-	-	-	-	-
1	32	200	-0.118098612	-	-	-	-	-	-
1	33	185	-0.109241216	-	-	-	-	-	-
1	34	170	-0.10038382	-	-	-	-	-	-

1	35	180	-0.106288751	-	-	-	-	-	-
1	36	150	-0.088573959	-	-	-	-	-	-
1	37	160	-0.09447889	-	-	-	-	-	-
1	38	145	-0.085621494	-	-	-	-	-	-
1	39	150	-0.088573959	-	-	-	-	-	-
1	40	140	-0.082669029	-	-	-	-	-	-
1	41	145	-0.085621494	-	-	-	-	-	-
1	42	120	-0.070859167	-	-	-	-	-	-
2	44	245	-0.0723354	-	-	-	-	-	-
1	45	115	-0.067906702	-	-	-	-	-	-
1	46	115	-0.067906702	-	-	-	-	-	-
1	47	95	-0.056096841	-	-	-	-	-	-
1	48	105	-0.062001771	-	-	-	-	-	-
1	49	90	-0.053144376	-	-	-	-	-	-
1	50	100	-0.059049306	-	-	-	-	-	-
1	51	90	-0.053144376	-	-	-	-	-	-
1	52	85	-0.05019191	-	-	-	-	-	-
1	53	90	-0.053144376	-	-	-	-	-	-
2	55	155	-0.045763212	-	-	-	-	-	-
1	56	75	-0.04428698	-	-	-	-	-	-
1	57	75	-0.04428698	-	-	-	-	-	-
1	58	75	-0.04428698	-	-	-	-	-	-
1	59	70	-0.041334514	-	-	-	-	-	-
2867	2926	2940	-0.000605528	7.5	4309.658256	232	513	7.06	6.3
2973	5899	30	-5.95856E-06	7.833333333	3915.000523	-	-	-	-
2836	8735	0	0	7.5	-	-	-	-	-
	Total	**12170**							

(at) Batch AT – Bed 2 (Tuesday, September 27, 2022)

Time Intervals	Cumulative	Collected	Effluent Flux	Sludge Deposit	TS (mg/L)	COD	NO_3	pH	DO

(min)	Time (min)	Volume (ml)	(cm/min)	Layer (cm)		(mg/L)	(mg/L)		(mg/L)
Influent	**-**	**30310**	**-**	**11.33333333**	**10795.65**	**5802**	**308**	**8.23**	**0.21**
4	4	150	-0.02214349	-	2676.672921	186	301	6.31	7.12
1	5	430	-0.253912017	-	-	-	-	-	-
1	6	500	-0.295246531	-	-	-	-	-	-
3	9	1290	-0.253912017	-	-	-	-	-	-
4	13	2450	-0.361677	-	-	-	-	-	-
2	15	1305	-0.385296723	-	-	-	-	-	-
2	17	1170	-0.345438441	-	-	-	-	-	-
1	18	580	-0.342485976	-	-	-	-	-	-
2	20	1110	-0.327723649	-	-	-	-	-	-
2	22	1105	-0.326247417	-	-	-	-	-	-
2	24	1095	-0.323294951	-	-	-	-	-	-
2	26	1060	-0.312961323	-	-	-	-	-	-
2	28	870	-0.256864482	-	-	-	-	-	-
2	30	670	-0.197815176	-	-	-	-	-	-
2	32	715	-0.21110127	-	-	-	-	-	-
2	34	470	-0.13876587	-	-	-	-	-	-
2	36	415	-0.12252731	-	-	-	-	-	-
2	38	300	-0.088573959	-	-	-	-	-	-
2	40	275	-0.081192796	-	-	-	-	-	-
2	42	235	-0.069382935	-	-	-	-	-	-
2	44	210	-0.062001771	-	-	-	-	-	-
2	46	185	-0.054620608	-	-	-	-	-	-
2	48	170	-0.05019191	-	-	-	-	-	-
2	50	160	-0.047239445	-	-	-	-	-	-
2	52	150	-0.04428698	-	-	-	-	-	-
2	54	160	-0.047239445	-	-	-	-	-	-
2	56	140	-0.041334514	-	-	-	-	-	-
2	58	135	-0.039858282	-	-	-	-	-	-
2	60	130	-0.038382049	-	-	-	-	-	-

2869	2929	6425	-0.001322383	11.33333333	2450.280712	200	308	6.99	6.89
2968	5897	185	-3.68063E-05	11.33333333	6331.317175	212	369	6.1	7.75
2837	8734	0	0	11.33333333	-	-	-	-	-
	Total	**24245**							

(au) Batch AU – Bed 3 (Tuesday, September 27, 2022)

Time Intervals (min)	Cumulative Time (min)	Collected Volume (ml)	Effluent Flux (cm/min)	Sludge Deposit Layer (cm)	TS (mg/L)	COD (mg/L)	NO_3 (mg/L)	pH	DO (mg/L)
Influent	**-**	**45470**	**-**	**11.83333333**	**10795.65**	**5802**	**308**	**8.23**	**0.21**
6	6	305	-0.030016731	-	3181.943046	114	327	6.49	3.88
3	9	400	-0.078732408	-	-	-	-	-	-
3	12	435	-0.085621494	-	-	-	-	-	-
3	15	410	-0.080700718	-	-	-	-	-	-
3	18	385	-0.075779943	-	-	-	-	-	-
2	20	260	-0.076764098	-	-	-	-	-	-
2	22	260	-0.076764098	-	-	-	-	-	-
2	24	230	-0.067906702	-	-	-	-	-	-
2	26	225	-0.066430469	-	-	-	-	-	-
2	28	225	-0.066430469	-	-	-	-	-	-
2	30	235	-0.069382935	-	-	-	-	-	-
2	32	235	-0.069382935	-	-	-	-	-	-
2	34	220	-0.064954237	-	-	-	-	-	-
2	36	205	-0.060525539	-	-	-	-	-	-
2	38	215	-0.063478004	-	-	-	-	-	-
2	40	220	-0.064954237	-	-	-	-	-	-
2	42	205	-0.060525539	-	-	-	-	-	-
2	44	205	-0.060525539	-	-	-	-	-	-
2	46	210	-0.062001771	-	-	-	-	-	-
2	48	210	-0.062001771	-	-	-	-	-	-
2	50	205	-0.060525539	-	-	-	-	-	-

2	52	210	-0.062001771	-	-	-	-	-	-
2	54	210	-0.062001771	-	-	-	-	-	-
2	56	210	-0.062001771	-	-	-	-	-	-
2	58	195	-0.057573074	-	-	-	-	-	-
2	60	190	-0.056096841	-	-	-	-	-	-
2878	2938	23640	-0.004850332	12	1224.076646	255	412	7.45	3.49
2956	5894	575	-0.000114862	12	7735.383447	134	363	6.5	7.69
2838	8732	75	-1.5605E-05	11	10394.81438	211	552	5.82	7.89
	Total	**30805**							

(av) Batch AV – Bed 1 (Monday, October 3, 2022)

Time Intervals (min)	Cumulative Time (min)	Collected Volume (ml)	Effluent Flux (cm/min)	Sludge Deposit Layer (cm)	TS (mg/L)	COD (mg/L)	NO_3 (mg/L)	pH	DO (mg/L)
Influent	**-**	**15150**	**-**	**7.5**	**10795.65**	**5802**	**308**	**8.23**	**0.21**
2	2	300	-0.088573959	-	9959.97817	270	887	7.51	4.05
1	3	425	-0.250959551	-	-	-	-	-	-
1	4	495	-0.292294066	-	-	-	-	-	-
1	5	570	-0.336581045	-	-	-	-	-	-
1	6	475	-0.280484204	-	-	-	-	-	-
1	7	430	-0.253912017	-	-	-	-	-	-
1	8	410	-0.242102155	-	-	-	-	-	-
2	10	890	-0.262769412	-	-	-	-	-	-
1	11	425	-0.250959551	-	-	-	-	-	-
1	12	390	-0.230292294	-	-	-	-	-	-
1	13	365	-0.215529968	-	-	-	-	-	-
2	15	720	-0.212577502	-	-	-	-	-	-
1	16	290	-0.171242988	-	-	-	-	-	-
1	17	280	-0.165338057	-	-	-	-	-	-
1	18	250	-0.147623265	-	-	-	-	-	-
1	19	235	-0.13876587	-	-	-	-	-	-

1	20	220	-0.129908474	-	-	-	-	-	-
1	21	210	-0.124003543	-	-	-	-	-	-
1	22	175	-0.103336286	-	-	-	-	-	-
1	23	165	-0.097431355	-	-	-	-	-	-
1	24	170	-0.10038382	-	-	-	-	-	-
1	25	145	-0.085621494	-	-	-	-	-	-
1	26	140	-0.082669029	-	-	-	-	-	-
2	28	225	-0.066430469	-	-	-	-	-	-
1	29	110	-0.064954237	-	-	-	-	-	-
4	33	320	-0.047239445	-	-	-	-	-	-
4	37	250	-0.036905816	-	-	-	-	-	-
3	40	155	-0.030508808	-	-	-	-	-	-
8	48	265	-0.019560083	-	-	-	-	-	-
4	52	110	-0.016238559	-	-	-	-	-	-
3	55	75	-0.014762327	-	-	-	-	-	-
36	91	430	-0.007053112	-	-	-	-	-	-
30	121	190	-0.003739789	-	-	-	-	-	-
228	349	465	-0.001204295	-	-	-	-	-	-
1228	1577	460	-0.000221194	8.5	9050.084	218	590	6.4	7.02
1378	2955	110	-4.71366E-05	8.166666667	8140.189547	204	1013	5.51	7.99
1678	4633	80	-2.81522E-05	7.666666667	-4070.65	196	1215	5.89	8.05
4314	8947	60	-8.2127E-06	7.833333333	-639.82	315	1324	5.94	7.93
	Total	**11480**							

(aw) Batch AW – Bed 2 (Monday, October 3, 2022)

Time Intervals (min)	Cumulative Time (min)	Collected Volume (ml)	Effluent Flux (cm/min)	Sludge Deposit Layer (cm)	TS (mg/L)	COD (mg/L)	NO_3 (mg/L)	pH	DO (mg/L)
Influent	**-**	**30310**	**-**	**11.33333333**	**10795.65**	**5802**	**308**	**8.23**	**0.21**
1	1	335	-0.197815176	-	6111.516922	271	692	7.81	3.07
1	2	1645	-0.971361087	-	-	-	-	-	-

1	3	1690	-0.997933274	-	-	-	-	-	-
1	4	2510	-1.482137585	-	-	-	-	-	-
1	5	2000	-1.180986123	-	-	-	-	-	-
1	6	2000	-1.180986123	-	-	-	-	-	-
2	8	2520	-0.744021258	-	-	-	-	-	-
4	12	4620	-0.682019486	-	-	-	-	-	-
5	17	2925	-0.345438441	-	-	-	-	-	-
2	19	405	-0.119574845	-	-	-	-	-	-
1	20	170	-0.10038382	-	-	-	-	-	-
1	21	145	-0.085621494	-	-	-	-	-	-
2	23	245	-0.0723354	-	-	-	-	-	-
2	25	210	-0.062001771	-	-	-	-	-	-
1	26	100	-0.059049306	-	-	-	-	-	-
2	28	170	-0.05019191	-	-	-	-	-	-
3	31	205	-0.040350359	-	-	-	-	-	-
3	34	125	-0.024603878	-	-	-	-	-	-
8	42	385	-0.028417479	-	-	-	-	-	-
7	49	215	-0.018136573	-	-	-	-	-	-
5	54	135	-0.015943313	-	-	-	-	-	-
3	57	75	-0.014762327	-	-	-	-	-	-
36	93	485	-0.007955254	-	-	-	-	-	-
30	123	245	-0.00482236	-	-	-	-	-	-
230	353	755	-0.001938358	-	-	-	-	-	-
1228	1581	830	-0.000399112	14	5341.024268	179	408	6.87	7.26
1379	2960	315	-0.000134884	12.66666667	4570.531613	175	612	5.16	7.77
1675	4635	190	-6.69813E-05	12.83333333	7078	170	530	5.5	7.8
4314	8949	75	-1.02659E-05	11.5	-2858	166	694	5.98	8.03
	Total	**25725**							

(ax) Batch AX – Bed 3 (Monday, October 3, 2022)

Time Intervals (min)	Cumulative Time (min)	Collected Volume (ml)	Effluent Flux (cm/min)	Sludge Deposit Layer (cm)	TS (mg/L)	COD (mg/L)	NO_3 (mg/L)	pH	DO (mg/L)
Influent	**-**	**45470**	**-**	**11**	**10795.65**	**5802**	**308**	**8.23**	**0.21**
1	1	415	-0.245054621	-	6132.701216	406	657	8.05	5.15
1	2	5465	-3.227044582	-	-	-	-	-	-
1	3	4400	-2.598169472	-	-	-	-	-	-
1	4	4050	-2.3914969	-	-	-	-	-	-
1	5	3325	-1.96338943	-	-	-	-	-	-
1	6	3000	-1.771479185	-	-	-	-	-	-
1	7	2700	-1.594331267	-	-	-	-	-	-
1	8	2190	-1.293179805	-	-	-	-	-	-
1	9	1955	-1.154413936	-	-	-	-	-	-
1	10	1490	-0.879834662	-	-	-	-	-	-
1	11	900	-0.531443756	-	-	-	-	-	-
1	12	630	-0.372010629	-	-	-	-	-	-
1	13	390	-0.230292294	-	-	-	-	-	-
1	14	360	-0.212577502	-	-	-	-	-	-
1	15	230	-0.135813404	-	-	-	-	-	-
1	16	275	-0.162385592	-	-	-	-	-	-
1	17	235	-0.13876587	-	-	-	-	-	-
1	18	200	-0.118098612	-	-	-	-	-	-
1	19	170	-0.10038382	-	-	-	-	-	-
1	20	140	-0.082669029	-	-	-	-	-	-
1	21	120	-0.070859167	-	-	-	-	-	-
1	22	110	-0.064954237	-	-	-	-	-	-
1	23	110	-0.064954237	-	-	-	-	-	-
1	24	75	-0.04428698	-	-	-	-	-	-
1	25	75	-0.04428698	-	-	-	-	-	-
1	26	75	-0.04428698	-	-	-	-	-	-
1	27	70	-0.041334514	-	-	-	-	-	-

8	35	365	-0.026941246	-	-	-	-	-	-
9	44	260	-0.017058688	-	-	-	-	-	-
12	56	265	-0.013040055	-	-	-	-	-	-
234	290	985	-0.002485623	-	-	-	-	-	-
1228	1518	895	-0.000430368	14	5254.185335	275	496.5	7.24	6.125
1379	2897	225	-9.63459E-05	13	4375.669455	144	336	6.43	7.1
1675	4572	165	-5.8168E-05	11.83333333	-7892	150	610	5	7.7
4315	8887	135	-1.84743E-05	11.33333333	-5609	138	769	5.5	7.82
	Total	**36450**							

(ay) Batch AY – Bed 4 (Monday, October 3, 2022)

Time Intervals (min)	Cumulative Time (min)	Collected Volume (ml)	Effluent Flux (cm/min)	Sludge Deposit Layer (cm)	TS (mg/L)	COD (mg/L)	NO_3 (mg/L)	pH	DO (mg/L)
Influent	**-**	**90940**	**-**	**10.33333333**	**10795.65**	**5802**	**308**	**8.23**	**0.21**
1	1	685	-0.404487747	-	4057.558772	210	557	7.71	2.09
1	2	875	-0.516681429	-	-	-	-	-	-
1	3	520	-0.307056392	-	-	-	-	-	-
1	4	415	-0.245054621	-	-	-	-	-	-
1	5	385	-0.227339829	-	-	-	-	-	-
1	6	300	-0.177147919	-	-	-	-	-	-
1	7	265	-0.156480661	-	-	-	-	-	-
1	8	240	-0.141718335	-	-	-	-	-	-
1	9	225	-0.132860939	-	-	-	-	-	-
1	10	205	-0.121051078	-	-	-	-	-	-
1	11	190	-0.112193682	-	-	-	-	-	-
1	12	185	-0.109241216	-	-	-	-	-	-
1	13	175	-0.103336286	-	-	-	-	-	-
1	14	165	-0.097431355	-	-	-	-	-	-
1	15	160	-0.09447889	-	-	-	-	-	-
1	16	155	-0.091526425	-	-	-	-	-	-

1	17	150	-0.088573959	-	-	-	-	-	-
1	18	140	-0.082669029	-	-	-	-	-	-
1	19	135	-0.079716563	-	-	-	-	-	-
1	20	140	-0.082669029	-	-	-	-	-	-
1	21	110	-0.064954237	-	-	-	-	-	-
1	22	120	-0.070859167	-	-	-	-	-	-
1	23	120	-0.070859167	-	-	-	-	-	-
1	24	115	-0.067906702	-	-	-	-	-	-
1	25	110	-0.064954237	-	-	-	-	-	-
1	26	110	-0.064954237	-	-	-	-	-	-
1	27	110	-0.064954237	-	-	-	-	-	-
1	28	105	-0.062001771	-	-	-	-	-	-
1	29	105	-0.062001771	-	-	-	-	-	-
1	30	100	-0.059049306	-	-	-	-	-	-
1	31	100	-0.059049306	-	-	-	-	-	-
1	32	95	-0.056096841	-	-	-	-	-	-
1	33	95	-0.056096841	-	-	-	-	-	-
1	34	95	-0.056096841	-	-	-	-	-	-
1	35	90	-0.053144376	-	-	-	-	-	-
1	36	90	-0.053144376	-	-	-	-	-	-
1	37	85	-0.05019191	-	-	-	-	-	-
1	38	85	-0.05019191	-	-	-	-	-	-
1	39	85	-0.05019191	-	-	-	-	-	-
1	40	85	-0.05019191	-	-	-	-	-	-
1188	1228	14800	-0.007356311	30	4426.506659	119	358	7.11	7.76
1363	2591	5225	-0.002263629	27.5	4795.454545	103	718	8.45	8.28
1680	4271	4180	-0.001469203	27.83333333	-5330.51544	100	716	7.8	8.1
3896	8167	7960	-0.001206449	27.5	-4496.739864	98	715	7.5	8
2939	11106	2960	-0.000594712	26	-4432.245057	95	714	7.4	7.93
1392	12498	4340	-0.001841049	25.33333333	-4367.750251	114	744	7.21	8.1
1515	14013	4090	-0.001594136	19.33333333	-3012.605375	105	1659	7	7.99

2804	16817	8920	-0.001878459	15.16666667	-6957.328386	96	781	7.32	7.85
2802	19619	6130	-0.001291835	14	-2128.543246	90	671	7.17	8.17
3112	22731	2910	-0.000552164	13.5	5115.259417	155	864	6.55	7.95
2814	25545	1370	-0.000287482	12.33333333	4063.916254	137	643	7.54	7.48
	Total	**70605**							

(az) Batch AZ – Bed 6 (Monday, October 3, 2022)

Time Intervals (min)	Cumulative Time (min)	Collected Volume (ml)	Effluent Flux (cm/min)	Sludge Deposit Layer (cm)	TS (mg/L)	COD (mg/L)	NO_3 (mg/L)	pH	DO (mg/L)
Influent	**-**	**45470**	**-**	**12.33333333**	**10795.65**	**5802**	**308**	**8.23**	**0.21**
5	5	0	0	-	-	-	-	-	-
1	6	190	-0.112193682	-	6667.55272	267	816	8.02	4.51
1	7	130	-0.076764098	-	-	-	-	-	-
1	8	230	-0.135813404	-	-	-	-	-	-
1	9	275	-0.162385592	-	-	-	-	-	-
1	10	255	-0.150575731	-	-	-	-	-	-
1	11	270	-0.159433127	-	-	-	-	-	-
1	12	260	-0.153528196	-	-	-	-	-	-
1	13	275	-0.162385592	-	-	-	-	-	-
1	14	285	-0.168290523	-	-	-	-	-	-
1	15	280	-0.165338057	-	-	-	-	-	-
1	16	280	-0.165338057	-	-	-	-	-	-
1	17	290	-0.171242988	-	-	-	-	-	-
1	18	285	-0.168290523	-	-	-	-	-	-
1	19	290	-0.171242988	-	-	-	-	-	-
1	20	290	-0.171242988	-	-	-	-	-	-
1	21	290	-0.171242988	-	-	-	-	-	-
1	22	290	-0.171242988	-	-	-	-	-	-
1	23	295	-0.174195453	-	-	-	-	-	-
1	24	290	-0.171242988	-	-	-	-	-	-

1	25	285	-0.168290523	-	-	-	-	-	-
1	26	270	-0.159433127	-	-	-	-	-	-
1	27	260	-0.153528196	-	-	-	-	-	-
1	28	265	-0.156480661	-	-	-	-	-	-
1	29	270	-0.159433127	-	-	-	-	-	-
1	30	240	-0.141718335	-	-	-	-	-	-
1	31	250	-0.147623265	-	-	-	-	-	-
1	32	250	-0.147623265	-	-	-	-	-	-
1	33	235	-0.13876587	-	-	-	-	-	-
1	34	235	-0.13876587	-	-	-	-	-	-
1	35	230	-0.135813404	-	-	-	-	-	-
1	36	235	-0.13876587	-	-	-	-	-	-
2	38	440	-0.129908474	-	-	-	-	-	-
1	39	235	-0.13876587	-	-	-	-	-	-
1	40	230	-0.135813404	-	-	-	-	-	-
1	41	235	-0.13876587	-	-	-	-	-	-
1	42	215	-0.126956008	-	-	-	-	-	-
1	43	210	-0.124003543	-	-	-	-	-	-
1	44	235	-0.13876587	-	-	-	-	-	-
1	45	230	-0.135813404	-	-	-	-	-	-
1	46	225	-0.132860939	-	-	-	-	-	-
1	47	215	-0.126956008	-	-	-	-	-	-
1	48	225	-0.132860939	-	-	-	-	-	-
1	49	230	-0.135813404	-	-	-	-	-	-
1	50	235	-0.13876587	-	-	-	-	-	-
1	51	245	-0.1446708	-	-	-	-	-	-
1	52	230	-0.135813404	-	-	-	-	-	-
1	53	250	-0.147623265	-	-	-	-	-	-
1	54	225	-0.132860939	-	-	-	-	-	-
1	55	225	-0.132860939	-	-	-	-	-	-
1	56	225	-0.132860939	-	-	-	-	-	-

1	57	220	-0.129908474	-	-	-	-	-	-
1	58	225	-0.132860939	-	-	-	-	-	-
1	59	225	-0.132860939	-	-	-	-	-	-
1	60	230	-0.135813404	-	-	-	-	-	-
195	255	17500	-0.052992967	-	-	-	-	-	-
22	277	545	-0.014628124	-	-	185	521	7.48	7.39
1200	1477	3095	-0.00152298	12.5	5802.600281	174	615	5.97	4.65
1379	2856	215	-9.20638E-05	12	4937.647842	160	700	6.5	5
1675	4531	290	-6.34839E-05	12.08333333	-6189.344425	150	800	7	6
4314	8845	255	-3.4904E-05	12	-3847.787522	139	911	7.43	7.81
2911	11756	30	-6.08547E-06	12.16666667	-6826.672698	215	1249	7.22	8.23
1392	13148	10	-4.24205E-06	12.17	-9805.557874	200	1710	7.48	7.75
	Total	**35475**							

(ba) Batch BA – Bed 1 (Sunday, October 9, 2022)

Time Intervals (min)	Cumulative Time (min)	Collected Volume (ml)	Effluent Flux (cm/min)	Sludge Deposit Layer (cm)	TS (mg/L)	COD (mg/L)	NO_3 (mg/L)	pH	DO (mg/L)
Influent	**-**	**15150**	**-**	**7.833333333**	**10795.65**	**5802**	**308**	**8.23**	**0.21**
16	16	0	0	-	-	-	-	-	-
2	18	70	-0.020667257	-	429.7202726	196	1113	6.85	3.79
1	19	50	-0.029524653	-	-	-	-	-	-
1	20	50	-0.029524653	-	-	-	-	-	-
1	21	50	-0.029524653	-	-	-	-	-	-
1	22	60	-0.035429584	-	-	-	-	-	-
1	23	65	-0.038382049	-	-	-	-	-	-
1	24	65	-0.038382049	-	-	-	-	-	-
1	25	65	-0.038382049	-	-	-	-	-	-
1	26	70	-0.041334514	-	-	-	-	-	-
1	27	65	-0.038382049	-	-	-	-	-	-
1	28	70	-0.041334514	-	-	-	-	-	-

1	29	65	-0.038382049	-	-	-	-	-	-
1	30	70	-0.041334514	-	-	-	-	-	-
1	31	75	-0.04428698	-	-	-	-	-	-
1	32	75	-0.04428698	-	-	-	-	-	-
1	33	75	-0.04428698	-	-	-	-	-	-
1	34	75	-0.04428698	-	-	-	-	-	-
1	35	70	-0.041334514	-	-	-	-	-	-
1	36	70	-0.041334514	-	-	-	-	-	-
1	37	65	-0.038382049	-	-	-	-	-	-
1	38	70	-0.041334514	-	-	-	-	-	-
1	39	75	-0.04428698	-	-	-	-	-	-
1	40	65	-0.038382049	-	-	-	-	-	-
1	41	70	-0.041334514	-	-	-	-	-	-
1	42	70	-0.041334514	-	-	-	-	-	-
1	43	65	-0.038382049	-	-	-	-	-	-
1	44	65	-0.038382049	-	-	-	-	-	-
1	45	65	-0.038382049	-	-	-	-	-	-
1	46	65	-0.038382049	-	-	-	-	-	-
1	47	70	-0.041334514	-	-	-	-	-	-
1	48	65	-0.038382049	-	-	-	-	-	-
1	49	65	-0.038382049	-	-	-	-	-	-
1	50	70	-0.041334514	-	-	-	-	-	-
1	51	70	-0.041334514	-	-	-	-	-	-
1	52	70	-0.041334514	-	-	-	-	-	-
1	53	65	-0.038382049	-	-	-	-	-	-
1	54	70	-0.041334514	-	-	-	-	-	-
1	55	65	-0.038382049	-	-	-	-	-	-
1	56	70	-0.041334514	-	-	-	-	-	-
1	57	65	-0.038382049	-	-	-	-	-	-
1	58	65	-0.038382049	-	-	-	-	-	-
1	59	65	-0.038382049	-	-	-	-	-	-

1	60	65	-0.038382049	-	-	-	-	-	-
1	61	70	-0.041334514	-	-	-	-	-	-
1	62	70	-0.041334514	-	-	-	-	-	-
1	63	75	-0.04428698	-	-	-	-	-	-
1	64	65	-0.038382049	-	-	-	-	-	-
1	65	65	-0.038382049	-	-	-	-	-	-
1	66	70	-0.041334514	-	-	-	-	-	-
1	67	70	-0.041334514	-	-	-	-	-	-
1	68	75	-0.04428698	-	-	-	-	-	-
1	69	65	-0.038382049	-	-	-	-	-	-
1	70	70	-0.041334514	-	-	-	-	-	-
1	71	70	-0.041334514	-	-	-	-	-	-
1	72	70	-0.041334514	-	-	-	-	-	-
2815	2887	8000	-0.001678133	8.5	-824.8374137	197	963	6.9	6.71
1409	4296	100	-4.19087E-05	7.666666667	-2079.3951	212	2340	7.08	8.05
1520	5816	75	-2.91362E-05	7.666666667	1361.667011	215	2623	7.24	8.06
2809	8625	40	-8.40859E-06	7.833333333	-2637.47	305	1825	6.92	7.91
	Total	**11920**							

(bb) Batch BB – Bed 2 (Sunday, October 9, 2022)

Time Intervals (min)	Cumulative Time (min)	Collected Volume (ml)	Effluent Flux (cm/min)	Sludge Deposit Layer (cm)	TS (mg/L)	COD (mg/L)	NO_3 (mg/L)	pH	DO (mg/L)
Influent	**-**	**30310**	**-**	**11.5**	**10795.65**	**5802**	**308**	**8.23**	**0.21**
4	4	0	0	-	-	-	-	-	-
1	5	145	-0.085621494	-	5410.641716	155	784	6.78	6.4
1	6	210	-0.124003543	-	-	187.5	875	7.19	6.46
1	7	500	-0.295246531	-	-	220	966	7.6	6.52
1	8	460	-0.271626808	-	-	156	1753	6.46	7.94
1	9	480	-0.28343667	-	-	288	2285	6.88	7.94
1	10	565	-0.33362858	-	-	272	1746.5	6.69	8.03

1	11	590	-0.348390906	-	-	256	1208	6.5	8.12
1	12	560	-0.330676115	-	-	-	-	-	-
1	13	500	-0.295246531	-	-	-	-	-	-
1	14	560	-0.330676115	-	-	-	-	-	-
1	15	560	-0.330676115	-	-	-	-	-	-
1	16	545	-0.321818719	-	-	-	-	-	-
1	17	555	-0.327723649	-	-	-	-	-	-
1	18	550	-0.324771184	-	-	-	-	-	-
1	19	485	-0.286389135	-	-	-	-	-	-
1	20	525	-0.310008857	-	-	-	-	-	-
1	21	455	-0.268674343	-	-	-	-	-	-
1	22	485	-0.286389135	-	-	-	-	-	-
1	23	465	-0.274579274	-	-	-	-	-	-
1	24	460	-0.271626808	-	-	-	-	-	-
1	25	455	-0.268674343	-	-	-	-	-	-
1	26	470	-0.277531739	-	-	-	-	-	-
1	27	445	-0.262769412	-	-	-	-	-	-
1	28	385	-0.227339829	-	-	-	-	-	-
1	29	425	-0.250959551	-	-	-	-	-	-
1	30	380	-0.224387363	-	-	-	-	-	-
1	31	425	-0.250959551	-	-	-	-	-	-
1	32	375	-0.221434898	-	-	-	-	-	-
1	33	365	-0.215529968	-	-	-	-	-	-
1	34	405	-0.23914969	-	-	-	-	-	-
1	35	335	-0.197815176	-	-	-	-	-	-
1	36	325	-0.191910245	-	-	-	-	-	-
1	37	370	-0.218482433	-	-	-	-	-	-
1	38	310	-0.183052849	-	-	-	-	-	-
1	39	315	-0.186005314	-	-	-	-	-	-
1	40	265	-0.156480661	-	-	-	-	-	-
1	41	325	-0.191910245	-	-	-	-	-	-

1	42	215	-0.126956008	-	-	-	-	-	-
1	43	235	-0.13876587	-	-	-	-	-	-
1	44	165	-0.097431355	-	-	-	-	-	-
1	45	175	-0.103336286	-	-	-	-	-	-
1	46	145	-0.085621494	-	-	-	-	-	-
1	47	145	-0.085621494	-	-	-	-	-	-
1	48	130	-0.076764098	-	-	-	-	-	-
1	49	110	-0.064954237	-	-	-	-	-	-
1	50	115	-0.067906702	-	-	-	-	-	-
1	51	100	-0.059049306	-	-	-	-	-	-
1	52	105	-0.062001771	-	-	-	-	-	-
1	53	85	-0.05019191	-	-	-	-	-	-
2841	2894	6435	-0.001337495	13.5	-1927.179142	220	966	7.6	6.52
1405	4299	205	-8.61574E-05	13.16666667	-9265	156	1753	6.46	7.94
1520	5819	85	-3.3021E-05	13.16666667	1415.428167	288	2285	6.88	7.94
2800	8619	60	-1.26534E-05	12.83333333	-1457	256	1208	6.5	8.12
	Total	**24540**							

(bc) Batch BC – Bed 3 (Sunday, October 9, 2022)

Time Intervals (min)	Cumulative Time (min)	Collected Volume (ml)	Effluent Flux (cm/min)	Sludge Deposit Layer (cm)	TS (mg/L)	COD (mg/L)	NO_3 (mg/L)	pH	DO (mg/L)
Influent	**-**	**45470**	**-**	**11.33333333**	**10795.65**	**5802**	**308**	**8.23**	**0.21**
2	2	765	-0.225863596	-	5294.748124	131	790	7.11	5
1	3	465	-0.274579274	-	-	-	-	-	-
1	4	465	-0.274579274	-	-	-	-	-	-
1	5	405	-0.23914969	-	-	-	-	-	-
1	6	410	-0.242102155	-	-	-	-	-	-
1	7	395	-0.233244759	-	-	-	-	-	-
1	8	435	-0.256864482	-	-	-	-	-	-
1	9	395	-0.233244759	-	-	-	-	-	-

1	10	380	-0.224387363	-	-	-	-	-	-
1	11	370	-0.218482433	-	-	-	-	-	-
1	12	340	-0.200767641	-	-	-	-	-	-
1	13	385	-0.227339829	-	-	-	-	-	-
1	14	315	-0.186005314	-	-	-	-	-	-
1	15	290	-0.171242988	-	-	-	-	-	-
1	16	290	-0.171242988	-	-	-	-	-	-
1	17	270	-0.159433127	-	-	-	-	-	-
1	18	240	-0.141718335	-	-	-	-	-	-
1	19	270	-0.159433127	-	-	-	-	-	-
1	20	260	-0.153528196	-	-	-	-	-	-
1	21	285	-0.168290523	-	-	-	-	-	-
1	22	300	-0.177147919	-	-	-	-	-	-
1	23	335	-0.197815176	-	-	-	-	-	-
1	24	270	-0.159433127	-	-	-	-	-	-
1	25	315	-0.186005314	-	-	-	-	-	-
1	26	275	-0.162385592	-	-	-	-	-	-
1	27	265	-0.156480661	-	-	-	-	-	-
1	28	280	-0.165338057	-	-	-	-	-	-
1	29	285	-0.168290523	-	-	-	-	-	-
1	30	260	-0.153528196	-	-	-	-	-	-
1	31	270	-0.159433127	-	-	-	-	-	-
1	32	250	-0.147623265	-	-	-	-	-	-
1	33	240	-0.141718335	-	-	-	-	-	-
1	34	280	-0.165338057	-	-	-	-	-	-
1	35	220	-0.129908474	-	-	-	-	-	-
1	36	210	-0.124003543	-	-	-	-	-	-
1	37	230	-0.135813404	-	-	-	-	-	-
1	38	210	-0.124003543	-	-	-	-	-	-
1	39	225	-0.132860939	-	-	-	-	-	-
1	40	205	-0.121051078	-	-	-	-	-	-

1	41	200	-0.118098612	-	-	-	-	-	-
1	42	200	-0.118098612	-	-	-	-	-	-
1	43	175	-0.103336286	-	-	-	-	-	-
1	44	155	-0.091526425	-	-	-	-	-	-
1	45	175	-0.103336286	-	-	-	-	-	-
1	46	190	-0.112193682	-	-	-	-	-	-
1	47	190	-0.112193682	-	-	-	-	-	-
1	48	185	-0.109241216	-	-	-	-	-	-
1	49	200	-0.118098612	-	-	-	-	-	-
1	50	200	-0.118098612	-	-	-	-	-	-
1	51	195	-0.115146147	-	-	-	-	-	-
1	52	200	-0.118098612	-	-	-	-	-	-
1	53	170	-0.10038382	-	-	-	-	-	-
1	54	190	-0.112193682	-	-	-	-	-	-
1	55	170	-0.10038382	-	-	-	-	-	-
1	56	175	-0.103336286	-	-	-	-	-	-
1	57	180	-0.106288751	-	-	-	-	-	-
1	58	180	-0.106288751	-	-	-	-	-	-
1	59	195	-0.115146147	-	-	-	-	-	-
1	60	195	-0.115146147	-	-	-	-	-	-
1	61	195	-0.115146147	-	-	-	-	-	-
1	62	180	-0.106288751	-	-	-	-	-	-
1	63	170	-0.10038382	-	-	-	-	-	-
1	64	165	-0.097431355	-	-	-	-	-	-
1	65	165	-0.097431355	-	-	-	-	-	-
1	66	165	-0.097431355	-	-	-	-	-	-
1	67	170	-0.10038382	-	-	-	-	-	-
2850	2917	18745	-0.003883787	13	860.3740622	313	1014	7.79	3.28
1393	4310	175	-7.41825E-05	11.66666667	-3230	138	1690	6.46	7.5
1520	5830	55	-2.13665E-05	11.66666667	403.25	297	1646	6.1	7.82
2865	8695	795	-0.000163854	11.5	2098.5	112	1058	6.88	7.44

Total	37055

(bd) Batch BD – Bed 5 (Wednesday, October 12, 2022)

Time Intervals (min)	Cumulative Time (min)	Collected Volume (ml)	Effluent Flux (cm/min)	Sludge Deposit Layer (cm)	TS (mg/L)	COD (mg/L)	NO_3 (mg/L)	pH	DO (mg/L)
Influent	**-**	**110000**	**-**	**10.83**	**10795.65**	**5802**	**308**	**8.23**	**0.21**
1	1	1945	-1.148509005	-	-962.3580522	251	2617	7.98	3.38
1	2	1325	-0.782403307	-	-	-	-	-	-
1	3	835	-0.493061707	-	-	-	-	-	-
1	4	455	-0.268674343	-	-	-	-	-	-
1	5	405	-0.23914969	-	-	-	-	-	-
1	6	305	-0.180100384	-	-	-	-	-	-
1	7	255	-0.150575731	-	-	-	-	-	-
1	8	380	-0.224387363	-	-	-	-	-	-
1	9	350	-0.206672572	-	-	-	-	-	-
1	10	280	-0.165338057	-	-	-	-	-	-
1	11	310	-0.183052849	-	-	-	-	-	-
1	12	345	-0.203720106	-	-	-	-	-	-
1	13	295	-0.174195453	-	-	-	-	-	-
1	14	265	-0.156480661	-	-	-	-	-	-
1	15	240	-0.141718335	-	-	-	-	-	-
1	16	230	-0.135813404	-	-	-	-	-	-
1	17	230	-0.135813404	-	-	-	-	-	-
1	18	230	-0.135813404	-	-	-	-	-	-
1	19	190	-0.112193682	-	-	-	-	-	-
1	20	200	-0.118098612	-	-	-	-	-	-
1	21	205	-0.121051078	-	-	-	-	-	-
1	22	175	-0.103336286	-	-	-	-	-	-
1	23	185	-0.109241216	-	-	-	-	-	-
1	24	175	-0.103336286	-	-	-	-	-	-

1	25	175	-0.103336286	-	-	-	-	-	-
1	26	170	-0.10038382	-	-	-	-	-	-
1	27	160	-0.09447889	-	-	-	-	-	-
1	28	160	-0.09447889	-	-	-	-	-	-
1	29	155	-0.091526425	-	-	-	-	-	-
1	30	155	-0.091526425	-	-	-	-	-	-
82	112	5985	-0.043098792	-	-	-	-	-	-
1402	1514	16255	-0.006846266	33.33333333	-3870.61782	162	1474	7.44	7.52
2762	4276	17950	-0.003837564	31.91666667	-3181.797372	163	700	6.68	3.7
2812	7088	36400	-0.007643651	30.5	5052.199069	254	996	7.94	3.27
3102	10190	2830	-0.000538715	13.66666667	5639.941037	163	822	6.07	7.9
2812	13002	1050	-0.00022049	12.83333333	4454.884173	182	935	7.66	7
3081	16083	400	-7.66625E-05	12.33333333	5052.199069	102	1195	7.96	7.18
2800	18883	70	-1.47623E-05	12.5	4601.325011	154	1552	8.01	7.72
2698	21581	0	0	12.41666667	-	-	-	-	-
4350	25931	0	0	12.33333333	-	-	-	-	-
1648	27579	0	0	12.41666667	-	-	-	-	-
2639	30218	0	0	12.33333333	-	-	-	-	-
3130	33348	0	0	12.16666667	-	-	-	-	-
2791	36139	0	0	12.16666667	-	-	-	-	-
2721	38860	0	0	12.16666667	-	-	-	-	-
	Total	**91725**							

(be) Batch BE – Bed 6 (Wednesday, October 12, 2022)

Time Intervals (min)	Cumulative Time (min)	Collected Volume (ml)	Effluent Flux (cm/min)	Sludge Deposit Layer (cm)	TS (mg/L)	COD (mg/L)	NO_3 (mg/L)	pH	DO (mg/L)
Influent	**-**	**45470**	**-**	**12.17**	**10795.65**	**5802**	**308**	**8.23**	**0.21**
4	4	0	0	-	-	-	-	-	-
2	6	65	-0.019191025	-	-4900.804571	185	2171	7.74	7.27
1	7	50	-0.029524653	-	-	-	-	-	-

1	8	50	-0.029524653	-	-	-	-	-	-
1	9	50	-0.029524653	-	-	-	-	-	-
1	10	50	-0.029524653	-	-	-	-	-	-
1	11	50	-0.029524653	-	-	-	-	-	-
1	12	45	-0.026572188	-	-	-	-	-	-
1	13	45	-0.026572188	-	-	-	-	-	-
1	14	45	-0.026572188	-	-	-	-	-	-
1	15	50	-0.029524653	-	-	-	-	-	-
1	16	50	-0.029524653	-	-	-	-	-	-
1	17	50	-0.029524653	-	-	-	-	-	-
1	18	50	-0.029524653	-	-	-	-	-	-
1	19	55	-0.032477118	-	-	-	-	-	-
1	20	55	-0.032477118	-	-	-	-	-	-
1	21	60	-0.035429584	-	-	-	-	-	-
1	22	60	-0.035429584	-	-	-	-	-	-
1	23	60	-0.035429584	-	-	-	-	-	-
1	24	60	-0.035429584	-	-	-	-	-	-
1	25	60	-0.035429584	-	-	-	-	-	-
1	26	60	-0.035429584	-	-	-	-	-	-
1	27	65	-0.038382049	-	-	-	-	-	-
1	28	65	-0.038382049	-	-	-	-	-	-
1	29	65	-0.038382049	-	-	-	-	-	-
1	30	65	-0.038382049	-	-	-	-	-	-
1	31	65	-0.038382049	-	-	-	-	-	-
1	32	65	-0.038382049	-	-	-	-	-	-
1	33	65	-0.038382049	-	-	-	-	-	-
1	34	65	-0.038382049	-	-	-	-	-	-
1	35	65	-0.038382049	-	-	-	-	-	-
1	36	65	-0.038382049	-	-	-	-	-	-
1	37	65	-0.038382049	-	-	-	-	-	-
1	38	65	-0.038382049	-	-	-	-	-	-

1	39	65	-0.038382049	-	-	-	-	-	-
1	40	65	-0.038382049	-	-	-	-	-	-
1	41	65	-0.038382049	-	-	-	-	-	-
1	42	65	-0.038382049	-	-	-	-	-	-
1	43	65	-0.038382049	-	-	-	-	-	-
1	44	65	-0.038382049	-	-	-	-	-	-
1	45	65	-0.038382049	-	-	-	-	-	-
1	46	65	-0.038382049	-	-	-	-	-	-
1	47	65	-0.038382049	-	-	-	-	-	-
1	48	65	-0.038382049	-	-	-	-	-	-
1	49	65	-0.038382049	-	-	-	-	-	-
1	50	65	-0.038382049	-	-	-	-	-	-
1	51	65	-0.038382049	-	-	-	-	-	-
1	52	65	-0.038382049	-	-	-	-	-	-
1	53	60	-0.035429584	-	-	-	-	-	-
1	54	60	-0.035429584	-	-	-	-	-	-
1	55	60	-0.035429584	-	-	-	-	-	-
1	56	60	-0.035429584	-	-	-	-	-	-
1	57	60	-0.035429584	-	-	-	-	-	-
1	58	60	-0.035429584	-	-	-	-	-	-
1	59	60	-0.035429584	-	-	-	-	-	-
1	60	60	-0.035429584	-	-	-	-	-	-
2	62	120	-0.035429584	-	-	-	-	-	-
1	63	60	-0.035429584	-	-	-	-	-	-
1	64	60	-0.035429584	-	-	-	-	-	-
1	65	60	-0.035429584	-	-	-	-	-	-
1	66	55	-0.032477118	-	-	-	-	-	-
1414	1480	29000	-0.012110537	14.16666667	-3660.186192	202	1900	7.83	6.14
2795	4275	5000	-0.001056338	13.83333333	230.1813829	146	700	6.55	6.2
2812	7087	305	-6.40471E-05	12.83333333	-3822.511493	145	1089	7.12	7.92
3103	10190	75	-1.42723E-05	12.66666667	5450.443407	151	850	6.06	7.55

2805	12995	0	0	12.66666667	-	-	-	-	-
	Total	**38025**							

(bf) Batch BF – Bed 1 (Saturday, October 15, 2022)

Time Intervals (min)	Cumulative Time (min)	Collected Volume (ml)	Effluent Flux (cm/min)	Sludge Deposit Layer (cm)	TS (mg/L)	COD (mg/L)	NO_3 (mg/L)	pH	DO (mg/L)
Influent	**-**	**15150**	**-**	**7.833333333**	**10795.65**	**5802**	**308**	**8.23**	**0.21**
1	1	95	-0.056096841	-	-2415.26	154	1371	6.92	6.34
1	2	460	-0.271626808	-	-	-	-	-	-
1	3	575	-0.33953351	-	-	-	-	-	-
1	4	605	-0.357248302	-	-	-	-	-	-
1	5	580	-0.342485976	-	-	-	-	-	-
1	6	590	-0.348390906	-	-	-	-	-	-
1	7	470	-0.277531739	-	-	-	-	-	-
1	8	470	-0.277531739	-	-	-	-	-	-
1	9	470	-0.277531739	-	-	-	-	-	-
1	10	465	-0.274579274	-	-	-	-	-	-
1	11	415	-0.245054621	-	-	-	-	-	-
1	12	365	-0.215529968	-	-	-	-	-	-
1	13	265	-0.156480661	-	-	-	-	-	-
1	14	205	-0.121051078	-	-	-	-	-	-
1	15	180	-0.106288751	-	-	-	-	-	-
1	16	160	-0.09447889	-	-	-	-	-	-
1	17	155	-0.091526425	-	-	-	-	-	-
1	18	140	-0.082669029	-	-	-	-	-	-
1	19	135	-0.079716563	-	-	-	-	-	-
1	20	135	-0.079716563	-	-	-	-	-	-
1	21	125	-0.073811633	-	-	-	-	-	-
1	22	135	-0.079716563	-	-	-	-	-	-
1	23	125	-0.073811633	-	-	-	-	-	-

1	24	120	-0.070859167	-	-	-	-	-	-
1	25	120	-0.070859167	-	-	-	-	-	-
1	26	95	-0.056096841	-	-	-	-	-	-
1	27	115	-0.067906702	-	-	-	-	-	-
1	28	105	-0.062001771	-	-	-	-	-	-
1	29	105	-0.062001771	-	-	-	-	-	-
1	30	100	-0.059049306	-	-	-	-	-	-
1	31	105	-0.062001771	-	-	-	-	-	-
1	32	100	-0.059049306	-	-	-	-	-	-
1	33	100	-0.059049306	-	-	-	-	-	-
1	34	95	-0.056096841	-	-	-	-	-	-
1	35	95	-0.056096841	-	-	-	-	-	-
2732	2767	3710	-0.000801877	8	-1926.1122	215	924	7.06	4.69
3117	5884	630	-0.000119349	7	5604.321404	217	1169	7.42	7.92
2810	8694	85	-1.78619E-05	7	4493.708808	234	864	7.06	7.5
	Total	**13000**							

(bg) Batch BG – Bed 2 (Saturday, October 15, 2022)

Time Intervals (min)	Cumulative Time (min)	Collected Volume (ml)	Effluent Flux (cm/min)	Sludge Deposit Layer (cm)	TS (mg/L)	COD (mg/L)	NO_3 (mg/L)	pH	DO (mg/L)
Influent	**-**	**30310**	**-**	**12.83333333**	**10795.65**	**5802**	**308**	**8.23**	**0.21**
1	1	45	-0.026572188	-	-4564	264	1146	6.55	6.96
1	2	1030	-0.608207854	-	-	-	-	-	-
1	3	900	-0.531443756	-	-	-	-	-	-
1	4	1590	-0.938883968	-	-	-	-	-	-
1	5	950	-0.560968409	-	-	-	-	-	-
1	6	945	-0.558015943	-	-	-	-	-	-
2	8	1795	-0.529967523	-	-	-	-	-	-
1	9	875	-0.516681429	-	-	-	-	-	-
1	10	880	-0.519633894	-	-	-	-	-	-

1	11	870	-0.513728964	-	-	-	-	-	-
1	12	740	-0.436964866	-	-	-	-	-	-
1	13	705	-0.416297609	-	-	-	-	-	-
1	14	890	-0.525538825	-	-	-	-	-	-
2	16	1300	-0.38382049	-	-	-	-	-	-
1	17	590	-0.348390906	-	-	-	-	-	-
1	18	500	-0.295246531	-	-	-	-	-	-
1	19	615	-0.363153233	-	-	-	-	-	-
1	20	620	-0.366105698	-	-	-	-	-	-
1	21	585	-0.345438441	-	-	-	-	-	-
1	22	495	-0.292294066	-	-	-	-	-	-
1	23	375	-0.221434898	-	-	-	-	-	-
1	24	350	-0.206672572	-	-	-	-	-	-
1	25	335	-0.197815176	-	-	-	-	-	-
1	26	300	-0.177147919	-	-	-	-	-	-
1	27	260	-0.153528196	-	-	-	-	-	-
1	28	220	-0.129908474	-	-	-	-	-	-
1	29	210	-0.124003543	-	-	-	-	-	-
1	30	195	-0.115146147	-	-	-	-	-	-
1	31	180	-0.106288751	-	-	-	-	-	-
1	32	180	-0.106288751	-	-	-	-	-	-
1	33	155	-0.091526425	-	-	-	-	-	-
2736	2769	4610	-0.000994946	12.66666667	449.7473478	179	735	6.91	6.5
3114	5883	700	-0.000132738	12.83333333	3663.305207	126	1027	7.41	7.66
2809	8692	145	-3.04811E-05	12.5	5695.311813	222	844	6.81	7.84
	Total	**25135**							

(bh) Batch BH – Bed 3 (Saturday, October 15, 2022)

Time Intervals (min)	Cumulative Time (min)	Collected Volume (ml)	Effluent Flux (cm/min)	Sludge Deposit Layer (cm)	TS (mg/L)	COD (mg/L)	NO_3 (mg/L)	pH	DO (mg/L)

Influent	**-**	**45470**	**-**	**11.5**	**10795.65**	**5802**	**308**	**8.23**	**0.21**
1	1	1145	-0.676114556	-	-3258	206	1382	7.62	4.84
1	2	1860	-1.098317095	-	-	-	-	-	-
1	3	1160	-0.684971952	-	-	-	-	-	-
1	4	2700	-1.594331267	-	-	-	-	-	-
1	5	3700	-2.184824328	-	-	-	-	-	-
1	6	2540	-1.499852377	-	-	-	-	-	-
1	7	2830	-1.671095365	-	-	-	-	-	-
1	8	1220	-0.720401535	-	-	-	-	-	-
1	9	1555	-0.918216711	-	-	-	-	-	-
1	10	1430	-0.844405078	-	-	-	-	-	-
1	11	1465	-0.865072335	-	-	-	-	-	-
1	12	1245	-0.735163862	-	-	-	-	-	-
1	13	1200	-0.708591674	-	-	-	-	-	-
1	14	1200	-0.708591674	-	-	-	-	-	-
1	15	1250	-0.738116327	-	-	-	-	-	-
1	16	1255	-0.741068792	-	-	-	-	-	-
1	17	700	-0.413345143	-	-	-	-	-	-
1	18	825	-0.487156776	-	-	-	-	-	-
1	19	730	-0.431059935	-	-	-	-	-	-
1	20	665	-0.392677886	-	-	-	-	-	-
1	21	605	-0.357248302	-	-	-	-	-	-
1	22	405	-0.23914969	-	-	-	-	-	-
1	23	350	-0.206672572	-	-	-	-	-	-
1	24	305	-0.180100384	-	-	-	-	-	-
1	25	265	-0.156480661	-	-	-	-	-	-
1	26	235	-0.13876587	-	-	-	-	-	-
1	27	220	-0.129908474	-	-	-	-	-	-
1	28	185	-0.109241216	-	-	-	-	-	-
1	29	155	-0.091526425	-	-	-	-	-	-
1	30	155	-0.091526425	-	-	-	-	-	-

1	31	150	-0.088573959	-	-	-	-	-	-
2738	2769	4400	-0.00094893	11.5	-320.9	169	815	7.02	3.39
3113	5882	350	-6.63902E-05	10.83333333	3362.489093	105	792	7.22	7.95
2809	8691	85	-1.78682E-05	10.83333333	5900.2095	226	836	7.17	7.7
	Total	**38540**							

(bi) Batch BI – Bed 1 (Friday, October 21, 2022)

Time Intervals (min)	Cumulative Time (min)	Collected Volume (ml)	Effluent Flux (cm/min)	Sludge Deposit Layer (cm)	TS (mg/L)	COD (mg/L)	NO_3 (mg/L)	pH	DO (mg/L)
Influent	**-**	**9345**	**-**	**7**	**17507.14**	**6465**	**470**	**7.43**	**0.15**
2	2	240	-0.070859167	-	3847.004201	168	866	7.09	4.2
1	3	410	-0.242102155	-	-	-	-	-	-
1	4	510	-0.301151461	-	-	-	-	-	-
1	5	440	-0.259816947	-	-	-	-	-	-
1	6	470	-0.277531739	-	-	-	-	-	-
1	7	340	-0.200767641	-	-	-	-	-	-
1	8	370	-0.218482433	-	-	-	-	-	-
1	9	280	-0.165338057	-	-	-	-	-	-
1	10	160	-0.09447889	-	-	-	-	-	-
1	11	120	-0.070859167	-	-	-	-	-	-
1	12	100	-0.059049306	-	-	-	-	-	-
1	13	130	-0.076764098	-	-	-	-	-	-
1	14	120	-0.070859167	-	-	-	-	-	-
1	15	100	-0.059049306	-	-	-	-	-	-
1	16	110	-0.064954237	-	-	-	-	-	-
1	17	80	-0.047239445	-	-	-	-	-	-
3027	3044	3820	-0.000745188	6.833333333	3852.749491	240	644	6.95	3.11
2814	5858	90	-1.88857E-05	6.833333333	3858.494781	406	830	5.93	7.68
2709	8567	0	0	6.5	5115.772605	-	-	-	-
	Total	**7890**							

(bj) Batch BJ – Bed 2 (Friday, October 21, 2022)

Time Intervals (min)	Cumulative Time (min)	Collected Volume (ml)	Effluent Flux (cm/min)	Sludge Deposit Layer (cm)	TS (mg/L)	COD (mg/L)	NO_3 (mg/L)	pH	DO (mg/L)
Influent	**-**	**18690**	**-**	**12.5**	**17507.14**	**6465**	**470**	**7.43**	**0.15**
4	4	80	-0.011809861	-	4517.607651	201	782	6.78	3.24
1	5	210	-0.124003543	-	-	-	-	-	-
1	6	310	-0.183052849	-	-	-	-	-	-
1	7	340	-0.200767641	-	-	-	-	-	-
1	8	410	-0.242102155	-	-	-	-	-	-
1	9	360	-0.212577502	-	-	-	-	-	-
1	10	430	-0.253912017	-	-	-	-	-	-
1	11	390	-0.230292294	-	-	-	-	-	-
1	12	400	-0.236197225	-	-	-	-	-	-
1	13	380	-0.224387363	-	-	-	-	-	-
1	14	380	-0.224387363	-	-	-	-	-	-
1	15	360	-0.212577502	-	-	-	-	-	-
1	16	340	-0.200767641	-	-	-	-	-	-
1	17	340	-0.200767641	-	-	-	-	-	-
1	18	220	-0.19486271	-	-	-	-	-	-
1	19	320	-0.18895778	-	-	-	-	-	-
1	20	310	-0.183052849	-	-	-	-	-	-
1	21	320	-0.18895778	-	-	-	-	-	-
1	22	280	-0.165338057	-	-	-	-	-	-
1	23	280	-0.165338057	-	-	-	-	-	-
1	24	260	-0.153528196	-	-	-	-	-	-
1	25	260	-0.153528196	-	-	-	-	-	-
1	26	210	-0.124003543	-	-	-	-	-	-
1	27	210	-0.124003543	-	-	-	-	-	-
1	28	210	-0.124003543	-	-	-	-	-	-
1	29	190	-0.112193682	-	-	-	-	-	-
1	30	180	-0.106288751	-	-	-	-	-	-

1	31	170	-0.10038382	-	-	-	-	-	-
1	32	160	-0.09447889	-	-	-	-	-	-
1	33	160	-0.09447889	-	-	-	-	-	-
3017	3050	6030	-0.001180203	12.83333333	3297.100679	187	583	6.42	5.04
2808	5858	245	-5.15209E-05	12.33333333	4459.036759	135	841	6.81	7.96
2709	8567	40	-8.71898E-06	12.16666667	2105.263158	223	961	7.01	7.42
	Total	**14785**							

(bk) Batch BK – Bed 3 (Friday, October 21, 2022)

Time Intervals (min)	Cumulative Time (min)	Collected Volume (ml)	Effluent Flux (cm/min)	Sludge Deposit Layer (cm)	TS (mg/L)	COD (mg/L)	NO_3 (mg/L)	pH	DO (mg/L)
Influent	**-**	**28040**	**-**	**10.83333333**	**17507.14**	**6465**	**470**	**7.43**	**0.15**
1	1	610	-0.360200768	-	3647.86505	123	759	7.09	3.95
1	2	790	-0.466489519	-	-	-	-	-	-
1	3	850	-0.501919102	-	-	-	-	-	-
1	4	820	-0.484204311	-	-	-	-	-	-
1	5	900	-0.531443756	-	-	-	-	-	-
1	6	820	-0.484204311	-	-	-	-	-	-
1	7	780	-0.460584588	-	-	-	-	-	-
1	8	760	-0.448774727	-	-	-	-	-	-
1	9	720	-0.425155004	-	-	-	-	-	-
1	10	740	-0.436964866	-	-	-	-	-	-
1	11	660	-0.389725421	-	-	-	-	-	-
1	12	600	-0.354295837	-	-	-	-	-	-
1	13	670	-0.395630351	-	-	-	-	-	-
1	14	580	-0.342485976	-	-	-	-	-	-
1	15	600	-0.354295837	-	-	-	-	-	-
1	16	640	-0.377915559	-	-	-	-	-	-
1	17	500	-0.295246531	-	-	-	-	-	-
1	18	500	-0.295246531	-	-	-	-	-	-

1	19	480	-0.28343667	-	-	-	-	-	-
1	20	500	-0.295246531	-	-	-	-	-	-
1	21	420	-0.248007086	-	-	-	-	-	-
1	22	410	-0.242102155	-	-	-	-	-	-
2	24	770	-0.227339829	-	-	-	-	-	-
1	25	360	-0.212577502	-	-	-	-	-	-
1	26	210	-0.124003543	-	-	-	-	-	-
1	27	220	-0.129908474	-	-	-	-	-	-
1	28	260	-0.153528196	-	-	-	-	-	-
1	29	240	-0.141718335	-	-	-	-	-	-
1	30	220	-0.129908474	-	-	-	-	-	-
1	31	220	-0.129908474	-	-	-	-	-	-
1	32	190	-0.112193682	-	-	-	-	-	-
1	33	190	-0.112193682	-	-	-	-	-	-
1	34	170	-0.10038382	-	-	-	-	-	-
1	35	160	-0.09447889	-	-	-	-	-	-
1	36	120	-0.070859167	-	-	-	-	-	-
3015	3051	6530	-0.001278912	13.16666667	-1926.6	171	579	6.85	3.14
2806	5857	30	-6.31318E-06	12.83333333	5269.5	206	956	6.38	7.53
2707	8564	0	0	11.83333333		-	-	-	-
	Total	**24240**							

(bl) Batch BL – Bed 4 (Friday, October 21, 2022)

Time Intervals (min)	Cumulative Time (min)	Collected Volume (ml)	Effluent Flux (cm/min)	Sludge Deposit Layer (cm)	TS (mg/L)	COD (mg/L)	NO_3 (mg/L)	pH	DO (mg/L)
Influent	**-**	**56080**	**-**	**12.33333333**	**17507.14**	**6465**	**470**	**7.43**	**0.15**
11	11	60	-0.003220871	-	2802.459212	127	527	6.94	3.13
1	12	50	-0.029524653	-	-	-	-	-	-
1	13	50	-0.029524653	-	-	-	-	-	-
1	14	60	-0.035429584	-	-	-	-	-	-

1	15	70	-0.041334514	-	-	-	-	-	-
1	16	70	-0.041334514	-	-	-	-	-	-
1	17	60	-0.035429584	-	-	-	-	-	-
1	18	70	-0.041334514	-	-	-	-	-	-
1	19	80	-0.047239445	-	-	-	-	-	-
1	20	80	-0.047239445	-	-	-	-	-	-
1	21	90	-0.053144376	-	-	-	-	-	-
1	22	80	-0.047239445	-	-	-	-	-	-
1	23	90	-0.053144376	-	-	-	-	-	-
1	24	80	-0.047239445	-	-	-	-	-	-
1	25	90	-0.053144376	-	-	-	-	-	-
1	26	90	-0.053144376	-	-	-	-	-	-
1	27	90	-0.053144376	-	-	-	-	-	-
1	28	90	-0.053144376	-	-	-	-	-	-
1	29	90	-0.053144376	-	-	-	-	-	-
1	30	90	-0.053144376	-	-	-	-	-	-
1	31	90	-0.053144376	-	-	-	-	-	-
1	32	90	-0.053144376	-	-	-	-	-	-
1	33	90	-0.053144376	-	-	-	-	-	-
1	34	80	-0.047239445	-	-	-	-	-	-
1	35	80	-0.047239445	-	-	-	-	-	-
1	36	80	-0.047239445	-	-	-	-	-	-
1	37	80	-0.047239445	-	-	-	-	-	-
1	38	80	-0.047239445	-	-	-	-	-	-
1	39	70	-0.041334514	-	-	-	-	-	-
1	40	70	-0.041334514	-	-	-	-	-	-
1	41	70	-0.041334514	-	-	-	-	-	-
1	42	70	-0.041334514	-	-	-	-	-	-
1	43	70	-0.041334514	-	-	-	-	-	-
1	44	70	-0.041334514	-	-	-	-	-	-
1	45	70	-0.041334514	-	-	-	-	-	-

1	46	70	-0.041334514	-	-	-	-	-	-
1	47	60	-0.035429584	-	-	-	-	-	-
1	48	60	-0.035429584	-	-	-	-	-	-
1	49	60	-0.035429584	-	-	-	-	-	-
1	50	60	-0.035429584	-	-	-	-	-	-
1	51	60	-0.035429584	-	-	-	-	-	-
1	52	60	-0.035429584	-	-	-	-	-	-
1	53	60	-0.035429584	-	-	-	-	-	-
1	54	60	-0.035429584	-	-	-	-	-	-
1	55	60	-0.035429584	-	-	-	-	-	-
1	56	50	-0.029524653	-	-	-	-	-	-
1	57	50	-0.029524653	-	-	-	-	-	-
1	58	60	-0.035429584	-	-	-	-	-	-
1	59	50	-0.029524653	-	-	-	-	-	-
2989	3048	20150	-0.003980741	25	2504.876296	129	442	7.2	7.22
2799	5847	20370	-0.004297372	16.16666667	1589.127026	234	413	6.62	7
2711	8558	4850	-0.001056397	15.5	-2808.529203	132	381	6.98	6.82
4341	12899	1870	-0.00025437	13.5	-500	125	500	7.05	6.87
1652	14551	470	-0.000167997	12.5	-514.0507197	111	596	7.03	7
2640	17191	650	-0.000145387	12.33333333	1385.361348	82	622	7.17	7.93
3130	20321	360	-6.79161E-05	11.83333333	897.7121165	74	643	7.1	7.2
2791	23112	180	-3.80827E-05	11.66666667	2692.687747	85	614	6.87	7.4
2721	25833	75	-1.6276E-05	11.5	15581.87917	197	732	7.17	7.78
	Total	**52485**							

(bm) Batch BM – Bed 6 (Friday, October 21, 2022)

Time Intervals (min)	Cumulative Time (min)	Collected Volume (ml)	Effluent Flux (cm/min)	Sludge Deposit Layer (cm)	TS (mg/L)	COD (mg/L)	NO_3 (mg/L)	pH	DO (mg/L)
Influent	**-**	**28040**	**-**	**12.66666667**	**17507.14**	**6465**	**470**	**7.43**	**0.15**
1	1	80	-0.047239445	-	3745.073704	200	759	7.36	3.42

1	2	240	-0.141718335	-	-	-	-	-	-
1	3	150	-0.088573959	-	-	-	-	-	-
1	4	120	-0.070859167	-	-	-	-	-	-
1	5	100	-0.059049306	-	-	-	-	-	-
1	6	80	-0.047239445	-	-	-	-	-	-
1	7	80	-0.047239445	-	-	-	-	-	-
1	8	100	-0.059049306	-	-	-	-	-	-
1	9	120	-0.070859167	-	-	-	-	-	-
1	10	120	-0.070859167	-	-	-	-	-	-
1	11	140	-0.082669029	-	-	-	-	-	-
1	12	140	-0.082669029	-	-	-	-	-	-
1	13	150	-0.088573959	-	-	-	-	-	-
1	14	160	-0.09447889	-	-	-	-	-	-
1	15	190	-0.112193682	-	-	-	-	-	-
1	16	190	-0.112193682	-	-	-	-	-	-
1	17	190	-0.112193682	-	-	-	-	-	-
1	18	190	-0.112193682	-	-	-	-	-	-
1	19	190	-0.112193682	-	-	-	-	-	-
1	20	190	-0.112193682	-	-	-	-	-	-
1	21	200	-0.118098612	-	-	-	-	-	-
1	22	200	-0.118098612	-	-	-	-	-	-
1	23	190	-0.112193682	-	-	-	-	-	-
1	24	200	-0.118098612	-	-	-	-	-	-
1	25	200	-0.118098612	-	-	-	-	-	-
1	26	210	-0.124003543	-	-	-	-	-	-
1	27	200	-0.118098612	-	-	-	-	-	-
1	28	200	-0.118098612	-	-	-	-	-	-
1	29	230	-0.135813404	-	-	-	-	-	-
1	30	220	-0.129908474	-	-	-	-	-	-
1	31	230	-0.135813404	-	-	-	-	-	-
1	32	240	-0.141718335	-	-	-	-	-	-

1	33	230	-0.135813404	-	-	-	-	-	-
1	34	220	-0.129908474	-	-	-	-	-	-
1	35	220	-0.129908474	-	-	-	-	-	-
1	36	220	-0.129908474	-	-	-	-	-	-
1	37	210	-0.124003543	-	-	-	-	-	-
1	38	210	-0.124003543	-	-	-	-	-	-
1	39	210	-0.124003543	-	-	-	-	-	-
1	40	210	-0.124003543	-	-	-	-	-	-
1	41	210	-0.124003543	-	-	-	-	-	-
1	42	200	-0.118098612	-	-	-	-	-	-
1	43	200	-0.118098612	-	-	-	-	-	-
1	44	200	-0.118098612	-	-	-	-	-	-
1	45	200	-0.118098612	-	-	-	-	-	-
1	46	200	-0.118098612	-	-	-	-	-	-
1	47	200	-0.118098612	-	-	-	-	-	-
1	48	200	-0.118098612	-	-	-	-	-	-
1	49	180	-0.106288751	-	-	-	-	-	-
1	50	190	-0.112193682	-	-	-	-	-	-
1	51	190	-0.112193682	-	-	-	-	-	-
1	52	200	-0.118098612	-	-	-	-	-	-
1	53	210	-0.124003543	-	-	-	-	-	-
1	54	210	-0.124003543	-	-	-	-	-	-
2999	3053	17180	-0.003382684	13.25	3714.205839	174	628	6.97	3.93
2798	5851	90	-1.89937E-05	13	5274.706726	178	873	7.22	7.5
2698	8549	0	0	13	-	-	-	-	-
4289	12838	0	0	13	-	-	-	-	-
	Total	**27230**							

(bn) Batch BN – Bed 1 (Thursday, October 27, 2022)

Time Intervals	Cumulative	Collected	Effluent Flux	Sludge Deposit	TS (mg/L)	COD	NO_3	pH	DO

(min)	Time (min)	Volume (ml)	(cm/min)	Layer (cm)		(mg/L)	(mg/L)		(mg/L)
Influent	**-**	**9345**	**-**	**6.5**	**17507.14**	**6465**	**470**	**7.43**	**0.15**
2	2	45	-0.013286094	-	3751.138739	179	661	6.24	2.93
1	3	180	-0.106288751	-	-	-	-	-	-
1	4	200	-0.118098612	-	-	-	-	-	-
1	5	190	-0.112193682	-	-	-	-	-	-
1	6	190	-0.112193682	-	-	-	-	-	-
1	7	195	-0.115146147	-	-	-	-	-	-
1	8	200	-0.118098612	-	-	-	-	-	-
1	9	200	-0.118098612	-	-	-	-	-	-
1	10	195	-0.115146147	-	-	-	-	-	-
1	11	190	-0.112193682	-	-	-	-	-	-
1	12	190	-0.112193682	-	-	-	-	-	-
1	13	175	-0.103336286	-	-	-	-	-	-
1	14	165	-0.097431355	-	-	-	-	-	-
1	15	165	-0.097431355	-	-	-	-	-	-
1	16	160	-0.09447889	-	-	-	-	-	-
1	17	155	-0.091526425	-	-	-	-	-	-
1	18	145	-0.085621494	-	-	-	-	-	-
1	19	140	-0.082669029	-	-	-	-	-	-
1	20	130	-0.076764098	-	-	-	-	-	-
1	21	125	-0.073811633	-	-	-	-	-	-
1	22	125	-0.073811633	-	-	-	-	-	-
1	23	100	-0.059049306	-	-	-	-	-	-
2	25	180	-0.053144376	-	-	-	-	-	-
1	26	85	-0.05019191	-	-	-	-	-	-
4306	4332	4100	-0.000562244	7.666666667	754.1111219	249	582	6.34	1.28
1652	5984	0	0	7.5	-	-	-	-	-
2641	8625	0	0	7.5	-	-	-	-	-
	Total	**7925**							

(bo) Batch BO – Bed 2 (Thursday, October 27, 2022)

Time Intervals (min)	Cumulative Time (min)	Collected Volume (ml)	Effluent Flux (cm/min)	Sludge Deposit Layer (cm)	TS (mg/L)	COD (mg/L)	NO_3 (mg/L)	pH	DO (mg/L)
Influent	**-**	**18690**	**-**	**12.16666667**	**17507.14**	**6465**	**470**	**7.43**	**0.15**
1	1	95	-0.056096841	-	742.7764986	183	729	6.89	3.48
1	2	105	-0.062001771	-	-	-	-	-	-
1	3	680	-0.401535282	-	-	-	-	-	-
1	4	440	-0.259816947	-	-	-	-	-	-
1	5	465	-0.274579274	-	-	-	-	-	-
1	6	475	-0.280484204	-	-	-	-	-	-
1	7	460	-0.271626808	-	-	-	-	-	-
1	8	460	-0.271626808	-	-	-	-	-	-
1	9	530	-0.312961323	-	-	-	-	-	-
1	10	415	-0.245054621	-	-	-	-	-	-
1	11	430	-0.253912017	-	-	-	-	-	-
1	12	470	-0.277531739	-	-	-	-	-	-
1	13	430	-0.253912017	-	-	-	-	-	-
1	14	445	-0.262769412	-	-	-	-	-	-
1	15	410	-0.242102155	-	-	-	-	-	-
1	16	430	-0.253912017	-	-	-	-	-	-
1	17	425	-0.250959551	-	-	-	-	-	-
1	18	400	-0.236197225	-	-	-	-	-	-
1	19	375	-0.221434898	-	-	-	-	-	-
1	20	370	-0.218482433	-	-	-	-	-	-
1	21	320	-0.18895778	-	-	-	-	-	-
1	22	275	-0.162385592	-	-	-	-	-	-
1	23	225	-0.132860939	-	-	-	-	-	-
1	24	200	-0.118098612	-	-	-	-	-	-
4309	4333	6130	-0.000840038	12.83	-471.1	225	656	6.52	3.25
1650	5983	0	0	12.16666667	-	-	-	-	-
2640	8623	0	0	12.16666667	-	-	-	-	-

Total	**15460**

(bp) Batch BP – Bed 3 (Thursday, October 27, 2022)

Time Intervals (min)	Cumulative Time (min)	Collected Volume (ml)	Effluent Flux (cm/min)	Sludge Deposit Layer (cm)	TS (mg/L)	COD (mg/L)	NO_3 (mg/L)	pH	DO (mg/L)
Influent	**-**	**28040**	**-**	**11.83333333**	**17507.14**	**6465**	**470**	**7.43**	**0.15**
1	1	3240	-1.91319752	-	0	248	585	7.26	1.91
1	2	3510	-2.072630647	-	-	-	-	-	-
1	3	2200	-1.299084736	-	-	-	-	-	-
1	4	1975	-1.166223797	-	-	-	-	-	-
1	5	1950	-1.15146147	-	-	-	-	-	-
1	6	1570	-0.927074107	-	-	-	-	-	-
1	7	1410	-0.832595217	-	-	-	-	-	-
1	8	1520	-0.897549454	-	-	-	-	-	-
1	9	1290	-0.76173605	-	-	-	-	-	-
1	10	750	-0.442869796	-	-	-	-	-	-
1	11	650	-0.38382049	-	-	-	-	-	-
1	12	350	-0.206672572	-	-	-	-	-	-
1	13	250	-0.147623265	-	-	-	-	-	-
1	14	210	-0.124003543	-	-	-	-	-	-
1	15	200	-0.118098612	-	-	-	-	-	-
1	16	160	-0.09447889	-	-	-	-	-	-
1	17	150	-0.088573959	-	-	-	-	-	-
1	18	140	-0.082669029	-	-	-	-	-	-
1	19	130	-0.076764098	-	-	-	-	-	-
4290	4309	2970	-0.000408803	13	774.8062984	250	418	6.1	2.34
1650	5959	0	0	12.5	-	-	-	-	-
2640	8599	0	0	12.33333333	-	-	-	-	-
	Total	**24625**							

(bq) Batch BQ – Bed 6 (Sunday, October 30, 2022)

Time Intervals (min)	Cumulative Time (min)	Collected Volume (ml)	Effluent Flux (cm/min)	Sludge Deposit Layer (cm)	TS (mg/L)	COD (mg/L)	NO_3 (mg/L)	pH	DO (mg/L)
Influent	**-**	**28040**	**-**	**13**	**17507.14**	**6465**	**470**	**7.43**	**0.15**
1	1	250	-0.147623265	-	48.85078528	461	660	7.88	1.74
1	2	340	-0.200767641	-	-	-	-	-	-
1	3	215	-0.126956008	-	-	-	-	-	-
1	4	150	-0.088573959	-	-	-	-	-	-
1	5	130	-0.076764098	-	-	-	-	-	-
1	6	125	-0.073811633	-	-	-	-	-	-
1	7	140	-0.082669029	-	-	-	-	-	-
1	8	125	-0.073811633	-	-	-	-	-	-
1	9	135	-0.079716563	-	-	-	-	-	-
1	10	135	-0.079716563	-	-	-	-	-	-
1	11	130	-0.076764098	-	-	-	-	-	-
1	12	140	-0.082669029	-	-	-	-	-	-
1	13	145	-0.085621494	-	-	-	-	-	-
1	14	140	-0.082669029	-	-	-	-	-	-
1	15	140	-0.082669029	-	-	-	-	-	-
1	16	140	-0.082669029	-	-	-	-	-	-
1	17	140	-0.082669029	-	-	-	-	-	-
1	18	135	-0.079716563	-	-	-	-	-	-
1	19	140	-0.082669029	-	-	-	-	-	-
1	20	135	-0.079716563	-	-	-	-	-	-
1	21	135	-0.079716563	-	-	-	-	-	-
1	22	135	-0.079716563	-	-	-	-	-	-
1	23	135	-0.079716563	-	-	-	-	-	-
1	24	135	-0.079716563	-	-	-	-	-	-
1	25	135	-0.079716563	-	-	-	-	-	-
1	26	135	-0.079716563	-	-	-	-	-	-
1	27	125	-0.073811633	-	-	-	-	-	-

1	28	130	-0.076764098	-	-	-	-	-	-
1	29	135	-0.079716563	-	-	-	-	-	-
1	30	125	-0.073811633	-	-	-	-	-	-
1	31	130	-0.076764098	-	-	-	-	-	-
1	32	130	-0.076764098	-	-	-	-	-	-
1	33	130	-0.076764098	-	-	-	-	-	-
1	34	130	-0.076764098	-	-	-	-	-	-
1	35	130	-0.076764098	-	-	-	-	-	-
1	36	135	-0.079716563	-	-	-	-	-	-
1	37	135	-0.079716563	-	-	-	-	-	-
1	38	140	-0.082669029	-	-	-	-	-	-
1	39	140	-0.082669029	-	-	-	-	-	-
1	40	135	-0.079716563	-	-	-	-	-	-
1	41	140	-0.082669029	-	-	-	-	-	-
1	42	135	-0.079716563	-	-	-	-	-	-
1	43	135	-0.079716563	-	-	-	-	-	-
1	44	135	-0.079716563	-	-	-	-	-	-
1	45	135	-0.079716563	-	-	-	-	-	-
1	46	140	-0.082669029	-	-	-	-	-	-
1	47	135	-0.079716563	-	-	-	-	-	-
1	48	135	-0.079716563	-	-	-	-	-	-
1	49	135	-0.079716563	-	-	-	-	-	-
1	50	130	-0.076764098	-	-	-	-	-	-
1	51	130	-0.076764098	-	-	-	-	-	-
1	52	130	-0.076764098	-	-	-	-	-	-
1	53	135	-0.079716563	-	-	-	-	-	-
1	54	135	-0.079716563	-	-	-	-	-	-
1	55	135	-0.079716563	-	-	-	-	-	-
1	56	135	-0.079716563	-	-	-	-	-	-
1	57	135	-0.079716563	-	-	-	-	-	-
1	58	135	-0.079716563	-	-	-	-	-	-

1	59	135	-0.079716563	-	-	-	-	-	-
1	60	140	-0.082669029	-	-	-	-	-	-
1	61	135	-0.079716563	-	-	-	-	-	-
1	62	135	-0.079716563	-	-	-	-	-	-
2	64	250	-0.073811633	-	-	-	-	-	-
1570	1634	13300	-0.005002266	13.5	-856.5624924	270	632	6.31	6.84
2639	4273	290	-6.48893E-05	13.3	1758.544231	163	547	6.47	6.89
3130	7403	0	0	13	-	-	-	-	-
2791	10194	0	0	13	-	-	-	-	-
2721	12915	0	0	13	-	-	-	-	-
	Total	**22600**							

(br) Batch BR – Bed 1 (Wednesday, November 2, 2022)

Time Intervals (min)	Cumulative Time (min)	Collected Volume (ml)	Effluent Flux (cm/min)	Sludge Deposit Layer (cm)	TS (mg/L)	COD (mg/L)	NO_3 (mg/L)	pH	DO (mg/L)
Influent	**-**	**9345**	**-**	**7.5**	**17507.14**	**6465**	**470**	**7.43**	**0.15**
1	1	130	-0.076764098	-	1366.763012	138	661	6.79	3.5
1	2	160	-0.09447889	-	-	-	-	-	-
1	3	140	-0.082669029	-	-	-	-	-	-
1	4	90	-0.078240331	-	-	-	-	-	-
1	5	125	-0.073811633	-	-	-	-	-	-
1	6	150	-0.088573959	-	-	-	-	-	-
1	7	125	-0.073811633	-	-	-	-	-	-
1	8	125	-0.073811633	-	-	-	-	-	-
1	9	130	-0.076764098	-	-	-	-	-	-
1	10	135	-0.079716563	-	-	-	-	-	-
1	11	115	-0.067906702	-	-	-	-	-	-
1	12	120	-0.070859167	-	-	-	-	-	-
1	13	125	-0.073811633	-	-	-	-	-	-
1	14	125	-0.073811633	-	-	-	-	-	-

1	15	125	-0.073811633	-	-	-	-	-	-
1	16	120	-0.070859167	-	-	-	-	-	-
1	17	120	-0.070859167	-	-	-	-	-	-
1	18	115	-0.067906702	-	-	-	-	-	-
1	19	120	-0.070859167	-	-	-	-	-	-
1	20	115	-0.067906702	-	-	-	-	-	-
1	21	115	-0.067906702	-	-	-	-	-	-
1	22	105	-0.062001771	-	-	-	-	-	-
1	23	110	-0.064954237	-	-	-	-	-	-
1	24	115	-0.067906702	-	-	-	-	-	-
1	25	105	-0.062001771	-	-	-	-	-	-
1	26	105	-0.062001771	-	-	-	-	-	-
1	27	100	-0.059049306	-	-	-	-	-	-
1	28	110	-0.064954237	-	-	-	-	-	-
1	29	100	-0.059049306	-	-	-	-	-	-
1	30	90	-0.053144376	-	-	-	-	-	-
1	31	100	-0.059049306	-	-	-	-	-	-
1	32	95	-0.056096841	-	-	-	-	-	-
1	33	95	-0.056096841	-	-	-	-	-	-
1	34	95	-0.056096841	-	-	-	-	-	-
1	35	95	-0.056096841	-	-	-	-	-	-
1	36	95	-0.056096841	-	-	-	-	-	-
1	37	95	-0.056096841	-	-	-	-	-	-
1	38	80	-0.047239445	-	-	-	-	-	-
1	39	90	-0.053144376	-	-	-	-	-	-
1	40	85	-0.05019191	-	-	-	-	-	-
1	41	85	-0.05019191	-	-	-	-	-	-
1	42	80	-0.047239445	-	-	-	-	-	-
1	43	85	-0.05019191	-	-	-	-	-	-
1	44	80	-0.047239445	-	-	-	-	-	-
1	45	80	-0.047239445	-	-	-	-	-	-

1	46	80	-0.047239445	-	-	-	-	-	-
1	47	80	-0.047239445	-	-	-	-	-	-
1	48	75	-0.04428698	-	-	-	-	-	-
1	49	75	-0.04428698	-	-	-	-	-	-
1	50	75	-0.04428698	-	-	-	-	-	-
1	51	70	-0.041334514	-	-	-	-	-	-
1	52	70	-0.041334514	-	-	-	-	-	-
1	53	75	-0.04428698	-	-	-	-	-	-
1	54	75	-0.04428698	-	-	-	-	-	-
1	55	65	-0.038382049	-	-	-	-	-	-
1	56	60	-0.035429584	-	-	-	-	-	-
1	57	70	-0.041334514	-	-	-	-	-	-
1	58	65	-0.038382049	-	-	-	-	-	-
1	59	65	-0.038382049	-	-	-	-	-	-
3025	3084	2710	-0.000529004	7.5	2122.356309	190	583	6.98	2.3
2803	5887	65	-1.36932E-05	7.666666667	2745.788015	156	863	6.87	7.48
2722	8609	0	0	7.5	-	-	-	-	-
	Total	**8675**							

(bs) Batch BS – Bed 2 (Wednesday, November 2, 2022)

Time Intervals (min)	Cumulative Time (min)	Collected Volume (ml)	Effluent Flux (cm/min)	Sludge Deposit Layer (cm)	TS (mg/L)	COD (mg/L)	NO_3 (mg/L)	pH	DO (mg/L)
Influent	**-**	**18690**	**-**	**12.16666667**	**17507.14**	**6465**	**470**	**7.43**	**0.15**
3	3	125	-0.024603878	-	2739.133569	151	420	6.6	3.81
1	4	295	-0.174195453	-	-	-	-	-	-
1	5	245	-0.1446708	-	-	-	-	-	-
1	6	220	-0.129908474	-	-	-	-	-	-
1	7	260	-0.153528196	-	-	-	-	-	-
1	8	270	-0.159433127	-	-	-	-	-	-
1	9	285	-0.168290523	-	-	-	-	-	-

1	10	295	-0.174195453	-	-	-	-	-	-
1	11	315	-0.186005314	-	-	-	-	-	-
1	12	260	-0.153528196	-	-	-	-	-	-
1	13	290	-0.171242988	-	-	-	-	-	-
1	14	275	-0.162385592	-	-	-	-	-	-
1	15	285	-0.168290523	-	-	-	-	-	-
1	16	260	-0.153528196	-	-	-	-	-	-
1	17	280	-0.165338057	-	-	-	-	-	-
1	18	260	-0.153528196	-	-	-	-	-	-
1	19	270	-0.159433127	-	-	-	-	-	-
1	20	275	-0.162385592	-	-	-	-	-	-
1	21	295	-0.174195453	-	-	-	-	-	-
1	22	275	-0.162385592	-	-	-	-	-	-
1	23	275	-0.162385592	-	-	-	-	-	-
1	24	260	-0.153528196	-	-	-	-	-	-
1	25	255	-0.150575731	-	-	-	-	-	-
1	26	250	-0.147623265	-	-	-	-	-	-
2	28	460	-0.135813404	-	-	-	-	-	-
1	29	250	-0.147623265	-	-	-	-	-	-
1	30	245	-0.1446708	-	-	-	-	-	-
1	31	230	-0.135813404	-	-	-	-	-	-
1	32	215	-0.126956008	-	-	-	-	-	-
1	33	205	-0.121051078	-	-	-	-	-	-
1	34	250	-0.147623265	-	-	-	-	-	-
1	35	205	-0.121051078	-	-	-	-	-	-
1	36	205	-0.121051078	-	-	-	-	-	-
1	37	195	-0.115146147	-	-	-	-	-	-
1	38	195	-0.115146147	-	-	-	-	-	-
1	39	190	-0.112193682	-	-	-	-	-	-
1	40	185	-0.109241216	-	-	-	-	-	-
1	41	180	-0.106288751	-	-	-	-	-	-

2	43	150	-0.04428698	-	-	-	-	-	-
3	46	135	-0.026572188	-	-	-	-	-	-
4	50	115	-0.016976676	-	-	-	-	-	-
5	55	105	-0.012400354	-	-	-	-	-	-
6	61	95	-0.009349473	-	-	-	-	-	-
7	68	90	-0.007592054	-	-	-	-	-	-
8	76	85	-0.006273989	-	-	-	-	-	-
9	85	80	-0.005248827	-	-	-	-	-	-
10	95	75	-0.004428698	-	-	-	-	-	-
11	106	70	-0.003757683	-	-	-	-	-	-
12	118	75	-0.003690582	-	-	-	-	-	-
13	131	75	-0.003406691	-	-	-	-	-	-
14	145	60	-0.002530685	-	-	-	-	-	-
15	160	65	-0.002558803	-	-	-	-	-	-
3032	3192	5510	-0.001073093	12.66666667	1835.61085	162	530	6.36	3.06
2797	5989	890	-0.000187894	12.83333333	3067.717973	133	677	6.51	7.44
2721	8710	65	-1.41059E-05	12.5	1487.5	207	696	6.72	7.89
	Total	**17325**							

(bt) Batch BT – Bed 3 (Wednesday, November 2, 2022)

Time Intervals (min)	Cumulative Time (min)	Collected Volume (ml)	Effluent Flux (cm/min)	Sludge Deposit Layer (cm)	TS (mg/L)	COD (mg/L)	NO_3 (mg/L)	pH	DO (mg/L)
Influent	**-**	**28040**	**-**	**12.33333333**	**17507.14**	**6465**	**470**	**7.43**	**0.15**
1	1	125	-0.073811633	-	1705.970898	134	474	6.96	3.78
1	2	140	-0.082669029	-	-	-	-	-	-
1	3	120	-0.070859167	-	-	-	-	-	-
1	4	100	-0.059049306	-	-	-	-	-	-
1	5	95	-0.056096841	-	-	-	-	-	-
1	6	95	-0.056096841	-	-	-	-	-	-
1	7	100	-0.059049306	-	-	-	-	-	-

1	8	105	-0.062001771	-	-	-	-	-	-
1	9	105	-0.062001771	-	-	-	-	-	-
1	10	100	-0.059049306	-	-	-	-	-	-
1	11	105	-0.062001771	-	-	-	-	-	-
1	12	110	-0.064954237	-	-	-	-	-	-
1	13	140	-0.082669029	-	-	-	-	-	-
1	14	135	-0.079716563	-	-	-	-	-	-
1	15	180	-0.106288751	-	-	-	-	-	-
1	16	185	-0.109241216	-	-	-	-	-	-
1	17	175	-0.103336286	-	-	-	-	-	-
1	18	180	-0.106288751	-	-	-	-	-	-
1	19	175	-0.103336286	-	-	-	-	-	-
1	20	180	-0.106288751	-	-	-	-	-	-
1	21	180	-0.106288751	-	-	-	-	-	-
1	22	180	-0.106288751	-	-	-	-	-	-
1	23	170	-0.10038382	-	-	-	-	-	-
1	24	175	-0.103336286	-	-	-	-	-	-
1	25	190	-0.112193682	-	-	-	-	-	-
1	26	185	-0.109241216	-	-	-	-	-	-
1	27	185	-0.109241216	-	-	-	-	-	-
1	28	180	-0.106288751	-	-	-	-	-	-
1	29	175	-0.103336286	-	-	-	-	-	-
1	30	185	-0.109241216	-	-	-	-	-	-
1	31	175	-0.103336286	-	-	-	-	-	-
1	32	180	-0.106288751	-	-	-	-	-	-
1	33	180	-0.106288751	-	-	-	-	-	-
1	34	170	-0.10038382	-	-	-	-	-	-
1	35	170	-0.10038382	-	-	-	-	-	-
1	36	170	-0.10038382	-	-	-	-	-	-
1	37	165	-0.097431355	-	-	-	-	-	-
1	38	165	-0.097431355	-	-	-	-	-	-

1	39	160	-0.09447889	-	-	-	-	-	-
1	40	160	-0.09447889	-	-	-	-	-	-
1	41	155	-0.091526425	-	-	-	-	-	-
1	42	155	-0.091526425	-	-	-	-	-	-
1	43	160	-0.09447889	-	-	-	-	-	-
1	44	155	-0.091526425	-	-	-	-	-	-
1	45	155	-0.091526425	-	-	-	-	-	-
1	46	160	-0.09447889	-	-	-	-	-	-
1	47	160	-0.09447889	-	-	-	-	-	-
1	48	160	-0.09447889	-	-	-	-	-	-
1	49	160	-0.09447889	-	-	-	-	-	-
1	50	155	-0.091526425	-	-	-	-	-	-
1	51	170	-0.10038382	-	-	-	-	-	-
1	52	145	-0.085621494	-	-	-	-	-	-
1	53	155	-0.091526425	-	-	-	-	-	-
1	54	150	-0.088573959	-	-	-	-	-	-
1	55	150	-0.088573959	-	-	-	-	-	-
1	56	150	-0.088573959	-	-	-	-	-	-
1	57	150	-0.088573959	-	-	-	-	-	-
1	58	150	-0.088573959	-	-	-	-	-	-
1	59	150	-0.088573959	-	-	-	-	-	-
1	60	150	-0.088573959	-	-	-	-	-	-
3027	3087	14940	-0.002914426	12.33333333	1487.006396	119	576	6.61	4.13
2797	5884	55	-1.16114E-05	12.5	2608.04769	169	1061	7.71	7.58
2721	8605	0	0	12.33333333	-	-	-	-	-
	Total	**24240**							

Appendix L: Graphs of Sludge Deposit Layer Thickness in Phase 1 Experiment.

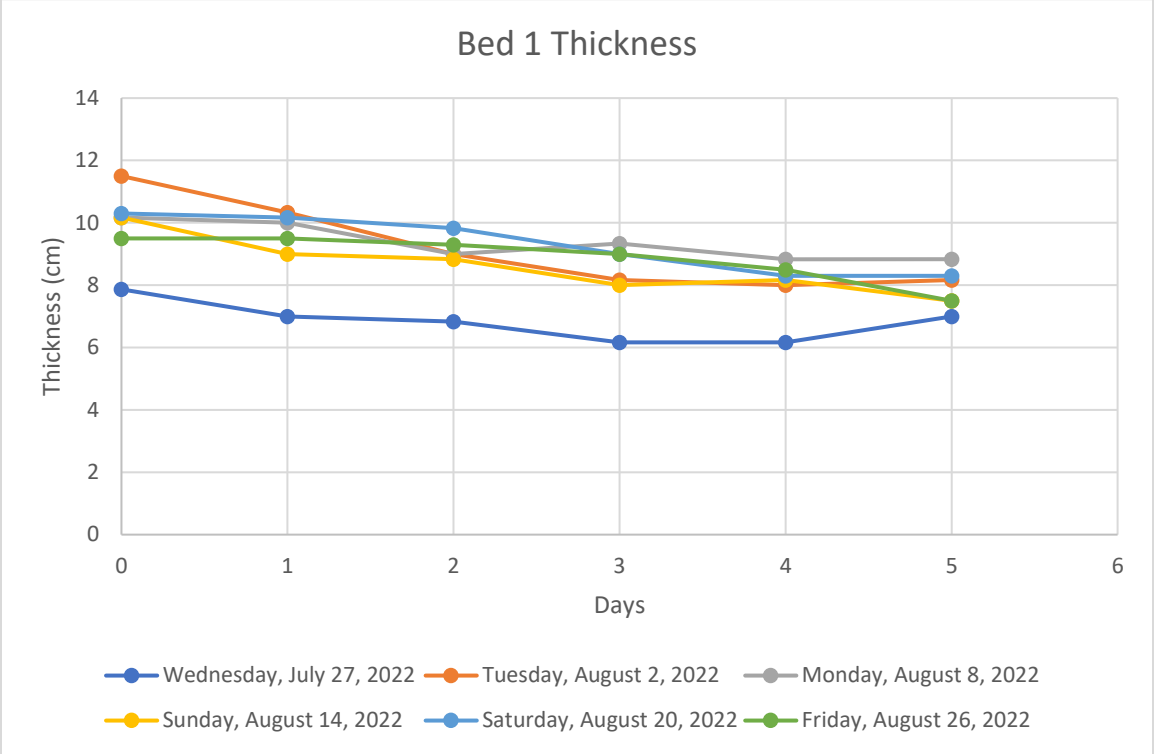

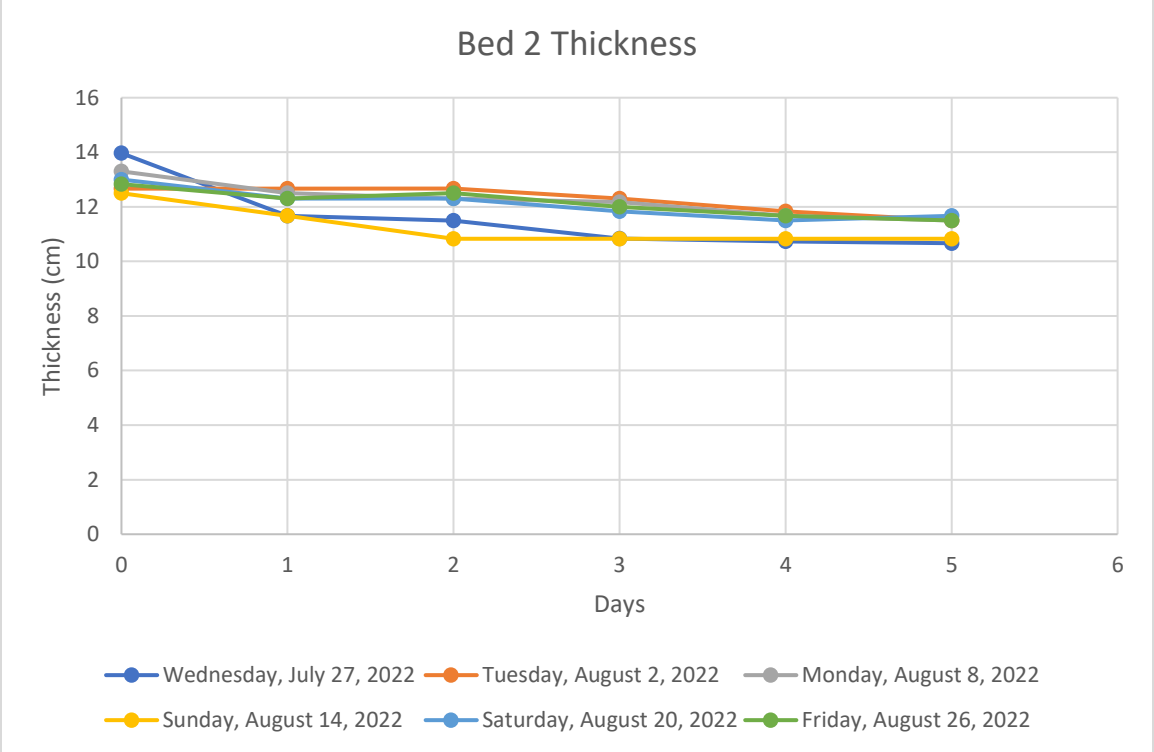

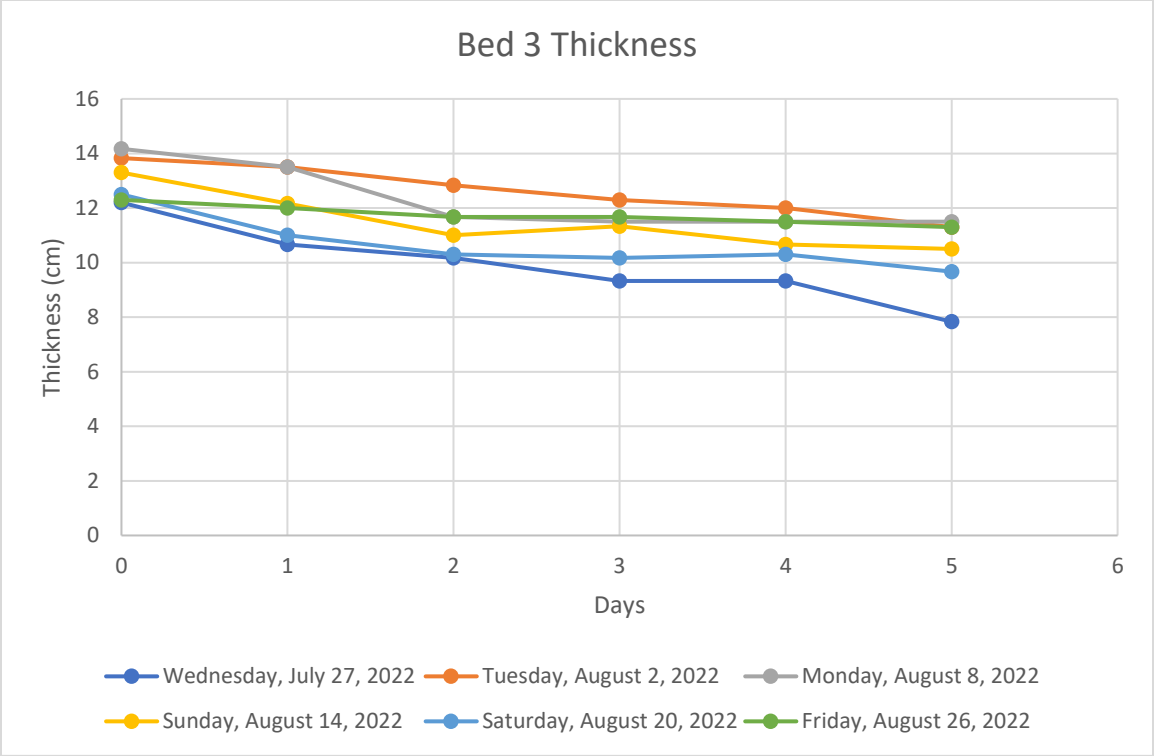
Bed 3 Thickness
Thickness (cm)
16
14
12
10
8
6
4
2
0
0
1
2
3
4
5
6
Days
Wednesday, July 27, 2022
Tuesday, August 2, 2022
Monday, August 8, 2022
Sunday, August 14, 2022
Saturday, August 20, 2022
Friday, August 26, 2022

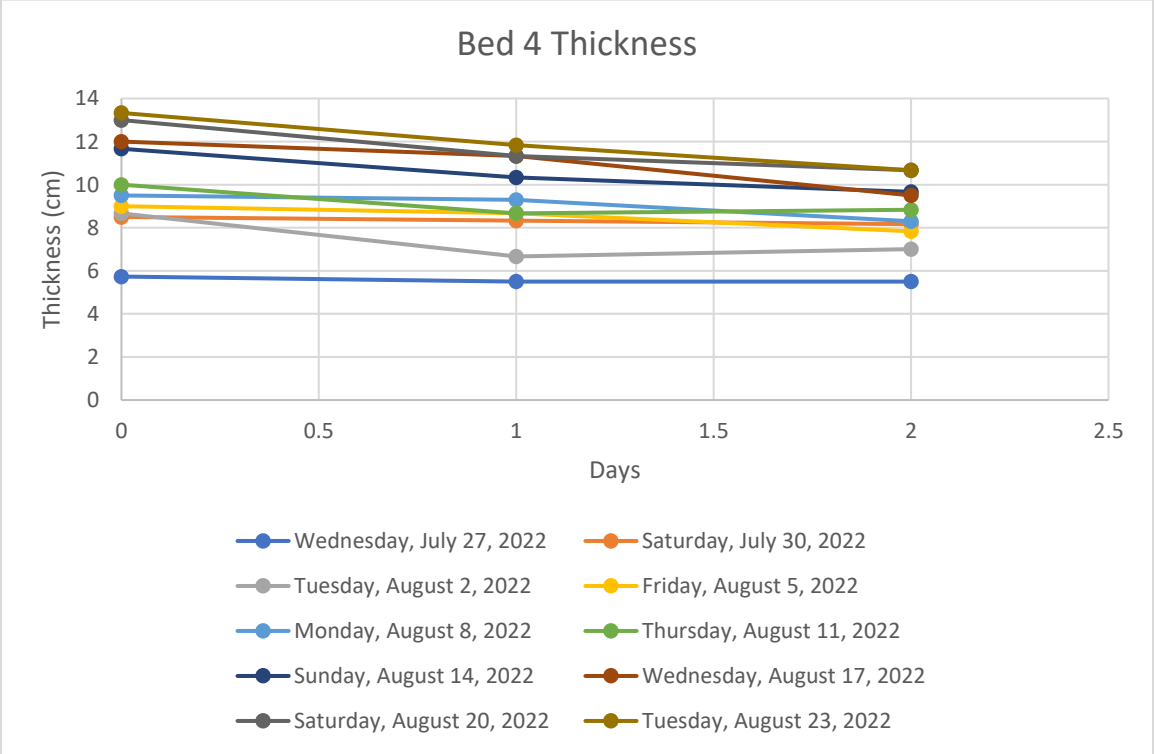
Bed 4 Thickness
Thickness (cm)
14
12
10
8
6
4
2
0
0
0.5
1
1.5
2
2.5
Days
Wednesday, July 27, 2022
Saturday, July 30, 2022
Tuesday, August 2, 2022
Friday, August 5, 2022
Monday, August 8, 2022
Thursday, August 11, 2022
Sunday, August 14, 2022
Wednesday, August 17, 2022
Saturday, August 20, 2022
Tuesday, August 23, 2022

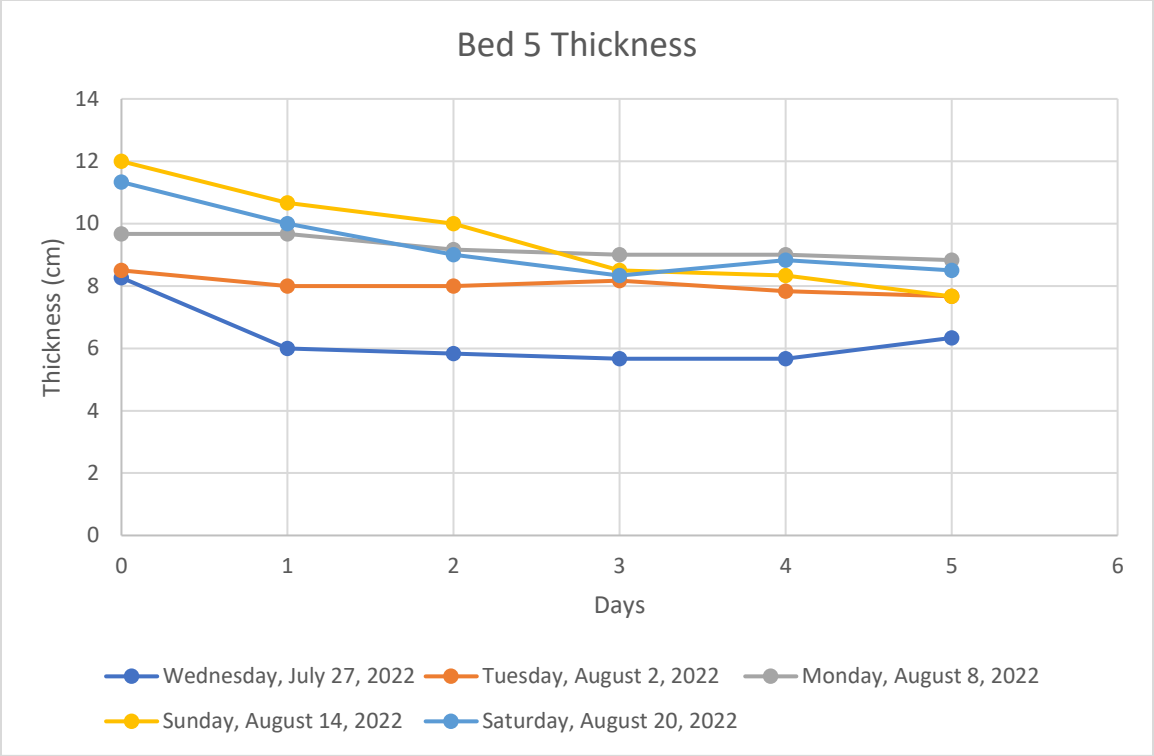
Bed 5 Thickness
Thickness (cm)
Days
Wednesday, July 27, 2022
Tuesday, August 2, 2022
Monday, August 8, 2022
Sunday, August 14, 2022
Saturday, August 20, 2022

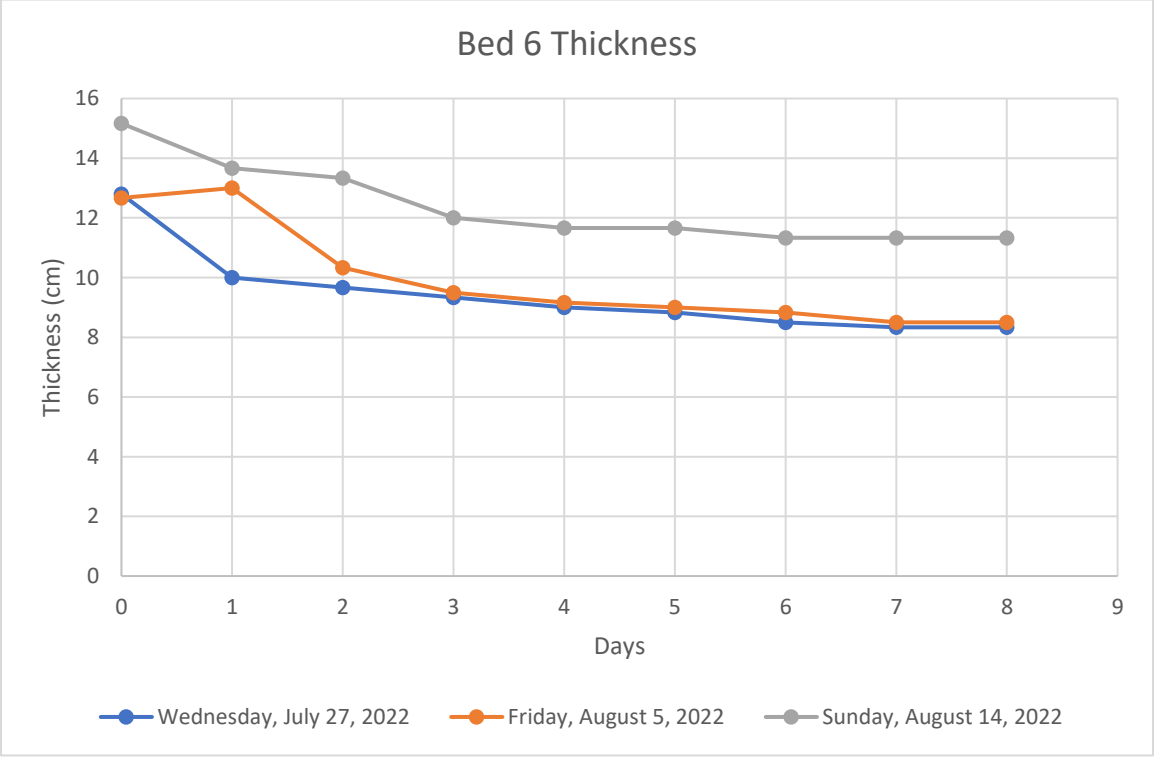
Bed 6 Thickness
Thickness (cm)
Days
Wednesday, July 27, 2022
Friday, August 5, 2022
Sunday, August 14, 2022

Appendix M: Graphs of Moisture Content of Sludge Deposit in Phase 1 Experiment.

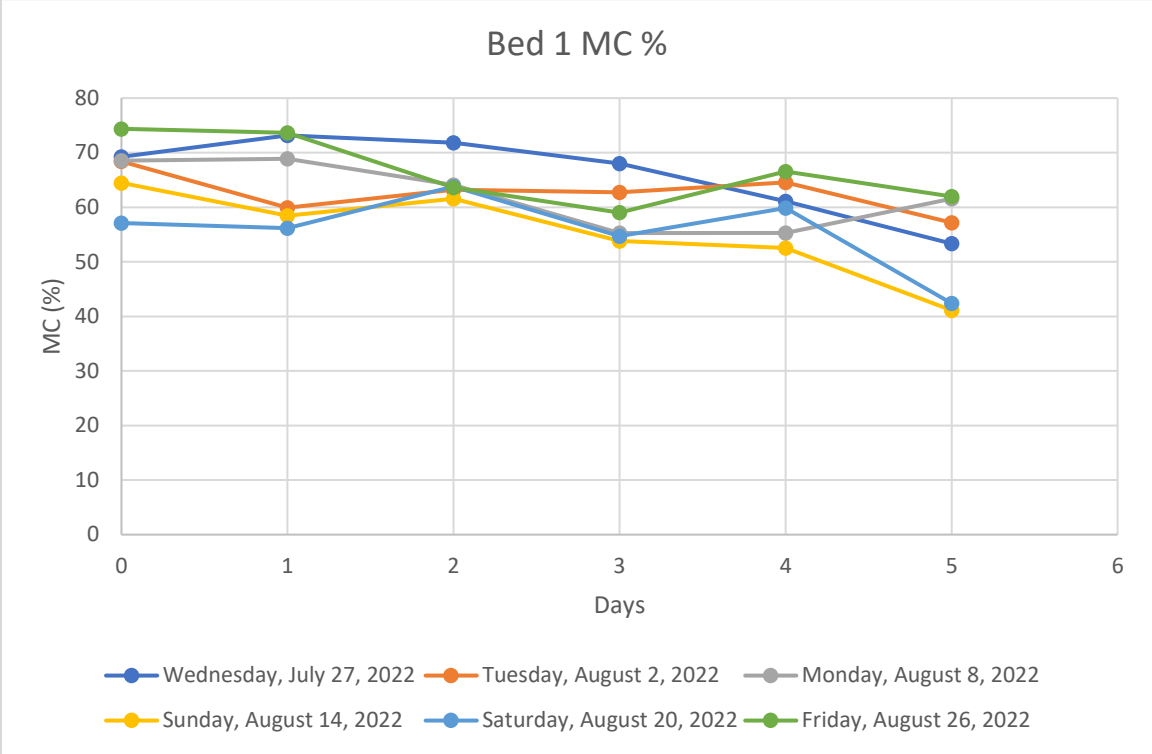

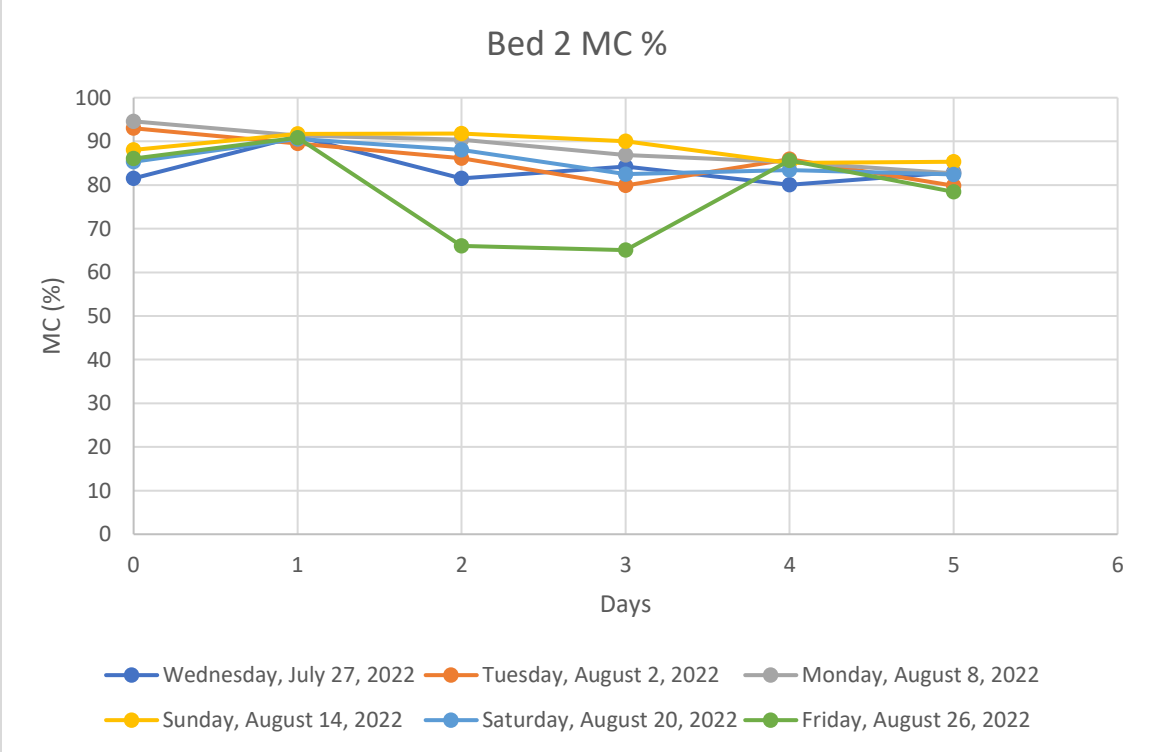

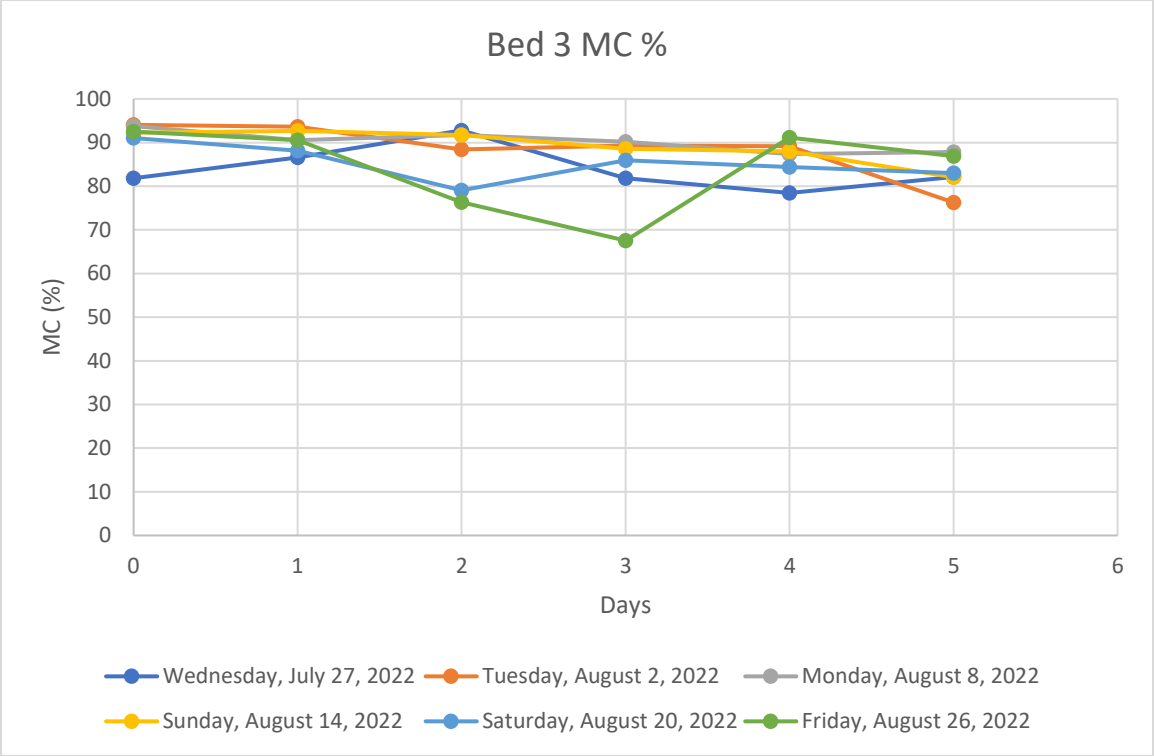
Bed 3 MC %
MC (%)
Days
Wednesday, July 27, 2022
Tuesday, August 2, 2022
Monday, August 8, 2022
Sunday, August 14, 2022
Saturday, August 20, 2022
Friday, August 26, 2022

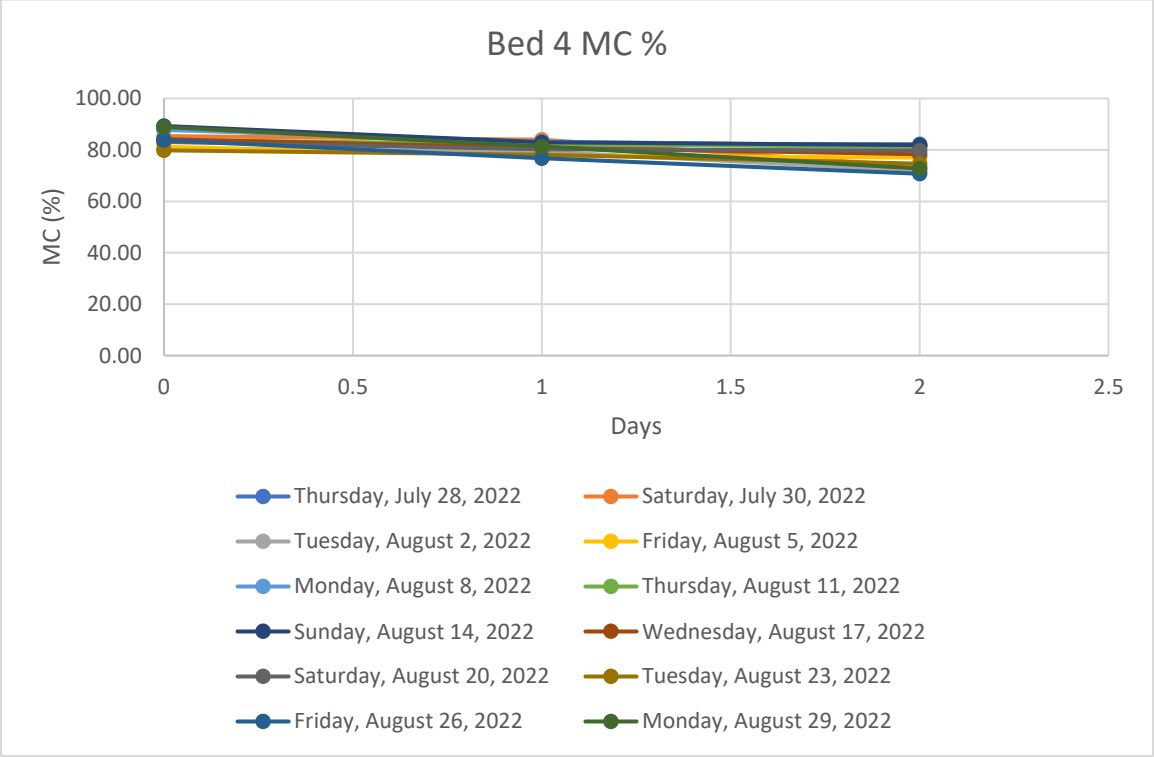
Bed 4 MC %
MC (%)
Days
Thursday, July 28, 2022
Saturday, July 30, 2022
Tuesday, August 2, 2022
Friday, August 5, 2022
Monday, August 8, 2022
Thursday, August 11, 2022
Sunday, August 14, 2022
Wednesday, August 17, 2022
Saturday, August 20, 2022
Tuesday, August 23, 2022
Friday, August 26, 2022
Monday, August 29, 2022

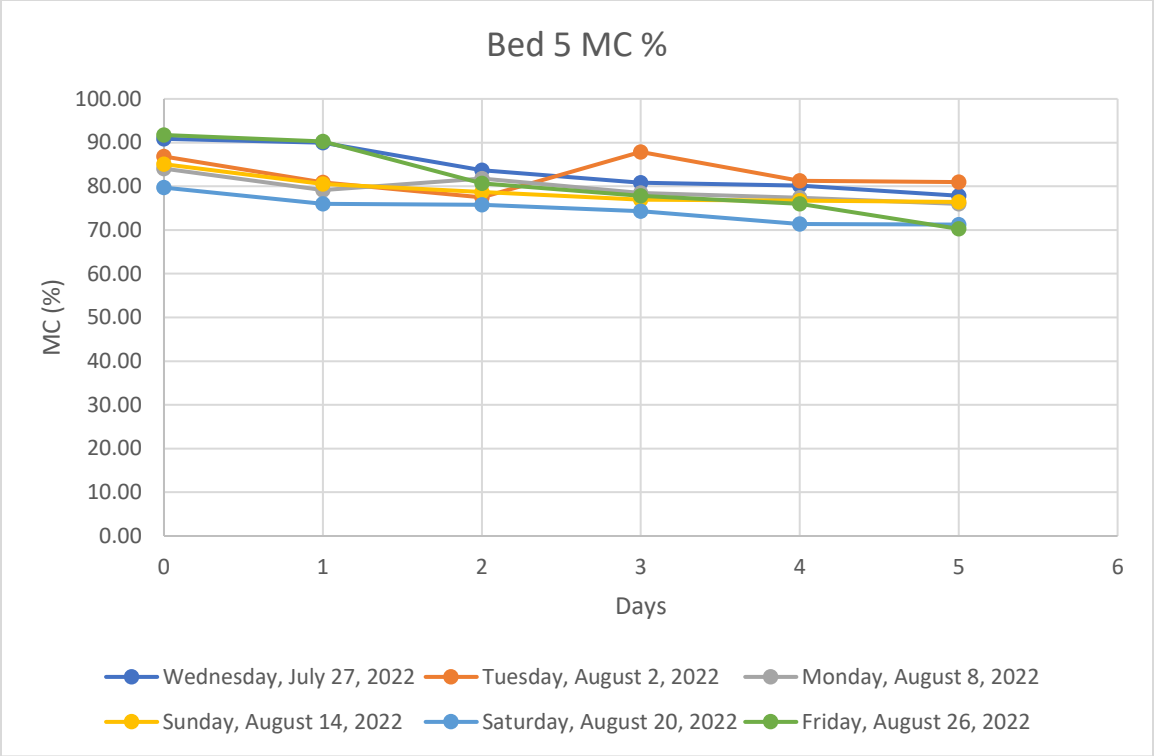
Bed 5 MC %
100.00
90.00
80.00
70.00
60.00
50.00
40.00
30.00
20.00
10.00
0.00
MC (%)
0
1
2
3
4
5
6
Days
Wednesday, July 27, 2022
Tuesday, August 2, 2022
Monday, August 8, 2022
Sunday, August 14, 2022
Saturday, August 20, 2022
Friday, August 26, 2022

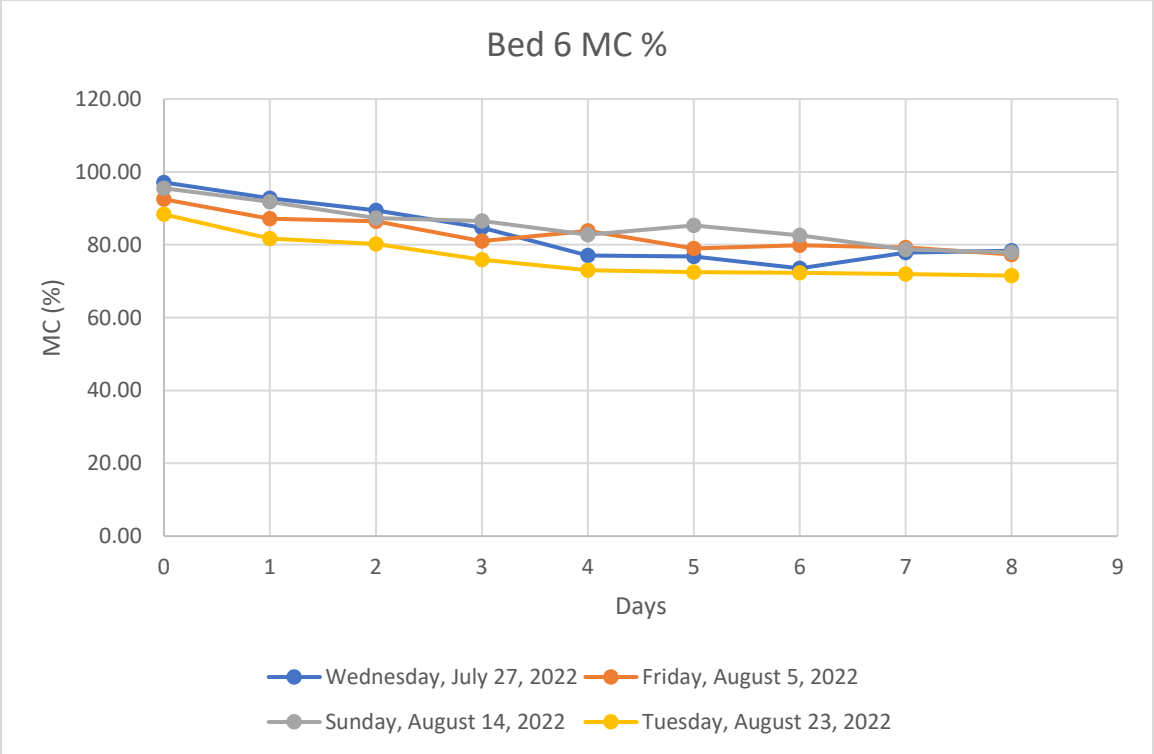
Bed 6 MC %
120.00
100.00
80.00
60.00
40.00
20.00
0.00
MC (%)
0
1
2
3
4
5
6
7
8
9
Days
Wednesday, July 27, 2022
Friday, August 5, 2022
Sunday, August 14, 2022
Tuesday, August 23, 2022

Appendix N: Graphs of Total Solids Content of Sludge Deposit in Phase 1 Experiment.

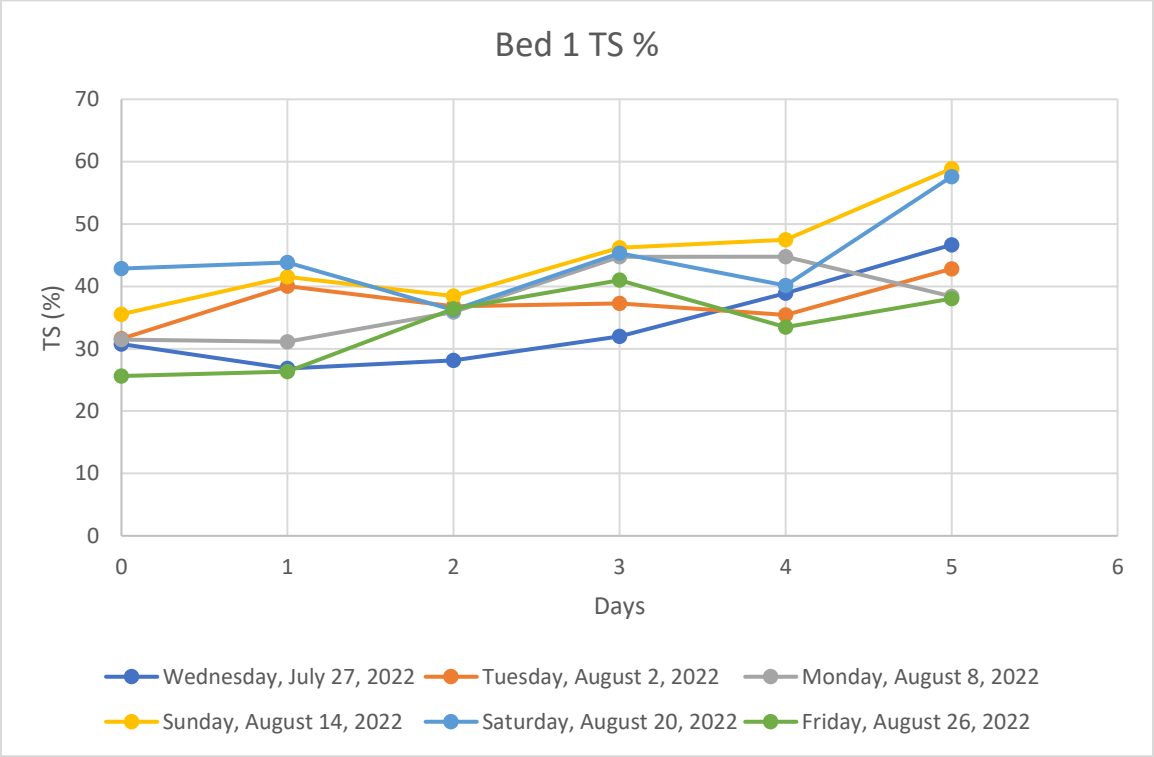

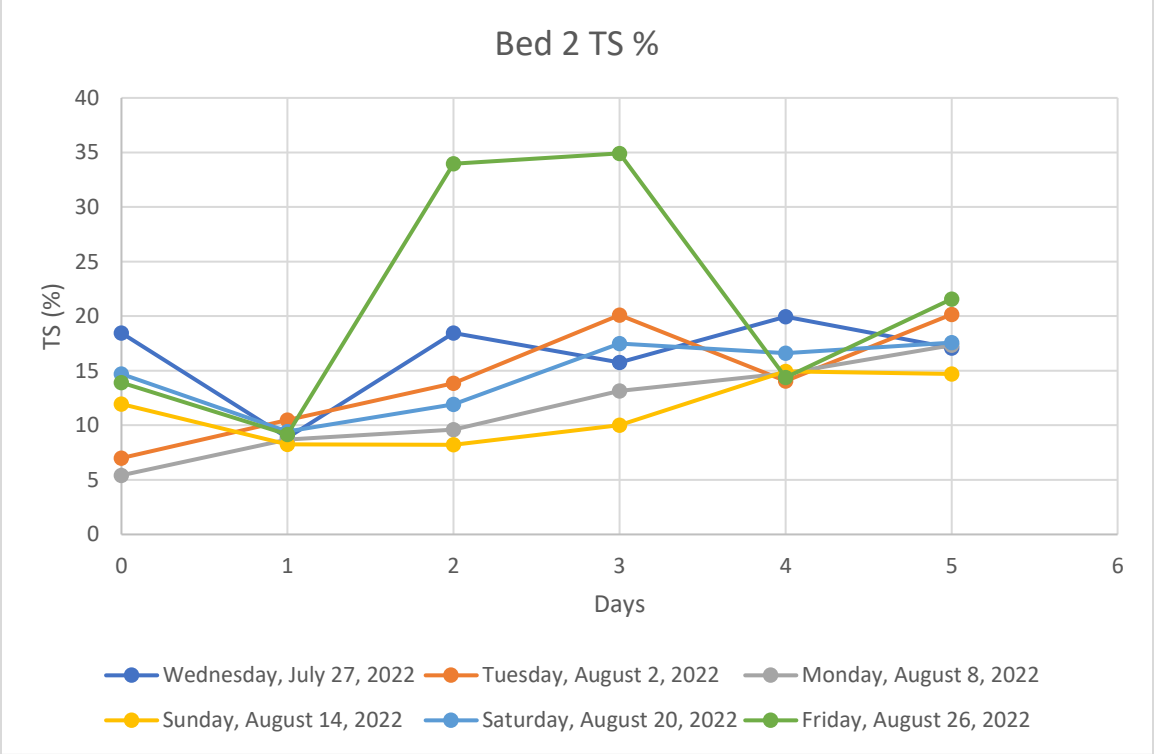

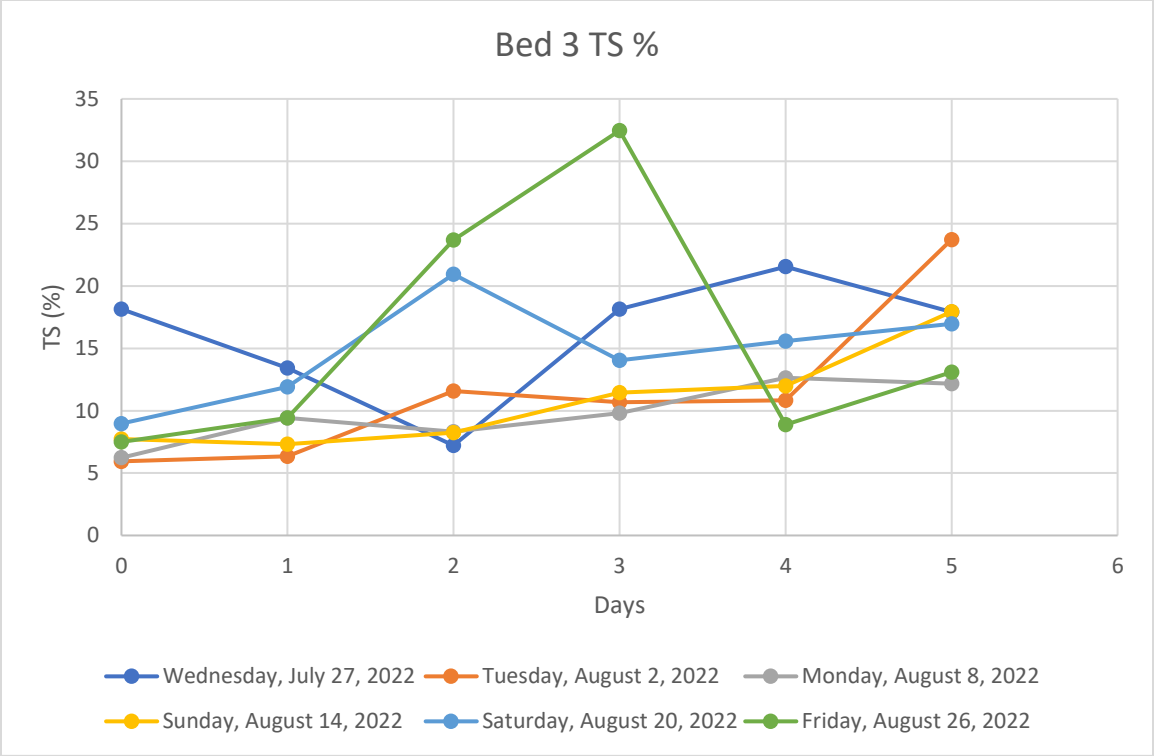
Bed 3 TS %
TS (%)
Days
Wednesday, July 27, 2022
Tuesday, August 2, 2022
Monday, August 8, 2022
Sunday, August 14, 2022
Saturday, August 20, 2022
Friday, August 26, 2022

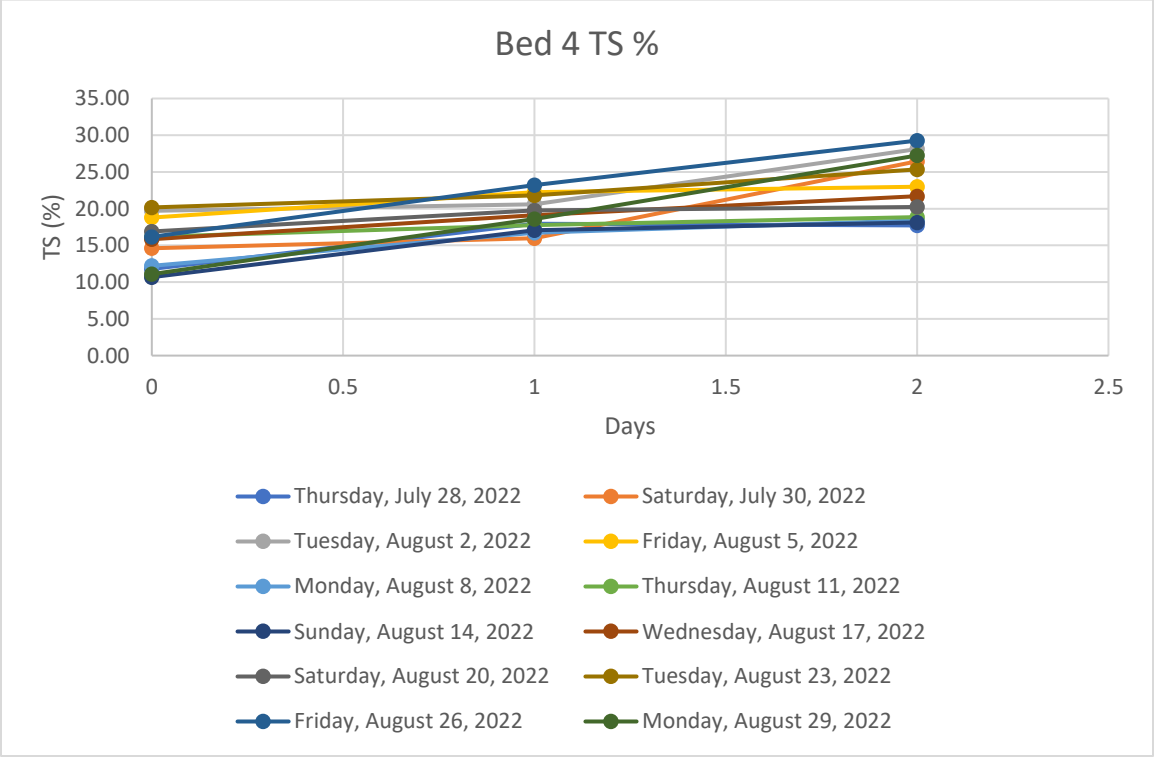
Bed 4 TS %
TS (%)
Days
Thursday, July 28, 2022
Saturday, July 30, 2022
Tuesday, August 2, 2022
Friday, August 5, 2022
Monday, August 8, 2022
Thursday, August 11, 2022
Sunday, August 14, 2022
Wednesday, August 17, 2022
Saturday, August 20, 2022
Tuesday, August 23, 2022
Friday, August 26, 2022
Monday, August 29, 2022

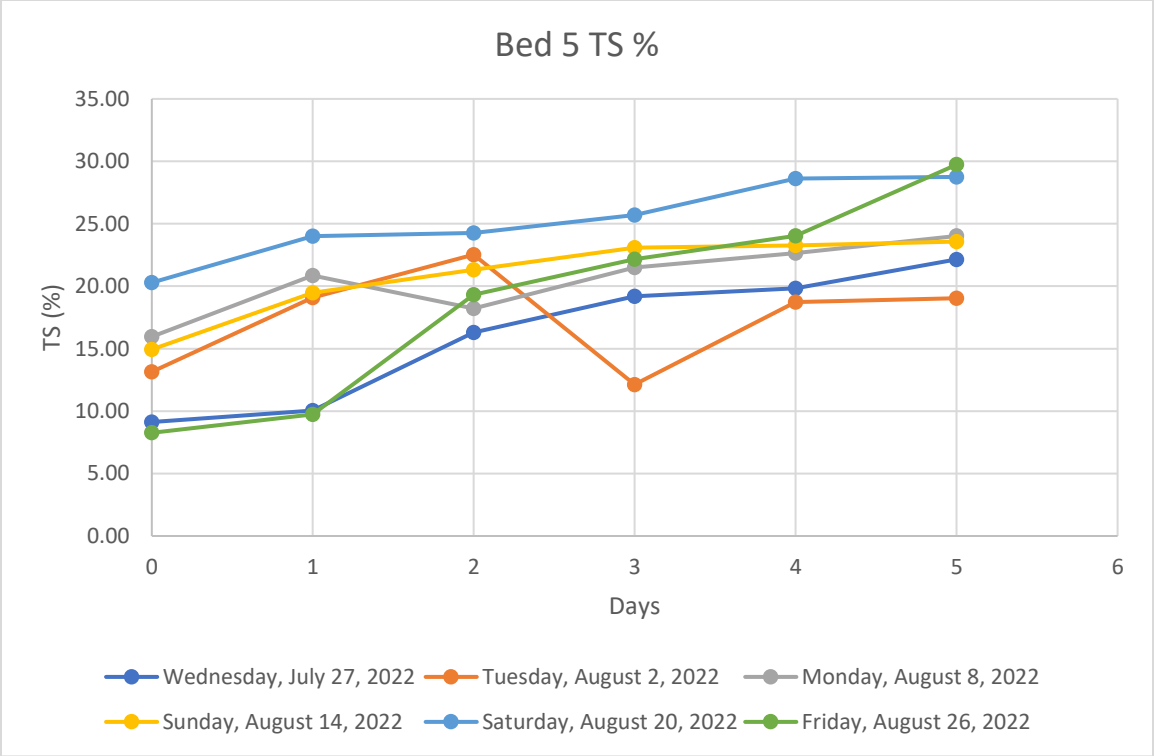
Bed 5 TS %
35.00
30.00
25.00
20.00
15.00
10.00
5.00
0.00
TS (%)
0
1
2
3
4
5
6
Days
Wednesday, July 27, 2022
Tuesday, August 2, 2022
Monday, August 8, 2022
Sunday, August 14, 2022
Saturday, August 20, 2022
Friday, August 26, 2022

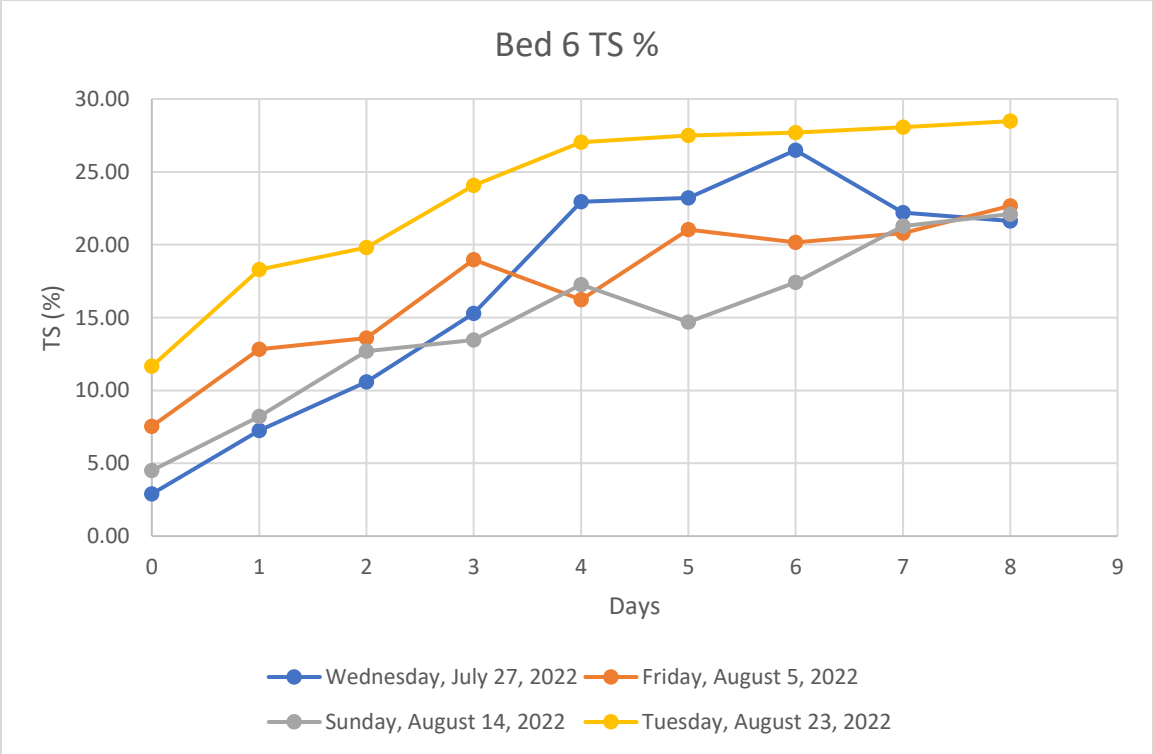
Bed 6 TS %
30.00
25.00
20.00
15.00
10.00
5.00
0.00
TS (%)
0
1
2
3
4
5
6
7
8
9
Days
Wednesday, July 27, 2022
Friday, August 5, 2022
Sunday, August 14, 2022
Tuesday, August 23, 2022

Appendix O: Graphs of Total Volatile Solids Content of Sludge Deposit in Phase 1 Experiment.

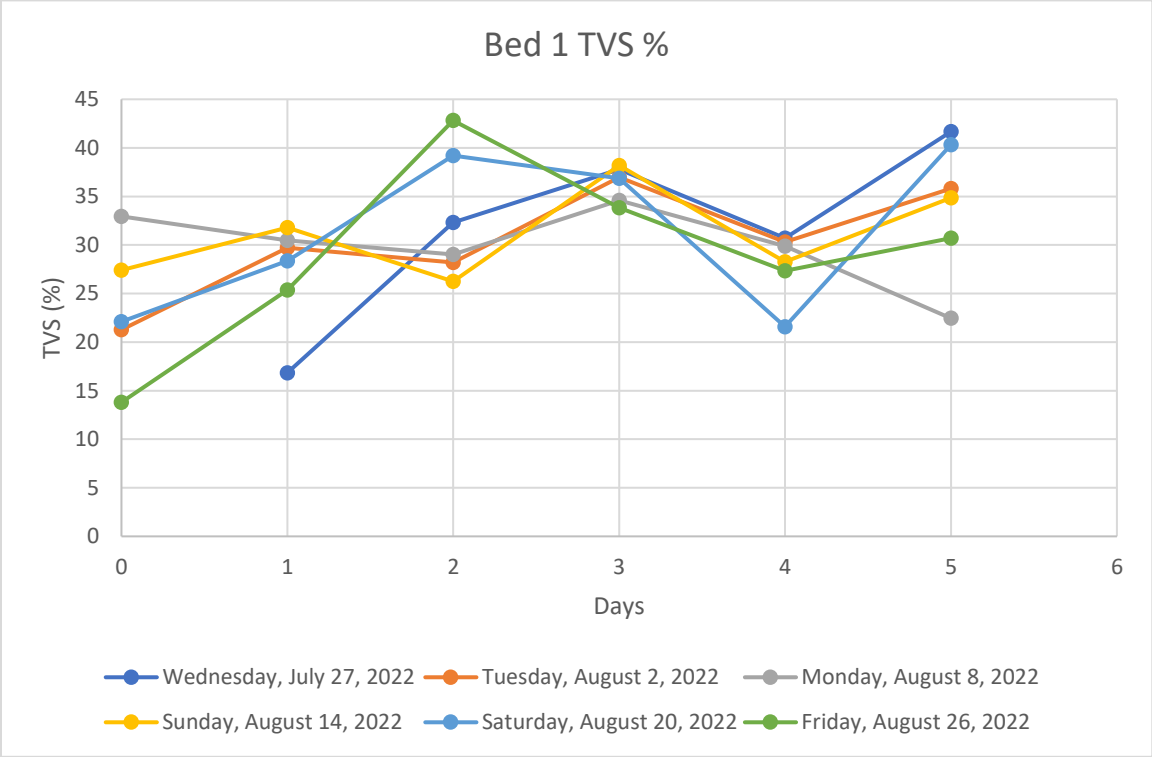

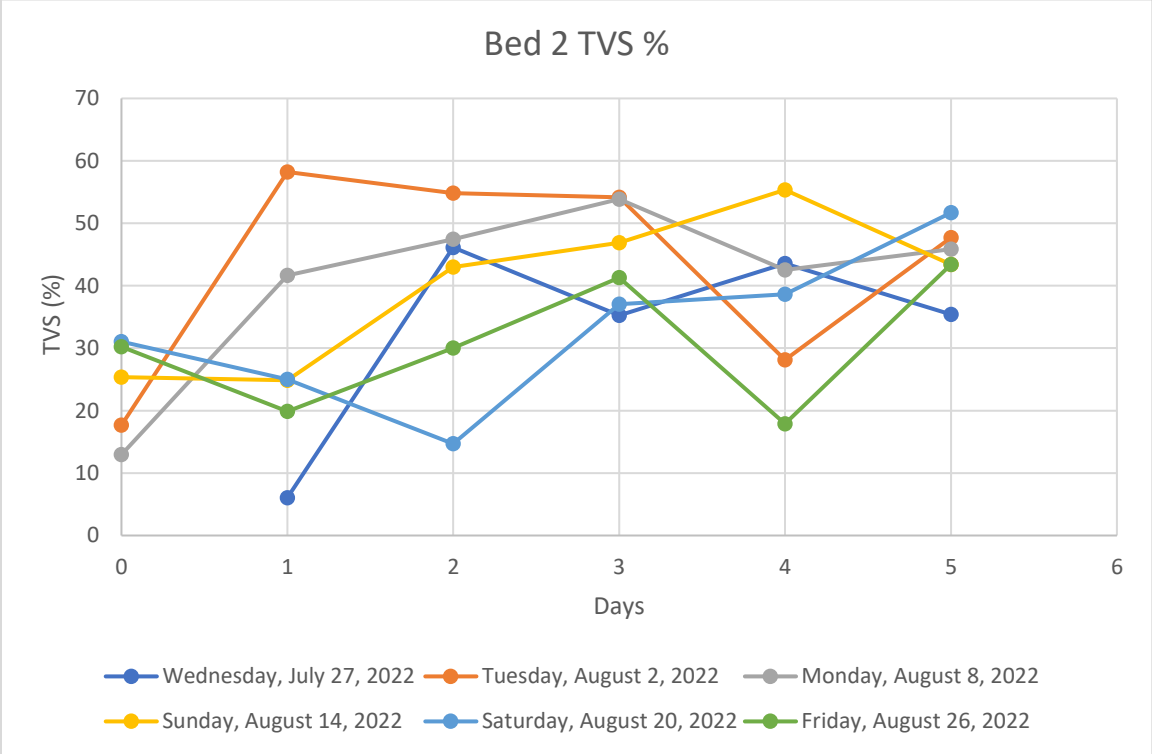

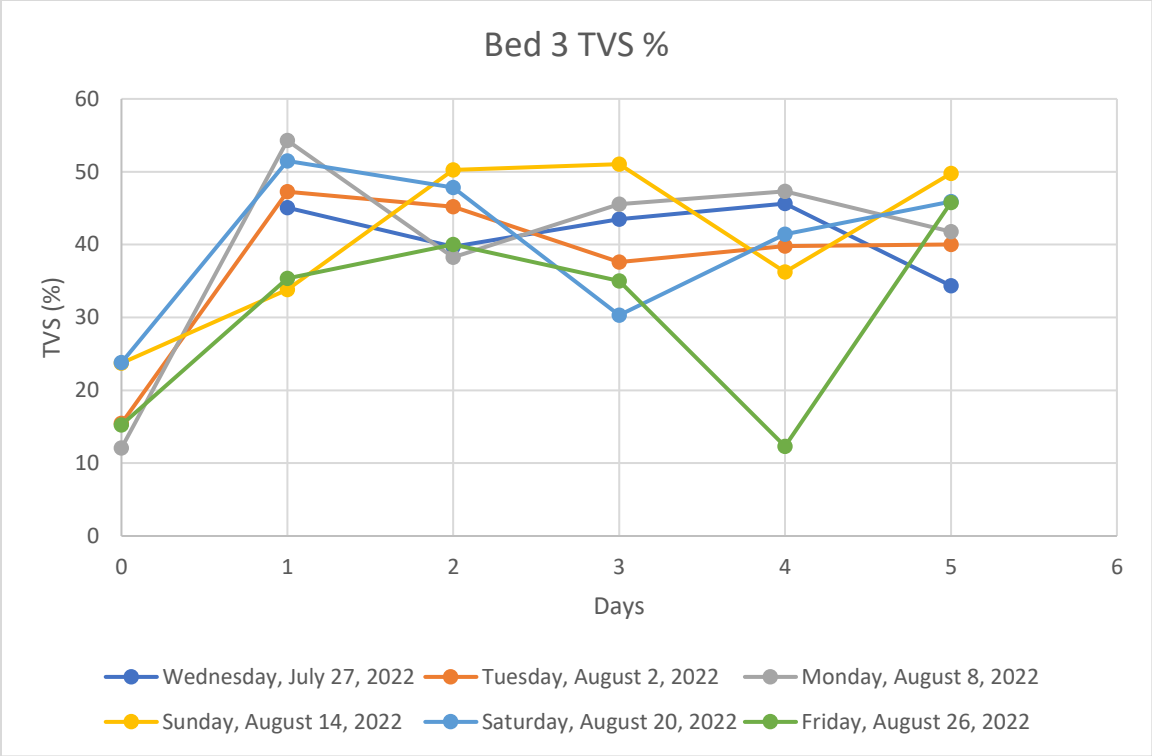
Bed 3 TVS %
TVS (%)
Days
0
10
20
30
40
50
60
0
1
2
3
4
5
6
Wednesday, July 27, 2022
Tuesday, August 2, 2022
Monday, August 8, 2022
Sunday, August 14, 2022
Saturday, August 20, 2022
Friday, August 26, 2022

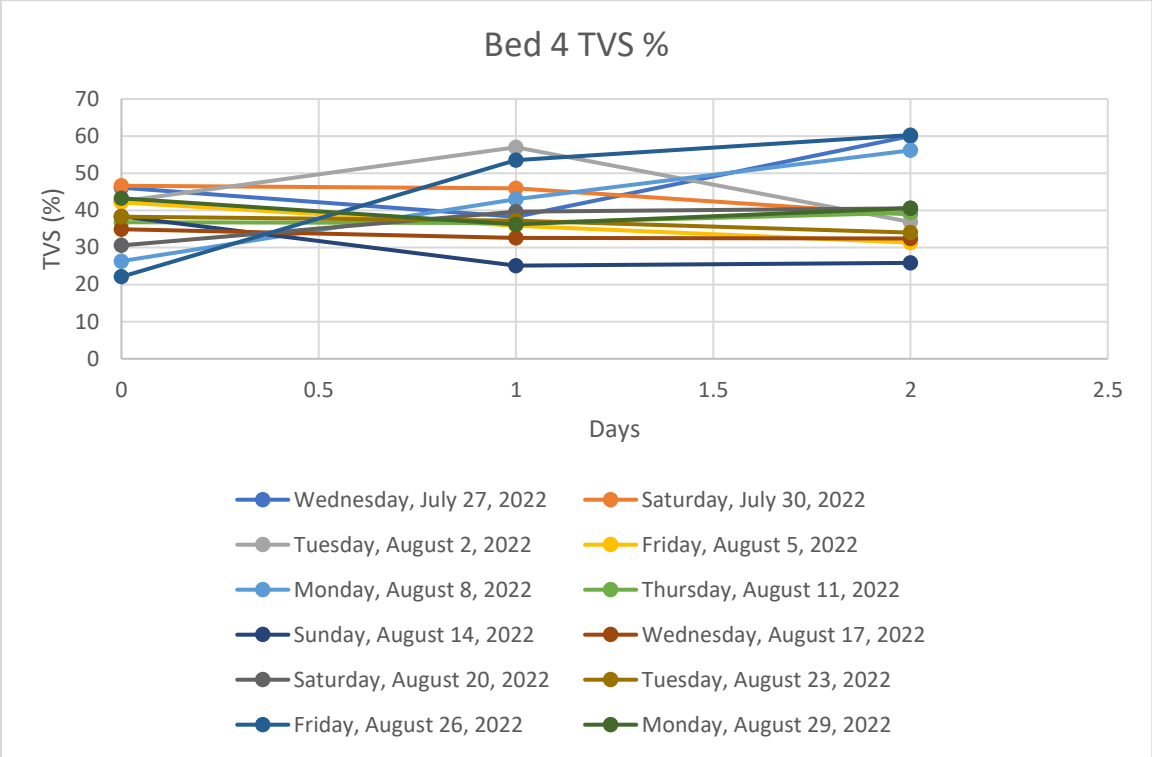
Bed 4 TVS %
TVS (%)
Days
0
10
20
30
40
50
60
70
0
0.5
1
1.5
2
2.5
Wednesday, July 27, 2022
Saturday, July 30, 2022
Tuesday, August 2, 2022
Friday, August 5, 2022
Monday, August 8, 2022
Thursday, August 11, 2022
Sunday, August 14, 2022
Wednesday, August 17, 2022
Saturday, August 20, 2022
Tuesday, August 23, 2022
Friday, August 26, 2022
Monday, August 29, 2022

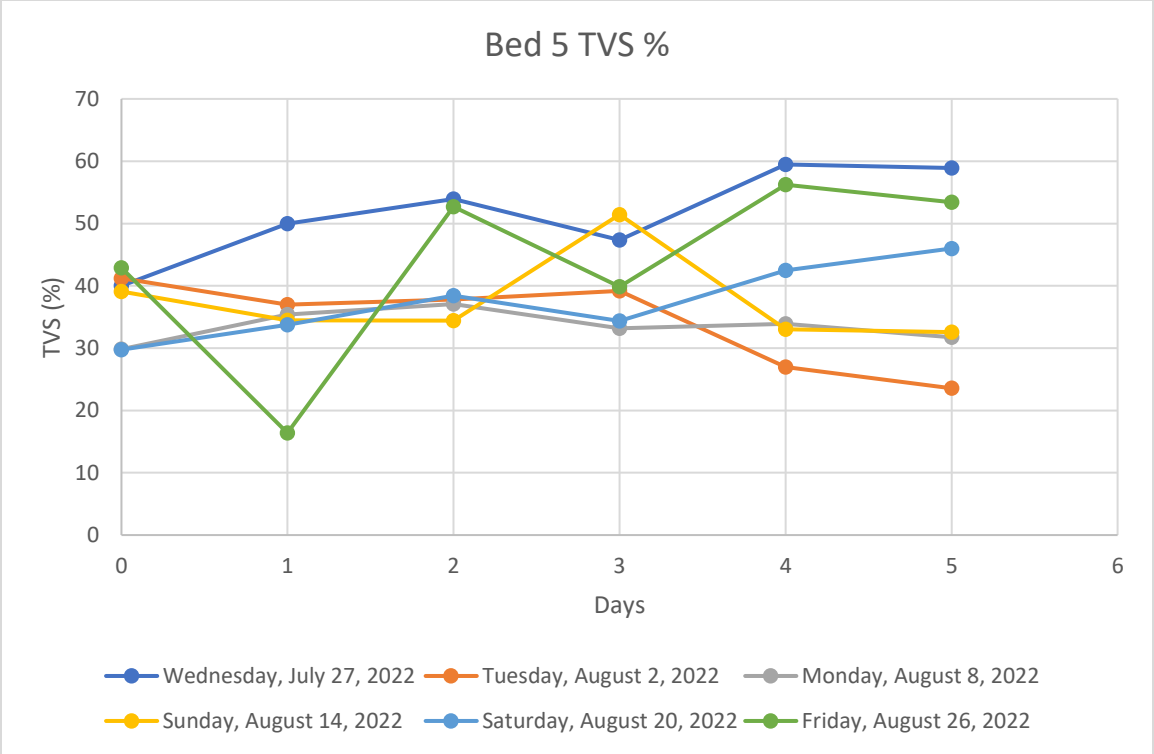
Bed 5 TVS %
TVS (%)
Days
0
10
20
30
40
50
60
70
0
1
2
3
4
5
6
Wednesday, July 27, 2022
Tuesday, August 2, 2022
Monday, August 8, 2022
Sunday, August 14, 2022
Saturday, August 20, 2022
Friday, August 26, 2022

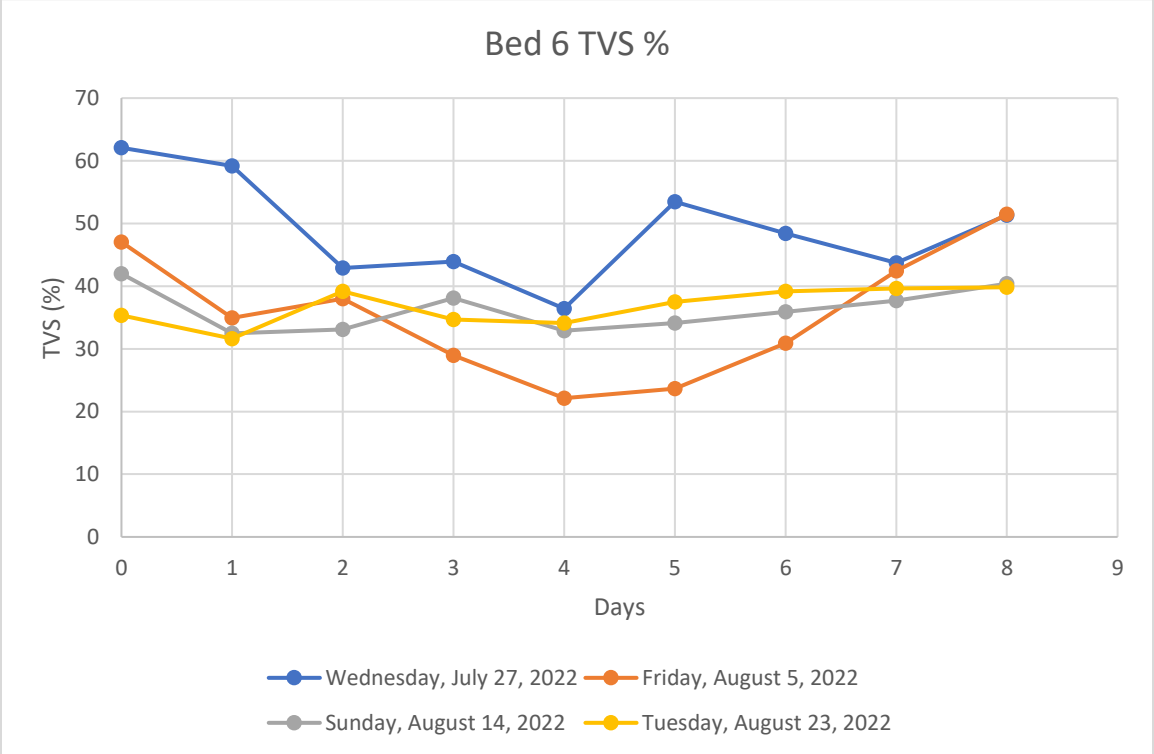
Bed 6 TVS %
TVS (%)
Days
0
10
20
30
40
50
60
70
0
1
2
3
4
5
6
7
8
9
Wednesday, July 27, 2022
Friday, August 5, 2022
Sunday, August 14, 2022
Tuesday, August 23, 2022

Appendix P: Graphs of Effluent Quality in Phase 1 Experiment.

(a) Chemical Oxygen Demand (COD)

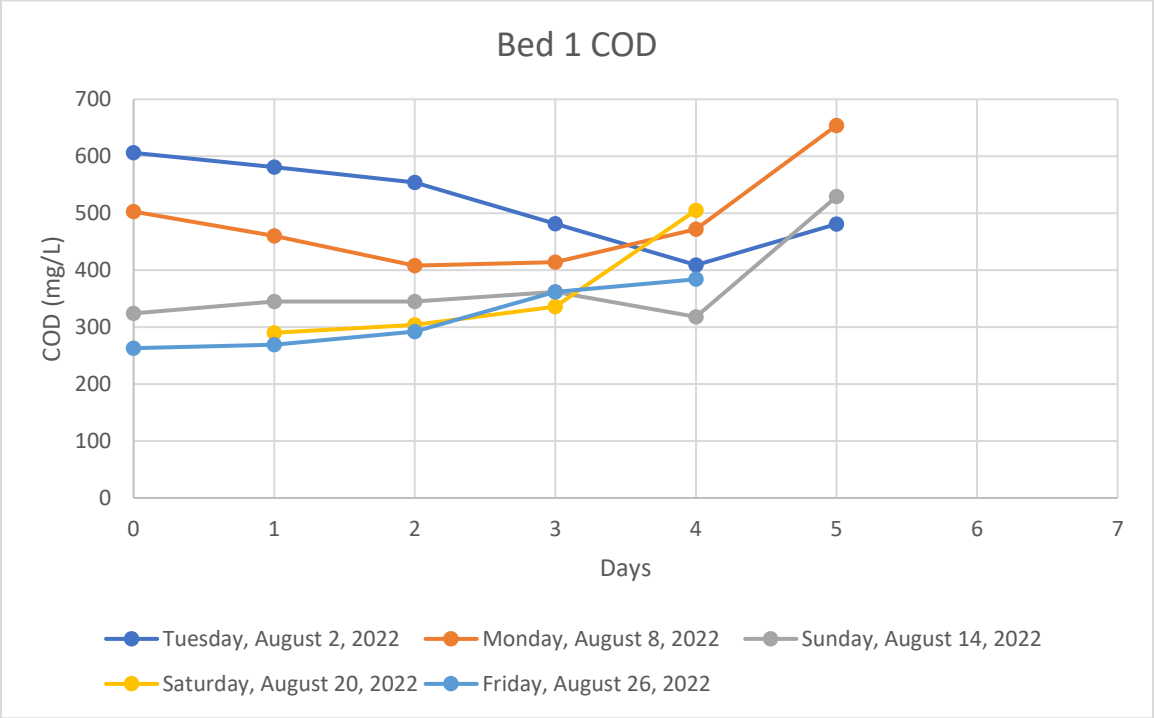

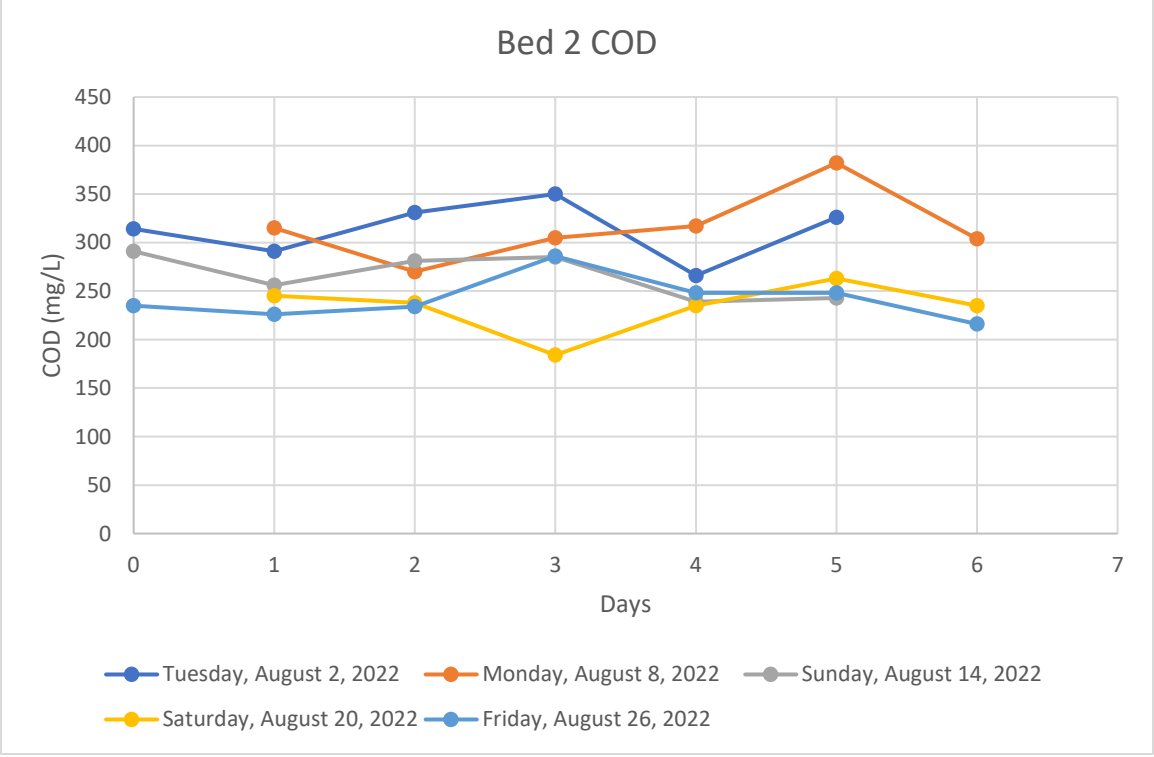

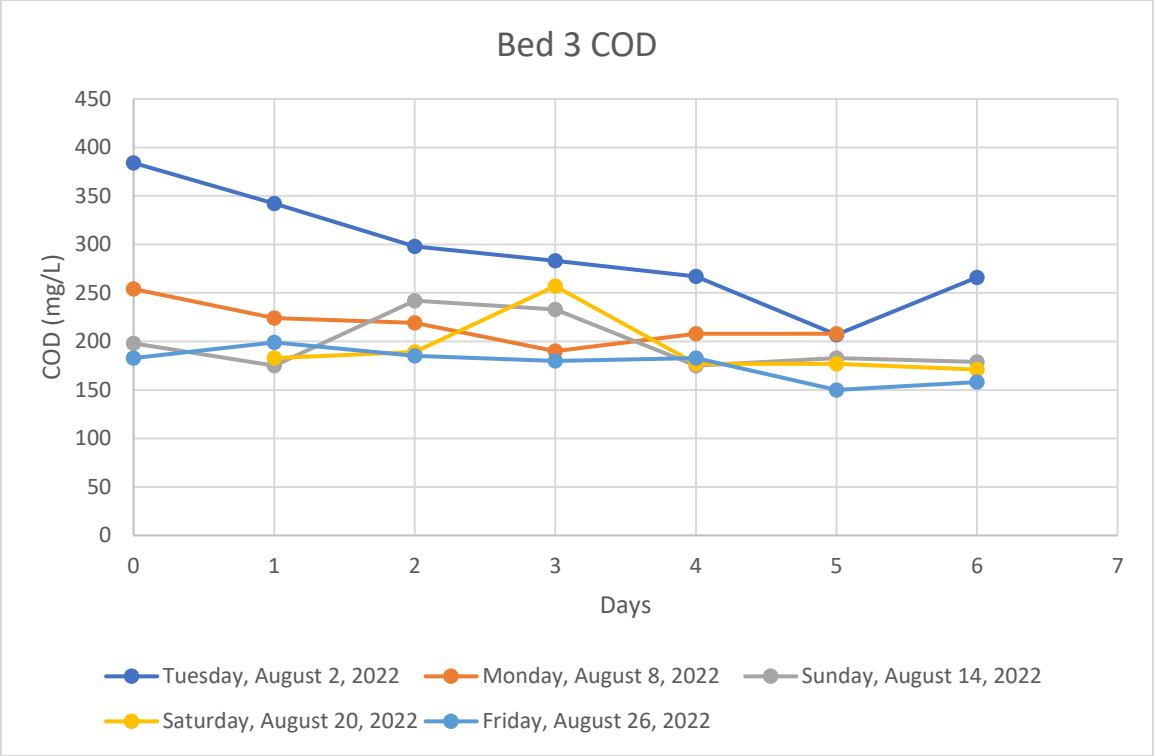
Bed 3 COD
COD (mg/L)
450
400
350
300
250
200
150
100
50
0
0
1
2
3
4
5
6
7
Days
Tuesday, August 2, 2022
Monday, August 8, 2022
Sunday, August 14, 2022
Saturday, August 20, 2022
Friday, August 26, 2022

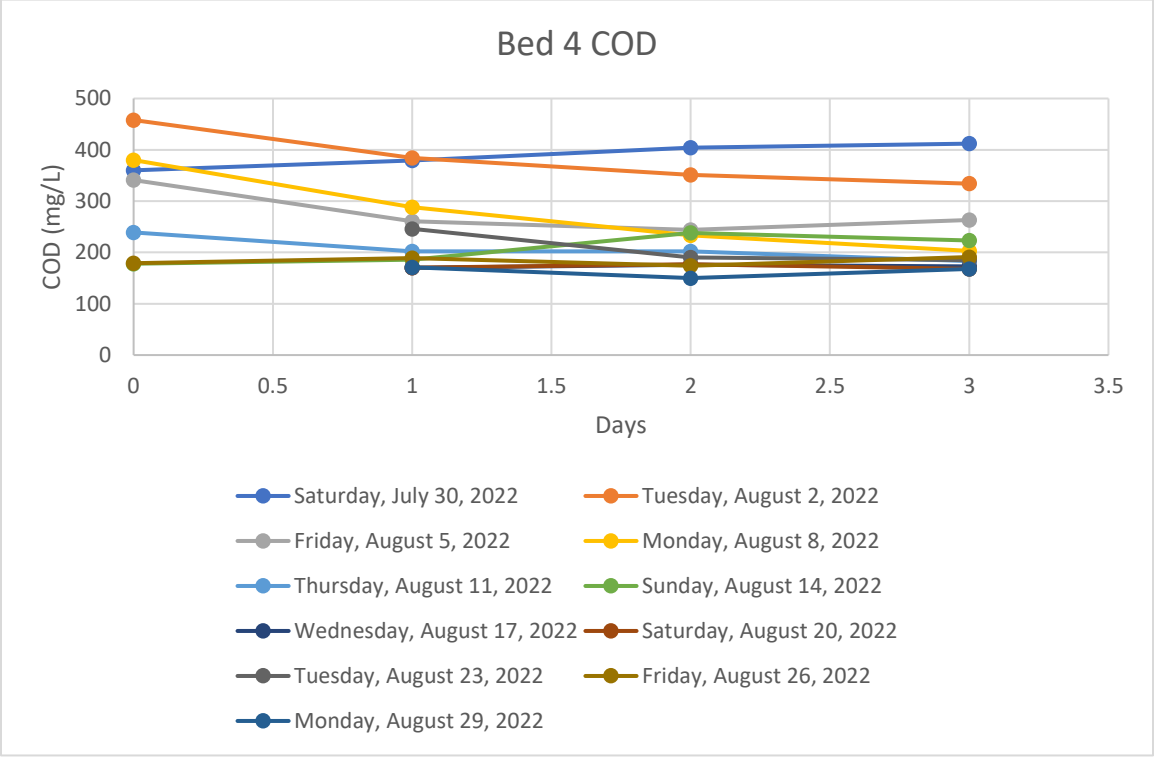
Bed 4 COD
COD (mg/L)
500
400
300
200
100
0
0
0.5
1
1.5
2
2.5
3
3.5
Days
Saturday, July 30, 2022
Tuesday, August 2, 2022
Friday, August 5, 2022
Monday, August 8, 2022
Thursday, August 11, 2022
Sunday, August 14, 2022
Wednesday, August 17, 2022
Saturday, August 20, 2022
Tuesday, August 23, 2022
Friday, August 26, 2022
Monday, August 29, 2022

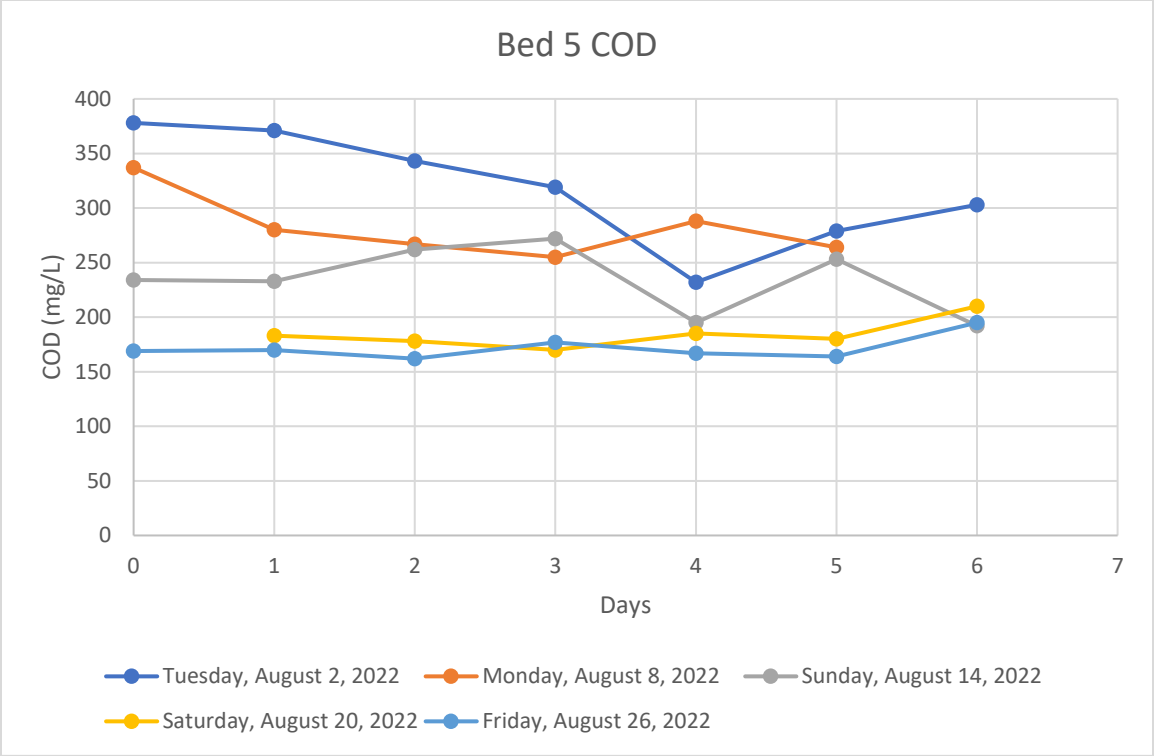
Bed 5 COD
COD (mg/L)
400
350
300
250
200
150
100
50
0
0
1
2
3
4
5
6
7
Days
Tuesday, August 2, 2022
Monday, August 8, 2022
Sunday, August 14, 2022
Saturday, August 20, 2022
Friday, August 26, 2022

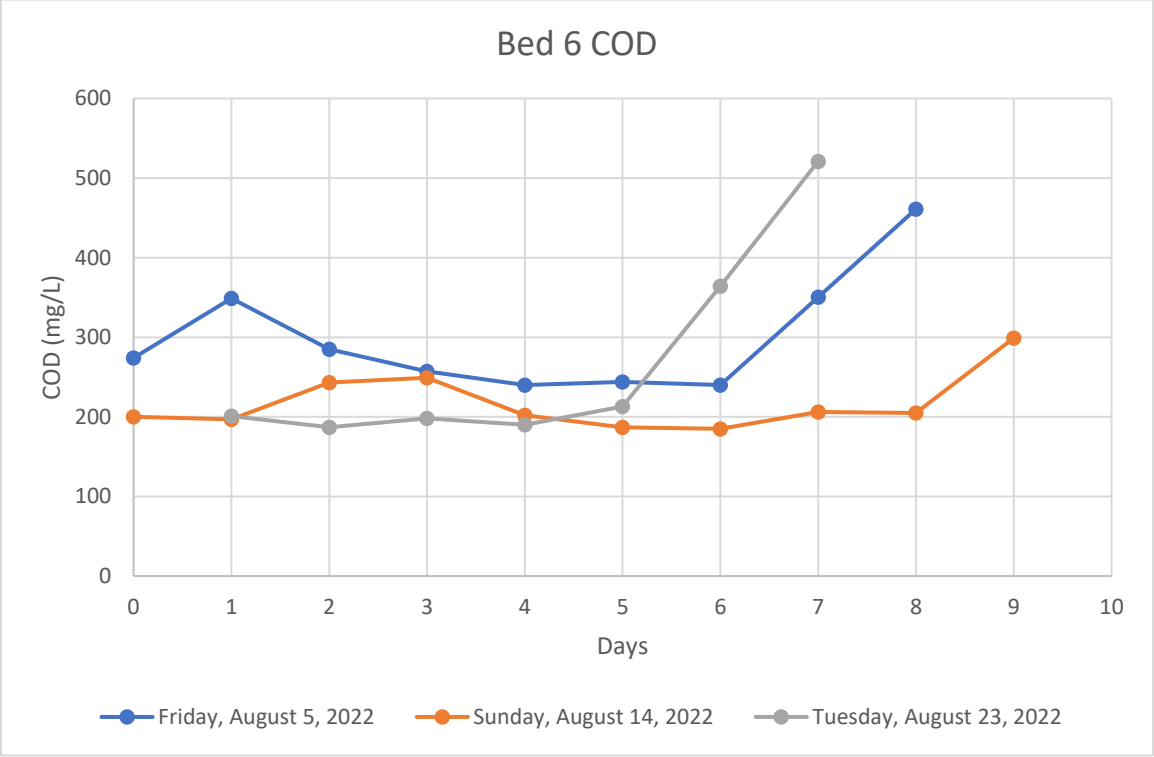
Bed 6 COD
COD (mg/L)
600
500
400
300
200
100
0
0
1
2
3
4
5
6
7
8
9
10
Days
Friday, August 5, 2022
Sunday, August 14, 2022
Tuesday, August 23, 2022

(b) Nitrates (NO_3)

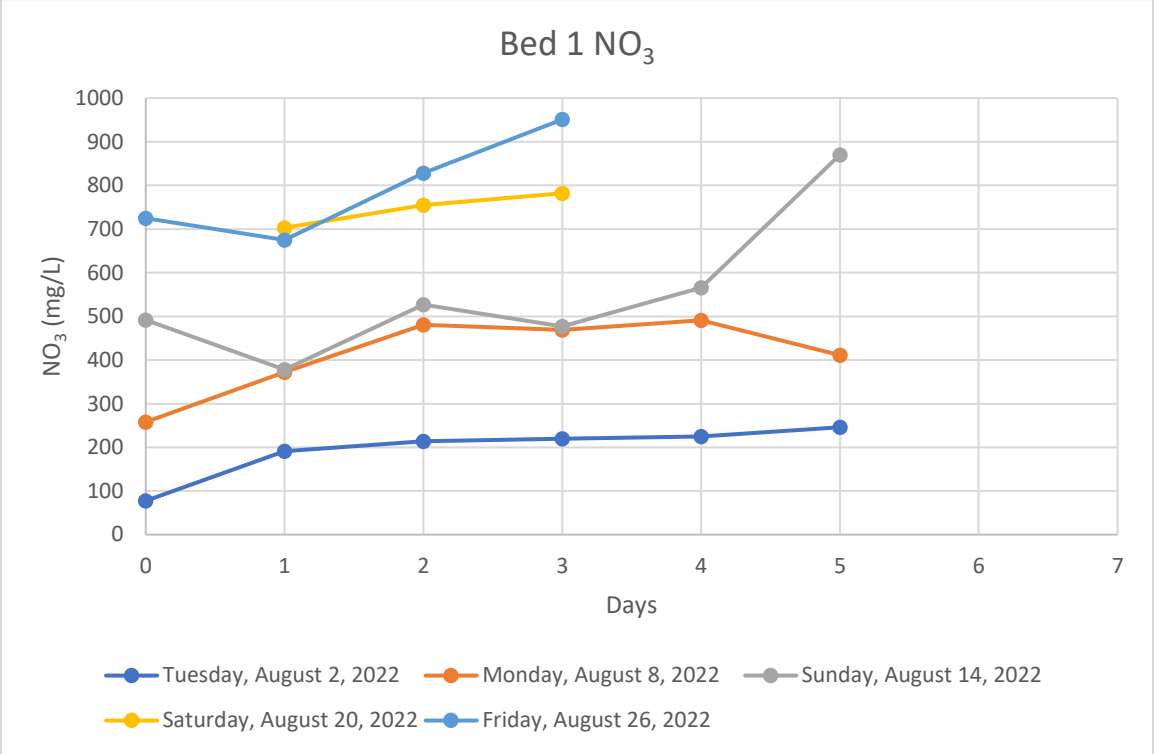

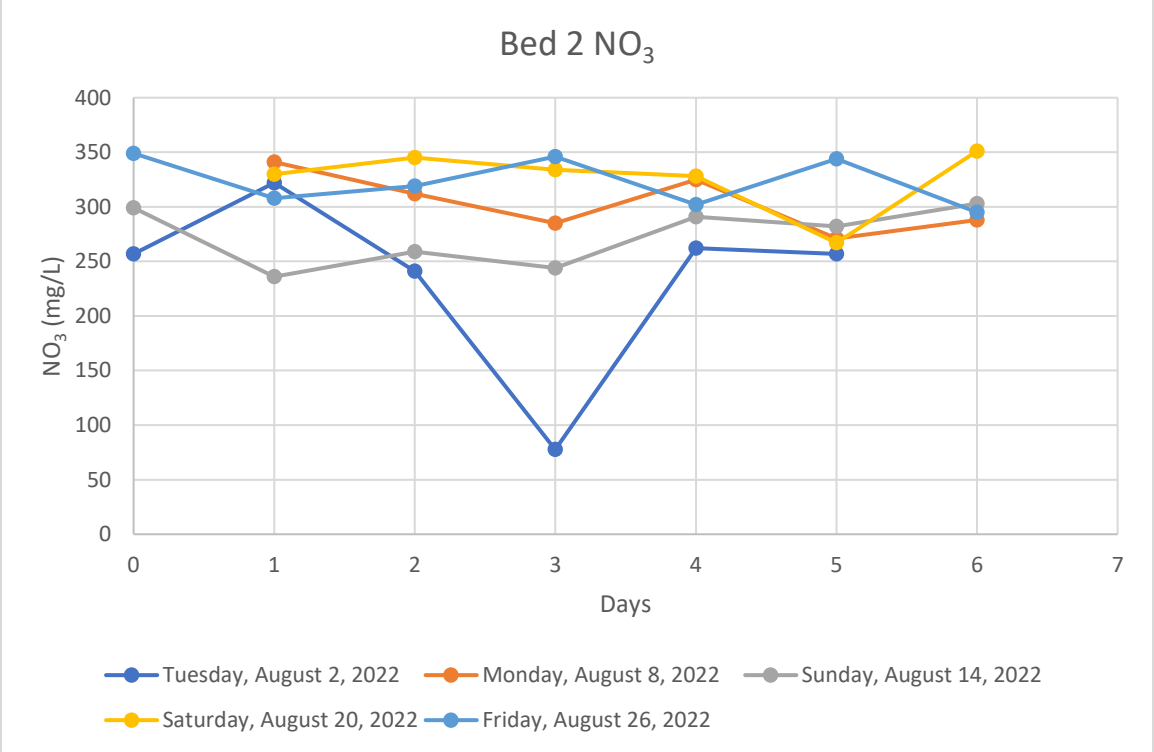

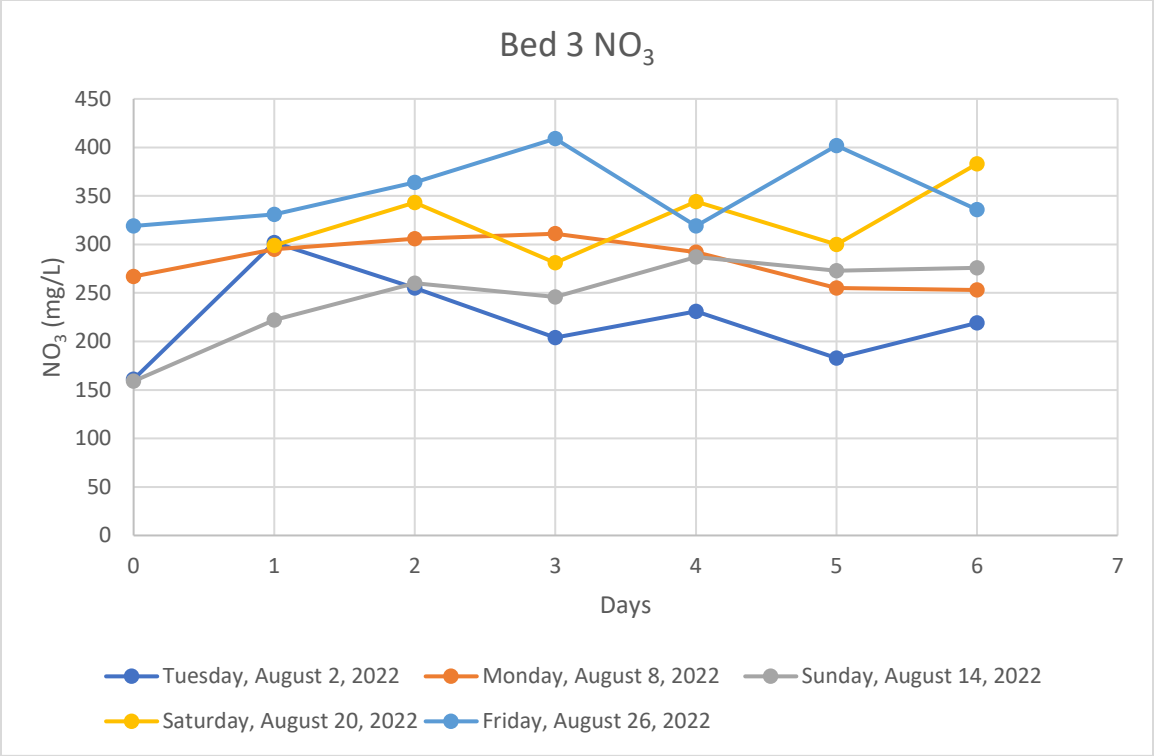
Bed 3 NO3
NO3 (mg/L)
450
400
350
300
250
200
150
100
50
0
0
1
2
3
4
5
6
7
Days
Tuesday, August 2, 2022
Monday, August 8, 2022
Sunday, August 14, 2022
Saturday, August 20, 2022
Friday, August 26, 2022

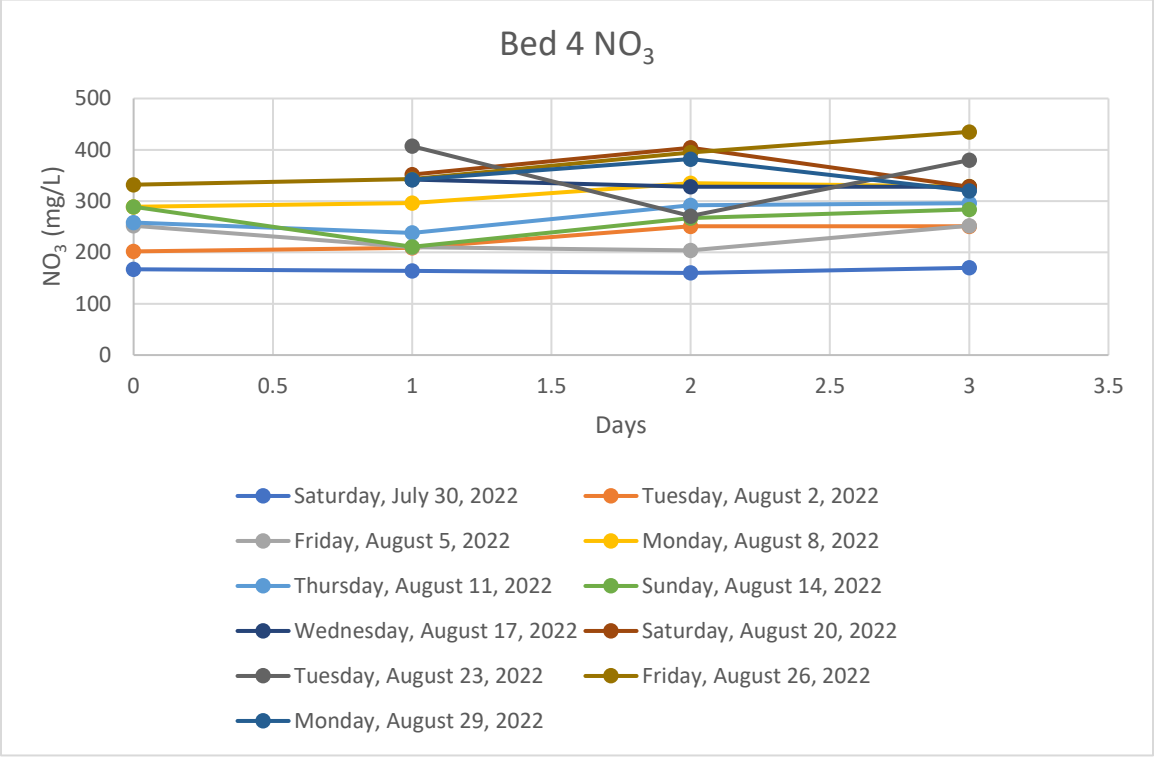
Bed 4 NO3
NO3 (mg/L)
500
400
300
200
100
0
0
0.5
1
1.5
2
2.5
3
3.5
Days
Saturday, July 30, 2022
Tuesday, August 2, 2022
Friday, August 5, 2022
Monday, August 8, 2022
Thursday, August 11, 2022
Sunday, August 14, 2022
Wednesday, August 17, 2022
Saturday, August 20, 2022
Tuesday, August 23, 2022
Friday, August 26, 2022
Monday, August 29, 2022

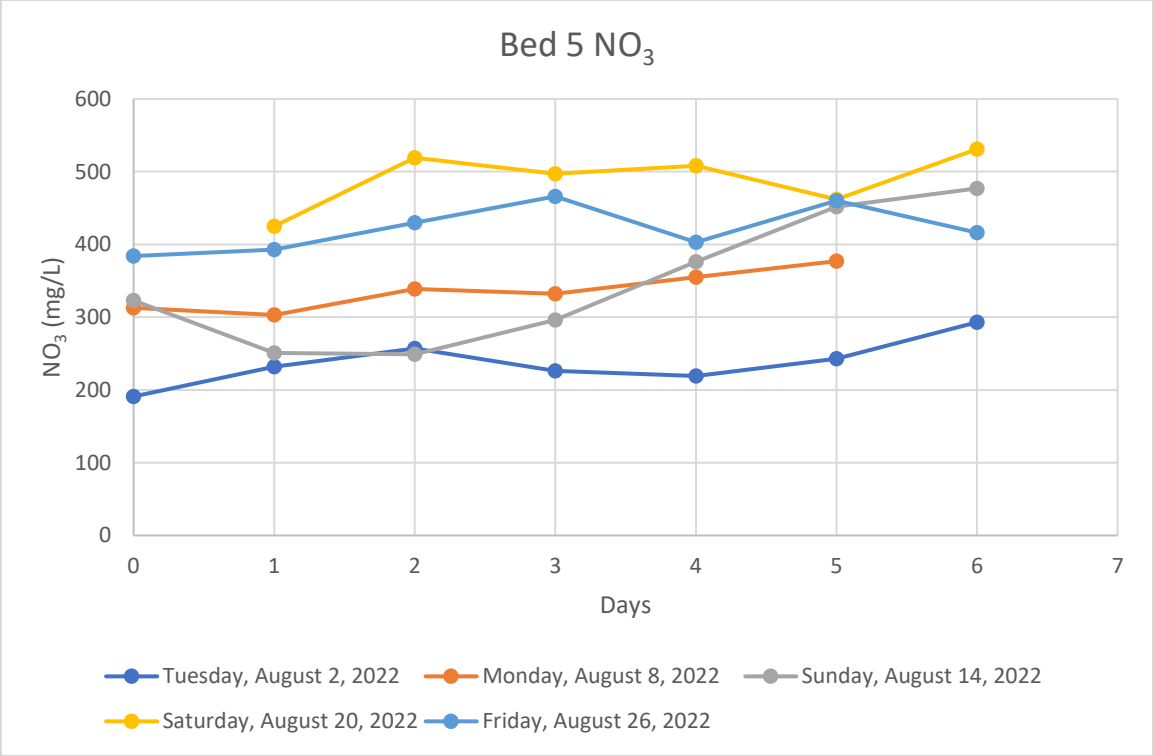
Bed 5 NO3
600
500
400
300
200
100
0
NO3 (mg/L)
0
1
2
3
4
5
6
7
Days
Tuesday, August 2, 2022
Monday, August 8, 2022
Sunday, August 14, 2022
Saturday, August 20, 2022
Friday, August 26, 2022

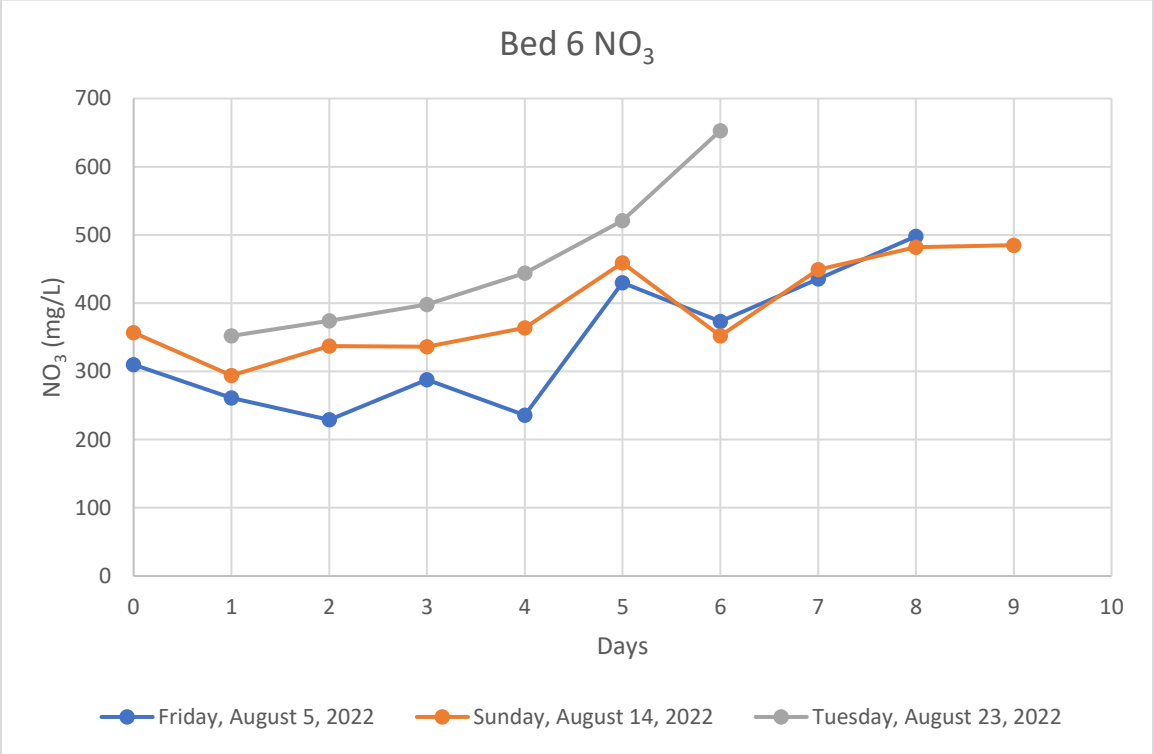
Bed 6 NO3
700
600
500
400
300
200
100
0
NO3 (mg/L)
0
1
2
3
4
5
6
7
8
9
10
Days
Friday, August 5, 2022
Sunday, August 14, 2022
Tuesday, August 23, 2022

(c) pH

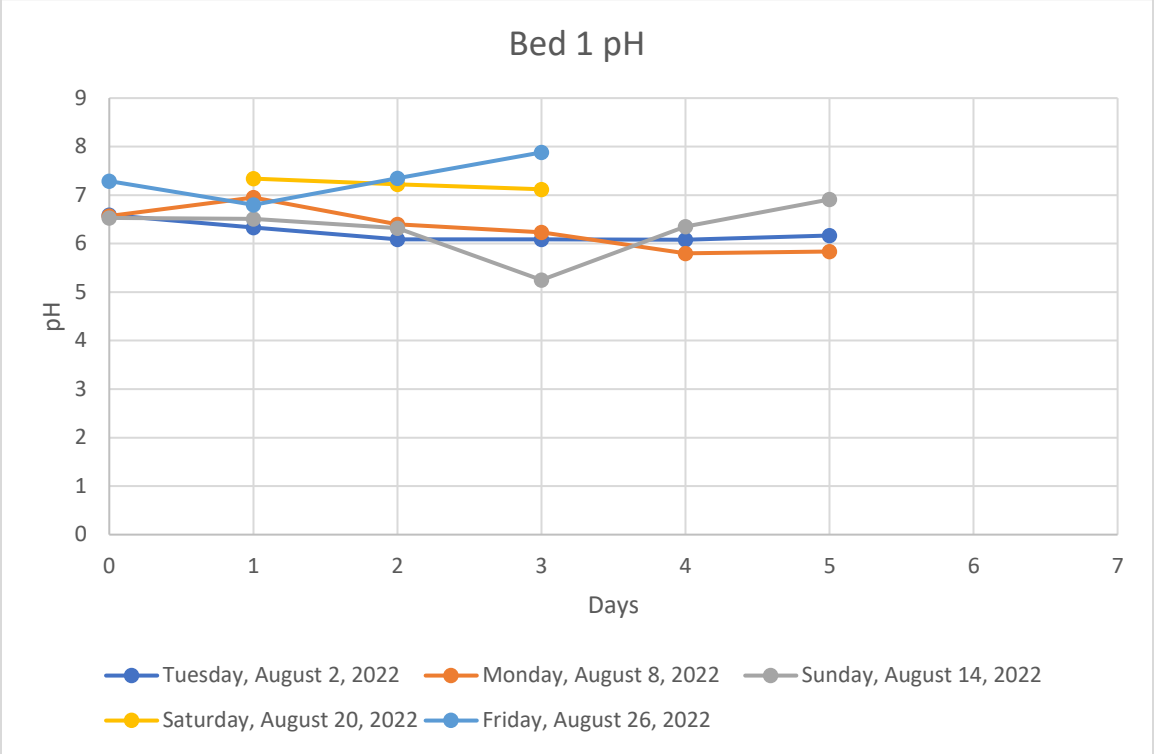
Bed 1 pH
pH
Days
0
1
2
3
4
5
6
7
8
9
Tuesday, August 2, 2022
Monday, August 8, 2022
Sunday, August 14, 2022
Saturday, August 20, 2022
Friday, August 26, 2022

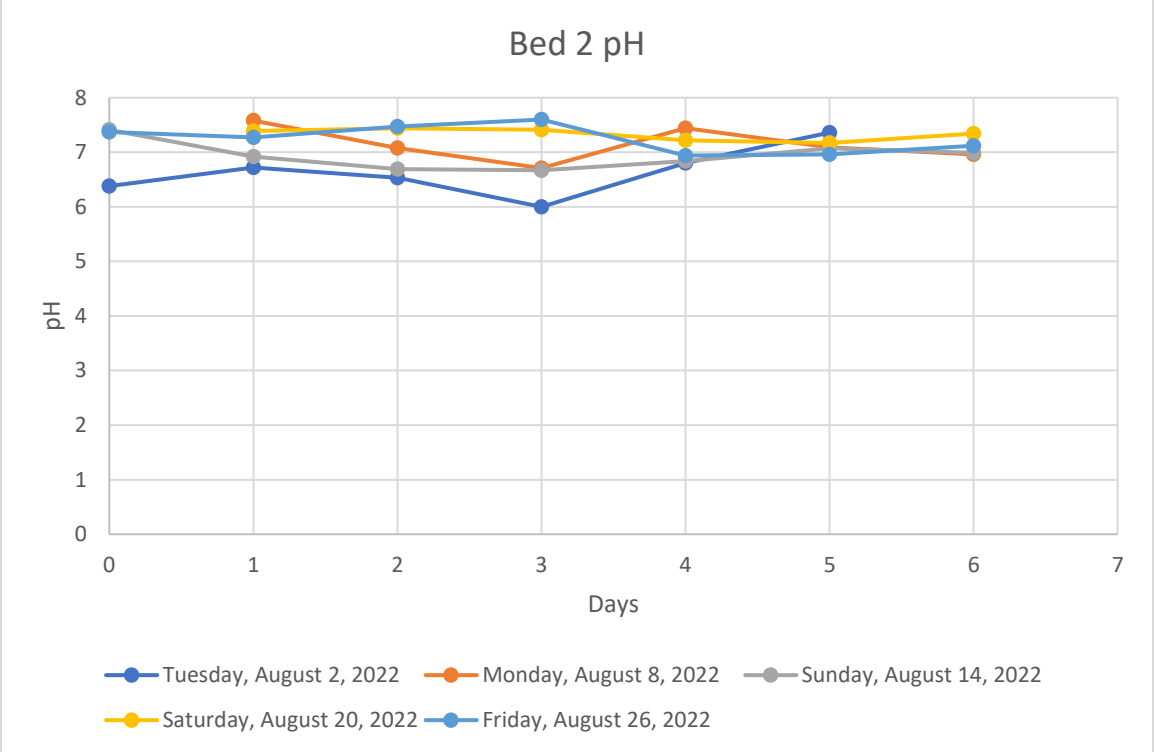
Bed 2 pH
pH
Days
0
1
2
3
4
5
6
7
8
Tuesday, August 2, 2022
Monday, August 8, 2022
Sunday, August 14, 2022
Saturday, August 20, 2022
Friday, August 26, 2022

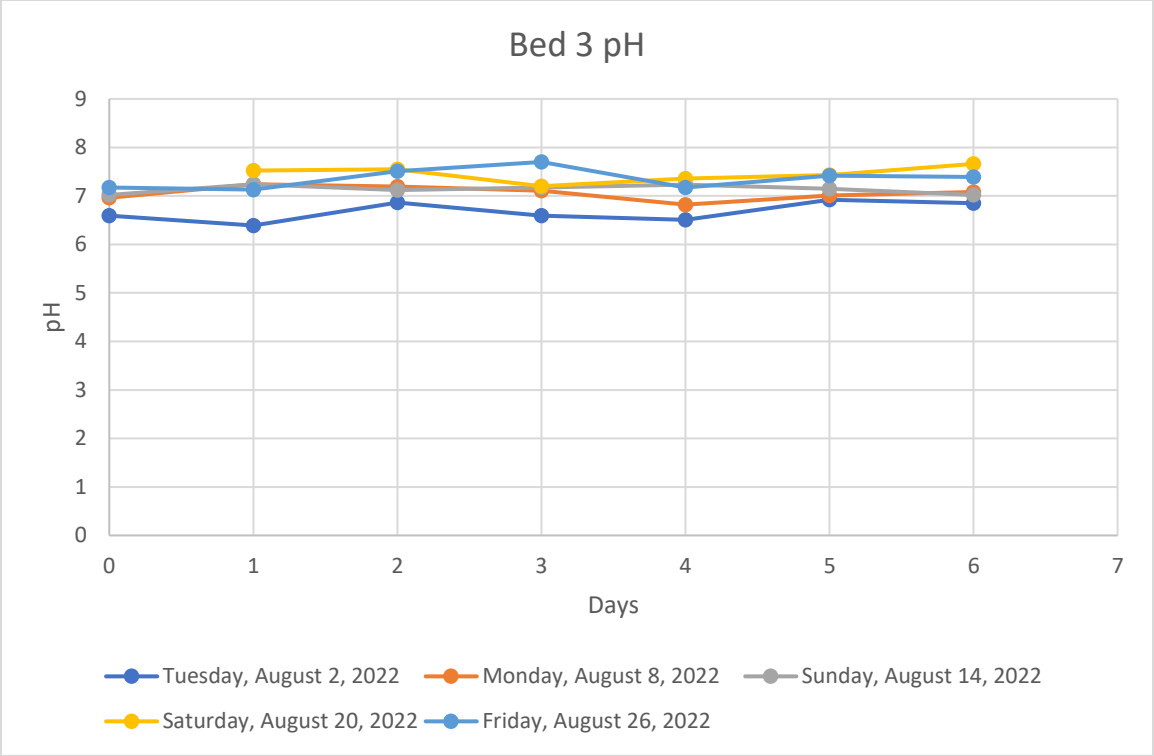
Bed 3 pH
pH
Days
Tuesday, August 2, 2022
Monday, August 8, 2022
Sunday, August 14, 2022
Saturday, August 20, 2022
Friday, August 26, 2022

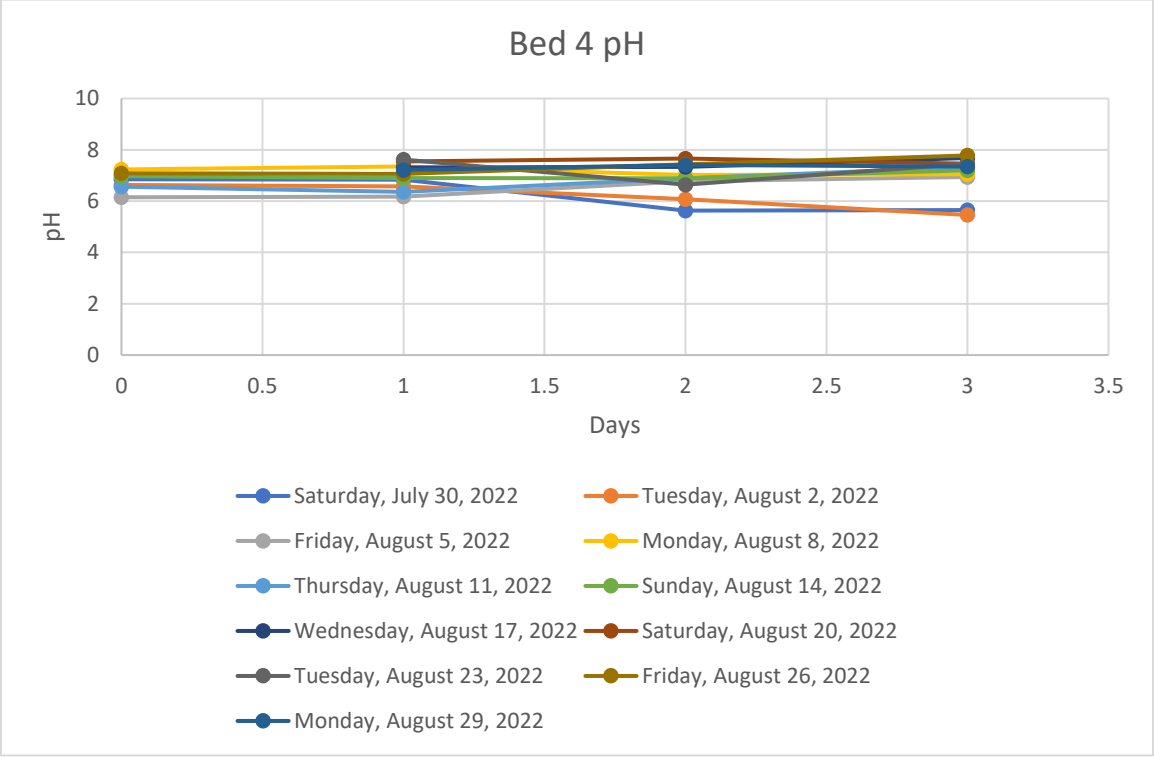
Bed 4 pH
pH
Days
Saturday, July 30, 2022
Tuesday, August 2, 2022
Friday, August 5, 2022
Monday, August 8, 2022
Thursday, August 11, 2022
Sunday, August 14, 2022
Wednesday, August 17, 2022
Saturday, August 20, 2022
Tuesday, August 23, 2022
Friday, August 26, 2022
Monday, August 29, 2022

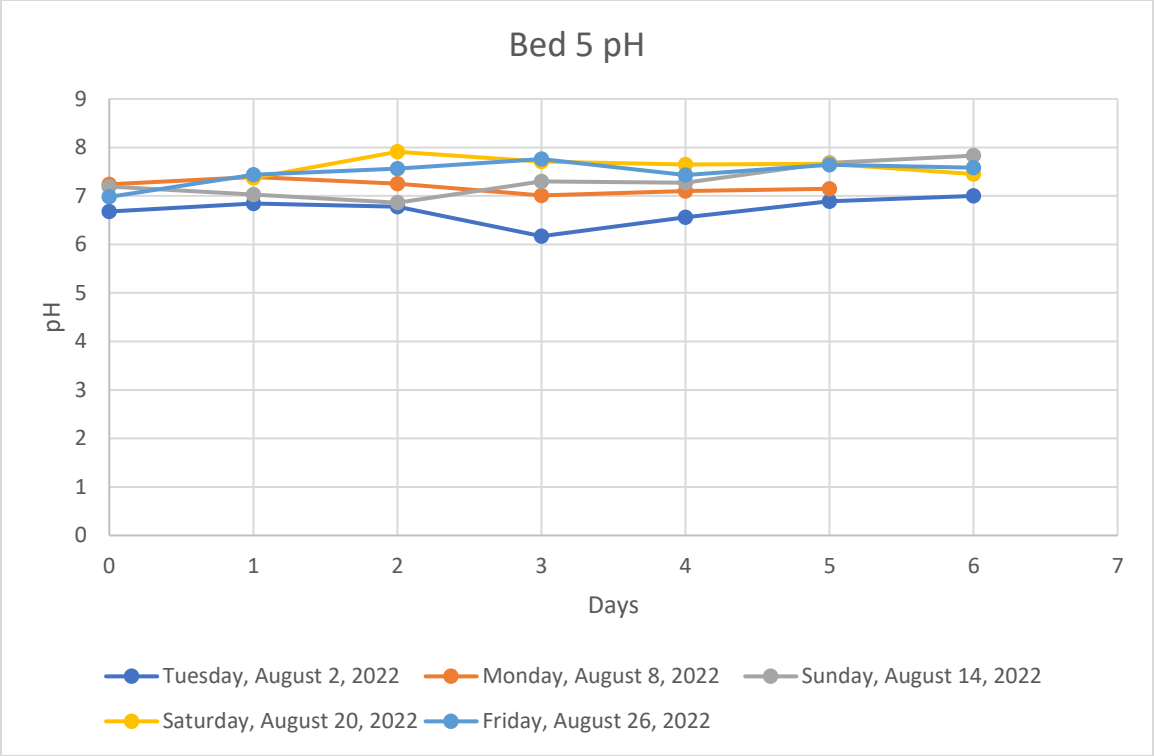
Bed 5 pH
pH
Days
Tuesday, August 2, 2022
Monday, August 8, 2022
Sunday, August 14, 2022
Saturday, August 20, 2022
Friday, August 26, 2022

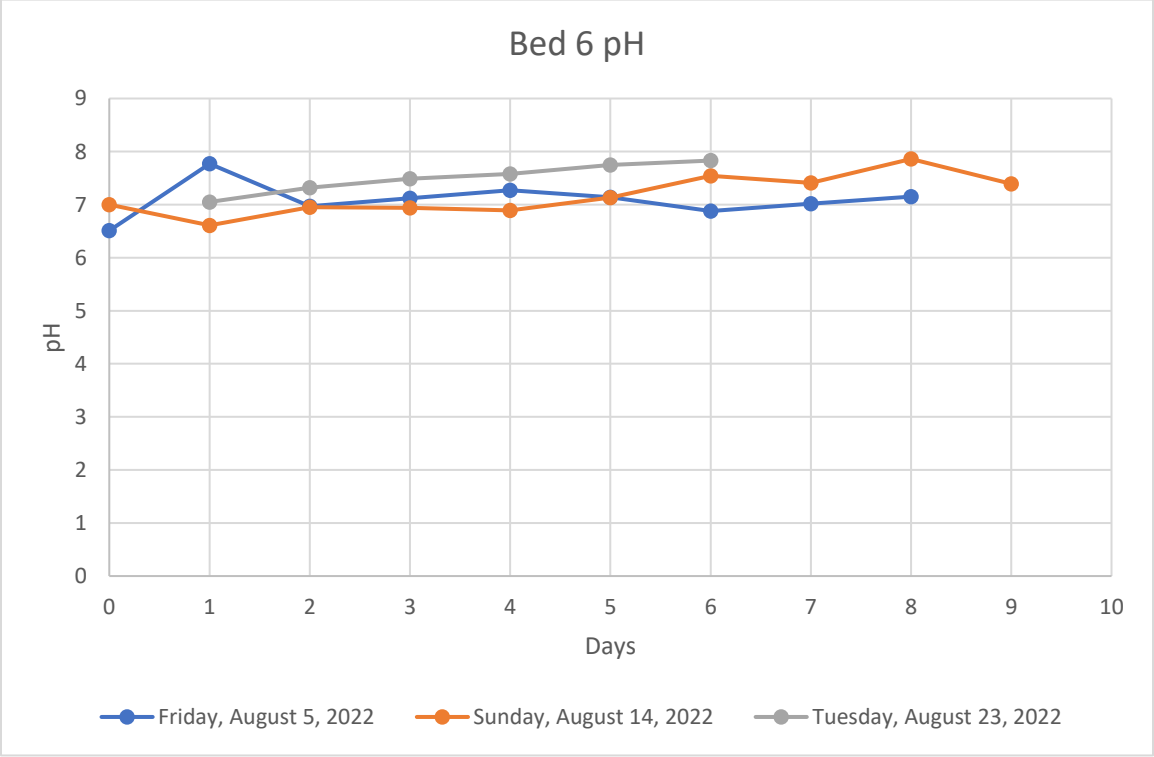
Bed 6 pH
pH
Days
Friday, August 5, 2022
Sunday, August 14, 2022
Tuesday, August 23, 2022

(d) Dissolved Oxygen (DO)

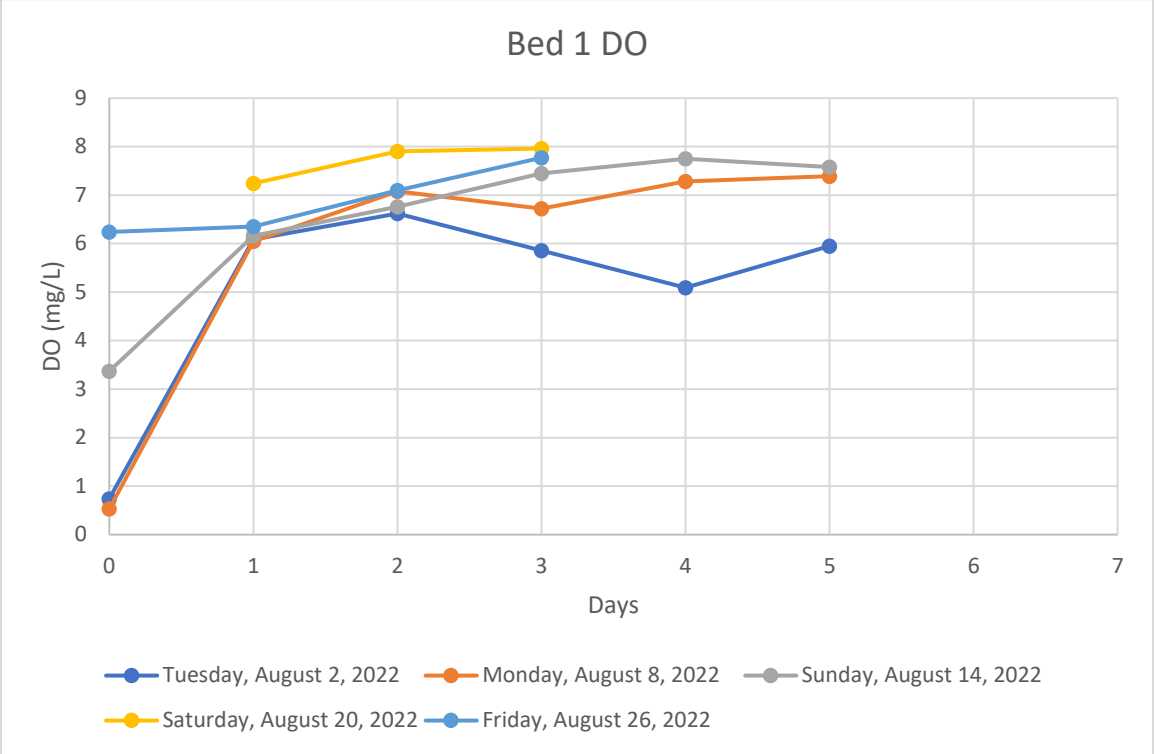

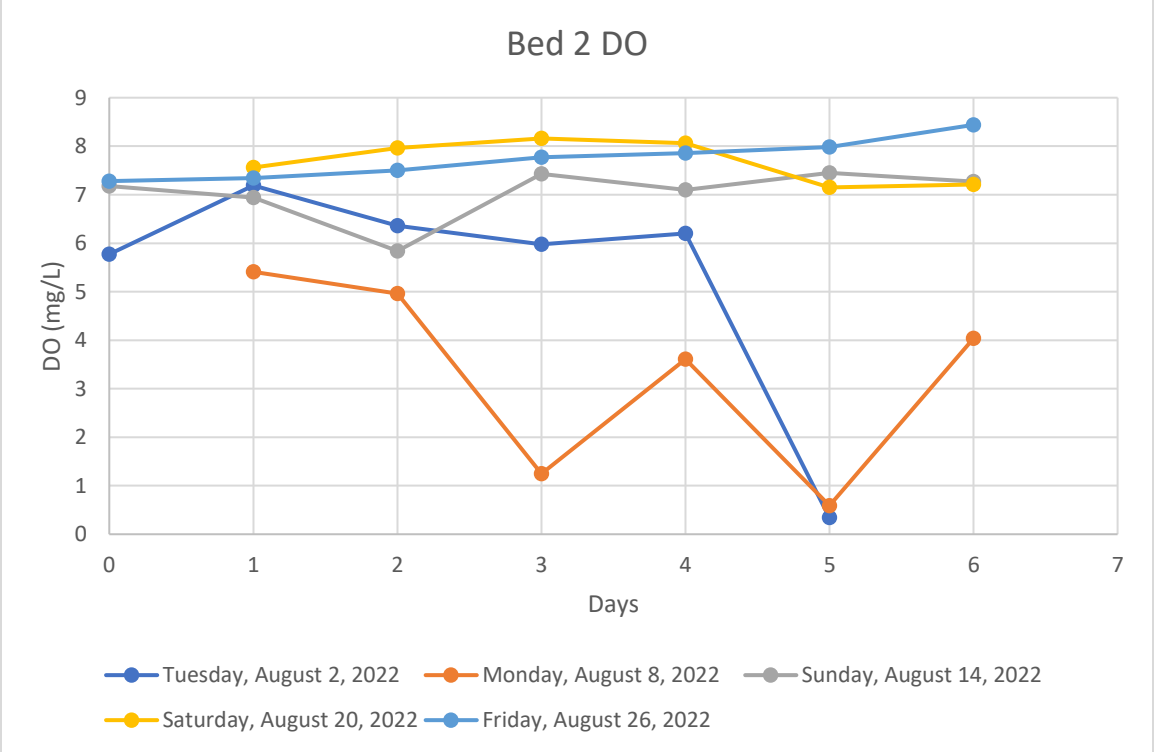

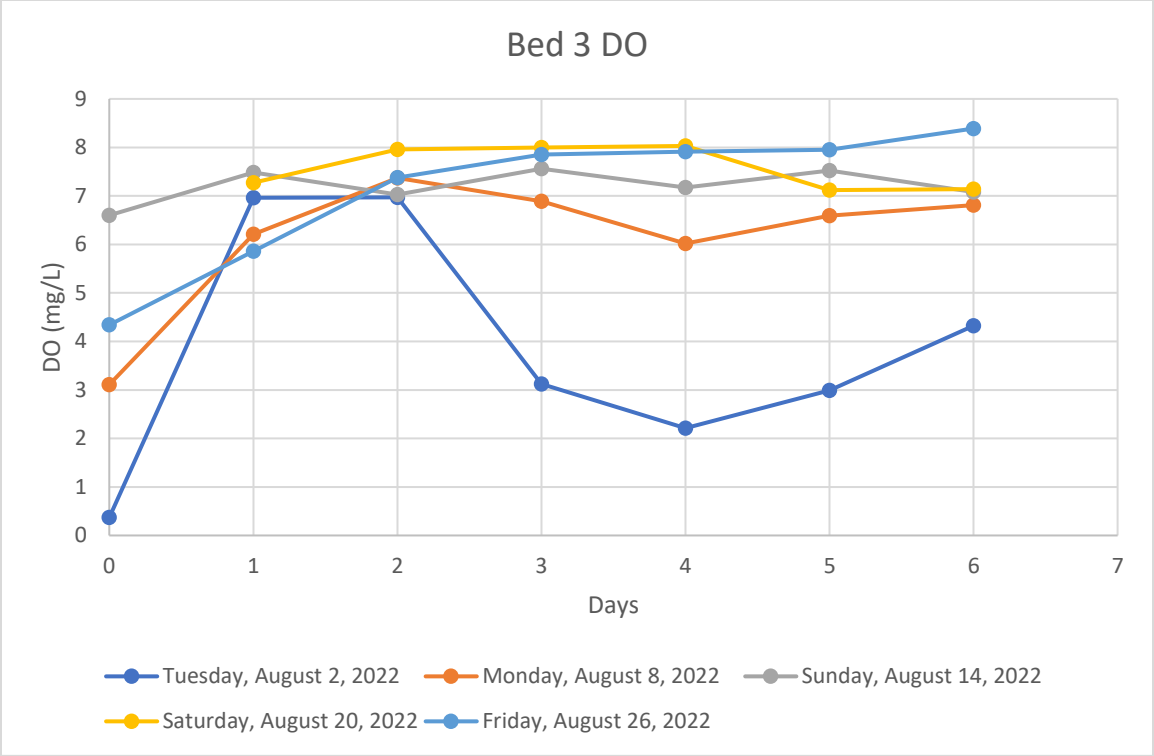
Bed 3 DO
DO (mg/L)
Days
Tuesday, August 2, 2022
Monday, August 8, 2022
Sunday, August 14, 2022
Saturday, August 20, 2022
Friday, August 26, 2022

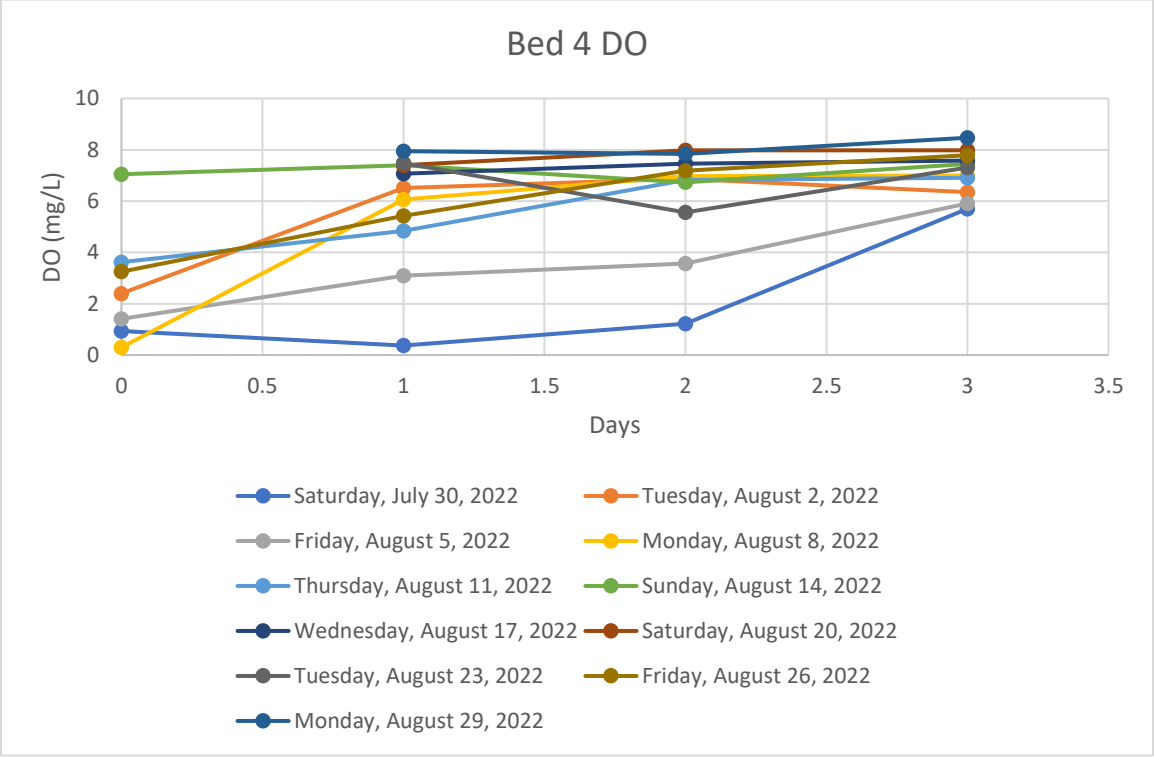
Bed 4 DO
DO (mg/L)
Days
Saturday, July 30, 2022
Tuesday, August 2, 2022
Friday, August 5, 2022
Monday, August 8, 2022
Thursday, August 11, 2022
Sunday, August 14, 2022
Wednesday, August 17, 2022
Saturday, August 20, 2022
Tuesday, August 23, 2022
Friday, August 26, 2022
Monday, August 29, 2022

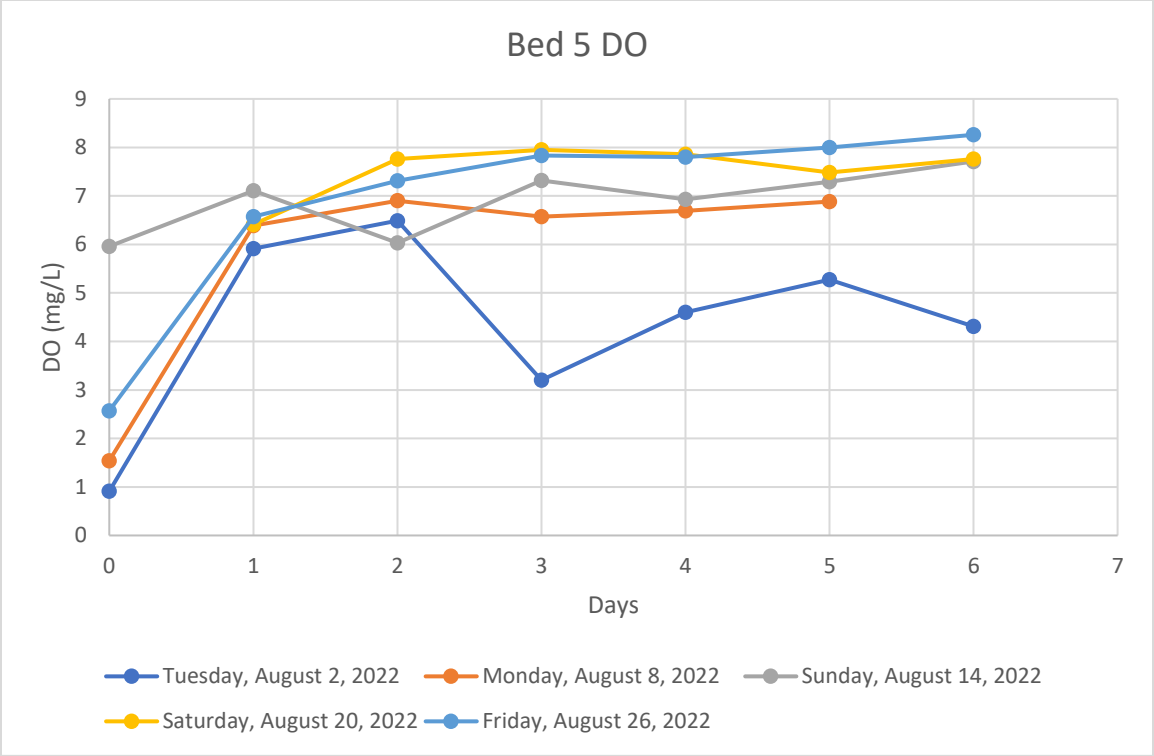
Bed 5 DO
DO (mg/L)
Days
Tuesday, August 2, 2022
Monday, August 8, 2022
Sunday, August 14, 2022
Saturday, August 20, 2022
Friday, August 26, 2022

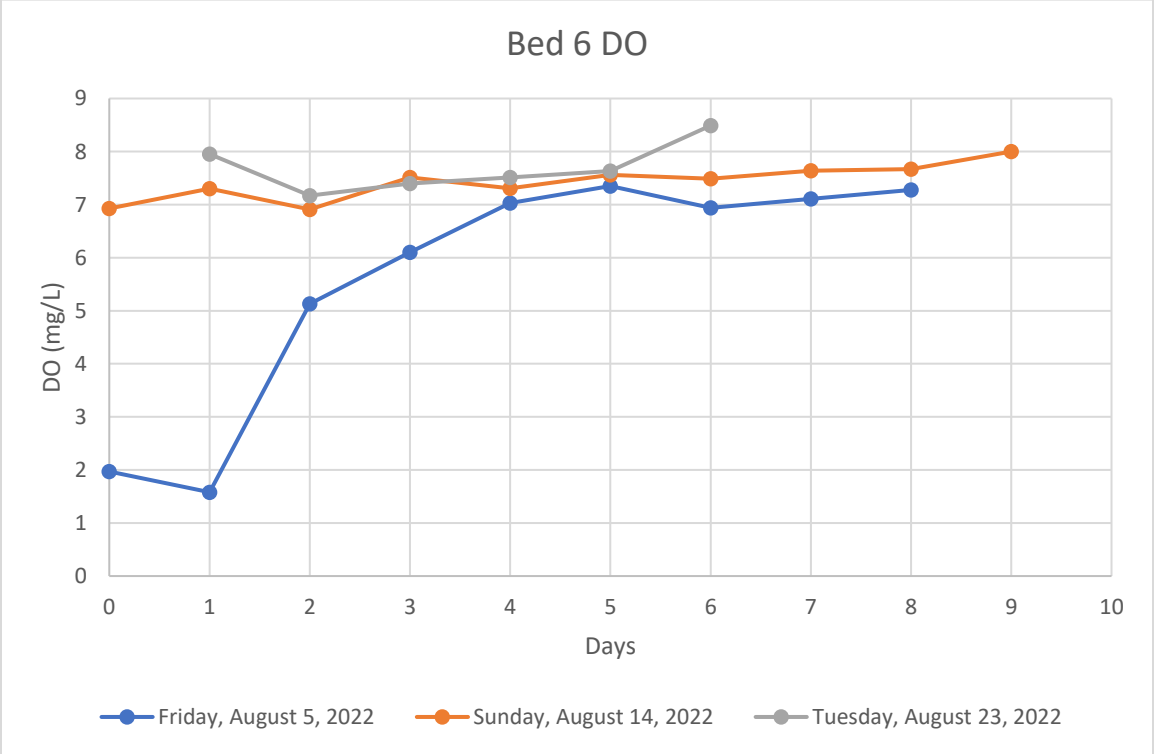
Bed 6 DO
DO (mg/L)
Days
Friday, August 5, 2022
Sunday, August 14, 2022
Tuesday, August 23, 2022

(e) Total Solids (TS)

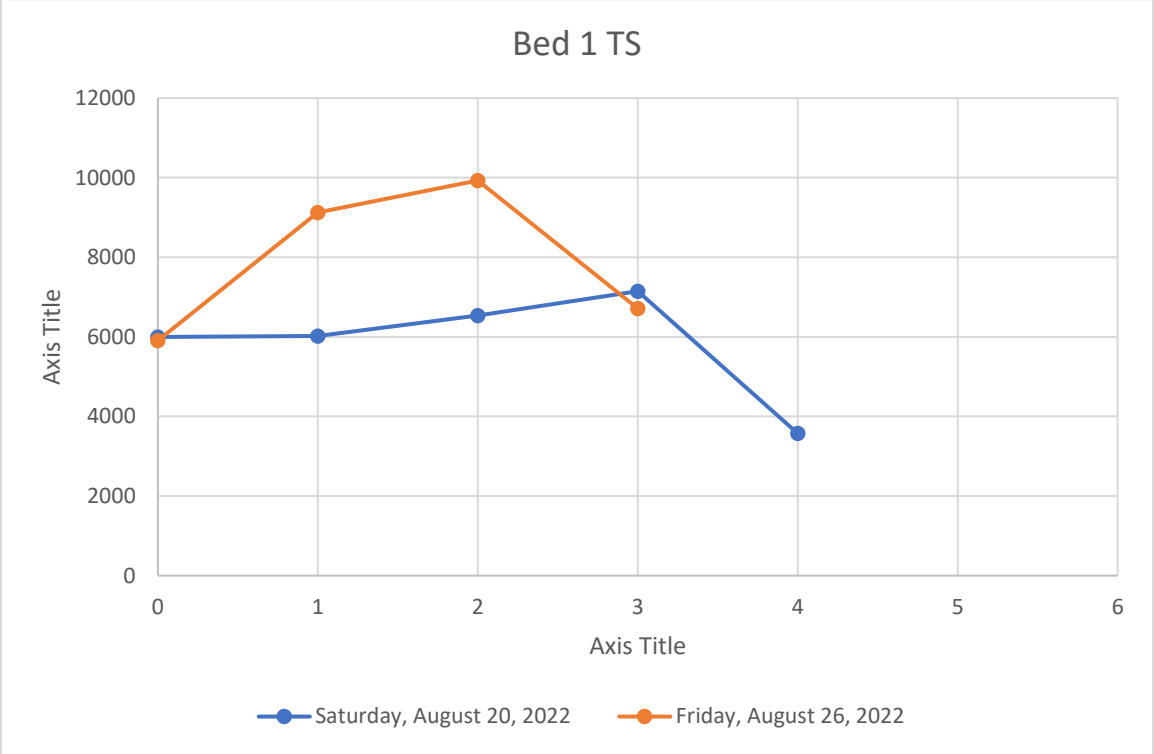

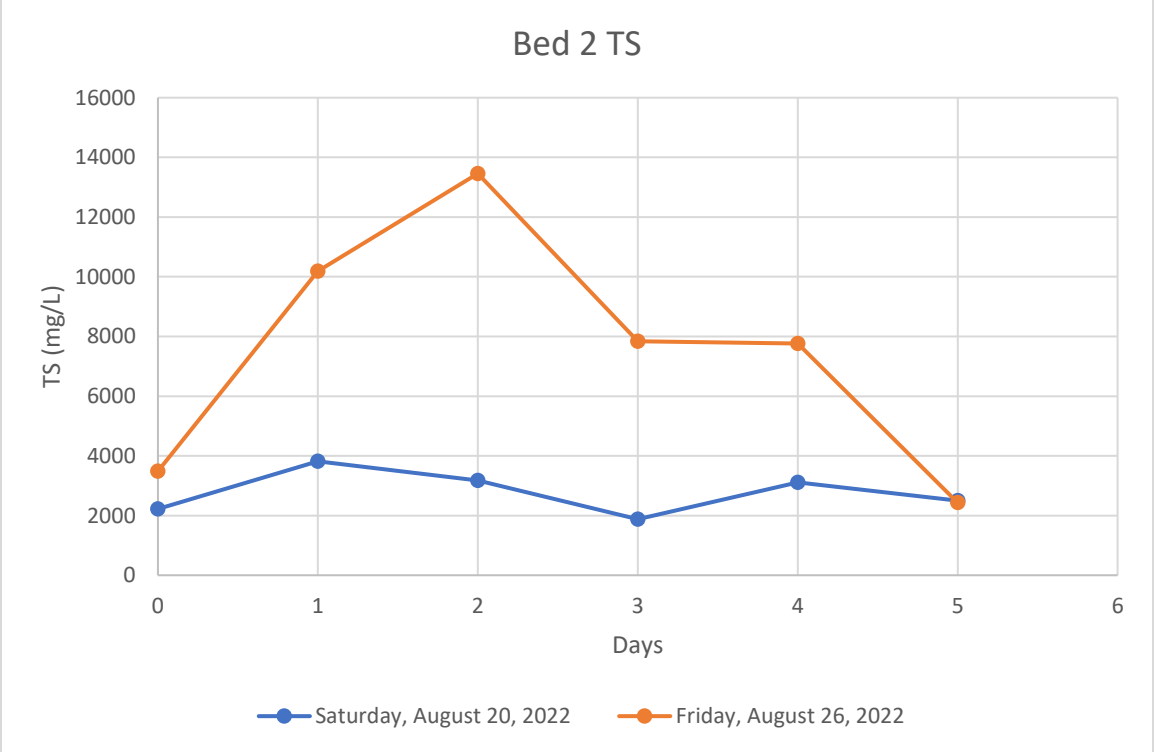

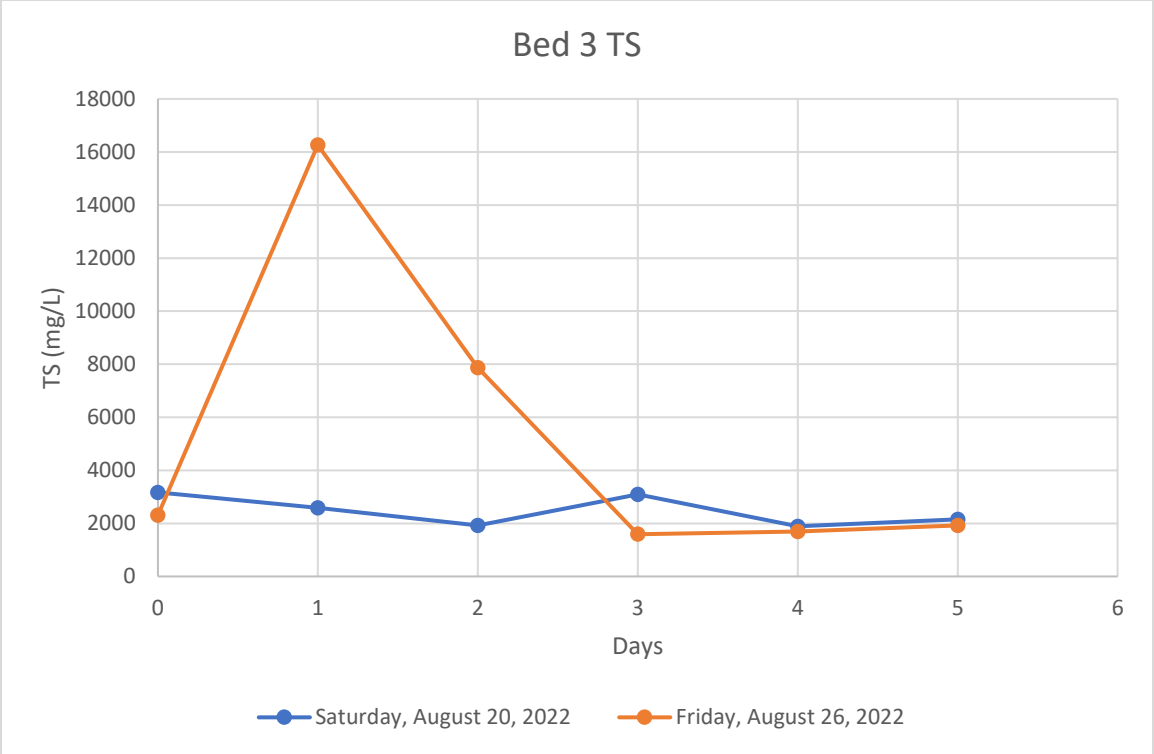
Bed 3 TS
18000
16000
14000
12000
10000
8000
6000
4000
2000
0
TS (mg/L)
0
1
2
3
4
5
6
Days
Saturday, August 20, 2022
Friday, August 26, 2022

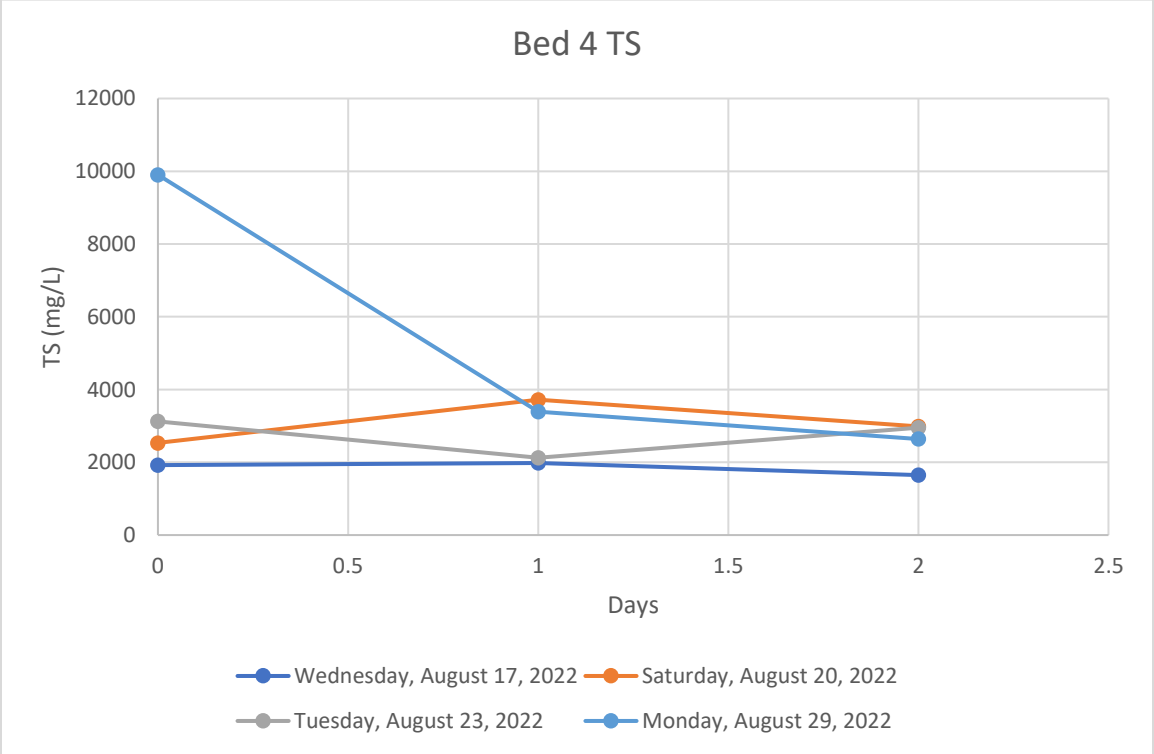
Bed 4 TS
12000
10000
8000
6000
4000
2000
0
TS (mg/L)
0
0.5
1
1.5
2
2.5
Days
Wednesday, August 17, 2022
Saturday, August 20, 2022
Tuesday, August 23, 2022
Monday, August 29, 2022

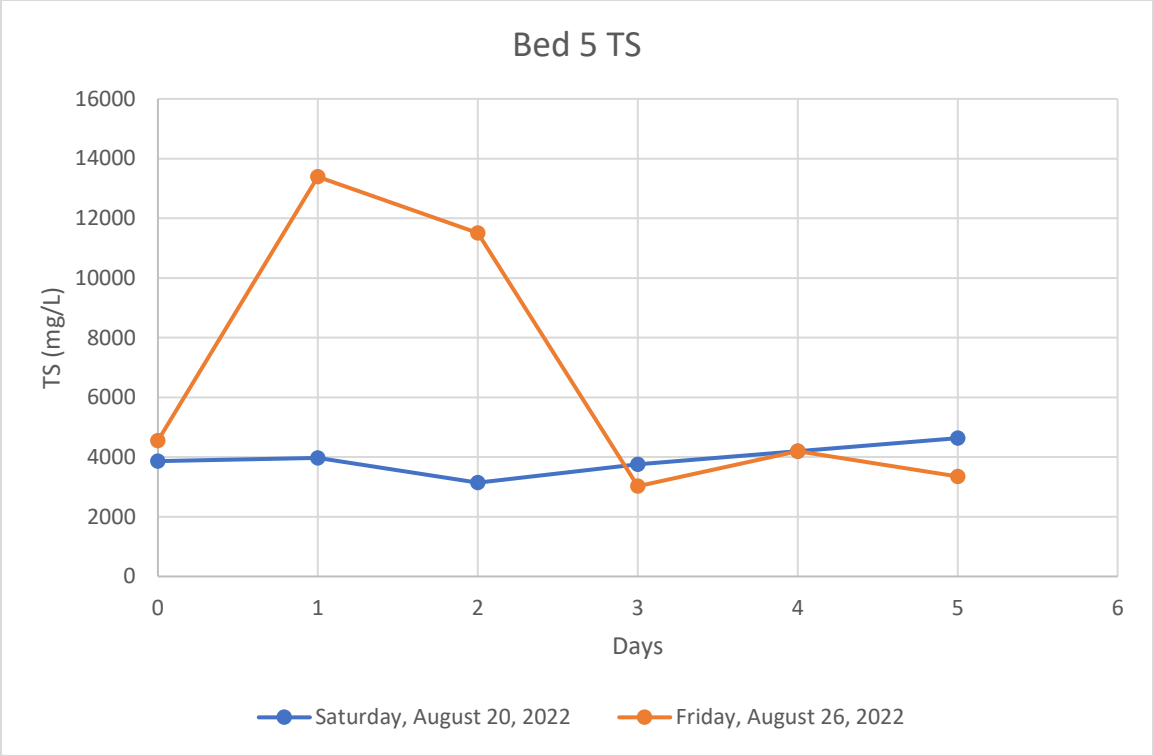
Bed 5 TS
16000
14000
12000
10000
8000
6000
4000
2000
0
TS (mg/L)
0
1
2
3
4
5
6
Days
Saturday, August 20, 2022
Friday, August 26, 2022

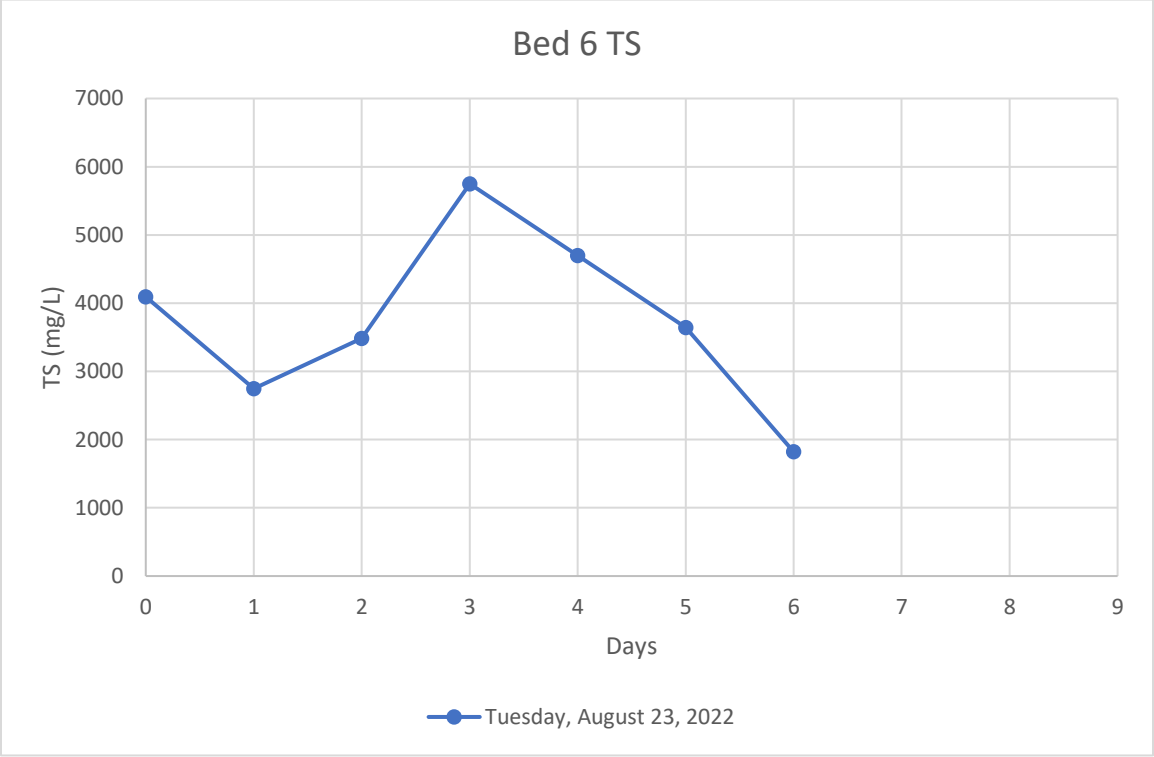
Bed 6 TS
7000
6000
5000
4000
3000
2000
1000
0
TS (mg/L)
0
1
2
3
4
5
6
7
8
9
Days
Tuesday, August 23, 2022

Appendix Q: Experimental Results in Phase 2 Experiment.

(a) Overall Effluent Flux

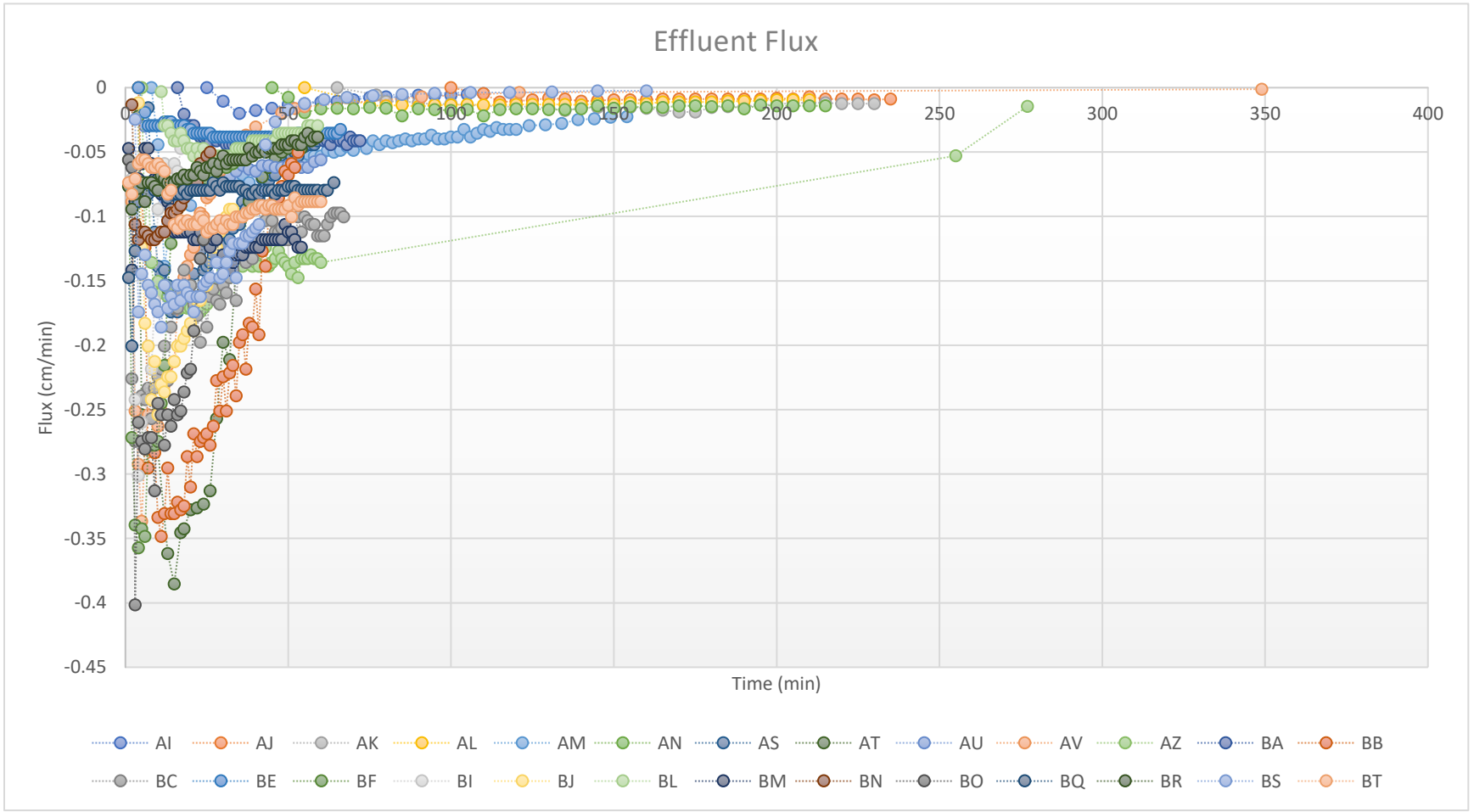

(b) Thickness of Sludge Deposit

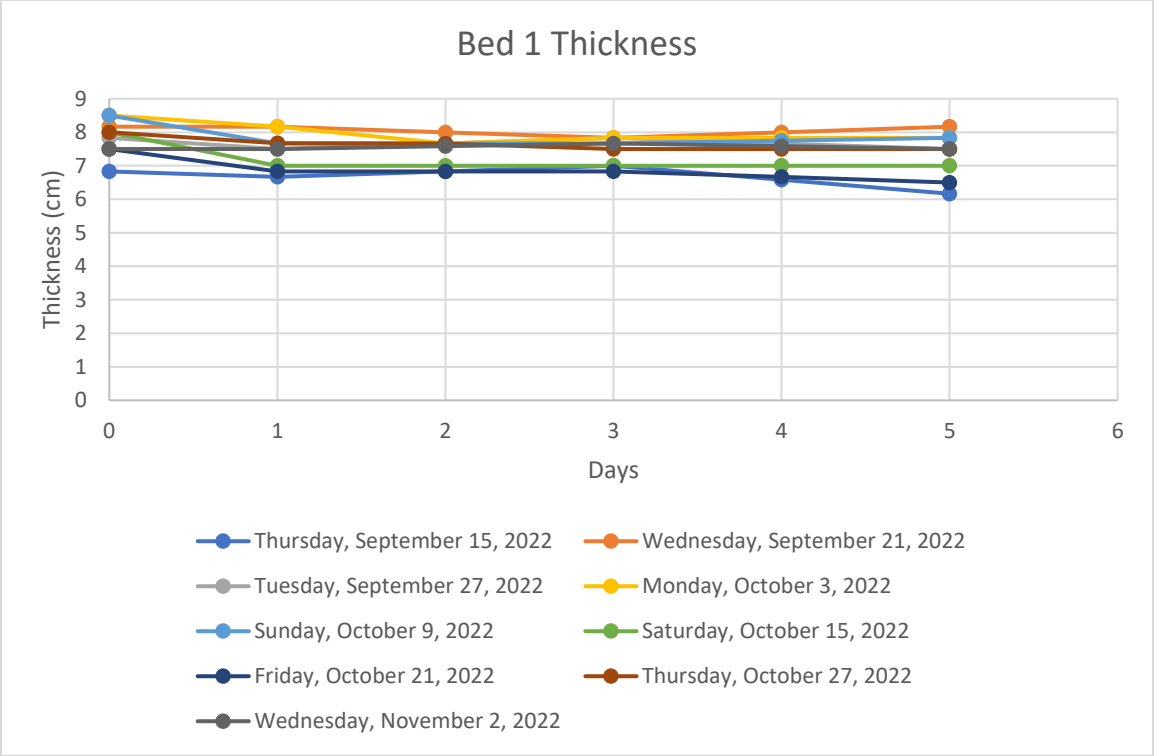

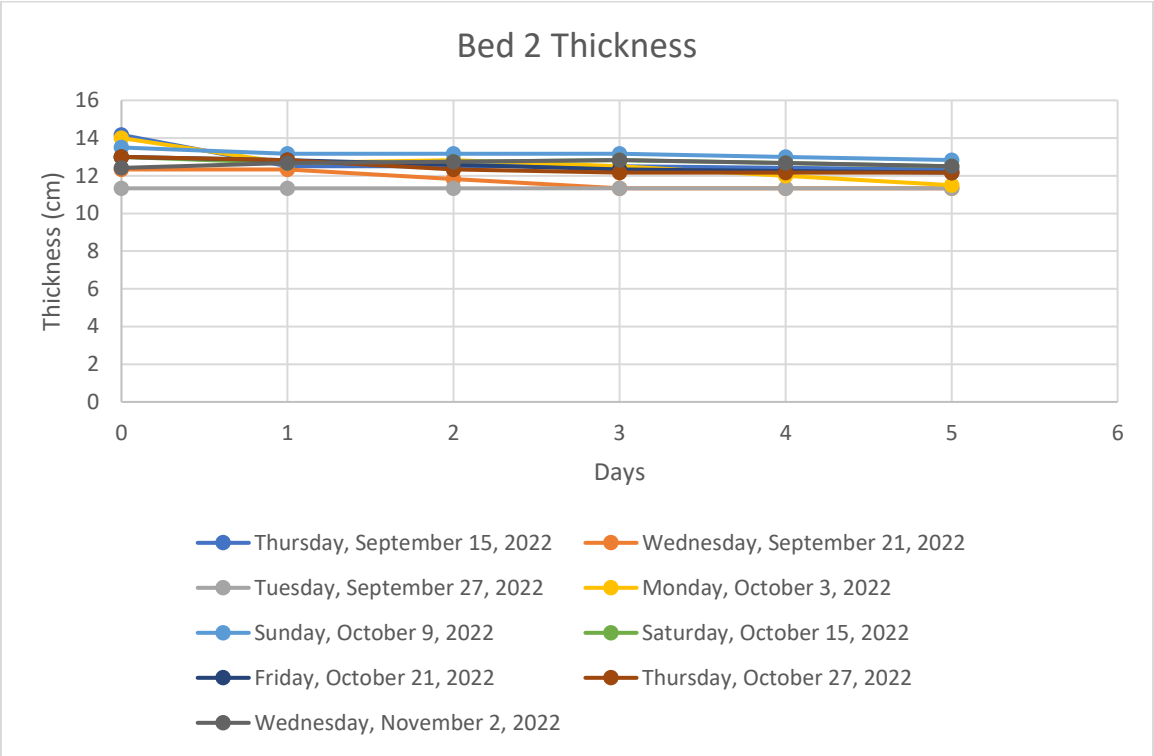

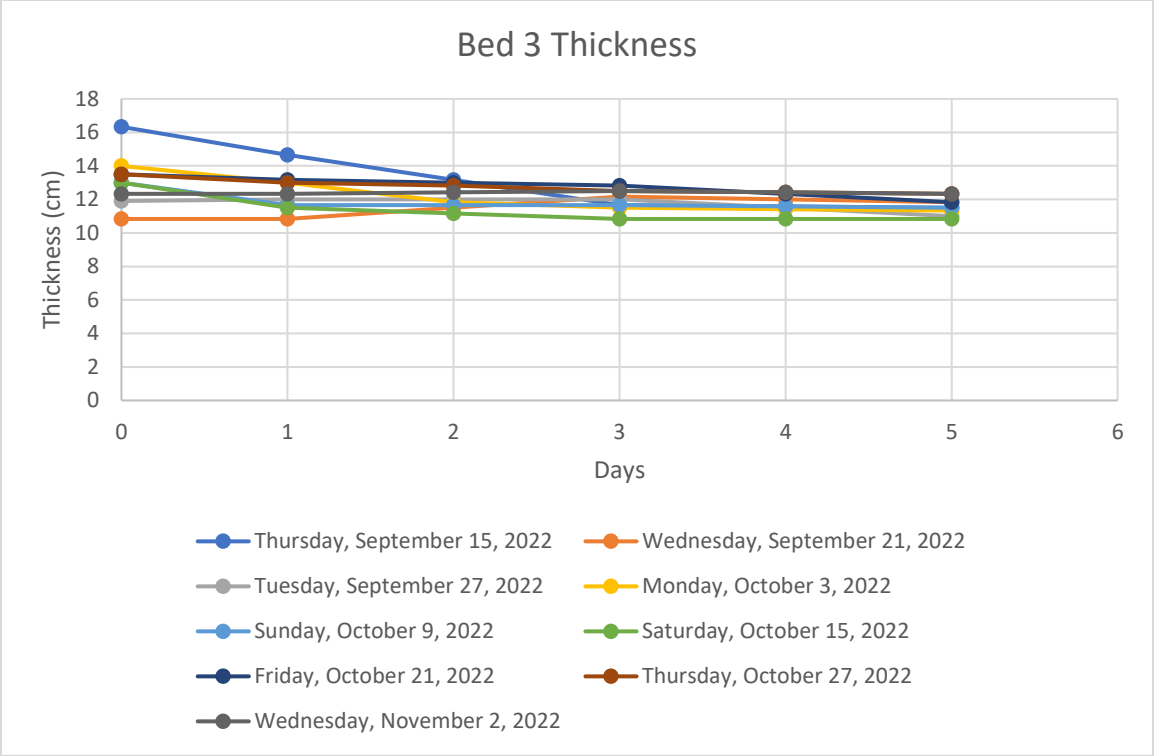
Bed 3 Thickness
Thickness (cm)
Days
Thursday, September 15, 2022
Wednesday, September 21, 2022
Tuesday, September 27, 2022
Monday, October 3, 2022
Sunday, October 9, 2022
Saturday, October 15, 2022
Friday, October 21, 2022
Thursday, October 27, 2022
Wednesday, November 2, 2022

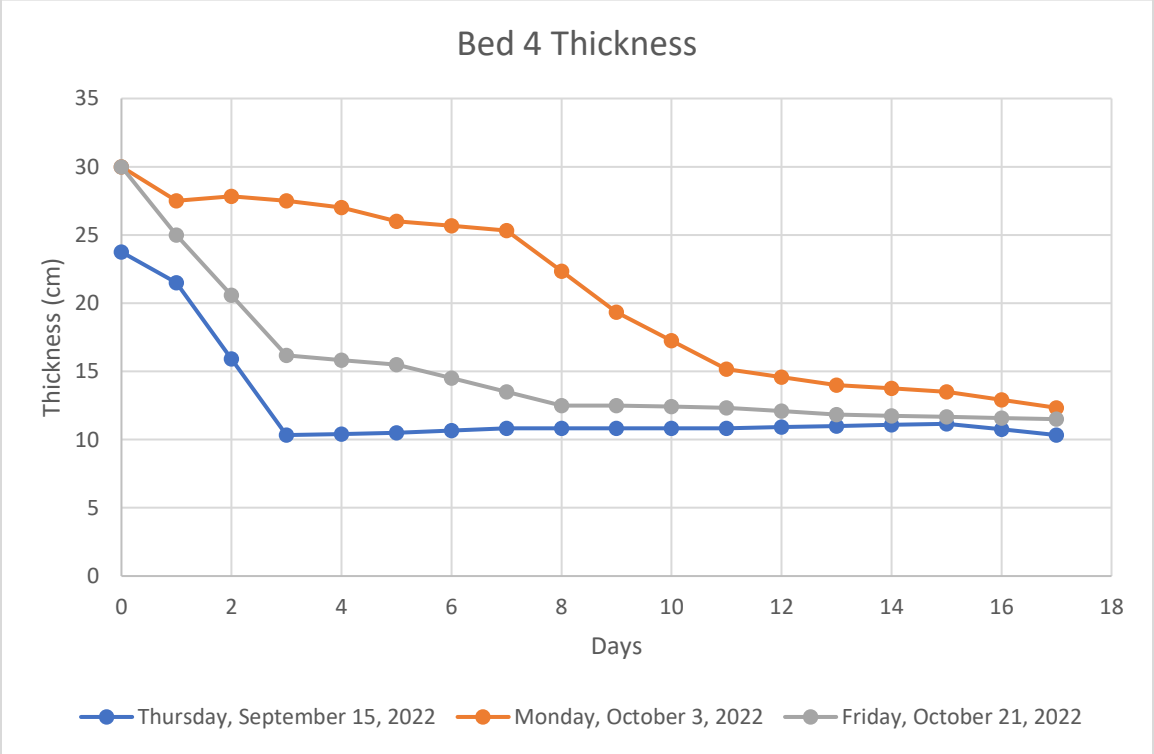
Bed 4 Thickness
Thickness (cm)
Days
Thursday, September 15, 2022
Monday, October 3, 2022
Friday, October 21, 2022

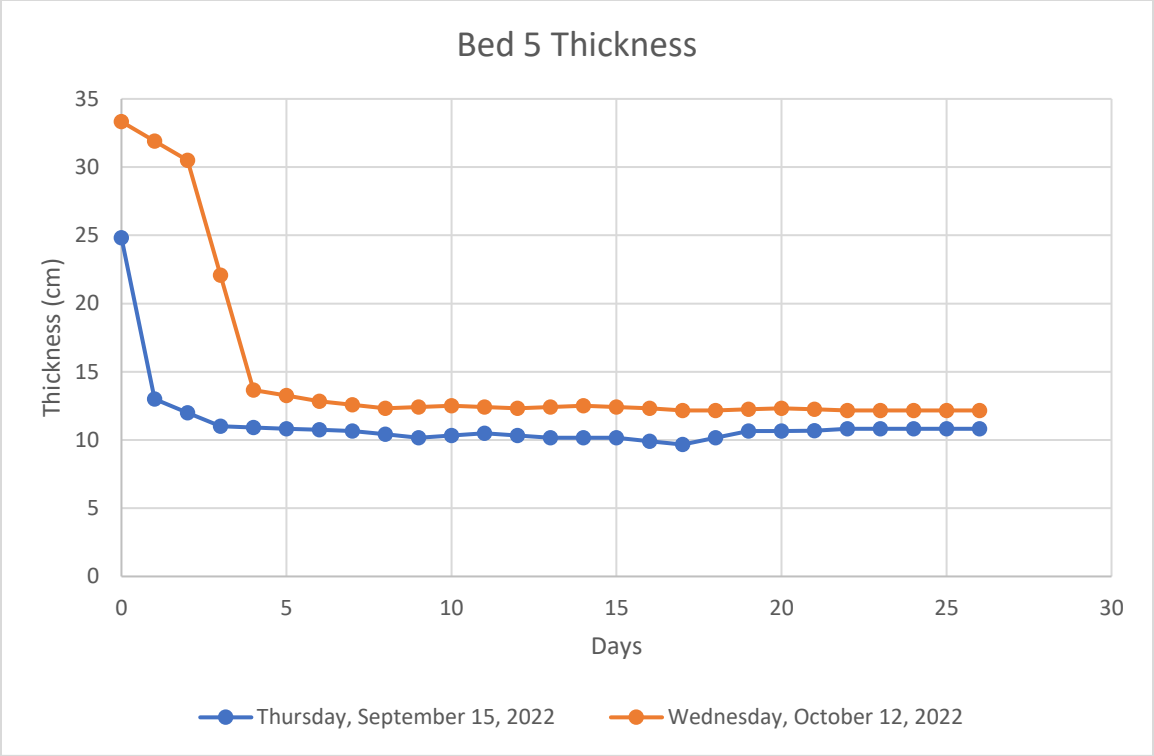
Bed 5 Thickness
Thickness (cm)
Days
0
5
10
15
20
25
30
35
Thursday, September 15, 2022
Wednesday, October 12, 2022

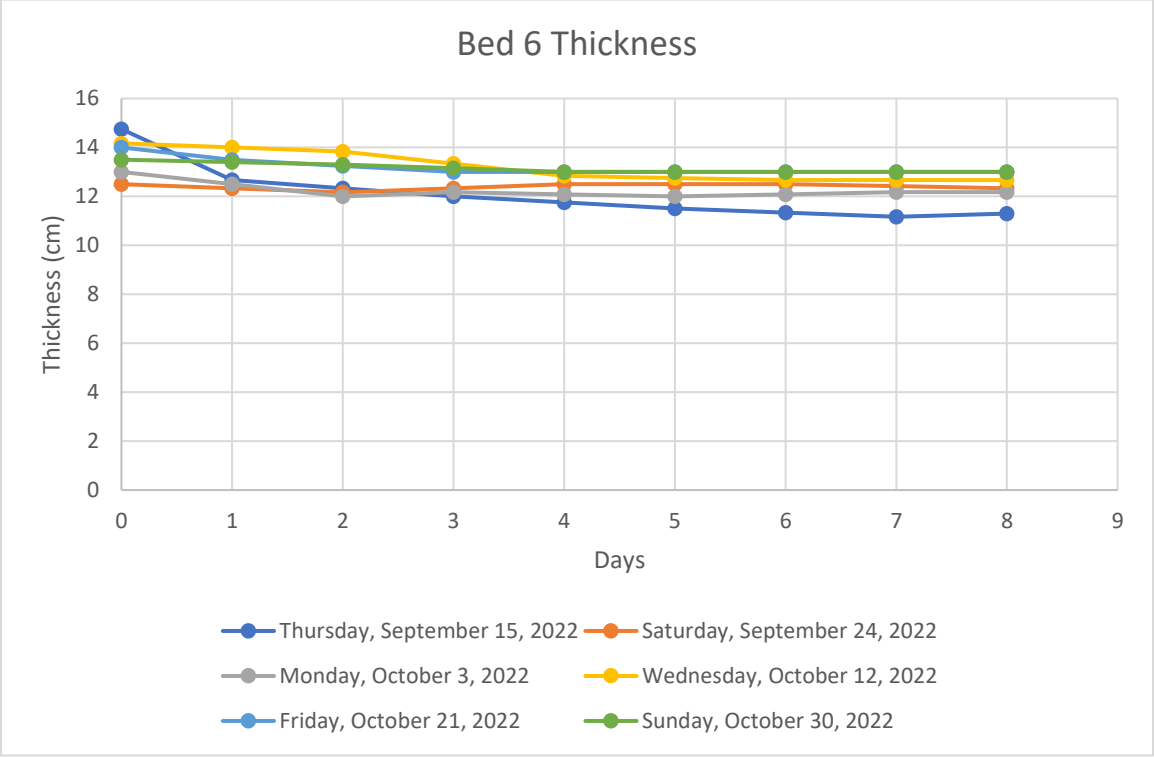
Bed 6 Thickness
Thickness (cm)
Days
0
2
4
6
8
10
12
14
16
0
1
2
3
4
5
6
7
8
9
Thursday, September 15, 2022
Saturday, September 24, 2022
Monday, October 3, 2022
Wednesday, October 12, 2022
Friday, October 21, 2022
Sunday, October 30, 2022

(c) Moisture Content

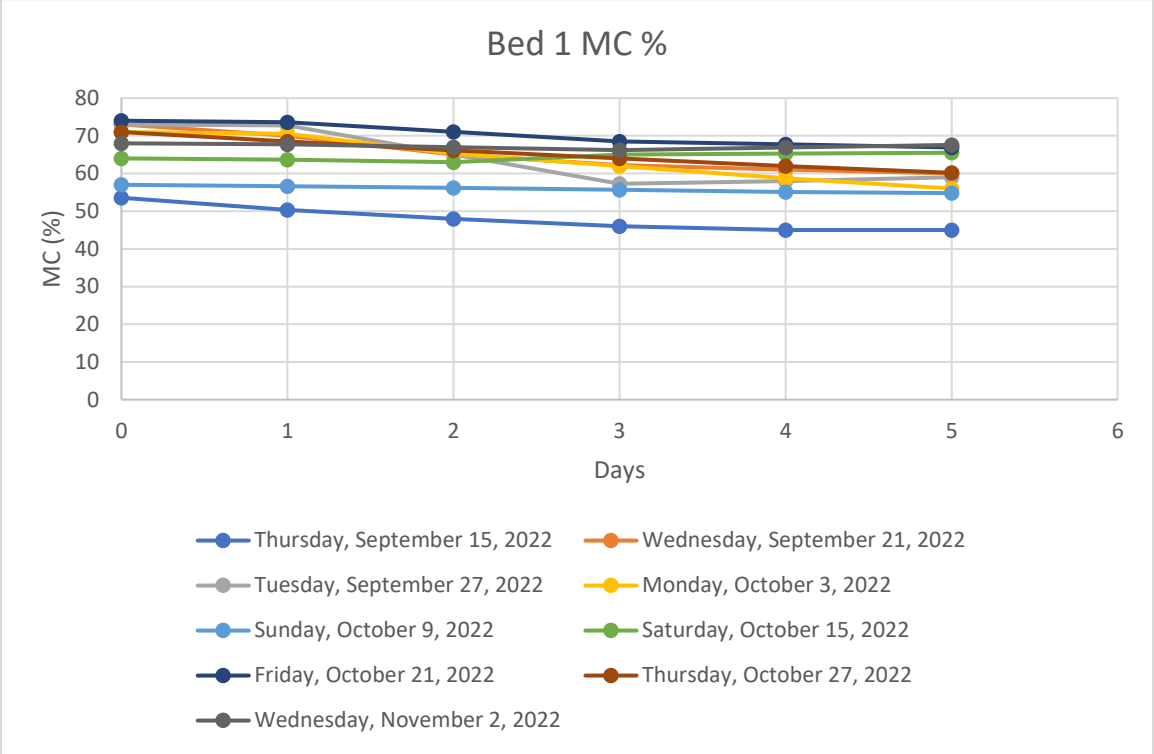

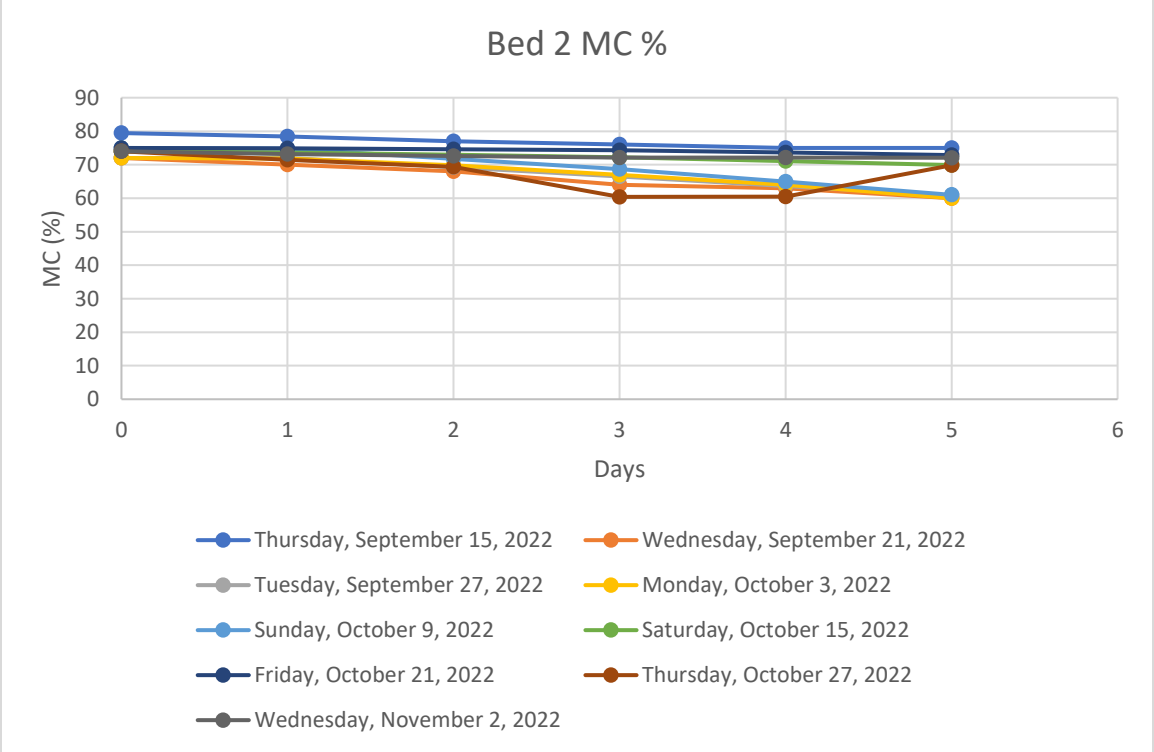

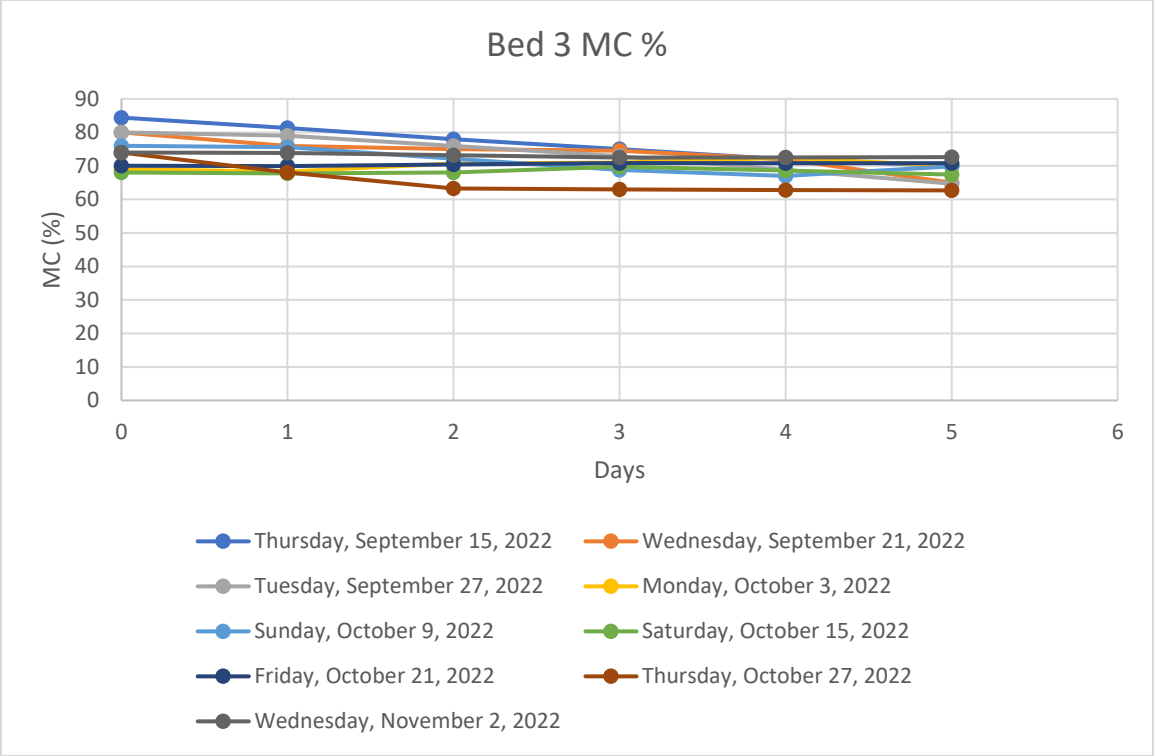
Bed 3 MC %
MC (%)
Days
Thursday, September 15, 2022
Wednesday, September 21, 2022
Tuesday, September 27, 2022
Monday, October 3, 2022
Sunday, October 9, 2022
Saturday, October 15, 2022
Friday, October 21, 2022
Thursday, October 27, 2022
Wednesday, November 2, 2022

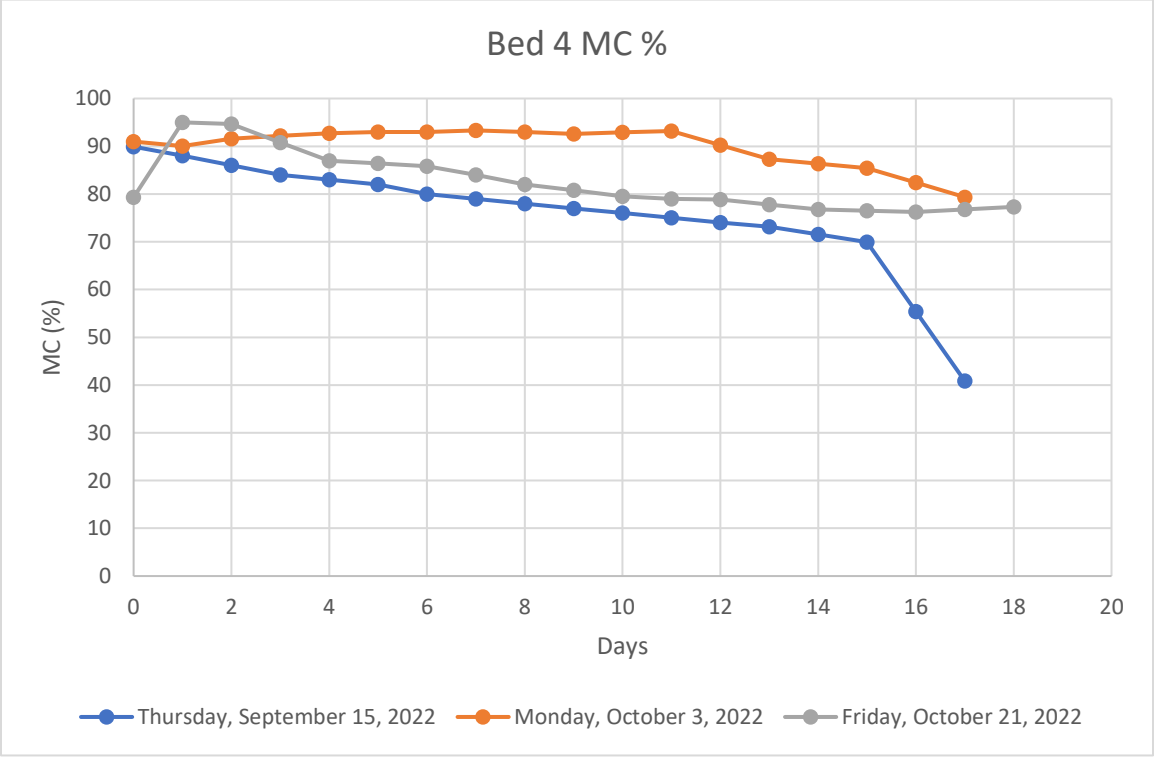
Bed 4 MC %
MC (%)
Days
Thursday, September 15, 2022
Monday, October 3, 2022
Friday, October 21, 2022

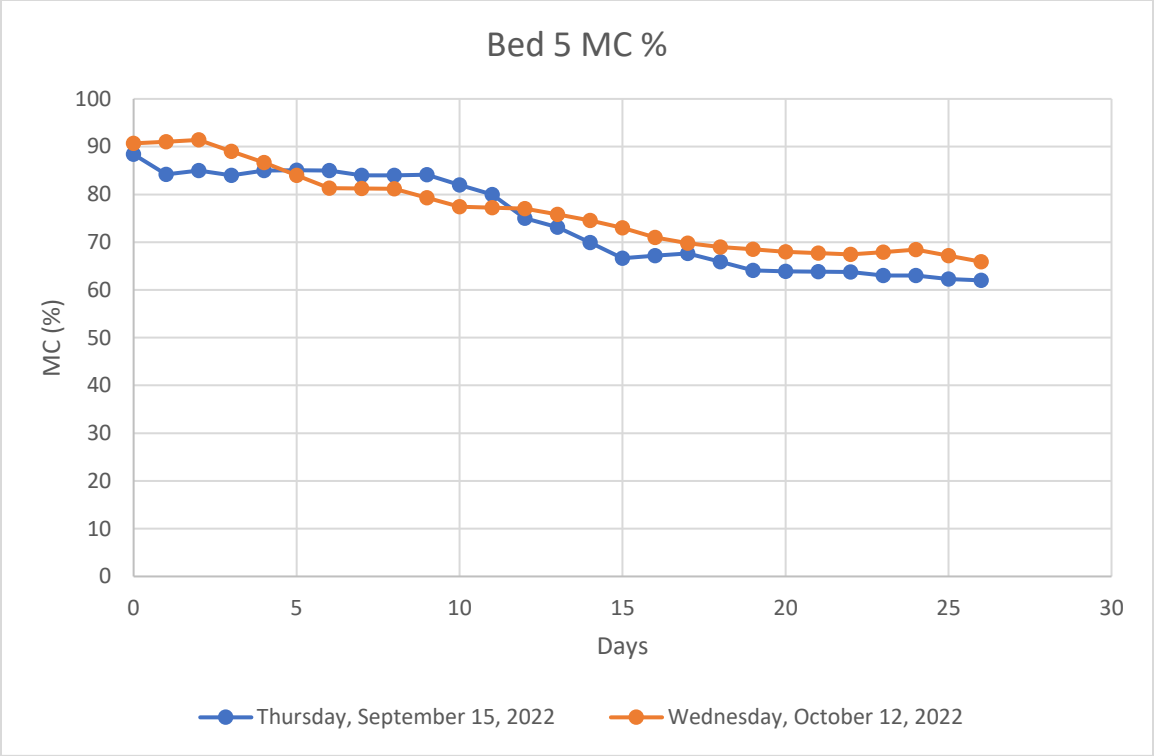
Bed 5 MC %
MC (%)
Days
0
10
20
30
40
50
60
70
80
90
100
0
5
10
15
20
25
30
Thursday, September 15, 2022
Wednesday, October 12, 2022

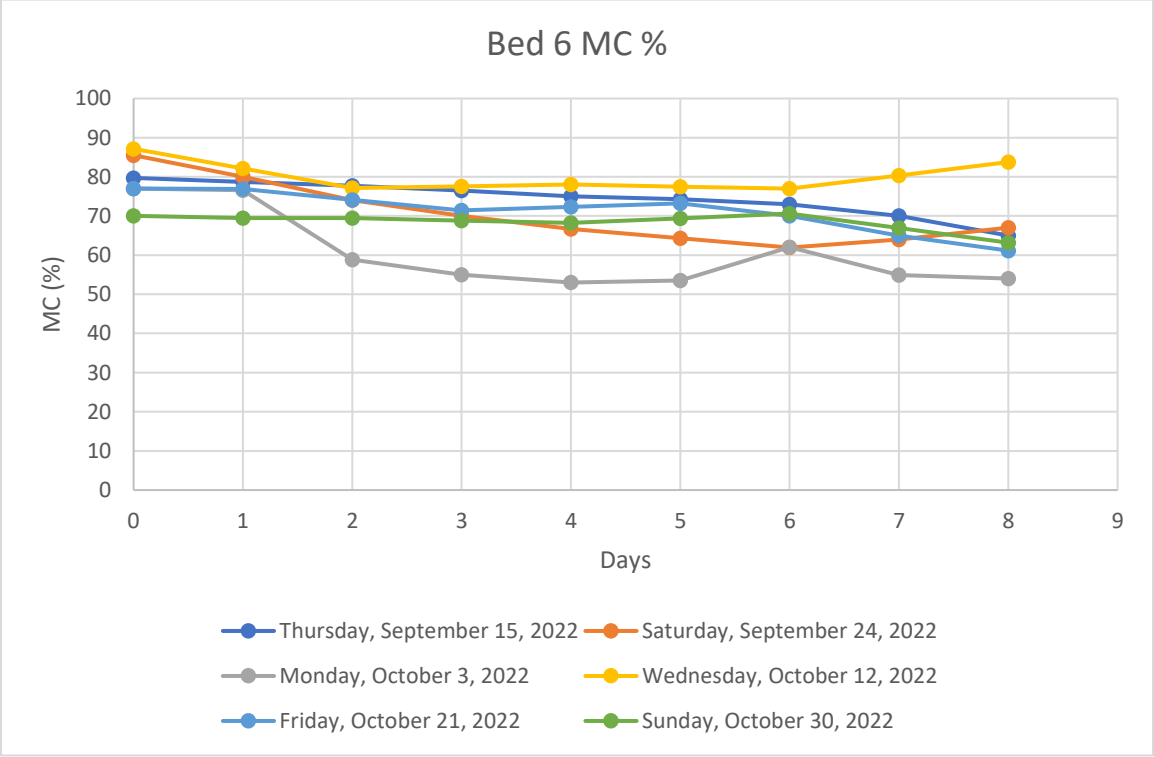
Bed 6 MC %
MC (%)
Days
0
10
20
30
40
50
60
70
80
90
100
0
1
2
3
4
5
6
7
8
9
Thursday, September 15, 2022
Saturday, September 24, 2022
Monday, October 3, 2022
Wednesday, October 12, 2022
Friday, October 21, 2022
Sunday, October 30, 2022

(d) Total Solids

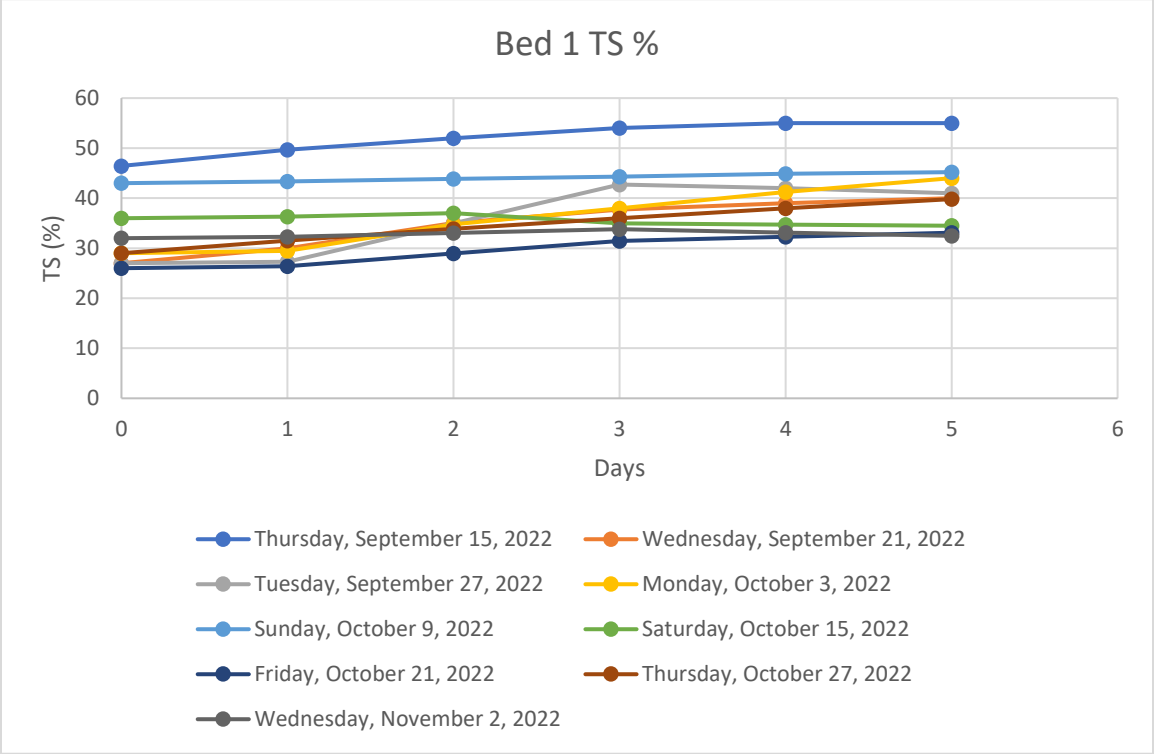

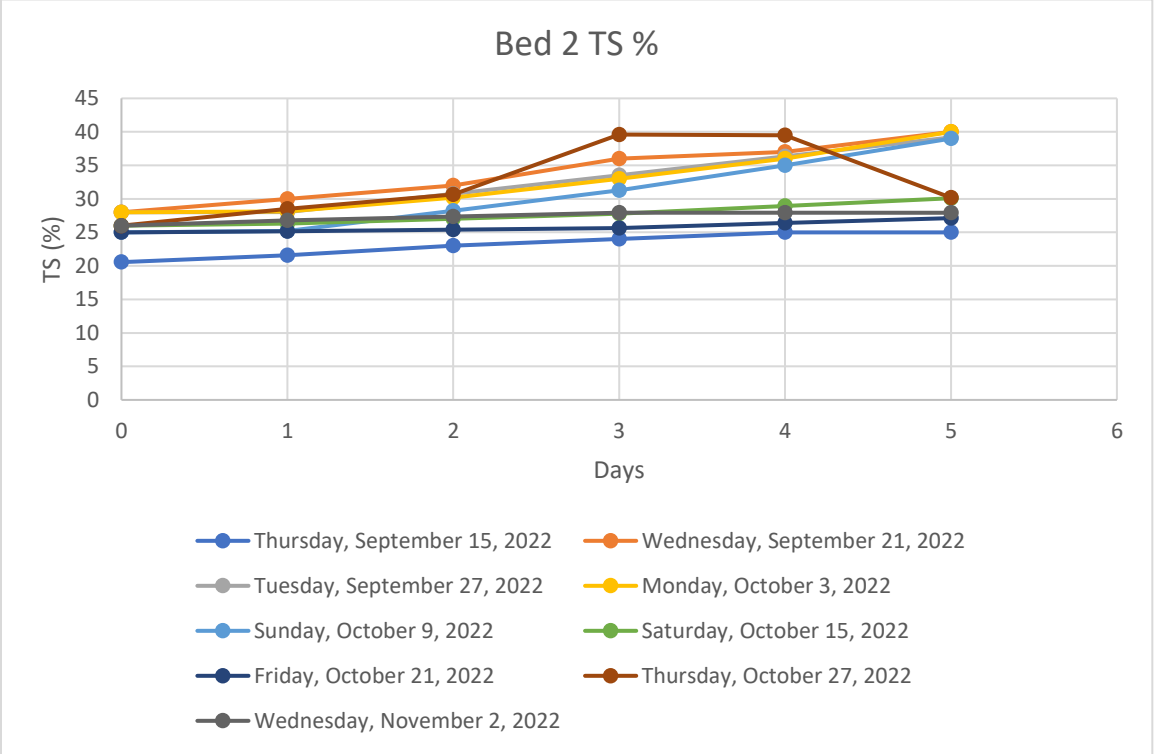

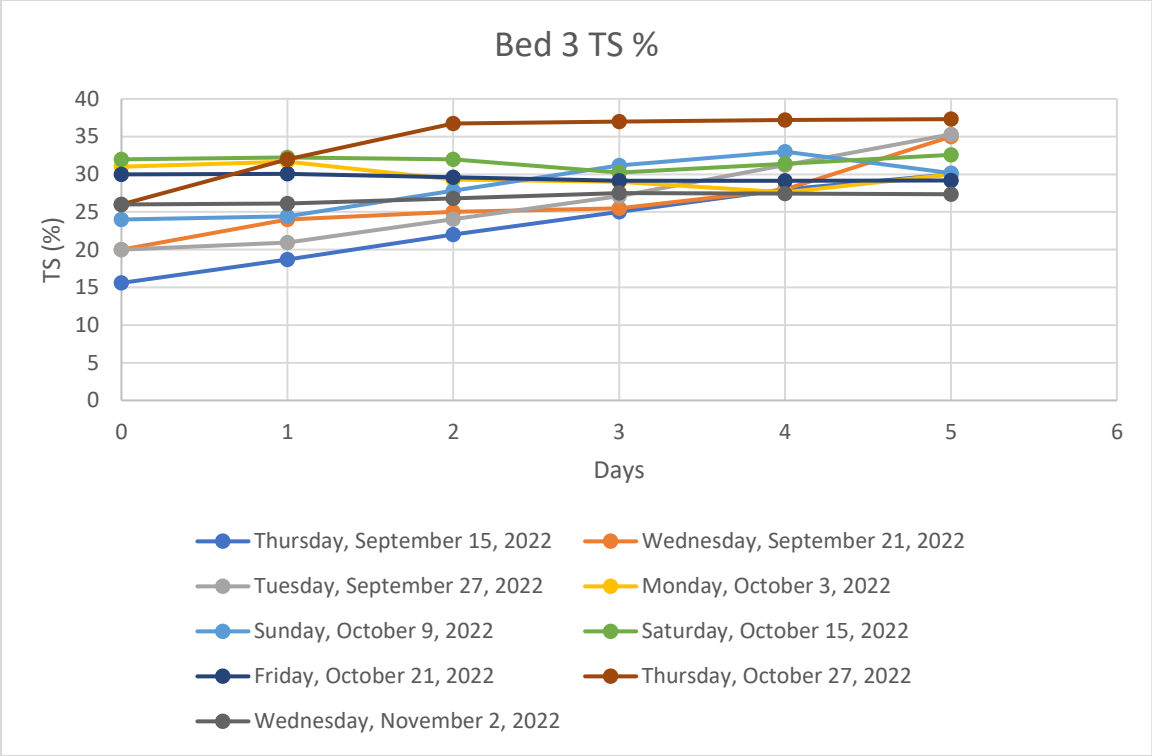
Bed 3 TS %
TS (%)
Days
0
5
10
15
20
25
30
35
40
0
1
2
3
4
5
6
Thursday, September 15, 2022
Wednesday, September 21, 2022
Tuesday, September 27, 2022
Monday, October 3, 2022
Sunday, October 9, 2022
Saturday, October 15, 2022
Friday, October 21, 2022
Thursday, October 27, 2022
Wednesday, November 2, 2022

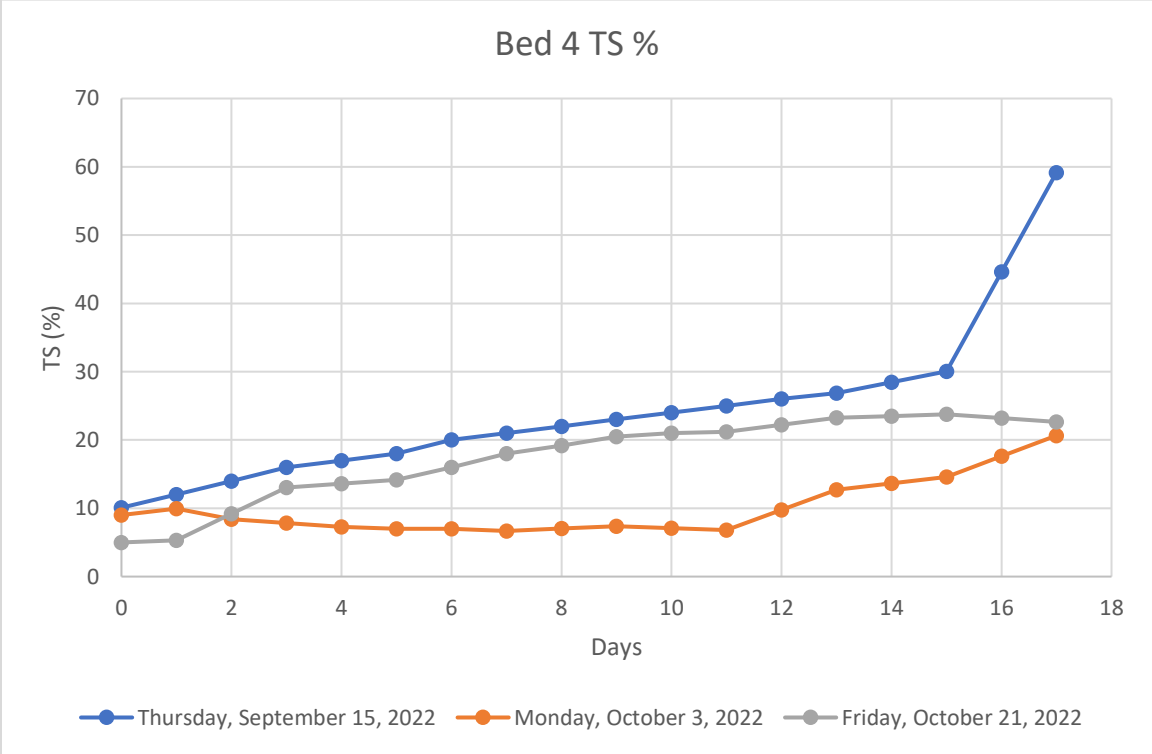
Bed 4 TS %
TS (%)
Days
0
10
20
30
40
50
60
70
0
2
4
6
8
10
12
14
16
18
Thursday, September 15, 2022
Monday, October 3, 2022
Friday, October 21, 2022

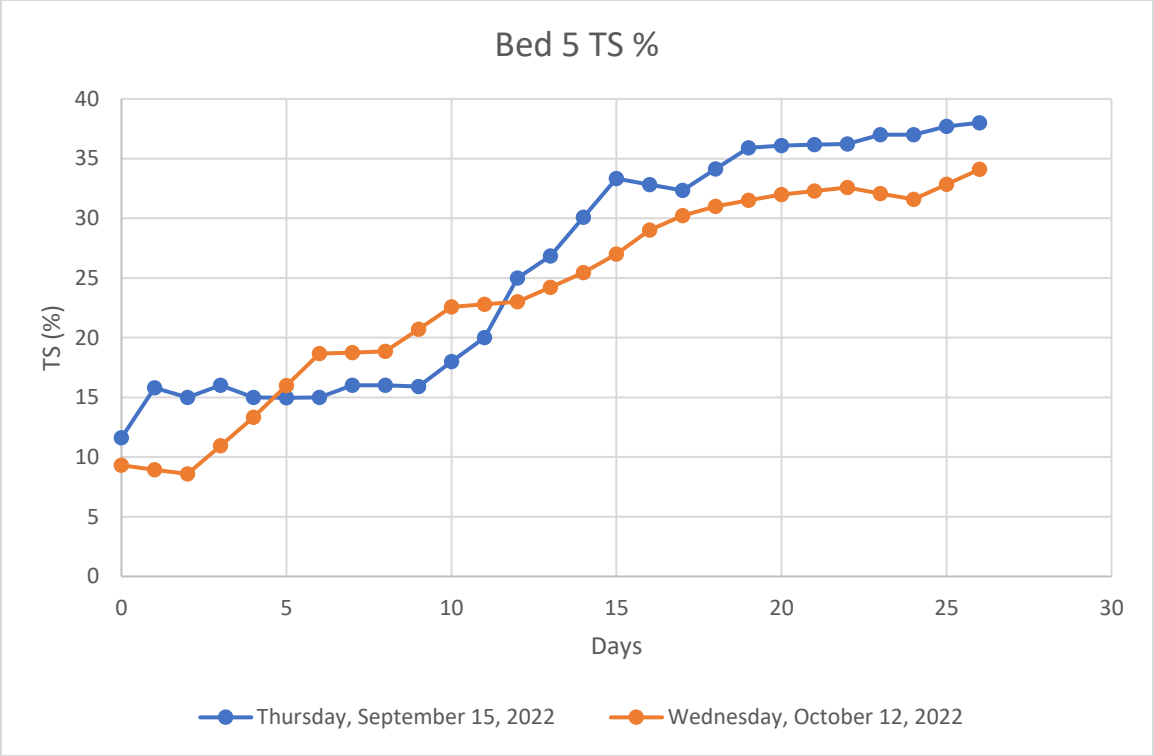
Bed 5 TS %
TS (%)
Days
0
5
10
15
20
25
30
35
40
Thursday, September 15, 2022
Wednesday, October 12, 2022

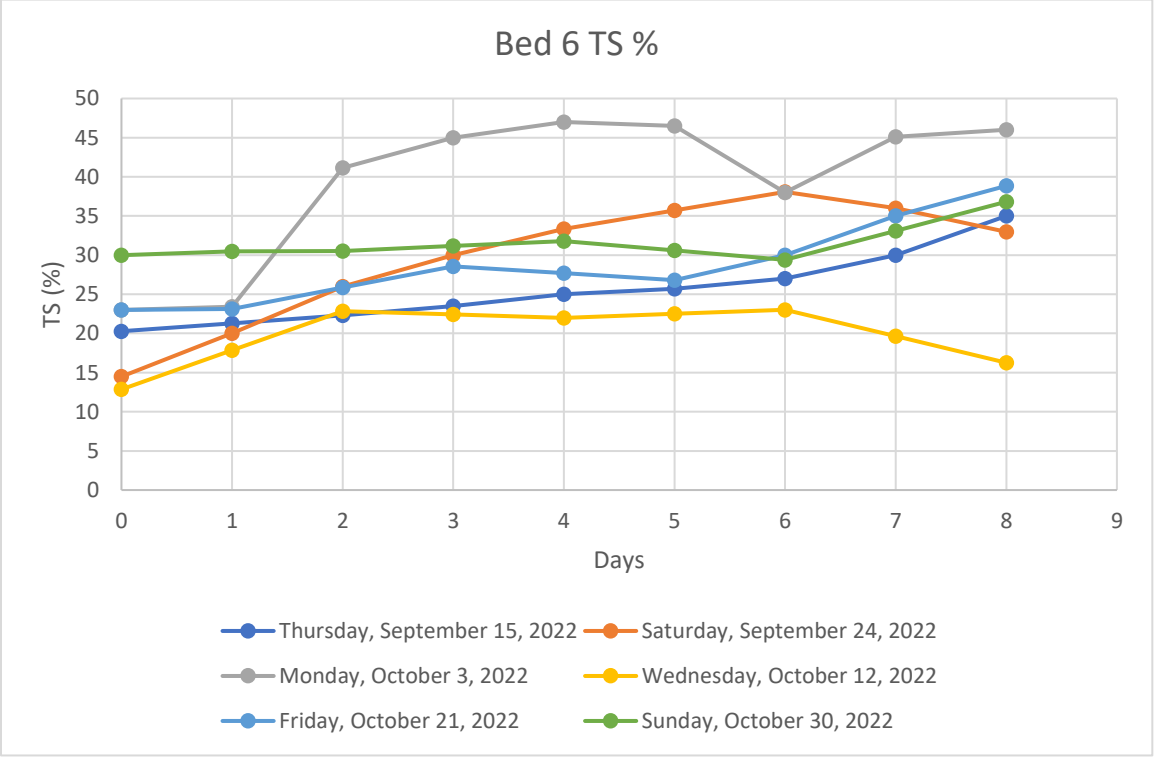
Bed 6 TS %
TS (%)
Days
0
5
10
15
20
25
30
35
40
45
50
0
1
2
3
4
5
6
7
8
9
Thursday, September 15, 2022
Saturday, September 24, 2022
Monday, October 3, 2022
Wednesday, October 12, 2022
Friday, October 21, 2022
Sunday, October 30, 2022

(e) Total Volatile Solids

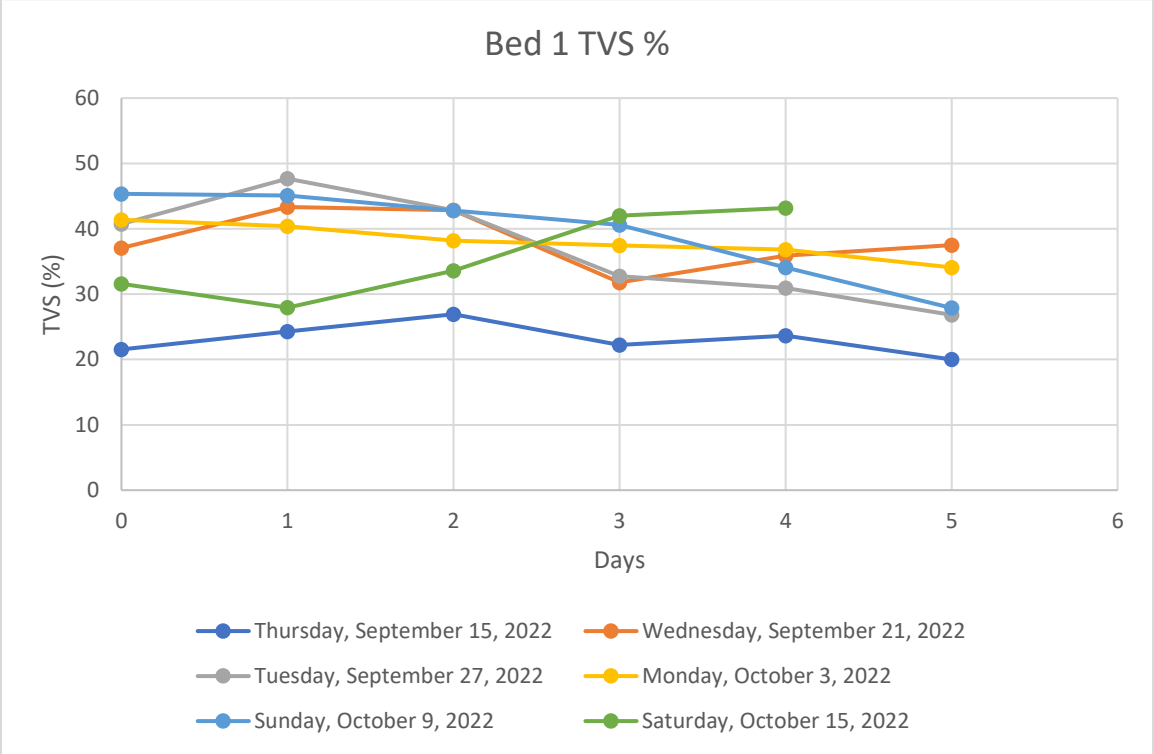

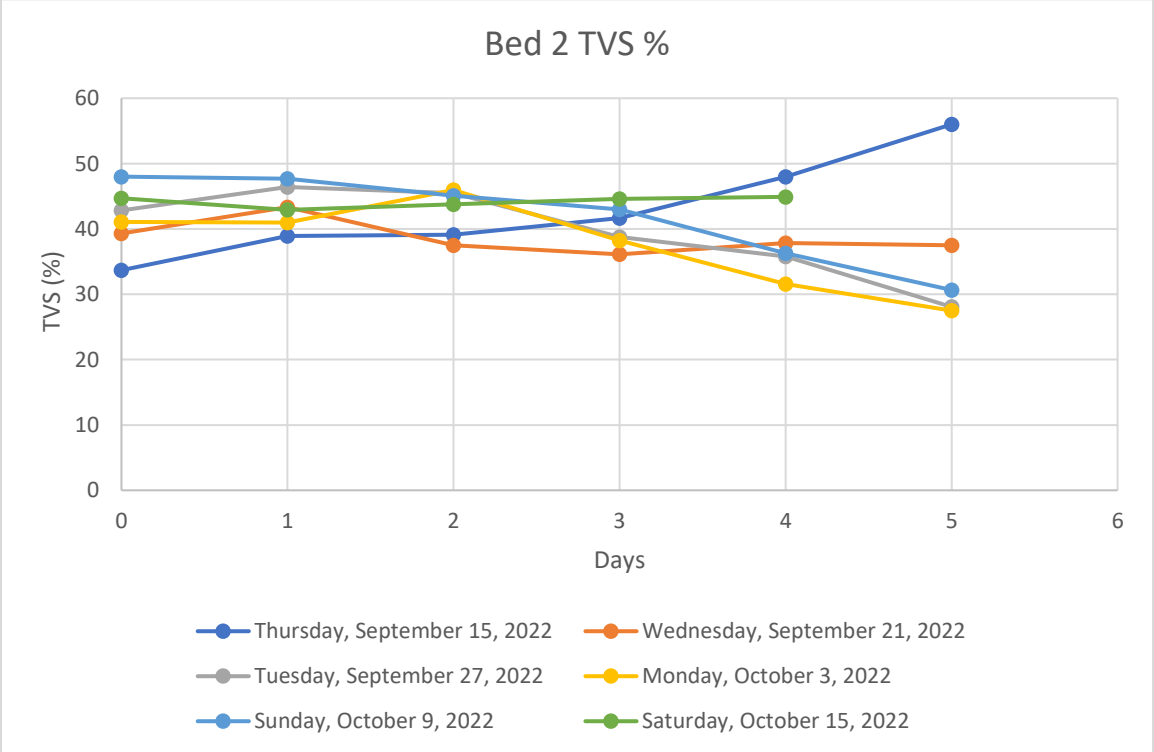

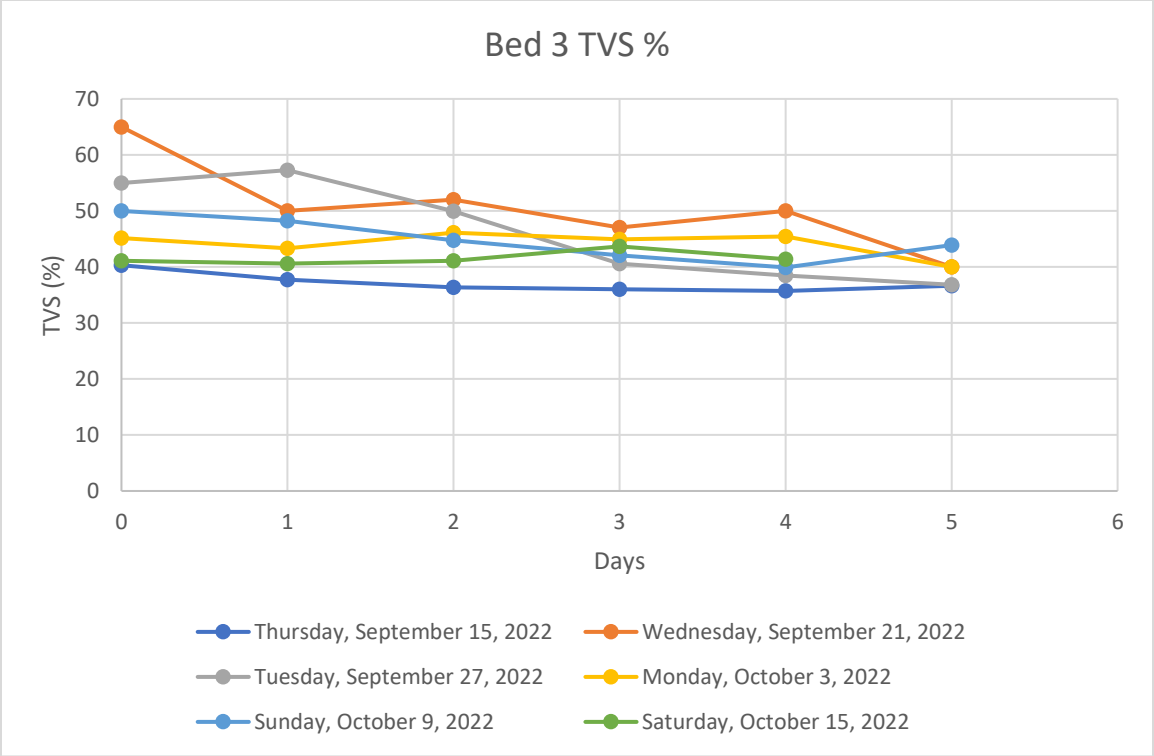
Bed 3 TVS %
TVS (%)
Days
0
10
20
30
40
50
60
70
0
1
2
3
4
5
6
Thursday, September 15, 2022
Wednesday, September 21, 2022
Tuesday, September 27, 2022
Monday, October 3, 2022
Sunday, October 9, 2022
Saturday, October 15, 2022

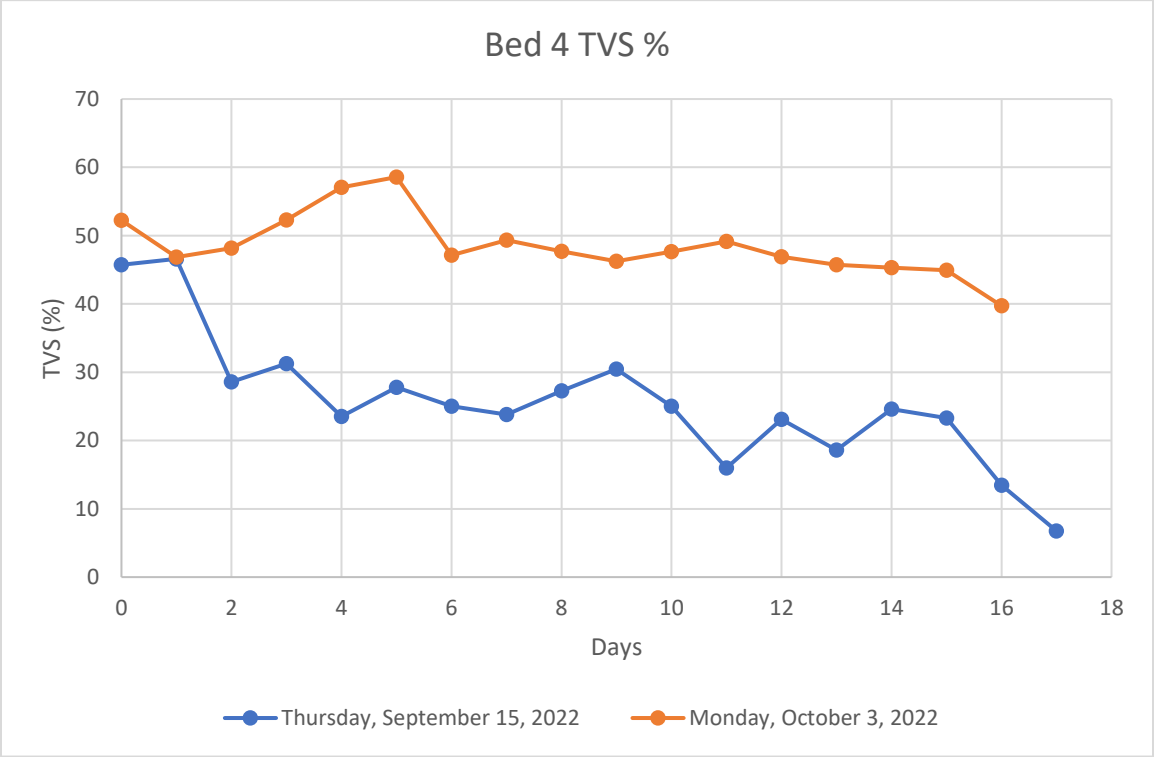
Bed 4 TVS %
TVS (%)
Days
0
10
20
30
40
50
60
70
0
2
4
6
8
10
12
14
16
18
Thursday, September 15, 2022
Monday, October 3, 2022

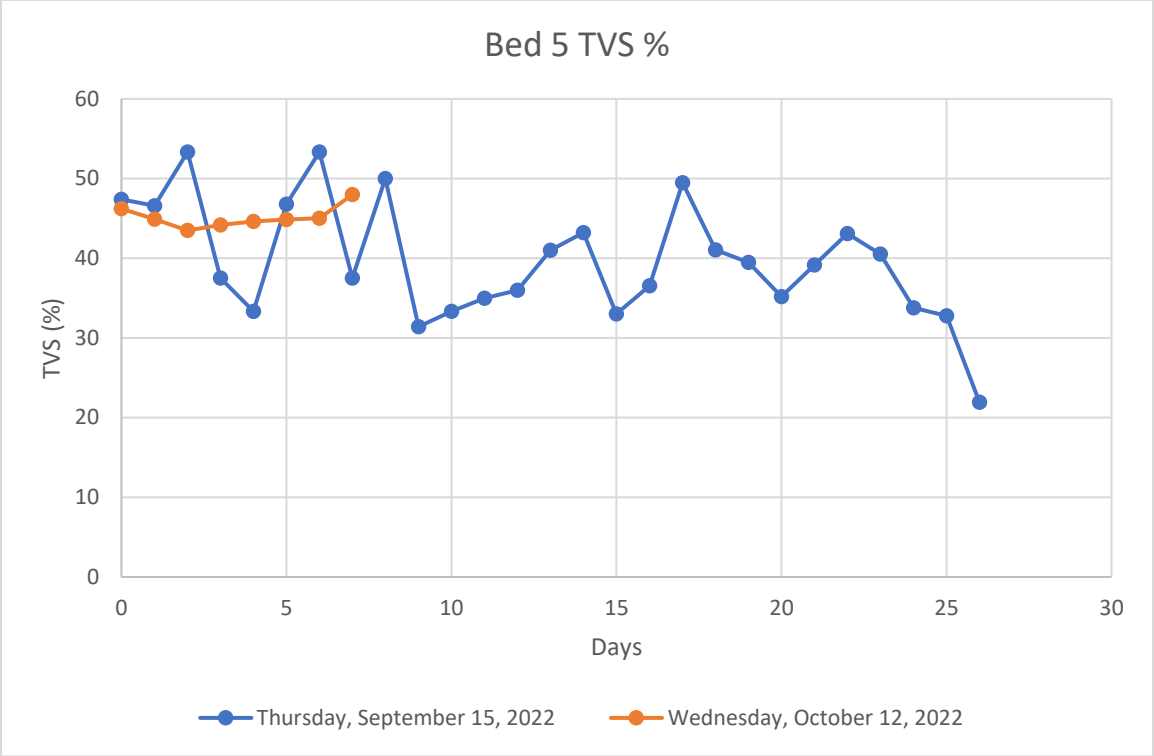
Bed 5 TVS %
TVS (%)
Days
0
10
20
30
40
50
60
0
5
10
15
20
25
30
Thursday, September 15, 2022
Wednesday, October 12, 2022

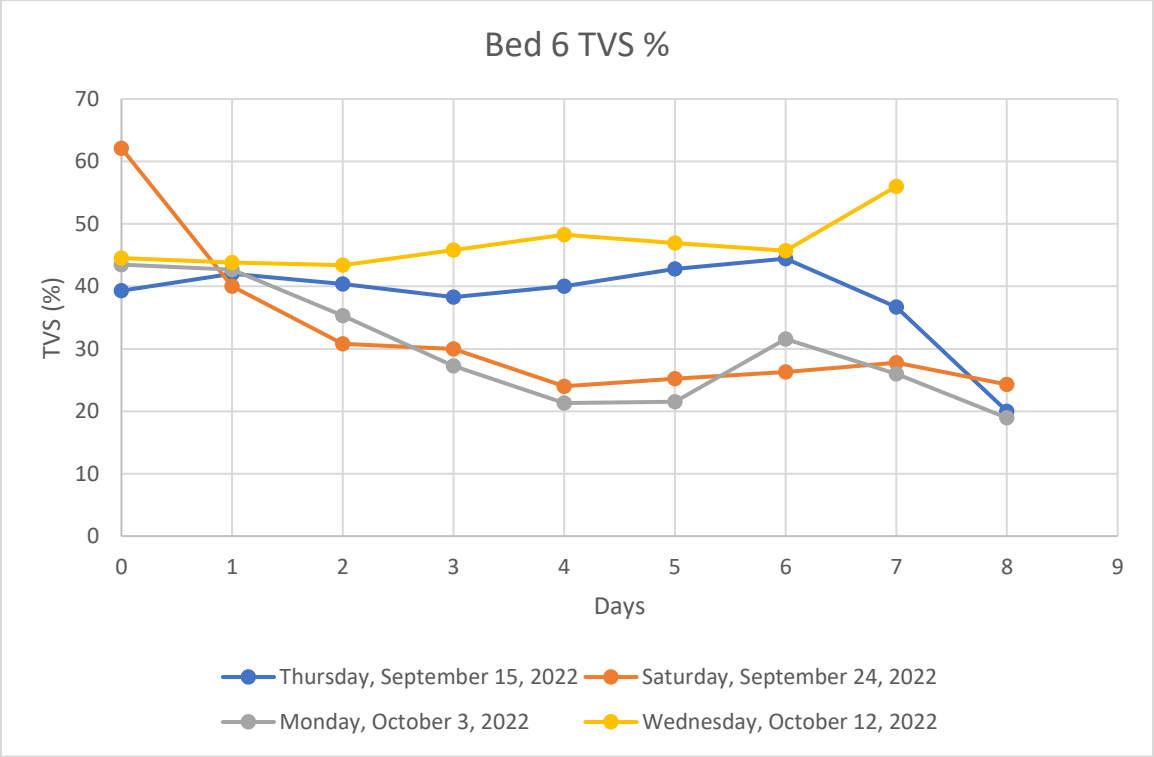
Bed 6 TVS %
TVS (%)
Days
0
10
20
30
40
50
60
70
0
1
2
3
4
5
6
7
8
9
Thursday, September 15, 2022
Saturday, September 24, 2022
Monday, October 3, 2022
Wednesday, October 12, 2022

(f) Effluent COD

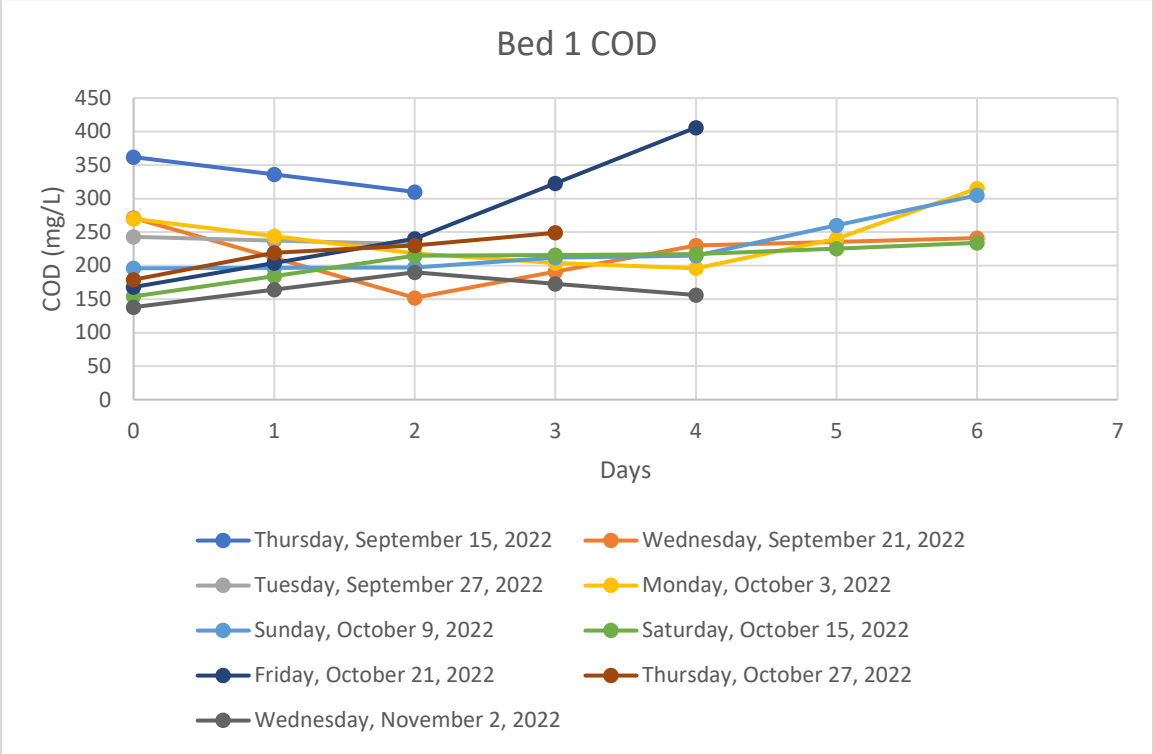

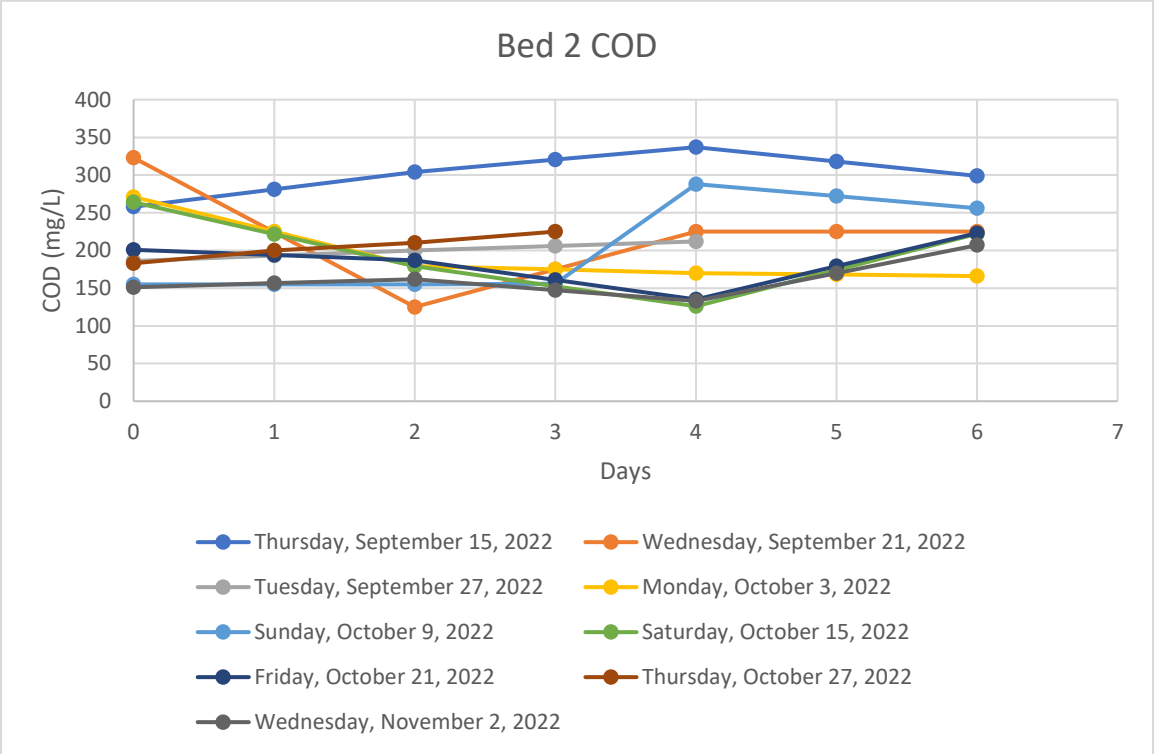

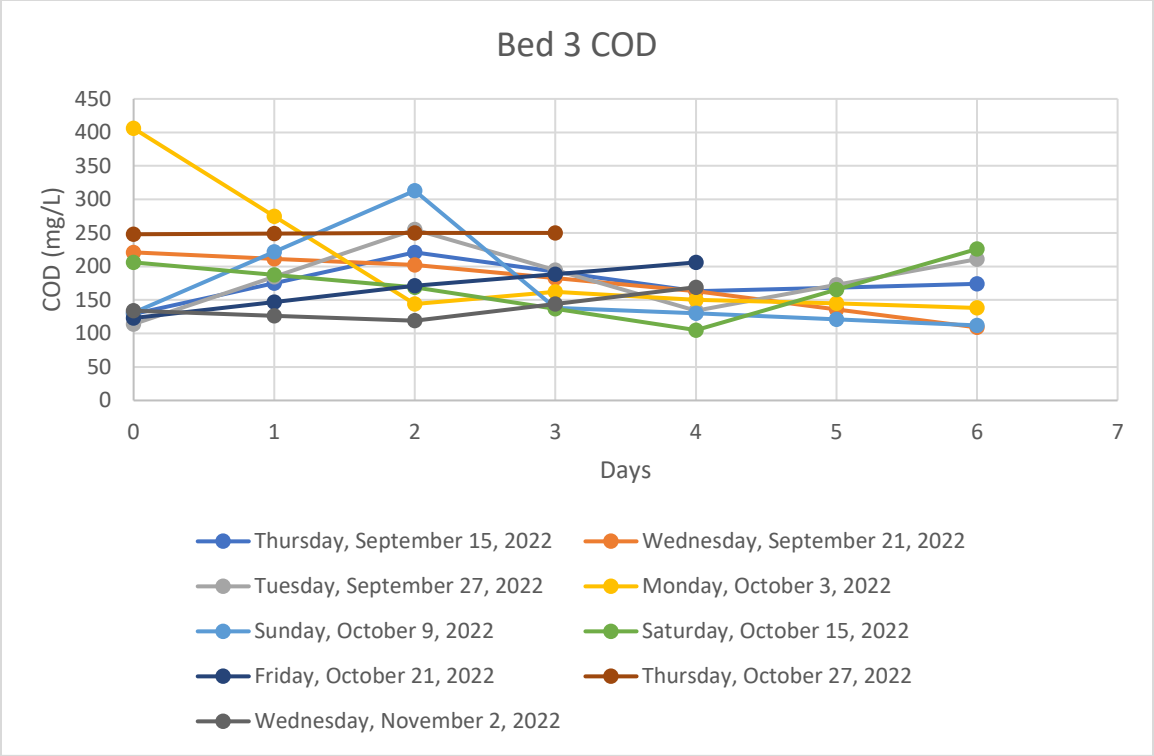
Bed 3 COD
COD (mg/L)
450
400
350
300
250
200
150
100
50
0
0
1
2
3
4
5
6
7
Days
Thursday, September 15, 2022
Wednesday, September 21, 2022
Tuesday, September 27, 2022
Monday, October 3, 2022
Sunday, October 9, 2022
Saturday, October 15, 2022
Friday, October 21, 2022
Thursday, October 27, 2022
Wednesday, November 2, 2022

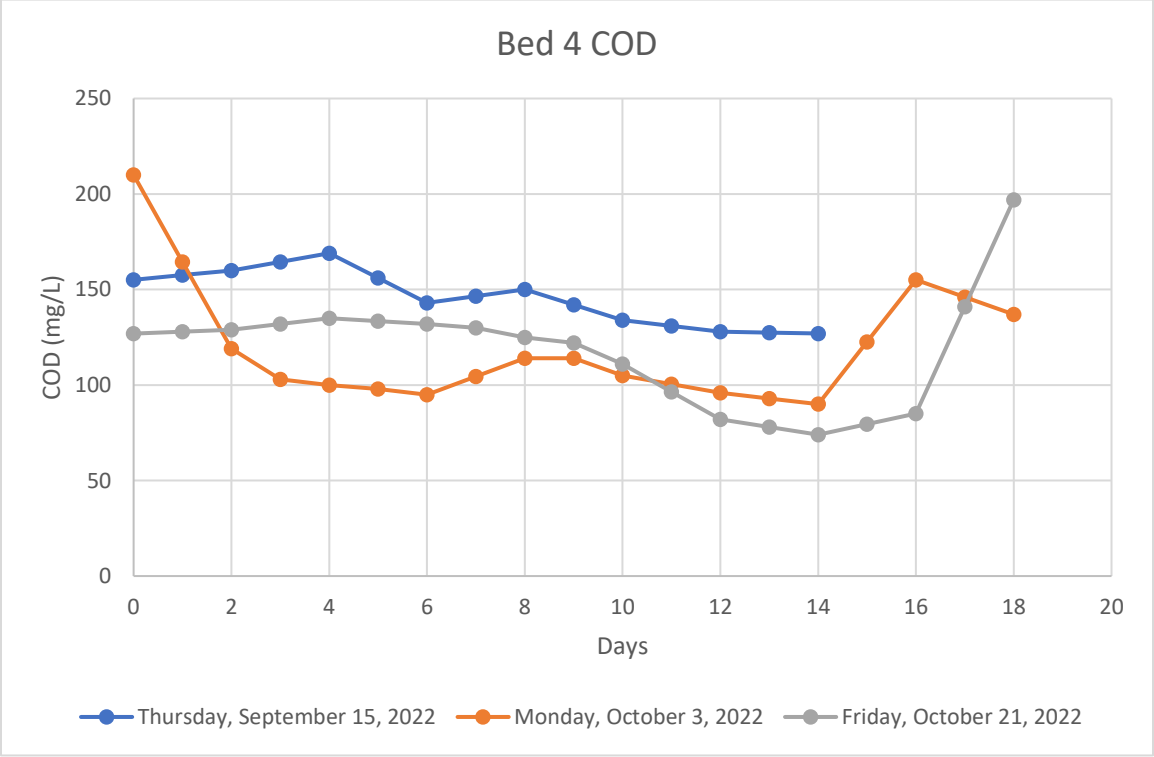
Bed 4 COD
COD (mg/L)
250
200
150
100
50
0
0
2
4
6
8
10
12
14
16
18
20
Days
Thursday, September 15, 2022
Monday, October 3, 2022
Friday, October 21, 2022

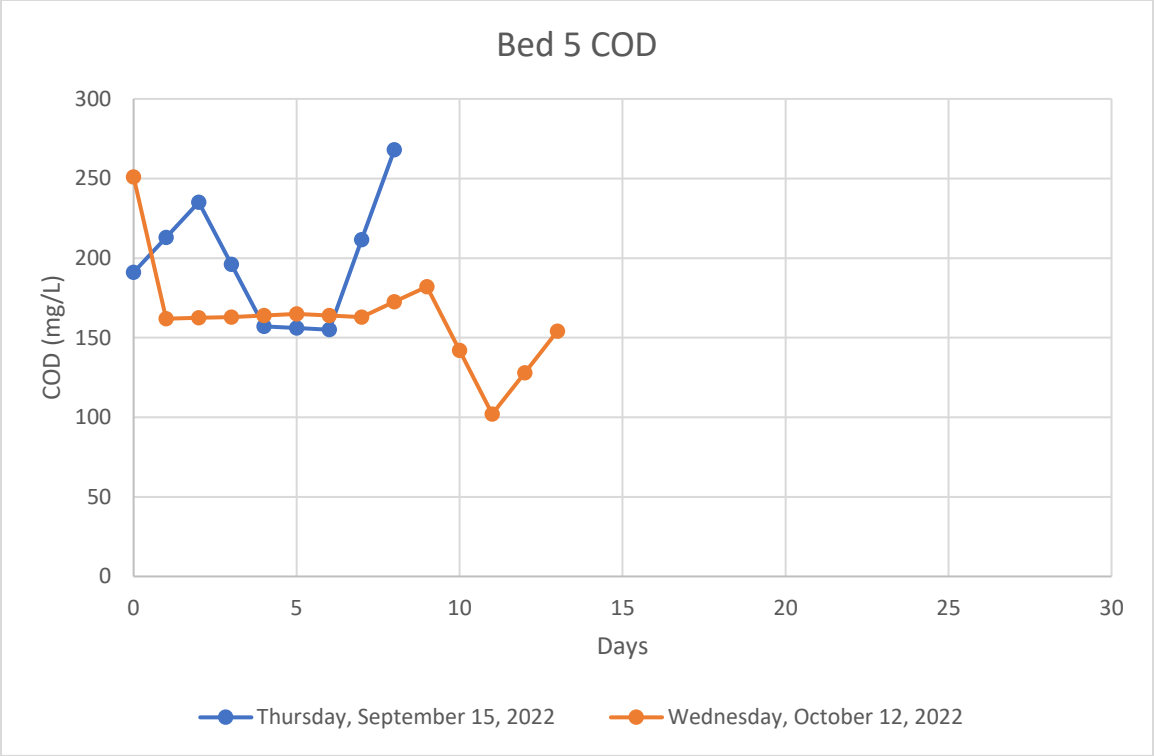
Bed 5 COD
COD (mg/L)
300
250
200
150
100
50
0
0
5
10
15
20
25
30
Days
Thursday, September 15, 2022
Wednesday, October 12, 2022

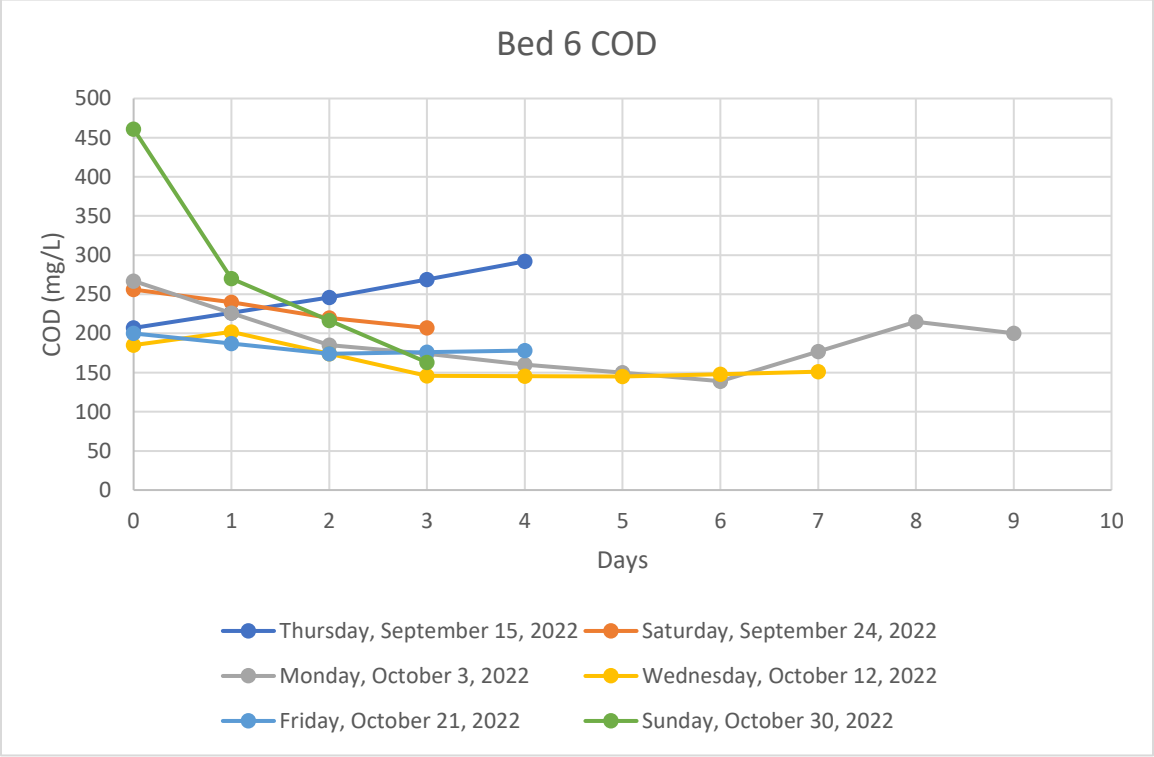
Bed 6 COD
COD (mg/L)
500
450
400
350
300
250
200
150
100
50
0
0
1
2
3
4
5
6
7
8
9
10
Days
Thursday, September 15, 2022
Saturday, September 24, 2022
Monday, October 3, 2022
Wednesday, October 12, 2022
Friday, October 21, 2022
Sunday, October 30, 2022

(g) Effluent NO_3

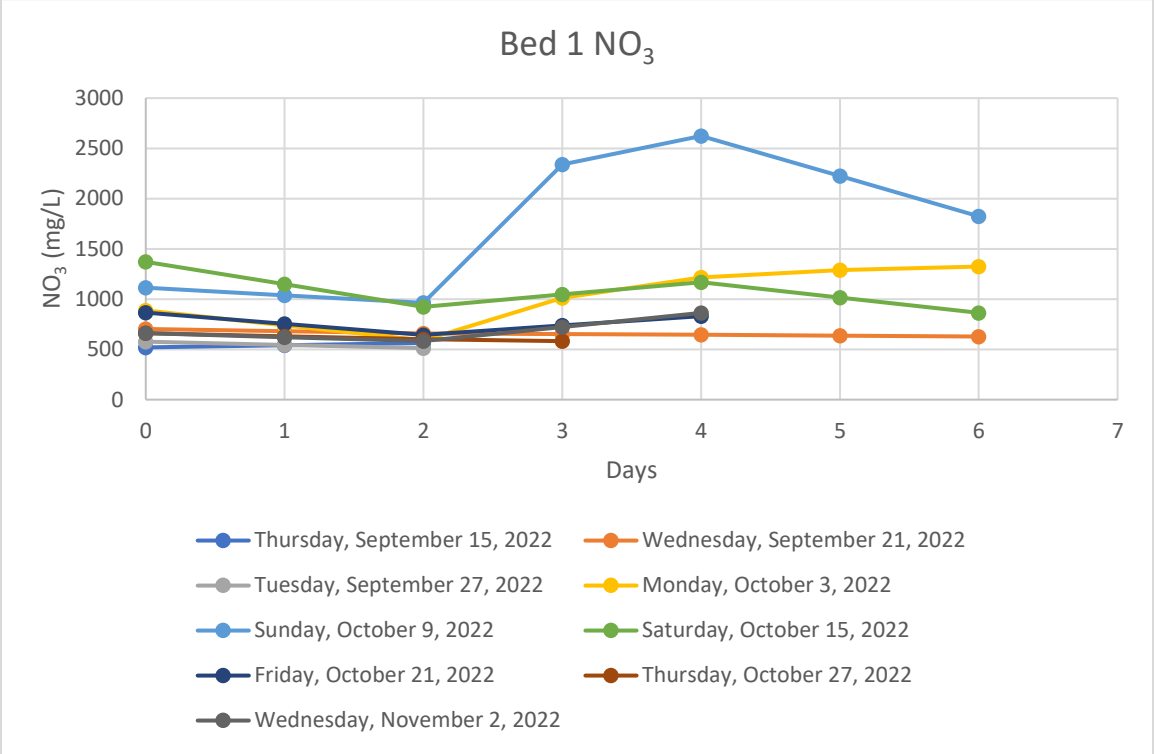

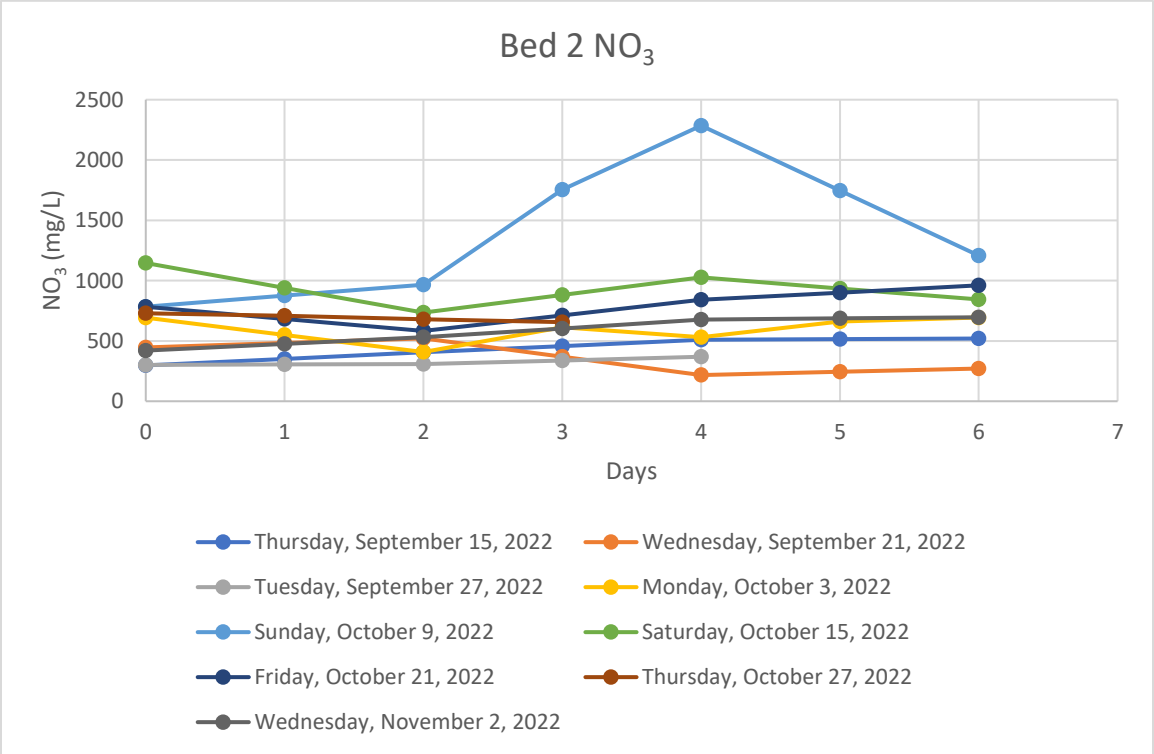

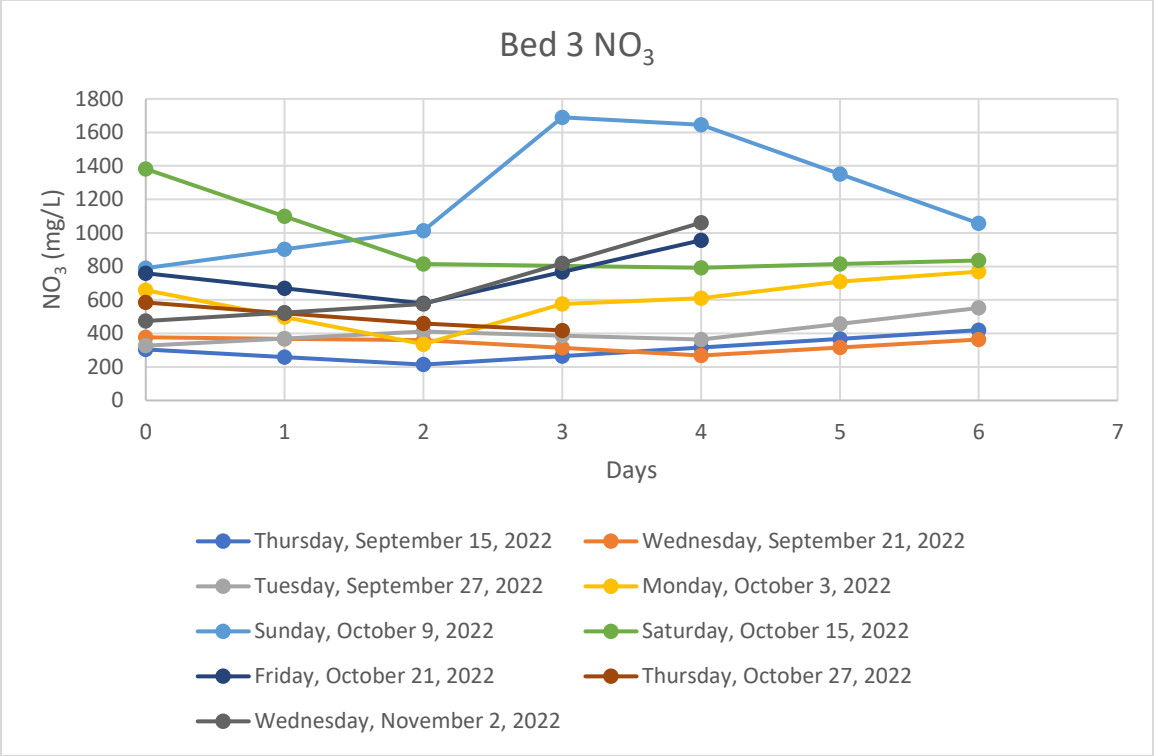
Bed 3 NO3
NO3 (mg/L)
1800
1600
1400
1200
1000
800
600
400
200
0
0
1
2
3
4
5
6
7
Days
Thursday, September 15, 2022
Wednesday, September 21, 2022
Tuesday, September 27, 2022
Monday, October 3, 2022
Sunday, October 9, 2022
Saturday, October 15, 2022
Friday, October 21, 2022
Thursday, October 27, 2022
Wednesday, November 2, 2022

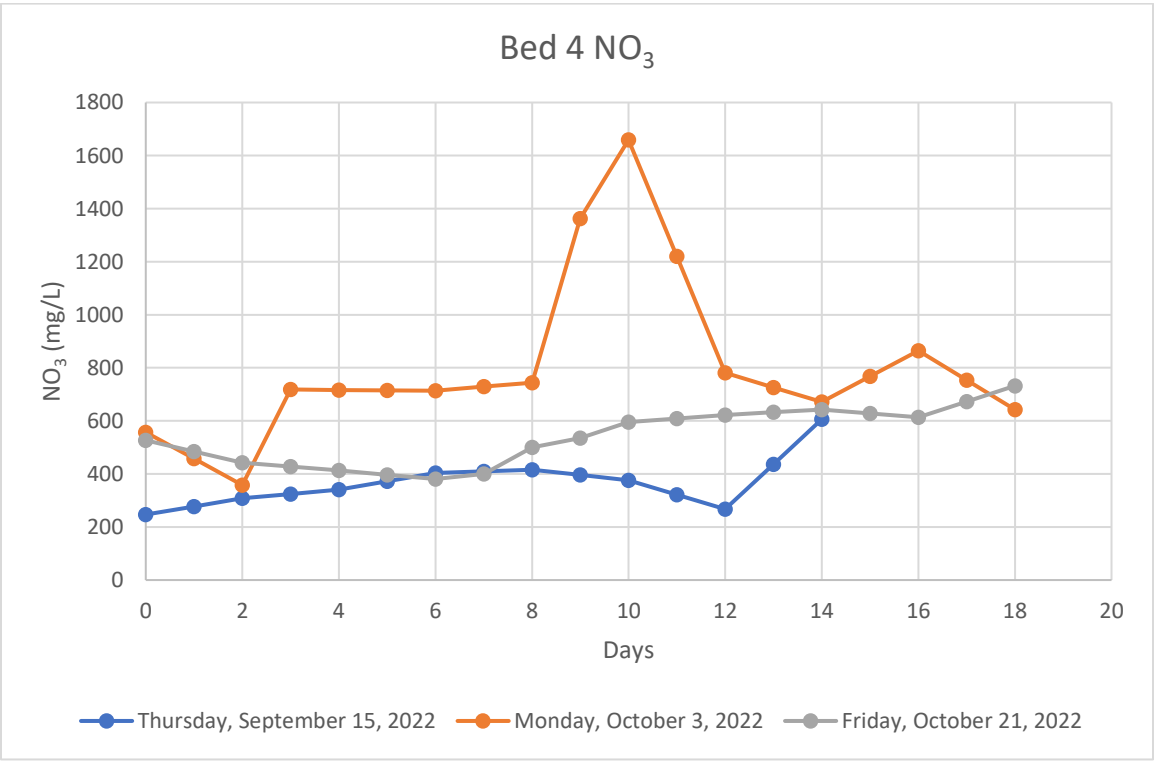
Bed 4 NO3
NO3 (mg/L)
1800
1600
1400
1200
1000
800
600
400
200
0
0
2
4
6
8
10
12
14
16
18
20
Days
Thursday, September 15, 2022
Monday, October 3, 2022
Friday, October 21, 2022

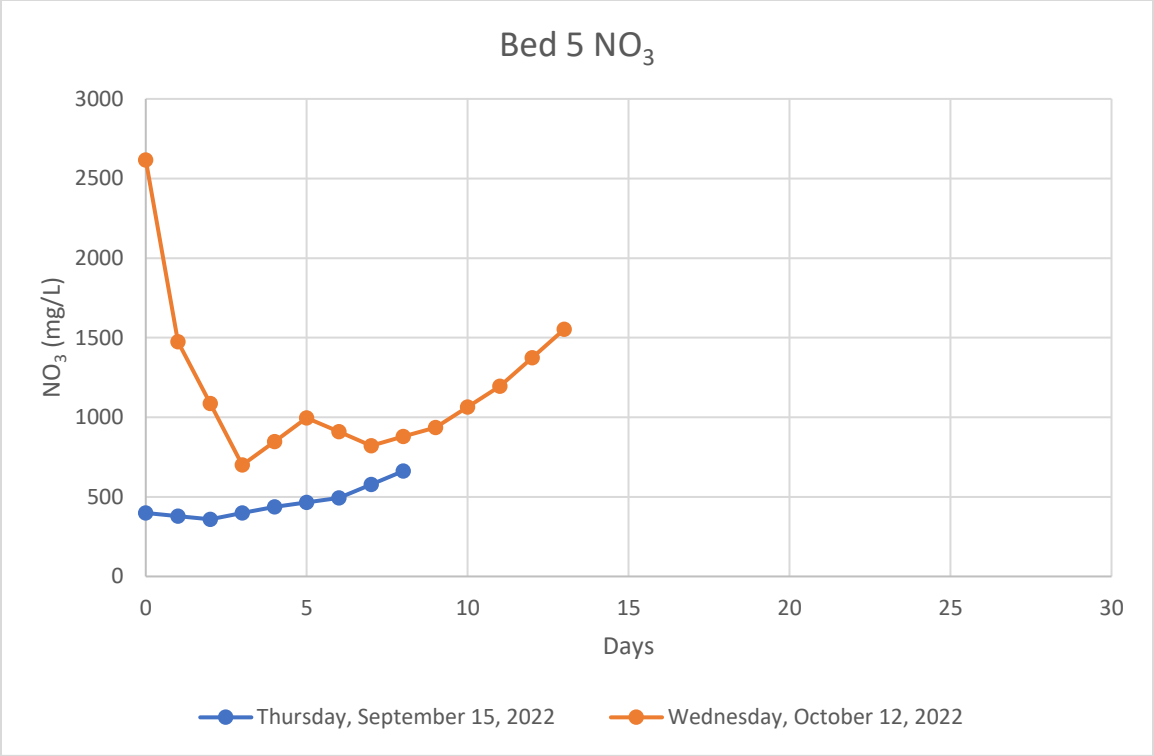
Bed 5 NO3
3000
2500
2000
1500
1000
500
0
NO3 (mg/L)
0
5
10
15
20
25
30
Days
Thursday, September 15, 2022
Wednesday, October 12, 2022

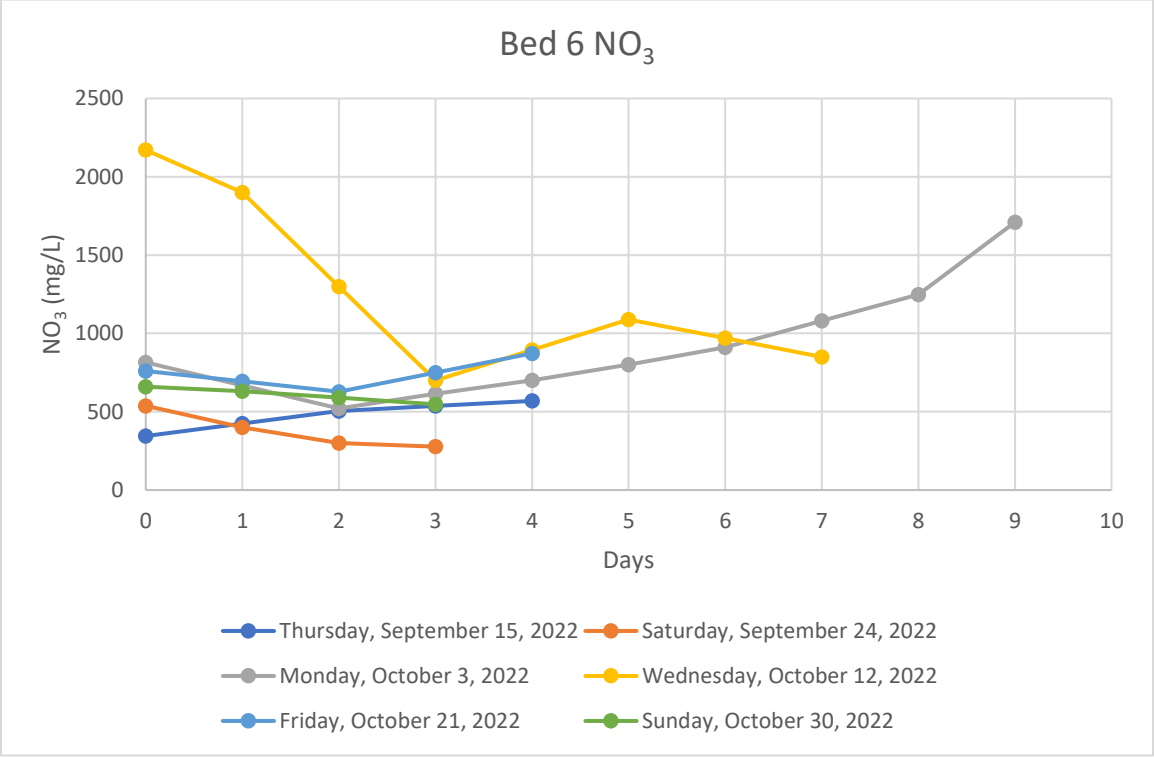
Bed 6 NO3
2500
2000
1500
1000
500
0
NO3 (mg/L)
0
1
2
3
4
5
6
7
8
9
10
Days
Thursday, September 15, 2022
Saturday, September 24, 2022
Monday, October 3, 2022
Wednesday, October 12, 2022
Friday, October 21, 2022
Sunday, October 30, 2022

(h) Effluent pH

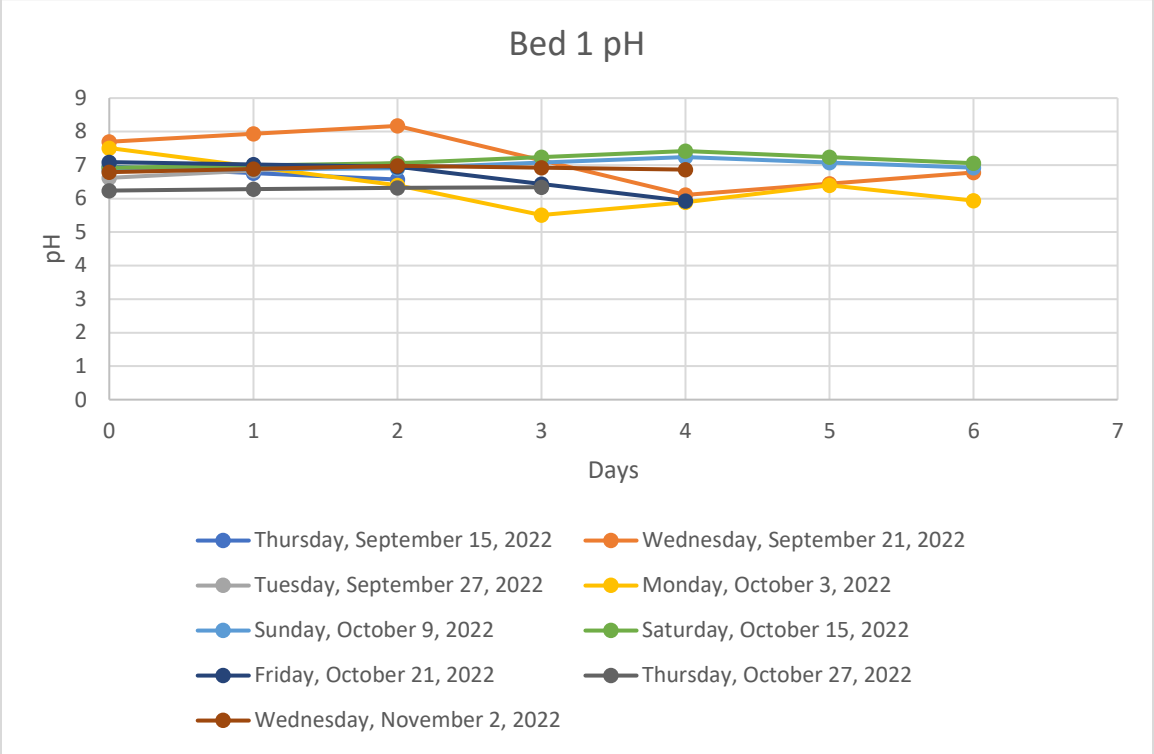

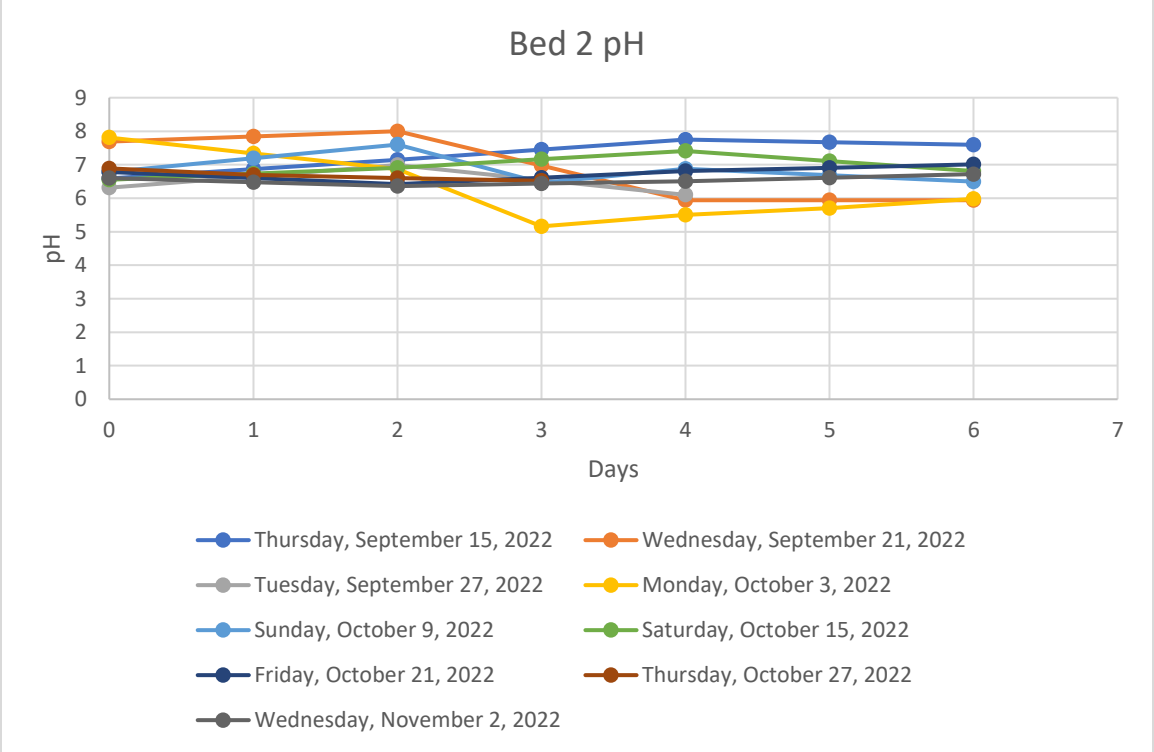

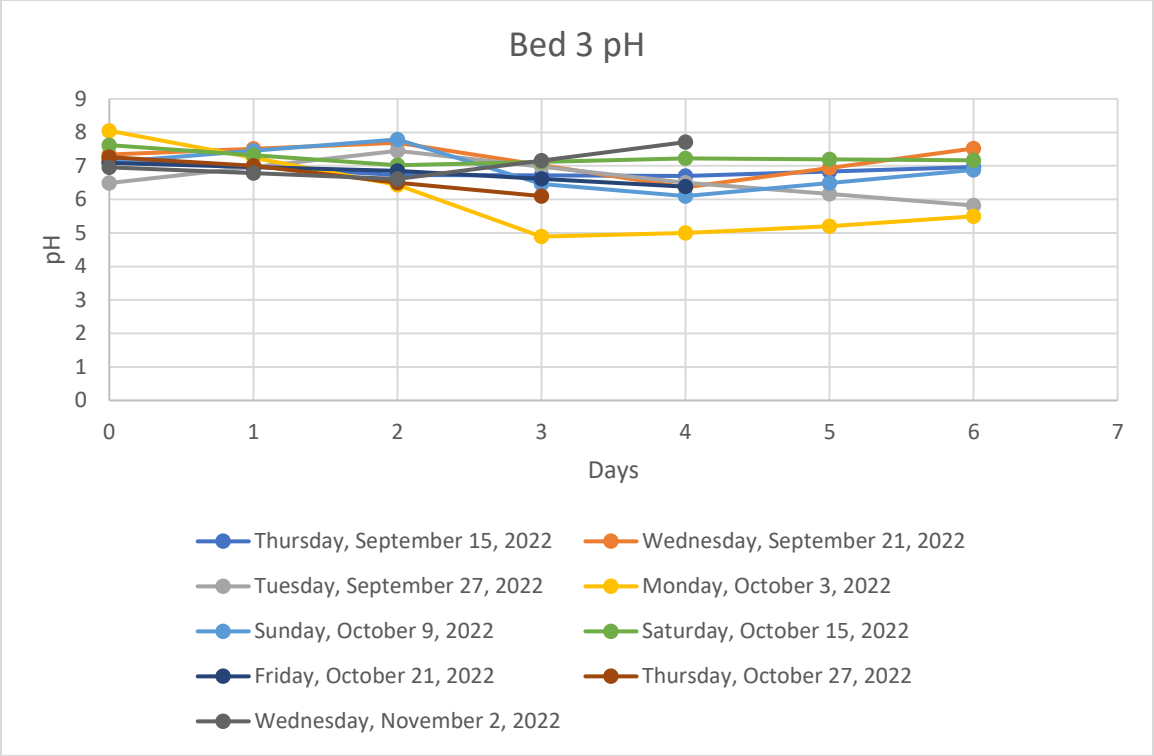
Bed 3 pH
pH
Days
0
1
2
3
4
5
6
7
8
9
Thursday, September 15, 2022
Wednesday, September 21, 2022
Tuesday, September 27, 2022
Monday, October 3, 2022
Sunday, October 9, 2022
Saturday, October 15, 2022
Friday, October 21, 2022
Thursday, October 27, 2022
Wednesday, November 2, 2022

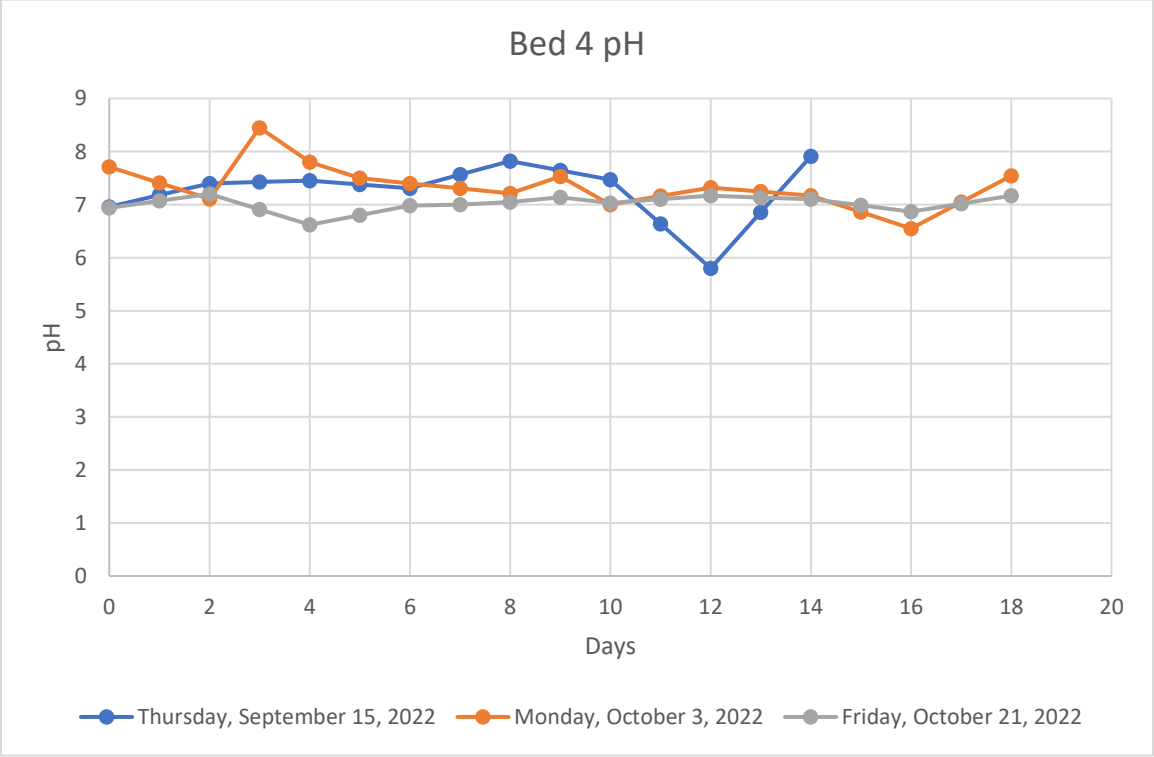
Bed 4 pH
pH
Days
0
2
4
6
8
10
12
14
16
18
20
Thursday, September 15, 2022
Monday, October 3, 2022
Friday, October 21, 2022

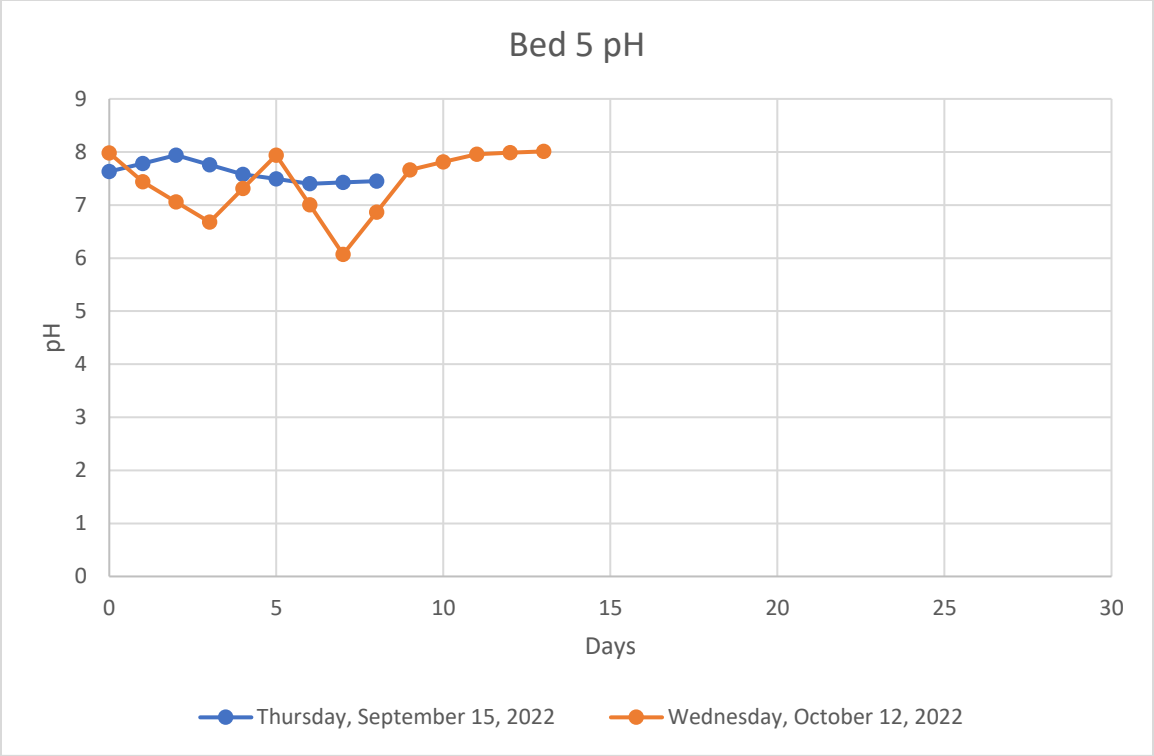
Bed 5 pH
pH
Days
0
1
2
3
4
5
6
7
8
9
0
5
10
15
20
25
30
Thursday, September 15, 2022
Wednesday, October 12, 2022

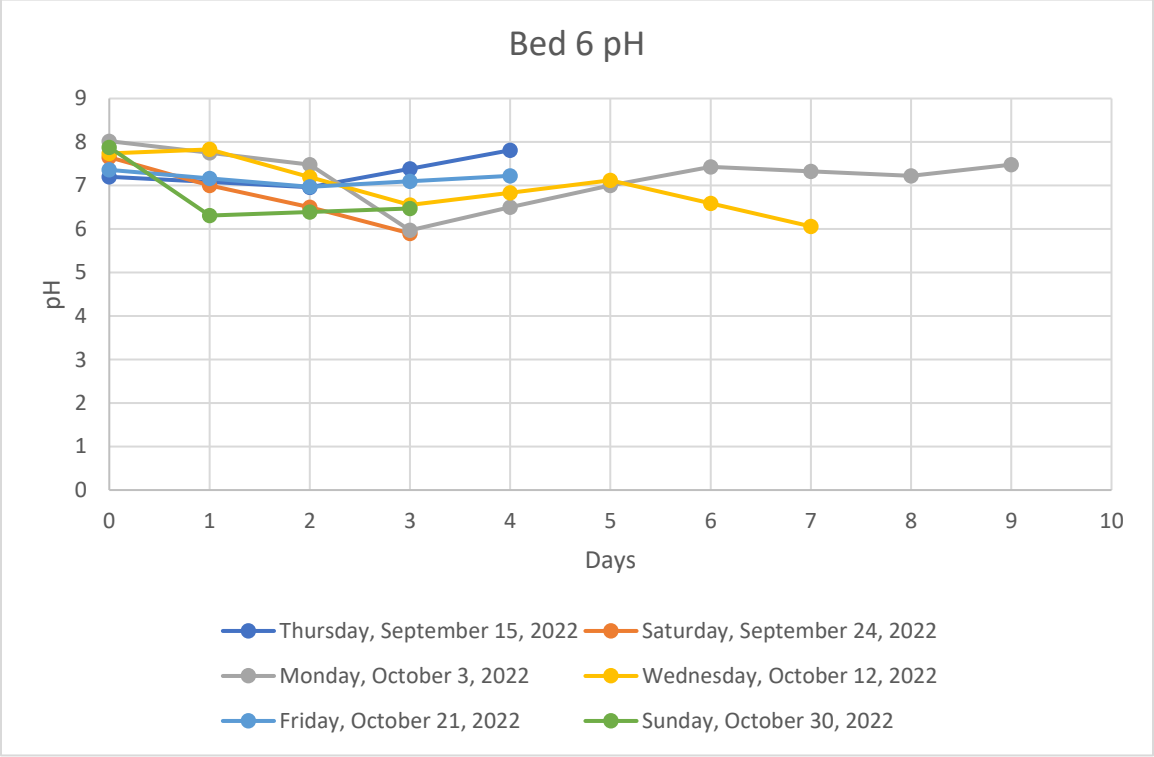
Bed 6 pH
pH
Days
0
1
2
3
4
5
6
7
8
9
10
Thursday, September 15, 2022
Saturday, September 24, 2022
Monday, October 3, 2022
Wednesday, October 12, 2022
Friday, October 21, 2022
Sunday, October 30, 2022

(i) Effluent DO

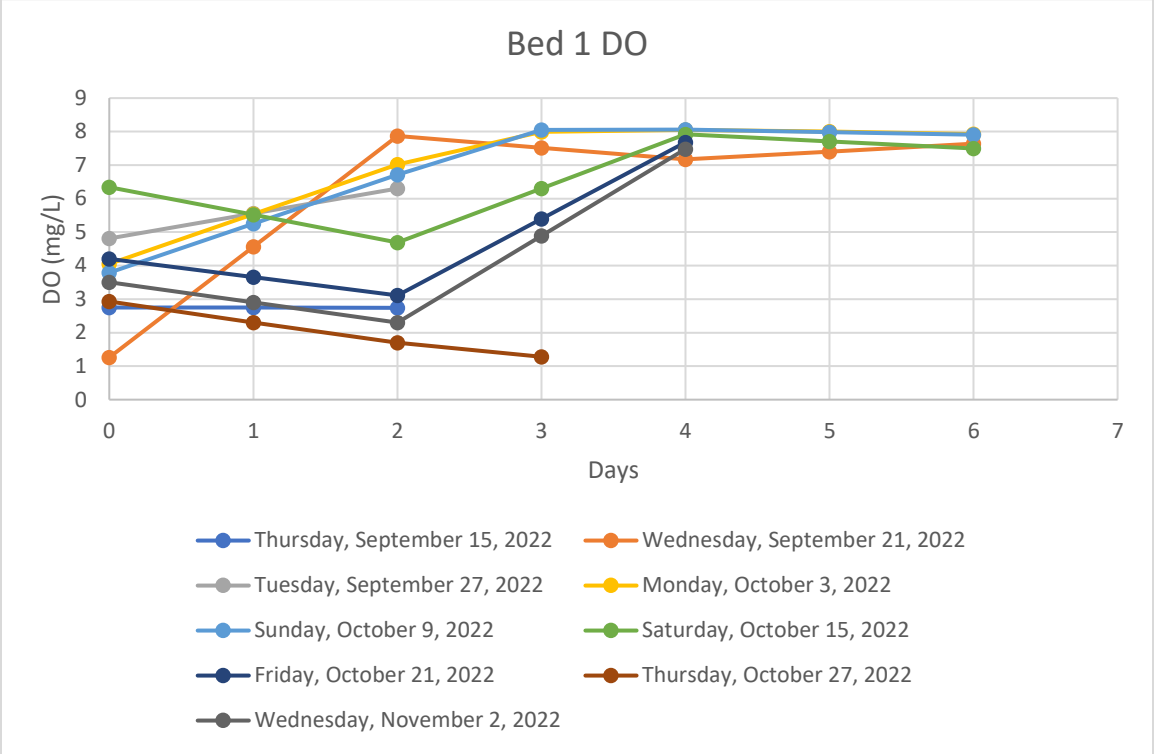

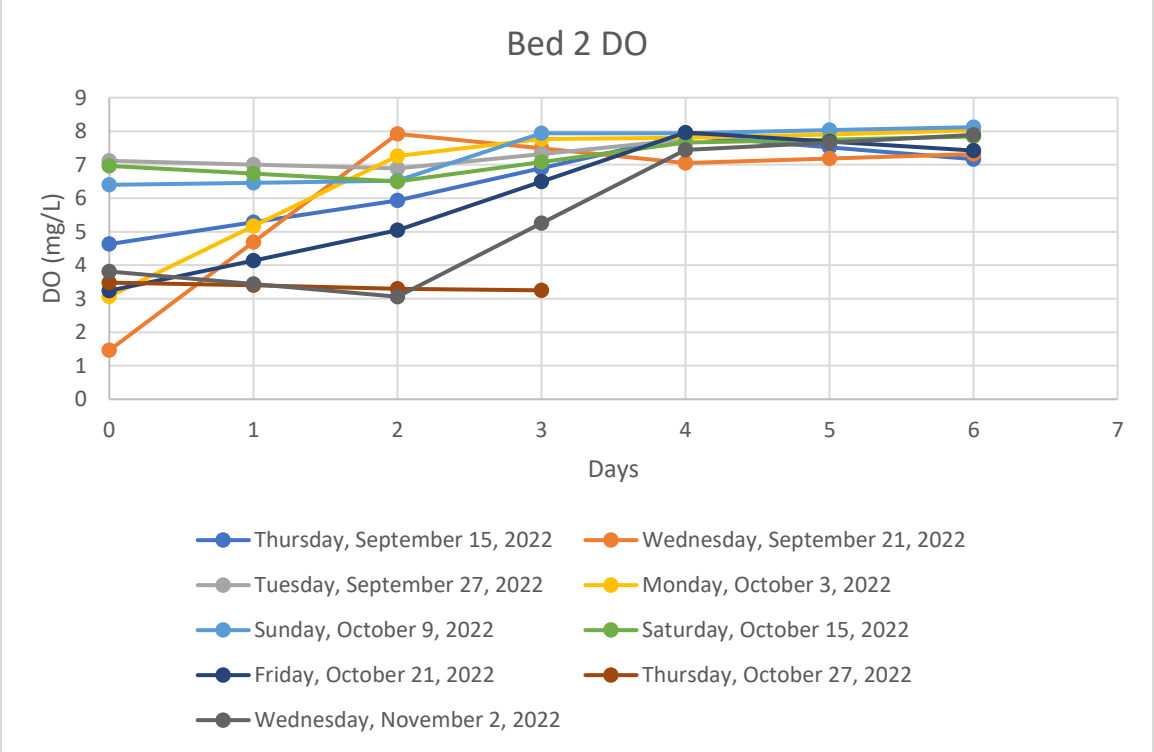

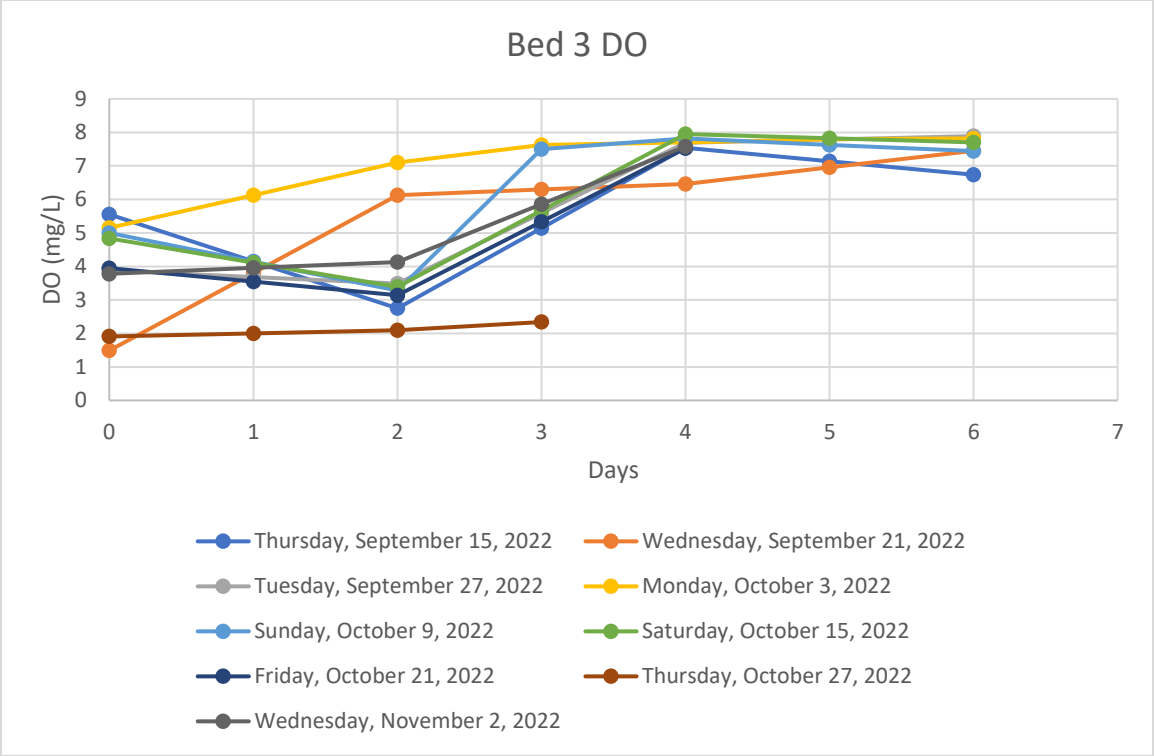
Bed 3 DO
DO (mg/L)
Days
Thursday, September 15, 2022
Wednesday, September 21, 2022
Tuesday, September 27, 2022
Monday, October 3, 2022
Sunday, October 9, 2022
Saturday, October 15, 2022
Friday, October 21, 2022
Thursday, October 27, 2022
Wednesday, November 2, 2022

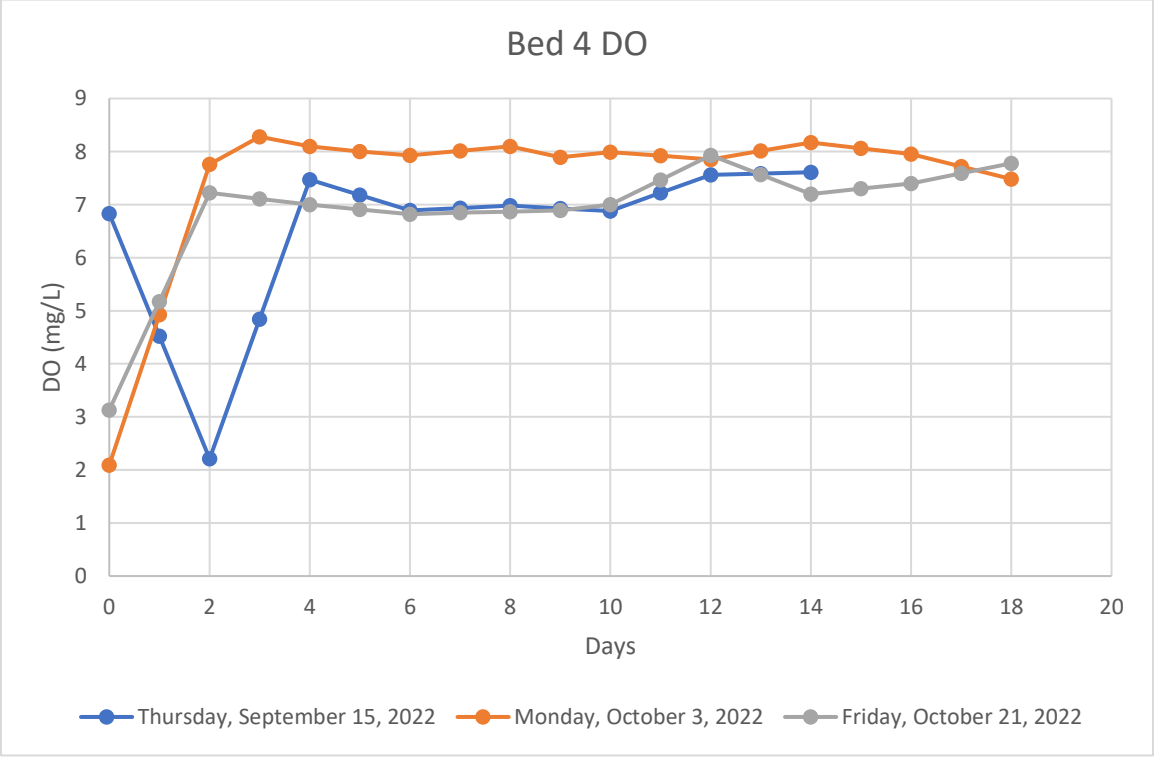
Bed 4 DO
DO (mg/L)
Days
Thursday, September 15, 2022
Monday, October 3, 2022
Friday, October 21, 2022

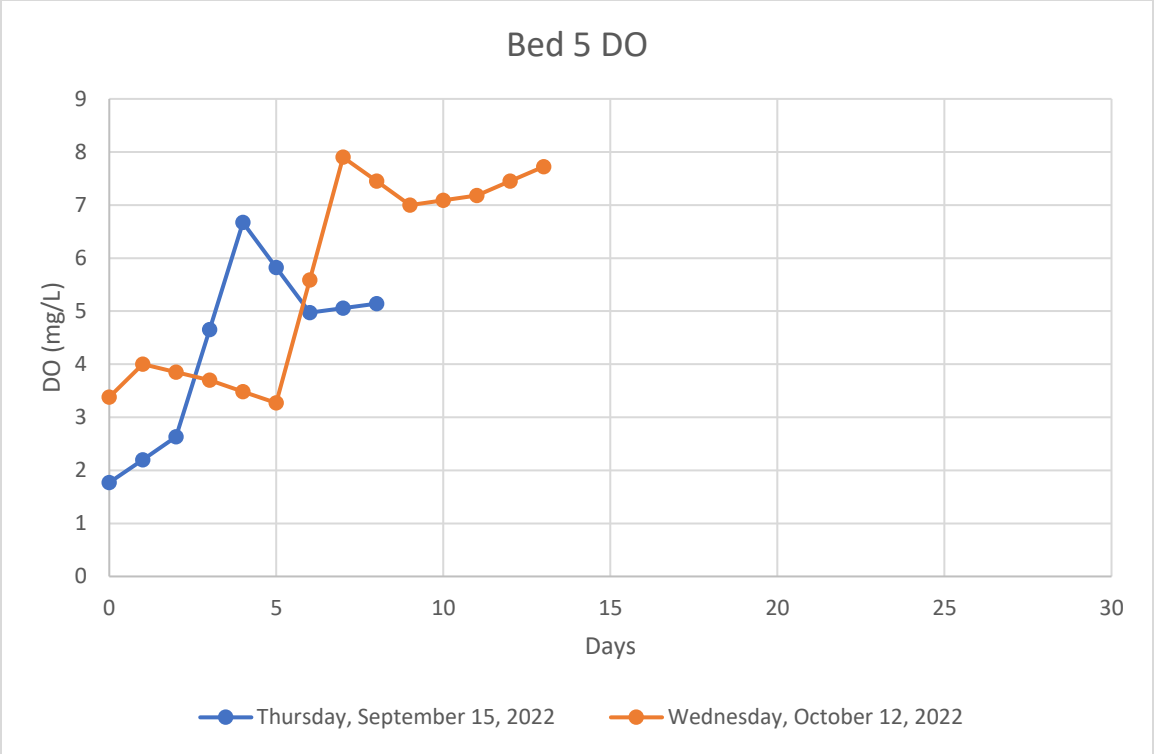
Bed 5 DO
DO (mg/L)
Days
Thursday, September 15, 2022
Wednesday, October 12, 2022

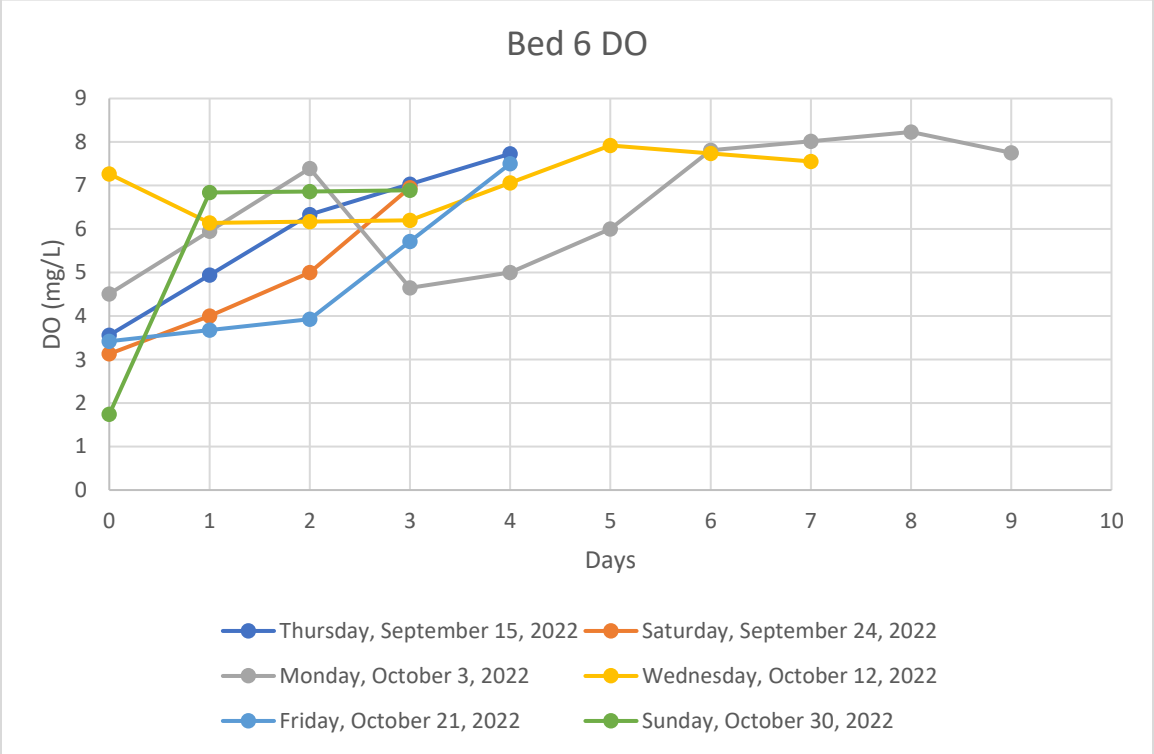
Bed 6 DO
DO (mg/L)
Days
Thursday, September 15, 2022
Saturday, September 24, 2022
Monday, October 3, 2022
Wednesday, October 12, 2022
Friday, October 21, 2022
Sunday, October 30, 2022

(j) Effluent TS

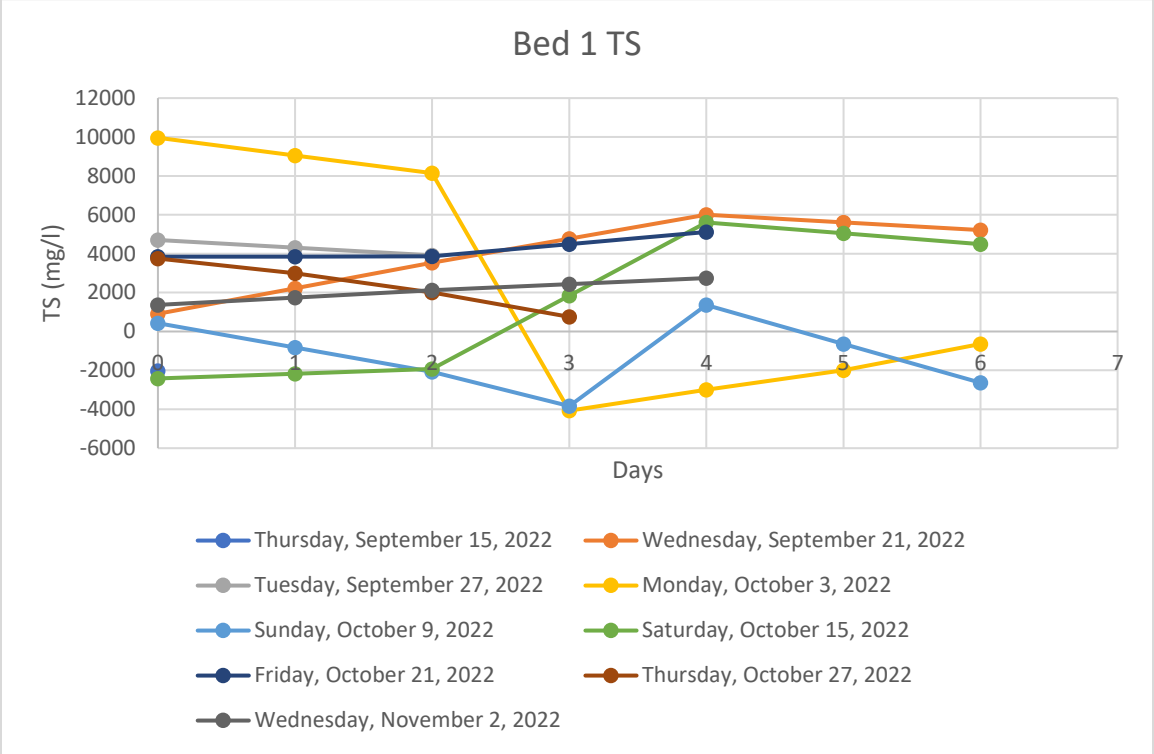

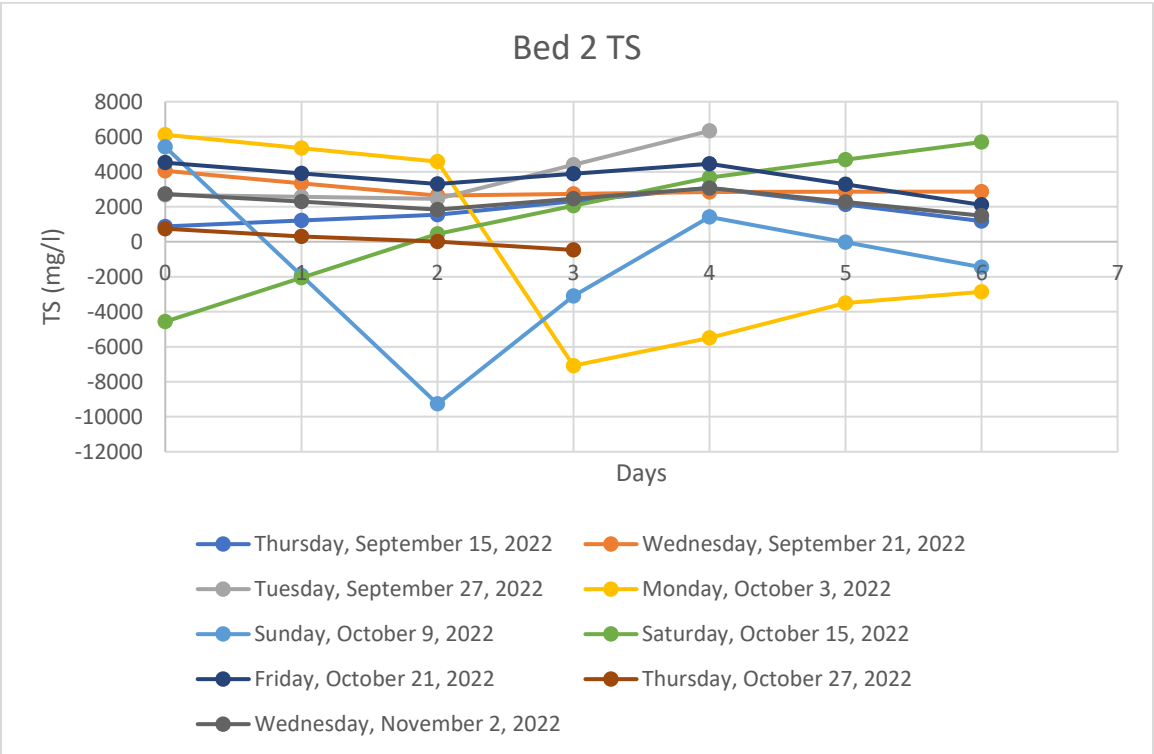

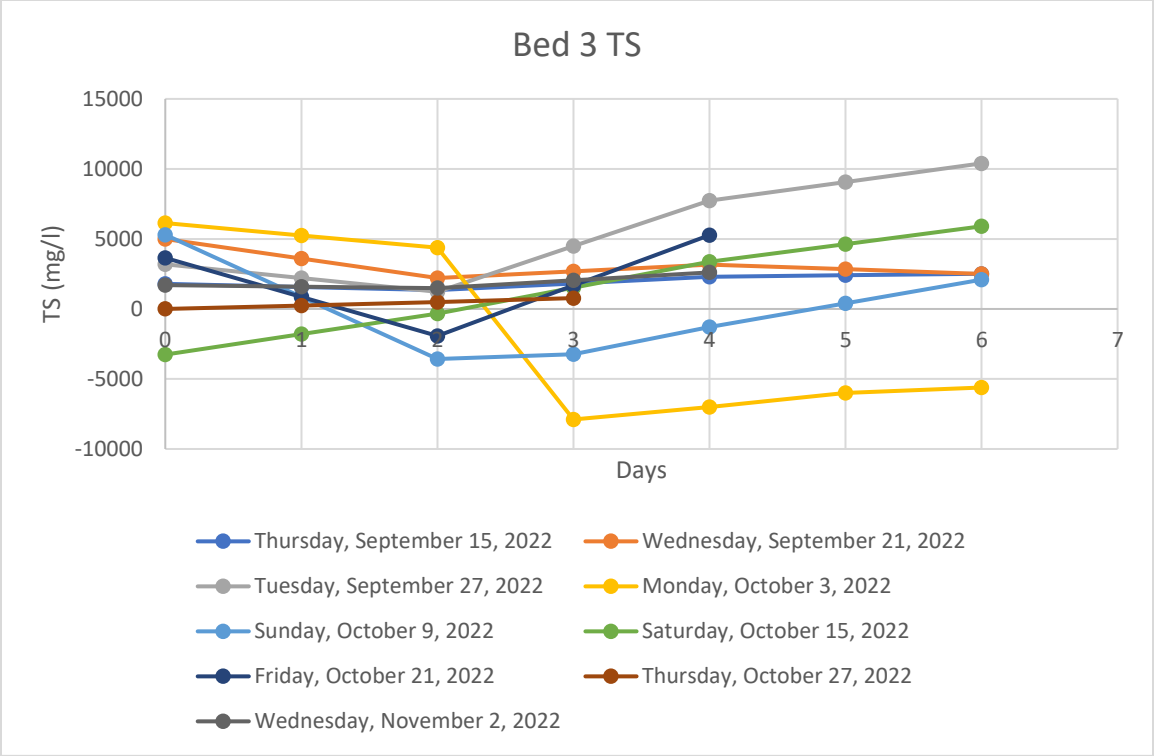
Bed 3 TS
15000
10000
5000
0
-5000
-10000
TS (mg/l)
0
1
2
3
4
5
6
7
Days
Thursday, September 15, 2022
Wednesday, September 21, 2022
Tuesday, September 27, 2022
Monday, October 3, 2022
Sunday, October 9, 2022
Saturday, October 15, 2022
Friday, October 21, 2022
Thursday, October 27, 2022
Wednesday, November 2, 2022

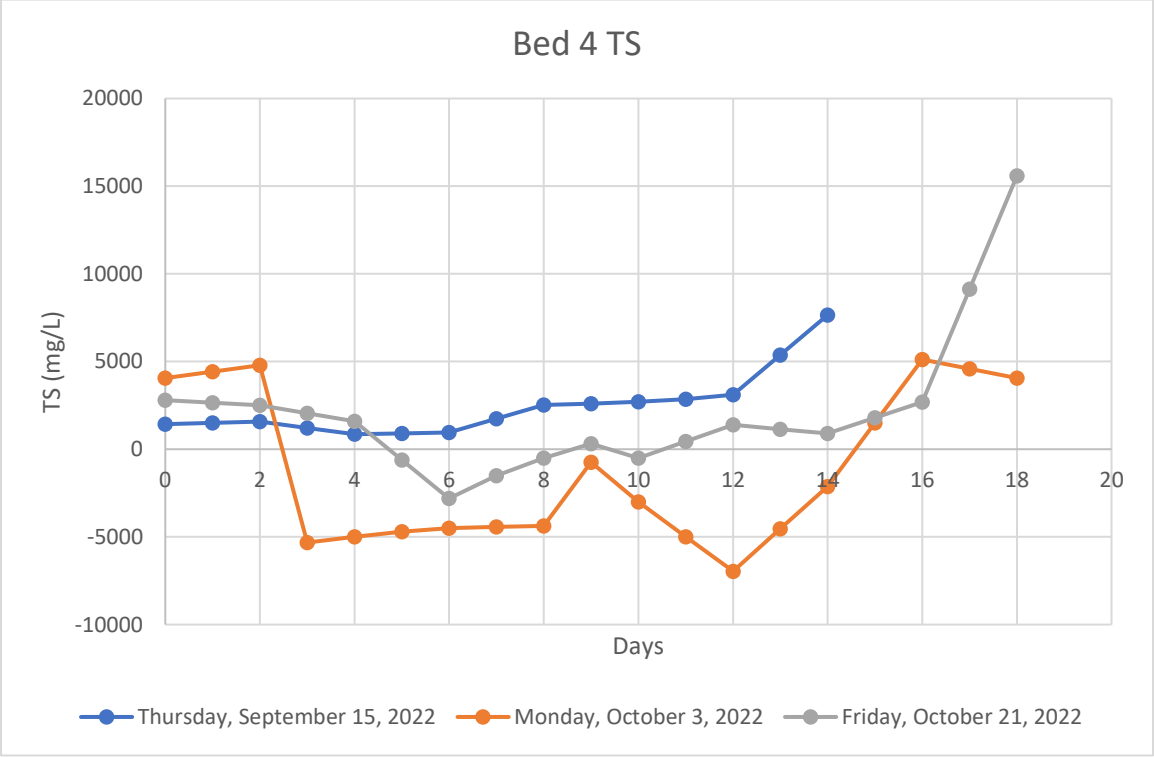
Bed 4 TS
20000
15000
10000
5000
0
-5000
-10000
TS (mg/L)
0
2
4
6
8
10
12
14
16
18
20
Days
Thursday, September 15, 2022
Monday, October 3, 2022
Friday, October 21, 2022

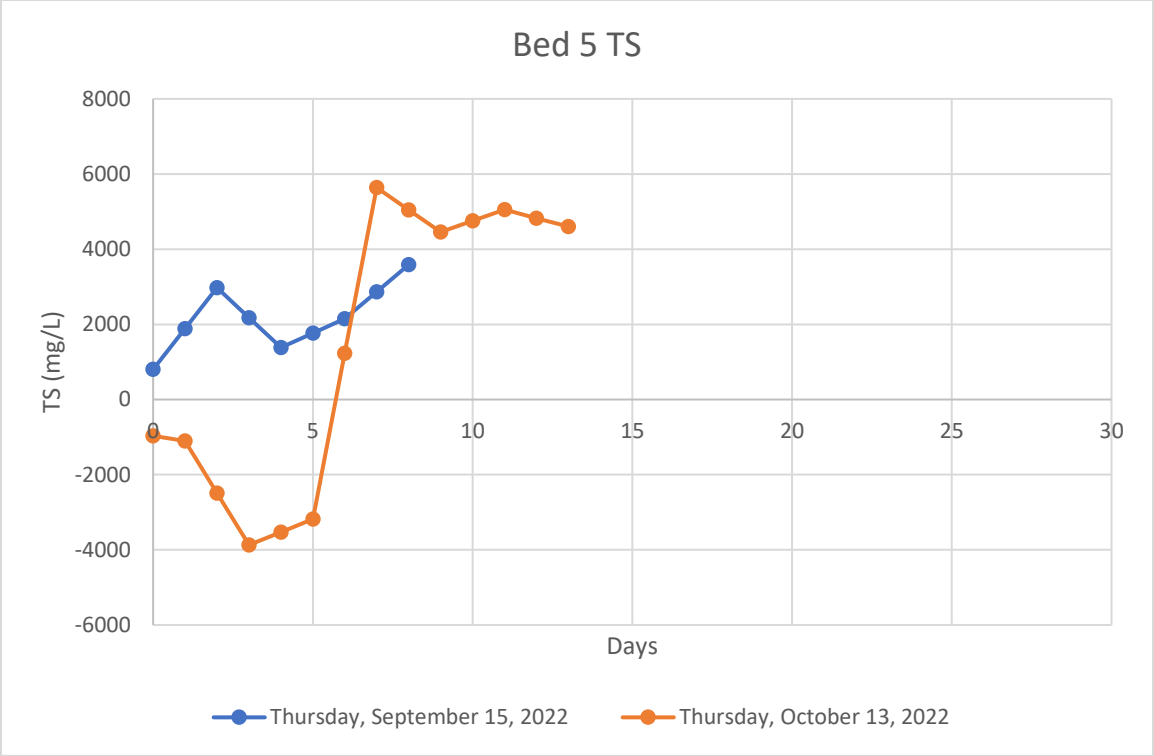
Bed 5 TS
8000
6000
4000
2000
0
-2000
-4000
-6000
TS (mg/L)
0
5
10
15
20
25
30
Days
Thursday, September 15, 2022
Thursday, October 13, 2022

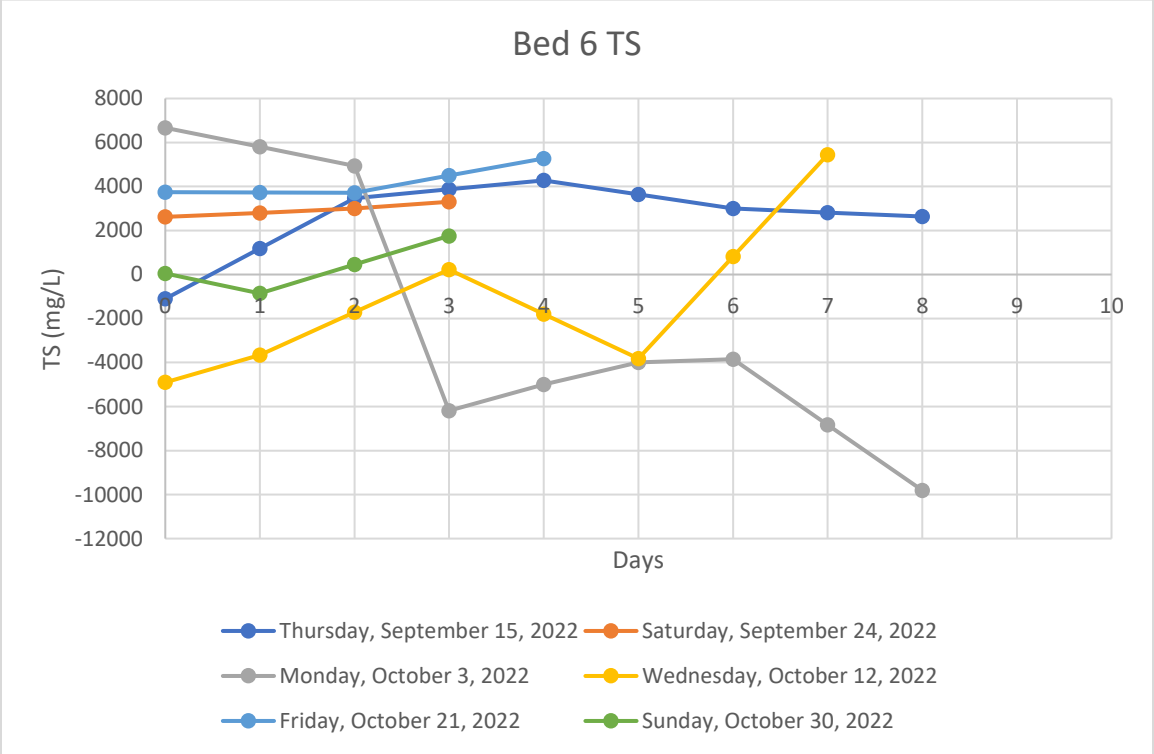
Bed 6 TS
8000
6000
4000
2000
0
-2000
-4000
-6000
-8000
-10000
-12000
TS (mg/L)
0
1
2
3
4
5
6
7
8
9
10
Days
Thursday, September 15, 2022
Saturday, September 24, 2022
Monday, October 3, 2022
Wednesday, October 12, 2022
Friday, October 21, 2022
Sunday, October 30, 2022

Appendix R: ANOVA

(a) Significance of water recovery

Groups	Count	Average (%)	Significance (p-value)	Status
PHASE 1				
50 kg/m^2/year	5	52.87	0.8693	Not significant
100 kg/m^2/year	5	50.11		
150 kg/m^2/year	5	55.29		
3-day	11	56.21	0.4602	Not significant
6-day	5	63.51		
9-day	3	64.45		
PHASE 2				
50 kg/m^2/year	10	78.18	0.7902	Not significant
100 kg/m^2/year	10	82.03		
150 kg/m^2/year	10	81.86		
6-day	10	82.03	0.8961	Not significant
9-day	7	76.93		
18-day	4	79.06		
27-day	3	79.98		
OVERALL				
Bed 1	15	69.74	0.6265	Not significant
Bed 2	15	71.39		
Bed 3	15	73.00		
Bed 4	15	62.30		
Bed 5	8	69.69		
Bed 6	10	73.18		

(b) Significance of flow delay

Groups	Count	Average (min)	Significance (p-value)	Status
PHASE 1				
50 kg/m^2/year	5	46.4	0.0050	Significant
100 kg/m^2/year	5	154.2		
150 kg/m^2/year	5	94.0		
3-day	11	119.6	0.4431	Not significant
6-day	5	78.8		
9-day	3	96.7		
PHASE 2				
50 kg/m^2/year	10	6.5	0.8307	Not significant
100 kg/m^2/year	10	13.2		
150 kg/m^2/year	10	9.2		
6-day	10	13.2	0.9185	Not significant

9-day	7	9.6		
18-day	4	20.3		
27-day	3	7.3		
OVERALL				
Bed 1	15	19.8	0.0245	Significant
Bed 2	15	60.2		
Bed 3	15	37.5		
Bed 4	15	93.1		
Bed 5	8	52.0		
Bed 6	10	35.7		

(c) Significance of flux peaks

Groups	Count	Average (cm/min)	Significance (p-value)	Status
PHASE 1				
50 kg/m^2/year	5	0.0120	0.0194	Significant
100 kg/m^2/year	5	0.0018		
150 kg/m^2/year	5	0.0035		
3-day	11	0.0025	0.0182	Significant
6-day	5	0.0142		
9-day	3	0.0040		
PHASE 2				
50 kg/m^2/year	10	0.2528	0.1394	Not significant
100 kg/m^2/year	10	0.6255		
150 kg/m^2/year	10	0.9606		
6-day	10	0.6255	0.3685	Not significant
9-day	7	0.1824		
18-day	4	0.1454		
27-day	3	0.3930		
OVERALL				
Bed 1	15	0.1726	0.0463	Significant
Bed 2	15	0.4176		
Bed 3	15	0.6416		
Bed 4	15	0.0406		
Bed 5	8	0.1563		
Bed 6	10	0.1289		

(d) Significance of sludge deposit layer thickness

Groups	Count	Average (cm)	Significance (p-value)	Status
PHASE 1				
50 kg/m^2/year	37	8.61	2.28E-17	Significant
100 kg/m^2/year	37	11.82		
150 kg/m^2/year	37	11.27		

3-day	31	9.16	7.14E-05	Significant
6-day	31	8.35		
9-day	31	10.78		
PHASE 2				
50 kg/m^2/year	55	7.48	2.83E-71	Significant
100 kg/m^2/year	55	12.49		
150 kg/m^2/year	55	12.30		
6-day	55	12.49	4.21E-05	Significant
9-day	55	12.79		
18-day	55	16.21		
27-day	55	13.50		
OVERALL				
Bed 1	92	7.94	6.12E-24	Significant
Bed 2	92	12.22		
Bed 3	92	11.88		
Bed 4	86	13.67		
Bed 5	86	11.64		
Bed 6	86	12.07		

(e) Significance of moisture content

Groups	Count	Average (%)	Significance (p-value)	Status
PHASE 1				
50 kg/m^2/year	36	61.43	1.90E-32	Significant
100 kg/m^2/year	36	84.92		
150 kg/m^2/year	36	86.88		
3-day	36	80.85	0.4128	Not significant
6-day	36	80.14		
9-day	36	81.93		
PHASE 2				
50 kg/m^2/year	55	62.60	2.76E-14	Significant
100 kg/m^2/year	55	70.62		
150 kg/m^2/year	55	71.78		
6-day	55	70.62	2.97E-14	Significant
9-day	55	71.03		
18-day	55	82.90		
27-day	55	75.57		
OVERALL				
Bed 1	91	62.14	4.38E-47	Significant
Bed 2	91	76.28		
Bed 3	91	77.76		
Bed 4	91	82.09		
Bed 5	91	77.38		

Bed 6	91	75.34		

(f) Significance of total volatile solids

Groups	Count	Average (%)	Significance (p-value)	Status
PHASE 1				
50 kg/m^2/year	35	30.57	0.0090	Significant
100 kg/m^2/year	35	36.89		
150 kg/m^2/year	35	38.34		
3-day	36	39.58	0.9930	Not significant
6-day	36	39.66		
9-day	36	39.41		
PHASE 2				
50 kg/m^2/year	55	30.55	0.0042	Significant
100 kg/m^2/year	55	33.40		
150 kg/m^2/year	55	36.19		
6-day	55	33.40	5.09E-08	Significant
9-day	55	35.87		
18-day	55	41.98		
27-day	55	40.52		
OVERALL				
Bed 1	90	30.56	1.43E-14	Significant
Bed 2	90	34.75		
Bed 3	90	37.03		
Bed 4	91	41.03		
Bed 5	91	40.18		
Bed 6	91	37.27		

(g) Significance of effluent COD

Groups	Count	Average (mg/L)	Significance (p-value)	Status
PHASE 1				
50 kg/m^2/year	27	416.7	2.38E-16	Significant
100 kg/m^2/year	30	272.6		
150 kg/m^2/year	31	216.3		
3-day	34	236.7	0.4525	Not significant
6-day	31	237.2		
9-day	26	259.5		
PHASE 2				
50 kg/m^2/year	44	224.9	0.0006	Significant
100 kg/m^2/year	52	205.9		
150 kg/m^2/year	51	180.0		
6-day	52	205.9	4.57E-14	Significant
9-day	36	210.0		

18-day	52	126.6		
27-day	24	183.1		
OVERALL				
Bed 1	71	297.8	2.93E-20	Significant
Bed 2	82	230.3		
Bed 3	82	193.7		
Bed 4	86	170.2		
Bed 5	55	213.6		
Bed 6	62	230.8		

(h) Significance of effluent NO_3

Groups	Count	Average (mg/L)	Significance (p-value)	Status
PHASE 1				
50 kg/m^2/year	25	495.4	1.01E-07	Significant
100 kg/m^2/year	30	290.8		
150 kg/m^2/year	31	288.5		
3-day	34	292.4	0.0002	Significant
6-day	31	360.5		
9-day	25	388.7		
PHASE 2				
50 kg/m^2/year	44	904.0	0.0030	Significant
100 kg/m^2/year	52	682.2		
150 kg/m^2/year	51	632.6		
6-day	52	682.2	0.0056	Significant
9-day	36	776.7		
18-day	52	581.0		
27-day	24	890.6		
OVERALL				
Bed 1	69	755.9	2.15E-05	Significant
Bed 2	82	539.0		
Bed 3	82	502.5		
Bed 4	86	466.9		
Bed 5	55	591.8		
Bed 6	61	617.7		

(i) Significance of effluent pH

Groups	Count	Average	Significance (p-value)	Status
PHASE 1				
50 kg/m^2/year	25	6.56	1.02E-05	Significant
100 kg/m^2/year	30	7.04		
150 kg/m^2/year	31	7.13		
3-day	34	6.97	0.0381	Significant

6-day	31	7.26		
9-day	25	7.22		
PHASE 2				
50 kg/m^2/year	44	6.83	0.9512	Not significant
100 kg/m^2/year	52	6.79		
150 kg/m^2/year	51	6.81		
6-day	52	6.79	1.00E-06	Significant
9-day	36	7.07		
18-day	52	7.20		
27-day	24	7.47		
OVERALL				
Bed 1	69	6.73	2.43E-10	Significant
Bed 2	82	6.88		
Bed 3	82	6.93		
Bed 4	86	7.11		
Bed 5	55	7.35		
Bed 6	61	7.13		

(j) Significance of effluent DO

Groups	Count	Average (mg/L)	Significance (p-value)	Status
PHASE 1				
50 kg/m^2/year	25	6.20	0.8196	Not significant
100 kg/m^2/year	30	6.22		
150 kg/m^2/year	31	6.50		
3-day	34	6.21	0.4237	Not significant
6-day	31	6.31		
9-day	25	6.84		
PHASE 2				
50 kg/m^2/year	44	5.30	0.0515	Not significant
100 kg/m^2/year	52	6.17		
150 kg/m^2/year	51	5.35		
6-day	52	6.17	5.62E-05	Significant
9-day	36	5.84		
18-day	52	6.97		
27-day	24	4.98		
OVERALL				
Bed 1	69	5.63	0.0073	Significant
Bed 2	82	6.19		
Bed 3	82	5.78		
Bed 4	86	6.67		
Bed 5	55	5.73		
Bed 6	61	6.25		

(k) Significance of effluent TS

Groups	Count	Average (mg/L)	Significance (p-value)	Status
PHASE 1				
50 kg/m^2/year	11	7130.9	0.0205	Significant
100 kg/m^2/year	16	4787.9		
150 kg/m^2/year	16	3210.4		
3-day	16	4004.9	0.2204	Not significant
6-day	15	4822.9		
9-day	14	3014.1		
PHASE 2				
50 kg/m^2/year	42	3415.8	0.5803	Not significant
100 kg/m^2/year	51	3071.2		
150 kg/m^2/year	50	2983.6		
6-day	51	3071.2	0.2402	Not significant
9-day	52	2712.0		
18-day	23	3058.1		
27-day	39	3519.8		
OVERALL				
Bed 1	53	4186.8	0.0861	Not significant
Bed 2	67	3481.2		
Bed 3	66	3038.6		
Bed 4	68	3016.2		
Bed 5	38	3754.7		
Bed 6	53	3386.2		

Appendix S: Simulated Results for General Case

HL = 9345 cm^3 h = -12 cm Ks1 = 0.02 (cm/min) T1 = 8 cm

(a) Flux profiles

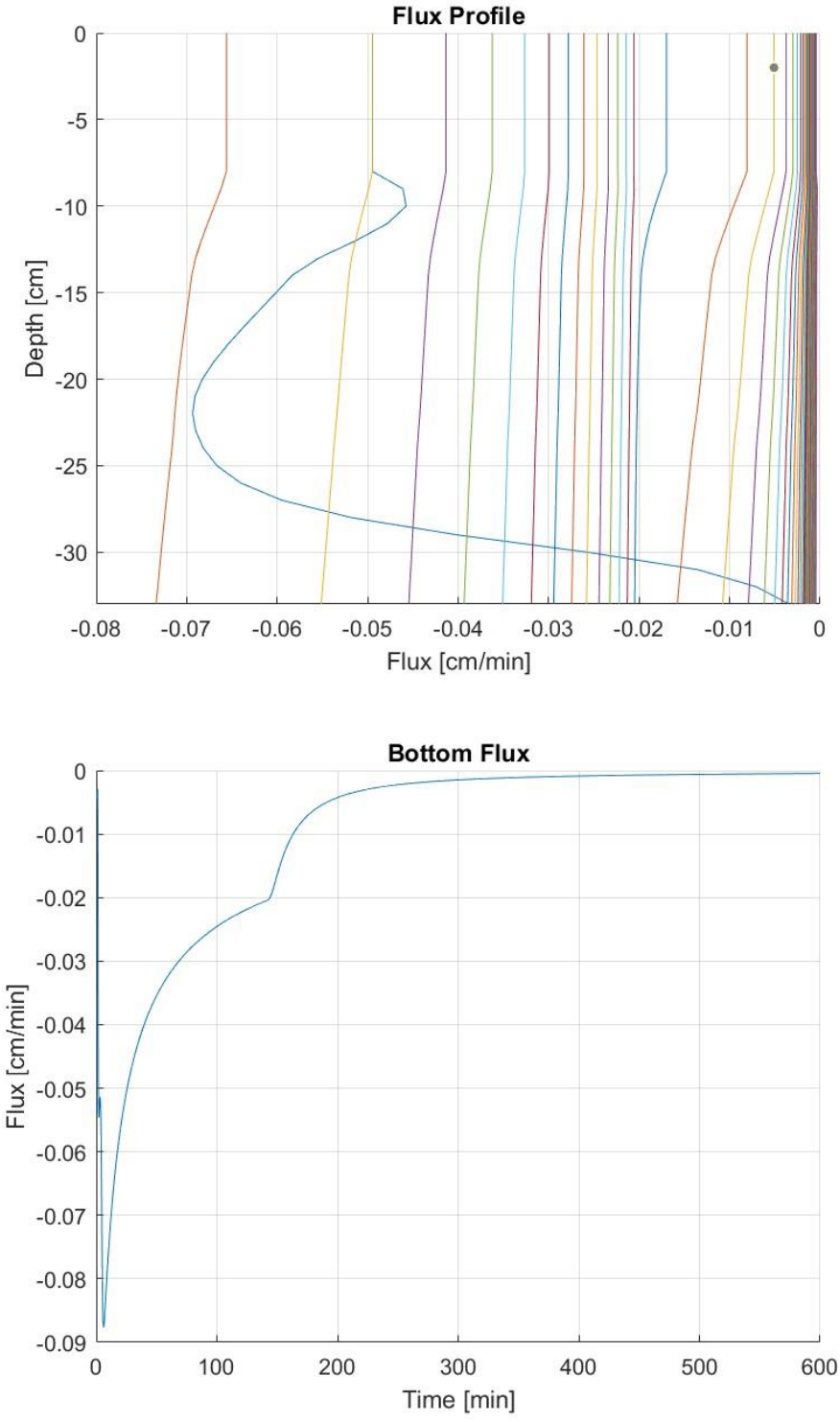

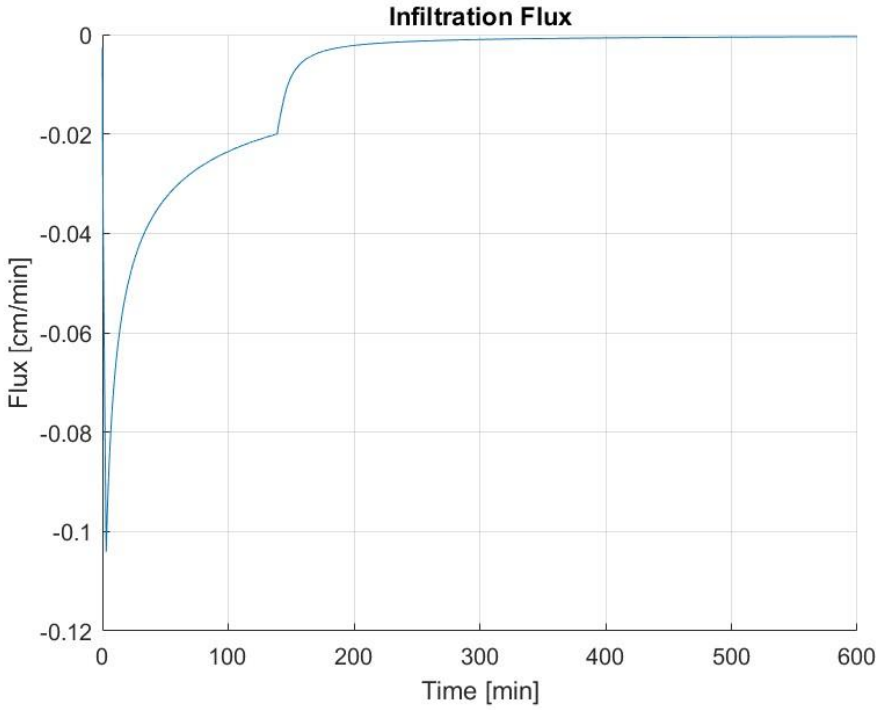

(b) Cumulative Flux Profile

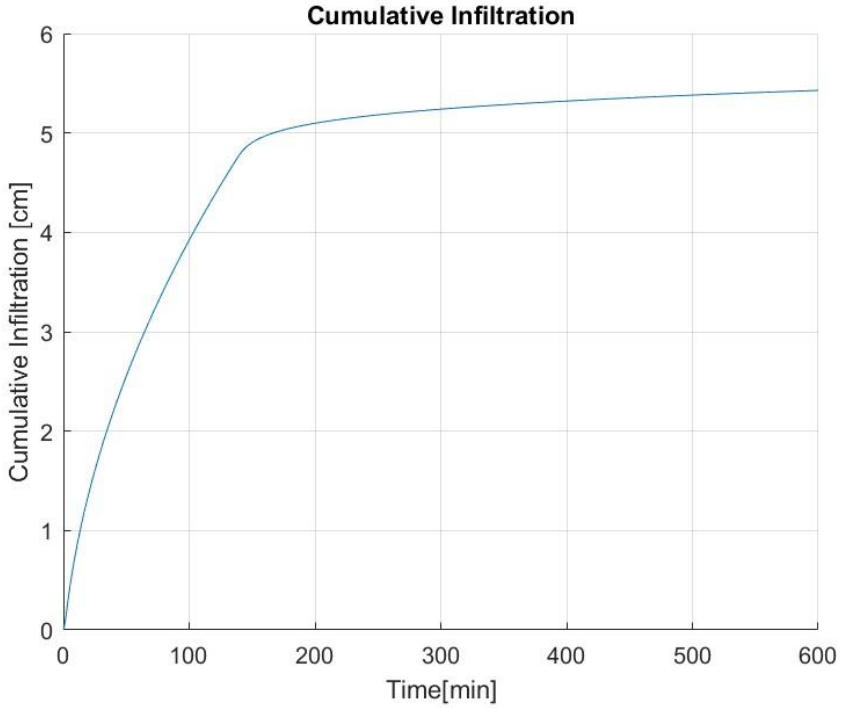

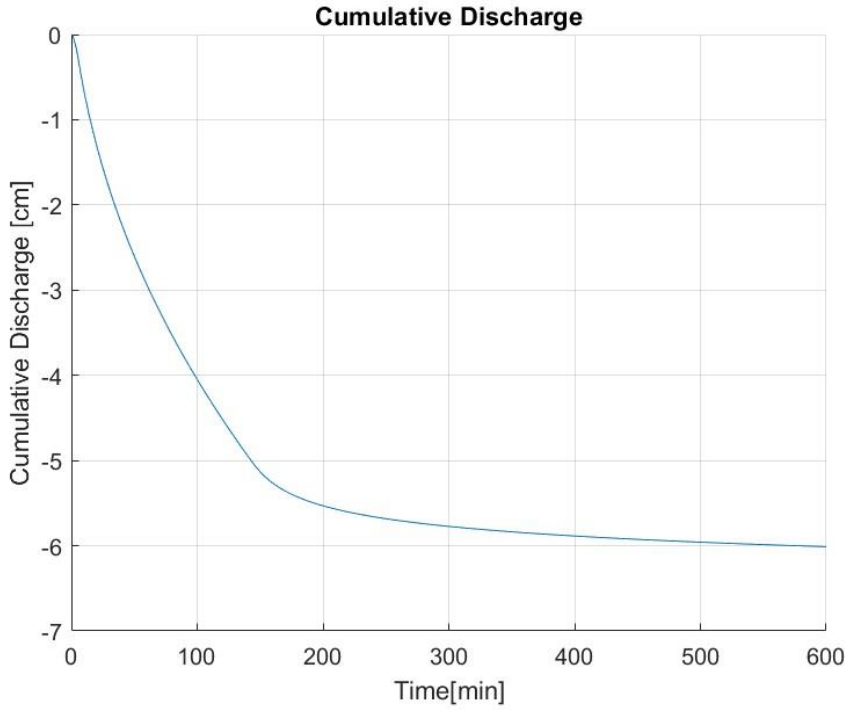

(c) Hydraulic Head Profile

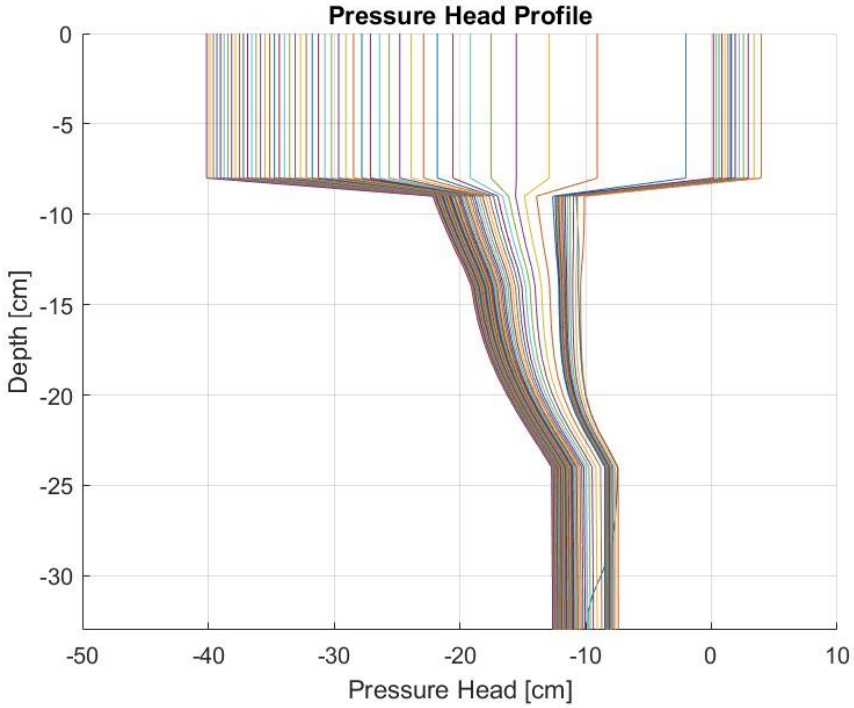

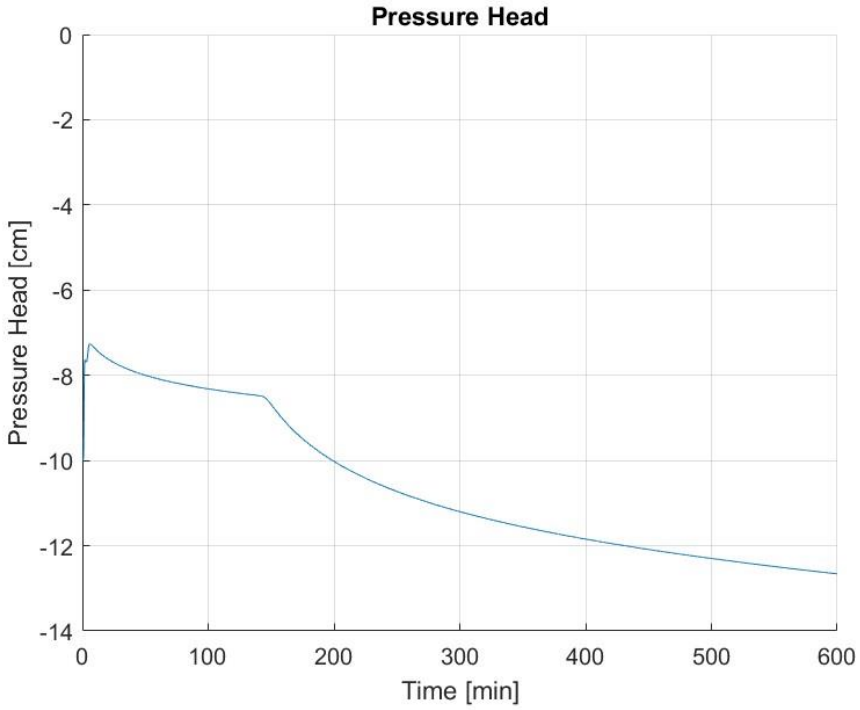

(d) Water Content Profile

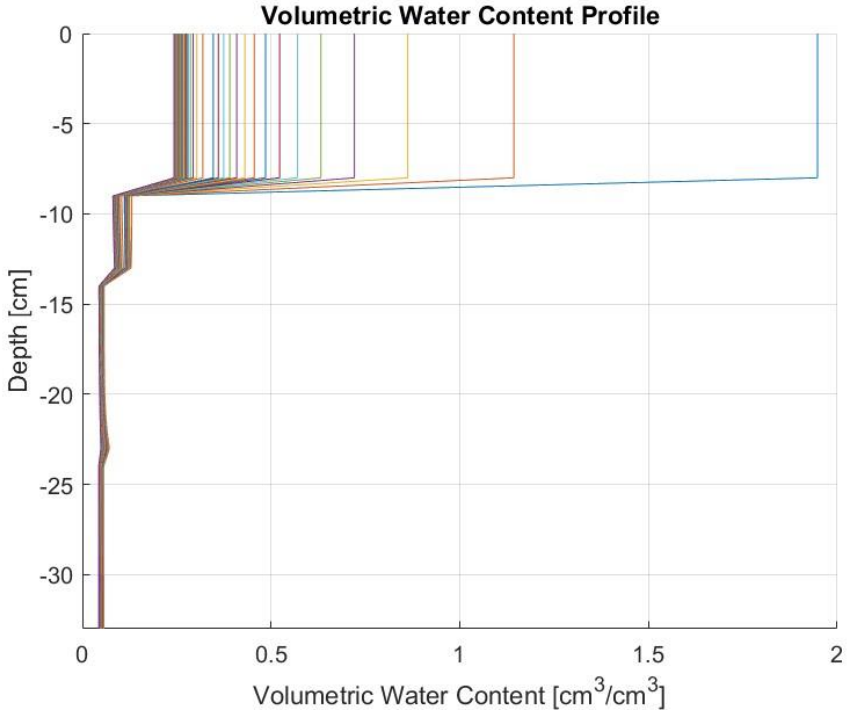

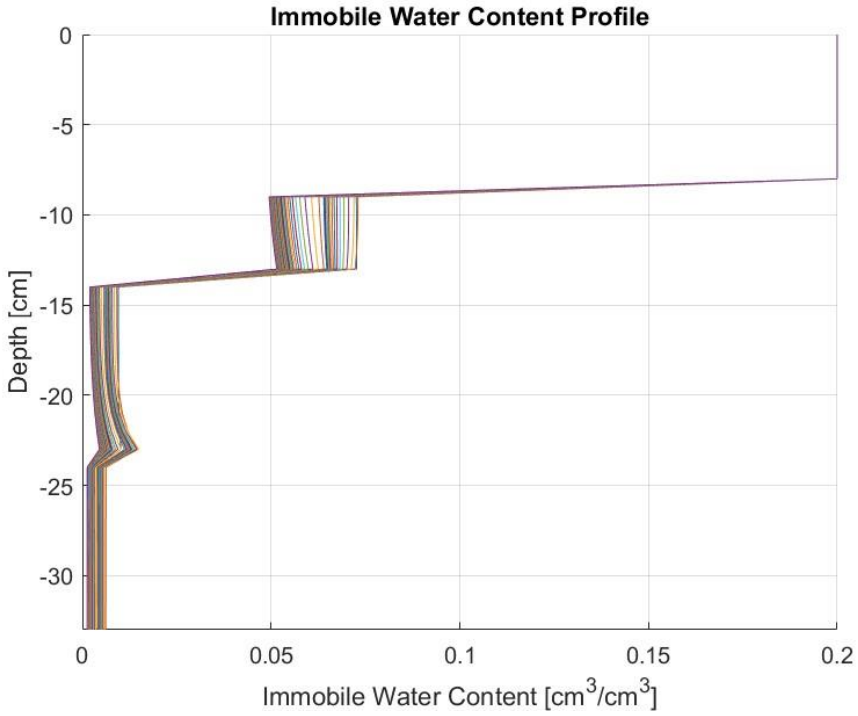
Immobile Water Content Profile
Depth [cm]
0
-5
-10
-15
-20
-25
-30
0
0.05
0.1
0.15
0.2
Immobile Water Content [cm3/cm3]

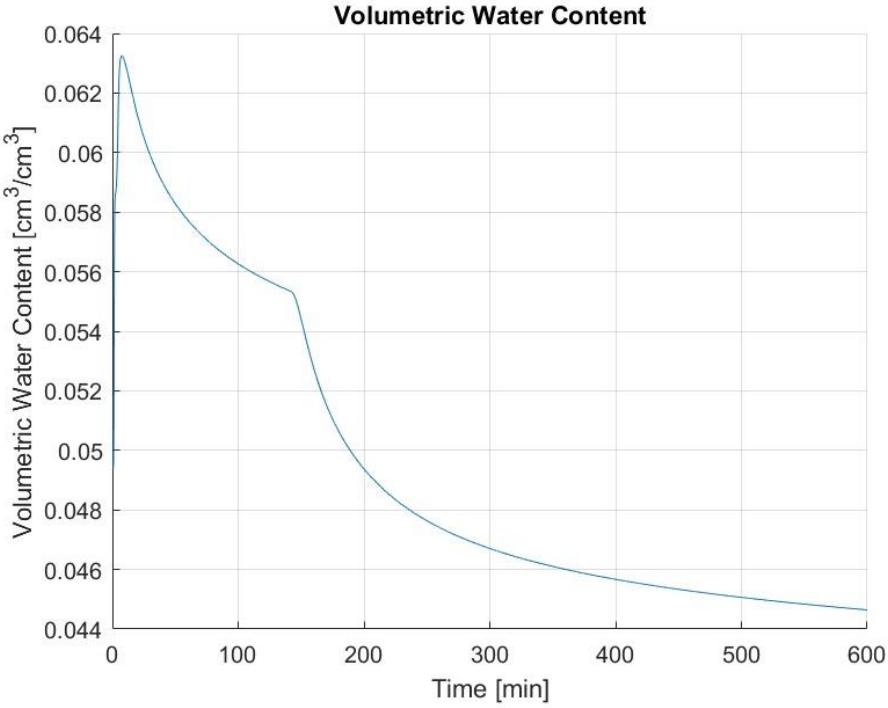
Volumetric Water Content
Volumetric Water Content [cm3/cm3]
0.064
0.062
0.06
0.058
0.056
0.054
0.052
0.05
0.048
0.046
0.044
0
100
200
300
400
500
600
Time [min]

(e) Root Water Uptake Profile

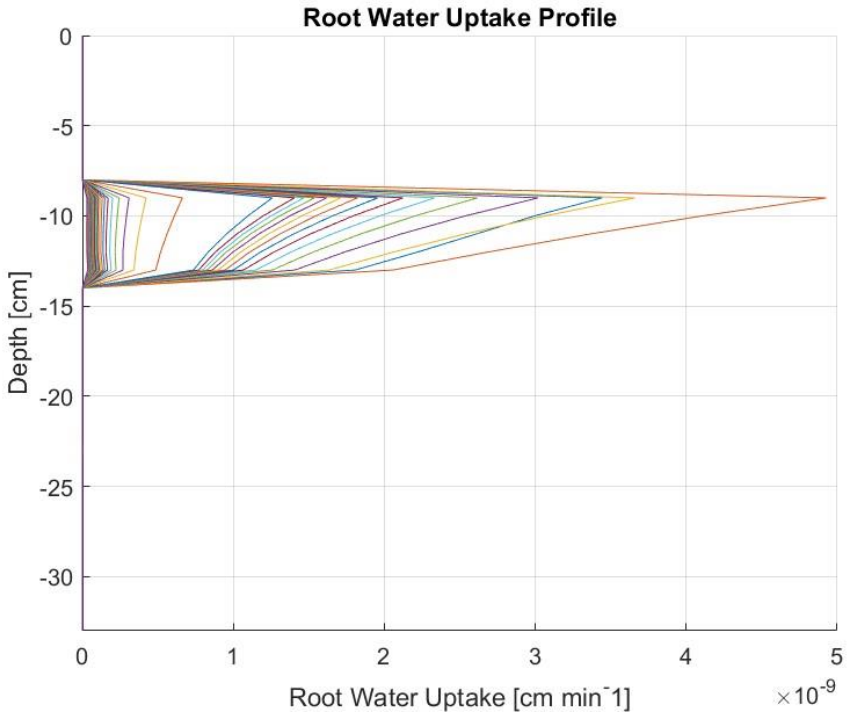

(f) Mass Transfer Rate Profile

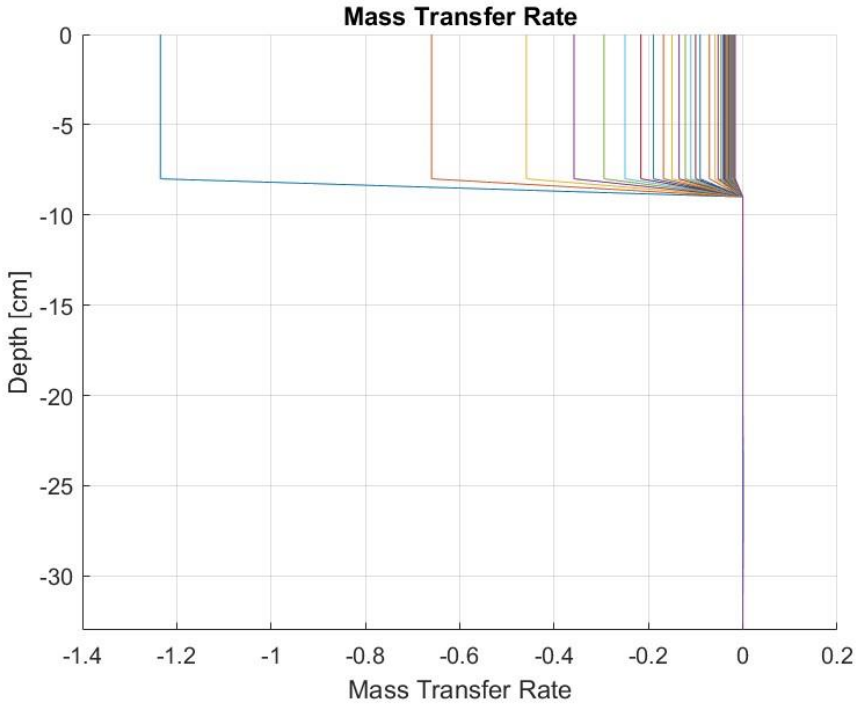

(g) Development of Sludge Profile

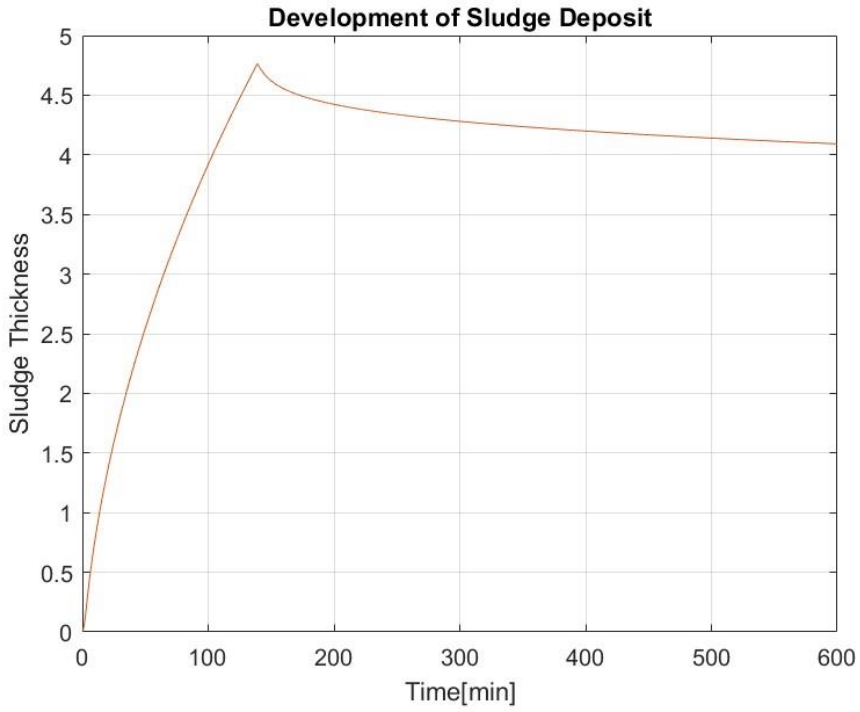

(h) Increment of dz Profile

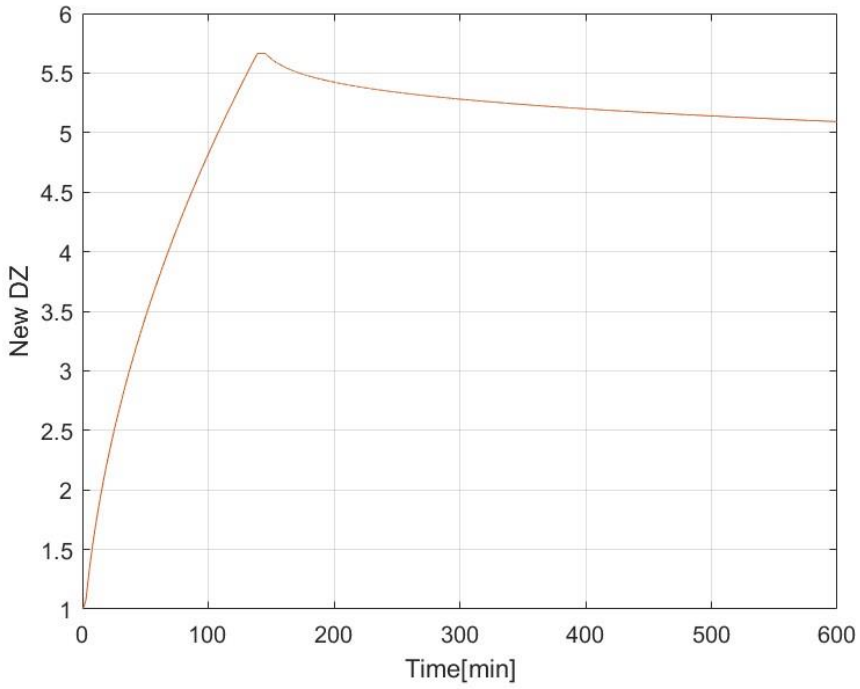

Appendix T: Summary of calibrated parameters and error analysis (RP=resting period, SLR=solids loading rate, HL=hydraulic load, T=sludge deposit layer thickness, WR=water recovery, FD=flow delay, FP=flux peak, $\tilde{V}$=average velocity).

Loading Batch | RP (days) | SLR (kg/m^2/year)			HL (cm^3)	T (cm)	WR (%)	FD (min)	FP (cm/min)	Calibrated h (cm)	Calibrated K_s (cm/min)	$\tilde{V}$ (cm/min)	MAE	MAE%	RMSE	R^2
SLR = 50 kg/m^2/year, Resting period = 6 days														
B	6	50	8,710	7.00	72.56	20	0.0199	-17	0.0060	-0.0097	0.00179	18.51	0.00272	0.8999
I	6	50	5,460	8.17	59.52	45	0.0081	-18	0.0025	-0.0042	0.00095	27.50	0.00138	0.7867
V	6	50	2,930	7.50	16.04	102	0.0001	-20	0.0001	0.0000	1.82E-05	12.47	2.35E-05	0.7331
AC	6	50	8,030	8.33	54.30	45	0.0153	-29	0.0030	-0.0065	0.00122	34.50	0.00191	0.7941
BA	6	50	15,150	7.83	78.68	18	0.0382	-29	0.0100	-0.0312	0.00593	16.92	0.00864	0.3650
BN	6	50	9,345	6.50	84.43	2	0.1019	-10	0.0250	-0.0700	0.00917	13.64	0.01388	0.8467
BR	6	50	9,345	7.50	92.83	1	0.0815	-10	0.0200	-0.0485	0.00665	11.12	0.01434	0.4895
Mean			**8,424**	**7.55**	**65.48**	**33**	**0.0379**	**-19**	**0.0095**	**-0.0243**	**0.00368**	**19.24**	**0.00613**	**0.7021**
Std Deviation			**3,789**	**0.64**	**25.61**	**35**	**0.0390**	**8**	**0.0095**	**0.0266**	**0.00352**	**8.66**	**0.00610**	**0.1981**
Minimum			**2,930**	**6.50**	**16.04**	**1**	**0.0001**	**-29**	**0.0001**	**-0.0700**	**0.00002**	**11.12**	**0.00002**	**0.3650**
Maximum			**15,150**	**8.33**	**92.83**	**102**	**0.1019**	**-10**	**0.0250**	**0.0000**	**0.00917**	**34.50**	**0.01434**	**0.8999**
SLR = 100 kg/m^2/year, Resting period = 6 days														
C	6	100	17,420	10.67	63.29	125	0.0051	-29	0.0004	-0.0021	0.00055	13.71	0.00078	0.7014
F	6	100	17,420	6.33	91.91	30	0.0199	-19	0.0015	-0.0086	0.00377	32.49	0.00550	0.1201
J	6	100	10,917	11.50	43.83	250	0.0005	-29	0.0001	-0.0003	0.00027	13.15	0.00030	0.4004
M	6	100	10,917	7.67	66.18	55	0.0326	-25	0.0014	-0.0084	0.00489	30.54	0.00896	0.3908
P	6	100	10,917	11.50	36.14	180	0.0004	-22	0.0001	-0.0003	0.00024	19.79	0.00028	0.1561
W	6	100	5,870	10.83	51.70	146	0.0003	-19	0.0001	-0.0002	0.00014	9.46	0.00016	0.4227
Z	6	100	5,870	7.67	43.78	144	0.0006	-22	0.0003	-0.0002	9.30E-05	28.05	0.00012	0.6784
AJ	6	100	16,070	11.00	54.39	110	0.0097	-29	0.0025	-0.0068	0.00106	10.97	0.00231	0.4381
BG	6	100	30,310	12.83	82.93	1	0.8098	-10	0.1000	-0.2716	0.07776	33.86	0.11715	0.6358
BJ	6	100	18,690	12.50	79.11	4	0.2190	-29	0.0500	-0.1298	0.02645	20.60	0.03592	0.7271
BO	6	100	18,690	12.17	82.72	1	0.3463	-10	0.0500	-0.1760	0.04874	26.45	0.07061	0.5633
Mean			**14,826**	**10.42**	**63.27**	**95**	**0.1313**	**-22**	**0.0188**	**-0.0549**	**0.01491**	**21.73**	**0.02201**	**0.4758**
Std Deviation			**7,006**	**2.19**	**18.84**	**83**	**0.2521**	**7**	**0.0334**	**0.0941**	**0.02592**	**9.01**	**0.03846**	**0.2084**
Minimum			**5,870**	**6.33**	**36.14**	**1**	**0.0003**	**-29**	**0.0001**	**-0.2716**	**0.00009**	**9.46**	**0.00012**	**0.1201**

Maximum			**30,310**	**12.83**	**91.91**	**250**	**0.8098**	**-10**	**0.1000**	**-0.0002**	**0.07776**	**33.86**	**0.11715**	**0.7271**
SLR = 150 kg/m^2/year, Resting period = 6 days														
D	6	150	26,140	7.83	69.93	20	0.0087	-15	0.0006	-0.0044	0.00036	11.10	0.00049	0.9382
K	6	150	16,380	11.33	47.31	145	0.0012	-25	0.0002	-0.0006	0.00035	12.84	0.00042	0.6191
Q	6	150	16,380	11.50	49.27	70	0.0010	-17	0.0001	-0.0006	0.00042	9.03	0.00048	0.2814
X	6	150	8,800	10.50	65.57	145	0.0006	-22	0.0002	-0.0003	0.00022	15.71	0.00025	0.5539
AK	6	150	24,110	11.00	59.21	77	0.0163	-29	0.0018	-0.0106	0.00367	28.31	0.00444	0.2057
AU	6	150	45,470	11.83	67.75	6	0.0738	-13	0.0065	-0.0508	0.00668	11.57	0.00850	0.8700
BC	6	150	45,470	11.33	81.49	2	0.2368	-9	0.0250	-0.1230	0.02372	16.33	0.03664	0.7433
BH	6	150	45,470	11.50	84.76	1	1.8844	-9	0.2000	-0.5049	0.21249	73.15	0.28728	0.6017
BK	6	150	28,040	10.83	86.45	1	0.4584	-10	0.0800	-0.2318	0.06559	30.63	0.10059	0.5455
BT	6	150	28,040	12.33	86.45	1	0.0968	-29	0.0175	-0.0748	0.02562	28.07	0.03115	0.2123
BW	6	150	28,040	12.33	96.47	1	0.2648	-8	0.0275	-0.1219	0.03638	28.14	0.04721	0.4653
Mean			**28,395**	**11.12**	**72.24**	**43**	**0.2766**	**-17**	**0.0327**	**-0.1022**	**0.03414**	**24.08**	**0.04704**	**0.5488**
Std Deviation			**12,535**	**1.23**	**16.19**	**58**	**0.5532**	**8**	**0.0603**	**0.1524**	**0.06264**	**18.19**	**0.08541**	**0.2469**
Minimum			**8,800**	**7.83**	**47.31**	**1**	**0.0006**	**-29**	**0.0001**	**-0.5049**	**0.00022**	**9.03**	**0.00025**	**0.2057**
Maximum			**45,470**	**12.33**	**96.47**	**145**	**1.8844**	**-8**	**0.2000**	**-0.0003**	**0.21249**	**73.15**	**0.28728**	**0.9382**
SLR = 100 kg/m^2/year, Resting period = 3 days														
A	3	100	8,710	5.50	69.06	30	0.0054	-18	0.0015	-0.0038	0.00089	19.85	0.00113	0.7004
E	3	100	8,710	8.17	51.38	50	0.0066	-20	0.0010	-0.0034	0.00093	19.13	0.00130	0.7302
G	3	100	8,710	7.00	113.61	40	0.0064	-20	0.0015	-0.0038	0.00118	24.89	0.00144	0.5631
L	3	100	5,460	7.83	66.85	145	0.0019	-21	0.0005	-0.0008	0.00030	14.23	0.00037	0.7130
N	3	100	5,460	8.33	48.08	90	0.0006	-18	0.0002	-0.0003	0.00016	28.27	0.00018	0.6304
R	3	100	5,460	8.83	57.60	175	0.0007	-20	0.0003	-0.0003	0.00025	27.77	0.00028	0.4679
U	3	100	2,930	9.67	45.56	250	0.0006	-25	0.0004	-0.0002	9.86E-05	12.02	0.00011	0.7841
Y	3	100	2,930	9.50	45.90	146	0.0003	-22	0.0002	-0.0001	5.67E-05	13.39	6.50E-05	0.9060
AA	3	100	2,930	10.67	65.19	250	0.0005	-22	0.0004	-0.0002	5.92E-05	13.81	8.88E-05	0.9620
AF	3	100	8,030	10.67	54.30	100	0.0041	-29	0.0008	-0.0021	0.00033	7.88	0.00051	0.8534
Mean			**5,933**	**8.62**	**61.75**	**128**	**0.0027**	**-22**	**0.0007**	**-0.0015**	**0.00043**	**18.12**	**0.00055**	**0.7311**
Std Deviation			**2,478**	**1.62**	**20.17**	**80**	**0.0026**	**3**	**0.0005**	**0.0016**	**0.00041**	**7.02**	**0.00054**	**0.1530**
Minimum			**2,930**	**5.50**	**45.56**	**30**	**0.0003**	**-29**	**0.0002**	**-0.0038**	**0.00006**	**7.88**	**0.00007**	**0.4679**
Maximum			**8,710**	**10.67**	**113.61**	**250**	**0.0066**	**-18**	**0.0015**	**-0.0001**	**0.00118**	**28.27**	**0.00144**	**0.9620**

SLR = 100 kg/m^2/year, Resting period = 9 days														
H	9	100	26,140	8.33	84.56	45	0.0076	-23	0.0009	-0.0053	0.00064	8.19	0.00124	0.7882
T	9	100	16,380	8.50	49.91	125	0.0031	-29	0.0004	-0.0013	0.00044	22.39	0.0006	0.7715
AB	9	100	8,800	11.33	58.86	250	0.0012	-22	0.0009	-0.0002	4.98E-05	4.94	7.54E-05	0.9607
AN	9	100	24,110	11.00	49.13	50	0.0188	-29	0.0030	-0.0120	0.00265	17.54	0.00435	0.3643
AZ	9	100	45,470	12.33	78.02	6	0.1502	-29	0.0200	-0.1086	0.03432	29.05	0.04282	0.4706
BE	9	100	45,470	12.17	83.63	6	0.0331	-12	0.0020	-0.0276	0.00707	23.37	0.00797	0.4850
BQ	9	100	28,040	13.00	80.60	1	0.1732	-9	0.0100	-0.0666	0.02057	27.95	0.02688	0.2968
BZ	9	100	28,040	13.00	78.78	2	0.0840	-9	0.0030	-0.0313	0.00616	17.29	0.00868	0.7869
Mean			**27,806**	**11.21**	**70.44**	**61**	**0.0589**	**-20**	**0.0050**	**-0.0316**	**0.00899**	**18.84**	**0.01158**	**0.6155**
Std Deviation			**12,719**	**1.86**	**15.18**	**87**	**0.0691**	**9**	**0.0068**	**0.0381**	**0.01225**	**8.71**	**0.01532**	**0.2407**
Minimum			**8,800**	**8.33**	**49.13**	**1**	**0.0012**	**-29**	**0.0004**	**-0.1086**	**0.00005**	**4.94**	**0.00008**	**0.2968**
Maximum			**45,470**	**13.00**	**84.56**	**250**	**0.1732**	**-9**	**0.0200**	**-0.0002**	**0.03432**	**29.05**	**0.04282**	**0.9607**
SLR = 100 kg/m^2/year, Resting period = 18 days														
AL	18	100	55,210	10.00	52.20	68	0.0163	-29	0.0008	-0.0081	0.00180	12.71	0.00300	0.6390
AY	18	100	90,940	10.33	77.64	1	0.4456	-6	0.0040	-0.0774	0.02179	19.95	0.03874	0.8020
BL	18	100	56,080	12.33	93.59	11	0.0458	-29	0.0033	-0.0305	0.00372	10.39	0.00536	0.8760
BX	18	100	56,080	11.50	92.80	1	0.0738	-9	0.0010	-0.0243	0.00778	25.08	0.01201	0.5989
Mean			**64,578**	**11.04**	**79.06**	**20**	**0.1454**	**-18**	**0.0023**	**-0.0351**	**0.00877**	**17.03**	**0.01478**	**0.7290**
Std Deviation			**17,580**	**1.07**	**19.35**	**32**	**0.2015**	**12**	**0.0016**	**0.0298**	**0.00903**	**6.74**	**0.01642**	**0.1316**
Minimum			**55,210**	**10.00**	**52.20**	**1**	**0.0163**	**-29**	**0.0008**	**-0.0774**	**0.00180**	**10.39**	**0.00300**	**0.5989**
Maximum			**90,940**	**12.33**	**93.59**	**68**	**0.4456**	**-6**	**0.0040**	**-0.0081**	**0.02179**	**25.08**	**0.03874**	**0.8760**
SLR = 100 kg/m^2/year, Resting period = 27 days														
AM	27	100	90,315	8.00	86.25	10	0.1197	-28	0.0040	-0.0360	0.00386	8.40	0.00786	0.8963
BY	27	100	84,120	12.17	70.30	11	0.0688	-29	0.0023	-0.0274	0.00277	6.08	0.00608	0.8954
Mean			**87,218**	**10.09**	**78.28**	**11**	**0.0943**	**-29**	**0.0032**	**-0.0317**	**0.00332**	**7.24**	**0.00697**	**0.8959**
Std Deviation			**4,381**	**2.95**	**11.28**	**1**	**0.0360**	**1**	**0.0012**	**0.0061**	**0.00077**	**1.64**	**0.00126**	**0.0006**
Minimum			**84,120**	**8.00**	**70.30**	**10**	**0.0688**	**-29**	**0.0023**	**-0.0360**	**0.00277**	**6.08**	**0.00608**	**0.8954**
Maximum			**90,315**	**12.17**	**86.25**	**11**	**0.1197**	**-28**	**0.0040**	**-0.0274**	**0.00386**	**8.40**	**0.00786**	**0.8963**
MAE% > 35%														
O	6	50	5,460	8.83	61.90	20	0.0168	-15	0.0035	-0.0053	0.00214	52.89	0.00273	0.6439
AI	6	50	8,030	7.00	28.77	30	0.0173	-29	0.0055	-0.0070	0.00402	63.39	0.00484	0.6857

AO	6	50	15,150	6.17	73.43	1	1.0008	-9	0.2400	-0.1676	0.20960	153.27	0.31130	0.1611
AS	6	50	15,150	8.17	80.33	7	0.1502	-29	0.0350	-0.0830	0.02277	42.10	0.03201	0.4313
AV	6	50	15,150	7.50	75.76	2	0.2903	-10	0.0500	-0.1038	0.02909	72.76	0.04093	0.7818
BF	6	50	15,150	7.83	85.81	1	0.3081	-9	0.0550	-0.1149	0.04481	54.41	0.05364	0.7068
BI	6	50	9,345	7.00	84.43	2	0.2597	-10	0.0700	-0.1035	0.05564	75.58	0.06781	0.5157
BU	6	50	9,345	7.50	96.95	1	0.2801	-9	0.0750	-0.1201	0.03532	67.42	0.04962	0.7504
S	6	100	10,917	8.83	59.77	70	0.0132	-29	0.0018	-0.0053	0.00209	44.12	0.00287	0.3872
AD	6	100	16,070	11.67	55.57	200	0.0028	-29	0.0005	-0.0008	0.00055	62.45	0.00085	0.5011
AG	6	100	16,070	8.50	55.91	95	0.0046	-29	0.0006	-0.0023	0.00062	84.44	0.00094	0.7087
AP	6	100	30,310	12.33	85.60	1	2.6050	-10	0.6000	-0.3481	0.30056	150.95	0.45437	0.6449
AT	6	100	30,310	11.33	79.99	4	0.3323	-29	0.0600	-0.1386	0.07135	69.28	0.08795	0.4326
AW	6	100	30,310	11.33	84.87	1	1.2783	-10	0.2500	-0.2525	0.14269	151.99	0.22358	0.7165
BB	6	100	30,310	11.50	80.96	5	0.3005	-29	0.0400	-0.1675	0.07103	43.36	0.08919	0.3346
BS	6	100	18,690	12.17	92.70	3	0.1604	-11	0.0250	-0.0882	0.03702	204.27	0.04106	0.5752
BV	6	100	18,690	12.50	97.03	2	0.1935	-10	0.0275	-0.1314	0.04786	40.84	0.05482	0.7279
AE	6	150	24,110	9.67	44.38	90	0.0059	-29	0.0007	-0.0028	0.00114	174.09	0.00183	0.4767
AQ	6	150	45,470	11.50	88.04	1	2.0041	-9	0.2500	-0.4892	0.29180	331.72	0.37440	0.7404
AX	6	150	45,470	11.00	80.16	1	2.7833	-13	0.4000	-0.4839	0.33655	287.70	0.56722	0.4754
BP	6	150	28,040	11.83	87.82	1	1.7876	-8	0.3500	-0.5013	0.33957	158.10	0.48975	0.2831
AH	3	100	8,030	10.67	50.75	170	0.0008	-29	0.0004	-0.0003	0.00023	109.56	0.00034	0.2067
AR	9	100	45,470	11.33	71.23	1	0.6952	-7	0.0500	-0.2351	0.09304	54.67	0.12246	0.5645
BM	9	100	28,040	12.67	97.11	1	0.1222	-29	0.0200	-0.0875	0.03665	35.15	0.04406	0.1231
BD	27	100	110,000	10.83	83.39	1	0.9906	-6	0.0400	-0.1233	0.18456	125.76	0.26515	0.2988
Mean			**25,163**	**9.99**	**75.31**	**28**	**0.6241**	**-17**	**0.1060**	**-0.1505**	**0.09443**	**108.41**	**0.13535**	**0.5150**
Std Deviation			**21,298**	**2.04**	**17.71**	**55**	**0.8350**	**10**	**0.1544**	**0.1552**	**0.11384**	**77.96**	**0.17290**	**0.1986**
Minimum			**5,460**	**6.17**	**28.77**	**1**	**0.0008**	**-29**	**0.0004**	**-0.5013**	**0.00023**	**35.15**	**0.00034**	**0.1231**
Maximum			**110,000**	**12.67**	**97.11**	**200**	**2.7833**	**-6**	**0.6000**	**-0.0003**	**0.33957**	**331.72**	**0.56722**	**0.7818**
Overall														
Mean			**24,077**	**10.00**	**70.33**	**55**	**0.2772**	**-19**	**0.0429**	**-0.0786**	**0.03902**	**48.25**	**0.05586**	**0.5898**
Std Deviation			**21,622**	**2.03**	**18.62**	**72**	**0.5756**	**8**	**0.1003**	**0.1231**	**0.07886**	**60.87**	**0.11702**	**0.2208**
Minimum			**2,930**	**5.50**	**16.04**	**1**	**0.0001**	**-29**	**0.0001**	**-0.5049**	**1.82E-05**	**4.94**	**2.35E-05**	**0.1201**
Maximum			**110,000**	**13.00**	**113.61**	**250**	**2.7833**	**-6**	**0.6000**	**0.0000**	**0.33957**	**331.72**	**0.56722**	**0.9620**

Appendix U: Weather Data

(a) Air Temperature

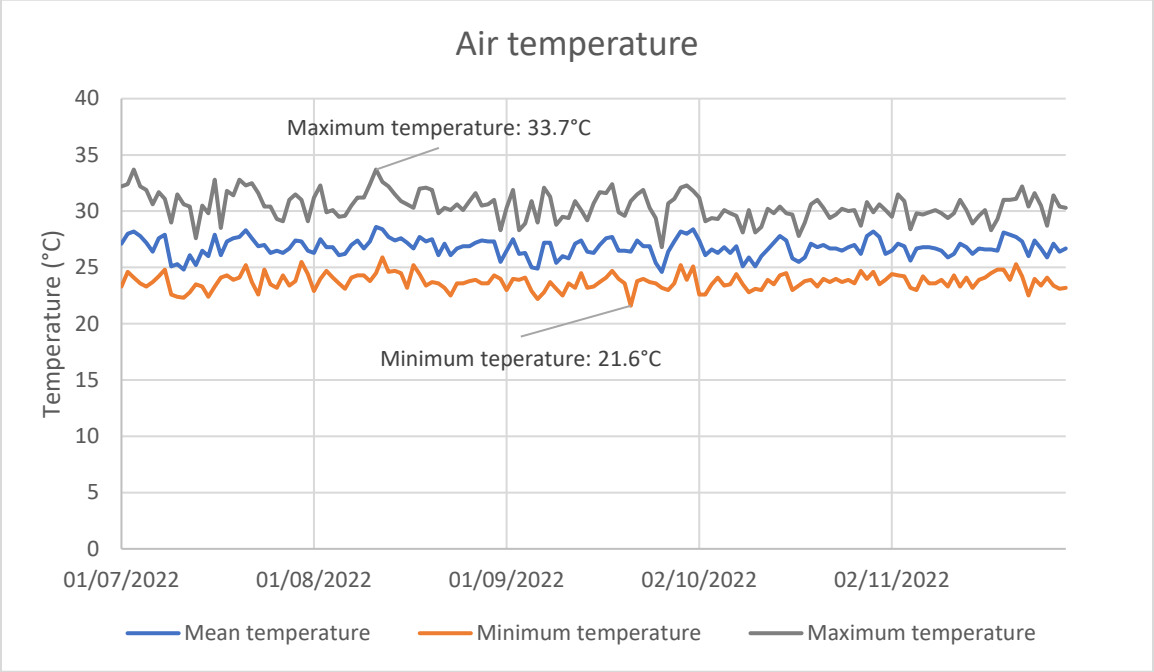

(b) Wind Speed

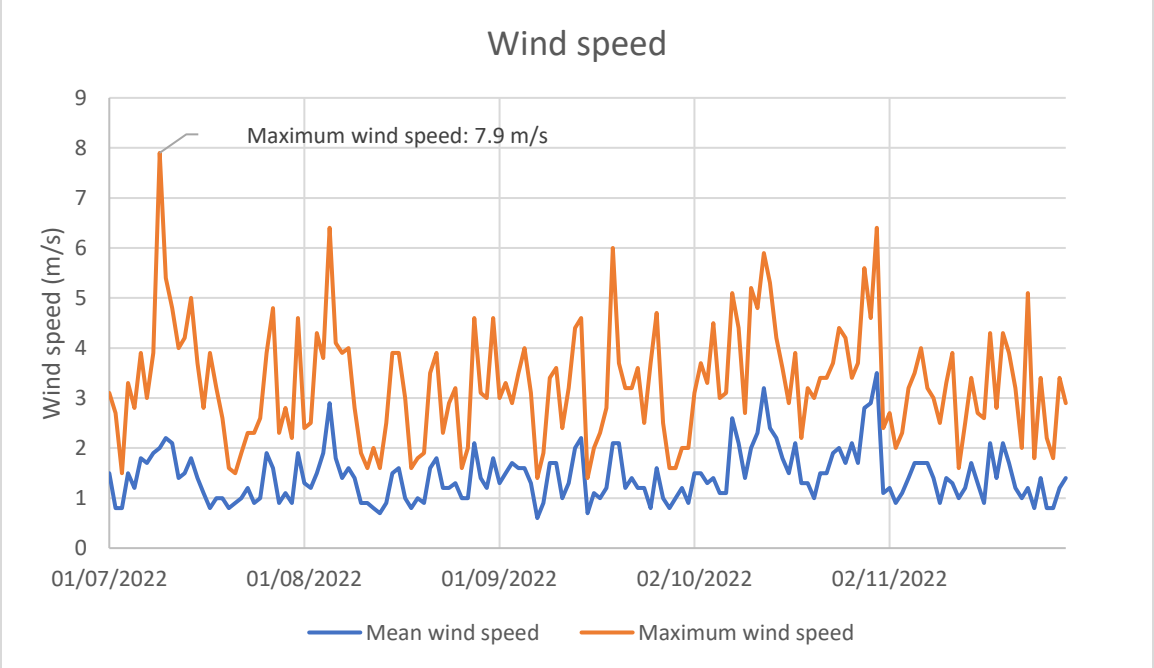

(c) Relative Humidity

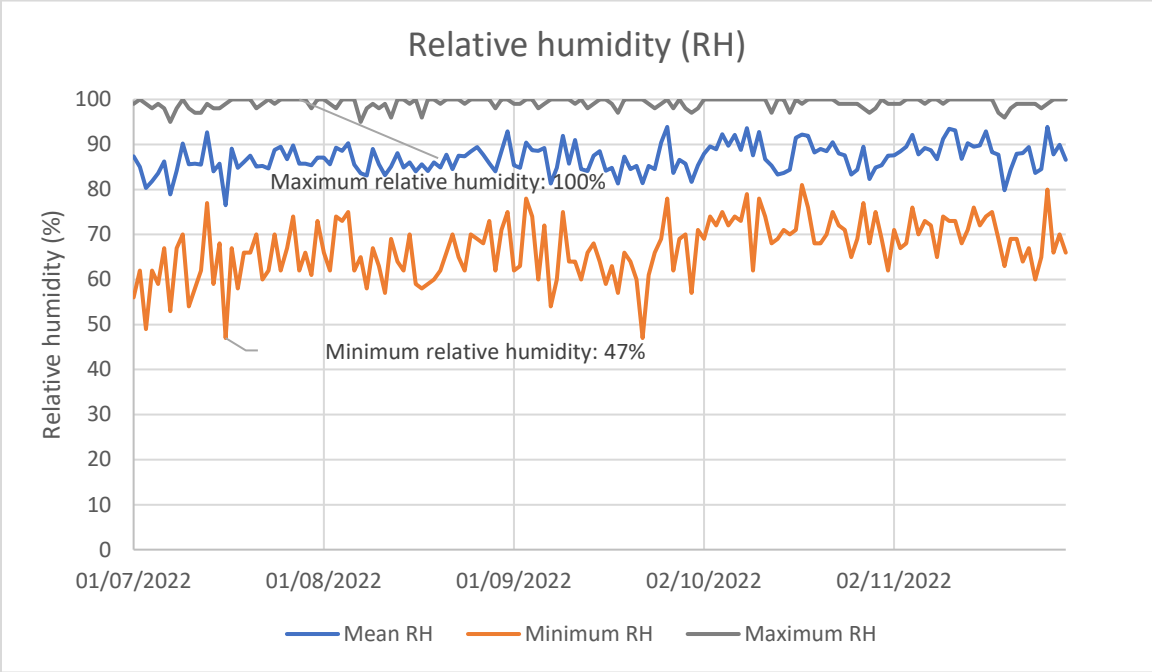

(d) Total Rainfall